Optimization and control of storage in smart grids

Md Umar Hashmi

PSL
UNIVERSITÉ PARIS

THÈSE DE DOCTORAT
DE L'UNIVERSITÉ PSL

Préparée à École Normale Supérieure

Optimization and Control of Storage in Smart Grids

Soutenue par
Md Umar Hashmi
Le 6 Décembre 2019

École doctorale n°386
Sciences Mathématiques de Paris Centre

Spécialité
Informatique

Composition du jury :

Daniel Kofman Télécom ParisTech	*Président du Jury*
Prabir Barooah University of Florida	*Rapporteur*
Luce Brotcorne Inria Lille	*Rapporteur*
Jean Maeght Réseau de Transport d'Electricité	*Examinateur*
Nadia Oudjane Électricité de France	*Examinateur*
Hrvoje Pandžić University of Zagreb	*Examinateur*
Ana Bušić INRIA de Paris	*Encadrante de thèse*
Marc Lelarge INRIA de Paris	*Directeur de thèse*

ENS | PSL

In the name of God, the most gracious, the most merciful

Dedicated to my parents, my sister and Aayan and Hamdan.

Contents

Abstract

The power system transformation brings new challenges and opportunities due to changes and uncertainties in electricity consumption and generation. High integration of intermittent solar and wind generation requires fast ramping resources to satisfy the growing demand, triggered by the electrification of the transportation sector. Energy storage is one possible solution to facilitate such a transformation. In this thesis Li-Ion battery, as energy storage, is used both at the level of individual consumers minimizing the cost of electricity and at the grid level for increasing reliability and stability of the power network. The cost of the batteries being still high, the importance is also given to the health of the battery taking into account its degradation in optimization and control formulations.

Electricity consumers with local renewable generation such a rooftop solar generation can use a battery to minimize their cost of operation. We formulate storage optimization problem under time-varying electricity prices with different net-metering policies. The strong Lagrangian theory based storage operation solution is developed with threshold-based structure of the optimal charging policy. The proposed algorithm is computationally efficient with quadratic worst-case complexity with respect to the horizon length.

Due to their high-cost batteries need to be used for more than one dedicated application for becoming financially viable. New billing mechanisms worldwide facilitate such a storage operation. In the co-optimization formulations, we consider storage performing energy arbitrage under net metering along with power factor correction, peak demand shaving, and energy backup for power outages. These formulations are evaluated on case studies using real data. To implement the above algorithms in real time, autoregressive forecast in context of receding/rolling horizon model predictive control is proposed. Further, prosumer storage applications are explored for low voltage consumers in Madeira and Uruguay. These control policies are tailored based on consumer contracts proposed by the utility.

Large-scale storage applications facilitating dynamic regulation and phase balancing using storage are proposed for increasing power system reliability. A distributed stochastic control is implemented for a fleet of geographically distributed batteries for tracking fast timescale supply and demand imbalance, while also ensuring that the mean charge level of the fleet stays close to the desired level. Based on real-world data case studies for a substation in Madeira and network-based simulations, we show that phase unbalance can be an outcome of ad hoc distributed generation and electric vehicle charging placement in the context of phase imbalance. Storage control architectures are proposed for reducing the phase imbalance.

Battery life is commonly quantified using cycle life and calendar life. In other words, battery degradation happens due to operational cycles and the age of the battery. To increase the operational life of the battery, age-based storage degradation should be matched with the operational cycle based degradation. We propose an effective mechanism to control the cycles of operation, thus reducing the stress on the battery. Such considerations of storage health are embedded in the control and the optimization design for the batteries.

Several case studies using real data are conducted to evaluate the performance of the storage control and optimization algorithms. We observe that the ever-decreasing prices of batteries and the growing share of intermittent renewables will only increase the relevance of this work for future power networks.

Résumé

La transformation du système électrique due aux changements et aux incertitudes de la consommation et de la production apporte de nouveaux défis et de nouvelles opportunités. La forte intégration de la production intermittente d'énergie solaire et éolienne nécessite des ressources à montée en puissance rapide afin de satisfaire la demande croissante, déclenchée par l'électrification du secteur des transports. Le stockage d'énergie est une solution possible pour faciliter une telle transformation. Dans cette thèse, la batterie Li-Ion est utilisée à la fois au niveau des consommateurs individuels, minimisant le coût de l'électricité, et au niveau du réseau pour accroître la fiabilité et la stabilité du réseau électrique. Le coût des batteries étant encore élevé, l'importance est également donnée à la durée de vie de la batterie, compte tenu de sa dégradation dans les formulations d'optimisation et de contrôle.

Les consommateurs d'électricité avec la génération renouvelable locale peuvent utiliser une batterie pour minimiser leurs coûts de fonctionnement. Nous formulons le problème d'optimisation du stockage sous des prix de l'électricité variables dans le temps avec différentes politiques de facturation nette. Basée sur la théorie lagrangienne forte, le contrôle optimal du stockage est développé, ayant une structure à seuils. L'algorithme proposé est efficace du point de vue calcule, avec une complexité quadratique dans le pire de cas par rapport à la longueur de l'horizon.

En raison de son coût élevé, les batteries doivent être utilisées dans plusieurs applications pour devenir plus pertinentes financièrement. Dans les formules de co-optimisation, nous considérons que le stockage effectue un arbitrage énergétique sous la facturation nette, ainsi que la correction du facteur de puissance, la réduction de la demande de pointe et la réserve de l'énergie en cas de coupures de courant. Ces formulations sont évaluées sur des études de cas utilisant des données réelles. Pour mettre en œuvre les algorithmes ci-dessus en temps réel, des prévisions autorégressives sont proposées dans le contexte du contrôle prédictif du modèle en recul / horizon glissant. De plus, des applications de stockage sont explorées pour les consommateurs à basse tension à Madère et en Uruguay. Ces politiques de contrôle sont adaptées en fonction des contrats de consommation proposés par le fournisseur.

Des applications de stockage à grande échelle, facilitant la régulation dynamique et l'équilibrage de phase, sont proposées pour accroître la fiabilité du système d'alimentation électrique. Un algorithme de contrôle stochastique distribué est mis en œuvre pour un parc de batteries réparties géographiquement afin de suivre les déséquilibres rapides de l'offre et de la demande, tout en veillant à ce que le niveau de charge moyen du parc reste proche du niveau souhaité. Sur la base d'une étude de cas réelle sur une sous-station à Madère et des simulations réseaux, nous montrons que le déséquilibre de phase peut résulter de la génération distribuée ad hoc et du placement de la charge de véhicules électriques dans un contexte de déséquilibre de phase. Des architectures de contrôle de stockage sont proposées pour réduire le déséquilibre de phase.

La durée de vie de la batterie est généralement quantifiée en se basant sur la durée de vie en cycle et en calendrier. Afin d'augmenter la durée de vie de la batterie, la dégradation du stockage en fonction de l'âge doit être adaptée à celle basée sur le cycle opérationnel. Nous proposons un mécanisme efficace pour contrôler les cycles de fonctionnement, réduisant ainsi les contraintes sur la batterie. Ces considérations sur la durée de vie du stockage sont intégrées dans l'optimisation et le contrôle des batteries.

Plusieurs études de cas utilisant des données réelles sont menées pour évaluer les performances des algorithmes de l'optimisation et le contrôle du stockage. Nous constatons que les prix en baisse constante des batteries et la part croissante des énergies renouvelables intermittentes ne feront que renforcer la pertinence de ce travail pour les futurs réseaux électriques.

Abbreviations

AEC	Area Control Error
ARIMA	Autoregressive integrated moving average
ARMA	AutoRegressive Moving Average
BESS	Battery Energy Storage System
BPA	Bonneville Power Administration
CAISO	California Independent System Operator
COFR	Continuous Operating Frequency Range
CPUC	California Public Utilities Commission
ENTOSE	European Network Transmission System Operators for Electricity
DER	Distributed Energy Resources
DoD	Depth-of-Discharge
DG	Distributed Generation
DSO	Distribution System Operators
EEM	Empresa de Electricidade da Madeira
EoL	End-of-Life
ERCOT	Electric Reliability Council of Texas
EV	Electric Vehicle
FERC	Federal Energy Regulatory Commission
FPL	Florida Power and Light
ISO	Independent system operator
ISO-NE	ISO New England
Li-Ion	Lithium Ion
LMP	Locational Marginal Prices
LP	Linear Programming
LQR	Linear Quadratic Regulator
LV	Low Voltage
MDP	Markov Decision Process
MISO	Midcontinent Independent System Operator
MPC	Model Pedictive Control
MV	Medium Voltage
MWh	Mega Watt hours
NEM	Net Energy Metering
NERC	North American Electric Reliability Corporation
NYISO	New York ISO
PF	Power Factor
PFC	Power Factor Correction
PPC	Peak Power Contract
PJM	Pennsylvania-New Jersey-Maryland
PV	PhotoVoltaic
RegD	Regulation Dynamic
RES	Renewable Energy Sources
RMSE	Root-Mean Square Error
RTP	Real Time electricity Price
QoS	Quality-of-Service
RES	Renewable Energy Source
RMC(P)CP	Regulation Market Capability (Performance) Clearing Price
SAIDI	System Average Interruption Duration Index
SoC	State-of-Charge
TOU	Time-Of-Use
VUF	Voltage Unbalance Factor

Some Notations

i	Index for time instant; $i \in \{1, 2, ..., N\}$
N	Total number of time instants in the time-horizon
h_i	Sampling time at time instant i; h without time index denotes constant sampling time.
T	Total time in the time-horizon; $T = \sum_{i=1}^{N} h_i$.
η_{ch}	Charging efficiency of battery; $\eta_{\text{ch}} \in (0, 1]$.
η_{dis}	Discharging efficiency of battery; $\eta_{\text{dis}} \in (0, 1]$.
δ_i	Change in battery capacity at time instant i; units Watts; $\delta_i \in [\delta_{\min}, \delta_{\max}]$
x_i	Change in battery capacity at time instant i; units Wh; $x_i = \delta_i h_i$
b_i	Battery capacity at time instant i; units watt-hour; $b_i = b_{i-1} + x_i$. $b_i \in [b_{\min}, b_{\max}]$.
$b_{\min}$	Minimum permissible battery capacity in watt-hours
$b_{\max}$	Maximum permissible battery capacity in watt-hours
b_{rated}	Rated battery capacity in watt-hour.
SoC_i	State-of-Charge at time i; $\text{SoC}_i = b_i/b_{\text{rated}}$.
$\text{SoC}_{\min}$	Minimum permissible state of charge of the battery.
$\text{SoC}_{\max}$	Maximum permissible state of charge of the battery.
$\delta_{\min}$	Minimum discharge rate in watts; $\delta_{\min} < 0$
$\delta_{\max}$	Minimum charge rate in watts; $\delta_{\max} > 0$
d_i	Inelastic consumer load at time instant i in joules
r_i	Renewable generation at time instant i in joules
z_i	Net load seen by the energy meter without storage at time instant i in joules; $z_i = d_i - r_i$
s_i	Output storage output at time instant i in joules; $s_i \in [S_{\min}, S_{\max}]$.
L_i	Total load behind the meter at time i in joules; $L_i = z_i + s_i$.
$S_{\min}$	Minimum energy output of storage in a time instant i with sampling time h.
$S_{\max}$	Maximum energy output of storage in a time instant i with sampling time h.
$p_{\text{elec}}(i)$	Electricity price at time instant i.
$p_b(i)$	Buying price of electricity at time instant i.
$p_s(i)$	Selling price of electricity at time instant i.
κ_i	Ratio of selling price and buying price of electricity at time instant i; $\kappa_i = p_s(i)/p_b(i)$.
S_h^i	Apparent power of consumer load at time i; $S_h^i = P_h^i + jQ_h^i$.
P_h^i	Active power consumed by the consumer load
Q_h^i	Reactive power consumed by the consumer load.
S_r^i	Apparent power output of the solar inverter
S_B^i	The apparent power output of energy storage (connected through a converter which is an inverter or a rectifier) is given as $S_B^i = P_B^i + jQ_B^i$.
P_B^i	Active power output of battery at time i; $P_B^i \in [P_B^{\min}, P_B^{\max}]$, $P_B^{\min} = \delta_{\min}\eta_{dis}$, $P_B^{\max} = \frac{\delta_{\max}}{\eta_{ch}}$
$S_B^{\max}$	The converter rating given by the maximum apparent power supplied/consumed.
Q_B^i	Reactive power output of storage converter; $Q_B^i \in [-S_B^{\max}, S_B^{\max}]$.
T_{cycle}	Cycle life of battery in 100% depth-of-discharge.
T_{calender}	Calender life of battery in years.
L_{cal}	Calender life of battery in days.
η_{fric}	Friction coefficient.
D_i	Aggregate demand at time i.
G_i	Aggregate generation at time i.
Δ_i	Mismatch between demand and generation at time i.
$R(i)$	Residual mismatch between demand and generation with storage output s_i.

List of Figures

List of Tables

Chapter 1

Introduction

Someone's sitting in the shade today because someone planted a tree a long time ago. -Warren Buffett

Electrical power system is undergoing a metamorphosis. The future power networks will have greater unpredictability due to the increased share of renewable generation either as bulk installations connected to high voltage (HV)[1] / medium voltage (MV)[2] electricity networks or as distributed generation and new loads such as electric vehicles connected to low voltage (LV)[3] electricity network. Due to intermittancy and uncertainty in renewable generation, large-scale integration of renewable generation and new loads alter the aggregate consumption behavior; such an evolution of power system brings unique *challenges* and *opportunities* for generation facilities, consumers, aggregators, and other power network participants. Energy storage devices could effectively mitigate the uncertainty caused due to such an evolution of power system. In this thesis we explore some of the different applications that energy storage, specifically Li-Ion batteries, can perform in future power systems. We present the motivation of the thesis in the next section and subsequently the contributions and outline of the thesis.

1.1 Motivation

Energy consumption can be broadly categorized in three categories: (a) electricity, (b) transportation and (c) non-electric heating and cooling. With the growth of electric vehicles, many believe that energy consumption due to transportation would be largely met by increased electricity usage, thus ensuring the reliability of electric energy is even more essential. Electricity is one of the major form of energy for humanity which will only become more important in future. Traditionally, electricity generation used fossil fuels which contribute to increased pollution, production of greenhouse gases. This leads us to question their sustainability. The Paris climate change agreement of 2015 aims to keep the increase in global temperature to below 2 degree Celsius compared to the pre-industrial levels [24]. In order to achieve the above mentioned goals, participants of the agreement which covers 195 countries made commitments to reduce greenhouse gas production, increase energy efficiency and reducing carbon footprint. We list the commitments made by France as an example of the climate change self-imposed obligations that participants have sworn to fulfill based on their *nationally determined contributions*. France made commitments listed as: (i) to ban all petrol and diesel vehicles by 2040, (ii) stop using coal for producing electricity post 2022, (iii) invest up to 4 billion euros for boosting energy efficiency, (iv) produce 23% of total energy needs from renewable energy sources by 2020. This commitment breaks down to 33% of energy used in heating and cooling sector, 27% of the electricity sector, and 10.5% in the transportation sector.

Clearly, to achieve the goals of the Paris Agreement, more electricity should be generated using renewable energy sources replacing the traditional fossil fuel based generators. Furthermore, renewable generators are becoming more and more financially competitive compared to conventional sources of generation. Thus, many countries are replacing their generation facilities reaching their operational age with new renewable energy sources. In 2016, new wind and solar installations beat investments in fossil fuels by 2-to-1. In 2015, renewable energy provided 19.3% of the total energy consumed worldwide. Presently, at least 30 nations already have renewable energy contributing more than 20% of energy supply [77]. Gradually, the share of renewables is further going to increase worldwide.

[1] IEC 60038 classifies voltage levels between 35 kV to 230 kV as high voltage or HV.
[2] IEC 60038 classifies voltage levels between 1000 V to 35 kV as medium voltage or MV.
[3] IEC 60038 classifies voltage levels upto 1000 V as low voltage or LV.

Some believe this transition in energy will mark the beginning of the fourth industrial revolution. The gravity with which this transition is required is not just about financial viability but is also essential to ensure a sustainable future for the newer generation. To materialize the commitments towards climate change, the developed countries affirmed to mobilize $100 billion a year in climate finance by 2020.[4] Another study estimates that the world will spend an extra $8 trillion over the next 25 years to prolong the use of non-renewable resources, a cost that would be eliminated by transitioning to greater share of renewable energy generation.[5]

Note that renewable sources consist of not only solar and wind but also geothermal, biomass, burnt waste, and small hydro plants. Based on this definition of renewable energy sources, not all of them are intermittent. Often hydro plants and/or pumped storage are integrated together with intermittent solar and wind plants. Hydro and pumped storage can be used as an energy storage for mitigating the intermittent behavior of solar and wind generators. For example, Lower Austria, one of the nine states of Austria with a population of more than 1.6 million claims to have a 100% renewable energy consumption. The total generation consist of 63% hydroelectricity, 26% wind, 9% biomass and 2% solar. In this generation mix majority of 72% could be scheduled to ramp up or ramp down. Furthermore, total installed capacity is often significantly higher than the peak demand, this is to ensure that if a fraction of generators is out of service, the total load will still be met. In this context, if there is a sudden drop in solar or wind generation due to a passing cloud or loss of wind then hydro and biomass generations could be ramped up to meet this unexpected drop in generation. Similarly, if solar and wind generate excess energy than forecasted values, then hydro reservoir could be used to store the excess generation. However, hydro and pumped storage are geography-specific and cannot be built in all places. In the absence of such storage, batteries are an alternative solution.

Batteries are becoming more and more attractive for power system applications with a larger share of renewable generation. The key attributes of batteries that make them so attractive are high energy density, low starting time, fast ramping ability compared to other storage technologies such as flywheels with high ramping capability but low energy capacity, pumped-hydro with a low ramping capability and a high energy capacity. Furthermore, LiIon batteries have significantly higher roundtrip efficiency compared to other forms of energy storage. In this thesis, we focus on using the batteries for different applications for:

- electricity consumers integrating energy storage for minimizing their cost of consumption and
- large-scale storage applications for the utility/the aggregator/generation facilities for ensuring the power system stability and reliability.

However, batteries are yet not cost effective due to their high initial cost. We, therefore, explore co-optimizing storage applications to improve revenue opportunities that energy storage owners can make. The new electricity consumer contracts indicate that inclusion of storage would indeed make financial sense for consumers. We present case-studies of Uruguay and Madeira in Portugal as examples for exploring possible roles energy storage could make in their power system. Furthermore, batteries should be used optimally to maximize the service provided, and the control design should prolong their operational life. Batteries degrade due to operational cycles and age. So tuning operational cycles can affect the long-term life of the battery. We consider the battery degradation in storage optimization and control design.

1.2 Contributions of the Thesis

In this thesis we explore various applications of energy storage in the context of the future power networks, taking into account storage health. Major contributions of this thesis are:

Optimal energy storage arbitrage: Under time-varying electricity price, consumers can operate battery to minimize their cost of consumption. This is referred to as energy arbitrage. We propose a computationally efficient algorithm for solving the optimal arbitrage problem. This formulation considers: (a) consumer load variation, (b) time-varying electricity price, (c) storage ramping, capacity constraints along with efficiency losses. We identify the exact threshold based structure of optimal storage operation governed by the price fluctuations, storage efficiency and consumer load (can also include the local renewable generation by the consumer). These thresholds are used to decide the envelope of possible solutions in a sub-horizon which is often smaller than the entire time horizon of optimization. The proposed

[4] https://www.wri.org/blog/2015/12/what-does-paris-agreement-do-finance
[5] https://news.nationalgeographic.com/news/energy/2010/11/101109-peak-oil-iea-world-energy-outlook/

methodology of solving the optimal energy arbitrage problem is computationally efficient with worst-case runtime complexity of quadratic and, therefore, several folds faster than a linear programming and convex optimization based benchmarks. This proposed algorithm is then generalized for different relationship of buying and selling price of electricity. In order to ensure the convexity of the arbitrage problem, selling price is assumed to be lower or equal to the buying price. This assumption is valid for most net-metering policies. In fact, we are unaware of a counterexample where the selling price is higher than the buying price.

Co-optimization of storage: Due to the high cost of batteries, co-optimizing storage for multiple tasks can increase the revenue stream thus increasing the financial viability of batteries. We propose three co-optimization formulations in this thesis.
Formulation 1: Arbitrage with power factor correction - Using convex relaxations we formulate the co-optimization problem for performing arbitrage along with power factor correction (PFC). Using data collected from households in Madeira we exhibit that solar inverters operating at unity power factor degrade the power factor seen by the grid. We validate our co-optimization formulations using numerical results and conclude that performing power factor correction does not affect the arbitrage gains noticeably and the control of active and reactive power is largely decoupled.
Formulation 2: Arbitrage with power factor correction and peak demand shaving - Co-optimizing formulation for arbitrage with PFC and peak demand shaving deals with different time scales of operation. A peak demand charge is applicable for a longer time scale, e.g. a month. However, arbitrage and PFC is applicable for smaller time scales of minutes to a few hours. We propose a heuristic to simplify this co-optimization by reducing the horizon to one day using a memory variable which tracks the past peak demand. This simplification makes the co-optimization problem computationally efficient.
Formulation 3: Arbitrage with peak demand shaving, energy backup and self-sufficiency - A case-study for consumer contracts in Madeira Portugal for co-optimization is performed. The storage also performs energy backup for power outages.

Case-studies for power networks: We analyze the low-voltage consumer contracts for two locations: Madeira in Portugal and Uruguay. We identify that consumers in Madeira and Uruguay can gain significantly by including energy storage. We also provide a case-study which can be used to recommend the suitable contracts created by the utility that consumers with/without given storage should opt for. The proposed optimization formulations for Madeira also consider energy storage used for power backup. Under this role, energy storage attempts to have a higher charge level for periods where load shedding or power outage is more probable. Due to the type of net-metering policy and time-of-use pricing of electricity consumer storage operation in Uruguay is insensitive to uncertainties. For storage applications in Uruguay, we show that pre-decided threshold based structure will be best-suited as the storage operation for both active and reactive energy is not affected by exogenous parameter variations.

Large-scale storage applications[6]: We consider two large-scale applications for batteries:
(a) Dynamic regulation tracking by using a distributed fleet of batteries. The hierarchical control consists of two levels: (i) feedback control based on the aggregate response of the fleet and (ii) local control for ensuring that charge level of the battery is within the target band for battery charge level. An additional control layer, drift compensation, is proposed to ensure that the aggregate charge level of the fleet of batteries remains close to the target charge level.
(b) Phase balancing: Haphazard growth of renewables and electric vehicles could cause power unbalance in three phases. This is due to most distributed generators and electric vehicles consume single phase electricity and thus causing unbalance in three-phases. Energy storage at building, substation or distribution feeder level could assist in phase balancing. We present the different architectures of storage control for phase balancing. Case of a substation in Madeira, Portugal is presented showing three phase imbalance due to DGs and EVs.

Health consideration in storage operation: Storage life is often described as a combination of cycle life and calender life. We propose controlling cycles of operation for equating cycling degradation to the age degradation thus in effect increasing operational life of the battery. We show that controlling the cycles of operation using proposed friction coefficient only eliminates the low returning transactions. This methodology is also applied for co-optimization formulation described above, where storage uses the majority of its cycles for performing arbitrage. We also present the mechanism for controlling cycles for storage performing dynamic regulation by adjusting ramping commitments.

[6]Large-scale storage application refers to those applications where storage size is more than 1 MW.

Financial feasibility of battery applications: Batteries are expensive with constraints due to cycle life, ramping, and capacity. Financial viability is an essential aspect for batteries. We observe using case studies for energy markets in the USA and Europe that performing only arbitrage is not profitable for storage owners. However, co-optimization of multiple applications using battery could drastically increase dollars per cycle that storage owners could make. Case studies for energy markets in Uruguay and Madeira exhibit that batteries are profitable in such markets. On the contrary to consumer-based storage applications, providing ancillary service is much more profitable. As a case-study for PJM ISO, we observe that performing dynamic regulation is more than 15 times profitable compared to performing arbitrage under the same ISO.

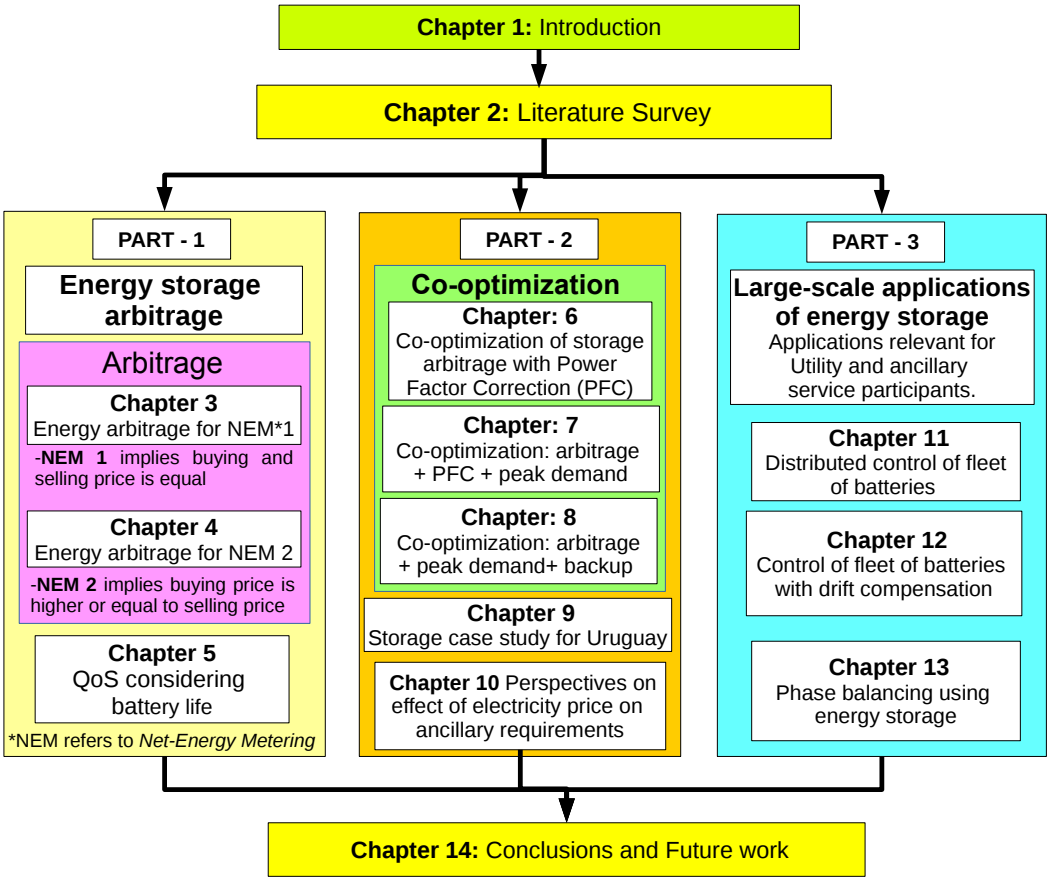

Figure 1.1: Organization of the thesis

1.3 Organization of the Thesis

The organization of the thesis is depicted in Fig. 1.1. In Chapter 2 we present a detailed literature review of the problems in power systems and why energy storage plays a pivotal role of technology enabler. We also explore bottlenecks associated with batteries which need to be addressed in modeling and financial evaluations.

The thesis is divided into three parts. In Part I and Part II we present the applications of battery energy storage for an energy consumer in LV/MV power network such as residential consumers, building consumers, and small industrial loads. We present a case-study of Uruguay that shows that storage applications in a region or country should take into account the policies applicable, consumption behavior, and local generation. In Part III we explore some of the large-scale applications of energy storage for the power utility and ancillary service participants perspectives. In Chapter 5 in Part I and Chapter 12 in Part III we also present how quality-of-service for batteries can be taken into account for some applications described. Part II of the thesis is concluded with a perspective on the effect of real-time electricity price on the ancillary service requirements which provides the need for applications discussed in Part III. The last chapter of the thesis concludes and provides perspectives for future extensions of the work.

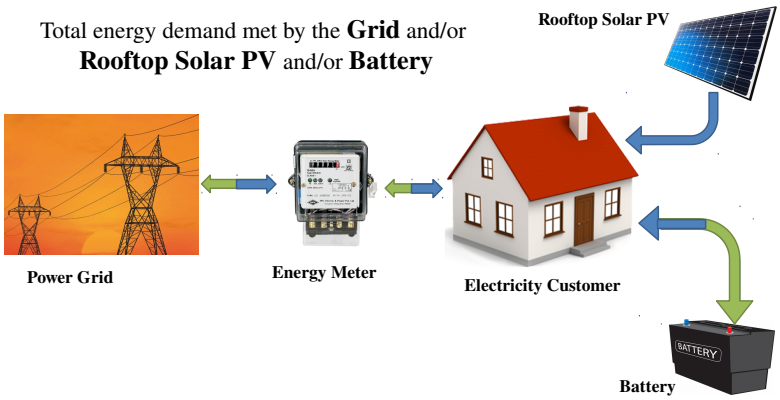

Figure 1.2: The system considered for storage applications in Part I and Part II of the thesis

1.3.1 Part I of the thesis: energy storage arbitrage

The system considered in Part I and Part II of this thesis, *i.e.*, electricity consumer/prosumer, is shown in Fig. 1.2. In this part storage performing energy arbitrage is discussed under contemporary net-metering policies with time-varying electricity price. Real-time implementation of the algorithm is proposed using model predictive control. This part covers Chapter 3 to Chapter 5. A brief outline of each of these chapters is as follows.

Chapter 3 describes **Energy arbitrage under NEM[7] 1.0:** Energy arbitrage using energy storage refers to buying electrical energy when the price of electricity is low so as to sell when prices are higher in order to make financial gains. In this chapter, we propose optimal energy storage control algorithm for NEM 1.0, which compensates the excess generation supplied to the grid at par to the buying price of electricity at that time instant. We observe that under such a net-metering policy minimizing the cost of consumption with energy storage to maximize the gains is equivalent to minimizing the total cost of consumption, thus storage operation is *independent* of inelastic load and renewable generation variation. Our algorithm is based on the discretization of optimal Lagrange multipliers of a convex problem and has a threshold based structure in which the optimal control decisions are independent of past or future prices beyond a certain time horizon. The proposed algorithm has the worst-case quadratic run-time complexity in terms of the time-horizon length. The proposed algorithm is found to be several folds faster than other benchmarks and hence has the potential to be used for in real-time [182]. Furthermore, we present three case-studies: (i) arbitrage financial potential in some European and USA energy markets, (ii) statistical quantification of sub-horizon based on CAISO price data for 2017 [183], (iii) mitigating uncertainty and comparison of scenario-based model predictive control with traditional forecasting with MPC on arbitrage gains [130].

Chapter 4 describes **Energy arbitrage under NEM 2.0: [183]** We extend the approach proposed for the optimal arbitrage under NEM 1.0 in Chapter 3 for NEM 2.0. In this case, the optimal storage operation is affected by the magnitude and sign of the inelastic load and renewable generation. We present a modular and computationally efficient algorithm for performing energy arbitrage under various net-metering schemes. We show that the optimal storage operation has threshold based structure and we list these thresholds for different conditions. The thresholds are a function of (i) electricity price, (ii) charging and discharging efficiency, (iii) storage ramp constraint, (iv) relationship of selling price, buying price and storage efficiency, and (v) inelastic load and renewable generation. We also observe that energy storage optimal operation depends on a period defined as a sub-horizon. The sub-horizon is the lookahead horizon which is required for taking optimal actions. The time instants outside the sub-horizon in past or future do not affect the optimal control decisions. We observe that the sensible value of this sub-horizon is governed by price variation and energy storage parameters like ramping and capacity. The length of sub-horizon is governed by (a) initial storage charge level, (b) electricity price, (c) charging and discharging efficiency, (d) ratio of ramp rate and rated capacity, and (e) sampling time.

[7]Net-Energy Metering or NEM: (a) NEM 1.0 refers to a policy where buying and selling prices are equal. (b) NEM 2.0 refers to a policy where the selling price is lower than or equal to the buying price. NEM 1.0 and NEM 2.0 are the two versions of net-metering policy in California. Similar compensation strategies are also applicable for many countries across the world, for example, France, Uruguay, rest of the US [22].

Chapter 5 describes **Considering battery life for arbitrage and regulation services:** Estimation of financial returns of energy storage is very essential due to its high cost. This chapters aims to identify the monetary potential of batteries in performing price based energy arbitrage and dynamic regulation, while considering the degradation of the battery over time and due to operational cycles. Based on the present compensation mechanism we calculate the dollar value of per cycle operation of a battery. We propose an algorithm for identifying the cycles of operation of the battery, taking into account the depth-of-discharge of the battery. This is essential as Li-Ion batteries have a nonlinear relationship between cycle life of the battery and the depth-of-discharge. Furthermore, we propose mechanisms to control the operational cycles of the battery for increasing their operational life [181].

1.3.2 Part II of the thesis: energy storage co-optimization

In modern power networks energy storage devices can perform many different tasks from price-based arbitrage, incentive based demand response, voltage and frequency regulation as ancillary service participants or peak demand shaving for consumers. This part consists of Chapter 6 to Chapter 10. In Chapter 6, Chapter 7, and Chapter 8 we deal with **co-optimizing** energy storage applications for multiple revenue streams. Chapter 9 provides a case-study using the new consumer contracts in Uruguay, where low voltage consumers can co-optimize for arbitrage and reactive energy compensation. The section ends with a perspective on the effect of real time electricity pricing on ancillary requirements in Chapter 10.

Chapter 6 describes **Co-optimization of arbitrage with power factor correction:** The large scale integration of distributed generation will drastically deteriorate power quality specifically power factor (PF) due to inverters producing only active power. PF norms which presently are applicable only to large and industrial loads will change in future with greater share of low voltage distributed generation. We use energy storage interfaced with a converter to correct the PF locally without deteriorating its ability to perform arbitrage or peak demand shaving. We use four-quadrant energy storage converter operation, i.e., energy storage converter generating or consuming both active and reactive power for maintaining the PF within permissible levels set by the utility. This work is submitted as [178].

Chapter 7 describes **Co-optimization for arbitrage, peak demand shaving and power factor correction:** We present a co-optimization formulation for energy storage devices for performing energy arbitrage and power factor correction in the time scale of minutes to hours along with peak demand shaving in the time scale of a month. The optimization problem, despite being non-convex, is solved using a penalized convex relaxation. In this chapter, we present a case-study with real data for a time scale of several months. This numerical experiment shows the effectiveness of energy storage devices performing multiple tasks simultaneously. In particular, we show that the energy storage can correct the power factor without significant change in arbitrage gains and peak demand charges [177].

Chapter 8 describes **Co-optimization for energy backup, peak demand shaving and self-sufficiency:** Energy storage applications and roles are explored from a prosumer perspective for the island of Madeira, Portugal. These applications can also be applicable to other isolated or mainland power networks. We formulate a convex optimization problem for energy arbitrage under zero feed-in tariff, increase self-sufficiency by increasing self-consumption of locally generated renewable energy, provide peak shaving, and act as a backup power source during anticipated and scheduled power outages [187].

Chapter 9 describes a **case-study applicable for LV consumers in Uruguay**. The objectives of the case-study are two-fold: (a) Understanding the contracts available for low voltage electricity consumers in Uruguay and (b) Energy storage applications and control for consumers with inelastic load and/or solar PV [179]. Furthermore, we provide suggestions to an electricity consumer in selecting such contracts and at the same time reducing their cost of consuming electricity. The presented case study depicts that the applications of energy storage need to be tailored based on region which decides the available contracts, consumption pattern, distributed generation available, and investment constraints for installing energy storage.

Chapter 10 describes perspective on the **Effect of real time electricity price on ancillary services:** We analyze the effect of real-time electricity price (RTP) on the amount of ancillary services required for load balancing in the presence of responsive users, information asymmetry and forecast errors in demand

and renewable generation. We consider a electricity price that is determined by the forecasted generation and ramping cost. A community choice aggregator manages the load of all the consumers by setting the price. The consumer's objective is to minimize their overall cost of consumption. Ancillary services are called upon to balance the load in real time. With zero RES in the power network and a high degree of load flexibility, the proposed RTP flattens and the volatility in demand vanishes. However, in presence of RES the volatility in price and demand is reduced up to an extent and ancillary services are required for load balancing. The amount of ancillary services required increases with forecast errors. We also propose a real time algorithm that approximates the optimal consumer behavior under the deterministic setting. Numerical simulations are provided using real data from Pecan Street and Elia Belgium [185].

1.3.3 Part III of the thesis: large-scale application

In this part we present some of the large-scale applications of energy storage for the power utility and ancillary service participants. This part of the thesis consists of Chapter 11 to Chapter 13. Chapter 12 presents the quality-of-service aspects of storage in the proposed distributed control design in Chapter 11. Chapter 13 provides storage application for phase balancing.

Chapter 11 describes **Distributed Control of Fleet of Batteries:** Battery storage is increasingly important for grid-level services such as frequency regulation, load following, and peak-shaving. The management of a large number of potentially geographically distributed batteries presents a control challenge. The proposed control solution respects battery constraints, and ensures that the aggregate power output tracks the desired grid-level signal [114], [135]. The system considered in this chapter is shown in Fig. 1.3. The geographically distributed fleet of batteries track the reference signal r_t denoting the instantaneous unbalance in supply and demand. This fleet of batteries do not have any communication among themselves. The objective of the control design is: scalability, robustness to disturbances, modularity, and low communication infrastructure.

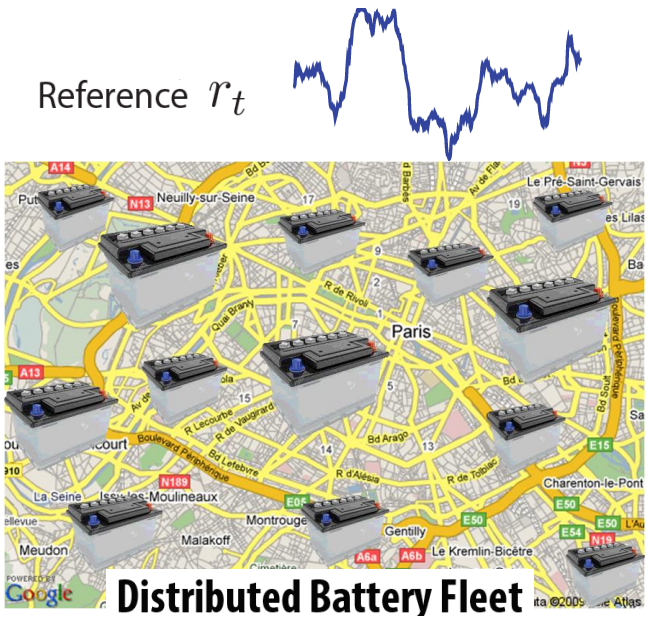

Figure 1.3: Geographically distributed fleet of batteries control design for providing ancillary service.

Chapter 12 describes **Drift Compensation:** Mean state-of-charge (SoC) of batteries drifts from the pre-decided optimal SoC level due to (a) charging and discharging efficiency losses and (b) non-zero mean regulation signal. Control proposed in Chapter 11 does not actively ensure maintaining the SoC. We propose a drift compensation control layer for stochastic control of geographically distributed fleet of batteries proposed in Chapter 11 [114], in order to maintain the charge level of batteries in the desired range. We show that the inclusion of the drift compensation leads to stable operation of providing dynamic regulation with a fleet of batteries with efficiency losses [175].

Chapter 13 describes **Phase Balancing:** Most bulk transmission of electrical energy is done in three phases. However, distribution of electrical energy in low voltage level is often performed in single-phase.

The three phases independently act as three single phase lines. Phase imbalance can introduce additional power losses and limit the loading capability of distribution transformer [102]. With ad hoc deployment of renewables the chances of power unbalance among phases will increase with the share of distributed renewable energy installations. A case study to demonstrate probable phase imbalance is also presented for a substation in Madeira, Portugal.

In this chapter, we consider balancing active and reactive power between phases using a battery. We consider a battery that is owned by the utility or building and placed at low voltage substations or building or in the distribution feeder. The system considered in this unpublished work, [180], is shown in Fig. 1.4.

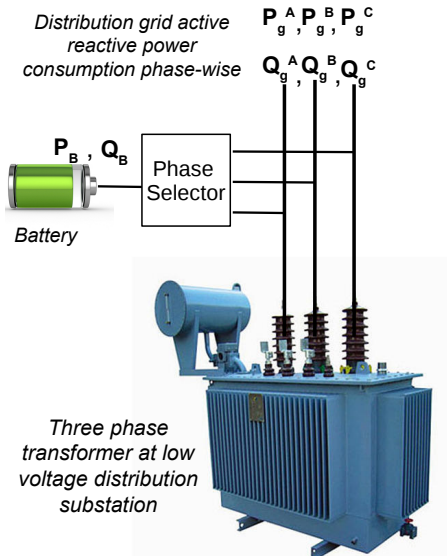

Figure 1.4: One of storage control architectures used at distribution level for balancing active and reactive power in the three phases [180].

1.3.4 Conclusion and future directions

Chapter 14 contains a summary of contributions made in this thesis and provide future directions for possible extension of this line of research.

1.4 Publications

Journal Publications:

(J1.) Md Umar Hashmi, Arpan Mukhopadhyay, Ana Bušić, and Jocelyne Elias. *Storage Optimal Control under Net Metering Policies.* submitted to IEEE Transactions on Smart Grid. https://arxiv.org/abs/2002.01524
Semi-finalist (2nd Runner-up) in the Student Research Competition at the 2018 Pecan Street Conference at the University of Texas at Austin on March 6, 2018.

(J2.) Md Umar Hashmi, Deepjyoti Deka, Lucas Pereira, Ana Bušić, Scott Backhus. *Arbitrage with Power Factor Correction using Energy Storage.* accepted in IEEE Transactions on Power System. https://ieeexplore.ieee.org/document/8972560

(J3.) Md Umar Hashmi, Jose Horta, Diego Kiedanski, Lucas Pereira, Ana Bušić, and Daniel Kofman. *Energy Storage Applications for LV Consumers in Uruguay.* To be submitted to Elsevier Applied Energy. https://arxiv.org/pdf/2002.04192.pdf

Conference Publications:

(C1.) Ana Bušić, Md Umar Hashmi, and Sean Meyn. *Distributed control of a fleet of batteries.* IEEE American Control Conference 2017, Seattle, USA. http://ieeexplore.ieee.org/abstract/document/7963473/.

(C2.) Md Umar Hashmi, Arpan Mukhopadhyay, Ana Bušić, and Jocelyne Elias. *Optimal Control of Storage under Time Varying Electricity Prices.* IEEE Smart Grid Communications 2017, Dresden, Germany. https://ieeexplore.ieee.org/document/8340703.

(C3.) Md Umar Hashmi and Ana Bušić. *Limiting energy storage cycles of operations.* IEEE GreenTech 2018, Austin, USA. https://ieeexplore.ieee.org/abstract/document/8373605.

(C4.) Md Umar Hashmi, Deepan Muthirayan, and Ana Bušić, *Effect of Real-Time Electricity Price on Ancillary Service Needs.* ACM e-Energy 2018, Karlsruhe, Germany. https://dl.acm.org/doi/abs/10.1145/3208903.3214350.

(C5.) Md Umar Hashmi, Wael Labidi, Ana Bušić, S.-E. Elayoubi, and T. Chahed. *Long-Term Revenue Estimation for Battery Performing Arbitrage and Ancillary Services.* SmartGridComm 2018 at Aalborg, Denmark. https://ieeexplore.ieee.org/abstract/document/8587562

(C6.) Yize Chen, Md Umar Hashmi, Deepjyoti Deka, and Michael Chertkov. *Stochastic battery operations using deep neural networks.* IEEE ISGT NA 2019, Washington, DC. https://ieeexplore.ieee.org/abstract/document/8791566

(C7.) Md Umar Hashmi, Lucas Pereira, and Ana Bušić, *Energy Storage Roles in Madeira, Portugal: Co-optimizing for Arbitrage, Self-Sufficiency, Peak Shaving and Energy Backup.* in IEEE PowerTech 2019. https://ieeexplore.ieee.org/abstract/document/8810531

(C8.) Md Umar Hashmi, Deepjyoti Deka, Lucas Pereira, Ana Bušić, and Scott Backhus. *Co-optimizing Energy Storage for Low Voltage Prosumers using Convex Relaxations.* at 20th International Conference on Intelligent Systems Applications to Power Systems, New Delhi India. https://tinyurl.com/wv3vdjd

(C9) Md Umar Hashmi, Arpan Mukhopadhyay, Ana Bušić, Jocelyne Elias, and Diego Kiedanski. *Optimal Storage Arbitrage under Net Metering Policies using Linear Programming.* at IEEE SmartGridComm 2019, Beijing, China. https://arxiv.org/abs/1905.00418

(C10) Diego Kiedanski, Md Umar Hashmi, Ana Bušić, and Daniel Kofman. *Sensitivity to forecast errors in energy storage arbitrage for residential consumers.* IEEE SmartGridComm 2019, Beijing, China. https://hal.telecom-paristech.fr/hal-02163114/document.

(C11) Md Umar Hashmi, Jonathan Cavaleiro, Lucas Pereira and Ana Bušić. *Sizing and Profitability of Energy Storage for Prosumers in Madeira, Portugal.* in IEEE ISGT NA 2020 Washington DC. https://arxiv.org/pdf/1911.10458.pdf

Book Chapter:

• Yue Chen, Md Umar Hashmi, J Mathias, Ana Bušić, and Sean Meyn. May, 2017 *Distributed Control Design for Balancing the Grid Using Flexible Loads.* IMA volume Energy Markets and Responsive Grids, Springer. https://link.springer.com/chapter/10.1007/978-1-4939-7822-9_16.

Patent in preparation:

• Md Umar Hashmi, Deepjyoti Deka, Lucas Pereira, Ana Bušić, Scott Backhus. *Control of inverters in smart grids.*

In preparation:

• Md Umar Hashmi, *Load Flexibility for Price based Demand Response,* hal-01911254, 2018.

• Md Umar Hashmi, Ana Bušić, Sean Meyn. *Drift Compensation for Maintaining SoC of a Fleet of Batteries.* to be submitted.

• Md Umar Hashmi, Deepjyoti Deka, Lucas Pereira, and Ana Bušić. *Energy storage optimization for grid reliability.* submitted to ACM e-Energy 2020.

• Md Umar Hashmi, Jose Horta, Lucas Pereira, Zachary Lee and Ana Bušić and Daniel Kofman, *Towards Phase Balancing using Energy Storage.* https://arxiv.org/abs/2002.04177.

Chapter 2

Challenges and Literature Review

In the middle of difficulty lies opportunity. - Albert Einstein

Energy storage as technology enabler for smart electricity networks

What bank is for money, battery is for energy.

Energy storage in power system are buffers which can deliver and store electrical energy, therefore, can be used to store excess generation and supply excess demand. Many types of storage technologies are used in power networks worldwide. For instance hydroelectric pumped storage acts as mechanical energy storage, batteries store energy as chemical energy. Different energy storage technologies could serve different applications in power grid. Capacity[1], cost, energy density, efficiency level, discharging speed[2], self-discharge[3] technical and economic life are factors that determine in which context the storage technologies are most suitable.

Table 2.1: Energy Storage Specifications [259, 168, 275]

Storage Technology	Efficiency Level	Life	Self-discharge %(per-day)	Discharge Speed	Cost $/kWh	Energy Density	Start-up Time
Pumped Hydro	65-85	50+ yrs	0 - 0.5	1-24 hours	200-300	0.35-1.12 kWh/m^3	sec-min
Compressed Air	42-54	10-20 yrs	0 - 10	1-24 hours		0.5-0.8 kWh/m^3	min
Lithium-Ion	85-95	10-20 yrs/ 2-10,000 cycles	$\approx$ 0.067	min-hours	370-900	85-200 kWh/kg	-
Lead Acid	60-95	7 yrs/$\leq$ 1000 cyc.	$\approx$ 0.167	min-hours	100-300	33-42 kWh/kg	-
Flywheels	95	20 yrs	20-100 [93]	0.1-20 min	550-950	200 kWh/kg	ms
Super-capacitor	95	1 million+ cycles	2-4	0.001-3 sec	200-300	1-30 kWh/kg	ms

Table 2.1 lists some of the common storage technology along with the range of technical specifications. It is evident that storage type will govern the applications for which storage is used. For example pumped hydro will be more suitable for energy management applications facilitating bulk energy shift. However, pumped hydro will create less value in primary frequency regulation due to its slow ramping characteristics, see discharging speed in Table 2.1. On the contrary, batteries are best suited for most power grid applications, Fig. 2.1 presented in NERLs report [9] on energy storage shows a visual representation of storage characteristics and possible application for which the storage could be used. In this report they use capacity and discharge time to distinguish storage technologies. The storage applications are categorized into three primary goals: energy management or shifting energy in time, operational and ramping reserves for following load and frequency regulation[4] to ensure power quality. These roles can be further categorized for applications concerning generation end, transmission and distribution end and end-user level.

U.S. Energy Information Administration in its recent report explores market trends of large-scale battery storage in the US [315]. Large scale refers to system that are grid connected and have a nameplate power capacity greater than 1 MW. The report identifies that Lithium-ion represented more than 80% of the installed power and energy capacity of large-scale battery storage in operation in the United States at the end of 2016. This is due to Lithium-ion batteries having high-cycle efficiency and fast response times.

[1] Battery capacity is measured in Watt-hours which is a unit of energy.
[2] Discharge speed denotes the time required to discharge the battery from fully charged state at maximum discharge rate.
[3] Self-discharge refers to the deterioration of battery charge level even when idle due to internal chemical reactions.
[4] Frequency regulation refers to maintaining the power grid frequency within pre-set limits decided by the balancing authority or the Transmission System Operators (TSOs).

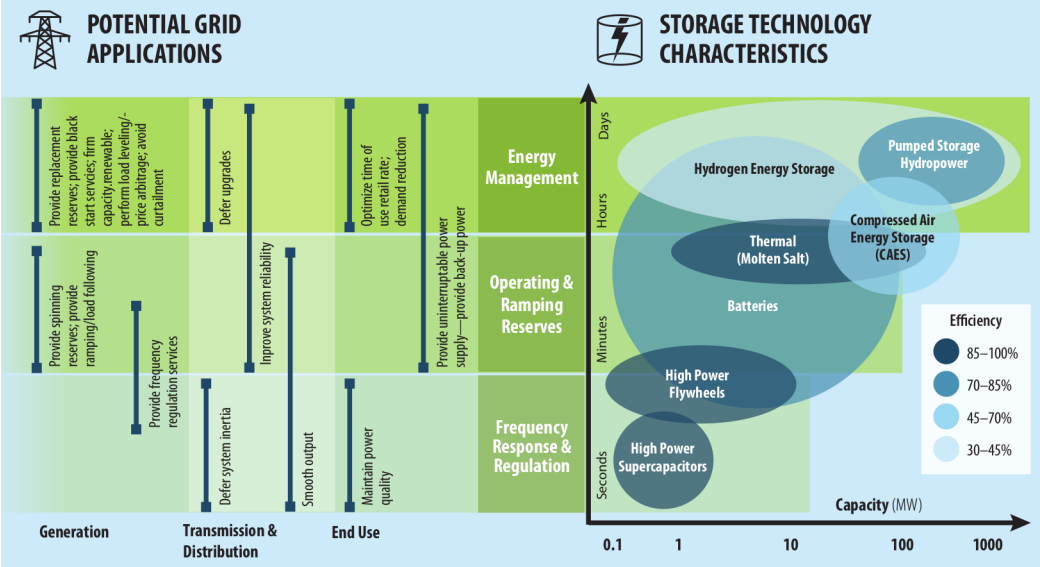

Figure 2.1: Classification of roles of energy storage in power system based on storage technology [9].

In addition, their high energy density makes them the current battery of choice for the portable electronic and electric vehicle industries. At the end of 2017, 708 MegaWatts (MW) of power capacity (maximum instantaneous power), representing 867 MegaWatthours (MWh) of energy capacity (total storage capacity), of large-scale battery storage capacity was in operation. Nearly 40% of existing large-scale battery storage power capacity (and 31% of energy capacity) lies in the Pennsylvania-New Jersey-Maryland Interconnection (PJM). Installations in California Independent System Operator (CAISO) territory accounted for 18% of existing U.S. large-scale battery storage power capacity in 2017, but they accounted for 44% of existing energy capacity. Market trend indicates the superiority of Li-Ion batteries. In this thesis we consider Li-Ion as energy storage for various power system applications.

This chapter is divided into five parts. The first part describes challenges specific to future power system and presents some of the roles of independent system operator (ISO). ISO would encourage active participation of different entities: commercial and residential consumers and generators facilitating reliable operation of power network. In the second part we describe the various roles energy storage can play in a smart grid. Energy participants could combine various roles in order to maximize their profit. A detailed segregation of these tasks based on high voltage (HV), medium voltage (MV) and low voltage (LV) is not performed in this thesis. In the third part we list the bottlenecks associated with Li-Ion energy storage based on cost, storage parameters and uncertainty in decision variables. Note that some of these bottlenecks will also be applicable for other types of storage. It is essential to consider these bottlenecks in modeling and evaluation of energy storage applications. In the fourth part, we present the strategy used to mitigate the effect of uncertainty and the storage operation used in the rest of the thesis. In the last part of this chapter, we present the notation and storage model used in this thesis.

2.1 Future Power System Challenges

Electrical power system is often considered the most complex man-made system and comprises of generation, transmission and distribution assets facilitating electricity consumers commercial and residential, to use electrical energy. In order to ensure the electrical *stability* and *reliability* of power network so as the power can be transported from generators to distribution networks and to loads, independent system operators or ISOs are created (in context of the US). ISOs being independent from ownership by generators or market participants bring fairness as they do not tend to favor one over other in setting norms. An ISO performs the following tasks (not complete list):

- (T1) instantaneous balancing of cumulative generation and load,
- (T2) power quality[5] in the system,

[5]Power quality involves magnitude, frequency, and waveform of voltage and current. Well known indices such as frequency, power factor, total harmonic distortion etc are frequently used as indicators of power quality.

- (T3) power grid upgrade for future. Often an ISO divides the responsibility to several Distribution System Operators or DSOs. DSO handles reliable operation of power network at a regional level. In cases where DSOs are unable to ensure power reliability, ISOs take the role at regional level too.

The power network is undergoing a transformation at generation and load sides simultaneously. Distributed generation (DG) facilities which consist of primarily renewable energy sources like wind and solar are being integrated in the power network. The share of DG is expected to increase. This transformation of traditional centralized generation to distributed generation will require a re-design of the system to attain the same levels of reliability. Contemporary power networks have very high reliability. Furthermore, more and more fossil fuel based generators will reach their usable life and will not be replenished by the same level of fossil fuel based generation due to environmental concerns. Large scale renewables will cause the aggregate generation intermittent and more challenging to achieve a balance between generation and demand. The renewable generation at electric consumer end is often interfaced via a converter which operates at close to unity power factor[6] [172] leading to deterioration of power factor seen by the grid which meets all the consumer reactive power and only a fraction of active power. At the load side, new loads like Electric Vehicles or EVs will evolve in large-scale in near future. Effect of such loads needs to be evaluated. Both of these directions of power system transformation are heavily researched.

We summarize the effects caused by the above mentioned transformation presented in the literature.

- Generation shift from *dispatchable units to intermittent renewables*: paradigm shift from traditional power network where generation used to follow load [202]. Furthermore, inverter interfaced renewable energy sources (RES) replacing rotor based generation will *reduce power system inertia* which implies higher rate of change of frequency during system disturbances. Distributed generation is intermittent, interfaced via single phase converter and solar PV also have a high impedance and low short circuit current making it more prone to cause unbalance[7] in the power network [229], [155].
- *Bulk centralized generation facilities to decentralized DGs*: For instance, in the UK electricity network is dominated by a centralized power generation model, where power flows from less than sixty large power stations to millions of consumers [26]. However, this will change with growth of DGs and small renewable generation plants. Due to growth of DGs compared to traditional power system with centralized generation the risk of local voltage problems and congestion will increase [202]. Central system operators will no longer have a system overview to effectively dispatch reserves and therefore, requiring localized corrective actions. Authors in [159] present case studies of how distributed generation should be considered for finding the feeder hosting capacity[8] to prevent over-voltages and transformer overload. The hosting capacity depends on the network topology, line parameters and transformer rating. In case of overproduction from the hosting capacity level, soft or hard curtailment of generation will be required in order to ensure stable operation.
- *Localized impact of DG outage*: this is the advantage the new power system with large amounts of DGs. Failure of DGs will have a localized effect, unlike presently power generation failures which can lead to cascaded effect leading to complete blackout. However, detailed analysis should be considered in redesigning the power grid, which has been designed for one way power flow, i.e. from bulk generation facilities to LV and MV consumers. The distribution feeders are designed such that the voltage magnitude becomes lower when moving along the feeder. Integrating DGs at distribution level makes the design condition of feeders invalid and thus over-voltages could occur [104].
- *Synchronized operation*: The connection of single phase electric vehicles (EVs) and DGs are random and often clustered in a certain area. Authors in [278] note that voltage imbalance caused by single phase EVs is unlikely to exceed the prescribed limits set provided EVs are reasonably distributed among three phases. However, such a distribution cannot be guaranteed. In addition both EVs and PVs (PhotoVoltaics) tend to be active in a synchronized manner, i.e., majority EVs tend to get charged in the evening when people reach their homes after work and all PVs generate electricity when it is sunny. Such a synchronized operation of these loads and generation aggravates the problems for distribution system operators who are obliged to ensure power quality at all times. Huge ramping reserves (both up and down) will be required to cope up with bulk DG and EV integration.

Fig. 2.2 shows two consecutive weeks of demand, generation and regulation required at Bonneville Power Administration (BPA) balancing authority. The left plots shows a week with negligible amount of wind

[6]Power factor measures the phase difference between the ac voltage and ac current.

[7]Voltage unbalance is used to measure unbalance in power networks. Voltage unbalance measure is referred as Voltage Unbalance Factor or VUF. In Chapter 8 we describe in detail the various definitions used to measure unbalance.

[8]Feeder hosting capacity refers to the amount of resources (generators or loads) that can be accommodated on a feeder without impacting system operation under existing control and infrastructure configuration [223].

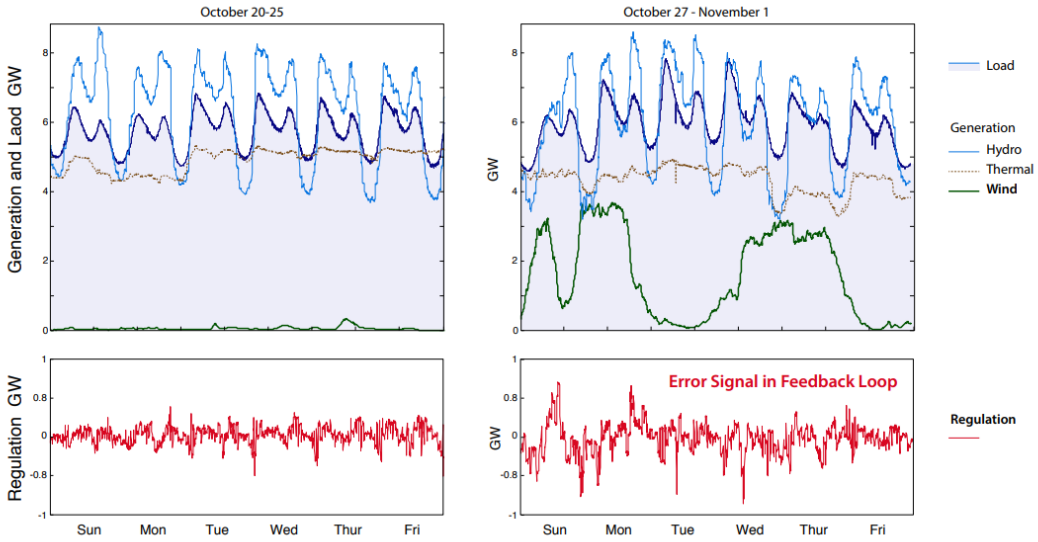

Figure 2.2: BPA demand supply mismatch with renewable generation for two consecutive weeks [5].

generation and the right plot shows significant amount of wind generation. Due to greater intermittancy brought by higher wind generation the amount of regulation required for achieving balancing between aggregate load and generation increases noticeably. The new power system will require active participation of grid participants: consumers and producers. More ancillary services[9] and greater responsiveness of participants will be required. Greater observability of power network with sensors, information system and communication protocols will be required for adaptive decision making in real time.

With increasing share of RES the problem of supply and load balancing will become more challenging, due to the additional intermittency in power generation by RES. The various solutions to this problem proposed in the literature are:

- *Solution S1*: Install new fast ramping generation infrastructure and upgrade in transmission and distribution grid infrastructure [168].
- *Solution S2*: Induce demand response participation by end-users in exchange of incentives [248, 265].
- *Solution S3*: Direct load control by the balancing authority or independent system operators [289, 256].
- *Solution S4*: Generation and/or demand curtailment.
- *Solution S5*: Perform ancillary service [114], demand response, arbitrage [182], load balancing, infrastructure deferral, generation and/or demand curtailment using batteries or storage devices.

In this thesis we focus on *Solution S5*.

Roles of ISO: The broad categorization of ISO tasks T1-T3 described previously, are coupled in nature. If T1 is not achieved then one or more indices of T2 will deviate beyond their prescribed limits. For instance in high voltage network where active power is coupled by frequency, if the active load exceeds active power generated then frequency will dip below 50/60 Hz [188]. The dip will be governed by the magnitude of unbalance between generated and consumed active power. The tasks T1 and T3 are coupled in a way that if power network does not have enough reserves than achieving T1 is not possible without load or generation shedding, a scenario which reduces power system reliability. ISO plans the growth of transmission, distribution and generation facilities taking into account the emergence of new loads, degradation of existing infrastructure, uncertainty in generation scheduling and intermittency of renewable generation. In this thesis we do not discuss T3.

For ensuring that tasks T1 and T2 are achieved, ISOs introduced new billing mechanisms for energy participants, created new energy markets, encouraged participation in ancillary service market and set power quality norms for different participating entities in the network. Below we describe the need and effect of these initiatives by ISOs. Fig. 2.3 shows the various ISOs in the US and Canada [34].

2.1.1 Need for innovative billing

In order to encourage electricity consumers to participate actively in facilitating goals T1 and T2 of the ISO, ISOs provides incentives (or penalties) to energy participants, i.e. consumers and/or generators, in

[9] Ancillary services includes frequency support, voltage support, and system restoration [304].

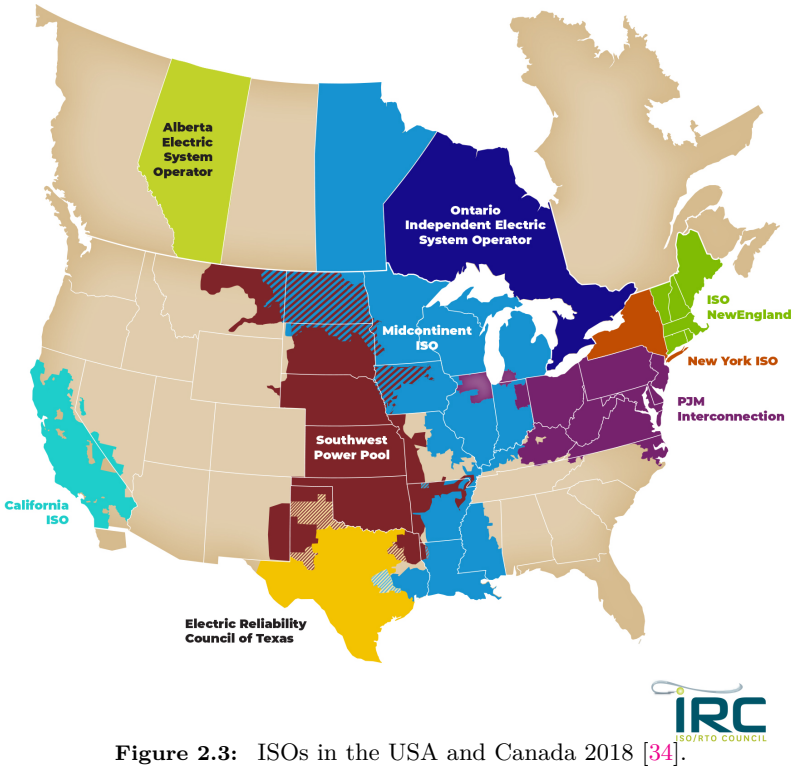

Figure 2.3: ISOs in the USA and Canada 2018 [34].

exchange of their services. The new electricity bills have few or all of the following revenue sources for active participants. ISO also sets Locational Marginal Prices for participants of energy markets which consists of large loads, generation facilities and utilities/retailers that buy energy for their consumers.

Wholesale Energy Markets: Wholesale energy markets exist in many power networks. The PJM energy markets consists of two markets: a day-ahead market and a real-time balancing market [230]. The day-ahead market is a forward market in which hourly clearing prices called as day-ahead LMPs[10] which are calculated for each hour of the next day based on offers and bids submitted into the day-ahead market. The real-time energy market based on real-time operation uses real-time LMPs calculated based on system operating conditions. All spot purchases and sales in balancing market are settled at real-time LMPs. Large loads and bulk generators participate in wholesale energy markets.

Electricity Price for Consumers: Traditionally utilities and ISOs used fixed electricity prices as most generators were developed to follow the load. However, with uncertainty in generation side, consumer responsiveness could help ISOs in avoiding developing new infrastructure to mitigate such intermittency. The real time electricity prices are set for consumers to incentivize their power consumption deviation.

- *Time-of-Use (ToU) Price*: ToU pricing is a variable rate structure that charges for energy depending on the time of day and the season when the energy is used. Responsive end-users shift their load to low rate times thus facilitating in load shifting from the historical peak consumption periods to off-peak periods. ToU can reduce the peak aggregate load [105]. However, ToU rate is inadequate to reflect the real time conditions of the grid, because the peak rate times are determined based on past aggregate consumption and may not correspond to the actual peak load. This will only exacerbate with more renewable sources in the grid. This is exemplified by the case study of Northern Italy by authors in [310] pointing the non-effectiveness of ToU pricing in shifting peak demand. Therefore, more dynamic price structure are proposed which reflects the real time condition of the grid.
- *Real Time Electricity Price*: electricity price vary dynamically with sampling time ranging from 5 minutes in CAISO to 15 minutes in NYISO to hourly variations in PJM [16]. Real time electricity price aim to reduce the peak- to-average load ratio, i.e. flatten the load, leading to peak shaving for the grid. For *ex-ante* type real time price (RTP) design where the electricity price set at the beginning

[10]Locational Marginal Price or LMP is defined as the marginal price for energy at the location where energy is delivered or received. In PJM LMP consists of three components: system energy price, congestion price and loss price [230].

of the time interval is most prevelent. Information asymmetry is caused by the time delay between setting RTP, consumption decision and intermittent generation. Setting RTP requires the prediction of aggregate demand and RES generation by the utility if the price is set *ex-ante* and prediction of price by the consumers if the price is set *ex-post* [287, 185]. Due to information asymmetry the application of RTP is limited in real-time load balancing [185], thus ancillary services are called for supply and demand balancing, see Section 2.1.2 and Chapter 10.

Peak Demand Charge: The maximum demand dictates the size of power grid infrastructure, i.e. generators, transmission lines, transformers, circuit breakers etc. Due to this many power utilities around the world have introduced peak demand charge that a consumer may seek to minimize over a longer period (weeks or months). For example in California, Pacific Gas and Electric company charge peak demand charges are applied based on the maximum demand over a month [295].

Peak Consumption Contract: In many places instead of peak demand charge, the utility offers peak demand contracts where the consumer should ensure their peak demand within the selected contract. In case the instantaneous power exceeds the contract level, the utility could either disconnect the consumer and/or penalize for contract violations. This contract level decides the fixed charge component of the end user electricity bill. For instance in Madeira in Portugal the utility *Empresa de Eletricidade da Madeira* (EEM) provides low voltage consumers with 8 peak power levels which consumers select as a contract [320]. In case the peak power of the consumer exceeds the consumer contract level, a localized disconnection happens. The consumer can manually reconnect. However, such disconnection could affect appliance life.

Demand Response Participation: There are several different mechanisms for implementation of demand response or DR[11] programs. The demand response can be (dr1) price based, (dr2) consumers opting for contracts where they respond to balancing authority's request and (dr3) consumers opting for contracts where the flexible resources are controlled directly using a centralized signal ensuring the local quality of service of consumer. There are many examples of demand response implementation worldwide. We list some literature on demand response type (dr1). Authors in [302] present how price-based demand-side management programs assist in the reduction of peak demand and present a case study of the impact of real-time pricing on a power network in the city of Gothenburg, Sweden. Note that demand-side management includes DR, energy-efficiency and conservation programs [319]. Authors in [224] present results for price structures from the Ameren Illinois Power Company, showing a reduction of up to 39% in overall domestic energy costs. Authors in [205] show that demand-side resources like space heating can be incentivized to alter their consumption pattern pertaining to variations in the price of electricity, leading to a reduction in the cost of consumption for the end user, while performing price-based DR for the grid. Authors in [337] proposes controller for residential HVAC[12] systems for a significant reduction in peak loads and electricity bills with modest variations in thermal comfort. Authors in [279, 291] propose real-time electricity pricing scheme that reduces the peak-to-average load ratio, i.e. flattens the load, leading to peak shaving for the grid. In many cases, DR participants are informed prior to an event to reduce consumption thus deferring investment in peak ramping power plants. For example, consumers can enroll in Florida Power and Light (FPL) Residential On Call savings program where FPL-approved contractor installs the On Call device to reduce energy demand during emergencies. This of the form demand response (dr2) consumers could save up to $137 a year even if FPL never turns off the appliances chosen by consumers to participate. Historically, this program has been implemented a few times per year in early to late afternoons on weekdays [30]. Extensive works of demand response of the form (dr3) are available. Some works of direct load control are [94, 246].

Penalties for violating power quality indices: Many ISOs also include power quality penalties, in order to encourage consumers to maintain power quality at their point of common coupling. Such penalties are often levied upon large consumers and commercial loads, however, we believe that as the power network evolves such tasks will also be mandatory for smaller loads. Actively participating consumers should aim to minimize the penalties by abiding by the power quality norms set. In this introduction we provide rules for power factor violation and penalties, similar norms are available for other power quality indices.

Power Factor Rules: Power factor (PF) which denotes the ratio of active power and the apparent power

[11] Demand Response refers to change is the consumption of electricity by an energy participant to meet the needs of the grid. The participants receive incentives in exchange.

[12] HVAC refers to Heating, ventilation, and air conditioning loads.

is denoted as $\cos(\phi)$, where ϕ denotes the angle between active and reactive power. An alternate definition commonly used to denote the PF is $\tan(\phi)$ represented as $\texttt{tg}\ \phi$ in national and ISO level power norm documents. $\texttt{tg}\ \phi$ denotes the ratio of reactive power over active power. Note $|\cos(\phi)|$ denotes absolute value of PF and implies the rules for leading or lagging power factor are symmetrical. Maintaining PF of aggregate load seen by the transmission network is essential for reliable operation of distribution network. Power utilities worldwide have rules designed for consumers to comply with the minimum power factor that they should maintain. In case the consumer power factor goes below the pre-set limit defined by utility, the consumer has to pay a penalty under some utilities or the utility makes it compulsory for the consumer to install power factor correction equipment to improve the power factor within permissible limits. The cost of power factor correction devices are borne by the consumer and not the utility [12, 18].

Below we list in Table 2.2 the power factor norms in different regions:

Table 2.2: Power Factor Correction Rules

Utility Name	PF Limit	Penalty/Reactive Power Cost/Remarks
France [72]	$\lvert\text{tg}\ \phi\rvert \leq 0.4$	0.2 × Active Power Cost
Portugal [271]	$\lvert\cos(\phi)\rvert \geq 0.92$	0.016 to 0.18 × Active Power Cost
Germany [303]	$\lvert\cos(\phi)\rvert \geq 0.95$	Applicable for Solar Generators
CAISO	$\lvert\cos(\phi)\rvert \geq 0.95$	Applicable for bulk Wind Generators [28]
	$\lvert\cos(\phi)\rvert \geq 0.9$	for Producers in Distribution Grid [31],[33],[32]
	$\lvert\cos(\phi)\rvert \geq 0.85$	LV consumers in PG&E [23]
PJM [28]	$\lvert\cos(\phi)\rvert \geq 0.95$	Applicable for Wind Generators
ERCOT [239]	$\lvert\cos(\phi)\rvert \geq 0.95$	Applicable for all Generators since 2004
FirstEnergy, Ohio [12]	$\lvert\cos(\phi)\rvert \geq 0.85$	Consumers obliged for reactive power compensation
Alabama Power Company [1]	$\lvert\cos(\phi)\rvert \geq 0.9$	kW Billable = kW measured × $\frac{\text{90\% power factor}}{\text{Actual power factor in \%}}$
Lansing Board of Water and Light [18]	$\cos(\phi) \geq 0.85$	Consumers obliged for reactive power compensation
Hydro Ottawa, Canada [14]	$\lvert\cos(\phi)\rvert \geq 0.9$	kW Billable = kW measured × $\frac{\text{90\% power factor}}{\text{Actual power factor in \%}}$

Essential Services Commission in Australia have drafted a much more detailed rules and conditions for maintaining the power factor based on consumer size, supply voltage and leading or lagging power factor. The detailed list is presented as listed in [11] (Table 2, Page 13).

Traditionally, these rules of power factor where applicable for large loads like industrial facilities, commercial complexes etc. However, with the growth of DGs power factor correction will be essential for kW load levels. Since the economics of small loads in almost all contemporary electrical markets is based on active power, i.e., buy and/or sell of active power, the need for supplying reactive power has been completely overlooked. Furthermore, the growth of capacitive appliances and non-linear power consuming devices would aggravate the stress on distribution transformers in near future.

2.1.2 Need for ancillary services

Ancillary services are the specialty services and functions provided by the energy participants that facilitate and support the continuous flow of electricity so that supply will continuously meet demand. The term ancillary services is used to refer to a variety of operations beyond generation and transmission that are required to maintain grid stability and security. These services generally include, frequency control, spinning reserves and operating reserves. Ancillary services are called upon for load balancing in time scale of seconds to minutes.

Frequency Regulation in PJM: PJM must comply with standards set by North American Electric Reliability Corporation (NERC). The "Real Power Balancing Control Performance" standard requires each balancing authority to control its area control error (ACE) within specified limits in terms of yearly averages and on minute-by-minute basis [3]. Frequency regulation is the tool to smooth out the real-time supply and demand imbalances, or ACE. In 2011, FERC's Order 755 required grid operators to compensate frequency regulation providers, including new fast ramp-rate resources, according to their actual performance and technical ability to support the grid system. On October 1, 2012, with the purpose of incorporating accurate but energy-limited storage resources, PJM split the frequency regulation signal into two signals: slow-responding Regulation A (RegA) and fast-responding Regulation D (RegD). In the initial construction of this split-signal system, RegA was designed for resources "with the ability to sustain energy output for long periods of time, but with limited ramp rates," while RegD was designed for resources "with the ability to quickly adjust energy output, but with limited ability to sustain energy output for long periods of time" [218]. PJM developed a valuation system to determine the optimal mix of RegA and

RegD resources. PJM uses a study conducted by KEMA [17], that simulated different combinations of RegA and RegD for achieving load balancing. Regulation resources currently receive a two-part payment that consists of capability payment and performance payment, both of which are scaled according to the performance score. Performance score is a measure the quality of regulation provided by a participant.

2.2 Roles energy storage can play in a smart grid

Batteries in future smart grid will play many essential roles, such as reserves, load balancing, frequency regulation, microgrid stabilization, facilitating connection of renewable energy sources (RES) for the grid and perform load shifting, demand response and energy arbitrage for the end user. However, batteries are costly devices which consume some energy, act as inefficient buffers of energy and undergoes degradation, therefore, health of battery should be considered for maximizing operational life.

In the previous section, 2.1, we discuss the future challenges the power network will face due to growth of DGs and new loads such as EVs. In such power grids, balancing the load will be difficult. Energy storage devices act as energy buffers and can therefore be used for diversified tasks in future power grids. Batteries are an attractive solution as:

- *Expected reduction in cost*: The cost of batteries are expected to drop further in coming future, pertaining to the fact that intense research is going on in developing cost effective energy storage technology. Fig. 2.11 shows the decrease in storage cost, extrapolating this decrease which has a learning rate of 18%. The Li-Ion battery cost is projected to to be around $94/kWh by 2024 and $62/kWh by 2030 [103].
- *New avenues*: as indicated earlier, the innovative billing strategies provides energy participants with opportunity to reduce their cost of consumption by participating in grid based services. These opportunities are expected to increase for energy participants due to increased uncertainty and greater responsiveness required. For instance, the volatility of electricity price signal will increase with increased share of RES in total energy generation [185].
- *For large energy participants*: For big consumers or generators, the rules are well drafted by ISOs. Such energy participants can install energy storage to ensure that the power quality and operational norms are not violated.

Ideally, a battery which has a low cost, high energy density, high ramp rate, low maintenance, non-toxic in nature will instantly become the ultimate solution for the various storage applications in the future electricity grid. Although the research in achieving these goals are ongoing, batteries are becoming popular in smart grids. Few contemporary examples are:

- California planning billion dollar battery: "In 2013, the California Public Utilities Commission (CPUC) recognized the need to expand the role of energy storage in support of a carbon-free grid by establishing an energy storage procurement target of 1,325 megawatts for load serving entities. The investor-owned utilities, Pacific Gas and Electric Company, Southern California Edison and San Diego Gas & Electric, as well as energy service providers operating in California must procure storage resources by 2020 with installations completed by the end of 2024" [50].
- Hawaii island powered by Tesla battery and solar panels: The Kauai project consists of a 52 megawatt-hour battery installation plus a 13 megawatt SolarCity solar farm. Tesla and the Kauai Island Utility Cooperative, the power company that ordered the project, believe the project will reduce fossil fuel usage by 1.6 million gallons per year [64].

Next we describe some of the many energy storage applications for the future power networks.

2.2.1 Energy Arbitrage

Consider an electricity consumer with time varying electricity price. Electricity consumer could differ their consumption seen by the grid such that when prices are high they consume less and when prices are low they consume more, in effect reducing their cost of consumption without reducing total energy consumed. By responding to such a price signal the consumer is assisting the utility to reduce peak demand by shifting loads to off peak periods or from periods of more congestion to periods of less congestion in the network. Electricity price design and consumers responding to such prices serves several other objectives often difficult to quantify each ISO often has a different algorithm to generate RTPs. In Fig. 2.4 we show

the real-time and day ahead electricity price over a week in California. The relationship between day-ahead electricity price and aggregate load is clear. The morning and evening peak of aggregate load coincides with peaks of day-ahead electricity price. This is primarily because the variation of aggregate load is fairly predictable. However, the variation of real-time electricity price is much harder to quantify only using aggregate load.

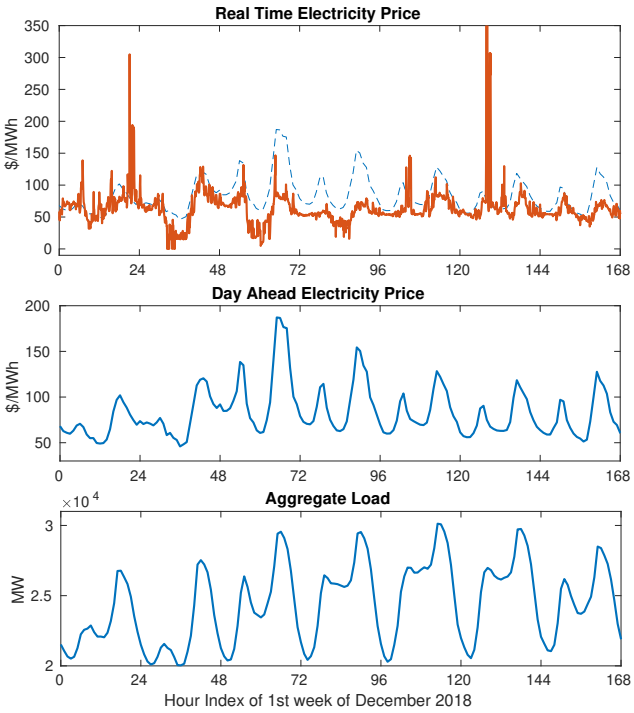

Figure 2.4: Real-time, day-ahead electricity price and aggregate load in CAISO during 1st week of December 2018 [16].

Although it would be beneficial for consumers to deviate consumption taking into account electricity price variation, it has been observed that consumption patterns of users do not change significantly with real time electricity price variations and hence consumers end-up paying more in their electricity bill [87]. Installing energy storage by an end user allows them to perform energy arbitrage, i.e., to buy energy when prices are low and sell it when it is expensive. The energy bought can be stored in the battery for later use when the demand arises. Hence, using the battery allows the user to keep the same consumption pattern without increasing their electricity bills under time-varying electricity prices [251]. Additionally, if the user is equipped with a renewable generation unit, then a battery also allows the user to reduce generation intermittence and uncertainty by storing excess generation. The value created by storage performing arbitrage will increase with the increase in the variability in electricity prices [251] for the same storage.

Energy Storage with Distributed Generation: The share of total energy consumed worldwide by buildings, which include commercial and residential end users, accounts for around 20% and it is projected to grow at an average of 1.4% per year from 2012 to 2040 [260]. The environmental benefit of connecting more and more renewable energy sources in meeting the global energy demand is therefore irrefutable. Consider a residential consumer with load, rooftop solar generation and a battery. The battery is controlled based on the levels of buying price applicable when power flow from the grid to residential consumer and selling price otherwise. The value of energy storage increases with DG installed locally as the selling price is often lower than buying price, facilitating self-consumption of locally generated renewable energy which otherwise would be wasted or supplied back to the grid at a low price, see Chapter 4 [183].

2.2.2 Dynamic Regulation and Reserves

Grid operator's role is to maintain a balance between the supply and the demand. Electric energy is unique in the sense that the demand and supply has to match approximately at every time instant such that the frequency and voltage of the grid is within a specified band, for example for a nominal frequency of 50 or 60 Hz the grid frequency can vary between lower and upper bound of frequency decided by grid norms of the country. Table below lists continuous operating frequency range (COFR) for some countries.

Table 2.3: Continuous operating frequency range

Country	COFR
Germany[234], China [194]	49.5 to 50.5 Hz
Australia [194]	47 to 52 Hz
India [194]	47.5 to 51.5 Hz
USA [234]	A-zone: 59.95 to 60.05 Hz, B-zone:59.8-59.95 & 60.05-60.02 Hz, C-zone: <59.8 Hz & >60.02Hz

To maintain reliability the ISO must continuously match the demand of electricity with supply on a second-by-second time-scale. In case of over-generation, excess generation curtailment maybe essential to ensure stability of power network. And in case of under-generation, load shedding maybe essential. In order to contain uncertainties in load and generation, additional resources are required for achieving load balancing at finer time-scales. Such resources should be able to ramp up or ramp down with very small response time. Traditionally, fast ramping gas turbines are used for such goals which can ramp up generation in a short time. Using energy storage devices for dynamic regulation facilitates ramping up (i.e. generating energy) and ramping down (i.e. consuming energy) capability simultaneously, thus holds greater potential to eliminate generation curtailment and load shedding.

Case of Elia in Belgium: Each system operator in ENTSO-E[13] synchronous area is responsible for balancing generation and consumption within its own control area. In Belgium, Elia assumes this responsibility. Elia divides the balancing responsibility to pre-designated access responsible parties or ARPs. These ARPs maintain a balance in their designated area at every 15 minutes time interval. ARP could be a producer, a major consumer, an energy supplier or a trader. Elia uses the measurement data to verify whether the ARPs are meeting their respective balance management obligations. Elia will apply imbalance tariffs if it observes a quarter-hourly imbalance between injections, imports, purchases and off-takes, exports and sales. Energy storage owners can track unbalance signal for assisting Elia achieves balance in net load and net generation. Similar to CAISO, Elia incentivizes ARPs and resources providing up-regulation and down-regulation by separate up-regulation tariff denoted as POS and down-regulation tariff denoted as NEG. Although, instantaneous values for POS and NEG are the same for most time instants. The amount and direction of regulation required is denoted by Net Regulation Volume or NRV. A positive value of NRV indicates a net upward regulation signal and a negative value indicates a net downward regulation signal [6].

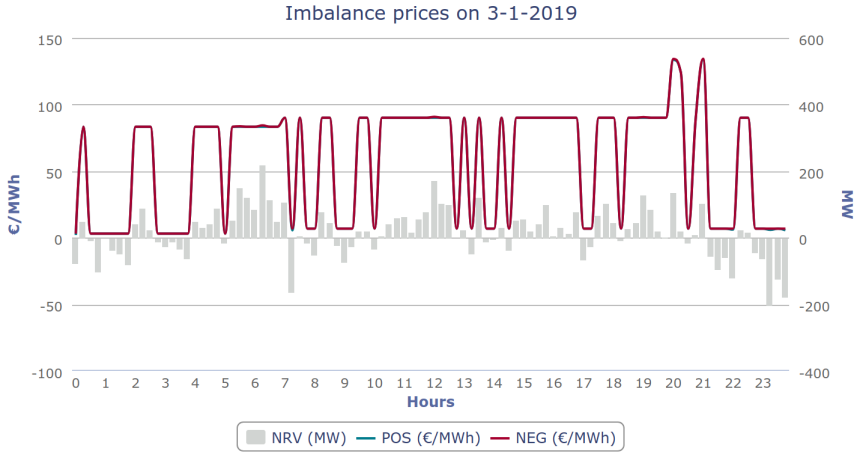

Figure 2.5: Imbalance prices and Net Regulation Volume for 3rd January, 2019 [15].

Fig. 2.5 shows the imbalance prices for up-regulation and down-regulation and NRV for 3rd January 2019. ARPs and resources should track NRV for facilitating balance in the power network.

Note that the imbalance signal in Elia is not energy neutral and therefore the price for up-regulation and down-regulation is settled separately. Contrary to this, in PJM ISO the regulation services combines

[13]ENTSO-E, the European Network of Transmission System Operators, represents 43 electricity transmission system operators (TSOs) from 36 countries across Europe.

up-regulation and down-regulation and they are not settled separately. Therefore, PJM attempts to ensure conditional neutrality of dynamic regulation signal [218]. Batteries commit capacity prior to regulation participation and get compensated based on committed capacity and performance of tracking. For Elia and CAISO battery owners commit up-regulation and down-regulation separately.

Reserves

Reserves enable power networks to maintain frequency and voltage at appropriate levels while managing balance and congestion in three different types of reserves [2]:

Primary reserve: The turbines at some production units can automatically detect frequency fluctuations and, where necessary, adjust production within 0 to 30 seconds.

Secondary reserve: The secondary reserve is automatically and continually activated both upstream and downstream (upward/downward regulation). It kicks in quickly (between 30 seconds and 15 minutes) and remains active as long as it is needed.

Tertiary reserve: The tertiary reserve enables ISOs to cope with a significant or systematic imbalance in the control area and/or resolve major congestion problems.

In France the total electricity produced in 2013 is 551 TWh, implying 62.9 GW average power production over the year [153]. The operating reserves used in French power network are [84]:

- Primary reserves with response time of less than 20 seconds and a cumulative capacity $\approx$ 500MW,
- Secondary reserves with response time of less than 3 minutes and a cumulative capacity $\approx$ 600MW,
- Tertiary reserves with response time of less than 15 minutes and a cumulative capacity $\approx$ 1500MW.

Thus total reserves in French power grid is $\approx 4.13\%$ of the average generation for year 2013.

Energy storage can be used as reserves in power networks. With growth of uncertainty, the amount of reserves will increase providing greater opportunity for energy storage devices.

2.2.3 Peak Demand Flattening

Previously, we discussed that the maximum demand dictates the size of power grid infrastructure, i.e. generators, transmission lines, transformers, circuit breakers etc. Due to this many power utilities around the world have introduced peak demand charge [295, 320, 228] that a consumer may seek to minimize over a longer period (weeks or months). The peak demand charge is applied to the average peak power level for a 5 min to an hour interval. The time scale varies from place to place. Authors in [294] note that energy storage can reduce peak demand cost without degrading the ability to perform other applications using energy storage.

Peak Power Contracts (PPC) for Low Voltage (LV) Consumers in Madeira, Portugal: As of 2018, LV customers can select between 8 levels of peak power contract (PPC). LV customers are subject to a maximum peak power contract (kVA), ranging from 3.45 kVA to 20.70 kVA (see Tab.2.4). The nominal PPC value is selected by the customer based of their estimated electricity needs and should not be exceeded since the supply is shut-down when that happens. The disconnection of power is done locally and consumer can restart their energy-meter, however, sudden interruptions should be avoided as it may damage appliances. The PPC can be changed upon formal request to EEM.

Table 2.4: Peak Power Contract for LV customer as of 2018.

Peak Power Contract (EUR/Day)		
PPC (kVA)	Single-rate (in euros)	Dual/Triple-rate (in euros)
3.45	0.1611	0.1643
4.60	0.2096	0.2132
5.75	0.2560	0.2590
6.90	0.3040	0.3080
10.35	0.4478	0.4532
13.80	0.5902	0.5981
17.25	0.7326	0.7436
20.70	0.8751	0.8892

Form Tab.2.4 it is evident that consumers can use energy storage device to lower their peak demand and in effect reduce the fixed cost associated with PPC contract selected by the consumer.

2.2.4 Fast ramping and low response time

California aims to generate 50% of retail electricity from renewable power by 2030 in order to reduce greenhouse gas emission to 1990 levels. Such goals would constitute increase in distributed generation and large scale inclusion of electric vehicles. Historically, the ISO directed controllable power plant units to track instantaneous demand. With growing penetration of renewables on the grid, there are higher levels of uncontrollable, variable generation resources. Because of that the ISO must use controllable resources to achieve a balance between both variable demand and variable supply. CAISO uses net load which is the difference between total load and renewable generation such as wind and solar. The net-load curve illustrates the variability and often referred as duck curve.

The CAISO performed an analysis on changing grid conditions by analyzing loads in past and near future [197]. With growing inverter based renewables the frequency response of the power network deteriorates. This study identifies inclusion of specific resource operational capabilities for mitigation of [197], [322] (i) oversupply risk, (ii) short and steep ramps. In order to mitigate the possible issues, the ISO needs a resource mix that can react quickly to adjust electricity production to meet the sharp changes in electricity demand.

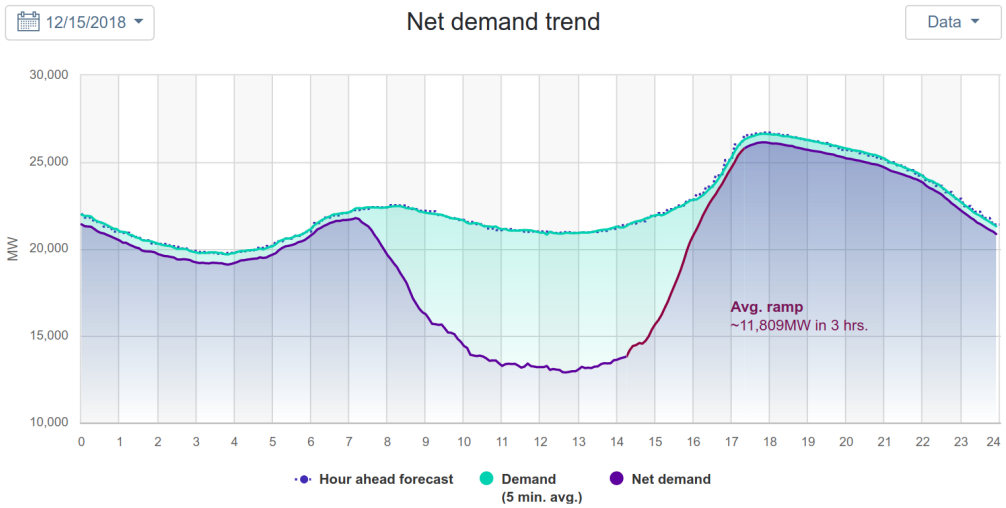

Figure 2.6: Aggregate load forecast with growing share of renewables in CAISO [35].

To ensure reliability under changing grid conditions, the ISO needs resources with ramping flexibility and ability to start and stop multiple times per day. Large scale solar integration in CAISO increases the chances of oversupply during mid-day. According to testimony given to the FERC, CAISO's minimum non-dispatchable power production is about 15,000 MW - meaning the power grid's online generators cannot produce less than 15,000 MW at any one time [113, 107]. Solar power significantly reduces the net-load on conventional generators during the day but not during the night, a surge in generation demand may occur as the sun sets [113]. In that time, average day-ahead hourly energy market prices during the 3 hour interval (5 p.m. to 8 p.m. during summer and 2 p.m. to 5 p.m. during winter) – the "neck" of the duck – have spiked to nearly $60 per megawatt-hour, compared to about $35 per megawatt-hour in the same period in 2016 [198]. The recent analysis on duck curve concludes that the increase in ramps is not seasonal and exists throughout the year. The ramps are most severe during weekend. Authors also point that duck curve which is observed in California will become also present in other parts of the world with high share of wind and solar generation [322]. This author also points that the evolution of ramping requirements is much faster than anticipated in prior studies such as [197]. Batteries can help to solve such ramping problems, which motivated growing installation of batteries in California in the last decade.

Fig. 2.6 shows the net load plot for 15th December 2018. The average ramp required for this day is $\approx 11,809$ MW. This ramp should be met with reserves which can respond rapidly. Energy storage is a solution which CAISO considers has huge potential.

2.2.5 Power Quality

Energy storage interfaced via a converter can be a source or sink of active and reactive power. The active power output is governed by ramping constraint of the storage and the reactive power output is governed

by it converter rating and instantaneous active power output.

Phase Balancing: Unbalance in power distribution network can be eliminated by design if the transmission lines are fully transposed and load is divided symmetrically in all phases, both of which is difficult to realize in low voltage distribution networks due to primarily single phase loads and DGs connected. Due to unbalanced loading and unequal feeder lengths, phase imbalance exists. Power utilities aim to contain the unbalance within pre-decided norms, rather than complete elimination of unbalance. Table 2.5 lists the norms derived from standards and utilities for voltage unbalance. Note the norms often are more detailed and are specific to the network and feeder. For instance in a radial distribution network, feeders away from the source have higher potential to cause unbalance than those close to the source. Table 2.5 shows simplified version of these norms and should not be generalized. Many traditional solutions are

Table 2.5: Voltage Unbalance Norms

Utility/Standard	Voltage Unbalance Factor Limit
American National Standard for electric power system and equipment ANSI C84.1	3%
PG&E [37]	2.5%
NEMA MG-1-1988 [21]	1%
UK - network unbalance UK - load point unbalance	2% 1.3%
BC Hydro - Standard Unbalance [10] BC Hydro - Rural Unbalance [10]	2% 3%
Europe EN 50160 - LV and MV [36] Europe EN 50160 - High Voltage [36]	2% 1%

available in the literature for solving unbalance problem in three phase networks. Inclusion of shunt or series connected compensators are widely used traditionally. Recent works present feeder reconfiguration for phase balancing [327]. Authors in [328] propose coordination of operation of data-center and DERs to reduce phase unbalance. Authors in [329] propose load balancing with EV chargers and PV inverters in unbalanced distribution grids by adaptively selecting the phase based on unbalance. Authors in [225] present the phase balancing using EVs interfaced to power network via a single phase connection that adaptively selects the phase to connect in LV Danish grid. Authors in [193] used solid state switch placement to achieve phase balancing in distribution grid. Authors in [306] used energy storage owned privately for performing arbitrage and phase balance considering battery degradation. Balancing the voltage helps in saving energy and money by increasing motor efficiency. Furthermore, transmission line capacity is better utilized, false trigger of protective relays are avoided and also prevents downtime due to motor failures.

Energy storage interfaced via a converter is capable of supplying active and reactive power for phase balancing of three phase network. Authors in [141] consider unbalance which could be caused by building integrated PV. Converter control is proposed for tracking voltage and phase angle mismatch. [140] mitigates voltage unbalance in low voltage distribution network with high penetration of PV system using energy storage. The controller minimizes the current flow in the neutral line and experimental study indicates improved Voltage Unbalance Factor or VUF.

2.2.6 Case-Study : EV Charging in Pasadena[14]

Phase unbalance can be an issue behind the meter as well. In this sub-section presents a case study around phase unbalance at the Adaptive Charging Network (ACN) testbed located at Caltech in Pasadena, California. A description of the testbed including its electrical topology and usage patterns is provided then provide examples of power unbalance between phases which occur do to usage patterns which lead to non-symmetric loading between phases. Finally a motivation is provided for the need for phase balancing techniques such as the energy storage which can account not only for instantaneous unbalances but also long term unbalances caused by differences in the total energy demand on each phase.

Electric vehicle charging EVs are expected to dominate future transportation. Charging EV batteries can place a massive load on the local electrical infrastructure. Table 2.6 lists some EVs and their battery characteristics. The batteries can either be charged using three-phase or single-phase AC connection. In

[14]This section is prepared by Zachary Lee at California Institute of Technology, Pasadena, California.

the case of AC level-2 charging, a single-phase connection is used by the AC/DC converter inside the EV. In the case of DC charging, a single-phase or three-phase connection can be used to feed an AC/DC converter outside the EV, which then feeds DC current directly to the EV's battery. Table 2.7 lists the standard single and three-phase EVSEs (charging ports) and their rated power transfer capability. For instance, Nissan Leaf can be completely charged within 4 hours using 1-phase 32A charging EVSE. All charging points in Caltech ACN Testbed are of single phase and 32A rated type.

Table 2.6: EV battery characteristics [70]

EV make	Warranty	Battery	Charge times
Nissan Leaf	8yrs./100,000 miles	30 kWh	8h at 230V AC, 15A,
Chevrolet Bolt	8yrs./100,000 miles	60 kWh	10h at 230V AC, 30A
Tesla model S	8yrs./unlimited miles	70, 90 kWh	9h with 10kW charger

Table 2.7: EV charging socket characteristics [73]

Charger type (230V AC)	Rated power	Time to charge 30kWh
1-ϕ 16 A	3.7 kW	8 hours
1-ϕ 32 A	7.4 kW	4 hours
1-ϕ 16A/ϕ	11kW	2h 45 min
3-ϕ 32A/ϕ	22 kW	1h 22 min

The Caltech ACN Testbed: The ACN testbed at Caltech was built in early 2016 and since then as delivered over 735 MWh of electricity to charge electric vehicles. The ACN currently has 54 EVSEs which are used for research. It is a three-phase system supplied by a 150 kVA delta-wye transformer. Each EVSE (charging port) is connected line-to-line. Early in the project, two EVSEs were replaced with pods of 8 EVSEs each to demonstrate the scalability of smart charging. This has led to a significant imbalance in the number of EVSEs on each leg of the delta, with AB having 26 EVSEs, BC and CA each having 14 a piece. This topology only exacerbates the power unbalance caused by randomness in user demands. More information about the ACN including its hardware, software, and algorithms can be found in [220]. Since 2016, the ACN framework has been commercialized by PowerFlex Systems which operates similar large-scale charging systems around the United States.

Examples of Unbalance To demonstrate the unbalance present in the Caltech ACN the authors considered two cases, uncontrolled charging and smart charging. In both cases they simulated the phase unbalance using ACN-Sim, an open-source simulator for EV charging research [221]. Each simulation was based on real usage data collected from the Caltech ACN available from from the ACN-Data dataset [222] (which can be downloaded at [219]) as well as models of the actual electrical infrastructure of the Caltech ACN. The current unbalance which results from uncontrolled charging is shown in the top panel of Fig. 2.7, while the unbalance from the smart charging algorithm used in the actual ACN (described in detail in [220]) is shown in the bottom panel. From the top panel it can be seen that the current unbalance from uncontrolled charging can be substantial, differing by as much as 280 A between phase A and phase C. In the actual system, a smart charging algorithm is used to schedule charging while accounting for infrastructure constraints as well as user provided deadlines and energy requests. While this algorithm does not explicitly try to reduce phase unbalance, it does implicitly reduce unbalance during times of congestion since more power can be delivered when phases are balanced. In the bottom panel of Fig. 2.7, it is observed that while the smart charging algorithm is able to lower the peak currents in the system to below the line limits (here 417 A), phase unbalances are still substantial.

Limitations of Smart Charging While smart charging algorithms can help to prevent line overloads and alleviate instantaneous current unbalance by shifting loads in time, it cannot fix the inherent imbalance in total load. For example, on September 5, 2018 the total energy demand on EVSEs on the AB leg of the delta was 408 kWh while BC was 178 kWh and CA was 232 kWh. These unbalanced energy demands mean require us to redistribute load between phases in order to balance currents. The proposed energy storage system is one way to do so.

2.2.7 Increasing Reliability and Inertia

With large-scale integration of renewables the frequency response of the power network deteriorates as (i) less resources are available to automatically adjust electricity production to maintain grid reliability, (ii)

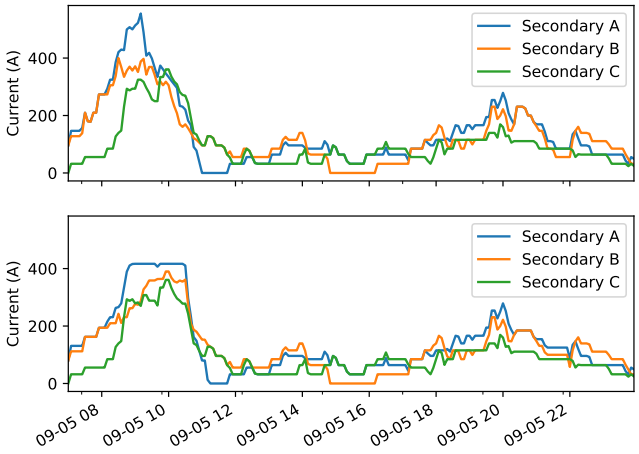

Figure 2.7: (top) Current unbalances for uncontrolled EV charging at the Caltech ACN. (bottom) Current unbalances for smart EV charging at the Caltech ACN. Both plots are simulated based on real data collected Sept. 5, 2018 at the Caltech ACN.

inverter based distributed generations do not add inertia thus the grid becomes more prone to fluctuations and (iii) distributed generation increases fluctuations.

The electrical power system globally is undergoing huge changes in operation. This change is attribute to integration of intermittent renewable energy sources in transmission and distribution side of power system. Especially the integration of DG is critical for stable operation of entire power system. Traditionally, the power system is designed for one way power flow, however, with DGs the direction of power flow can be reversed. This new power system will require more real time adaptive control for stable operation. Authors in [226] claim that smart grid with large share of renewables will bring the third industrial revolution worldwide. The concept of smart grid could be a reality with cheap DGs, affordable storage, advancements in communication and information theory.

2.2.8 Congestion and Voltage Support

Power networks were designed for one way power flow. Bulk power generators transmit power to consumers. Under such a power network the voltage level farther away from the generation with respect to point of connection in the network will be lower compared to all points before it. However, this will not be valid with integration of DGs in power network. Such a power network could have overvoltage issues at a local level and will require localized mitigation. Prior to this situation the voltage at the beginning of the feeder would have given a good estimation of voltage profile across the network, however, this will no longer be valid with DG integration. Furthermore, power system protections have been designed based on one way power flow assumption, a detailed study needs to be performed to understand the required modification in protective relay settings in order to avoid false tripping of relays.

Case Study for a Radial Distribution Network: We present a toy example to demonstrate this issue. We use a IEEE 33 bus radial distribution system shown in Fig. 2.8. The buses 1-18, 19-22 and 26-33 are part of single feeder. Under no DG the voltage magnitude in each of these feeders will drop as we go farther away from the connection point. For instance voltage magnitude will reduce from 1 to 18, bus 18 being the lowest in magnitude.

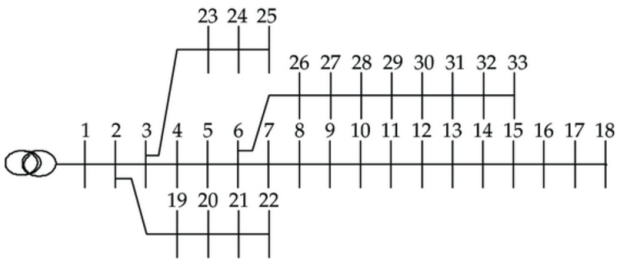

Figure 2.8: IEEE 33 bus radial distribution system

We identify the voltage profile of 3 different cases: (i) Nominal case, (ii) Change the load at bus 15 to 2 MW and (iii) add 2 MW generation at bus 15. We perform these simulations using MatPower toolbox [342]. The voltage profile for the 33 bus network under the three cases is described in Fig. 2.9. The blue and red lines show the expected voltage profile behavior of dropping voltage magnitude as we go farther away from point of connection. However, for the third case where a DG is emulated using a 2 MW generation, the voltage profile peaks at that point. If generation is further increased, the voltage will go beyond permissible limits set by utility. Note that the voltage measurement at the bus 1 (generation bus) might not be able to provide indication of such localized over-voltages.

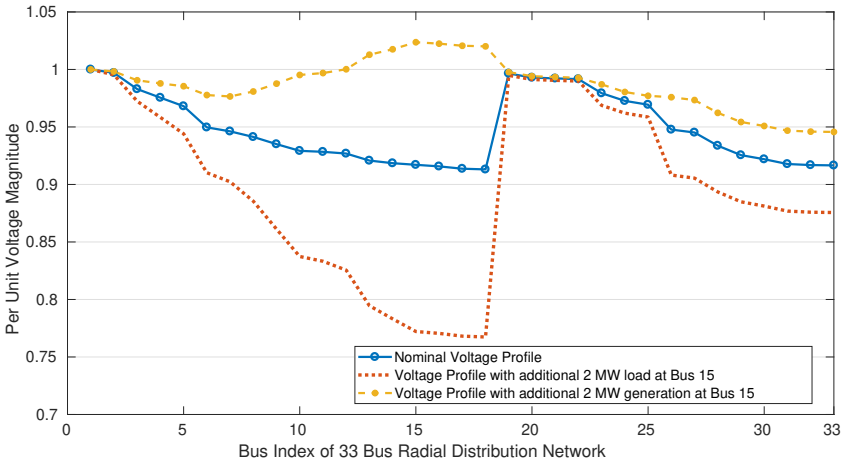

Figure 2.9: Voltage profile plot for IEEE 33-bus radial distribution network for (i) Nominal flow, (ii) 2 MW load at bus 15, (iii) 2 MW DG connected at bus 15.

Form Fig. 2.9 it is clear that overvoltage issues would be localized. Such problems could be efficiently solved using distributed energy storage devices and/or load flexibility at local level.

2.2.9 Infrastructure Deferral

All the above problems described could be solved using more traditional solutions like adding more fast ramping power plants, curtailment of excess generation, load-shedding (affecting power network reliability), power quality improvement infrastructure. However, the capital required for such an upgrade of power network will be several folds higher than using energy storage in a smart grid with ample amount of information for adaptive decision making. Thus adding storage will provide power utilities to defer the infrastructure development cost which otherwise they would need in order to cope with the new power grid with more volatility and uncertainty [86].

Transmission and distribution deferral keeps the loading of the transmission or distribution system equipment lower than a specified maximum. This allows for delays or completely avoids the need to upgrade a transmission system or avoids congestion-related costs and charges [315].

There are several other applications of energy storage such as microgrid stabilization, spinning reserves, island and off-grid storage, black-start services etc., which have not been discussed in detailed.

2.3 Bottlenecks with energy storage: Li-Ion battery

Li-Ion battery could be used for many power system applications, however, there are various bottlenecks associated with Li-Ion battery and energy storage in general. Firstly, energy storage is a costly solution making it financially infeasible if deployed for many of the applications. Careful financial evaluation is essential. Secondly, due to energy storage parameters and chemistry batteries consume cycling losses, degrade over time and have limited life time. Furthermore, batteries require maintenance at regular intervals. Battery health and thus its life is affected by temperature, humidity, charging and discharging pattern to name a few. Thirdly, there is uncertainty in system variables based on which battery mode of operation is selected. Note that optimal storage operation of energy storage requires look-ahead in time. If the parameters based on which mode of operation of battery is decided are drastically different, then the mode decided might not be optimal. Thus due to inaccurate information the storage returns could be

undermined. Forecasting is a heavily research area in power systems. However, the forecast models are not modular, i.e., a forecast model in a region could be of little use in forecasting the same parameters in a different region.

2.3.1 High Cost

Batteries are expensive with per kWh cost ranging from US $ 400 to several thousands. The cost of Li-ion battery depends on the technical specifications and the type of application. The price of Tesla's Powerwall from 2017 are listed in Table 2.8.

Table 2.8: Ramp Rates as listed in datasheets

Manufacturer	Cost ($)	Cost per kWh	Wh per US $
Tesla Powerwall 1 [66]	$ 3000	470	2.13
Tesla Powerwall 2 [66]	$ 5500	398	2.51

Researchers are optimistic about future dip in price of batteries. Fig. 2.10 shows the forcast of price dip from 2015.

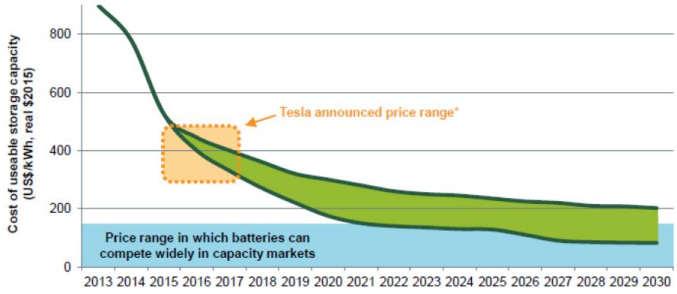

Figure 2.10: IHS Benchmark Battery Module Price Forecast in 2015 (US$/kWh) [47].

A similar projection is presented in BloombergNEF report 2019 shown in Fig. 2.11.

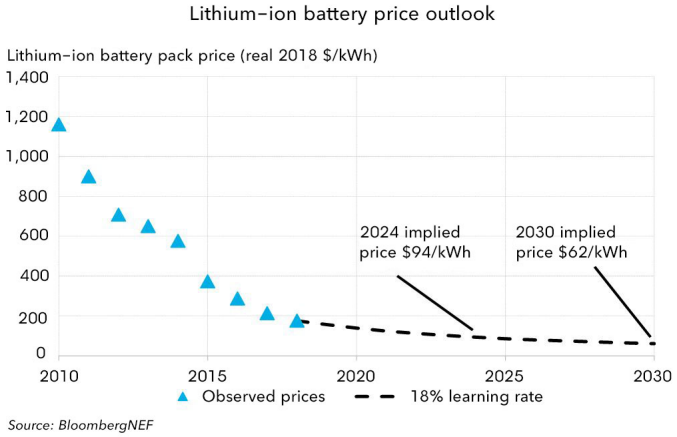

Figure 2.11: The price of an average LiIon battery pack is projected to be around $94/kWh by 2024 and $62/kWh by 2030 [103] (Mar 2019. Source: https://about.bnef.com/blog/behind-scenes-take-lithium-ion-battery-prices/)

US Energy Information Administration in it report, [315], state that the cost of the battery storage technology depends on power and energy capacity of the battery. The battery cost is the maximum of the costs decided by battery power and energy ratings.

2.3.2 Battery life and parameters

Batteries degrade as a function of its operational trajectories, i.e. charging and discharging cycles, exogenous condition such as temperature, humidity and the age of the battery. There are many degradation models for Li-Ion storage available in the literature.

The usable life of a Li-Ion battery is commonly referred as End-of-Life or EoL[15]. The battery should be operated in a way that the EoL of the battery is maximized.

The objective of this subsection is to list the internal bottlenecks related to Li-Ion batteries such as efficiency losses, cycle life, calender life, capacity, size and ramp rate rate specifications and their approximate relationships. Here we also present the effect of temperature and mode of operation which should be considered in designing the charge controller. We explore the datasheets of Li-Ion batteries for electrical power system. Some of the experience gained from this exercise will be used in battery models used in the rest of this thesis.

We use xC-yC notation to represent the relationship between ramp rate and battery capacity. xC-yC implies battery takes 1/x hours to charge and 1/y hours to discharge completely. Higher value of x and y implies faster the battery is to charge and discharge. For example 2C-1C battery implies the battery takes 0.5 hours to charge and 1 hour to discharge completely.

Efficiency Losses: Batteries store electrical energy as chemical energy. When a battery is charging, electrical energy is converted into chemical energy and when a battery is discharging, chemical energy is converted into electrical energy. These energy conversions are not completely efficient and thus induce losses denoted by charging and discharging efficiency. The roundtrip battery efficiency of the battery is the product of charging and discharging efficiency. The battery produces or consumes direct-current or DC, however, the majority of power network is alternating current or AC. In order to use batteries in AC networks, a converter is required which converts AC to DC (i.e. acts as a rectifier) while the battery is charging and performs DC to AC conversion (i.e. acts as a inverter) while battery is discharging. These AC to DC and DC to AC conversions also induce losses. Battery manufacturers use system efficiency to denote the product of charging, discharging and converter efficiency.

The loss of energy in charging and discharging cycle is shown in Fig. 2.12. Note as the battery is charged its cell voltage increases. In fact cell voltage is a primary variable used in many state-of-charge or SoC[16] estimation algorithms. Fig. 2.12 also denotes the SoC operating window confined due to high stress in extremely low and high SoC regions. We will discuss this in more details in modes of operations of a Li-Ion battery.

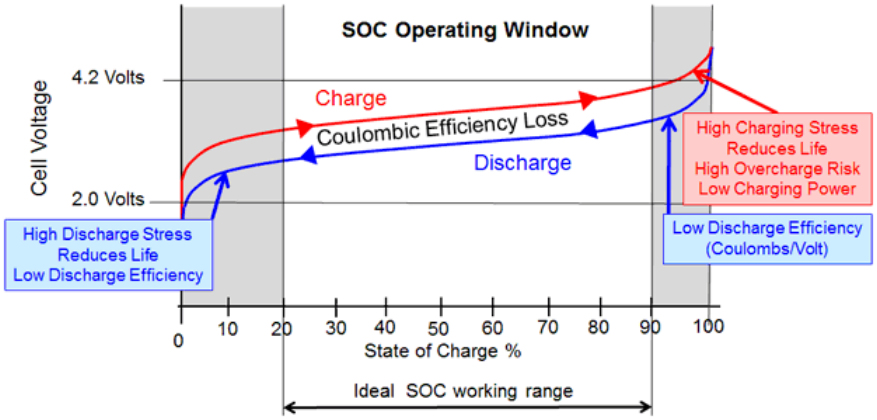

Figure 2.12: Charge and discharge cycle losses and optimal range of SoC [53].

Table 2.9 lists the efficiency information provided in battery datasheets. The values of efficiencies listed indicate that at best 85 to 95 % of charging energy could be discharged. AES Advancion [42] claims that slower ramp rates lead to greater roundtrip efficiency. Tesla Powerwall specifications are applicable when the battery is brand new. Powerwall specifies that age of the product, temperatures above or below 25 deg. C, and charge rates or discharge rates above 2 kW would lower this value of efficiency, thus decreasing the system performance. Table 2.9 shows that battery efficiency of a Li-Ion battery is affected by ramp rates and temperature as most of the efficiency listed in datasheets where applicable for a specific operating condition.

Cycles of operation: One of the indexes which decides the life of operation is the rated cycles of operation of a battery. This is an information often provided by manufacturers in their datasheets,

[15]EoL is the state of the battery when the maximum battery capacity reduces to 80% of its initial rated capacity in watt-hours.

[16]SoC denotes battery charge level in a scale of 0 to 1, where 0 denotes fully discharged and 1 denotes fully charged battery.

Table 2.9: Efficiency of Li-Ion battery

Manufacturer	Efficiency	Remarks
LI TEL 48-170C C&D Techno[48]	η_{charging}=98%	for 35 deg.C
AES Advancion[42]	$\eta_{\text{roundtrip}}$ >85-90%	depends on ramp rate
Saft Evolion Li-ion[62]	$\eta_{\text{roundtrip}}$ >95%	-
LG Chem RESU 6.4EX [51]	$\eta_{\text{roundtrip}}$ >95%	For ramp rate C/3 and 25 deg. C
QINOUS Li-ion [59]	η_{system} >88%, $\eta_{\text{roundtrip}}$ >96%	-
Tesla Powerwall 1 [66]	$\eta_{\text{roundtrip}} \approx$ 92.5%	for battery voltage 400-450V
Tesla Powerwall 2 [66]	$\eta_{\text{roundtrip}} \approx$ 89%	for 25 deg. C
Tesvolt Li-phosphate [67]	$\eta_{\text{roundtrip}}$ >90%	-
aentron Li-ion [41]	η_{system} >97%	for 25 deg. C
Bosch Storage [44]	$\eta_{\text{roundtrip}}$ >95%	-
BYD [45]	η_{inverter} ≈93%, η_{system} ≈89%	-
REFU [60]	η_{inverter} ≈95%, $\eta_{\text{discharge}}$ ≈96%, η_{charge} ≈93%	for 25 deg. C

measured under controlled environment. This value of cycles will with high probability lead to the EoL of the battery.

Table 2.10: Cycles of operation as listed in datasheets

Manufacturer	Cycles of operation	Remarks
C&D Techno [48]	4,300 cycles	20 deg. C and 80 % DoD
AES Advancion [42]	2000 to 3000	at 80% DOD
LG Chem RESU 6.4 [51]	> 6000	90% DoD and 25 deg. C
QINOUS Li-ion [59]	4000 cycles	at 1C/1C at 80% DoD, 25 deg.C
Tesla Powerwall 1 [66]	5000 cycles	daily cycle application
Tesvolt Li-phosphate [67]	8000 cycles 5000 cycles	for 70% DoD for 90% DoD
Forsee Power HE48 [49]	6 000, excluding calendar aging 5 000, including calendar aging 4400, including calendar aging	25 deg.C, 70% DOD 25 deg.C, 70% DOD, 2 cycles/day 25 deg.C, 70% DOD, 1 cycles/day
aentron Li-ion [41]	3000	50% DoD, 20 deg. C
Bosch Storage [44]	4500	-
REFU [60]	6000	80% DoD, 20 deg.C, max discharge=0.5C

The important thing to note from Table 2.10 is that the manufactures describe the cycles of operation of a battery with respect to a particular temperature (implying if temperature is not maintained then operational life will be lower), number of cycles of operation per day, depth of discharge or DoD[17], calender aging, rate of charge and discharge. If we say a battery is 100% fully charged, it means the DoD of this battery is 0%, If we say the battery has delivered 30% of its energy, we say the DoD of this battery is 30% [43]. Slower the charge or discharge rate, slower will be the stress on the battery and thus longer the life of battery.

From Table 2.10 we observe that the factors affecting the rated cycles of operation are: (i) Battery type, i.e. chemical composition of the battery, (ii) Depth of discharge of Operational cycles, (iii) Temperature, (iv) Ramp rate and (v) Cycles per day.

***Calender life in years*:** Calender life refers to the number of years the battery is expected to last till the battery will reach EoL. It is independent of how much the battery is charged and discharged. However, calender life is dependent on the state of charge of the battery and the temperature. As shown in Fig. 2.13, observe that below 35 deg. C expected life is independent of SoC.

The life of a battery will be a combined function of cycle life, calender life, temperature, SoC. Fig. 2.13 shows how the calender life of the battery is a function of SoC level and temperature. An interesting observation is that a high SoC level affects the calender life drastically at high temperatures.

[17]The depth of discharge of the battery measures how deeply depleted the battery is, compared to a state of full discharge when it would have discharged all of its energy capacity. When a battery has discharged its full energy capacity, the DoD 100%.

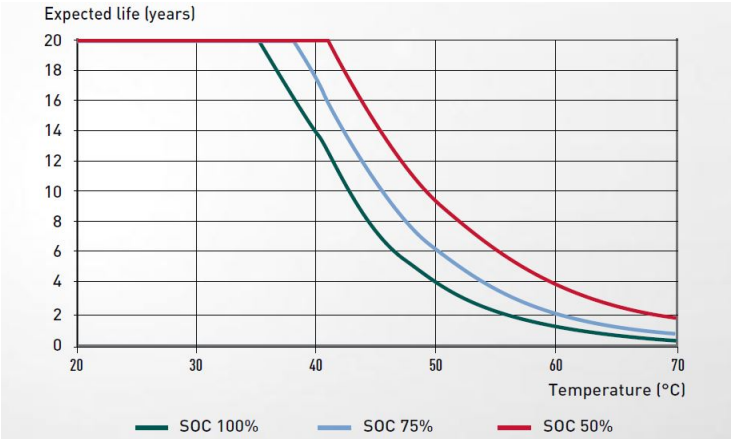

Figure 2.13: Expected life for Li-ion cells with temperature (EoL for capacity loss of 20%) [49]

Table 2.11: Calender Life as listed in datasheets

Manufacturer	Calender life and Remarks
AES Advancion [42]	7-8 years Lifespan
Evolion Li-ion battery [62]	at 20 deg. C is 20 years at 40 deg. C is > 10 years
LG Chem's RESU 6.4 EX [51]	at 25 deg. C is > 10 years
Tesla Powerwall 2 [66]	warranty of 10 years
Tesvolt Li-phosphate [67]	10 years
Forsee Power Li-ion HE48 [49]	10 years
Aentron off grid Li-ion [41]	10 years at 20 deg. C, Warranty 5 years
Bosch Storage Solutions [44]	> 10 years
BYD [45]	Warranty of 5 years

Table 2.11 indicates that the typical value of calender life is around 10 years. The calender life deteriorates drastically with temperature as shown in Table 2.11 for Evolion Li-ion battery.

Capacity, size and ramp rate: Capacity and size of the battery is a critical component of selection as the area occupied by one or a fleet of batteries acts as a constraint. We enlist in Table 2.12 some of lithium based batteries to understand the relationship between the dimension and capacity of batteries.

Table 2.12: kWh, Ah Capacity of the battery and its size and weight

Manufacturer	Energy	Capacity	Dimension (w, d, h)	Weight	m^3/kWh
Li TEL 48-170 C [48]	8.2 kWh	173 Ah	0.564, 0.564, 0.172m	72.6 kg	0.00667
Evolion Li-ion battery [62]	3.9 kWh	74 Ah	0.216, 0.404, 0.260m	30 kg	0.00582
LG Chem RESU 6.4 [51]	6.4 kWh	126 Ah	0.406, 0.165, 0.664m	60 kg	0.00695
Tesla Powerwall 1 [66]	6.4 kWh	-	1.3,0.86,0.18m [65]	97 kg	0.03144
Tesla Powerwall 2 [66]	13.5 kWh	-	1.15,0.755,0.155m	122 kg	0.00997
Tesvolt Li-phosphate [67]	120 kWh	2400 Ah	3,2.45,2.9m	4800 kg	0.17763
Qinous Li-ion [59]	44 to 331 kWh	-	-	-	-
Forsee Power HE48 [49]	2.7 to 27 kWh	-	0.483, 0.526, 0.088m	-	0.00828
aentron Off grid Li-ion [41]	4 to 12 kWh	50-500 Ah	0.8, 0.6, 0.4m	-	0.04800
Bosch Storage [44]	2 MWh	-	14,2.4,2.9m	80000 kg	0.04872
BYD [45]	8 kWh	-	-	-	-
Panasonic [57]	4 kWh-1 MWh	-	-	-	-
REFU [60]	3 kWh	-	1.023, 0.738, 0.290m	70 kg	0.07298

Table 2.13 lists the rated ramp rates for charging and discharging of some batteries. Typical charging time ranges from 1 hour to 4 hours. As can be observed for Forsee Li-ion battery that discharging is twice faster than rated charging time.

Table 2.13: Ramp Rates as listed in datasheets

Manufacturer	Charging Rate	Disharging Rate
LG Chem's RESU 6.4 EX [51]	0.3C	0.3C
Tesla Powerwall 1 [66]	-	0.313C continuous
Tesla Powerwall 2 [66]	-	0.52C peak/ 0.37C continuous
Tesvolt Li-phosphate [67]	0.417C	0.417C
Forsee Power Li-ion HE48 [49]	0.5C	1C
REFU [60]	≈1C or 3200 W	3000 W

Temperature effects: Prevention of excessive temperature rise in Lithium chemistry cell packs has always been a major design issue. Most Lithium-Ion cells must not be charged above 45 deg. C or discharged above 60 deg. C. These limits can be pushed a bit higher, but at the expense of drastically reducing the cycle life. In the worst case, if cell temperatures get too high, venting may occur, resulting in battery failure or even a cell fire [52].

Li TEL 48-170 C [48] has an operating temperature is between -30 deg. C to 50 deg. C. The typical optimal operating temperature of Li-ion battery is between 20 to 30 deg.C. LG Chem's RESU 6.4 EX [51] has an optimal operating temperature ranging from 15 to 30 deg.C. The cooling can be natural convection.

ABB ESS Pro [40] has the cooling requirements. The cooling can be forced air, chiller, HVAC depending on rating spanning from 50 kW to 6 MW of continuous power.

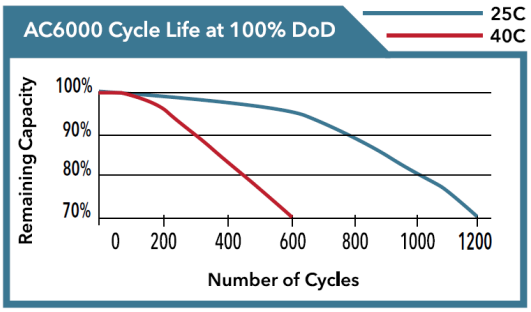

Figure 2.14: Effect of temperature on number of cycles of operation [54].

Fig. 2.14 shows increase of temperature from 25 deg. C to 40 deg. C will reduce the number of cycles with 100% DoD from 1200 cycles to almost 600 cycles. This plot is for Activenergy's AC6000 [54]. However, similar trends will be present for Li-ion batteries of other manufacturers. The key take away is temperature adversely affects cycle life Li-ion battery. Therefore maintaining temperature for the batteries is essential for long operational battery life and making best use of these expensive devices.

Li-Ion Charging operation: Mechanism of charging and discharging is essential for long operational life of Li-ion battery. The commonly used method for charging of Lithium-Ion cells is constant current - constant voltage (CC-CV). This means charging with constant current until a predefined threshold is reached by the cell and continuing with constant voltage until the current drops to zero. The charge time depends on the charge level of the battery and varies from 1-4 hours for full charge from the starting state of minimum charge level. Also Li-Ion cannot be charged very fast, as this will increase their temperature above safety limits. Charging time increases at lower temperatures.

Li-Ion battery chemistries utilize a constant, or controlled, current and constant voltage algorithm that can be broken-up into four stages:

Stage 1: *Trickle Charge* – Trickle charge restores charge to deeply depleted cells.

Stage 2: *Constant Current Charge* – For Li-Ion batteries, after the cell voltage has risen above the trickle charge threshold, the charge current increases in order to perform constant current charging. The constant current charge should be in the 0.2C to 1.0C range.

Stage 3: *Constant Voltage* – For Li-Ion batteries, constant current charge ends and the constant voltage stage begins when the cell voltage reaches predefined threshold (4.2V for single cell). In order to maximize performance, the voltage regulation tolerance should be better than ±1%.

Stage 4: *Charge Termination* – When the timed trickle charge is complete, charge termination is then necessary.

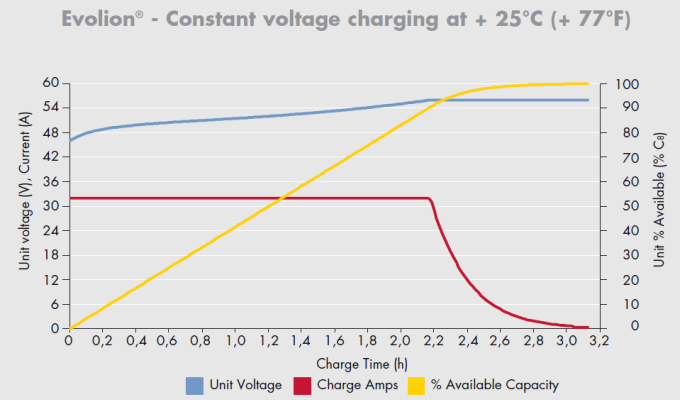

Figure 2.15: Mode of charging a battery [63].

Fig. 2.15 shows the charging current, SoC, battery voltage with time for a Evolion Li-ion battery [63].

Over-charging and over-discharging Li-Ion batteries increases stress in the battery and affect the life of the battery significantly. In order to maximize operational life Li-Ion battery should not be over-charged or over-discharged. The SoC of the battery should lie within minimum SoC level denoted as SoC_{min} and maximum SoC level denoted as SoC_{max}. The upper and lower band of SoC will depend on the electrochemical composition of the battery, type of load, external conditions such as temperature and humidity. These levels can be dynamic or chosen as constant fixed thresholds to minimize control design complexity. This physical characteristic of Li-Ion battery is used to design the nominal battery model presented in Chapter 11.

2.4 Uncertainty in parameters

Energy storage is bounded by capacity and ramping constraints. Any decision to charge or discharge affects the battery capacity available in subsequent time steps. This implies look-ahead in time is essential for optimal decision making. Look-ahead variables need to be forecasted and due to their non-stationarity accuracy of forecast cannot be guaranteed. The inaccuracy in forecast of information required for selection of mode of operation of the storage leads to sub-optimal results.

Forecasting: The variables required for decision making can be fairly accurately forecasted in near future compared to long time ahead in future. We demonstrate this with an example below.

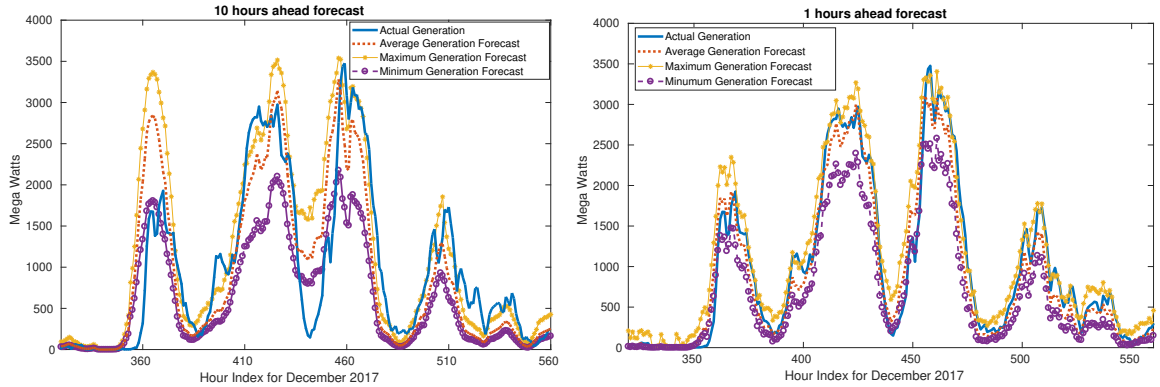

Figure 2.16: Wind generation forecast 10 hour ahead and 1 hour ahead published by BPA

Based on BPA Centralized Wind Power Forecasting Initiative, the historical information is being provided for the benefit of academics and researchers. The wind forecast information provided represents the expected aggregate generation level of wind generators in BPA's balancing authority area. For each month's historical data BPA publishes maximum, minimum and average forecast values for the next 72 hours as a rolling horizon window. The Average forecast represents the expected average hourly generation and the Maximum and Minimum forecast denotes the predictive interval. We show in Fig. 2.16 the actual wind generation values for hour ahead and 10-hour ahead forecast for several days in the month of

December 2017 [5],[38]. It is evident from the plots that the accuracy of forecast in close vicinity of the present time is much more accurate compared to farther away in time.

We represent this idea in a quantitative way in Fig. 2.17. Fig. 2.17 presents the root-mean square error (RMSE) of actual generation values with respect to mean, maximum and minimum forecast values. It is clear that the forecast in vicinity of 1-3 hours is significantly better compared to forecasts made more away from present time. Note that the RMSE of the different forecasts saturates after few time intervals.

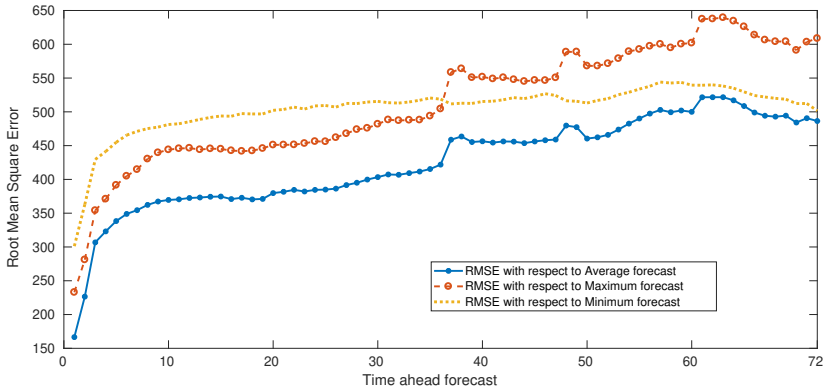

Figure 2.17: Root-mean square error of wind generation forecast based on look-ahead period under BPA for the month of December 2017 [38].

Effect of Uncertainty on Storage Control: Optimal usage of energy storage of power grid applications requires two components: (i) optimal control algorithm and (ii) accurate information of system parameters, exogenous variables based on which step (i) is implemented. Note that the two components are coupled in nature. Inaccuracy in system parameters and variables would diminish energy storage operational value and thus in effect affect the gains made by the storage owner.

In our works [114],[130],[183] we identify that the effect of uncertainty on energy storage control depends on the relationship between charge or discharge time and the sampling time of control decisions. For example, if the charging and discharging time at maximum ramp rate is 2 hours and the sampling time is 2 seconds, implying the sampling time is significantly lower than charge or discharge time, the storage control is not strongly affected by stochastic nature of future decisions. This is shown in Chapter 11 where the the regret of the control decision lies with 4% with a myopic control design. The regret of controller is expressed as the fraction of deteriorated gains with respect to maximum gains storage owners could have made in deterministic case. In Chapter 3.6 we show as the value of charge or discharge times become comparable to the sampling time, the effect of uncertainty in control decisions increase, thus regret increases.

Mitigation of Uncertainty: As pointed earlier, due to mismatch in forecasted and actual parameter values, the storage gains will be lower than the deterministic optimal gains. In this thesis we mitigate the effect of uncertainty using improving forecast generated at each time state implemented along with Model Predictive Control or MPC. This idea of new forecast at time instant is based on the fact that the accuracy of forecast in vicinity of present time could be done with fair amount of accuracy, compared to farther away in time, denoted in Fig. 2.17. MPC is used to optimize the decisions in current time slots, while taking into account future time slots. In the receding or rolling horizon the forecast is updated and implemented again, till end time is reached.

Inaccurate estimation of storage states: Note that in this work we do not consider the effect of uncertainty in measurement and estimation of system parameters. For instance the state of the battery can only be estimated with certain accuracy.

2.4.1 AutoRegressive Forecasting and Model Predictive Control

In this section, we describe the AutoRegressive Moving Average (ARMA) and AutoRegressive Integrated Moving Average (ARIMA) forecast models we used in this thesis. The forecast information is used to calculate storage control actions in real-time. The pseudo algorithm is presented as `ForecastwithMPC`.

We define the mean behavior of past values of net load without storage at time step i as

$$\bar{z}_i = \frac{1}{D}\sum_{p=1}^{D} z_{(i-pN)} \quad \forall i \in \{k, ..., N\}, k \geq 1, \tag{2.4.1}$$

where N is the number of points in a time horizon of 1 day, and D is the number of days in the past whose values are considered in calculating $\bar{z}$. The actual value of net load without storage is given as

$$z_i = \bar{z}_i + X_i \quad \forall i \in \{k, ..., N\}, k \geq 1, \tag{2.4.2}$$

where X_i represents the actual difference from the mean behavior. The forecasted value of net load without storage is given as

$$\hat{z}_i = \bar{z}_i + \hat{X}_i \quad \forall i \in \{k, ..., N\}, k \geq 1, \tag{2.4.3}$$

where $\hat{X}_i$ represents the forecasted difference from the mean behavior. We define $\hat{X}_i, \forall i \in \{k, ..., N\}$ as

$$\hat{X}_k = \alpha_1 X_{k-1} + \alpha_2 X_{k-2} + \alpha_3 X_{k-3} + \beta_1 \delta_k^1 + \beta_2 \delta_k^2 + \beta_3 \delta_k^3, \tag{2.4.4}$$

where $\delta_k^m = (z_{k-mN} - \bar{z}_{k-mN})$ and $\alpha_i, \beta_i \forall i \in \{1, 2, 3\}$ are constant. Our forecast model uses the errors in net load without storage for the past three time steps and the error in the same time step for past three days. At time step $i = k - 1$ we calculate $\hat{X}_k$ as shown in Eq 2.4.4. We also need to calculate $\hat{X}_{k+1}$ till $\hat{X}_N$ in order to update the forecast signal to be fed to MPC.

$$\hat{X}_{k+1} = \alpha_1 \hat{X}_k + \alpha_2 X_{k-1} + \alpha_3 X_{k-2} + \sum_{q=1}^{3} \beta_q \delta_{k+1}^q,$$

$$\hat{X}_{k+2} = \alpha_1 \hat{X}_{k+1} + \alpha_2 \hat{X}_k + \alpha_3 X_{k-1} + \sum_{q=1}^{3} \beta_q \delta_{k+2}^q, \quad ...$$

$$\hat{X}_N = \alpha_1 \hat{X}_{N-1} + \alpha_2 \hat{X}_{N-2} + \alpha_3 \hat{X}_{N-3} + \sum_{q=1}^{3} \beta_q \delta_N^q.$$

We calculate $\hat{z}$ using Eq. 2.4.3. The vector $\hat{z}$ is fed to MPC for calculating optimal energy storage actions for time step $i = k - 1$. At the time step $i = k$, we can calculate $X_k = z_k - \bar{z}_k$. Similar steps are done for $i \in \{k + 1, ..., N\}$, till the end of time horizon is reached.

The forecasted end user consumption without storage is fed to the online algorithm, `ForecastwithMPC`. The online algorithm is executed sequentially and uses model predictive control to identity the optimal modes of operation of storage.

We define the mean behavior of past values of active power at time step i as

$$\overline{P}^i = \frac{1}{D}\sum_{p=1}^{D} P_{(i-pN)} \quad \forall i \in \{k, ..., N\}, k \geq 1, \tag{2.4.5}$$

where N is the number of points in a time horizon of 1 day, and D is the number of days in the past whose values are considered in calculating $\overline{P}$.

We define the mean behavior of past values of reactive power at time step i as

$$\overline{Q}^i = \frac{1}{D}\sum_{p=1}^{D} Q_{(i-pN)} \quad \forall i \in \{k, ..., N\}, k \geq 1, \tag{2.4.6}$$

The actual value of active power is given as

$$P^i = \overline{P}^i + X^i \quad \forall i \in \{k, ..., N\}, k \geq 1, \tag{2.4.7}$$

where X^i represents the difference from the mean behavior.

The actual value of reactive power is given as

$$Q^i = \overline{Q}^i + Y^i \quad \forall i \in \{k, ..., N\}, k \geq 1, \tag{2.4.8}$$

where Y^i represents the actual difference from the mean behavior.

The forecast value of forecast variable z with $\hat{M}^i$ as the difference from mean behavior is given as

$$\hat{z}_i = \bar{z}_i + \hat{M}_i \quad \forall i \in \{k, ..., N\}, k \geq 1, \tag{2.4.9}$$

We define $\hat{M}_i, \forall i \in \{k, ..., N\}$ as

$$\hat{M}_k = \alpha_1 M_{k-1} + \alpha_2 M_{k-2} + \alpha_3 M_{k-3} + \beta_1 \delta_k^1 + \beta_2 \delta_k^2 + \beta_3 \delta_k^3, \tag{2.4.10}$$

where $\delta_k^m = (z_{k-mN} - \bar{z}_{k-mN})$ and $\alpha_i, \beta_i, \ \forall i \in \{1, 2, 3\}$ are constant. Our forecast model uses the errors in net load without storage for the past three time steps and the error in the same time step for past three days. At time step $i = k - 1$ we calculate $\hat{X}_k$ as shown in Eq 7.4.3. We also need to calculate $\hat{M}_{k+1}$ till $\hat{M}_N$ in order to update the forecast signal as

$$\hat{M}_{k+1} = \alpha_1 \hat{M}_k + \alpha_2 M_{k-1} + \alpha_3 M_{k-2} + \sum_{q=1}^{3} \beta_q \delta_{k+1}^q,$$

$$\hat{M}_{k+2} = \alpha_1 \hat{M}_{k+1} + \alpha_2 \hat{M}_k + \alpha_3 M_{k-1} + \sum_{q=1}^{3} \beta_q \delta_{k+2}^q, \quad ...$$

$$\hat{M}_N = \alpha_1 \hat{M}_{N-1} + \alpha_2 \hat{M}_{N-2} + \alpha_3 \hat{M}_{N-3} + \sum_{q=1}^{3} \beta_q \delta_N^q.$$

The weights used in ARMA model, $\alpha_i, \beta_i, \ \forall i \in \{1, 2, 3\}$, are tuned by minimizing Eq. 7.4.4

$$\min \sum_i \{||z_i - \hat{z}_i||_2 + ||\text{norm}([\alpha_i, \beta_i])||_1\} \tag{2.4.11}$$

We calculate $\hat{z}$ using Eq. 2.4.9. The vector $\hat{z}$ is fed to MPC for calculating optimal energy storage actions for time step $i = k - 1$. At the time step $i = k$, we can calculate $M_k = z_k - \bar{z}_k$. Similar steps are done for $i \in \{k + 1, ..., N\}$, till the end of time horizon is reached.

We use AutoRegressive Integrated Moving Average (ARIMA) model of 8^{th} lag order and one degree of differencing for forecasting electricity price. The ARIMA model is developed using training data and tested for test dataset. For price forecast the moving average window is set to zero. This model is denoted as

$$\Delta X_{t+1} = \gamma_1 \Delta X_t + \gamma_2 \Delta X_{t-1} + ... + \gamma_8 \Delta X_{t-7} \tag{2.4.12}$$

where $\Delta X_t = X_t - X_{t-1}$.

Algorithm 1 `ForecastwithMPC`

Inputs: Time horizon, sampling time, historical data, real time information, system variables and parameters

1: Tune forecast model using training data,
2: Generate forecast ARMA and ARIMA,
3: Run the model using forecast data,
4: Select the first action calculated in Line 3,
5: Update states and increment time and Goto 2.

2.5 Notation and battery model

The system considered in Chapter 3 to Chapter 8 consists of an electricity consumer with inelastic demand, renewable generation (rooftop solar) and battery. The electricity consumer is shown in block diagram in Fig. 2.18. We consider operation of storage over a total duration T, with operations divided into N steps indexed by $i \in \{1, ..., N\}$. The duration of a step is denoted as h. Hence, $T = hN$.

The inelastic load for time i is denoted as d_i. The renewable generation for time i is denoted as r_i. The total active energy in one sample seen by the energy meter with storage is denoted as $z_i = d_i - r_i$. The total active power seen by the energy meter without storage is denoted as $P^i = z_i/h$. The reactive power at time i without storage is denoted as Q^i. We denote the battery using ramping and capacity constraint, considering charging and discharging efficiency. The ramping constraint is denoted as

$$\delta_i \in [\delta_{\min}, \delta_{\max}], \tag{2.5.1}$$

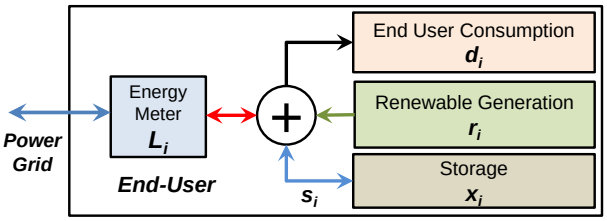

Figure 2.18: Consumer with renewable generation model used in Chapters 3 to 8

where $\delta_{\min}$ denotes minimum ramping rate or the maximum discharge rate and $\delta_{\max}$ denotes the maximum charge rate in units of watts (i.e. power), where $\delta_{\min} \leq 0, \delta_{\max} \geq 0$ are the minimum and the maximum ramp rates (kW).

The instantaneous battery charge level is denoted as b_i for time instant i. The battery charge level should satisfy

$$b_i \in [b_{\min}, b_{\max}], \tag{2.5.2}$$

where $b_{\min}$ and $b_{\max}$ denotes the minimum and maximum battery charge level. The battery charge level evolution with time depends the ramp rate of the battery and the battery charge level in the previous time instant and is given as

$$b_i = b_{i-1} + x_i, \tag{2.5.3}$$

where $x_i = \delta_i h$ denotes the change in charge level of the battery. A value $x_i > 0$ implies charging and $x_i < 0$ implies discharging. x_i/h denotes the corresponding storage ramp rate with $\delta_{\min} \leq 0$ and $\delta_{\max} \geq 0$ as the minimum and maximum ramp rates (kW) respectively. h denotes the sampling time. The state-of-charge (SoC) of the battery is defined as

$$\text{SoC}_i = \frac{b_i}{b_{\text{rated}}}, \tag{2.5.4}$$

where b_{rated} is the rated battery capacity. For LiIon battery health consideration, it should not be over-charged or over-discharged beyond a certain level [114], we define $\text{SoC}_{\min} = b_{\min}/b_{\text{rated}}$ and $\text{SoC}_{\max} = b_{\max}/b_{\text{rated}}$.

We define two more variables. The time required for the energy storage to completely discharge from $b_{\max}$ to $b_{\min}$ at the maximum discharge rate is given as

$$T_{dis} = \frac{b_{\max} - b_{\min}}{|\delta_{\min}|}. \tag{2.5.5}$$

The time required for the energy storage to completely charge from $b_{\min}$ to $b_{\max}$ at the maximum charge rate is given as

$$T_{ch} = \frac{b_{\max} - b_{\min}}{\delta_{\max}}. \tag{2.5.6}$$

The active power output of the battery is denoted as

$$P_B^i = \frac{[x_i]^+}{h\ \eta_{ch}} - \frac{[x_i]^- \eta_{dis}}{h}, \tag{2.5.7}$$

where η_{ch} and η_{dis} denote charging and discharging efficiency of the battery and lie in the range $(0, 1]$. The function $[a]^+$ denotes $\max(0, a)$ and $[a]^-$ denotes $-\min(0, a)$.

The active power ramp rate constraint is given as

$$P_B^i \in [P_B^{\min}, P_B^{\max}] \quad \text{with } P_B^{\min} = \delta_{\min}\eta_{dis}, P_B^{\max} = \frac{\delta_{\max}}{\eta_{ch}} \tag{2.5.8}$$

Though the battery charge level is not affected by the reactive power output Q_B^i of the connected inverter, the amount of active power supplied or consumed is dependent upon it, due to the line current limitations [208]. The converter rating is given by maximum apparent power supplied/consumed denoted as $S_B^{\max}$. The instantaneous apparent power of battery S_B^i should satisfy

$$(S_B^{\max})^2 \geq (S_B^i)^2 = (P_B^i)^2 + (Q_B^i)^2, \tag{2.5.9}$$

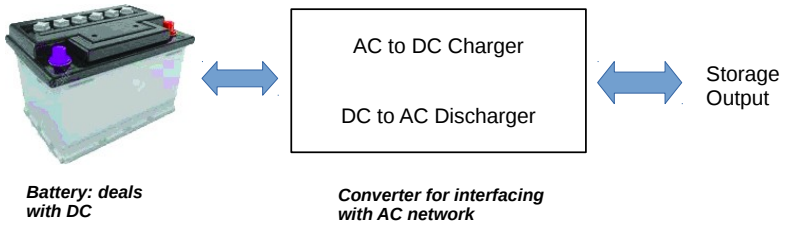

Figure 2.19: Energy storage interfaced via a converter; the converter acts as AC to DC battery charger and DC to AC power source.

Stress on battery: Authors in [242, 164] identify that the internal storage losses depends square of the current supplied by the battery. Thus the storage operational profile which reduces the sum of square of currents over the time horizon would minimize the losses and thus we consider reduce the stress on the battery.

The block diagram of the electricity consumer in terms of active and reactive power is shown in Fig. 2.20. The apparent power of the load shown in Fig. 2.20, at i^{th} time instant is denoted as $S_h^i = P_h^i + jQ_h^i$, where P_h^i and Q_h^i are the active and reactive power consumed. Apparent power of the solar inverter is given as $S_r^i = P_r^i$ where P_r^i is the active power supplied by solar inverter. We assume the solar inverter operates at unity PF. Let us denote the combined load and renewable active and reactive power by $P^i = P_h^i - P_r^i$ and $Q^i = Q_h^i$ respectively. The power factor seen by the grid is the ratio of real power supplied or extracted by the grid over the apparent power seen by the grid. In the absence of storage it is given by

$$\text{pf}_{\text{bc}}^i = P^i / \sqrt{P^{i2} + Q^{i2}}. \tag{2.5.10}$$

Observe that PF before correction, pf_{bc}^i, degrades as P_r^i and Q_h^i increases in magnitude.

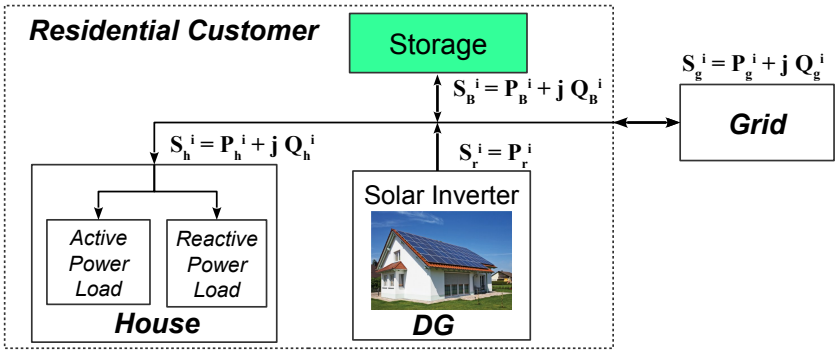

Figure 2.20: Residential load block diagram with DG and storage

Battery Model: We use xC-yC notation to represent the relationship between ramp rate and battery capacity. xC-yC implies battery takes 1/x hours to charge and 1/y hours to discharge completely. For example, 2C-1C battery takes 0.5 hours to charge fully (from completely discharged state) and 1 hour to discharge fully (from completely charge state). Commercial data-sheets often use this notation to denote the ramp rate with respect to battery capacity.

Part I

Energy Storage Arbitrage for Electricity Consumers

Chapter 3

Energy Arbitrage - Net Metering 1.0

One man's "magic" is another man's engineering. "Supernatural" is a null word. -Robert A. Heinlein

Summary: End users equipped with storage may exploit time variations in electricity prices to earn profit by doing energy arbitrage. We propose an algorithm to find an optimal solution of the energy arbitrage problem under given time varying electricity prices. Our algorithm is based on the discretization of optimal Lagrange multipliers of a convex problem and has a structure in which the optimal control decisions are independent of past or future prices beyond a certain time horizon, referred as *sub-horizon*. The proposed algorithm has a run time complexity of $O(N^2)$ in the worst case, where N denotes the time horizon. To show the efficacy of the proposed algorithm, we compare its run-time performance with other algorithms used in MATLAB's constrained optimization solvers and linear programming (LP). The LP formulation is detailed in Appendix B. Our algorithm is found to be several folds faster compared to other benchmarks, and hence has the potential to be used for in real-time. Using the proposed algorithm, we also evaluate the benefits of doing energy arbitrage over an extended period of time for which price signals are available from some ISO's in the USA and Europe. We present case-study for heuristically identifying the length of sub-horizon. Sub-horizon denotes optimal look-ahead required for performing arbitrage. We observe that faster ramping battery requires smaller lookahead horizon for performing arbitrage compared to faster ramping batteries, however, such a battery are more prone to uncertainties.

3.1 Introduction

Net-energy metering (NEM) or Net-metering compensates consumer for solar surplus production. Utilities in order to encourage consumers to install rooftop solar panels apply a compensation rate for surplus production that is equal to the retail rate. This version of NEM is referred as NEM 1.0, which relies on volumetric rates to recover fixed costs put by electric utilities [192]. Utilities aimed to increase renewable production from consumer end. NEM is a *noticeable* success, by end of 2018 more than 913,481 California electricity consumers opted for solar installations along with NEM. The total installed capacity of these consumers exceed 7.6 GW[1]. Fig. 3.1 (downloaded on June 5th, 2019) shows the growth of installed solar capacity in California [71]. There are many distributed generation interconnection programs offered by the California Investor Owned Utilities (IOUs) which include Pacific Gas & Electric (PG&E), Southern California Edison (SCE), and San Diego Gas & Electric (SDG&E) [2]. In this chapter, we formulate the optimal energy arbitrage problem under NEM 1.0 compensation mechanism.

Dynamic pricing of electricity in wholesale electricity markets has the potential to reduce peak demand [106]. An end user operating under such pricing has to alter its consumption pattern to reduce cost of operation by shifting its peak demand to hours of low price. However, it has been observed that consumption patterns of users do not change significantly with real time electricity price variations and hence consumers end-up paying more in their electricity bill [87]. Installing energy storage by an end user allows them to perform energy arbitrage. The energy bought can be stored in the battery for later use when the demand arises. Hence, using the battery allows the user to keep the same consumption pattern without increasing their electricity bills under time-varying electricity prices [251]. Additionally, if the

[1] https://www.californiadgstats.ca.gov/, January, 2019
[2] https://www.californiadgstats.ca.gov/programs/, January, 2019

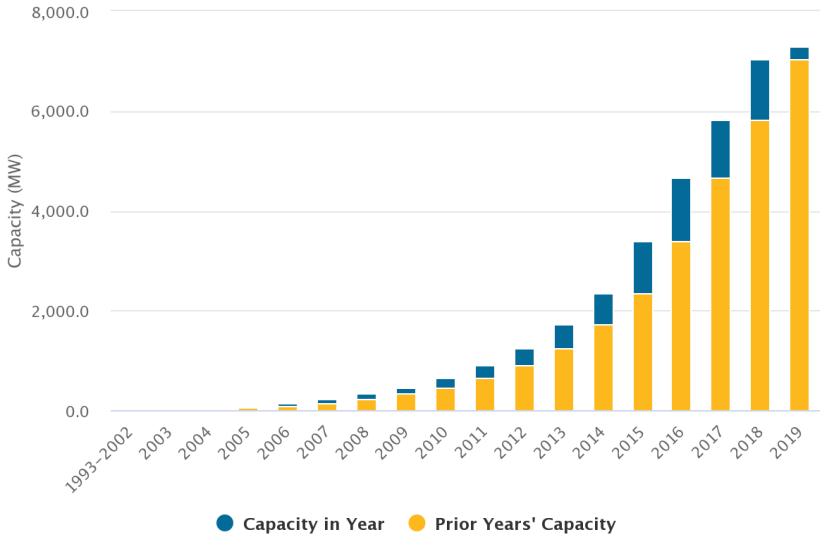

Figure 3.1: Growth of installed solar in CAISO; 65.26% in residential (sample size =448k), 24.54% in commercial (sample size: 8698), 5.29% in educational (sample size: 989), 2.12% in industrial (sample size: 181), 1.73% in other government bodies (sample size: 263), 0.77% in non-profit (sample size: 575) [71].

user is equipped with a renewable generation unit, then a battery also allows the user to reduce energy uncertainty by storing excess generations.

Combining energy storage with renewables holds several benefits for storage owners. For example, the Salt Lake Project in Phoenix Arizona (1995) demonstrated that the consumption peak and the solar PhotoVoltaic (PV) generation peak are not aligned; the use of energy storage for load matching is proposed in [266]. In a more recent study [283], renewables have been identified as primary contributors to the environmental aspect, and energy storage adds economic value from an end user's perspective. Renewables are intermittent in terms of power generation, and dependent on exogenous parameters like solar irradiance or wind speed. The design of real time electricity prices, as pointed out in [106, 185], indicates that energy storage can be profitable due to the increased volatility caused by greater integration of renewables.

In this chapter, we consider storage operation in the presence of time-varying electricity price, consumer load and renewable generation. Compensation for surplus supplied back to the grid is according to NEM 1.0. Under this setting, the optimization cost function is piecewise linear. Cruise et.al. [146] considered a general (strictly) convex objective function. Similar to Cruise et.al., we also consider the optimal energy arbitrage problem for an end user as a convex problem and propose a solution based on finding the optimal Lagrange multipliers. However, due to piecewise linear cost structure the search of optimal Lagrange multipliers can limited by electricity price levels and storage efficiency. We take the approach from Cruise and exploit the piecewise-linear cost structure to obtain an efficient algorithm with provable complexity analysis, see Chapter 4 Section 4.12. Our algorithm is much faster in practice than the simplex algorithm for linear programming (LP). This LP formulation is presented in Appendix B. The real time optimal storage arbitrage requires (i) an optimal control algorithm and (ii) accurate information about the present and future states. Collectively these two requirements affect the end user arbitrage gains. We formulate the energy arbitrage algorithm which allows users to perform energy arbitrage optimally and efficiently under time-varying electricity prices. In order to deal with the uncertainty of information we use model predictive control with forecasting. The key contributions/insights in the chapter are the following:

• *Lagrange multipliers*: Exploiting the piecewise linear cost structure of the arbitrage problem we find that the optimal Lagrange multipliers can only take a discrete set of values corresponding to buying and selling prices of electricity. This transforms the continuous optimization problem into a discrete optimization problem. We indicate how to tune the Lagrange multiplier variables for given prices.

• *Complexity*: Using the discrete nature of the optimization, we explicitly characterize the worst case running time complexity of the proposed arbitrage algorithm. The worst case run-time complexity is found to be quadratic in the number of instants for which price values are available. Numerical simulations show that our algorithm computes the optimal solution at least ten times faster than standard MATLAB optimization solver and several folds faster than LP formulation summarized in Appendix B.

• *Sub-horizon*: From the structure of solution obtained using Lagrangian dual, we observe that to find optimal control decisions in a certain period within the total period it is sufficient to consider prices only

within a sub-horizon much smaller than the whole duration. In the proposed algorithm, we show how to calculate these sub-horizons.
• *Arbitrage*: Using the proposed algorithm, we evaluate the benefits of performing energy arbitrage for an extended duration of operation (e.g. 5 years). We use real price data and also incorporate realistic losses in the battery.
• *Heuristic quantification of length of sub-horizon*: we present a heuristic based analysis to quantify the lookahead required based on storage type. We observe in this case-study that the optimal lookahead for performing arbitrage depends on the ratio of ramp rate over capacity. For batteries with high ratio of ramp rate over capacity, the lookahead required is smaller compared to batteries with lower ratio of ramp rate over capacity.
• *Influence of uncertainty with storage parameters*: For small sampling time (compared to charge/ discharge time of the battery), batteries with higher ramp rates are more prone to uncertainties. For cases where sampling time of the decision making is of the order of charge/discharge time, uncertainty in future parameters does not have a significant effect of arbitrage gains. We observe that for fast ramping batteries with small sampling time compared to charge or discharge time, it is crucial to model uncertainty which would drastically influence the arbitrage gains in absence of considerations of uncertainty.

The problem of optimal energy arbitrage using storage has been the subject of many recent works e.g., [317, 280, 210, 148, 251, 91, 331, 206, 314]. In [317], the demand and price of electricity are assumed to be correlated and stochastic. However, in this setting the user is not allowed to sell energy to the grid. In [280], a closed form solution based on stochastic dynamic programming has been found for the arbitrage problem without considering the ramp constraints of the battery. The objective in [210] is to reduce operational cost of the grid, where demands arrive randomly in time. The work closest to the current chapter is [148], where the energy arbitrage problem has been considered for a single battery user incorporating ramp and capacity constraints of the battery, for strictly convex cost function. In the current chapter, we consider a special case where the cost function is piecewise-linear which allows us to discretize the optimal Lagrange multiplier values and characterize the complexity of the optimal arbitrage algorithm.

In [91, 331, 323], the authors consider application of energy storage for not only energy arbitrage but also for providing ancillary services to the grid. Authors in [196] propose a deterministic setting of revenue maximization using spot market prices of electricity available one day ahead. Authors in [314] investigate control of energy storage in context of data-centers. Their model assumes that the battery is fully efficient.

The rest of the chapter is organized as follows. The battery model is described in Chapter 2.5. Section 3.2 presents a mathematical framework and the proposed algorithm for solving the arbitrage problem. Section 3.3 presents the numerical results. Section 3.4 analyses financial feasibility of energy storage performing arbitrage. Section 3.5 quantifies the length of sub-horizon based on a case-study. Section 3.6 presents the third case-study on effect and mitigation of uncertainty due to price variations with battery parameters. Section 3.7 concludes the chapter.

3.2 Arbitrage under NEM 1.0

We consider the operation of a single household user of electricity over a fixed period of time. The user is assumed to be equipped with a renewable generation unit and a battery to store excess generation. It is also connected to the electricity grid from where it can buy or to which it can sell energy. The objective is to minimize the cost or maximize the profit of the user's operation over a fixed period of time. Qualitatively, the optimal decisions consist of buying energy from the grid when electricity prices are low and selling energy to the grid when the electricity prices are high. Our objective is to find an efficient algorithm for user to make optimal decisions over a period of varying electricity prices. We assume that the energy consumed or sold by the end user over period of constant price is too small to affect the price of the electricity in the same period. So in our case the end user acts as a price-taker.

The total duration, T, of operation is divided into N steps, where in each step $i \in \{1, ..., N\}$ the price of electricity is assumed to be constant at p_i. This assumption is in sync with NEM 1.0 compensation in California where the selling price equals the retail rate for each time instant. The duration of step i is denoted as h_i. Hence, $T = \sum_{i=1}^{N} h_i$. The time duration T of the user's operation is typically chosen as one day [196] since the pattern in electricity prices repeats with a period of one day; being high during the day and low during the night. We assume each user has a non-elastic demand of d_i units of energy in time instant i and it generates r_i units of energy through renewable sources in the same time instant. We define $z_i = d_i - r_i \in \mathbb{R}$. This difference between the demand and the generation can be satisfied either by buying energy from the grid (at price p_i) or by the energy obtained from a battery installed at the user's home.

In case of excess energy generation, it can be either stored in the battery or sold to the grid. The effciency of charging and discharging of the battery are denoted by $\eta_{\text{ch}} \in (0,1]$ and $\eta_{\text{dis}} \in (0,1]$, respectively. We denote the change in the energy level of the battery at i^{th} instant by $x_i = h_i\delta_i$, where δ_i denotes the storage ramp rate at i^{th} instant; $\delta_i > 0$ implies charging and $\delta_i < 0$ implies discharging. Battery charge level is denoted as b_i and its evolution is given in Eq. 2.5.3. Amount of energy that comes from the grid or renewables or goes out to the grid or end user from the battery at i^{th} instant is given by

$$s_i = \frac{1}{\eta_{\text{ch}}}[x_i]^+ - \eta_{\text{dis}}[x_i]^-, \tag{3.2.1}$$

where function $[a]^+ = \max(0,a)$ and function $[a]^- = -\min(0,a)$. Hence, the net energy consumption at i^{th} instant is given as $P_{\text{em}}(i) = d_i - r_i + s_i$. The cost at i^{th} instant without the battery is given by $C_1(i) = z_i p_i$. Similarly, the cost at i^{th} instant with the battery is given by $C_2(i) = (z_i + s_i)\, p_i$. The objective of the energy arbitrage problem is to minimize $\sum_{i=1}^{N} C_2(i)$ with respect to x_i.

3.2.1 Optimal Energy Arbitrage Problem: NEM 1.0

The optimal arbitrage problem with battery is defined as the minimization of $\sum_{i=1}^{N} C_2(i)$ subjected to the battery constraints. We have

$$\sum_{i=1}^{N} C_2(i) = \sum_{i=1}^{N} (z_i + s_i)\, p_i = \sum_{i=1}^{N} C_1(i) + C^{(i)}_{\text{storage}}(x_i), \tag{3.2.2}$$

where $C^{(i)}_{\text{storage}}(x_i)$ is defined as

$$C^{(i)}_{\text{storage}}(x_i) = s_i p_i = p_i\Big(\frac{1}{\eta_{\text{ch}}}[x_i]^+ - \eta_{\text{dis}}[x_i]^-\Big). \tag{3.2.3}$$

Hence, minimizing $\sum_{i=1}^{N} C_2(i)$ is equivalent to minimizing $\sum_{i=1}^{N} C^{(i)}_{\text{storage}}(x_i)$ as $C_1(i)$ is a constant for every i. This implies the storage control under NEM 1.0 is independent of inelastic load and renewable generation variation. In this formulation, the only stochastic variable is the variation in electricity price. In this section, we formulate the energy arbitrage problem for deterministic price variation. The effect of uncertainty is mitigated using forecasting along with model predictive control, presented in Section 3.6. Therefore, the optimal arbitrage problem is given as

$$\begin{aligned} &\underset{x_i \in [X_i^{\min}, X_i^{\max}], \forall i}{\text{Minimize}} && \sum_{i=1}^{N} C^{(i)}_{\text{storage}}(x_i) \\ &\text{subject to} && b_{\min} \le b_i \le b_{\max}, \quad \forall i, \end{aligned} \tag{P_{NEM1}}$$

where $X_i^{\min} = h_i\delta_{\min}$ and $X_i^{\max} = h_i\delta_{\max}$ for all i. From Eq. 3.2.3 it is clear that $C^{(i)}_{\text{storage}}(x_i)$ is a piecewise linear, continuous increasing function in x_i for all i. Hence, the objective function for the above problem is convex. Fig. 3.2 shows the cost function. It is evident from Fig. 3.2 that the cost function is convex with respect to x_i. The Lagrangian of problem Eq. P_{NEM1} is given as

$$\mathscr{L}(x,\alpha,\beta) = \sum_{i=1}^{N} \Big(C^{(i)}_{\text{storage}}(x_i) + \alpha_i(b_{\min} - b_i) + \beta_i(b_i - b_{\max})\Big). \tag{3.2.4}$$

Hence, the Lagrangian dual of Eq. P_{NEM1} is given by

$$\begin{aligned} &\text{(LD)} && \max \quad \phi(\alpha,\beta) \\ &\text{subject to,} \quad \alpha_i, \beta_i \ge 0 \quad \forall i \quad \text{where} && \phi(\alpha,\beta) = \inf_{x_i \in [X_i^{\min}, X_i^{\max}]} \mathscr{L}(x,\alpha,\beta) \end{aligned}$$

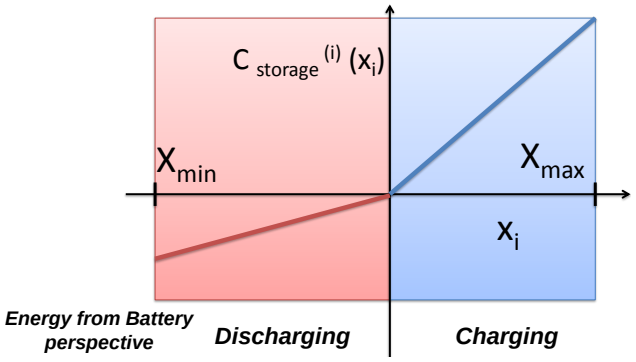

Figure 3.2: Cost Function for NEM 1.0

Theorem 3.2.1

There exists a pair (x^*, μ^*) with $\mu^* = (\mu_1^*, \ldots, \mu_N^*)$ such that:
(1.) $x^* = (x_1^*, ..., x_N^*)$ is a feasible solution of optimal arbitrage problem Eq. P_{NEM1} implying $x_i^* \in [X_i^{\min}, X_i^{\max}]$ and $b_i^* = b_0 + \sum_{j=1}^{i} x_j^* \in [b_{\min}, b_{\max}]$ for all i.
(2.) For each i, x_i^* minimizes $C_{storage}^{(i)}(x) - \mu_i^* x$. Here, μ_i^* is called the optimal accumulated Lagrange multiplier for time instant i and is related to the dual optimal solution (α^*, β^*) as follows $\mu_i^* = \sum_{j=i}^{N}(\alpha_j^* - \beta_j^*)$.
(3.) Optimal accumulated Lagrange multiplier, μ_i^*, at any time instant i satisfies the following recursive conditions:

- $\mu_{i+1}^* = \mu_i^*$, *if* $b_{\min} < b_i^* < b_{\max}$
- $\mu_{i+1}^* \leq \mu_i^*$, *if* $b_i^* = b_{\min}$
- $\mu_{i+1}^* \geq \mu_i^*$, *if* $b_i^* = b_{\max}$

where $b_i^* = b_0 + \sum_{j=1}^{i} x_j^*$
(4.) Additionally, the optimal accumulated Lagrange multiplier μ_N at the last instant N satisfies

- $\mu_N^* = 0$, *if* $b_{\min} < b_N^* < b_{\max}$
- $\mu_N^* \geq 0$, *if* $b_N^* = b_{\min}$

For any pair (x^*, μ^*) satisfying the above conditions, x^* solves the optimal arbitrage problem Eq. P_{NEM1}.

The proof of Theorem 3.2.1 is provided in Appendix A.1. We note that the optimality conditions stated in Theorem 3.2.1 are valid as long as $C_{\text{storage}}^{(i)}(x_i)$ is a convex function with respect to x_i for each i. Next, we characterize, for each instant i, the relationship between the optimal decision x_i^* and the optimal accumulated Lagrange multiplier μ_i^* using the particular nature of the cost function $C_{\text{storage}}^{(i)}(x_i)$. This will be useful in formulating the optimal arbitrage algorithm.

Remark 1. From condition (2) of Theorem 3.2.1 we have that the optimal control decision x_i^* in the ith instant minimizes the function $C_{\text{storage}}^{(i)}(x) - \mu_i^* x$ for $x \in \left[X_i^{\min}, X_i^{\max}\right]$. Now from Eq. 3.2.3 we obtain that for a given $\mu_i^* = \mu$ the optimal decision $x_i^*(\mu)$ is given by

$$x_i^*(\mu) = \begin{cases} \left[X_i^{\min}, X_i^{\min}\right], & \text{if } \mu < p_{\text{dis}}(i), \\ \left[X_i^{\min}, 0\right], & \text{if } \mu = p_{\text{dis}}(i), \\ [0, 0], & \text{if } p_{\text{ch}}(i) > \mu > p_{\text{dis}}(i), \\ \left[0, X_i^{\max}\right], & \text{if } \mu = p_{\text{ch}}(i), \\ \left[X_i^{\max}, X_i^{\max}\right], & \text{if } \mu > p_{\text{ch}}(i), \end{cases} \tag{3.2.5}$$

where $p_{\text{ch}}(i) = p_i/\eta_{\text{ch}}$ and $p_{\text{dis}}(i) = p_i \eta_{\text{dis}}$. Note that $x_i^*(\mu)$ is a set-valued function in μ: for $\mu = p_{\text{ch}}(i)$ or $\mu = p_{\text{dis}}(i)$, $x_i^*(\mu)$ takes an *envelope* of values and for any other value of μ it is a singleton set. It is also important to note from Eq. 3.2.5 that if $\mu_1 \leq \mu_2$ then $x_i^*(\mu_1) \preceq x_i^*(\mu_2)$, where for two sets A and B we say $A \preceq B$ (resp, $A \prec B$) if $a \leq b$ (resp $a < b$) for all $a \in A$ and for all $b \in B$. The above monotonicity property

also holds for the sets $b_i^*(\mu)$, defined recursively as $b_i^*(\mu) = b_{i-1}^*(\mu) + x_i^*(\mu)$ for $i \geq 1$ and $b_0^*(\mu) = b_0$. Here, addition of two intervals $[a, b]$ and $[c, d]$ denotes the interval $[a + c, b + d]$.

3.2.2 Proposed Algorithm under NEM 1.0

We now propose an algorithm which finds a pair (x^*, μ^*) that satisfies all the conditions in Theorem 3.2.1 and therefore solves Eq. P_{NEM1}. The pseudo code of the proposed algorithm is shown as Algorithm 2 below. Note from Theorem 3.2.1 condition (3) that μ_{i+1}^* may differ from μ_i^* only when $b_i^* = b_{\max}$ or $b_i^* = b_{\min}$. Hence, if the battery level at the end of a time instant lies strictly within the battery capacity limits, then there is no change in the value of the optimal accumulated Lagrange multiplier. Using this key idea, in the proposed algorithm, we divide the total duration T into groups, indexed as $\{1, 2, \ldots, M\}$, of consecutive time instants such that for all instants i belonging to the same group $K \in \{1, 2, \ldots, M\}$ the value of the accumulated Lagrange multiplier μ_i^* is the same, denoted as μ_K. We call each such group as a sub-horizon. At the end of each sub-horizon, the battery energy level touches either $b_{\max}$ or $b_{\min}$. The number M of sub-horizons, the start and end instants of each sub-horizon K, and the value of μ_K and optimal actions in each sub-horizon K depend on the problem instance and are determined recursively as described below.

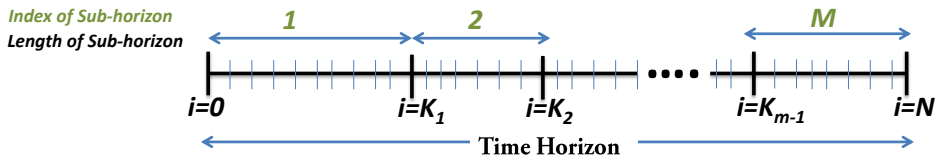

Figure 3.3: M sub-horizons in total horizon of length T

Suppose we have identified the first $K-1$ ($K \geq 1$) sub-horizons and the optimal actions in all instants belonging to these sub-horizons. Call the last instant identified to be in the $(K-1)$th sub-horizon as i_{K-1}. If $i_{K-1} = N$, then we have already covered whole period T. If $i_{K-1} < N$, then we proceed to identify the next sub-horizon K, i.e., the values of i_K, μ_K, and the optimal decisions for the time instants $i \in [i_{K-1} + 1, i_K]$. To identify the sub-horizon K, we start with instant $i_{K-1} + 1$ and a guess value of $\mu_K \geq 0$ for that sub-horizon.[3] Now, for the chosen value of μ_K, the values of $x_i^*(\mu_K)$ and $b_i^*(\mu_K)$ are computed as described in Remark 1 for all consecutive time instants $i > i_{K-1}$ until we reach a time instant $i = i_{\text{break}}$ for which one of the following conditions is satisfied (we call these as the *violation conditions*):

C1: $b_{i_{\text{break}}}^*(\mu_K) \prec \{b_{\min}\}$.
C2: $\{b_{\max}\} \prec b_{i_{\text{break}}}^*(\mu_K)$.
C3: $i_{\text{break}} = N, b_{\min} \notin b_N^*(\mu_K), \mu_K > 0$.

If no such i is found even after reaching $i = N$, then K is identified as the last sub-horizon and we set $i_K = N$ (and lines 24–30 of the pseudo code are executed). If $\mu_K > 0$, then $b_N^* = b_{\min}$; else b_N^* is taken to be some value in the set $[b_{\min}, b_{\max}) \cap b_N^*(\mu_K)$ to satisfy condition (4) of Theorem 3.2.1. The optimal decisions x_i^* and b_i^* for $i \in [i_{K-1} + 1, N]$ are then found by using the algorithm `BackwardStep`, shown as in Algorithm 3 below. The proposed algorithm then terminates. The algorithm `BackwardStep` will be discussed in more detail later.

If condition C1 above is satisfied, then for the chosen value of μ_K, the battery capacity limit is violated at the instant i_{break} since the set $b_{i_{\text{break}}}(\mu)$ lies strictly below $b_{\min}$. The value of μ_K is then increased to

$$\mu_K = \min \{p > \mu : p \in (p_{\text{ch}}(i), p_{\text{dis}}(i); i_{K-1} < i \leq i_{\text{break}})\}.$$

Otherwise, if C2 or C3 above is satisfied, then μ_K is decreased to

$$\mu_K = \max \{p < \mu : p \in (p_{\text{ch}}(i), p_{\text{dis}}(i); i_{K-1} < i \leq i_{\text{break}})\}.$$

With the updated value of μ_K we again repeat the same process as discussed above to obtain a new value of i_{break}. Since $x_i^*(\mu_K)$ and $b_i^*(\mu_K)$ are monotonically non-decreasing functions in μ_K, the potential effect

[3] For the first sub-horizon $K = 1$ (that includes the first time instant) the starting guess value of μ_1 is taken to be 0 and for every other sub-horizon $K > 1$, the starting guess value of μ_K is taken to be equal to μ_{K-1}. Note that these choices are arbitrary and the algorithm does not depend on these choices.

of the update of μ_K is that i_{break} is pushed to a later instant. The update of μ_K is repeated so long as i_{break} increases (or remains the same) as compared to its old value (stored in i_{memory}). If the value of i_{break} decreases with an updated value of μ_K, then for the previous value μ_{memory} of μ_K there must have been an instant $i \in [i_{K-1}+1, i_{\text{memory}}]$, where $b_{\max} \in b_i^*(\mu_K)$ (if the violation occurred due to C1) or $b_{\min} \in b_i^*(\mu_K)$ (if violation occurred due to C2 or C3). This is because both μ_{memory} and μ_K always lie in the range $[p_{\text{dis}}(i), p_{\text{ch}}(i)]$ for all $i > i_{K-1}$. Since $b_i^*(p_{\text{ch}}(i)) \cap b_i^*(p_{\text{dis}}(i)) \neq \emptyset$ an update of μ_K cannot cause $b_i^*(\mu_K)$ to completely go above $b_{\max}$ or below $b_{\min}$ if $\{b_{\min}\} \prec b_i^*(\mu_{\text{memory}}) \prec \{b_{\max}\}$.

At this point in the algorithm, μ_K and i_{break} are switched back to their previous values stored in μ_{memory} and i_{memory}, respectively. This value of μ_K is identified to be the final value of the optimal accumulated Lagrange multiplier in the sub-horizon K. We set i_K to be the latest time instant $i \in [i_{K-1}+1, i_{\text{break}}]$ for which $b_{\min} \in b_i^*(\mu_K)$ or $b_{\max} \in b_i^*(\mu_K)$. The value of $b_{i_K}^*$ is chosen to be $b_{\min}$ in the former case and $b_{\max}$ in the later case.

Finally, for each i in the range $i_{K-1}+1 \leq i < i_K$, the optimal battery level b_i^* is found from b_{i+1}^* through the function `BackwardStep` which uses the backward recursion $b_i^* = (b_{i+1}^* - x_{i+1}^*(\mu_K)) \cap b_i^*(\mu_K) \cap [b_{\min}, b_{\max}]$. If the above backward recursion returns a set, then any arbitrary value in the set is chosen to be the optimal battery level. We note here that the optimal solution to Eq. P_{NEM1} need not be unique since its objective function is not strictly convex.

Complexity Analysis: For any sub-horizon starting from instant i, there may be at most $N-i+1$ more time instants which may be included in the same sub-horizon. Hence, in order to find the optimal accumulated Lagrange multiplier for the sub-horizon, we may have to update the value of μ_K in the sub-horizon at most $2(N-i+1)$ times (for each instant i two possible values $p_{\text{dis}}(i)$ $p_{\text{ch}}(i)$ may be checked). For each update, a basic set of operation is performed. Furthermore, there may be separate sub-horizon starting from every time instant $i \in [1, N]$. Hence, a crude upper bound on the number of times the basic set of operations are needed to be repeated is $\sum_{i=1}^{N} 2(N-i+1) = O(N^2)$. Hence, the worst case time complexity of the proposed algorithm is $O(N^2)$. In most situations, however, the number of instants included in a sub-horizon does not grow with N. Hence, in most cases the the proposed algorithm would be performed in linear in time, see Chapter 4 Section 4.12.

3.2.3 Open Source Code

The optimal arbitrage algorithm developed in this chapter is made open source. The link for the code is https://github.com/umar-hashmi/netmetering1.

3.2.4 Stylized Example of Proposed Algorithm

Here we present a stylized example to demonstrate the operation of the proposed optimal arbitrage algorithm which is composed of Algorithm 2 and Algorithm 3. Algorithm 2 is used to identify a sub-horizon and returns the lower and the upper envelope of battery charge level in the sub-horizon. Algorithm 3 is implemented once for a sub-horizon to identify the optimal battery charge level. We present Remark 2 as the special case of Remark 1 for lossless battery, i.e., $\eta_{ch} = \eta_{dis} = 1$.

Remark 2. The optimal control decision x_i^* in the ith instant minimizes the function $C_{\text{storage}}^{(i)}(x) - \mu_i^* x$ for $x \in \left[X_{\min}^i, X_{\max}^i\right]$ and for battery with $\eta_{ch} = \eta_{dis} = 1$ is given as:

$$x_i^*(\mu) = \begin{cases} [X_{\min}^i, X_{\min}^i], & \text{if } \mu < p_i, \\ \left[X_{\min}^i, X_{\max}^i\right], & \text{if } \mu = p_i, \\ [X_{\max}^i, X_{\max}^i], & \text{if } \mu > p_i, \end{cases} \tag{3.2.6}$$

where $C_{\text{storage}}^{(i)}(x_i) = s_i p_{\text{elec}}(i)$. For $\mu = p_{\text{elec}}(i)$, $x_i^*(\mu)$ takes an *envelope* of values. This threshold based structure has a sub-gradient. For any other value of μ it is a singleton set.

This example considers a lossless battery under equal buying and selling price of electricity. For this example the price of electricity is assumed to be in ascending order (worst case), i.e., $0 < p_1 < p_2 < p_3 ...$ and so on. The accumulated Lagrange multiplier (μ) is initiated from zero. Fig. 3.4 shows the battery charge level trajectory for $\mu = 0$. The battery charge level has a feasible trajectory till $i = 1$. The temporary sub-horizon has sample between $i = 0$ and $i = 1$. Since $p_1 > \mu$ therefore, battery should discharge at maximum rate, based on the threshold based structure.

In the next iteration of the algorithm the accumulated Lagrange multiplier should be increased to the price level in the identified sub-horizon, i.e. p_1. The value of μ is increased because of the lower

Algorithm 2 `OptimalArbitrageNEM1`

Inputs: N, T, $h = (h_1, h_2, \ldots, h_N)$, $p = (p_1, p_2, \ldots, p_N)$, b_0
Parameters: $b_{\max}, b_{\min}, \delta_{\max}, \delta_{\min}$
Outputs: $x^* = (x_1^*, x_2^*, \ldots, x_N^*)$, $b^* = (b_1^*, b_2^*, \ldots, b_N^*)$, $\mu^* = (\mu_1^*, \mu_2^*, \ldots, \mu_K^*)$
Initialize: $K = 1$; $\mu_K = \mu_{\text{memory}} = 0$; $i_{K-1} = i_K = i_{\text{memory}} = 0$; `BreakFlag` $= 0$

while $i_K < N$ **do**
  for $i = i_{K-1} + 1$ to N **do**
    Compute $x_i^*(\mu_K)$ and $b_i^*(\mu_K)$
    if C1 or C2 or C3 holds **then**
      `BreakFlag` $\leftarrow 1$; $i_{\text{break}} \leftarrow i$
      Break
    end if
  end for
  if `BreakFlag` $= 1$ and $i_{\text{break}} \geq i_{\text{memory}}$ **then**
    `BreakFlag` $\leftarrow 0$; $i_{\text{memory}} \leftarrow i_{\text{break}}$; $\mu_{\text{memory}} \leftarrow \mu_K$
    if $b_i^*(\mu_K) \prec \{b_{\min}\}$ **then**
      $\mu_K \leftarrow \min\{p > \mu : p \in (p_{\text{ch}}(i), p_{\text{dis}}(i); i_{K-1} < i \leq i_{\text{break}})\}$
    else
      $\mu_K \leftarrow \max\{p < \mu : p \in (p_{\text{ch}}(i), p_{\text{dis}}(i); i_{K-1} < i \leq i_{\text{break}})\}$
    end if
  else if `BreakFlag` $= 1$ and $i_{\text{break}} < i_{\text{memory}}$ **then**
    if C1 is True **then**
      $i_K \leftarrow \max\{i \in [i_{K-1} + 1, i_{\text{memory}}] : b_{\max} \in b_i^*(\mu_{\text{memory}})\}$
      $b_{i_K}^* = b_{\max}$
    else if C2 or C3 is True **then**
      $i_K \leftarrow \max\{i \in [i_{K-1} + 1, i_{\text{memory}}] : b_{\min} \in b_i^*(\mu_{\text{memory}})\}$
      $b_{i_K}^* = b_{\min}$
    end if
    $\mu_K \leftarrow \mu_{\text{memory}}$; `BreakFlag` $\leftarrow 0$; $i_{\text{break}} \leftarrow i_{\text{memory}}$
    $i_{\text{memory}} \leftarrow i_K$
    `BackwardStep`$(\mu_K, i_{K-1}, i_K, b^*, x^*, \mu^*)$
    $\mu_{K+1} \leftarrow \mu_K$; $K \leftarrow K + 1$
  else
    $i_K \leftarrow N$;
    if $\mu_K > 0$ **then**
      $b_N^* \leftarrow b_{\min}$
    else
      $b_N^* \leftarrow [b_{\min}, b_{\max}) \cap b_N^*(\mu_K)$
    end if
    `BackwardStep`$(\mu_K, i_{K-1}, i_K, b^*, x^*, \mu^*)$
  end if
end while

Algorithm 3 `BackwardStep`$(\mu_K, i_{K-1}, i_K, b^*, x^*, \mu^*)$

Inputs: $\mu_K, i_{K-1}, i_K, b^*, x^*, \mu^*$
Function: Computes components of the optimal vectors b^*, x^* in the range $[i_{K-1} + 1, i_K - 1]$ using backward recursion
Initialize: $i \leftarrow i_K - 1$

while $i \geq i_{K-1} + 1$ **do**
  $b_i^* \leftarrow (b_{i+1}^* - x_{i+1}^*(\mu_K)) \cap b_i^*(\mu_K) \cap [b_{\min}, b_{\max}]$
  $x_{i+1}* \leftarrow b_{i+1}^* - b_i^*$
  $\mu_i^* \leftarrow \mu_K$
end while

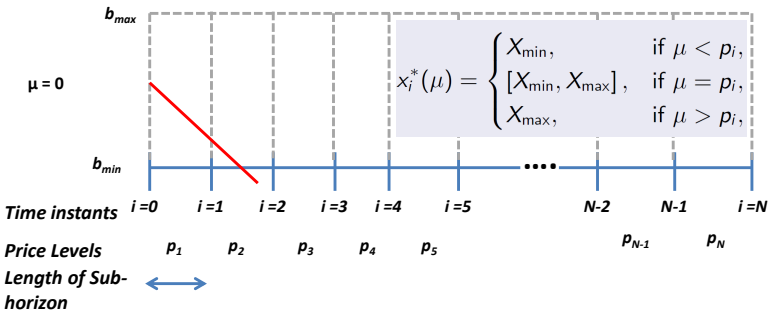

Figure 3.4: Battery charge level trajectory for $\mu = 0$

capacity violation in Fig. 3.5, see Condition 4 of Theorem 3.2.1. With this alteration of μ, the temporary sub-horizon has increased from $i = 0$ to $i = 2$, as no feasible charge level exists at $i = 3$.

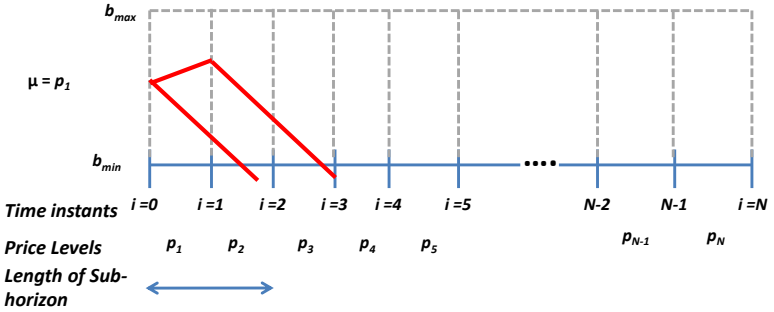

Figure 3.5: Battery charge level trajectory for $\mu = p_1$

In the next iteration the value of μ is increased to p_2. For the first time instant the battery should charge as $\mu > p_1$. For the second time instant the battery charge level has an envelope based structure between $i = 1$ to $i = 2$. For the third time $\mu < p_3$ therefore, the battery should discharge. The new temporary sub-horizon has increased from $i = 0$ to $i = 4$, as shown in Fig. 3.6.

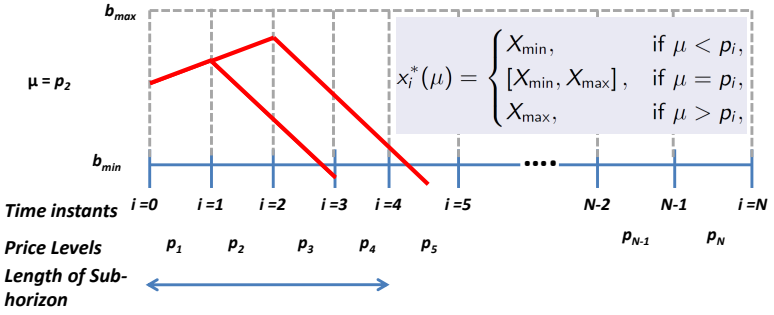

Figure 3.6: Battery charge level trajectory for $\mu = p_2$

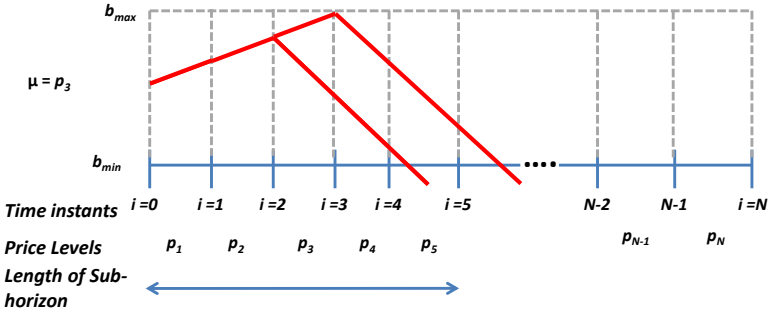

Figure 3.7: Battery charge level trajectory for $\mu = p_3$

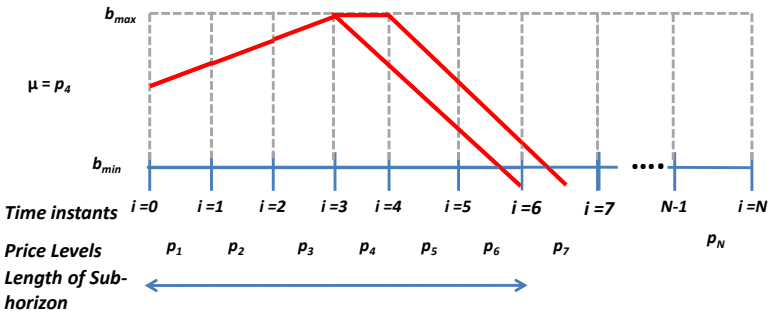

Figure 3.8: Battery charge level trajectory for $\mu = p_4$

Similar adjustment of μ is performed till the sub-horizon keeps increasing, see Fig. 3.4 to 3.8. Any further increase in μ from the case denoted in Fig. 3.8 decreases the length of the sub-horizon, see Fig. 3.9.

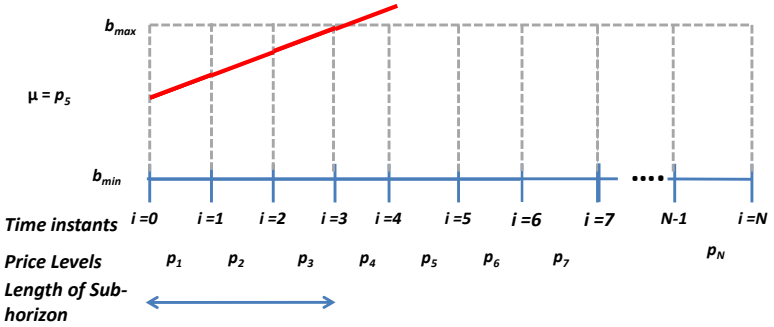

Figure 3.9: Battery charge level trajectory for $\mu = p_5$

The value of μ associated with case shown in Fig. 3.8 is called the optimal accumulated Lagrange multiplier denoted as μ^* for the sub-horizon. For this example $\mu^* = p_4$. The value of battery charge level trajectory associated with μ^* is the input to Algorithm 3. Note the value of μ^* acts as the shadow price and remains constant for a sub-horizon. Note the value of μ^* is selected from finite number of discrete levels of electricity price in the sub-horizon. This makes the proposed algorithm computationally very efficient due to this discretization of a continuous optimization problem.

Algorithm 3 takes as input the envelope of battery charge level and identifies the optimal solution. `BackwardStep` algorithm fix the last time instant in the sub-horizon at $b_{\min}$ and back-calculates the optimal battery charge level. For time instant where μ^* is equal to the price level, anything from $X_{\min}$ to X_{max} is possible. Note neither charging or discharging is profitable or loss here, however, the battery could charge some more if there are possible discharging opportunities in adjacent time periods in the sub-horizon. Similarly, the battery could discharge here if there are lower discharging opportunities in adjacent time periods in the sub-horizon. This period provides a slack in adjusting battery charge level. It is essential to note that in this period intermediate ramp rate could be possible, contrary to all prior works on threshold based optimal decision making. The optimal battery capacity is shown in Fig. 3.10.

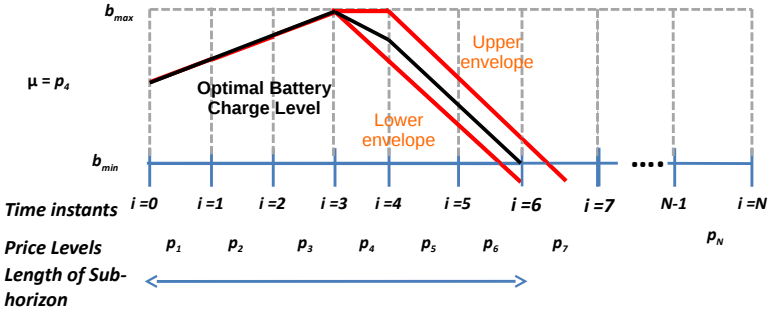

Figure 3.10: Optimal Battery charge level

The next sub-horizon begins at $i = 7$ as the optimal actions have been identified from $i = 0$ to $i = 6$.

3.3 Numerical Evaluation

We solve the optimal arbitrage problem using the proposed algorithm described in Section 3.2.2. The performance of the proposed algorithm is compared with Linear Programming (LP) and Matlab's Fmincon based constrained minimization (function evaluations set to 9600), in terms of run time and energy arbitrage gains. However, LP can only be evaluated for lossless battery as the objective function of Eq. P_{NEM1} is linear in the lossless case.

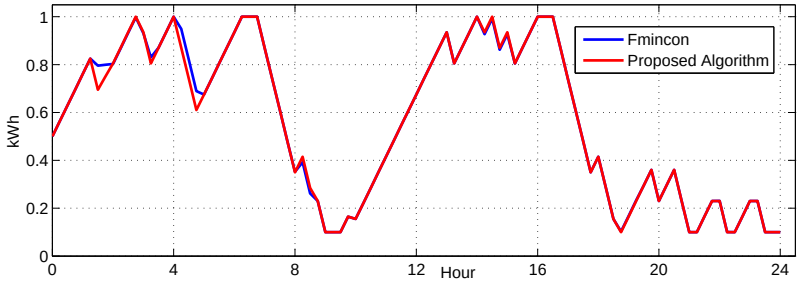

(a) Comparison of optimal battery level (b^*)

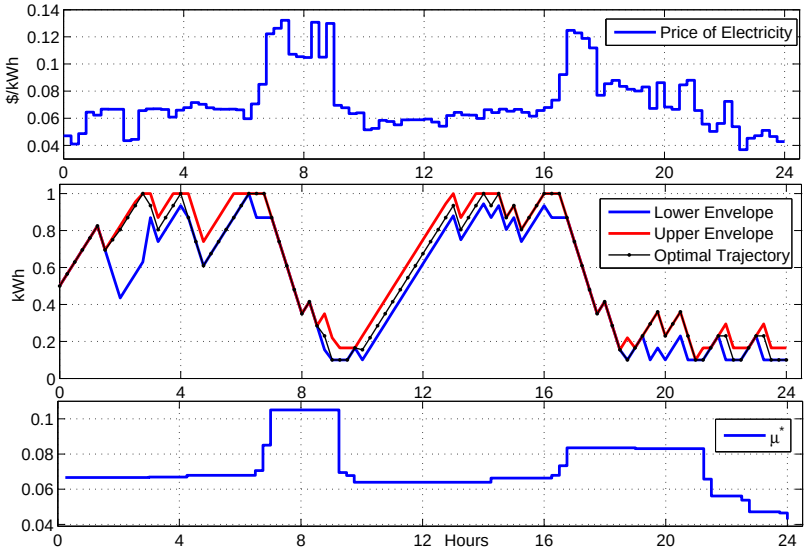

(b) Proposed algorithm results for lossless battery

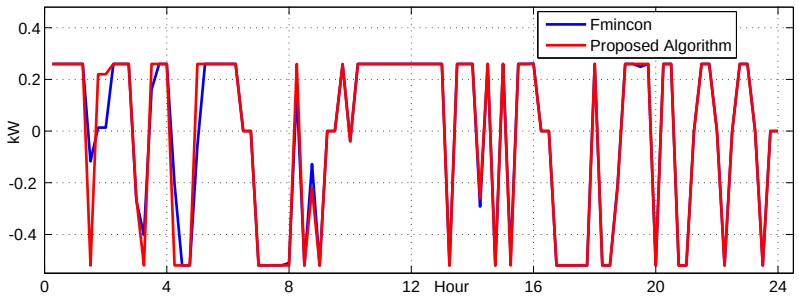

(c) Comparison of optimal ramp rates

Figure 3.11: Comparison for lossless battery

The battery parameters used for numerical evaluation are: $b_{\max} = 1$ kWh, $b_{\min} = 0.1$ kWh, $\delta_{\max} = 0.26$ kW, $\delta_{\min} = -0.52$ kW. Real-Time locational marginal pricing data for 21st December 2016 from NYISO [29] is used to calculate optimal ramping trajectory. The sampling time of price signal is $h = 0.25$ hours. Simulations are done using a laptop PC with Intel Core i5-4200M, 2.50GHz processor and 8 GB RAM.

Fig 3.11 shows the results for lossless battery, i.e. $\eta_{\text{ch}} = 1, \eta_{\text{dis}} = 1$. The first plot of Fig 3.11b shows the electricity price for a day [29], and the other plots show the optimal trajectory of battery level and the

value of μ with time. It can be observed from Fig 3.11a and 3.11c that the proposed algorithm has not violated the constraints for the battery and the results are using proposed algorithm and Matlab's Fmincon are very similar. The details of linear programming formulation is provided in Appendix B. However, the run time of the proposed algorithm is significantly lower than other methods as shown in Table 3.1.

Table 3.1: Comparison of performance for lossless battery

Algorithm Type	Run Time (sec)	Profit ($)
Proposed Algo	0.1967	0.1403245
Linear Programming	1.4873	0.1403245
Matlab's Fmincon	23.0526	0.14027568

Fig 3.12 shows the results of the proposed algorithm for a lossy battery, i.e. $\eta_{\text{ch}} = 0.95, \eta_{\text{dis}} = 0.95$.

Table 3.2: Comparison of performance for lossy battery

Algorithm Type	Run Time (sec)	Profit ($)
Proposed Algo	0.164189	0.1193289
Linear Programming	1.255490	0.1193289
Matlab's Fmincon	23.41217	0.11923956

From numerical evaluation it is observed that the proposed algorithm significantly reduces the run time compared to Matlab's Fmincon with reasonable number of evaluations, 9600 in this case. Table 3.2 provides a comparison of results for a lossy battery.

3.4 Case Study 1: Feasibility of Energy Arbitrage

Energy storage is expensive, so its financial feasibility analysis is essential. We present an approximate methodology to consider the net average capacity of the battery over its entire life. Using this average available capacity, we calculate energy arbitrage gains in a deterministic setting for a 1 kWh rated capacity battery with 1 day as optimization horizon.

3.4.1 Net Average Available Battery Capacity

The average battery capacity available over its entire life to the user will be close to 50 to 70 % of the original storage capacity when the battery is new. Oversizing is a crucial factor jeopardizing the financial viability of energy storage. We consider following sources of discounting:
(1.) Efficiency of Cycling : The losses incurred during cycles of charging and discharging ($\approx$ 70 to 95%)
(2.) Efficiency of Converter : AC to DC and DC to AC conversion incurs losses ($\approx$ 90 to 98 %)
(3.) Performance Degradation: Battery reaches End-of-Life (EoL) if the maximum battery capacity reduces to 80 % of the rated battery capacity. Life of a battery in years ranges from 5-20 years and in cycles from 1000 to 20000 cycles depending on type of battery, *whatever is achieved first marks EoL.*
(4.) Optimal SoC Band: overcharging or over-discharging a battery significantly affect its life.

The discount factors assumed are: (1.) $\eta_{\text{ch}} = 0.95, \eta_{\text{dis}} = 0.95$, thus the roundtrip battery efficiency equals 0.9025, (2.) Converter Efficiency = 0.95, (3.) Average Capacity due to Degradation = 0.9, (4.) $[B_{max} - B_{min}]$/Capacity = $[0.98 - 0.1]/1 = 0.88$. Therefore Net Available Capacity = 0.679. This implies that the earnings of 0.679 kWh available capacity in 5 years should match price paid by end user in buying 1 kWh, for achieving 5 yrs. simple payback period. Discount factors due to maintenance cost and self-discharge will further reduce the net average capacity of the battery.

3.4.2 Evaluation

The present battery cost is around $ 350 - 500 per kWh. One year (2016) simulations for real time electricity prices of Nord Pool, PJM, ISONE, MISO, NYISO, ERCOT, CAISO and PG&E's TOU prices are done to calculate the value of energy storage. The discounted returns calculated for Battery model

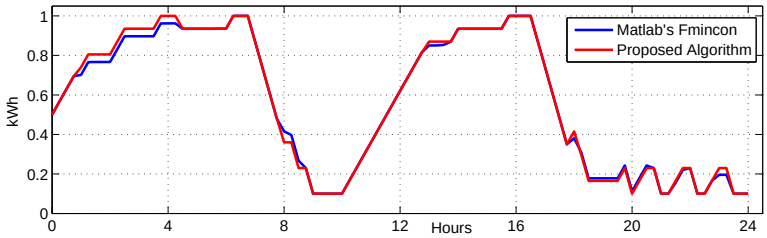

(a) Comparison of optimal battery level (b^*)

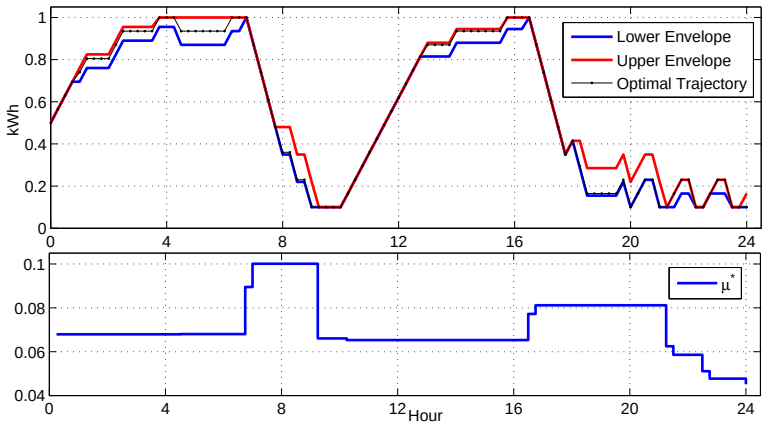

(b) Proposed algorithm results for lossless battery

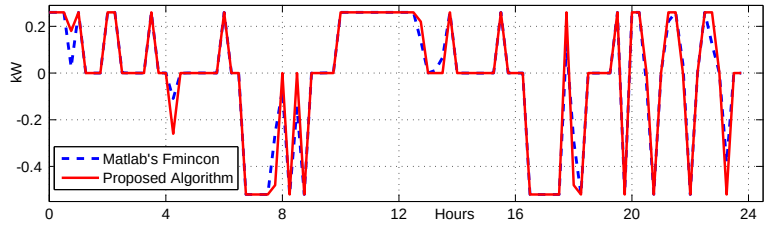

(c) Comparison of optimal ramp rates

Figure 3.12: Comparison for lossy battery

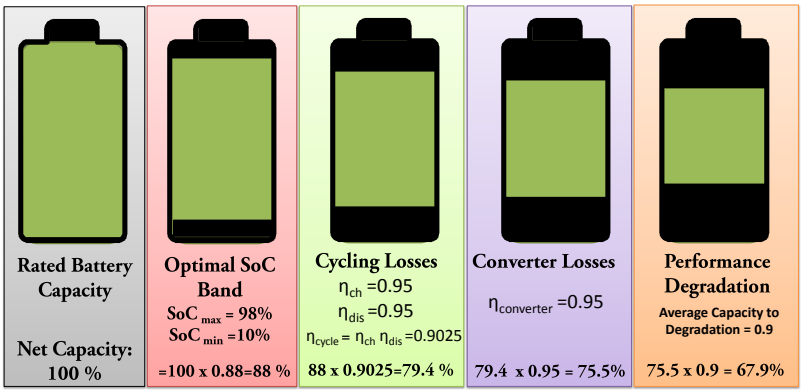

Figure 3.13: Average battery capacity due to: SoC constraint, cycling and converter losses and degradation

Table 3.3: The price signals evaluated are listed below

Region/ISO	Pricing	Sample
NordPool [76]	Real Time	1 hour
PG&E [295]	ToU	-
CAISO (Average Price) [16]	Real Time	5 min
PJM (Zone AEP) [16]	Real Time	1 hour
ERCOT (Zone LZ-Huston) [16]	Real Time	1 hour
ISONE (Zone .Z.SEMASS) [16]	Real Time	1 hour
MISO(Zone Michigan Hub) [16]	Real Time	1 hour
NYISO (Zone N.Y.C.) [16]	Real Time	1 hour

Table 3.4: Battery 1: δ_{max}=0.26 kW, δ_{min}=-0.52 kW

Region or ISO	Cumulative Gains in 2016	Operational Cycles in 2016	Discounted Gains in 5 yrs
NordPool	€ 0.991	1748	€ 4.3
PG&E	$ 4.38	184	$ 18.7
CAISO	$ 37.9	914	$ 162.0
PJM	$ 11.2	573	$ 47.9
ERCOT	$ 18.6	430	$ 79.5
ISONE	$ 15.3	687	$ 65.4
MISO	$ 10.5	595	$ 44.9
NYISO	$ 23.3	700	$ 99.6

Table 3.5: Battery 2: $\delta_{max} = 1kW$, $\delta_{min} = -1kW$

Region or ISO	Cumulative Gains in 2016	Operational Cycles in 2016	Discounted Gains in 5 yrs
NordPool	€ 1.09	2836	€ 4.7
PG&E	$ 4.38	184	$ 18.7
CAISO	$ 73.2	2008	$ 312.9
PJM	$ 16.1	825	$ 68.8
ERCOT	$ 25.02	534	$ 107.0
ISONE	$ 23.51	1082	$ 100.5
MISO	$ 15.52	860	$ 66.34
NYISO	$ 36.32	1225	$ 155.3

Table 3.6: Battery 3: $\delta_{max} = 2kW$, $\delta_{min} = -2kW$

Region or ISO	Cumulative Gains in 2016	Operational Cycles in 2016	Discounted Gains in 5 yrs
CAISO	$ 125.03	3240	$ 534.4

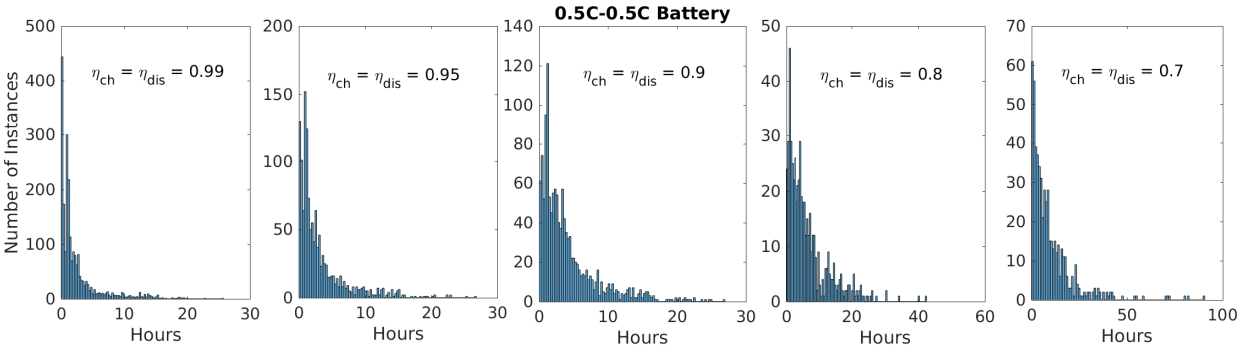

Figure 3.14: Histogram of sub-horizon spread for 0.5C-0.5C battery for CAISO in 2017

1, 2, 3 listed in Table 3.4, 3.5 and 3.6. The results take into account the net average battery capacity calculated in section 3.4.1. The discounted returns are significantly lower than the present cost of a battery. CAISO, NYISO and ERCOT is relatively more profitable but still lower than the initial investment made by end user. For small price variations arbitrage could still be profitable if (Selling Price) > (Buying Price)/(Round-trip Efficiency), but the revenue generated with per cycle of operation of the battery will be small. It is evident from Table 3.4, 3.5 that the arbitrage gains are lower than the cost of a battery, therefore subsides would be required for end user participation. For battery model 3, energy arbitrage using CAISO prices tend to over use the battery, which is evident from the cycles of operation shown in Table 3.6. Note that for other ISOs the gains remain as in Table 3.5, due to the one hour sampling time. Energy storage arbitrage could become more profitable if the price of energy storage decreases drastically *or/and* the price of electricity becomes more volatile *or/and* cycle life of batteries increase significantly.

3.5 Case Study 2: Quantifying length of a sub-horizon

Identifying optimal look-ahead horizon for performing arbitrage would be essential for maximizing the gains by performing arbitrage. Prior works [251] indicate selecting a time horizon of 1 day is sensible since the electricity pattern repeats with a period of one day approximately, being high during peak consumption hours during the day and low during the night [196]. In this work we claim that the optimal control actions for energy storage device depends on electricity price and load variations in a smaller part of a larger time horizon and independent of all points in past or beyond the sub-horizon, as shown in Fig. 3.3. However, identifying this optimal look-ahead period is challenging as it is governed by variation of electricity price, load and battery parameters. Next we present a case study for understanding the influence of battery parameters on length of a sub-horizon.

3.5.1 Case Study: CAISO 2017 for equal buying and selling price of electricity

We consider 2017 electricity price for CAISO and identify the variation of sub-horizon over a year with different energy storage parameters. The variable considered here in this case study are:

- Electricity price for CAISO in 2017,
- Ramp rate of the battery: in this case study we consider 1 kWh capacity battery with 3 different ramp rates. xC-yC represents that battery takes 1/x hours to completely charge and 1/y hours to completely discharge.
- Efficiency of the battery: we consider 5 levels of efficiency (η): 0.99, 0.95, 0.9, 0.8 and 0.7. Here $\eta = \eta_{ch} = \eta_{dis}$.

The performance indices used in this case study are:

- T_{mean}: denotes the mean length of a sub-horizon over the whole year,
- $T_{99\%}$: denotes the 99% quartile,
- T_{worst}: denotes the worst case length of a sub-horizon,

- $/cycle: denotes dollars per cycle gain and
- Gain: denoted total arbitrage gain.

Table 3.7: Quantifying the length of sub-horizon

Efficiency η	T_{mean} hours	$T_{99\%}$ hours	T_{worst} hours	$/cyc	Gains $
0.5 C - 0.5C Battery					
0.99	2.45	15.33	25.75	0.037	32.80
0.95	3.20	17.50	26.75	0.046	30.21
0.9	4.11	20.50	26.92	0.055	27.54
0.8	6.68	26.70	42.42	0.068	23.21
0.7	9.73	69.83	90.58	0.075	19.62
1 C - 1 C Battery					
0.99	1.76	11.83	18.75	0.036	59.52
0.95	2.14	13.00	18.75	0.047	54.84
0.9	2.79	14.83	23.08	0.059	50.04
0.8	4.52	18.67	33.58	0.077	42.29
0.7	6.37	30.67	63.50	0.085	35.86
2 C - 2 C Battery					
0.99	1.21	6.92	12.75	0.034	103.60
0.95	1.61	9.17	14.17	0.048	95.28
0.9	2.10	11.00	16.33	0.062	87.02
0.8	3.32	16.83	26.42	0.085	73.76
0.7	4.60	23.00	58.50	0.093	62.65

It is evident from Fig. 3.14 and Table 3.7 that the length of look ahead required for optimal energy storage arbitrage reduces as the ramping rate increases and as the energy storage becomes more efficient. As pointed in [174] that the efficiency creates a dead band in threshold based structure and increase in efficiency implies battery should not operate during low returning transactions as it would not be profitable. Dollars per cycle calculated using prior work [181] (detailed in Chapter 5) shows increase as the efficiency decreases. For more details refer to Chapter 5, [174] and [181]. As the ramping of battery increases and battery becomes more efficient the optimal look-ahead period decreases making it more prone to inaccuracies in forecast information. This observation is in sync with [130].

Table 3.7 compares the look-ahead window required in hours for three batteries. xC-yC battery implies battery takes 1/x hours to charge and 1/y hours to discharge completely. All the three batteries have the same capacity but different ramping rates. The arbitrage gains increases as the battery becomes more efficient and as the ramping rate increases. The $/cycle calculated here takes into account battery degradation due to operational cycles. Note the look-ahead window for 0.5C-0.C battery with 95% efficiency (i.e. $\eta_{ch} = \eta_{dis} = 0.95$) is 15.5 hours or below for 99% of sub-horizons over the whole year (CAISO, 2017), this decrease to 13 hours for 1C-1C battery and further reduces to just 9.17 hours for 2C-2C battery. This case study indicates that the optimal look-ahead window for performing arbitrage is not only governed by price variation but also battery ramping rate and round trip efficiency. Fig. 3.14 shows the spread of sub-horizons for 0.5C-0.5 battery with varying efficiency. For a highly efficient battery the spread is much more compact compared to less efficient one.

3.6 Case study 3: Effect of Uncertainty on Arbitrage

In recent years, energy storage has become an integral part of modern grid operations. Several pioneering research papers have studied the economic benefits brought by operating energy storage [297, 109]. The main obstacle here arise due to imperfections in the uncertainty modeling of forecast prices. Under NEM 1.0 the uncertainty is due to the variation of electricity price. Electricity price can be forecast based on historical observations and market signals, yet any off-the-shelf forecasting methods would bring prediction errors into subsequent battery control and arbitrage decisions. Battery owners need to design a strategy that maximizes accumulated profits for the overall operation period where designed charging/discharging

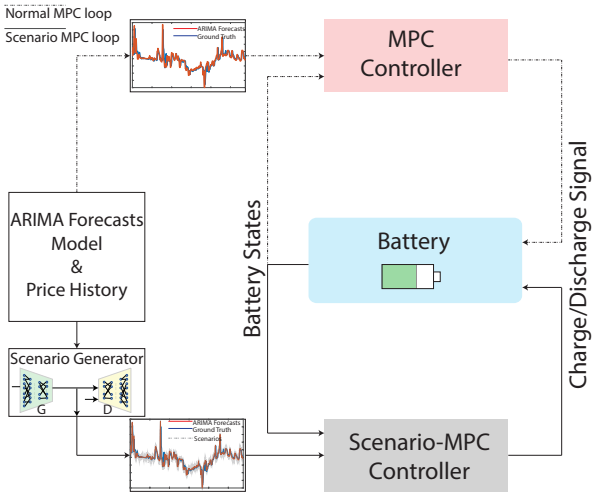

Figure 3.15: Schematic plot for our scenario-based battery controller, with a comparison to normal MPC controller using point forecasts [130].

actions are coupled in time due to finite size of inventory or capacity, inaccurate forecasts can lead to sub-optimal and hence less profitable sequential decisions.

To deal with such forecasting uncertainties, researchers have tried to design algorithms that are more robust to predictions errors, such as ones based on model predictive control (MPC) and dynamic programming (DP). The authors in [280, 317] maximize the expected value in presence of uncertain parameters, though the solutions are very sensitive to the accuracy of given point forecast algorithms. The authors in [92] propose multi-stage forecast for receding horizon control to mitigate the effects of forecasting errors, however, explicit quantification of uncertainty is still difficult. In [324], the authors use a data-driven reinforcement learning algorithm to maximize the arbitrage, yet both battery charging level and charge/discharge actions are discrete which simplifies the control. From another perspective, other researchers tried to handle the uncertainties explicitly via robust optimization [100], chance-constraints [292] or scenario-based optimization [123]. The scenario-based approach often avoids the conservative solutions achieved by robust optimization. It uses independent, identically distributed future realizations (*scenarios*) to expressively represent the uncertainties. Moreover, with an appropriate choice of the number of the scenarios, the solution of the scenario-based problem can be made a feasible solution of the corresponding chance-constrained problem [123]. Scenario approach can also ease the subsequent control and optimization problem with convex and linear formulations that are easy to scale. In [82, 213], authors use scenario-based maximization for selecting control decisions for arbitrage problem.

The goal of this case-study is two-fold. Firstly, mitigation of uncertainties leading to reduction in arbitrage gains for consumers compensated based on NEM 1.0 using model predictive control (MPC). We propose two algorithms applicable for: (i) point forecast with MPC and (ii) scenario based MPC. Fig. 3.15 compares the classical MPC control algorithm with design the scenario-MPC controller, and derive the optimal charge/discharge actions with respect to certain number of future price scenarios. Second goal of this case-study is to understand the effect of storage parameters on how prone performing arbitrage is towards uncertainty. For this evaluation we use four different simulation types: (a) Deterministic simulation based on actual price values, (b) Day-ahead price predictions used for fixing control decisions, (c) AutoRegressive Integrated Moving Average (ARIMA) based price forecast with MPC and (d) Model free scenario generation along with MPC based on [132, 131].

3.6.1 Threshold based structure for negative prices

In some cases with high penetration of renewables, there may exist negative prices. Note that under such cases, the cost function of the optimization is no longer convex. Here we make a realistic assumption that negative prices are rare[4], and assume the optimal action for the consumer under negative prices is to charge. For instance in Germany and in California the negative prices comprised of 2.6% of total hourly

[4]Negative electricity prices occur when high inflexible power generation which cannot be shut down and restarted in a quick and efficient manner meets low demand [158]. Such instances are on the rise with the growth of renewables, however, the share of instants with negative price over the total number of time instants still remain within 3%.

prices for the year 2017[5] [6]. Under this condition the threshold-based structure, used for selecting optimal control decisions in Section 3.2, is modified to Eq. 3.6.1 in Remark 3.

Remark 3. The storage control decision x_i^* in the ith instant minimizes the function $C^{(i)}_{\text{storage}}(x) - \mu_i^* x$ for $x \in [X_{\min}, X_{\max}]$. The storage control decision $x_i^*(\mu)$ is

$$x_i^*(\mu) = \begin{cases} \begin{cases} X_{\min}, & \text{if } \mu < p_{\text{dis}}(i), \\ [X_{\min}, 0], & \text{if } \mu = p_{\text{dis}}(i), \\ 0, & \text{if } p_{\text{ch}}(i) > \mu > p_{\text{dis}}(i), \text{ if } p_i \geq 0 \\ [0, X_{\max}], & \text{if } \mu = p_{\text{ch}}(i), \\ X_{\max}, & \text{if } \mu > p_{\text{ch}}(i), \end{cases} \\ \begin{cases} [0, X_{\max}], & \text{if } \mu \leq p_{\text{ch}}(i), \\ X_{\max}, & \text{if } \mu > p_{\text{ch}}(i), \end{cases} \quad \text{if } p_i < 0 \end{cases} \tag{3.6.1}$$

where $p_{\text{ch}}(i) = p_i/\eta_{\text{ch}}$, $p_{\text{dis}}(i) = p_i\eta_{\text{dis}}$, $C^{(i)}_{\text{storage}}(x_i) = s_i p_i$ and μ represents the shadow price of the transaction.

Note that for $\mu = \hat{p}_i^{ch}$ or $\mu = \hat{p}_i^{dis}$, $u_i^*(\mu)$ takes an *envelope* of values. For any other value of μ it is a singleton set. In order to find optimal decisions among an envelope of possible solutions based on the price variations, a backward Step algorithm is used as described in detail in Section 3.2.2, refer to `OptimalArbitrageNEM1` algorithm.

Though the `OptimalArbitrageNEM1` algorithm could provide resiliency to forecast uncertainties by iteratively solving the MPC, it still heavily relies on the performance of forecasts, and the point forecast errors can still lead to unsatisfactory charging/discharging actions. Next we present two algorithms used for the analysis mentioned.

3.6.2 Point Forecast with MPC

We use AutoRegressive Integrated Moving Average (ARIMA) model of 8^{th} lag order and one degree of differencing for forecasting electricity price. The ARIMA model is described in Section 2.4.1. The ARIMA model is developed using training data and tested for test dataset. Note that for price forecast the moving average window is set to zero. This model is denoted as

$$\Delta X_{i+1} = \gamma_1 \Delta X_i + \gamma_2 \Delta X_{i-1} + ... + \gamma_8 \Delta X_{i-7} \tag{3.6.2}$$

where $\Delta X_i = X_i - X_{i-1}$.

Algorithm 4 `PointForecastMPC`

Global Inputs: $\eta_{\text{ch}}, \eta_{\text{dis}}, \delta_{\max}, \delta_{\min}, b_{\max}, b_{\min}, b_0$
Inputs: $h, N, T, i = 0$

1: **while** $i < N$ **do**
2: $i = i + 1$
3: Forecast $\hat{p}_{elec}$ from time step i to N using ARIMA
4: Find x^* by solving `OptimalArbitrageNEM1` using inputs $\hat{p}_{elec}, b_0, h$, battery parameters
5: ${b_i}^* = b_{i-1} + x_i^*$
6: Update $b_0 = {b_i}^*$
7: **end while**

3.6.3 Scenario-Based MPC

Scenario approach has been introduced into optimization problems to replace the uncertainty set of variables by a finite number of scenarios. In [123, 268] different approaches have been proposed to formulate the uncertainty set as scenarios either in objectives or constraints. Model-free scenario generation is based on [131]. We advise interested readers to follow details of the model with respect to arbitrage in [130].

We can now bridge the machine learning scenario generation algorithm `ModelFreeScenarios` with the optimal control algorithm `OptimalArbitrageNEM1` into the SMPC formulation. We term the entire process as `ScenarioMPC` algorithm for real-time battery arbitrage.

[5] https://tinyurl.com/y9xq5gul
[6] https://tinyurl.com/y87t578b

Algorithm 5 `ScenarioMPC`

Global Inputs: $\eta_{\text{ch}}, \eta_{\text{dis}}, \delta_{\max}, \delta_{\min}, b_{\max}, b_{\min}, b_0, K$
Inputs: h, total horizon $N, T, t = 0$

while $i < N$ **do**
  Update $i = i + 1$
  $k = 1$
  while $k < K$ **do**
    Get forecasts $\hat{\mathbf{p}}_{\text{elec}}$ starting from i
    $\hat{\mathbf{p}}^{\mathbf{k}}_{\text{elec}} = \texttt{ModelFreeScenarios}(\hat{\mathbf{p}}_{\text{elec}}, i)$ [131]
    $k = k + 1$
  end while
  $\mathbf{x}^* = \texttt{OptimalArbitrageNEM1}(\hat{\mathbf{p}}^{\mathbf{k}}_{\text{elec}}, h, N), \forall\ k$
  Calculate $b_{i+1} = b_i + \mathbf{x}^*_i$
  Update $b_0 = b_{i+1}$
end while

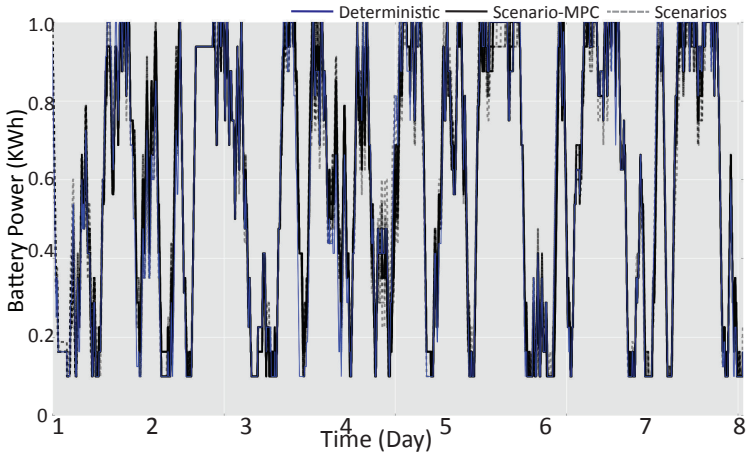

Figure 3.16: One-week charging/discharging signals under deterministic, single scenario and scenario-MPC control frameworks.

3.6.4 Simulation Results

We validate the performance of our algorithm on three battery model with varying ramp rates: $0.25kW, 1kW$ and $4kW$. The other battery parameters are $b_0 = 0.5kWh, B_{rated} = 1kWh$, $SoC_{\max} = 0.98$, $SoC_{\min} = 0.1$, $h = \frac{1}{12}$ hour, η_{ch}=η_{dis}=0.95. We use one-year locational marginal pricing data from CAISO[7] as training data for scenarios, and test the three battery's arbitrage performance on 1-week's separate data. We generate $1,000$ independent scenarios at each time-step. This number is selected in our case as we don't observe significant improvement in control performance with more scenarios. During testing on standalone 1-week test data, we also use public available day-ahead forecasts to compare the arbitrage performance.

We firstly validate if the proposed algorithm can make profits for batteries of varying ramp rates and compare the results with control using full knowledge of price (the deterministic case). As shown in Fig. 3.17, all three batteries are making profits, but the profits vary a lot depending on the ramp rate. This corresponds to our expectation, since battery with greater ramping rates are able to catch the opportunities of extreme prices (e.g., sell more energy when price are high). We define regret as the ratio of difference on arbitrage gains. The regret comparison is shown in Table 3.8. From Table 3.8 we can observe that inaccuracies in uncertainty model affect faster ramping battery (e.g., ultra-capacitor) much more significantly compared to slow ramping battery (e.g., hydro storage). Observe the regret for 4 kW ramping battery is more than 58% using SMPC, however, for 0.25 kW ramping battery the regret is less than 3%.

In all settings, we observe better performance by using proposed data-driven `ScenarioMPC` algorithm over MPC using point forecasts (ARIMA) and day-ahead price. More interestingly, when battery ramp rate is lower, `ScenarioMPC` could achieve nearly the benchmark of using real future price information. When ramp rate is higher, the battery are reacting more strongly to forecast errors, and scenarios can only compensate part of such uncertainties on forecasts.

[7] http://www.energyonline.com/Data/

Table 3.8: Comparison of regret on one-week profits

Max Ramp Rate	Day Ahead	ARIMA	SMPC
0.25 KW	0.657	0.133	**0.028**
1 kW	0.855	0.237	**0.134**
4 kW	0.922	0.730	**0.588**

We then look into the details of how `ScenarioMPC` affects the battery charging/discharging decisions in Fig. 3.16, where we show the actions for the battery with $0.25kW$ ramp rate. The decision of each single scenario may deviate from the deterministic version's strategy, while by integrating scenarios into `ScenarioMPC`, the final decision is getting closer to the deterministic solution.

3.6.5 Key Observation

In this case-study, we use optimal arbitrage framework proposed in this chapter for solving the battery arbitrage problem which is often faced with uncertainties in price forecasts. By utilizing data-driven scenarios in the optimal control problem, simulation results demonstrate our algorithm can achieve better performance than classical MPC algorithms with a basic ARIMA forecast. We observe that battery with higher ramp rate has a greater sensitivity towards uncertainty. In such cases the modeling of uncertainty is much more essential. However, if the sampling time of decision making is large than the effect of uncertainty is low. For instance modeling of uncertainty is more essential for places where electricity price varies every 5 minutes compared to places where the variation of electricity price happens hourly.

3.7 Conclusion and Perspectives

We formulate the optimal arbitrage algorithm for storage operation and propose an efficient algorithm to find an optimal solution. The method transforms a continuous, convex optimization problem into a discrete one by exploiting the piecewise linear structure of the cost function. This structure provides the derivative of the cost function which is unique or has a sub-gradient like structure. We observe that optimal storage control decisions do not depend on prices beyond a certain sub-horizon. In the proposed algorithm, we indicate a method to calculate these sub-horizons and finding the optimal solution in the sub-horizon using backwards step algorithm. The worst case run-time complexity of the proposed algorithm is found to be quadratic in terms of the number of time instants for which price values are available. The proposed algorithm outperforms even the simplex based LP formulation summarized in Appendix B.

Using the proposed algorithm, we conducted extended simulations for three case-studies. In first case-study we use real price data from several ISOs in the USA and Europe for the year 2016. We extrapolate the arbitrage gains for an end user for a five year period, considering detailed losses in the battery. The numerical evaluation suggests that only arbitrage cannot create positive net present value for storage, thus subsidies are required to incentivize investment.

In second case-study we quantify the length of a sub-horizon for CAISO price for the year 2017. We observe the sub-horizon required for faster ramping batteries are significantly lower compared to slow ramping batteries. However, in the third case-study we observe that faster ramping batteries are more prone to uncertainty compared to slower ramping batteries. This could be used to infer that short-term accurate forecasting is essential for maximizing arbitrage gains for faster ramping energy storage devices.

We also identify the effect of uncertainty on storage operation in association with the ramping capability of storage. Fast ramping batteries have a greater influence of parameter uncertainty and therefore, would require more rapid correction in its operation. Batteries could contribute if the lookahead forecast is accurate. Although, the central goal of the thesis is not to develop tools for forecasting, however, realizing the storage control algorithms in the real world should consider combining reliable forecasting tools with storage control.

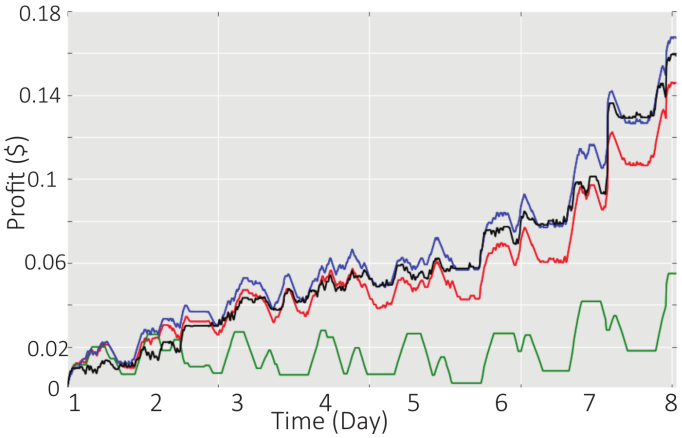

(a) Comparison of cumulative profit for battery 0.25C-0.25C

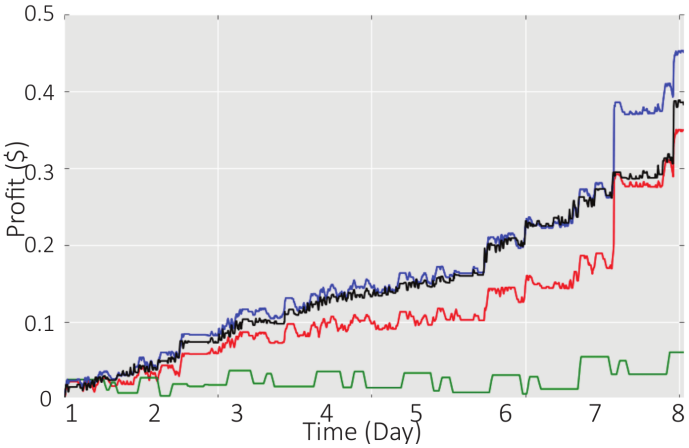

(b) Comparison of cumulative profit for battery 1C-1C

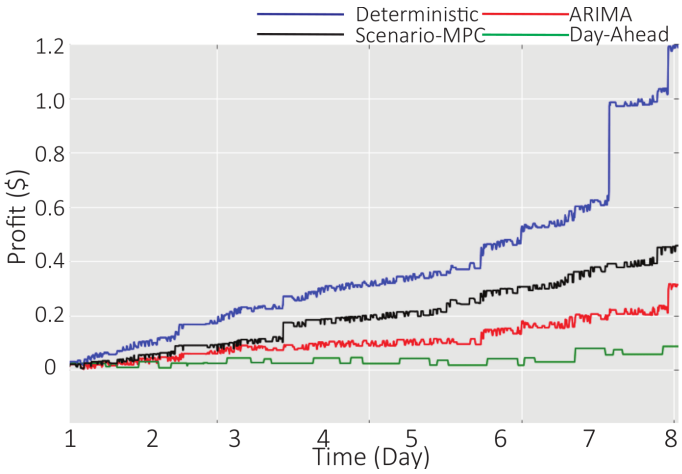

(c) Comparison of cumulative profit for battery 4C-4C

Figure 3.17: Case studies on one-week profits of 3 batteries with varying ramp rate. By incorporating scenarios to account for the forecasting uncertainties, scenario-MPC outperforms control algorithms using pure ARIMA or day-ahead forecasts information. Legend: (i) Blue shows deterministic case, (ii) Black shows scenario MPC, (iii) Red shows MPC using ARIMA forecast, (iv) Green shows cumulative gains using day-ahead price predictions.

Chapter 4

Energy Arbitrage - Net Metering 2.0

Never mistake a clear view for a short distance. - Paul Saffo

Summary: Electricity prices and the end user net load vary with time. End users equipped with energy storage devices can perform energy arbitrage, i.e., buy when energy is cheap or when there is a deficit of energy, and sell it when it is expensive or in excess, taking into account future variations in price and net load. Net metering policies indicate that many of the utilities in order to compensate excess power generated by end users apply a rate lower than or equal to the retail rate. In Chapter 3 we introduced net-metering policies specifically applicable for NEM 1.0. This chapter formulates the optimal arbitrage problem for NEM 2.0, where selling price is lower than or equal to buying price of electricity. Under such a case the consumer inelastic load and renewable generation cannot be ignored, unlike the optimal arbitrage formulation presented in Chapter 3. We propose a computationally efficient algorithm, with worst case run time complexity of $O(N^2)$, that computes the optimal energy ramping rates in a time horizon. The proposed algorithm exploits the problem's convexity properties and is based on the discretization of optimal Lagrange multipliers. The levels of discretization are governed by electricity price and storage efficiency. The solution has a threshold-based structure in which optimal control decisions are independent of past or future price as well as of net load values beyond a certain time horizon, defined as a sub-horizon. The threshold is governed by inelastic load, renewable generation, electricity price and storage parameters. Numerical results show the effectiveness of the proposed model and algorithm.

Furthermore, we investigate the impact of forecasting errors on the proposed technique. We consider an Auto-Regressive Moving Average (ARMA) based forecasting of net load together with the Model Predictive Control (MPC). We numerically show that adaptive forecasting and MPC significantly mitigate the effects of forecast error on energy arbitrage gains. In numerical results we present the sensitivity analysis of storage performing arbitrage with varying ramping batteries and different ratio of selling and buying price of electricity.

4.1 Introduction

The share of total energy consumed worldwide by buildings, which include commercial and residential end users, accounts for around 20% and it is projected to grow at an average of 1.4% per year from 2012 to 2040 [260]. The environmental benefit of connecting more and more renewable energy sources in meeting the global energy demand is therefore irrefutable. Nowadays, utilities encourage end users to install DG sources like solar PV, wind, biogas, biomass, geothermal energy or small hydro [98]; any excess power generated by such sources are bought back by the grid and compensated at every billing cycle (monthly or yearly). This can be achieved by *Net Metering*, which facilitates bi-directional power flow to and from an end user. Net metering is a policy designed to encourage private investment in renewable energy [22]. Authors in [151] identify that the future adoption of distributed generation (DG) is highly sensitive to the compensation mechanism, and an increase in retail rate would accelerate DG deployment. Incentivizing DG owners pushes utilities to increase charges per kWh for all the customers, creating a disparity for non-DG owners [156]. Utilities have to make a bargain in promoting DG and penalizing non-DG owners with higher electricity rates [78]. Therefore, net metering policies vary significantly by country and by state or province. For instance, in the US each state has its own mechanism to deal with distributed generation by consumers. The compensation for an excess generation by an end user can be categorized based on selling price as [78, 22]:

Retail Rate: The selling price is equal to the buying price of electricity for the end user for each time instant. This compensation mechanism also referred as NEM 1.0 is considered for storage operation in Chapter 3. States in the US where the NEM compensation equals retail rate: Connecticut, Delaware, Florida, DC, Illinois, Indiana, Iowa, Kansas, Kentucky, Maine, Maryland, Minnesota, Montana, Nevada, New Jersey, North Carolina, Vermont, Virginia, Washington, West Virginia, Wyoming,
Lower than the Retail rate: (referred as NEM 2.0). There are various compensation mechanisms where the selling price is lower than the buying price, such as (a.) selling price could be a function of buying price. States: Rhode Island, Michigan, Alabama, California, Colorado, Massachusetts, Oregon, Texas, (b.) *Avoided Cost*: is the minimum amount an electric utility is required to pay an end user. States where NEM compensation is based on the avoided cost are: Arizona, Louisiana, Missouri, Nebraska, New Hampshire, New Mexico, North Dakota, Oklahoma, (c.) *Generation Rate*: selling price is approximately half the retail rate, states: Ohio, Pennsylvania. Note that within a state there could be multiple utilities, the rules for net metering can differ for different utilities, for example, net metering in California is discussed in [55].

While originally intended to promote the growth of distributed solar which NEM 1.0 has irrefutably achieved, electric utilities have felt NEM 1.0 puts them in a disadvantaged position by increasing financial stress. Utilities claim that large-scale renewable generation facilities are at least 50% cheaper compared to buying surplus generation from consumers. NEM creates cross-subsidies between consumer classes, quite similar to those created during the 1960s in the US to promote electric heating instead of using oil and gas for heating. Utilities claimed that the increased sales resulting from consumers switching from gas to electric heating offset the costs of the incentive programs. The utilities offered rebates to consumers who switched to electric heating and promoted the concept of total electric home. The utilities were able to capitalize on the fact that electric homes used 2.5 to 3 times as much energy as their nonelectric counterparts, which would increase the sales for decades to come [192]. However, NEM contrary to increasing electricity sales actually decreases them. Arizona Public Services reported that for a typical solar consumer prior to installation of solar had 1,545 kWh and 8.9 kW average monthly energy and power needs, which reduces to 491 kWh and 8.5 kW average monthly energy and power needs [89]. Note although average power demand underwent non-noticeable change, the energy consumption reduced by more than 68%. Such a reduction in volumetric energy consumption makes it impossible for a fixed cost to be recovered. Investor-owned utilities which includes privately held companies such as PG&E claim that solar customers are being compensated more than they generate and propose a re-evaluation of NEM programs. The next generation NEM is referred to commonly as NEM 2.0. In this chapter, we formulate the optimal energy arbitrage problem under NEM 2.0 compensation mechanism.

In this chapter, we generalize the threshold based structure of storage operation introduced in Chapter 3 to NEM 2.0 net-metering compensation policies. We use a similar search strategy for finding the shadow price levels in a sub-horizon. Sub-horizon denotes a smaller portion of the longer time horizon where storage control actions are coupled. These levels of shadow price required to identify a sub-horizon are equivalent to the derivative of consumption cost paid by the consumer with respect to the optimization variable. In this chapter we use the change in storage charge level as the optimization variable, therefore, the shadow price defined takes the value which is governed by the price levels in the sub-horizon and storage charging and discharging efficiency. We formulate the storage arbitrage problem applicable for storage control under net-metering NEM 2.0, where the cost function has a piecewise linear structure. Our setting also considers a consumer with inelastic load and renewable generation. Based on the selection of optimization variable, we show the convexity of the objective function of operating energy storage in the presence of inelastic consumer load and renewable generation. The objective function is not strictly convex, so it does not have a unique derivative at the point of change of slope of the cost function, at these points the derivate has a sub-gradient like structure. Due to this attribute of the cost function, an only forward algorithm for storage control would not suffice. These points act as slack in optimizing storage operation. This is illustrated using a stylized example provided in Chapter 3. We observe that at these points the storage could have a ramp rate which is neither maximum, minimum nor zero, a notion (that optimal storage actions consist of these 3 storage operation levels) many believed to be true [170, 325], [272], we demonstrate this claim using a numerical experiment in Chapter 4.6. This claim assumes that the storage ramp rates can only be changed at decision epochs and not in between the sampling time. In order to identify storage actions in these points, we have a combination of a forward algorithm (Algorithm 6) which identifies the sub-horizon and envelope of storage actions and a backward algorithm (Algorithm 7) which runs one time in the identified sub-horizon to decide the storage control trajectory in that sub-horizon. Algorithm 6 and Algorithm 7 together performs optimal arbitrage. We observe that the power level seen by energy meter in the absence of energy storage affects the storage control decisions under net-metering. We list exact thresholds based on price variation, load, and renewable variation and storage parameters.

An alternative definition of energy arbitrage could be for reshaping renewable energy generation combined with energy storage operated to adjust the grid injection to maximize the profitability of the facility [253]. The proposed algorithm could also be used for increasing self-consumption of local distributed generation as pointed in [160] under zero selling price, thus reducing reliance on the utility.

4.1.1 General applicability of proposed algorithm

Note that the proposed solution is generally applicable for any system with finite capacity performing arbitrage. In any market of commodities a market participant buys the commodity and stores it in its inventory, in order to sell the commodity in the future to make profit. Performing such a transaction has a coupling in buying and selling decisions. This coupling in time is due to the finite size of the inventory, much like energy storage performing arbitrage. At any time, due to infrastructure constraint, the market participant can buy or sell no more than a given limit, much like the ramp rate constraint of a battery. Usage of inventory incurs some cost which decides the efficiency of buy and sell decisions, analogous to charging and discharging efficiency of a battery. The exogenous variables such as inelastic load and renewable generation is analogous to the operational cost and income for the inventory problem.

4.1.2 Contributions of the chapter

The key contributions of this chapter are as follows:
• *Generalized Buy and Sell Prices*: The Lagrangian theory for performing optimal arbitrage is proposed in [145], [146]. Our main contribution is the development of a computationally efficient algorithm applicable for different net-metering policies for consumer with inelastic load and renewable generation considering storage ramp and capacity constraints.
• *Sub-horizon*: We observe that in order to determine optimal control decisions in a certain period within the total time horizon it is sufficient to consider prices only within a sub-horizon which is often much smaller than the entire horizon. The length of sub-horizon depends on (a) initial storage capacity, (b) electricity price variation, (c) storage efficiency, (d) ratio of ramp rate over capacity and (e) sampling time of decision making.
• *Computationally efficient algorithm*: Due to the discrete nature of the optimization problem, we explicitly characterize the worst case run time complexity of the proposed arbitrage algorithm to be quadratic in the number of time steps. The discretization is governed by electricity price levels in the sub-horizon and storage charging and discharging efficiency.
• *Threshold based structure*: The threshold-based structure of the proposed solution provides a set of feasible solutions in a sub-horizon. A backward step is, therefore, used for selecting the optimal trajectory in a sub-horizon. We provide the conditions for optimally selecting these thresholds. Storage thresholds for optimal arbitrage is a function of (a) price for buying and selling, (b) storage charging and discharging efficiency, (c) ramping constraint, (d) the relationship between the ratio of selling and buying price with respect to round-trip storage efficiency and (e) consumption level seen by energy meter without storage.
• *The effect of forecast error on arbitrage gains*: We implement auto-regressive based forecast model along with MPC and numerically analyze their effect on arbitrage gains using real data from Pecan Street [58] and ERCOT price signal [16], and real data from a household in Madeira in Portugal and electricity price from California ISO [16]. The effect of uncertainty on arbitrage gains is more pronounced for cases where selling price is higher compared to cases where selling price is closer to zero.
• *Sensitivity of ratio of selling and buying price*: We numerically analyze the effect of the ratio of buying and selling price of electricity on the value of storage integration with inelastic load and renewable generation. We observe that the value of storage performing arbitrage significantly increases in the presence of load and renewable generation with the increasing disparity of selling and buying price of electricity, compared to only storage performing arbitrage. Inclusion of storage in the presence of load and renewable could be profitable even for cases where the selling price is zero or small compared to buying price. For the same case, only storage performing arbitrage would not be profitable.

Prior Work: As in Chapter 3, optimal arbitrage problem can be seen as LP (see App. B) and also as a convex optimization problem. The work closest to this chapter is [146], [148], where the energy arbitrage problem has been considered for a single battery user incorporating storage ramping and capacity constraints. In this chapter, we deal with a special case, for NEM 2.0, of optimal arbitrage problem dealt in [146] along with consumer load and/or generation. Authors in [146] propose a forward storage control algorithm, based on Lagrangian theory used to manage the storage capacity constraint, which could be applied for strictly convex cost function which has a unique derivative of the cost function. Authors in

[146] use strong Lagrangian theory for identifying storage control decisions. The key difference of our work compared to [146] are: discretizing the continuous optimization problem of performing arbitrage and presenting a threshold based structure of the optimal solution. Furthermore, we also consider inelastic consumer load and renewable generation which influence storage operations for cases where the selling price is lower than the buying price of electricity. The problem of optimal energy arbitrage using storage has been the subject of many recent works e.g., [317, 148, 251, 91, 206]. Works [317, 280], [272, 166] identify that the optimal decisions for arbitrage have a threshold based structure. In our work, we present an efficient way of finding such thresholds (refer to Remark 4-7). In Chapter 3, we consider equal buy and sell price of electricity, which simplifies the optimal arbitrage problem, as the optimal storage control becomes independent of consumer load and renewable generation [335]. The system in [317, 282, 249] has rooftop solar PV and energy storage for a residential setting, similar to the system considered in this work.

Modeling uncertainty with storage control is essential for real-time operation. Authors in [325] use reinforcement learning for real-time energy arbitrage. Authors in [91], [81] use receding horizon dynamic programming for mitigating uncertainty. We used model predictive control with forecasting for reducing the effect of uncertainty over arbitrage gains.

The system considered in this chapter is described in Chapter 2.5. The chapter is organized as follows. Section 4.2 presents a mathematical framework and proposes an algorithm for solving the arbitrage problem. Section 4.3 presents an online algorithm using the proposed optimal arbitrage algorithm using ARMA forecasting in the MPC framework. Section 4.4 discusses numerical results. Section 4.5 compares run-time of proposed algorithm with convex optimization and linear programming formulations. Section 4.6 and Section 4.7 provides two case-studies providing more insights about the features of arbitrage problem. Finally, section 4.8 concludes the chapter.

4.2 Optimal Arbitrage Problem

We consider the operation of a single residential user of electricity over a fixed period of time. The user is assumed to be equipped with a rooftop solar PV and a battery to store excess generation. It is also connected to the electricity grid from where it can buy or to which it can sell energy. The objective is to find an efficient algorithm for a user to make optimal decisions over a period of varying electricity prices considering variations in the solar generation and end user load. The time duration T of the user's operation is typically chosen as one day [251, 196] since the approximate pattern of electricity prices repeats with a period of one day. The price of electricity, $p_{\text{elec}}(i)$, equals the buying price, $p_b(i)$, if the consumption is positive; otherwise $p_{\text{elec}}(i)$ equals the selling price, $p_s(i)$. Note p_{elec} is ex-ante. The ratio of selling and buying price is denoted as $\kappa_i = \frac{p_s(i)}{p_b(i)}$. The end user inelastic consumption is denoted as d_i and generates r_i units of energy through renewable sources in time step i. Net energy consumption without storage is denoted as $z_i = d_i - r_i \quad \in \mathbb{R}$. Energy consumed by the storage in the i^{th} instant is given by

$$s_i = f(x_i) = \frac{1}{\eta_{\text{ch}}}[x_i]^+ - \eta_{\text{dis}}[x_i]^-, \tag{4.2.1}$$

where $x_i = \delta_i h_i$ must lie in the range from $X^i_{\min} = \delta_{\min} h_i$ to $X^i_{\max} = \delta_{\max} h_i$. Alternatively, we can write $x_i = \eta_{\text{ch}}[s_i]^+ - \frac{1}{\eta_{\text{dis}}}[s_i]^-$. The limits on s_i are given as $s_i \in [S^i_{\min}, S^i_{\max}]$, where $S^i_{\min} = \eta_{\text{dis}}\delta_{\min} h_i$ and $S^i_{\max} = \frac{\delta_{\max} h_i}{\eta_{\text{ch}}}$. The capacity of the battery imposes the constraint $b_i \in [b_{\min}, b_{\max}], \forall i$. The total energy consumed between time step i and $i+1$ is $L_i = z_i + s_i$. The optimal arbitrage problem (denoted as P_{NEM2}) is defined as the minimization of the cost of the total consumed energy, $\min \sum_{i=1}^{N} L_i p_{\text{elec}}(i)$, subject to the battery constraints. It is given as follows:

$$(\text{P}_{\text{NEM2}}) \quad \min \sum_{i=1}^{N} C^i_{nm}(x_i),$$

subject to, $b_{\min} - b_0 \leq \sum_{j=1}^{i} x_j \leq b_{\max} - b_0, \forall i \in \{1, .., N\}$, and $x_i \in \left[X^i_{\min}, X^i_{\max}\right] \forall i \in \{1, .., N\}$ $C^i_{\text{nm}}(x_i)$ is equal to cost of consumption, i.e. $[z_i + f(x_i)]^+ p_b(i) - [z_i + f(x_i)]^- p_s(i)$ denotes cost function at the i^{th} instant. We first show that the optimal arbitrage problem is convex in $x = (x_i, i = 1 : N)$. For this convexity to hold we require $p_b(i) \geq p_s(i)$ for all $i = 1 : N$, i.e., $\kappa \in [0, 1]$. This is generally the case in most practical net metering policies [22],[56].

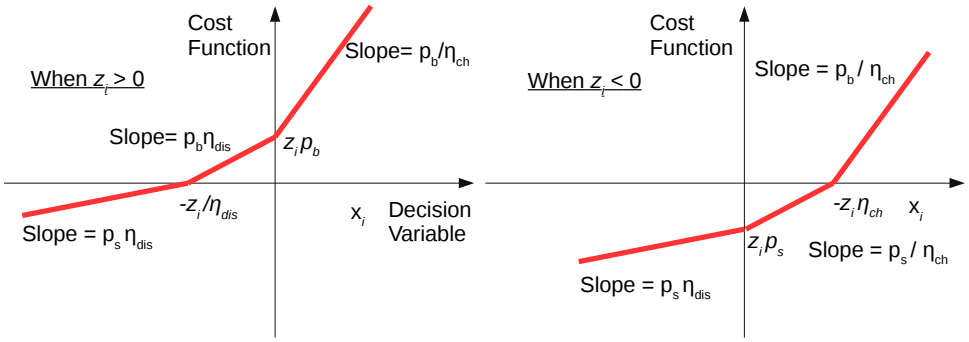

Figure 4.1: Convexity of cost function: pictorial representation

Theorem 4.2.1

If $p_b(i) \geq p_s(i)$ for all $i = 1 : N$, then problem (P_{NEM2}) is convex in x.

The proof of Theorem 4.2.1 is provided in Appendix A.3. It is evident from Fig. 4.1 that as κ_i exceeds 1, the plots will become concave. Therefore, in this work we assume $\kappa_i \in [0, 1]$. This assumption ensures that the cost function is convex. The convexity of (P_{NEM2}) established above helps us exploit the strong duality property with the dual problem (D) defined below. Finally, using this duality we find the structure of the optimal solution of (P_{NEM2}). The Lagrangian of the optimization problem described for generalized buy and sell electricity price is given as $\mathscr{L}(x, \alpha, \beta) = \sum_{i=1}^{N} \Big(C_{\text{nm}}^{(i)}(x_i) + \alpha_i \Big((b_{\min} - b_0) - \sum_{j=1}^{i} x_j \Big) + \beta_i \Big(\sum_{j=1}^{i} x_j - (b_{\max} - b_0) \Big) \Big)$. The Lagrangian dual of primal problem is (D) $\max \phi(\alpha, \beta)$, subject to, $\alpha_i, \beta_i \geq 0 \quad \forall i$, where $\phi(\alpha, \beta) = \inf_{f(x_i) \in [S_{\min}^i, S_{\max}^i]} \mathscr{L}(x, \alpha, \beta)$

Theorem 4.2.2

There exists a tuple (s^*, x^*, μ^*) with $\mu^* = (\mu_1^*, \ldots, \mu_N^*)$ such that:
(1.) $s^* = f(x^*) \quad \forall\ i$ (Refer Eq. 4.2.1).
(2.) $s^* = (s_1^*, ..., s_N^*)$ is a feasible solution of the optimal arbitrage problem (P_{NEM2}) implying $s_i \in \Big[\eta_{dis}\delta_{\min} h, \frac{\delta_{\max} h}{\eta_{ch}} \Big]$ and $b_i^* = b_0 + \sum_{j=1}^{i} x_j^* \in [b_{\min}, b_{\max}]$ for all i.
(3.) For each i, x_i^* minimizes $C_{nm}^{(i)}(x) - \mu_i^* x$. Here, μ_i^* is called the optimal accumulated Lagrange multiplier for time i and is related to the dual optimal solution (α^*, β^*) as follows $\mu_i^* = \sum_{j=i}^{N} (\alpha_j^* - \beta_j^*)$.
(4.) The optimal accumulated Lagrange multiplier, μ_i^*, at any time step i satisfies the following recursive conditions:

- $\mu_{i+1}^* = \mu_i^*$, *if* $b_{\min} < b_i^* < b_{\max}$,
- $\mu_{i+1}^* \leq \mu_i^*$, *if* $b_i^* = b_{\min}$,
- $\mu_{i+1}^* \geq \mu_i^*$, *if* $b_i^* = b_{\max}$.

(5.) Additionally μ_N^* at the last instant N satisfies

- $\mu_N^* = 0$, *if* $b_{\min} < b_N^* < b_{\max}$,
- $\mu_N^* \geq 0$, *if* $b_N^* = b_{\min}$.

For any pair (s^*, μ^*) satisfying the above conditions, s^* solves the optimal arbitrage problem (P_{NEM2}).

The proof of Theorem 4.2.2 is provided in Appendix A.4. We note that the optimality conditions stated in Theorem 4.2.2 do not depend on the particular structure of the cost function $C_{\text{nm}}^{(i)}(x_i)$ and are valid as long as it is a convex function with respect to x_i for each i. Theorem 4.2.2 is motivated from [148] and is a generalized representation of our prior work [182].

To compute the optimal solution (i.e., the optimal control decisions), we introduce the idea of a *sub-horizon* and propose a mechanism to identify such sub-horizons (see Theorem 4.2.2). A sub-horizon is a portion of time-horizon where the shadow price[1] remains constant. The shadow price is selected iteratively from discrete levels based on the price of electricity and the battery charging and discharging efficiencies

[1] In optimization, the shadow price is the value of the Lagrange multiplier at the optimal solution.

in the sub-horizon. The optimal control decisions have a threshold based structure, and these thresholds are calculated in function of the shadow prices. The accumulated Lagrange multiplier (μ^*) is considered as the shadow price of transaction.

4.2.1 Threshold Based Structure of the Optimal Solution

From condition (2) of Theorem 4.2.2 we have that the optimal control decision x_i^* in the ith instant minimizes the function $C_{\text{nm}}^{(i)}(x) - \mu_i^* x$ for $f(x_i) \in \left[S_{\min}^i, S_{\max}^i\right]$. This implies x_i^* is a function of accumulated Lagrange multiplier μ_i for time instant i. In all these cases we find out the expression for $s_i^*(\mu)$ can be directly mapped to $x_i^*(\mu)$. Below we observe that the relationship between s_i^* and μ is based on different threshold values of μ. Prior works [317, 280, 166] also indicates that the optimal actions for an energy storage device performing energy arbitrage have a threshold-based structure. We now present the different cases that may arise in terms of ratio κ_i. In the cases below we present the threshold based structure governed by the relationship between buying and selling price, battery charging and discharging efficiency and net load without storage.

Case 1: $\kappa_i = 1$

$\kappa_i = 1$ implies buying and selling price for time instant i are the same. This case is considered in Chapter 3. For equal buying and selling price, minimizing the total cost of consumption, i.e., $\sum(z_i + s_i)p_{\text{elec}}(i)$, is equivalent to minimizing the cost of operation of storage, $\sum s_i p_{\text{elec}}(i)$. Here the price of electricity, $p_{\text{elec}}(i) = p_s(i) = p_b(i)\ \forall\ i$ [182]. The threshold based structure of the optimal control decisions are presented in Remark 4.

Remark 4. Optimal control decision x_i^* minimizes the function $C_{\text{storage}}^{(i)}(s) - \mu_i^* x$ for $s \in \left[S_{\min}^i, S_{\max}^i\right]$. $s_i^*(\mu)$ is given in Eq. 4.2.2.

$$s_i^*(\mu) = \begin{cases} [S_{\min}^i, S_{\min}^i], & \text{if } \mu < p_s(i)\eta_{\text{dis}}, \\ \left[S_{\min}^i, 0\right], & \text{if } \mu = p_s(i)\eta_{\text{dis}}, \\ [0, 0], & \text{if } p_s(i)\eta_{\text{dis}} < \mu < p_b(i)/\eta_{\text{ch}}, \\ \left[0, S_{\max}^i\right], & \text{if } \mu = p_b(i)/\eta_{\text{ch}}, \\ [S_{\max}^i, S_{\max}^i], & \text{if } \mu > p_b(i)/\eta_{\text{ch}}, \end{cases} \tag{4.2.2}$$

where $C_{\text{storage}}^{(i)}(s_i) = s_i p_{\text{elec}}(i)$. Note for $\mu = p_b(i)/\eta_{\text{ch}}$ or $\mu = p_s(i)\eta_{\text{dis}}$, $s_i^*(\mu)$ takes an *envelope* of values and for any other value of μ it is a singleton set.

We would like to highlight here that for case concerning only storage device performing arbitrage in absence of any load, Eq. 4.2.2 can be applied for $\kappa_i \in [0, 1]$.

Note that $s_i^*(\mu)$ is a set-valued function in μ. It is also important to note that if $\mu_1 \leq \mu_2$ then $s_i^*(\mu_1) \preceq s_i^*(\mu_2)$, where for two sets A and B we say $A \preceq B$ (resp, $A \prec B$) if $a \leq b$ (resp $a < b$) for all $a \in A$ and for all $b \in B$. Note $x_i^* = f^{-1}(s_i^*)$. The above monotonicity property also holds for the sets $b_i^*(\mu)$, defined recursively as $b_i^*(\mu) = b_{i-1}^*(\mu) + x_i^*(\mu)$ for $i \geq 1$ and $b_0^*(\mu) = b_0$. Here, the addition of two intervals $[a, b]$ and $[c, d]$ denotes the interval $[a + c, b + d]$. Note that when μ lies between $p_s(i)\eta_{\text{dis}}$ and $p_b(i)/\eta_{\text{ch}}$, the optimal action for the battery is to do nothing, thus the cycles of operation that a battery performs can be controlled by introducing a friction coefficient facilitating the elimination of low returning transactions [174]. In [181] we show that this friction term can be tuned to maximize the battery life.

Case 2: $\kappa_i \in [0, \eta_{\text{ch}}\eta_{\text{dis}})$

For $\kappa_i \in [0, \eta_{\text{ch}}\eta_{\text{dis}})$ implies $p_s(i)/\eta_{ch} < p_b(i)\eta_{dis}$. Since $\eta_{ch} < 1, \eta_{dis} < 1$, therefore, $p_b > p_s$ is valid. The optimal thresholds based on the value of μ are given by Remark 5.

Remark 5. *The optimal control decision s_i^* minimizes the function $C_{nm}^{(i)}(f(x)) - \mu_i^* x$ for $f(x) \in \left[S_{\min}^i, S_{\max}^i\right]$. The optimal decision $s_i^*(\mu)$ is given by Eq. 4.2.3.*

$$
s_i^*(\mu) \in \begin{cases}
\begin{cases} \left[S^i_{\min}, S^i_{\min}\right], & \text{if } \mu < \eta_{\text{dis}} p_s(i), \\ \left[S^i_{\min}, \max(-z_i, S^i_{\min})\right], & \text{if } z_i \geq 0, \\ \left[S^i_{\min}, 0\right], & \text{if } z_i < 0, \end{cases} & \text{if } \mu = \eta_{\text{dis}} p_s(i) \\
\begin{cases} \left[\max(-z_i, S^i_{\min}), \max(-z_i, S^i_{\min})\right], & \text{if } z_i \geq 0, \\ [0, 0], & \text{if } z_i < 0, \end{cases} & \text{if } \eta_{\text{dis}} p_s(i) < \mu < \frac{p_s(i)}{\eta_{\text{ch}}} \\
\begin{cases} \left[\max(-z_i, S^i_{\min}), \max(-z_i, S^i_{\min})\right], & \text{if } z_i \geq 0, \\ \left[0, \min(-z_i, S^i_{\max})\right], & \text{if } z_i < 0, \end{cases} & \text{if } \mu = \frac{p_s(i)}{\eta_{\text{ch}}} \\
\begin{cases} \left[\max(-z_i, S^i_{\min}), \max(-z_i, S^i_{\min})\right], & \text{if } z_i \geq 0, \\ \left[\min(-z_i, S^i_{\max}), \min(-z_i, S^i_{\max})\right], & \text{if } z_i < 0, \end{cases} & \text{if } \frac{p_s(i)}{\eta_{\text{ch}}} < \mu < \eta_{\text{dis}} p_b(i) \\
\begin{cases} \left[\max(-z_i, S^i_{\min}), 0\right], & \text{if } z_i \geq 0, \\ \left[\min(-z_i, S^i_{\max}), \min(-z_i, S^i_{\max})\right], & \text{if } z_i < 0, \end{cases} & \text{if } \mu = \eta_{\text{dis}} p_b(i) \\
\begin{cases} [0, 0], & \text{if } z_i \geq 0, \\ \left[\min(-z_i, S^i_{\max}), \min(-z_i, S^i_{\max})\right], & \text{if } z_i < 0, \end{cases} & \text{if } \eta_{\text{dis}} p_b(i) < \mu < \frac{p_b(i)}{\eta_{\text{ch}}} \\
\begin{cases} \left[0, S^i_{\max}\right], & \text{if } z_i \geq 0, \\ \left[\min(-z_i, S^i_{\max}), S^i_{\max}\right], & \text{if } z_i < 0, \end{cases} & \text{if } \mu = \frac{p_b(i)}{\eta_{\text{ch}}} \\
\left[S^i_{\max}, S^i_{\max}\right], & \text{if } \mu > \frac{p_b(i)}{\eta_{\text{ch}}}
\end{cases}
\tag{4.2.3}
$$

Proof. For a given $\mu_i^* = \mu$ the optimal decision $s_i^*(\mu)$ is given by minimizing Eq. 4.2.4.

$$
[z_i + s_i]^+ p_b(i) - [z_i + s_i]^- p_s(i) - \mu\left(\eta_{\text{ch}}[s_i]^+ - \frac{1}{\eta_{\text{dis}}}[s_i]^-\right) \tag{4.2.4}
$$

Hence, in order to minimize Eq. 4.2.4 we consider the sign of $(z_i + s_i)$ and s_i. This will provide the following cases

J1: $s_i(p_b(i) - \mu\eta_{\text{ch}})$ s.t. $z_i + s_i \geq 0$ and $s_i \in [0, S_{\max}]$,

J2: $s_i(p_s(i) - \mu\eta_{\text{ch}})$ s.t. $z_i + s_i \leq 0$ and $s_i \in [0, S_{\max}]$,

J3: $s_i\left(p_b(i) - \frac{\mu}{\eta_{\text{dis}}}\right)$ s.t. $z_i + s_i \geq 0$ and $s_i \in [S_{\min}, 0]$,

J4: $s_i\left(p_s(i) - \frac{\mu}{\eta_{\text{dis}}}\right)$ s.t. $z_i + s_i \leq 0$ and $s_i \in [S_{\min}, 0]$.

The accumulated Lagrange multiplier, μ, can be viewed as the shadow price of decision making. Based on conditions J1 to J4, the value of μ will divide the price levels into nine cases. Table 4.1 lists the constraints and minimizing conditions, we will use this table to find optimal value of s_i^*. From Table 4.1 we can see the conditions of desired

Table 4.1: Conditions to check

Tag	$[z_i + s_i]$	$[s_i]$	min Condition	Desired scenario
J1	+ve	+ve	$s_i(p_b(i) - \mu\eta_{\text{ch}})$	$(p_b(i) - \mu\eta_{\text{ch}}) \leq 0$
J2	-ve	+ve	$s_i(p_s(i) - \mu\eta_{\text{ch}})$	$(p_s(i) - \mu\eta_{\text{ch}}) \leq 0$
J3	+ve	-ve	$s_i(p_b(i) - \frac{\mu}{\eta_{\text{dis}}})$	$(p_b(i) - \frac{\mu}{\eta_{\text{dis}}}) \geq 0$
J4	-ve	-ve	$s_i(p_s(i) - \frac{\mu}{\eta_{\text{dis}}})$	$(p_s(i) - \frac{\mu}{\eta_{\text{dis}}}) \geq 0$

scenarios. Based on conditions J1 to J4, we observe four distinct levels in price signal which will subsequently divide the real line into nine possible levels for the accumulated Lagrange multiplier (μ) as shown in Fig 4.2.

Region 1: $\mu < \eta_{\text{dis}} p_s(i)$: The minimizing conditions will be achieved by J3 and J4 as shown below:

Tag	$[z_i + s_i]$	$[s_i]$	min Condition	Sign	Comment
J1	+ve	+ve	$s_i(p_b(i) - \mu\eta_{\text{ch}})$	+ (+)	Undesired
J2	-ve	+ve	$s_i(p_s(i) - \mu\eta_{\text{ch}})$	+ (+)	Undesired
J3	+ve	-ve	$s_i(p_b(i) - \frac{\mu}{\eta_{\text{dis}}})$	- (+)	Desired
J4	-ve	-ve	$s_i(p_s(i) - \frac{\mu}{\eta_{\text{dis}}})$	- (+)	Desired

From J4 if $(z_i + s_i) < 0$ then $s_i^* = [S_{\min}, S_{\min}]$ and from J3 if $(z_i + s_i) \geq 0$ then $s_i^* = [S_{\min}, S_{\min}]$. Therefore, irrespective the sign of z_i the optimal value is $[S_{\min}, S_{\min}]$.

Region 2: $\mu = \eta_{\text{dis}} p_s(i)$: The minimizing conditions will be achieved by J3 and J4 is a don't care condition with only constraint on s_i being negative or zero.

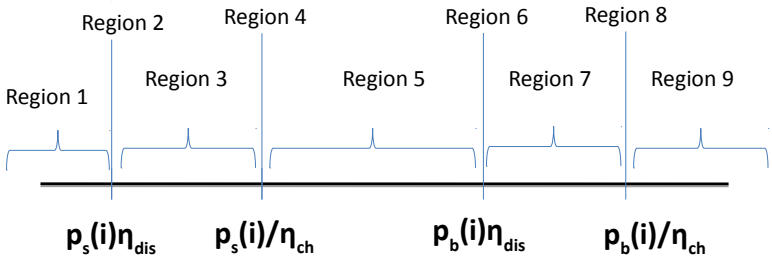

Figure 4.2: Cases based on levels of μ

Tag	$[z_i + s_i]$	$[s_i]$	min Condition	Sign	Comment
J1	+ve	+ve	$s_i(p_b(i) - \mu\eta_{\text{ch}})$	+ (+)	Undesired
J2	-ve	+ve	$s_i(p_s(i) - \mu\eta_{\text{ch}})$	+ (+)	Undesired
J3	+ve	-ve	$s_i(p_b(i) - \frac{\mu}{\eta_{\text{dis}}})$	- (+)	Desired
J4	-ve	-ve	$s_i(p_s(i) - \frac{\mu}{\eta_{\text{dis}}})$	- (0)	Don't Care

Sub-Case 1: from J3 and J2 if $z_i \geq 0$ then $s_i^* = [S_{\min}, \max(-z_i, S_{\min})]$.

Sub-Case 2: from J4 if $z_i < 0$ then $s_i^* = [S_{\min}, 0]$.

Region 3: $\mu \in (\eta_{\text{dis}} p_s(i), \frac{p_s(i)}{\eta_{\text{ch}}})$: The minimizing conditions will be achieved by minimizing J3. All other conditions, i.e., J1, J2 and J4 are undesired.

Tag	$[z_i + s_i]$	$[s_i]$	min Condition	Sign	Comment
J1	+ve	+ve	$s_i(p_b(i) - \mu\eta_{\text{ch}})$	+ (+)	Undesired
J2	-ve	+ve	$s_i(p_s(i) - \mu\eta_{\text{ch}})$	+ (+)	Undesired
J3	+ve	-ve	$s_i(p_b(i) - \frac{\mu}{\eta_{\text{dis}}})$	- (+)	Desired
J4	-ve	-ve	$s_i(p_s(i) - \frac{\mu}{\eta_{\text{dis}}})$	- (-)	Undesired

Sub-Case 1: from J3 if $z_i \geq 0$ then $s_i^* = [\max\{-z_i, S_{\min}\}, \max\{-z_i, S_{\min}\}]$.

Sub-Case 2: from J2 and J4 $s_i^* = [0, 0]$.

Region 4: $\mu = \frac{p_s(i)}{\eta_{\text{ch}}}$: The minimizing conditions will be achieved by minimizing J3. J2 is a don't care condition.

Tag	$[z_i + s_i]$	$[s_i]$	min Condition	Sign	Comment
J1	+ve	+ve	$s_i(p_b(i) - \mu\eta_{\text{ch}})$	+ (+)	Undesired
J2	-ve	+ve	$s_i(p_s(i) - \mu\eta_{\text{ch}})$	+ (0)	Don't Care
J3	+ve	-ve	$s_i(p_b(i) - \frac{\mu}{\eta_{\text{dis}}})$	- (+)	Desired
J4	-ve	-ve	$s_i(p_s(i) - \frac{\mu}{\eta_{\text{dis}}})$	- (-)	Undesired

Sub-Case 1: from J3 if $z_i \geq 0$ then $s_i^* = [\max\{-z_i, S_{\min}\}, \max\{-z_i, S_{\min}\}]$.

Sub-Case 2: from J2, if $z_i < 0$ then $s_i^* = [0, \min\{-z_i, S_{\max}\}]$.

Region 5: $\mu \in (\frac{p_s(i)}{\eta_{\text{ch}}}, \eta_{\text{dis}} p_b(i))$: The minimizing conditions will be achieved by minimizing J2 and J3.

Tag	$[z_i + s_i]$	$[s_i]$	min Condition	Sign	Comment
J1	+ve	+ve	$s_i(p_b(i) - \mu\eta_{\text{ch}})$	+ (+)	Undesired
J2	-ve	+ve	$s_i(p_s(i) - \mu\eta_{\text{ch}})$	+ (-)	Desired
J3	+ve	-ve	$s_i(p_b(i) - \frac{\mu}{\eta_{\text{dis}}})$	- (+)	Desired
J4	-ve	-ve	$s_i(p_s(i) - \frac{\mu}{\eta_{\text{dis}}})$	- (-)	Undesired

Sub-Case 1: from J3 if $z_i \geq 0$ then $s_i^* = [\max\{-z_i, S_{\min}\}, \max\{-z_i, S_{\min}\}]$.

Sub-Case 2: from J2, if $z_i < 0$ then $s_i^* = [\min\{-z_i, S_{\max}\}, \min\{-z_i, S_{\max}\}]$.

Region 6: $\mu = \eta_{\text{dis}} p_b(i)$: The minimizing conditions will be achieved by J2 and J3 is a don't care condition with only constraint on s_i being negative or zero.

Tag	$[z_i + s_i]$	$[s_i]$	min Condition	Sign	Comment
J1	+ve	+ve	$s_i(p_b(i) - \mu\eta_{\text{ch}})$	+ (+)	Undesired
J2	-ve	+ve	$s_i(p_s(i) - \mu\eta_{\text{ch}})$	+ (-)	Desired
J3	+ve	-ve	$s_i(p_b(i) - \frac{\mu}{\eta_{\text{dis}}})$	- (0)	Don't Care
J4	-ve	-ve	$s_i(p_s(i) - \frac{\mu}{\eta_{\text{dis}}})$	- (-)	Undesired

Sub-Case 1: from J3 if $z_i \geq 0$ then $s_i^* = [\max\{-z_i, S_{\min}\}, 0]$.
Sub-Case 2: from J2 if $z_i < 0$ then $s_i^* = [\min\{-z_i, S_{\max}\}, \min\{-z_i, S_{\max}\}]$.

Region 7: $\mu \in (\eta_{\text{dis}} p_b(i), \frac{p_b(i)}{\eta_{\text{ch}}})$: The minimizing conditions will be achieved by J2. All other cases will be undesirable.

Tag	$[z_i + s_i]$	$[s_i]$	min Condition	Sign	Comment
J1	+ve	+ve	$s_i(p_b(i) - \mu\eta_{\text{ch}})$	+ (+)	Undesired
J2	-ve	+ve	$s_i(p_s(i) - \mu\eta_{\text{ch}})$	+ (-)	Desired
J3	+ve	-ve	$s_i(p_b(i) - \frac{\mu}{\eta_{\text{dis}}})$	- (-)	Undesired
J4	-ve	-ve	$s_i(p_s(i) - \frac{\mu}{\eta_{\text{dis}}})$	- (-)	Undesired

Sub-Case 1: from J2 if $z_i < 0$ then $s_i^* = [\min\{-z_i, S_{\max}\}, \min\{-z_i, S_{\max}\}]$.
Sub-Case 2: if $z_i \geq 0$ then do nothing, $s_i^* = [0, 0]$. This is because J1 and J3 covers two direction of movement i.e. charging and discharging, both of which will increase the objective function.

Region 8: $\mu = \frac{p_b(i)}{\eta_{\text{ch}}}$: The minimizing conditions will be achieved by J2 and J1 is a don't care condition.

Tag	$[z_i + s_i]$	$[s_i]$	min Condition	Sign	Comment
J1	+ve	+ve	$s_i(p_b(i) - \mu\eta_{\text{ch}})$	+ (0)	Don't Care
J2	-ve	+ve	$s_i(p_s(i) - \mu\eta_{\text{ch}})$	+ (-)	Desired
J3	+ve	-ve	$s_i(p_b(i) - \frac{\mu}{\eta_{\text{dis}}})$	- (-)	Undesired
J4	-ve	-ve	$s_i(p_s(i) - \frac{\mu}{\eta_{\text{dis}}})$	- (-)	Undesired

Sub-Case 1: from J2 and J1 if $z_i < 0$ then $s_i^* = [\min\{-z_i, S_{\max}\}, S_{\max}]$.
Sub-Case 2: from J1 is $z_i \geq 0$ then $s_i^* = [0, S_{\max}]$.

Region 9: $\mu > \frac{p_b(i)}{\eta_{\text{ch}}}$: The minimizing conditions will be achieved by J2 and J1.

Tag	$[z_i + s_i]$	$[s_i]$	min Condition	Sign	Comment
J1	+ve	+ve	$s_i(p_b(i) - \mu\eta_{\text{ch}})$	+ (-)	Desired
J2	-ve	+ve	$s_i(p_s(i) - \mu\eta_{\text{ch}})$	+ (-)	Desired
J3	+ve	-ve	$s_i(p_b(i) - \frac{\mu}{\eta_{\text{dis}}})$	- (-)	Undesired
J4	-ve	-ve	$s_i(p_s(i) - \frac{\mu}{\eta_{\text{dis}}})$	- (-)	Undesired

Irrespective of sign of z_i, $s_i^* = [S_{\max}, S_{\max}]$. □

Case 3: $\kappa_i \in (\eta_{\text{ch}}\eta_{\text{dis}}, 1)$

For $p_b(i) > p_s(i)$ and $p_s(i)/\eta_{ch} > p_b(i)\eta_{\text{dis}}$ optimal thresholds based on the value of μ are given by Remark 6.

Remark 6. *The optimal control decision s_i^* minimizes the function $C_{nm}^{(i)}(f(x)) - \mu_i^* x$ for $f(x) \in \left[S_{\min}^i, S_{\max}^i\right]$. The optimal decision $s_i^*(\mu)$ is given by Eq. 4.2.5.*

$$
s_i^*(\mu) \in \begin{cases}
\left\{ \left[S_{\min}^i, S_{\min}\right]^i, \quad \text{if } \mu < \eta_{\text{dis}} p_s(i), \right. \\
\begin{cases} \left[S_{\min}^i, \max(-z_i, S_{\min}^i)\right], & \text{if } z_i \geq 0, \\ \left[S_{\min}^i, 0\right], & \text{if } z_i < 0, \end{cases} \quad \text{if } \mu = \eta_{\text{dis}} p_s(i) \\
\begin{cases} \left[\max(-z_i, S_{\min}^i), \max(-z_i, S_{\min}^i)\right], & \text{if } z_i \geq 0, \\ [0, 0], & \text{if } z_i < 0, \end{cases} \quad \text{if } \eta_{\text{dis}} p_s(i) < \mu < \eta_{\text{dis}} p_b(i) \\
\begin{cases} \left[\max(-z_i, S_{\min}^i), 0\right], & \text{if } z_i \geq 0, \\ [0, 0], & \text{if } z_i < 0, \end{cases} \quad \text{if } \mu = \eta_{\text{dis}} p_b(i) \\
\left\{ [0, 0], \quad \text{if } \eta_{\text{dis}} p_b(i) < \mu < \frac{p_s(i)}{\eta_{\text{ch}}} \right. \\
\begin{cases} [0, 0], & \text{if } z_i \geq 0, \\ \left[0, \min(-z_i, S_{\max}^i)\right], & \text{if } z_i < 0, \end{cases} \quad \text{if } \mu = \frac{p_s(i)}{\eta_{\text{ch}}} \\
\begin{cases} [0, 0], & \text{if } z_i \geq 0, \\ \left[\min(-z_i, S_{\max}^i), \min(-z_i, S_{\max}^i)\right], & \text{if } z_i < 0, \end{cases} \quad \text{if } \frac{p_s(i)}{\eta_{\text{ch}}} < \mu < \frac{p_b(i)}{\eta_{\text{ch}}} \\
\begin{cases} \left[0, S_{\max}^i\right], & \text{if } z_i \geq 0, \\ \left[\min(-z_i, S_{\max}^i), S_{\max}^i\right], & \text{if } z_i < 0, \end{cases} \quad \text{if } \mu = \frac{p_b(i)}{\eta_{\text{ch}}} \\
\left\{ \left[S_{\max}^i, S_{\max}^i\right], \quad \text{if } \mu > \frac{p_b(i)}{\eta_{\text{ch}}}, \right.
\end{cases}
\tag{4.2.5}
$$

The proof of Remark 4 is provided in Appendix A.5. Note by substituting $p_b(i) = p_s(i)$ in Eq. 4.2.5 and taking the union of the ranges, Case 3 can be simplified to Case 1.

Case 4: $\kappa_i = \eta_{\mathbf{ch}}\eta_{\mathbf{dis}}$

For $p_b(i) > p_s(i)$ and $p_s(i)/\eta_{ch} = p_b(i)\eta_{\text{dis}}$ optimal thresholds based on the value of μ are given by Remark 7.

Remark 7. *The optimal control decision s_i^* minimizes the function $C_{nm}^{(i)}(f(x)) - \mu_i^* x$ for $f(x) \in \left[S_{\min}^i, S_{\max}^i\right]$. The optimal decision $s_i^*(\mu)$ is given by Eq. 4.2.6.*

The proof of Remark 4 is provided in Appendix A.6.

$$
s_i^*(\mu) \in \begin{cases}
\left\{ \left[S_{\min}^i, S_{\min}\right]^i, & \text{if } \mu < \eta_{\text{dis}} p_s(i), \\
\begin{cases} \left[S_{\min}^i, \max(-z_i, S_{\min}^i)\right], & \text{if } z_i \geq 0, \\ \left[S_{\min}^i, 0\right], & \text{if } z_i < 0, \end{cases} & \text{if } \mu = \eta_{\text{dis}} p_s(i) \\
\begin{cases} \left[\max(-z_i, S_{\min}^i), \max(-z_i, S_{\min}^i)\right], & \text{if } z_i \geq 0, \\ [0, 0], & \text{if } z_i < 0, \end{cases} & \text{if } \eta_{\text{dis}} p_s(i) < \mu < \eta_{\text{dis}} p_b(i) \\
\begin{cases} \left[\max(-z_i, S_{\min}^i), 0\right], & \text{if } z_i \geq 0, \\ \left[0, \min(-z_i, S_{\max}^i)\right], & \text{if } z_i < 0, \end{cases} & \text{if } \mu = \eta_{\text{dis}} p_b(i) \\
\begin{cases} [0, 0], & \text{if } z_i \geq 0, \\ \left[\min(-z_i, S_{\max}^i), \min(-z_i, S_{\max}^i)\right], & \text{if } z_i < 0, \end{cases} & \text{if } \frac{p_s(i)}{\eta_{\text{ch}}} < \mu < \frac{p_b(i)}{\eta_{\text{ch}}} \\
\begin{cases} \left[0, S_{\max}^i\right], & \text{if } z_i \geq 0, \\ \left[\min(-z_i, S_{\max}^i), S_{\max}^i\right], & \text{if } z_i < 0, \end{cases} & \text{if } \mu = \frac{p_b(i)}{\eta_{\text{ch}}} \\
\left\{ \left[S_{\max}^i, S_{\max}^i\right], & \text{if } \mu > \frac{p_b(i)}{\eta_{\text{ch}}}, \end{cases}
\end{cases} \tag{4.2.6}
$$

By substituting $p_b\eta_{dis} = p_s/\eta_{ch}$ in Eq. 4.2.5 and taking the union of the ranges, Case 3 can be simplified to Case 4.

4.2.2 Proposed Algorithm

In this section we describe the algorithm we propose to solve the optimal energy arbitrage problem formulated previously. The objective of the algorithm is to find a tuple (s^*, x^*, μ^*) that satisfies conditions (1)-(5) of Theorem 4.2.2, and therefore solves (P_{NEM2}). The proposed algorithm is developed for Case 1 to 4, described in the previous section, using Remark 4, 5, 6 and 7 for lossy battery. The presented algorithm could be operated for a variable value of κ_i, such that $\kappa_i \in [0, 1]\ \forall\ i$, covering all net-metering compensation scheme. Algorithm 6 illustrates its main steps. Based on the value of κ_i the lower and upper bound of the envelope is selected, lines 4–8 of the pseudo code of Algorithm 6. From condition (4) of the theorem, we can see that μ_{i+1}^* may differ from the optimal accumulated Lagrange multiplier, μ_i^*, only when $b_i^* = b_{\max}$ or $b_i^* = b_{\min}$. This means that the value of μ remains constant as long as the battery level at a time instant lies strictly within the battery capacity limits. Based on this key idea, the whole duration T is divided into M periods, indexed as $\{1, 2, \ldots, M\}$. Each period contains a number of consecutive time instants, such that for all instants i belonging to the same period $K \in \{1, 2, \ldots, M\}$ the value of the accumulated Lagrange multiplier μ_i^* remains the same, denoted as μ_K. Each such period is called *sub-horizon*. It follows that at the end instant of each sub-horizon, the battery energy level touches either $b_{\max}$ or $b_{\min}$. Note that the number of sub-horizons (M), the start and end instants of each sub-horizon K, the μ_K value, and the optimal actions in sub-horizon K depend on the problem instance and are determined recursively, as described below.

Assume that we have already identified the first $K-1$ ($K \geq 1$) sub-horizons and determined the values of s_i^* and μ_i^* in all instants i belonging to these sub-horizons (for $i \in [1, i_{K-1}]$). The index i_{K-1} denotes the last instant in the $(K-1)$th sub-horizon. Hence:

If $i_{K-1} = N$, then we have already covered the whole period T and the algorithm terminates.

If $i_{K-1} < N$, then we proceed to identify the next sub-horizon K, i.e., the values of i_K (the last instant in sub-horizon K), μ_K, and the optimal decisions for the time instants $i \in [i_{K-1} + 1, i_K]$.

To determine sub-horizon K, we start with instant $i_{K-1}+1$ and an initial value of $\mu_K \geq 0$ for that sub-horizon[2]. We compute the values of $s_i^*(\mu_K)$ and $b_i^*(\mu_K)$[3] according to the method described in Remark 4, 5, 6 and 7, for all consecutive time instants $i > i_{K-1}$ until we reach a time instant $i = i_{\text{break}}$, for which one of the following conditions is satisfied (we call these as the *violation conditions*):

C1: $b^*_{i_{\text{break}}}(\mu_K) \prec \{b_{\min}\}$.

C2: $\{b_{\max}\} \prec b^*_{i_{\text{break}}}(\mu_K)$.

C3: $i_{\text{break}} = N, b_{\min} \notin b_N^*(\mu_K), \mu_K > 0$.

If no i_{break} is found even after reaching $i = N$, then K is the last sub-horizon and we set $i_K = N$ (and lines 36–43 of the pseudo code are executed). From condition (5) of Theorem 4.2.2, if $\mu_K > 0$, then $b_N^* = b_{\min}$; else b_N^* can take any value in the set $[b_{\min}, b_{\max}) \cap b_N^*(\mu_K)$. The optimal decisions of x_i^* and b_i^*, for $i \in [i_{K-1}+1, N]$, are calculated by using Algorithm 7, discussed in more detail later.

Tuning μ value: Since the cost function in problem (P_{NEM2}) is piecewise linear, the optimal values of the accumulated Lagrange multipliers μ_i^* are chosen from a discrete set of values corresponding to buying and selling prices of electricity. This feature transforms (P_{NEM2}) from a continuous optimization problem to a discrete one. Therefore, in the proposed solution, we specify how to tune the Lagrange multipliers to these prices to find their optimal values (lines 18, 20 in the pseudo code). Now, if condition C1 holds; for the chosen value of μ_K, the battery capacity limit is violated from below at instant i_{break} since the set $b_{i_{\text{break}}}(\mu)$ lies strictly below $b_{\min}$. The strategy here is to increase μ_K value to the

$$\mu_K = \min\{p > \mu : p \in p_{\text{s}}(i)\eta_{\text{dis}}, p_{\text{s}}(i)/\eta_{\text{ch}}, p_{\text{b}}(i)\eta_{\text{dis}}, p_{\text{b}}(i)/\eta_{\text{ch}}; i_{K-1} < i \leq i_{\text{break}}\}.$$

Otherwise, if condition C2 or condition C3 holds, then μ_K is decreased to

$$\mu_K = \max\{p < \mu : p \in p_{\text{s}}(i)\eta_{\text{dis}}, p_{\text{s}}(i)/\eta_{\text{ch}}, p_{\text{b}}(i)\eta_{\text{dis}}, p_{\text{b}}(i)/\eta_{\text{ch}}; i_{K-1} < i \leq i_{\text{break}}\}.$$

After updating μ_K value, we repeat the same process as before until we reach a new time instant i_{break}, for which one of the above conditions is satisfied. Note there is a one-to-one mapping of s_i and x_i, therefore, $x_i^*(\mu_K)$ and consequently $b_i^*(\mu_K)$ are monotonically non-decreasing functions in μ_K, the potential effect of the update of μ_K is that i_{break} is pushed to a later instant. The update of μ_K is repeated as long as i_{break} increases (or remains the same), compared to its previous value, stored in i_{mem}. This part of the proposed algorithm is mirrored in lines 15–21 of the pseudo-code of Algorithm 6. If the value of i_{break} decreases after updating μ_K, then for the previous value μ_{mem} of μ_K there must have been an instant $i \in [i_{K-1}+1, i_{\text{mem}}]$, where $b_{\max} \in b_i^*(\mu_K)$ (violation occurred due to C1) or $b_{\min} \in b_i^*(\mu_K)$ (violation occurred due to C2 or C3). This is due to the fact that both μ_{mem} and μ_K always lie in the range $\{p_{\text{s}}(i)\eta_{\text{dis}}, p_{\text{s}}(i)/\eta_{\text{ch}}, p_{\text{b}}(i)\eta_{\text{dis}}, p_{\text{b}}(i)/\eta_{\text{ch}}\}$, for all $i > i_{K-1}$. At this point of the algorithm (lines 22–34 of the pseudo-code), μ_K and i_{break} are switched back to their previous values, which are saved, respectively, in μ_{mem} and i_{mem}. This value of μ_K is selected as the final value of the optimal accumulated Lagrange multiplier corresponding to sub-horizon K. The end instant of sub-horizon K, i_K, is set equal to the latest time instant $i \in [i_{K-1}+1, i_{\text{break}}]$, for which $b_{\min} \in b_i^*(\mu_K)$ or $b_{\max} \in b_i^*(\mu_K)$, and $b^*_{i_K}$ takes the value $b_{\min}$ in the former case and $b_{\max}$ in the later case.

Using Algorithm 6 we find the optimal battery capacity in a sub-horizon, $b^*(\mu_K)$. $b^*(\mu_K) \cap [b_{\min}, b_{\max}]$ contains information of the lower and upper feasible envelope of battery capacity. We propose a novel method based on backward step to find the optimal solution among infinite possibilities, described as `BackwardStep`, in Algorithm 7. Note that the `BackwardStep` algorithm is implemented only one time for a sub-horizon. For each i in the range $i_{K-1}+1 \leq i < i_K$, the optimal battery level b_i^* is found from b_{i+1}^* through the function `BackwardStep` which uses the backward recursion $b_i^* = (b_{i+1}^* - x_{i+1}^*(\mu_K)) \cap b_i^*(\mu_K) \cap [b_{\min}, b_{\max}]$. If the above backward recursion returns a set, then any arbitrary value in the set is chosen to be the optimal battery level. We note here that the optimal solution to (P) needs not be unique since its objective function is not strictly convex. We also found out that intermediate ramp rates could be optimal contrary to [170, 325], wherein optimal actions have three possibilities i.e. stay idle or charge or discharge at a maximum possible rate. A stylized example demonstrating the operation of proposed optimal arbitrage algorithm is presented in Appendix 3.2.4.

[2]For the first sub-horizon K=1 (that includes the first time instant) the starting guess value of μ_1 is taken to be 0 and for every other sub-horizon $K > 1$, the starting guess value of μ_K is taken to be equal to μ_{K-1}. Note that these choices do not affect the solution given by the algorithm.

[3]$b_i^*(\mu_K)$ is a set containing the values of lower and upper envelope of optimal battery capacity for the scalar value of μ_K.

Complexity Analysis: Using the discrete nature of the optimization problem, we explicitly characterize the worst case run time of the proposed algorithm. For any sub-horizon starting from instant i, there may be at most $N-i+1$ more time instants which may be included in the same sub-horizon. Hence, in order to find the optimal accumulated Lagrange multiplier for the sub-horizon, we may have to update the value of μ_K in the sub-horizon at most $2(N-i+1)$ times (for each instant i two possible values $p_{\text{dis}}(i)$, $p_{\text{ch}}(i)$ may be checked for equal buying and selling price of electricity and four possible values $p_{\text{s}}(i)\eta_{\text{dis}}, p_{\text{s}}(i)/\eta_{\text{ch}}, p_{\text{b}}(i)\eta_{\text{dis}}, p_{\text{b}}(i)/\eta_{\text{ch}}$ may be checked for selling price strictly lower than buying price). For each update, a basic set of operations is performed. Furthermore, there may be separate sub-horizons starting from every time instant $i \in [1, N]$. Hence, a crude upper bound on the number of times the basic set of operations are needed to be repeated is $\sum_{i=1}^{N} 2(N-i+1) = O(N^2)$. Hence, the worst case time complexity of the proposed algorithm is $O(N^2)$. In most situations, however, the number of instants included in a sub-horizon does not grow with N. Hence, in most cases the proposed algorithm would be performed linearly in time. Run-time comparison of convex optimization, linear programming and proposed algorithm for performing arbitrage is shown in Appendix 4.5, it is observed that run-time complexity grows approximately linearly with number of samples in optimization horizon. The proposed algorithm outperforms the other benchmarks.

4.2.3 Open Source Codes

The optimal arbitrage algorithm developed in this chapter is made open source. The link for the code is https://github.com/umar-hashmi/NetMetering. The benchmarks used for optimal arbitrage algorithm are also made open source for evaluation. The linear programming formulation can be found here https://github.com/umar-hashmi/linearprogrammingarbitrage. The LP formulation details are provided in Appendix B. The convex optimization formulation can be found here https://github.com/umar-hashmi/ArbitrageConvex. The CVX formulation details are provided in Appendix A.8.

4.3 Online Implementation of Proposed Algorithm

The problem of real time energy arbitrage consists of two coupled problems: firstly, optimal arbitrage algorithm and secondly, forecasting future parameters like electricity price, end user demand and solar PV generation required for performing optimal arbitrage. Due to the mismatch in forecasted and actual parameter values, the arbitrage gains will likely be lower than deterministic optimal arbitrage gains. In this section we present an online algorithm which uses incrementally improving forecasting of parameters along with Model Predictive Control (MPC) to decide optimal control actions. MPC is used to optimize the decisions in current time slots, while taking into account future time slots. In the receding horizon the forecast is updated and MPC is implemented again, till end time is reached. In our proposed optimal arbitrage algorithm, `OptimalArbitrage`, we emphasized that the optimal control decisions are independent of past or future values of price, solar generation and consumer inelastic demand beyond the considered sub-horizon. This suggests we only need to accurately forecast for time instants in proximity to the current time instant, as optimal actions beyond the current sub-horizon are not influenced by parameters in future sub-horizons. However, quantifying the length of a sub-horizon is challenging since it is governed by storage parameters and variation of prices. A sub-horizon denotes the optimal lookahead in future intervals for selecting control decisions. In Section 3.5 we present a heuristic based analysis to quantify the lookahead required based on storage type. We observe in this case-study that the optimal lookahead for performing arbitrage depends on the ratio of ramp rate over capacity, battery efficiency, sampling time and κ. For batteries with high ratio of ramp rate over capacity, the lookahead required is smaller compared to batteries with lower ratio of ramp rate over capacity.

The deterministic arbitrage gains is denoted as V_a^*. This denotes the maximum value obtained by arbitrage for actual value of parameters under complete information about future variations of parameters. It is given as $V_a^* = \sum_{i=1}^{N} p_{\text{elec}}(i)(z_i - L_i^*(z_i, p_{\text{elec}}(i)))$, where L_i^*. The real arbitrage gains that the end user would make using optimal actions are calculated using forecasted parameters. Due to forecast errors, the end user's energy arbitrage gains are affected. Realistic arbitrage gain,V_r, is the energy arbitrage gain made by following the same actions as calculated for forecasted signals and is denoted as $V_r = \sum_{i=1}^{N} p_{\text{elec}}(i)(z_i - \hat{L}_i^*(\hat{z}_i, \hat{p}_{\text{elec}}(i)))$. $\hat{L}_i^*$ is the optimal end user net consumption for the forecasted price signal, $\hat{p}_{\text{elec}}(i)$, and forecasted load vector, $\hat{z}$. It is evident that $V_a^* \geq V_r$. In this section we show how adaptive forecasting and MPC can efficiently mitigate the effects of forecast error on user's arbitrage gains.

Our objective is to calculate energy arbitrage gains sequentially with incrementally improving the

Algorithm 6 `OptimalArbitrage`(p_b, p_s, b_0)

Inputs: N, T, $h = (h_1, h_2, \ldots, h_N)$, $p_b = (p_b^1, p_b^2, \ldots, p_b^N)$, $p_s = (p_s^1, p_s^2, \ldots, p_s^N)$, b_0, $z = (z_1, z_2, ..., z_N)$,
Parameters: $b_{\max}, b_{\min}, \delta_{\max}, \delta_{\min}, \eta_{\text{ch}}, \eta_{\text{dis}}$
Outputs: s^*=$(s_1^*, s_2^*, .., s_N^*)$, b^*=$(b_1^*, b_2^*, .., b_N^*)$, μ^*=$(\mu_1^*, \mu_2^*, .., \mu_K^*)$
Initialize: K=1; μ_K=μ_{mem}=0; i_{K-1}=i_K=i_{mem}=0; `BreakFlag`=0

while $i_K < N$ **do**
  for $i = i_{K-1} + 1$ to N **do**
    Compute $\kappa_i = p_s(i)/p_b(i)$
    if $\kappa_i = 1$ **then** Find $s_i^*(\mu_K)$ using Remark 4, Eq. 4.2.2
    else if $\kappa_i \in [0, \eta_{\text{ch}}\eta_{\text{dis}})$ **then** Find $s_i^*(\mu_K)$ using Remark 5, Eq. 4.2.3
    else if $\kappa_i \in (\eta_{\text{ch}}\eta_{\text{dis}}, 1)$ **then** Find $s_i^*(\mu_K)$ using Remark 6, Eq. 4.2.5
    else if $\kappa_i = \eta_{\text{ch}}\eta_{\text{dis}}$ **then** Find $s_i^*(\mu_K)$ with Rmk. 7, Eq. 4.2.6
    end if
    $x_i^* = f^{-1}(s_i^*(\mu_K))$and $b_i^*(\mu_K) = b_{i-1}^* + x_i^*$
    if C1 or C2 or C3 holds **then**
      `BreakFlag` $\leftarrow 1$; $i_{\text{break}} \leftarrow i$
      Break
    end if
  end for
  if `BreakFlag` = 1 and $i_{\text{break}} \geq i_{\text{mem}}$ **then**
    `BreakFlag` $\leftarrow 0$; $i_{\text{mem}} \leftarrow i_{\text{break}}$; $\mu_{\text{mem}} \leftarrow \mu_K$
    if $b_i^*(\mu_K) \prec \{b_{\min}\}$ **then**
      $\mu_K \leftarrow \min\{p > \mu_K : p \in (p_{\text{s}}(i)\eta_{\text{dis}}, p_{\text{s}}(i)/\eta_{\text{ch}}, p_{\text{b}}(i)\eta_{\text{dis}}, p_{\text{b}}(i)/\eta_{\text{ch}}; i_{K-1} < i \leq i_{\text{break}})\}$
    else
      $\mu_K \leftarrow \max\{p < \mu_K : p \in (p_{\text{s}}(i)\eta_{\text{dis}}, p_{\text{s}}(i)/\eta_{\text{ch}}, p_{\text{b}}(i)\eta_{\text{dis}}, p_{\text{b}}(i)/\eta_{\text{ch}}; i_{K-1} < i \leq i_{\text{break}})\}$
    end if
  else if `BreakFlag` = 1 and $i_{\text{break}} < i_{\text{mem}}$ **then**
    if C1 is True **then**
      $i_K \leftarrow \max\{i \in [i_{K-1} + 1, i_{\text{mem}}] : b_{\max} \in b_i^*(\mu_{\text{mem}})\}$
      $b_{i_K}^* = b_{\max}$
    else if C2 or C3 is True **then**
      $i_K \leftarrow \max\{i \in [i_{K-1} + 1, i_{\text{mem}}] : b_{\min} \in b_i^*(\mu_{\text{mem}})\}$
      $b_{i_K}^* = b_{\min}$
    end if
    $\mu_K \leftarrow \mu_{\text{mem}}$; `BreakFlag` $\leftarrow 0$; $i_{\text{break}} \leftarrow i_{\text{mem}}$
    $i_{\text{mem}} \leftarrow i_K$
    `BackwardStep`$(\mu_K, i_{K-1}, i_K, b^*, x^*, \mu^*)$
    $s^* = f(x^*)$ using Eq 4.2.1
    $\mu_{K+1} \leftarrow \mu_K$; $K \leftarrow K + 1$
  else
    $i_K \leftarrow N$;
    if $\mu_K > 0$ **then**
      $b_N^* \leftarrow b_{\min}$
    else
      $b_N^* \leftarrow [b_{\min}, b_{\max}) \cap b_N^*(\mu_K)$
    end if
    `BackwardStep`$(\mu_K, i_{K-1}, i_K, b^*, x^*, \mu^*)$
    $s^* = f(x^*)$ using Eq 4.2.1
  end if
end while

Algorithm 7 `BackwardStep`$(\mu_K, i_{K-1}, i_K, b^*, x^*, \mu^*)$

Inputs: $\mu_K, i_{K-1}, i_K, b^*, x^*, \mu^*$
Function: Computes components of the optimal vectors b^*, x^* in the range $[i_{K-1} + 1, i_K - 1]$ using backward recursion
Initialize: $i \leftarrow i_K - 1$

while $i \geq i_{K-1} + 1$ **do**
  $b_i^* \leftarrow (b_{i+1}^* - x_{i+1}^*(\mu_K)) \cap b_i^*(\mu_K) \cap [b_{\min}, b_{\max}]$
  $x_{i+1}* \leftarrow b_{i+1}^* - b_i^*$
  $\mu_i^* \leftarrow \mu_K$
  $i - -$
end while

forecast model. To this aim, we implement the forecast model using the AutoRegressive Moving Average (ARMA) model. In this work, we focus on and develop a forecast model for the net load consumption of the end user without storage. Note that similar forecasting model can be developed for electricity price. The details of autoregressive forecast model is presented in Section 2.4.1.

The forecasted end user load without storage is fed to the online algorithm, `ForecastPlusMPCnem2`, given below. The online algorithm is executed sequentially and uses MPC to identity the optimal modes

Algorithm 8 `ForecastPlusMPCnem2`

Global Inputs: $\eta_{\text{ch}}, \eta_{\text{dis}}, \delta_{\max}, \delta_{\min}, b_{\max}, b_{\min}, b_0$
Inputs: $h, N, T, i = 0$

1: **while** $i < N$ **do**
2: $i = i + 1$
3: Forecast $\hat{p}_{elec}, \hat{z}$ from time step i to N using ARMA model described in Section 2.4.1.
4: $s^* = \texttt{OptimalArbitrage}(\hat{p}_{elec}, \hat{z}, h, N, T)$
5: $b_i^* = b_{i-1} + f(s^*)$ and Update $b_0 = b_i^*$
6: **end while**

of operation of storage.

4.4 Numerical Results

For the numerical evaluation, we use a single end user having an inelastic power and energy demand and a rooftop solar generation. The end user's consumption data with solar generation data are downloaded from the Pecan Street's online data repository [58]. We use the data corresponding to user id 379 for May 2, 2016. This is one of the days when the solar generation exceeds the end user's consumption for some amount of time. We solve the optimal arbitrage problem using `OptimalArbitrage` described in the previous section. The battery parameters are set as follows: $b_{\max}$= 1 kWh, $b_{\min}$= 0.1 kWh, $\delta_{\max}$= 0.26 kW, $\delta_{\min}$=−0.52 kW. Real-time locational marginal pricing data from NYISO [29] is used to calculate the optimal ramping trajectory. The sampling time of the price signal is h=15 minutes. Simulations are conducted using a laptop PC with Intel Core i7-6600 CPU, 2.6 GHz processor and 16 GB RAM. The results obtained by our algorithm for a lossy battery with $\eta_{\text{ch}} = \eta_{\text{dis}} = 0.95$ and for the case of zero selling price are shown in the figures below. Fig. 4.3 shows the electricity buying price[4] and the shadow price,

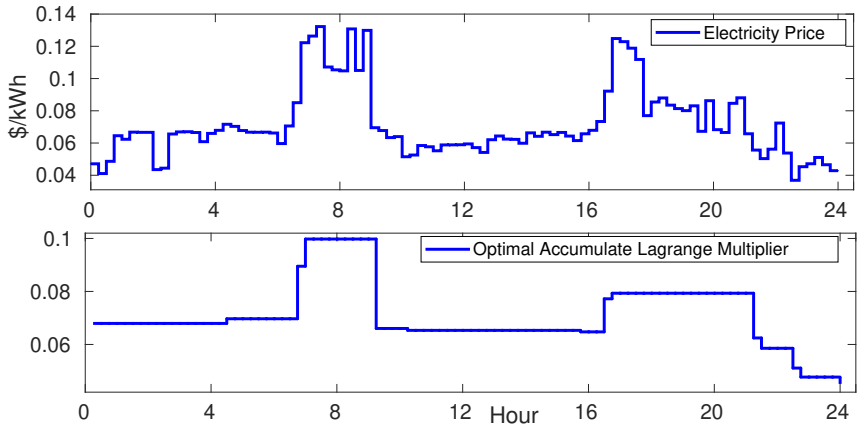

Figure 4.3: Price Signal and accumulated Lagrange Multiplier

i.e. μ^*, calculated using the proposed algorithm for initial battery charge level $b_0 = 0.5$. Since we assume zero selling price, implying that it is not beneficial for the end user to supply power back to the grid, we can observe from Fig. 4.4 that in the afternoon when the end user generates more than the consumption, it still supplies power back to the grid, as the user has no flexibility in form of storage. However, with the inclusion of energy storage we can observe the modification in the total energy consumption curve. In fact, since it is not beneficial to sell electricity, the total consumption is saturated at zero as the lower limit.

[4]NYISO Real Time Electricity Price Data, https://tinyurl.com/2flowo6

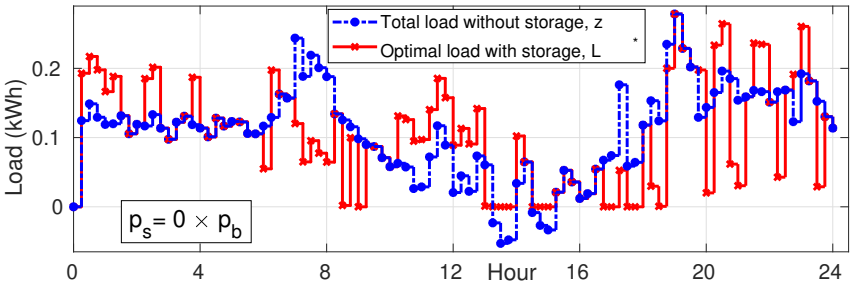

Figure 4.4: Demand without storage and with optimal storage control

Table 4.2 compares the run-time of the proposed algorithm with CVX[5], YALMIP and Matlab's Fmincon optimization tool.

Table 4.2: Comparison of runtime

Algorithm Type	Run Time (sec)
Proposed Algo	0.019
Linear Program [184]	0.025
CVX	0.536
YALMIP [231] with Gurobi	3.700
Matlab's Fmincon	5.693

Fig. 4.5 shows the solar generation, the end user demand and the energy consumed from the grid. Now,

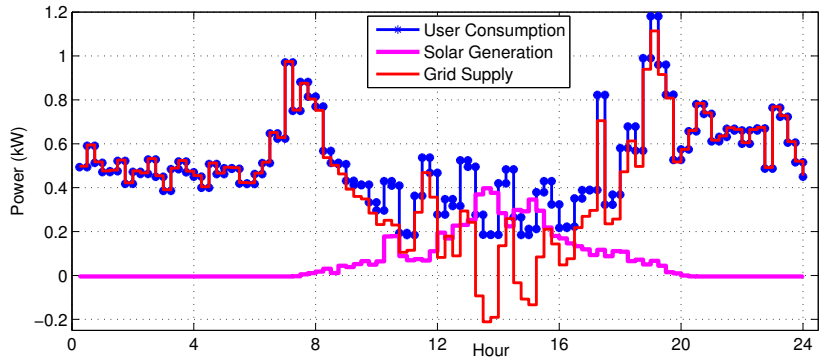

Figure 4.5: Pecan Street Data of a home with solar generation

consider a hypothetical scenario, when this end user might have had energy storage installed. How much gains could an end user make by installing an energy storage?

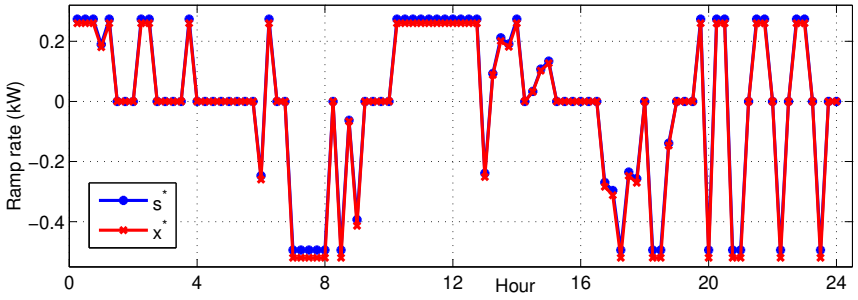

Figure 4.6: Ramp rate for optimal arbitrage

Fig. 4.6 shows the ramp rate of the battery. It is evident from Fig. 4.6 that the ramping constraints for the battery are met and intermediate ramp rates could also be optimal. Fig. 4.7 shows the optimal

[5]CVX Matlab Toolbox, http://cvxr.com/cvx

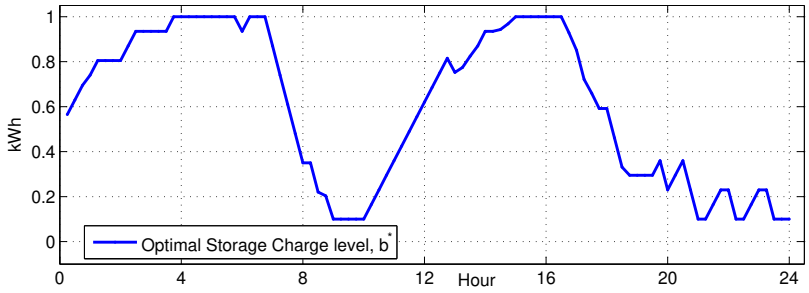

Figure 4.7: Optimal Energy level

battery capacity trajectory. Note from Fig. 4.3 that the price has two peaks in the whole day, thus the battery does 2 cycles of charge and discharge, as shown in Fig. 4.7.

The comparison of the change in valuation of only storage and only solar with the variation in the ratio of the selling price and buying price from an end user's perspective is studied. Fig. 4.8 shows the variation

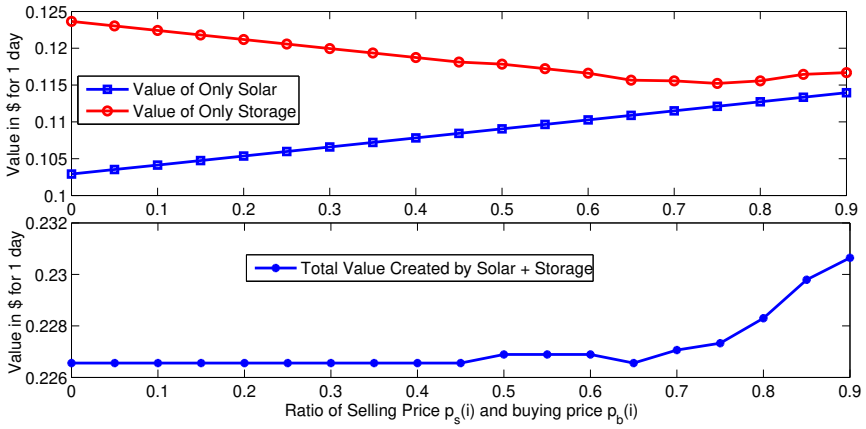

Figure 4.8: Value of Solar and Storage with the ratio of p_s and p_b

of value of only storage and only renewable with the change in the selling price of electricity. We define the value of solar as the difference between cost of consumption with only load and cost of consumption with load and solar. Similarly, the value of storage is defined as the difference between the cost of consumption with load and solar and the cost of consumption with load, solar and battery. The value of storage is defined as $\sum_{i=1}^{N}\{p_b[z_i]^+ - p_s[z_i]^-\} - \sum_{i=1}^{N}\{p_b[z_i+s_i]^+ - p_s[z_i+s_i]^-\}$. We would like to highlight that when selling price is low there is an increase in the storage value which comes at the cost of decrease in the value of renewables connected. For zero selling price the value of energy storage for the numerical evaluation is \$0.1237.

As the share of renewables connected to power network increases the volatility in electricity prices will increase in order to incentivize users to differ their consumption. Fig. 4.9 shows that as the variance

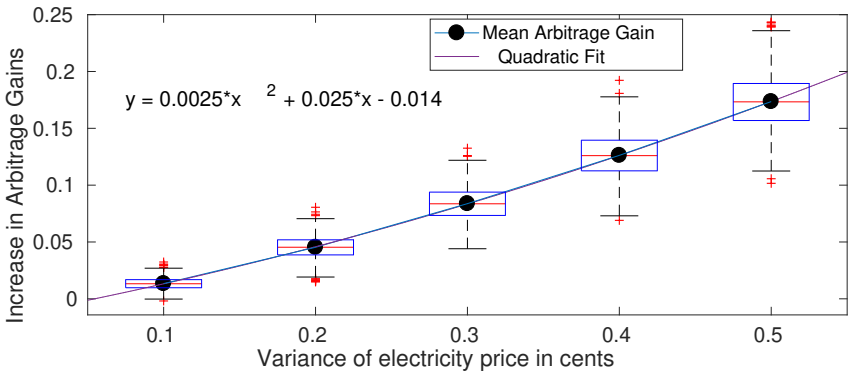

Figure 4.9: Increase in arbitrage gains with volatility in price

in electricity price increases, i.e. price volatility increases, the amount of arbitrage gains for consumers,

with full information about price variation, will increase. The increase in arbitrage gains with respect to variance can be approximated using a quadratic fit. Installing energy storage would provide more financial returns under increased volatility.

Forecast Error and Loss of Opportunity: It is expected that mismatch between forecast and actual values will create a loss of possible opportunity for the user. Loss of opportunity is defined as the per unit variation of ideal versus actual arbitrage gain with respect to ideal arbitrage gains. Loss of opportunity is denoted as Loss of Opportunity $= \frac{V_a^* - V_r}{V_a^*}$. In order to understand the effect of forecast error in electricity price on the arbitrage gains we conduct a performance evaluation based on 10,000 simulations for equal buying and selling prices with battery having 95% charging and discharging efficiency for different variance of forecast error (= actual price - forecasted price). Fig. 4.10 shows that with increasing variance of forecast error the loss of opportunity for the user will increase. Black dots in Fig. 4.10 represent the mean value of loss of opportunity corresponding to the variance in forecast error, which could be fitted with a linear function.

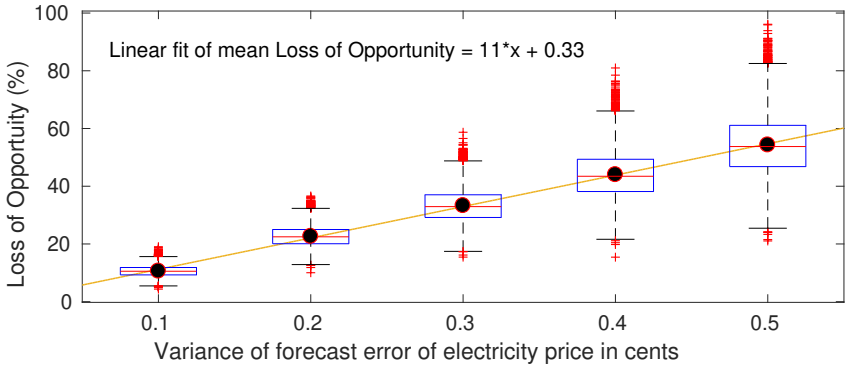

Figure 4.10: Relationship of Loss of Opportunity and Forecast Error

4.4.1 MPC with incrementally improving forecast

We use the Pecan Street data [58] for hourly consumption for house id 379 for the month of June and July 2016. The day ahead electricity prices in the ERCOT data is used for the same period [16]. It is assumed that the selling price is half that of the buying price. The factors in Eq. 2.4.4 are $\alpha_1 = \beta_1 = \frac{0.5\times x}{x+x^2+x^3} = 0.27185$, $\alpha_2 = \beta_2 = \frac{0.5\times x^2}{x+x^2+x^3} = 0.14780$ and $\alpha_3 = \beta_3 = \frac{0.5\times x^3}{x+x^2+x^3} = 0.08036$, note the factors are selected such that $x + x^2 + x^3 = 1$. The value of $D = 7$ days and $N = 24$. We use the same parameters of the battery as described in the previous numerical results. The simulation results for ARMA based forecasting

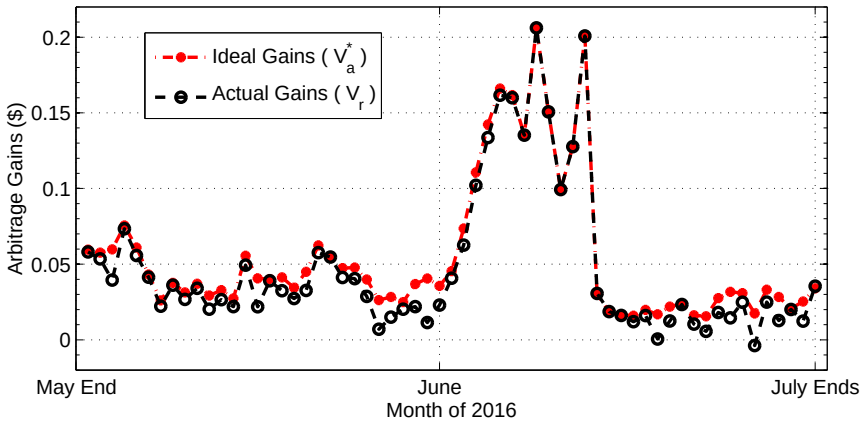

Figure 4.11: Comparison of arbitrage gains for ideal and actual case

with MPC are shown in Fig. 4.11. It can be observed that $V_r \leq V_a^*$.

Gain Type	Mean ($)	STD
Ideal (V_a^*)	0.05481	0.04673
Actual (V_r)	0.04783	0.04922

The table reports the mean and standard deviation of arbitrage gains over a period of 2 months (see Fig. 4.11), V_a^* and V_r. Due to inaccuracies in forecasting, end user incurs $\approx 12.7\%$ of loss in possible opportunity during the period of 2 months. The run time for forecasting and MPC for the whole period is 9.699 seconds. Fig 4.11 shows that actual and ideal arbitrage gains are in sync with each other. It should be noted that the forecast model using ARMA uses mean behavior over the past week as the starting point, however, the mean behavior provides a very crude indicator of future behavior. Even with this model along with MPC, we could significantly mitigate the effects of forecast error on arbitrage gains.

4.5 Comparing Run-Time of Algorithms

We compare the run-time of three optimal arbitrage algorithms for a given battery and present the run-times with different number of samples in the time horizon of optimization. The three algorithms compared here are:
(a) *Proposed algorithm* in this work which shows the structure of optimal arbitrage solution based on price and net-load variation.
(b) *Linear Programming*: We use the LP formulation proposed in Appendix B and [184]. The LP formulation is possible due to piecewise linear convex cost functions. In this formulation we consider: (i) net-metering compensation (with selling price at best equal to buying price) i.e. $\kappa_i \in [0, 1]$, (ii) inelastic load, (iii) consumer renewable generation, (iv) storage charging and discharging losses, (v) storage ramping constraint and (vi) storage capacity constraint. Using numerical results we perform sensitivity analysis of batteries with varying ramp rates and varying ratio of selling and buying price of electricity.
(c) *Convex optimization*: There could be several different ways of formulating optimal arbitrage problem using convex optimization toolbox. We propose one of the many ways of solving optimal arbitrage problem with convex piecewise linear cost function using CVX. Since in the optimization formulation we do not have any binary variable, this optimization problem could be solved using the default solver, SDPT3[6]. The decision variable x_i is fragmented into two variable given as $x_i = x_i^{ch} - x_i^{ds}$, where $x_i^{ch} \in [0, X_{\max}]$ and $x_i^{ds} \in [0, -X_{\min}]$, denotes the charging and discharging values.

For the numerical evaluation we use a battery with initial charge level, b_0=500 Wh, $b_{\max}$=3000 Wh, $b_{\min}$=100 Wh, η_{ch}=η_{dis}=0.9 and sampling time is equal to 1 hour.

Table 4.3: Sub-horizon characteristics in number of samples

Samples in time horizon	Mean no. of samples in sub-horizon	STD of sub-horizon length
10	5	7.07
100	10	6.29
1000	10.99	7.19
10000	11.09	7.27
100000	11.11	7.28

Fig. 4.12 shows the run-time in seconds for the three approaches for performing optimal arbitrage algorithm. It is evident that the proposed algorithm outperforms the other two approaches described significantly. The complexity of linear programming (LP) based algorithms is polynomial [203]. However, with a significantly longer time horizon LP might not be tractable. The CVX based convex optimization problem also becomes intractable for optimization horizon greater than 10^4 samples.

Fig. 4.13 shows the run-time in seconds for optimal arbitrage algorithm without and with load. It is evident that the complexity of the proposed algorithm grows approximately linearly with the number of samples. The quantification of mean and standard deviation of sub-horizon is shown in Table 4.3.

4.6 Case Study 1: Intermediate ramp rate

Several works on energy storage arbitrage use set thresholds according to which storage operation could be selected from 3 cases, i.e., charge at maximum rate, discharge at minimum rate or stay idle. We believe energy storage performing arbitrage could also have intermediate ramping rates which are neither minimum

[6]https://tinyurl.com/yfqclqz

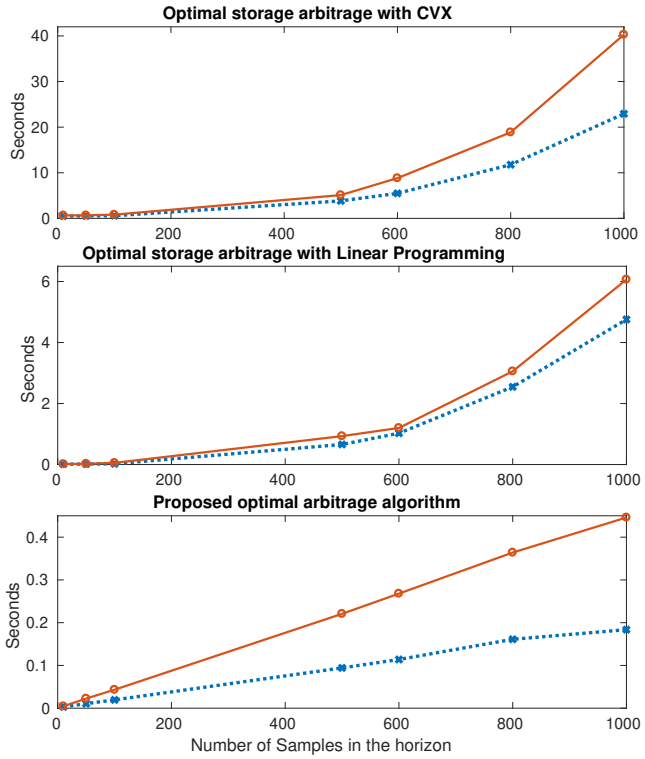

Figure 4.12: Comparison of run-time for CVX based optimization, linear programming and the proposed algorithm with variation of samples in time horizon of optimization for storage arbitrage. The run-time without load in blue and with load in red is shown.

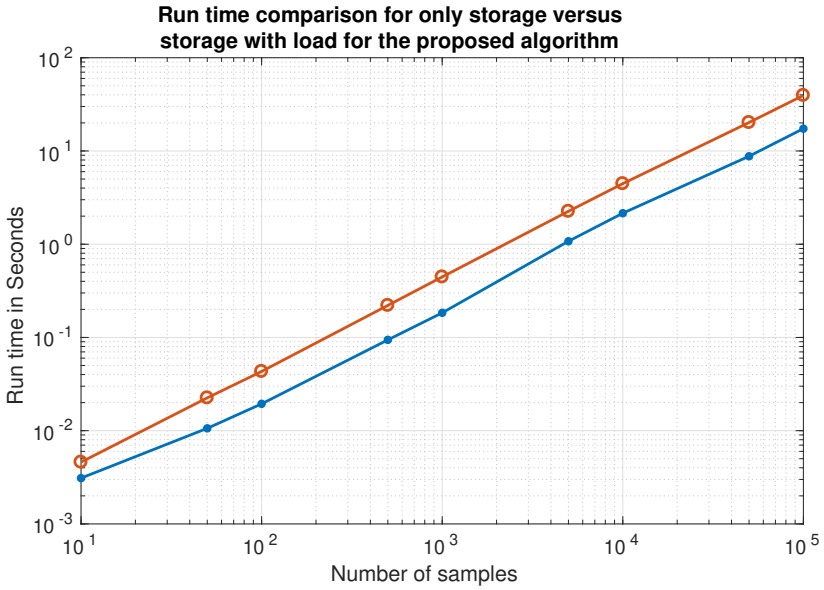

Figure 4.13: Proposed algorithm run-time comparison for with load (in red) and no load (in blue).

or maximum nor zero, making the optimal storage ramping selection a continuous set from minimum to maximum ramp rate, assuming storage ramp rate is same for a decision epoch.

We demonstrate this claim with a stylized example. In this example we consider only storage case with equal buying and selling price of electricity, in order to have analytical tractability. Consider the electricity price signal shown in the first plot of Fig. 4.14. The battery parameters are as follows: $b_0 = 500$Wh, $b_{\max} = 3000$Wh, $b_{\max} = 100$Wh, $\eta_{ch} = \eta_{dis} = 0.9$, $\delta_{\max} = -\delta_{\min} = 1000$W. The electricity price values for hour 1 to 10 are provided here: [1, 0.9, 1.5, 0.8, 0.6, 5, 4.9, 6, 5, 8]. We intend to provide all details of the results presented in order to ease the reproducibility of the claims made here.

The price signal is carefully designed to have values between 1 to 2 cent/kWh for hour 1 to 5 and higher levels of electricity price for hour 6 to 10. This could be analogous to low electricity price during the night and significantly higher price levels during the evening peak. Note that the electricity price for 7th and 9th hour are at the same level, i.e. 5 cents/kWh. The second plot of Fig. 4.14 shows the optimal storage charge level considering electricity price variation and storage parameters. The third plot of Fig. 4.14 shows the ramp rate in x which affects the change in battery charge level in blue and s, output power of storage in red which considers the charging and discharging efficiency losses. Points marked P1, P2 and P3 shows ramping of the battery which are neither at maximum, minimum or zero level of ramp rate.

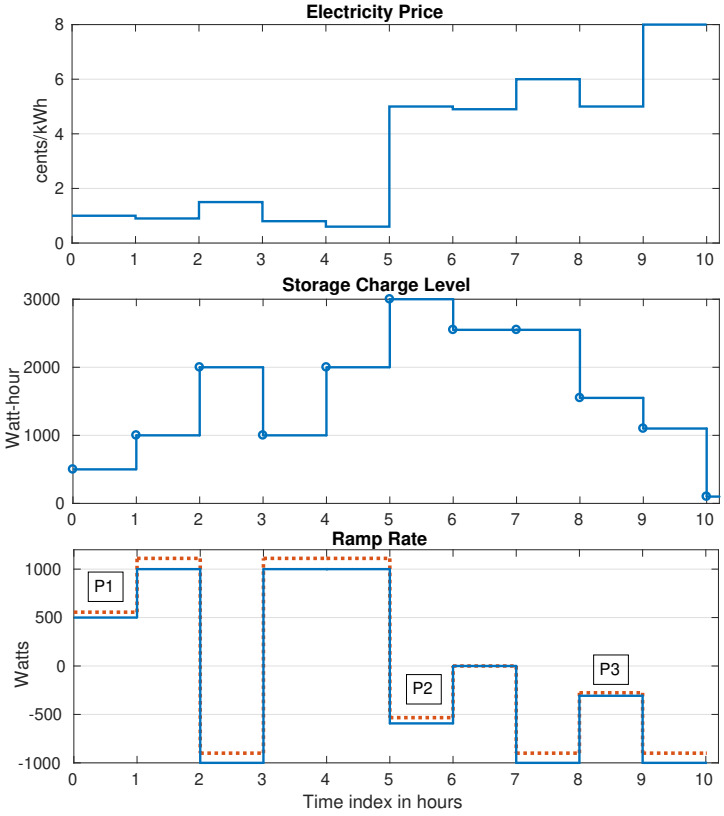

Figure 4.14: Toy example to show the intermediate ramp rate of energy storage. Plot 1 shows the electricity price. Plot 2 shows the optimal storage charge level. Plot 3 shows the storage ramp rate.

Clearly, based on the price variation for this example storage needs to be completely charged at the end of 5th hour. In order to discharge during higher price levels for interval 6 to 10 hour. The order of price levels in 0 to 5 hour are in this order: $p_{elec}(5) < p_{elec}(4) < p_{elec}(2) < p_{elec}(1) < p_{elec}(3)$. Starting from $b_0 = 500$Wh, storage needs 2500 Wh of energy to be fully charged at the end of 5th hour. The battery charges at a ramp rate of 500 W in hour 1. This level is lower than the max level of ramp rate. The battery reaches a charge level of 1000 Wh. $p_{elec}(2)$ is the third lower price in hour 1 to 5 and the battery charges at maximum rate in order to discharge during hour 3 to capture gains as $p_{elec}(3)$ is the local peak. In subsequent 4th and 5th hour the battery charges at max level to unity state-of-charge at the end of 5th hour.

The order of price levels in 6 to 10 hour are in this order: $p_{elec}(7) < p_{elec}(6) = p_{elec}(8) < p_{elec}(8) < p_{elec}(10)$. Clearly, battery should should discharge maximum possible during 10th hour and then 8th hour. If the battery is still not completely discharged than during 6th and 9th hour. The incentive of discharging during hour 6 and 9 are equal so multiple solutions could be possible if the battery is not discharging at

its peak rate. This could be seen in Fig. 4.15 where two distinct solutions are plotted (with infinite other combinations possible). All such combinations provide the same level of arbitrage gains which for this example is 14.89 cents. Since hour 7 has the lowest price level in the interval 6 to 10 hour and the battery could be discharged completely in slightly less than 3 hours. Thus storage remains idle during 7th hour.

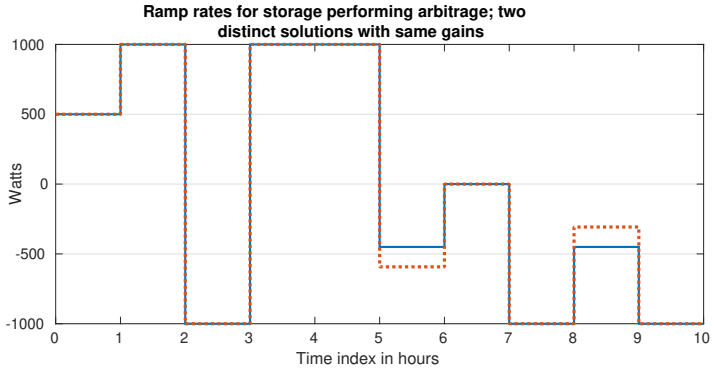

Figure 4.15: Two distinct optimal ramping solution for performing energy arbitrage for the electricity price shown in Fig. 4.14.

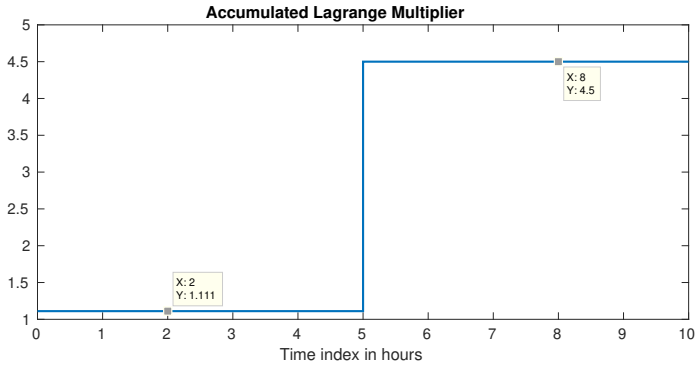

Figure 4.16: Shadow price (accumulated Lagrange multiplier) for the electricity price shown in Fig. 4.14.

Fig. 4.16 presents the shadow price (accumulated Lagrange multiplier) for the 2 sub-horizons for this example. First sub-horizon has $\mu_1 = 1.111$ is applicable for hour 1 to 5 and $\mu_2 = 4.5$ is applicable for hour 6 to 10. Since the intermediate ramp rate is observed at 1st hour with $p_{elec}(1) = 1$ cents/kWh and the battery is charging therefore, $\mu_1 = p_{elec}(1)/\eta_{ch} = 1.111$. Similarly, the intermediate ramp rate in the second sub-horizon is observed at 6th or 9th (as same price level) hour with $p_{elec}(6) = p_{elec}(9) = 5$ cents/kWh and the battery is discharging therefore, $\mu_2 = p_{elec}(6)\eta_{dis} = p_{elec}(9)\eta_{dis} = 4.5$.

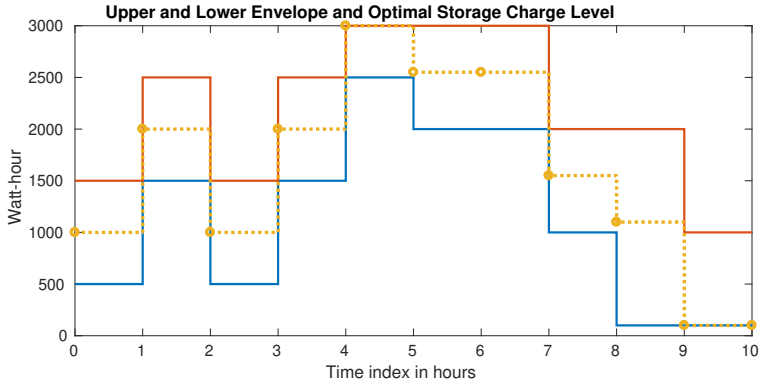

Figure 4.17: Lower, upper and optimal charge level for the electricity price signal shown in Fig. 4.14.

Fig. 4.17 shows the upper and lower envelopes of storage charge level along with the selected optimal storage charge level. The envelope of solutions is due to the piecewise linear cost structure of the cost function which provides sub-gradient like solution at point where the cost function changes its slope.

4.7 Case study 2: Sensitivity analysis for varying κ

For the numerical evaluation, we use battery parameters listed in Table 4.4. The performance indices used for evaluating simulations are:
• *Arbitrage Gains:* denotes the gains (made in absence of load and renewable) or reduction in the cost of consumption (made in presence of load and renewable) due to storage performing energy arbitrage under time-varying electricity prices,
• *Cycles of operation*: In our prior work [181] we develop a mechanism to measure the number of cycles of operation based on depth-of-discharge (DoD) of energy storage operational cycles. Equivalent cycles of 100% DoD are identified. This index provides information about how much the battery is operated.

We use xC-yC notation to represent the relationship between ramp rate and battery capacity. xC-yC implies battery takes 1/x hours to charge and 1/y hours to discharge completely. We perform sensitivity analysis with (a) four battery models with the different ramping capability listed in Table 4.4 and (b) 5 levels of the ratio of selling price and buying price of electricity, i.e., $\kappa \in \{1, 0.75, 0.5, 0.25, 0\}$. In this work we assume the selling price is equal to the product of scalar variable κ and the buying price of electricity. The optimization problem, P_{LP}, is solved using `linprog` in MATLAB[7]. `linprog` uses dual-simplex [90] (default) algorithm.

Table 4.4: Battery Parameters

$b_{\min}$, $b_{\max}$	200Wh, 2000 Wh
b_0	1000 Wh
$\eta_{ch} = \eta_{dis}$	0.95
$\delta_{\max} = -\delta_{\min}$ (4 battery model)	500 W for 0.25C-0.25C, 1000 W for 0.5C-0.5C 2000 W for 1C-1C, 4000 W for 2C-2C

4.7.1 Deterministic Simulations

The price data for our simulations in this subsection is taken from NYISO [29]. The load and generation data is taken from data collected at Madeira, Portugal. Fig. 4.18 shows the electricity price and energy consumption (includes inelastic load and rooftop solar generation) data used for deterministic simulations. Table 4.5 and Table 4.6 lists the energy storage arbitrage without and with energy consumption load for the electricity price data shown in Fig. 4.18. The observations are:

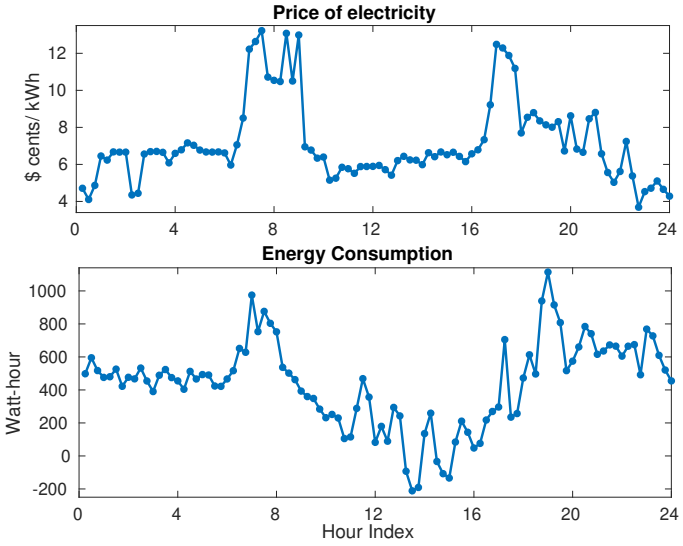

Figure 4.18: Electricity price and consumer net load data used for deterministic simulations.

[7] https://www.mathworks.com/help/optim/ug/linprog.html

• The value of storage in presence of load and renewable increases as κ decreases. Note that for $\kappa = 0$, the only storage operation provides zero gain (see Table 4.5), however, for the same buying and selling levels, the consumer would make significant gains when operated with inelastic load and renewable generation (see Table 4.6),
• The cycles of operation for faster ramping batteries are higher compared to slower ramping batteries. This implies that faster ramping batteries should be compared in terms of gains per cycle with slower ramping batteries. Observing only gains could be misleading.
• As κ decreases, the cycles of operation decrease, thus the effect on storage operation in the cases presented is similar to η_{fric} in reducing cycles of operation.
• Note that for $\kappa = 1$, the arbitrage gains with and without load are the same. This observation is in sync with claims made in [182]. Authors in [182] observe that storage operation becomes independent of load and renewable variation for equal buying and selling case.

Table 4.5: Performance indices for only storage

κ	2C-2C	1C-1C	0.5C-0.5C	0.25C-0.25C
Arbitrage gains in $ cents for 1 day				
1	44.445	33.760	25.636	17.536
0.75	18.842	17.668	14.077	9.921
0.5	7.682	7.088	6.253	5.219
0.25	2.513	2.502	2.483	2.422
0	0	0	0	0
Cycles of operation for 1 day				
1	6.586	3.856	2.237	1.620
0.75	2.401	1.742	1.484	0.795
0.5	1.539	1.099	0.714	0.386
0.25	0.182	0.171	0.164	0.160
0	0	0	0	0

Table 4.6: Performance indices for storage + load

κ	2C-2C	1C-1C	0.5C-0.5C	0.25C-0.25C
Arbitrage gains in $ cents for 1 day				
1	44.445	33.760	25.636	17.536
0.75	37.848	33.023	26.469	18.337
0.5	39.045	34.105	27.696	19.344
0.25	40.272	35.332	28.923	20.351
0	41.500	36.560	30.150	21.358
Cycles of operation for 1 day				
1	6.586	3.835	2.263	1.620
0.75	5.986	4.039	2.338	1.652
0.5	5.986	4.033	2.364	1.660
0.25	5.986	4.033	2.364	1.660
0	5.986	4.033	2.364	1.660

Fig. 4.19 and Fig. 4.20 show the arbitrage gains, gains per cycle and cycles of operation with varying κ for storage performing arbitrage without and with inelastic load and renewable generation. The gains per cycle are nearly flat with varying κ. Slow ramping batteries, 0.25C-0.25C and 0.5C-0.5C, have significantly higher gains per cycle compared to faster ramping batteries, 1C-1C and 2C-2C.

4.7.2 Results with Uncertainty

The forecast model is generated for load with solar generation and for electricity price. The ARMA based forecast uses 9 weeks of data (starting from 29th May, 2019) for training and generates forecast for the next week. `ForecastMPClinearProgram` is implemented in receding horizon. The electricity price data used for this numerical experiment is taken from CAISO [79] for the same days of load data. To compare the effect of forecasting net load and electricity prices with perfect information, we present average arbitrage gains and cycles of operation starting from 1st June 2019. Rolling horizon time-period of optimization, N_{opt},

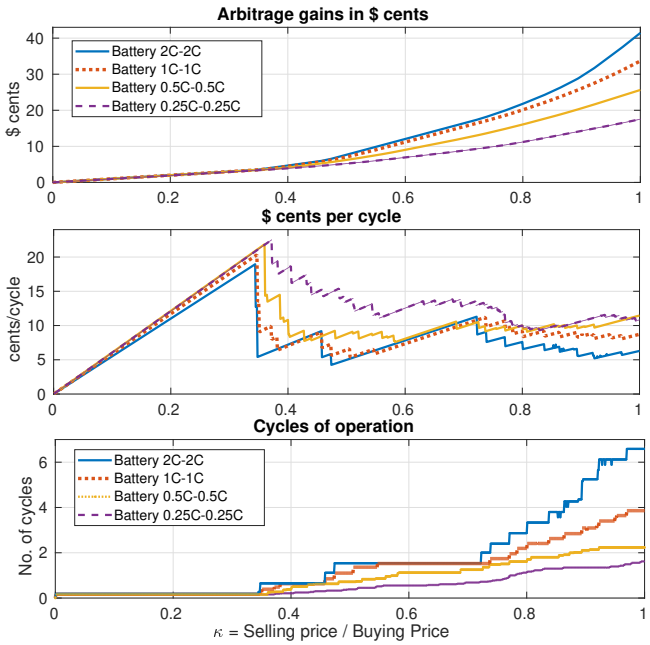

Figure 4.19: Performance indices for only storage performing arbitrage with varying κ for 1 day.

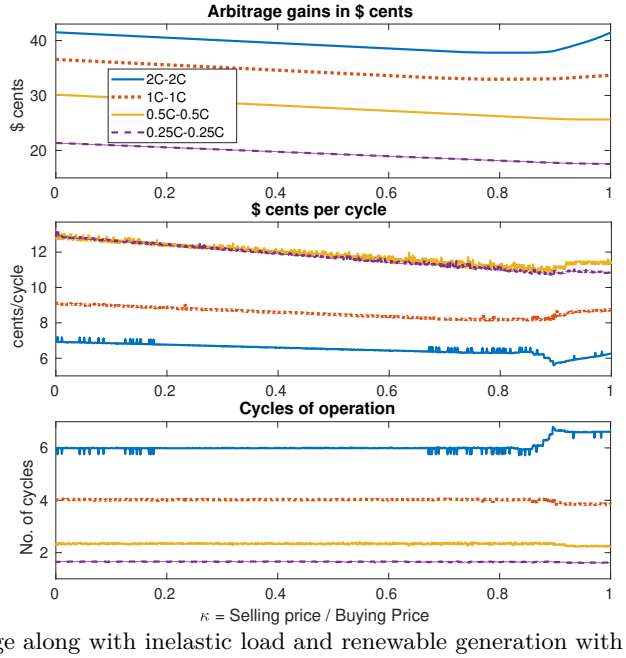

Figure 4.20: Storage along with inelastic load and renewable generation with varying κ for 1 day.

is selected as 1 day. This implies at 13:00 h today, the storage control decisions are based on parameter variation forecasts till 13:00 h tomorrow.

Table 4.7: Deterministic arbitrage gains for only storage

κ	2C-2C	1C-1C	0.5C-0.5C	0.25C-0.25C
Arbitrage gains in $ for 1 week				
1	9.411	7.059	4.784	3.065
0.75	5.729	4.491	3.168	2.082
0.5	3.166	2.550	1.833	1.217
0.25	1.124	0.941	0.688	0.456
0	0	0	0	0
Cycles of operation for 1 week				
1	58.729	37.257	21.324	12.107
0.75	23.462	16.341	10.746	7.519
0.5	12.689	9.770	7.579	6.174
0.25	7.727	6.229	4.558	3.464
0	0	0	0	0

Table 4.8: Deterministic arbitrage gains for storage with load

κ	2C-2C	1C-1C	0.5C-0.5C	0.25C-0.25C
Arbitrage gains in $ for 1 week				
1	9.411	7.059	4.784	3.065
0.75	7.462	6.269	4.540	3.025
0.5	6.641	5.987	4.468	3.019
0.25	6.350	5.904	4.451	3.019
0	6.313	5.902	4.451	3.019
Cycles of operation for 1 week				
1	58.700	37.294	21.324	12.107
0.75	28.583	20.809	14.382	10.229
0.5	19.296	16.629	13.007	9.971
0.25	16.591	15.348	12.498	9.968
0	16.041	15.201	12.484	9.968

Table 4.9: Stochastic indices for only storage

κ	2C-2C	1C-1C	0.5C-0.5C	0.25C-0.25C
Arbitrage gains in $ for 1 week				
1	6.035	4.684	3.469	3.000
0.75	5.024	4.118	3.081	1.904
0.5	3.004	2.367	1.692	1.110
0.25	1.067	0.891	0.618	0.442
Cycles of operation for 1 week				
1	64.323	38.979	22.622	12.850
0.75	24.870	16.169	10.570	7.733
0.5	11.393	8.891	7.013	6.099
0.25	6.429	5.557	4.359	3.395

The deterministic results for without and with load are presented in Table 4.7 and Table 4.8. Compare the deterministic results with stochastic results presented in Table 4.9 and Table 4.10. The primary numerical observations are:

• Effect of uncertainty on arbitrage gains for a faster ramping battery is greater compared to a slower ramping battery, this observation is in sync with conclusions drawn in [130],

• Combining storage with inelastic load with renewable generation provides greater gains for decreasing κ. Furthermore, the effect of uncertainty for lower κ is lower compared to higher values of κ.

• Profitability of operating only storage deteriorates sharply with decrease of κ. For only storage case under zero selling price case ($\kappa = 0$) no arbitrage would be possible and the gain remains zero.

Table 4.10: Stochastic indices for storage with load

κ	2C-2C	1C-1C	0.5C-0.5C	0.25C-0.25C
Arbitrage gains in $ for 1 week				
1	6.034	4.684	3.496	3.000
0.75	4.827	4.075	3.400	2.987
0.5	4.168	3.711	3.292	2.975
0.25	4.204	3.943	3.348	3.002
0	4.427	3.896	3.396	3.009
Cycles of operation for 1 week				
1	64.322	38.979	22.622	12.850
0.75	41.613	30.322	19.948	11.980
0.5	34.658	27.627	18.744	11.348
0.25	31.429	26.370	18.476	11.396
0	32.958	28.255	19.845	11.372

4.8 Conclusion and Perspectives

We formulated the optimal arbitrage problem for storage operation for an end user with load and renewable generation in presence of net-metering pricing policy. We proposed an efficient algorithm to find an optimal solution, using a method that transforms a continuous, convex optimization problem into a discrete one by exploiting the piecewise linear structure of the cost function, which leads to efficient algorithm that has worst case quadratic complexity with respect to the time horizon. This optimal solution structure is similar to Chapter 3. However, the thresholds for NEM 2.0 is more complex with more number of cases due to dependency os inelastic load and renewable generation compared to thresholds for NEM 1.0 described in Chapter 3. We introduced a method for determining the sub-horizons in the whole duration and showed that optimal storage control decisions do not depend on price of electricity and load variations beyond a sub-horizon. We observe that the complexity of the proposed algorithm is quadratic in worst case, however, numerical experiment indicate the complexity of the algorithm can be approximated to be linear in terms number of samples in the horizon of optimization. This computationally superiority compared to simplex for LP and CVX based benchmarks is striking. Furthermore, to find an optimal solution among infinite possibilities, we described a novel methodology using backward step algorithm, which is done only once in a sub-horizon. The worst case run-time complexity of the proposed algorithm is found to be quadratic in the number of time instants for which price signals are available. We also presented an application of the proposed algorithm to implement a MPC based control for reducing the effects of the forecast error on energy arbitrage gains significantly.

By conducting extensive numerical simulations, we analyze the sensitivity of energy storage with varying ramp rates and varying ratio of selling and buying price of electricity. We observe that the value of storage in presence of load and renewable increases as the ratio of selling and buying price decreases. We also perform stochastic simulation for real-time implementation and compare the stochastic results to the deterministic ones. Net-load and electricity price are modeled with AutoRegressive models for model predictive control. The effect of uncertainty on slow ramping batteries is observed to be lower compared to faster ramping batteries. Furthermore, as the ratio of selling and buying price decreases, arbitrage gains becomes less sensitive to uncertainty.

Chapter 5

Battery Degradation and Valuation

Earth provides enough to satisfy every man's needs, but not every man's greed. -Mahatma Gandhi

Summary: Battery life is often described a combination of cycle life and calendar life. In this chapter we propose a mechanism to limit the number of cycles of operation over a time horizon in a computationally efficient manner. We propose a modification in an optimal arbitrage algorithm proposed in Chapter 3 and Chapter 4 to efficiently control the number of cycles of operation of a battery. The cycles of operation have to be tuned based on price volatility to maximize the battery life and arbitrage gains. We propose a mechanism to distinguish arbitrage returns.

Energy storage revenue estimation is essential for analyzing financial feasibility of investment in batteries. We quantify the cycles of operation considering depth-of-discharge (DoD) of operational cycles and provide an algorithm to calculate equivalent 100% DoD cycles. This facilitates in comparing cycles of different DoDs. We propose a battery capacity degradation model based on the cycle and the calendar life and operational cycles. Using equivalent 100% DoD cycles and revenue generated, we calculate the dollars per cycle revenue of storage performing electricity price based arbitrage and ancillary services for load balancing in real time. Using PJM's (a regional transmission organization in the US) real data we calculate short term and long term financial potential for the year of 2017. We observe that participating in ancillary services is significantly more beneficial for storage owners compared to participating in arbitrage.

5.1 Introduction

With increased share of power coming from Renewable Energy Sources (RES), the uncertainty in power networks is increasing. This variability makes the power, frequency and voltage regulation more challenging. Inverter based RES has small inertia compared to conventional synchronous power generators, reducing the capability of the future power grid to withstand perturbation. The future power network will need fast dynamic ancillary services to avoid additional infrastructure development in installing fast ramping power generators. Distributed energy storage devices such as batteries are suitable for assisting the grid because of its fast ramping capability. Authors in [154] and in Chapter 2 we highlight the diverse roles energy storage technologies can play in future power networks. Energy storage not only improves the reliability of power network but also facilitates arbitrage and increases the value of renewable energy sources in the energy markets. Authors in [334] point that battery owners participating in electricity markets should consider cycle aging of batteries. This is due to finite battery cycle life, which is affected by charge-discharge operational cycles, temperature etc. Using a case study on ISO New England energy and reserve markets, authors demonstrate that participants maximize their operational profit while considering cycle aging cost.

The variability in the price is due to the variable generation cost and demand and supply mismatch components caused due to scheduling delays and errors in forecast of RES. This variability in the price can be used by batteries for performing arbitrage. However, sometimes charge and discharge cycles generate very small revenue and it would be beneficial for the battery to be idle. Maximizing idle time would lower stress on the battery and maximize the cycle life of the battery, observed in Chapter 11 [114].

Estimation of financial returns of energy storage is very essential due to its high cost. In modern power networks energy storage devices can perform many different tasks from price based arbitrage, incentive based demand response, voltage and frequency regulation as ancillary service participants or peak demand

shaving for consumers [125]. The goal of this chapter is to identify the monetary potential of energy storage devices, specifically batteries, in performing price based energy arbitrage and dynamic regulation, while considering the degradation of batteries over time and due to operational cycles. Based on the present compensation mechanism we calculate the dollar value of per cycle operation of a battery.

Prior work by Sandia National Laboratories [119] analyses the financial potential of batteries performing arbitrage and regulation in CAISO, California during 2010-11. The authors discovered that participating in dynamic regulation is four times more beneficial compared to participating in arbitrage. However, their work does not consider battery degradation. Furthermore, volatility in prices have changed significantly compared to rates in 2011. And without huge investment in energy storage and flexible load control, the volatility is expected to increase even more as the share of renewable increases in power network [185]. Prior work [332] on energy storage valuation for performing ancillary services concludes that in presence of performance based compensation and battery degradation, installing batteries are a profitable investment.

The authors in [308] optimize the DoD for a battery operating in a dynamic pricing environment that can perform one or two cycles per day and evaluate the gains per cycle. In [161], the authors evaluate the impact of cycle and calendar life on the gain achieved by arbitrage in smart grid networks for both Lead-acid and Lithium batteries. In [190], the authors proposed a linear programming algorithm to optimize the charge and discharge decisions for battery performing regulation and evaluates the return on investment taking into account the battery performances degradation due to the aging effect.

We believe it is essential to take into account the cycles of operation of the battery, due to finite battery cycle and calendar life. The value of cycle and calendar life is often provided by the manufacturers in their data-sheets [48, 49]. These values represent an upper limit of cycles of operation and age of battery by which the battery will reach its End-of-Life (EoL) with high probability. EoL is defined as a state of the battery when the maximum capacity of the battery reduces to 80% of its rated initial capacity. Calendar life refers to the number of years the battery is expected to last until the battery will reach EoL. It is independent of how much the battery is charged and discharged. However, calendar life is dependent on the state of charge of the battery and the temperature. Cycle life limits the number of cycles of operation a battery could perform before reaching EoL. It is governed by charge-discharge trajectory and temperature. In this chapter we do not consider the effect of temperature on battery degradation. The number of cycles of operation will depend on storage parameters and charging and discharging efficiency losses. Refer to Chapter 2 Section 2.3.2 for parameter details and dependencies described in their data-sheets by battery manufacturers. Batteries performing more cycles each day would imply the gains per cycles will be lower. In lithium-ion batteries the growth of solid-electrolyte inter-phase layer increases the impedance of the battery and therefore, reduces the battery capacity because of the consumption of cyclable lithium from the battery. The battery capacity thus degrades [299]. There are various models providing the remaining battery capacity as a combination of cycle life and calendar life: (i) summation of calendar and cycling degradation, (ii) greater of calendar or cycling degradation [300], or (iii) a multiplicative coupling between calendar and cycling degradation. In this chapter we consider the second model where the greater of cycling and calendar degradation decides the remaining battery capacity and the EoL of the battery. This chapter is a qualitative study to compare dollars per cycle a storage would make if they participate in dynamic regulation or in energy arbitrage.

Note the volatility of electricity price across days in a year can vary drastically, implying battery should perform more cycles when the volatility is high. The number of cycles of operation ideally should be selected adaptively ensuring maximizing gains and battery's operational life. The cycles should be controlled based on volatility. In this chapter, we propose a framework to eliminate low returning transaction for battery performing arbitrage using friction coefficient. This friction coefficient needs to be tuned based on nominal operation of battery with no cycles limitations. The battery life can at maximum be equal to its calender life. If the battery is over-used, then the battery EoL is achieved due to cycle life and if the battery is under-used than EoL is achieved due to calender life. In order to maximize the battery's operational life, the degradation due to aging and cycles of operation should be equal in per unit of time. The value of friction coefficient is calculated based on past data, assuming the mean volatility across a longer time horizon in the past will be equal in the future. We consider the longer time scale as a year as it would cover the effects of seasonality too. Similarly, batteries performing dynamic regulation in the ancillary service market should consider maximizing battery life by eliminating low returning transactions. For PJM interconnection it is observed that unlike arbitrage the amount of regulation required is independent of seasonality and remains fairly constant over the year, see Fig.5.9. The key contributions of this chapter are:

• *Financial potential of batteries*: We use real data to calculate dollar per cycle potential of storage performing arbitrage versus ancillary service market participation.

• *Equivalent 100% DoD cycles*: Battery operates with no fixed DoD. We propose a computationally efficient algorithm to calculate equivalent 100% cycles for varying DoD operational cycles. It is essential to consider DoD in comparing cycles, as the relationship between different DoD cycles and equivalent 100% DoD cycles is not linear.
• *Controlling cycles of operation*: Considering cycle and calendar degradation and DoD of each cycle we calculate the battery degradation and provide a mechanism to control cycles of operation to maximize gains and operational life of battery performing arbitrage and ancillary services. We present a mechanism for calculating the friction coefficient for calculating arbitrage gains. By introducing *friction coefficient*, η_{friction} in energy arbitrage control we can efficiently control the cycles of operation. If the battery is operating more number of cycles per day then η_{friction} is decreased so that the battery on average operates for lower number of cycles. Note the selection of η_{friction} will governed by variability of price, number of cycles of operation in absence of any friction, i.e., $\eta_{\text{friction}} = 1$.
• *Distinguishing arbitrage returns*: We present a mechanism to eliminate low returning transactions to maximize battery life. In this chapter we highlight how at the cost of small portion of arbitrage gains, the battery cycle life can be significantly improved.

For ancillary services, participants commit in advance the amount of regulation they can provide. The regulation provided should be achieved with high performance score. By adjusting ramping commitment, storage owners can control the cycles of operation for storage performing regulation.

This chapter is organized as follows. In Section 5.2 we describe the degradation model of the battery. Section 5.3 describes the rationale of eliminating low returning transactions for storage performing arbitrage. Section 5.4 deals with storage performing energy arbitrage using the optimal arbitrage algorithm proposed in [182]. We also propose a mechanism to control cycles of operation by tuning the friction coefficient. Section 5.5 presents energy storage performing ancillary services for the grid. Section 5.6 presents the numerical results. Section 5.7 concludes the chapter.

5.2 Battery degradation and mathematical model

In this section we present the battery model and the need to control cycles of operation. We present an algorithm to identify cycles based on DoD and calculate the equivalent 100% DoD cycles. We observe that storage operation with short cycles significantly increases the cycle life of battery. We present the mathematical model of a battery combining short and long time scales. Degradation of a battery is insignificant in shorter time scale, while it cannot be ignored in longer time horizon.

5.2.1 Battery Degradation

Batteries are energy storage devices which convert electrical energy into chemical energy while charging and chemical energy into electrical energy while discharging. These conversions are not completely efficient, incurring charging and discharging losses in shorter time frame. Furthermore, for longer time horizon batteries degrade because of time and operational cycles, providing us with distinct calendar and cycle life of the battery.

Degradation due to cycles of operation: What is a cycle for a battery? One would say if the battery at State of Charge (SoC) level x_1 charges to level x_2 and then discharges back to x_1 is called a cycle. But how could we differentiate between cycles; cycles with more change in SoC compared to cycles with less change in SoC. The change in SoC for the cycle example presented is $x_2 - x_1$, this is also called the DoD. Let the cycle life, T_{cycle}, at 100% DoD be given as N_{100} cycles. The proposed cycle degradation model of battery used in this chapter is derived from prior work [190]. The number of cycles at d DoD that the battery can operate if N_{100} is the rated cycle life at 100% DoD is assumed to be [190]

$$f(d) = N_{100} d^{-k_p}, \tag{5.2.1}$$

where k_p is a constant that ranges from 0.8 to 2.1.

DoD plays a significant role in deciding the cycle life especially because the growth in cycle life for a battery performing higher DoD cycles to smaller DoD cycles is not linear, as shown in Eq.(5.2.1) (would be linear if $k_p = 1$). We will demonstrate this with an example. In Forsee Power's Li-Ion battery system HE 48 V data-sheet [49], they show the relationship between cycle life with DoD. At 100% DoD the battery performs approximately 1500 cycles and at 5% DoD the battery performs $\approx 10^6$ cycles. We used the battery life model given by Eq.(5.2.1) to fit the DoD vs. cycle life plot in [49]. Fig. 5.1 shows an

approximate fit for $k_p = 1.1$. In Fig. 5.1 we also show the linear battery model which assumes for instance 10 cycles of 10% DoD as equivalent to 1 cycle of 100% DoD. From Fig. 5.1 it is evident that a battery model ignoring the effect of DoD in counting cycles of operation would hugely underestimate the life of battery and thus would be very pessimistic. If a battery performs n_d cycles at d DoD then this is equivalent to

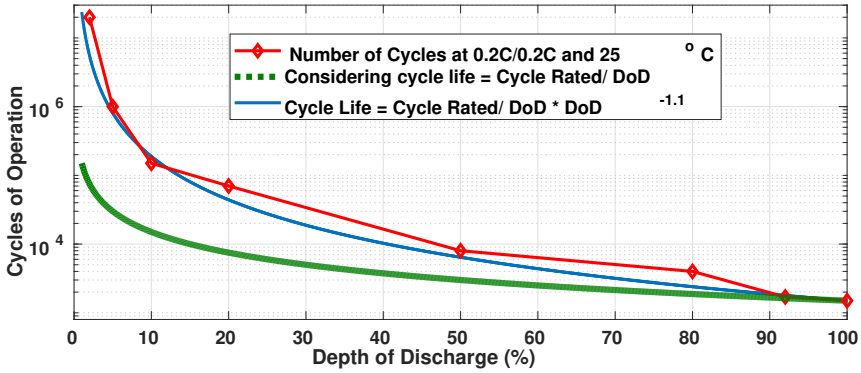

Figure 5.1: Li-ion cycle of operation with DoD [49].

n_{100} cycles at 100% DoD, this is given as $n_{100} = n_d d^{k_p}$. By this analogy T_{cycle} at 100% DoD is N_{100} then T_{cycle} at d% DoD is $N_{100} d^{k_p}$.

We propose an algorithm to calculate DoD efficiently. The new algorithm calculates DoD based on the change in SoC of the battery between mode reversals, i.e., from charging to discharging or vice versa. The Algorithm 9 finds the half cycle DoD and calculates equivalent 100% DoD cycles using Eq. 5.2.1. The input to the algorithm is the charge-discharge trajectory with respect to the rated storage capacity and the output is cumulative number of equivalent 100% DoD cycles the storage operated.

5.2.2 Battery Model

The total duration on shorter time-scale of a day is denoted as T, of operations divided into N steps indexed by $i \in \{1, ..., N\}$. The duration of time-step is denoted as h. Hence, $T = hN$. The total duration of storage operation on longer time-scale is denoted as τ, represents the day index. The day index, $\tau \in \{1, ..., L_{cal}\}$, where L_{cal} is the calendar life in days.

The efficiency of charging and discharging of battery is denoted by $\eta_{ch}, \eta_{dis} \in (0, 1]$. We denote the change in the energy level of the battery at i^{th} instant by $x_i^\tau = h\delta_i^\tau$, where δ_i^τ denotes the storage ramp rate at the i^{th} instant such that $\delta_i^\tau \in [\delta_{\min}, \delta_{\max}] \forall i$ and $\delta_{\min} \leq 0$ and $\delta_{\max} \geq 0$ are the minimum and maximum ramp rates (kW); $\delta_i^\tau > 0$ implies charging and $\delta_i^\tau < 0$ implies discharging. Energy consumed by the storage in the i^{th} instant is given by $s_i^\tau = \frac{[x_i^\tau]^+}{\eta_{ch}} - \eta_{dis}[x_i^\tau]^-$. Let b_i^τ denote the energy stored in the battery at the i^{th} step. Then, $b_i^\tau = b_{i-1}^\tau + x_i^\tau$. The rated battery capacity at the beginning of battery life is denoted by B_{rated}. The available battery capacity at day τ is approximated as

$$B_a(\tau) = B_{rated} - 0.2 \times \left(\max \left(\frac{O_{cy}(\tau)}{L_{cy}}, \frac{\tau}{L_{cal}} \right) \right) \tag{5.2.2}$$

where $O_{cy}(\tau)$ is the number of cycles operated until day index τ, L_{cy} denotes the battery cycle life for 100% DoD and L_{cal} is the calendar life of the battery in days. Eq. (5.2.2) assumes a linear capacity degradation. When the battery is new $B_a(0) = B_{rated}$ and when the battery reaches EoL then the battery capacity is denoted as $B_a(EoL) = 0.8 \times B_{rated}$. The state-of-charge of the battery is denoted as $SoC_i^\tau = \frac{b_i^\tau}{B_a(\tau)}$. The SoC is bounded by $SoC_i^\tau \in [SoC_{\min}, SoC_{\max}]$, therefore, $b_i^\tau \in [SoC_{\min} B_a(\tau), SoC_{\max} B_a(\tau)]$. The cycles of operation is calculated as $O_{cy}(\tau) = \sum_{j=1}^{\tau} n_{100}^j$, where n_{100}^j represents the equivalent 100% DoD cycles for j^{th} day.

5.2.3 Tuning Cycles of Operation

The cycles of operation have to be tuned based on price volatility across a longer time-horizon (months or years) to maximize the battery life and arbitrage gains. The ideal number of cycles of operation on average per unit of time (I_{op}) is approximated as the ratio of cycle life and calender life. Let us define I_N as the number of cycles of operation per unit of time that the battery performs with no cycle limitations.

Algorithm 9 $total^{100}_{cycle} = \texttt{DoDofVector}(x)$

Inputs: x
Function: Equivalent 100% DoD Cycles
Initialize: $a_{minus} = 0, a_{plus} = 0, vec = [\,], i = 1, N =$length$(x)$

while $i < N$ **do**
  if $x(i) >= 0$ **then** C1 = 1,
    if $a_{plus} == 0$ **then** $a_{plus} = x(i)$
    end if
  else C1 = 0,
    if $a_{minus} == 0$ **then** $a_{minus} = x(i)$
    end if
  end if
  if x(i+1) >= 0 **then** C2 = 1,
  else C2 = 0,
  end if
  if C1 == 1 and C2 ==1 **then** $a_{plus} = a_{plus} + x(i+1)$
  else if C1 == 0 and C2 ==0 **then** $a_{minus} = a_{minus} + x(i+1)$
  else if C1 == 1 and C2 ==0 **then** vec = [vec a_{plus}], $a_{plus} = 0, a_{minus} = 0$
  else if C1 == 0 and C2 ==1 **then** vec=[vec a_{minus}], $a_{plus} = 0, a_{minus} = 0$
  end if
  $i = i + 1$
end while
Calculate $dod_{\text{half}} =$ abs(vec)
Calculate $eq^{dod_{100}}_{cyc}(j) = 0.5 * (dod_{\text{half}}(j))^{k_p}, \forall j \in [1, .., \text{length}(vec)]$
Return $total^{100}_{cycle} = sum(eq^{dod_{100}}_{cyc})$

The scenarios of operations are:
• $I_N >> I_{op}$: for example Lead Acid with calendar life of 6 years and cycle life of 1500 cycles. In this case the storage cycles of operation should be controlled in such a way that calendar life equals cycle life. If no cycle control is implemented then battery will reach EoL due to over use, prior to reaching its calendar life. It is essential to ensure that the strategy to limit cycles should only eliminate storage operation for low returning transactions.
• $I_N \approx I_{op}$: for example Li-Ion with calendar life of 10 years and cycle life of 6000 cycles. In this case no control is required as the number of cycles of operation without controlling cycles approximates the optimal cycles of operation per unit of time.
• $I_N << I_{op}$: in such a case controlling the cycles of battery operation is again not required. In this case the battery will reach EoL due to under-use. The battery owner should consider using the battery for multiple applications in order to maximize its gains. This case is not dealt with in this chapter. However, the storage co-optimization formulations proposed in Chapter 7 and Chapter 8 will increase the storage operational cycles.

5.3 Eliminating Low Returning Arbitrage Gains

There are two distinct, but inter-related ways that are used to measure the life of Li-ion batteries deployed in energy storage system applications for smart grid - calendar life and cycle life.

5.3.1 Cycle Life

One of the indexes which decides the life of operation is the rated cycles of operation of a battery. This information is often provided by manufacturers in their data-sheets. In Section 2.3.2 we list the values of the cycle of operation provided by the manufacturers under controlled environment. This value of cycles will with probably lead to the EoL of the battery. The factors affecting the rated cycles of operation are: (a) Battery type: Chemical composition of the battery, (b) Depth of discharge (DoD): Operational cycles, (c) Temperature should be maintained, (d) Ramp rate: affects the stress on the battery, (e) Cycles per day. The cycles life for grid based batteries are listed in Table 2.10. Fig. 5.1 shows the effect of number of cycles of operation with variation in DoD. It should be noted that 10 cycles of 10% DoD will be equal to 1 cycle of 100% DoD, in terms of energy exchange.

5.3.2 Calendar Life

Calendar life refers to the number of years the battery is expected to last till the battery will reach EoL. It is independent of how much the battery is charged and discharged. However, calendar life is dependent on the state of charge of the battery and the temperature. Data-sheet [63] shows how the calendar life of the battery is a function of SoC level and temperature. An interesting observation is that a high SoC level affects the calendar life drastically at high temperatures. It can be observed that below 35^oC expected life is independent of SoC. In this chapter we assume temperature is controlled and SoC is regulated in the optimal band of operation. The calendar life for grid based batteries are listed in Table 2.11.

5.3.3 Optimal Storage Control

An optimal control problem for an energy storage device such as a battery is proposed in [148, 145] using convexity property of the optimization function and saddle point inequality. In Chapter 3 and Chapter 4 we formulate the optimal energy arbitrage problem and propose an efficient algorithm and we show that a time horizon of optimization can be sub-divided into sub-horizons. In each of these sub-horizons, the shadow price is a function of price levels in a sub-horizon and is independent of all past and future sub-horizons. This value of the shadow price is altered only when the battery capacity reaches its maximum or minimum permissible charge levels. Based on the value of shadow price in a sub-horizon, the optimal control decisions are selected depending on the level of price of electricity at that instant.

The threshold based structure of the optimal solution is presented in Remark 1 in Chapter 3.

5.3.4 Limiting Cycles of Operation

The life of a battery will be a function of cycle life and calendar life. If the battery operates more cycles per unit of time then the battery EoL will be achieved due to cycle life limitations and vice versa. In other words, if the battery is used a lot then the battery will last less. To increase the operational life, the average number of cycles of operation per unit of time (I_{op}) should be set to

$$I_{op} = \frac{\text{Cycle Life}}{\text{Calendar Life}}. \tag{5.3.1}$$

EoL of a battery operating more than I_{op} will be caused by the limitation on cycle life of the battery, implying the battery is over-used. If the battery is under-used, EoL will be caused by the calendar life. We assume that if cycle life equals calendar life of the battery than the operational life the battery is increased. This criterion will be met if battery operates I_{op} cycles per unit time on average, shown in Eq. 5.3.1. Desired cycles of operation for unit of time matches the battery calendar life degradation to that of the operational cycling degradation.

Note the volatility across all days in a year can vary drastically, implying battery should perform more cycles when the volatility is high. It is interesting that a scalar selection the friction coefficient will ensure storage performing more cycles under more volatile price compared to less volatile price.

We propose limiting the operation of the battery by adding friction in mode changes for the battery. Adding friction will ensure that the battery does not operate for lower returns. This idea of creating dead-band of no operation is motivated by Eq. 5.3.2. The threshold based structure of the optimal solution indicates that the optimal decision for the battery when the condition $p_{\text{ch}}(i) > \mu > p_{\text{dis}}(i)$ is true, is to do nothing. This band signifies the additional profit the charge discharge cycle of a battery should make in order to compensate the losses incurred due losses in charging and discharging. Increase of this band will indicate eliminating low returns transactions in arbitrage. We define modified charging and discharging cost as a function of friction coefficient denoted as

$$p^L_{\text{ch}}(i) = p_{\text{ch}}(i)/\eta_{\text{friction}} = \frac{p_i}{\eta_{\text{ch}}\eta_{\text{friction}}}, \quad p^L_{\text{dis}}(i) = p_{\text{dis}}(i)\eta_{\text{friction}} = p_i\eta_{\text{dis}}\eta_{\text{friction}}.$$

The threshold based structure of the solution is modified as

$$x^*_i(\mu) = \begin{cases} X_{\min}, & \text{if } \mu < p^L_{\text{dis}}(i), \\ [X_{\min}, 0], & \text{if } \mu = p^L_{\text{dis}}(i), \\ 0, & \text{if } p^L_{\text{ch}}(i) > \mu > p^L_{\text{dis}}(i), \\ [0, X_{\max}], & \text{if } \mu = p^L_{\text{ch}}(i), \\ X_{\max}, & \text{if } \mu > p^L_{\text{ch}}(i), \end{cases} \tag{5.3.2}$$

The selection of η_{friction} will be governed by: volatility of the price, maximizing operational life of the battery and arbitrage gains. Note the value of $\eta_{\text{friction}} \in (0, 1]$. The control of η_{friction} should only be considered if the cycles of operation per day is higher than I_{op}. Fig. 5.2 shows the ramping profile difference for the same price single for no losses and with losses (refer to numerical experiment in Chapter 3 for details).

Figure 5.2: Comparison of ramp rates for same price signal without and with efficiency losses

5.3.5 Numerical Results

In this section we present a numerical example demonstrating the effect of friction coefficient on arbitrage gains, number of cycles of operation and the shadow price of transaction. The battery parameters used for the numerical evaluation is listed in Table 5.1. Consider the battery has a cycle life of 6000 cycles

Table 5.1: Battery Parameters

Parameter	Value	Parameter	Value
δ_{max}	0.5 kW	δ_{min}	-0.5 kW
$b_{\max}$	1 kWh	$b_{\min}$	0.1 kWh
η_{ch}	0.95	η_{dis}	0.95
h	0.25 hour	b_0	0.1 kWh

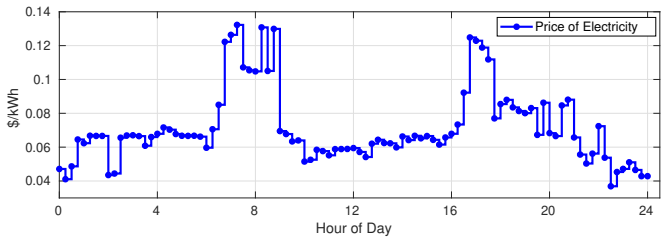

Figure 5.3: Electricity price data from NYISO [29].

and calendar life of 10 years. The optimal number of cycles the battery should operate per day should be $I_{op} = 1.644$ per day, using Eq. 5.3.1. Real-time 15-minute locational marginal price data for 21st December, 2016 from NYISO [29] is used for simulation analysis. The electricity price is plotted in Fig. 5.3. Fig. 5.4 shows the variation of cycles of operation and arbitrage gains with friction coefficient. When friction coefficient is 1 implies battery operates more and the arbitrage gains are higher. As the coefficient is reduced the decrease in gains and cycles of operation can be observed. For I_{op} cycles per day, the optimal value of friction coefficient for this numerical example is $\eta_{\text{friction}_{opt}} = 0.855$ as shown in Fig. 5.4. Note that for achieving I_{op} cycles the reduction in arbitrage gains is $\approx 10\%$ and the cycles of operation decreases by $\approx 36\%$. A risk averse user may prefer to maximize it's current gains, for example for $\eta_{\text{friction}} = 0.918$,

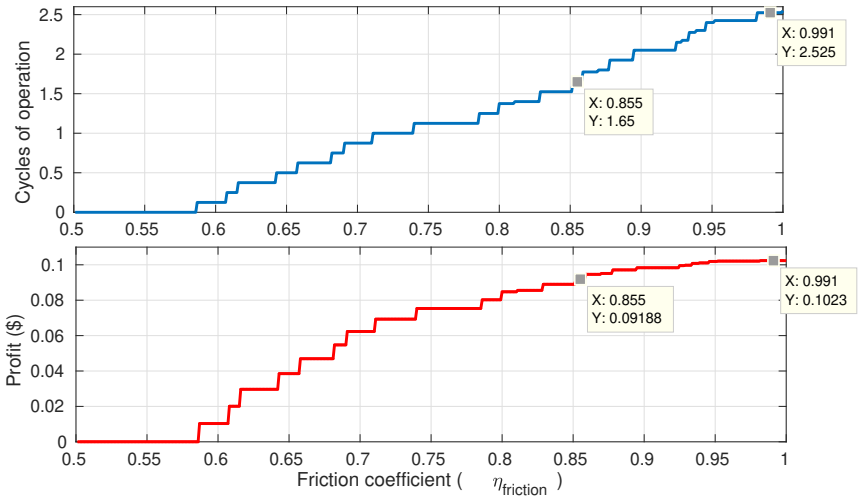

Figure 5.4: Variation of cycles and gains with η_{friction}

the reduction in gains is 1.47% and the reduction in cycles of operation will be 11.7%. Fig. 5.5 shows the variation of shadow price across the time horizon of 1 day as the friction coefficient is varied. Note as the friction coefficient is reduced, the shadow price converges to a single level. Fig. 5.6 shows the variation of

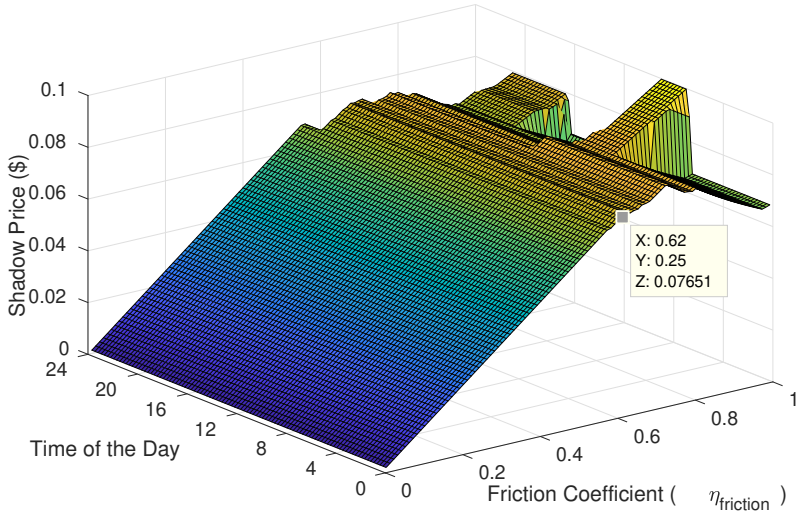

Figure 5.5: The shadow price in a day vary with η_{friction}

ramp rate of the battery with η_{friction}. On comparing Fig. 5.6 with respect to price variations in Fig. 5.3, it is evident that battery operates only when the gains are significantly higher for lower values of η_{friction}. As the η_{friction} is reduced the battery operates only around midnight to charge in order to discharge during morning peak and during evening peak. The friction coefficient distinguishes arbitrage gains based on the returns. Inclusion of η_{friction} ensures battery operates for only when the gains are high enough.

5.3.6 Observations

We propose a mechanism to compare arbitrage gains and cycles of operation for a battery. The users can tune the coefficient of friction according the price volatility over a period to maximize operational life of a battery and its arbitrage gains. The inclusion of friction coefficient ensures that low returning transactions are eliminated and battery operates only when returns are higher.

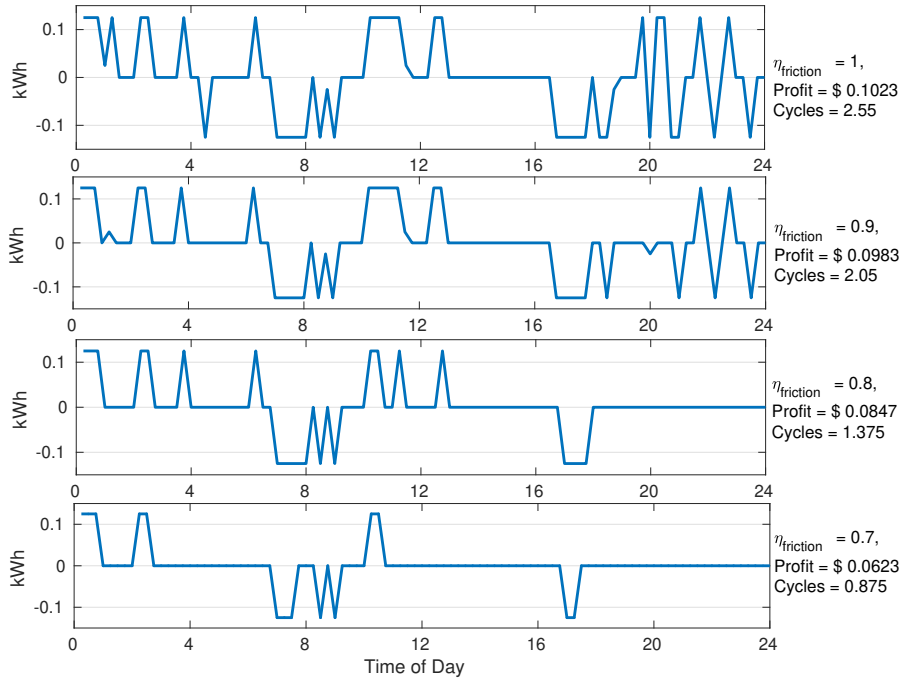

Figure 5.6: Variation of ramp rate of the battery with η_{friction}

5.4 Controlling Arbitrage Cycles

In this section we present the threshold based mechanism to identify the optimal arbitrage decisions and efficiently controlling the cycles of operation. We present an iterative framework to tune the number of cycles of operation to maximize battery life by matching calendar life degradation to cycle life degradation.

5.4.1 Energy Storage Arbitrage Algorithm with Negative Prices

Extension of the threshold based structure proposed in Chapter 3 for negative electricity prices is introduced in Section 3.6.1 and Remark 3. The threshold for day τ is given as Remark 8.

Remark 8. The storage control decision x_i^* for some day τ in the ith instant minimizes the function $C^{(i)}_{\text{storage}}(x) - \mu_i^* x$ for $x \in [X_{\min}, X_{\max}]$. The storage control decision $x_i^*(\mu)$ is [182]

$$x_i^*(\mu) = \begin{cases} \begin{cases} X_{\min}, & \text{if } \mu < p_{\text{dis}}(i), \\ [X_{\min}, 0], & \text{if } \mu = p_{\text{dis}}(i), \\ 0, & \text{if } p_{\text{ch}}(i) > \mu > p_{\text{dis}}(i), \text{ if } p_i \geq 0 \\ [0, X_{\max}], & \text{if } \mu = p_{\text{ch}}(i), \\ X_{\max}, & \text{if } \mu > p_{\text{ch}}(i), \end{cases} \\ \begin{cases} [0, X_{\max}], & \text{if } \mu \leq p_{\text{ch}}(i), \\ X_{\max}, & \text{if } \mu > p_{\text{ch}}(i), \end{cases} \quad \text{if } p_i < 0 \end{cases} \tag{5.4.1}$$

where $p_{\text{ch}}(i) = p_i^\tau / \eta_{\text{ch}}$, $p_{\text{dis}}(i) = p_i^\tau \eta_{\text{dis}}$, $C^{(i)}_{\text{storage}}(x_i) = s_i p_i^\tau$ and μ represents the shadow price of the transaction. Note for $\mu = p_{\text{ch}}(i)$ or $\mu = p_{\text{dis}}(i)$, $x_i^*(\mu)$ takes an *envelope* of values and for any other value of μ it is a singleton set. In order to find optimal decisions among an envelope of possible solutions based on the price variations, the Backward Step algorithm is used one time. The details of the algorithm can be found in Chapter 3 [182].

5.4.2 Controlling Cycles of Operation

The average monthly arbitrage gains is shown in Fig. 5.7. It is evident that opportunity for users is different for different months of the year. The results are for 1C/1C battery and the price signal used is

for the year 2016. For instance, it will be beneficial for users in MISO and NEISO to operate more number of cycles during August than any other month. However, for CAISO it is November. Storage in PJM in 2016 performing arbitrage would earn almost 15% of the total gains in the year for just the month of April. In our prior work [174], we proposed a mechanism to eliminate the low returning transactions of

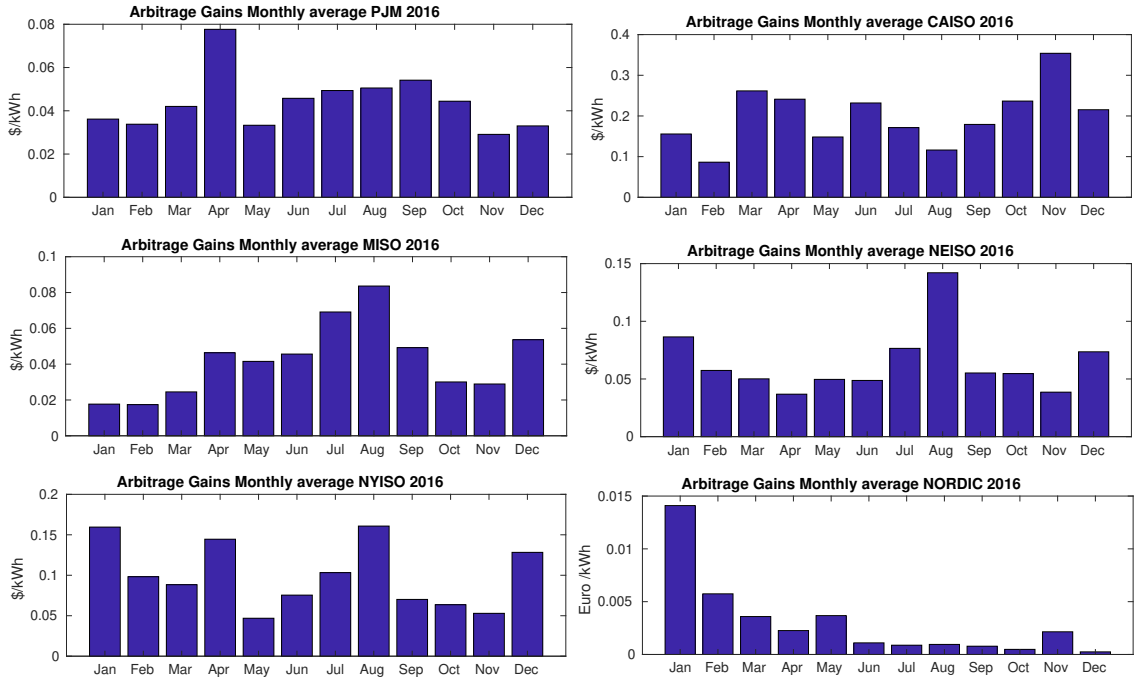

Figure 5.7: Monthly Average Arbitrage Gains

Algorithm 10 `OptimalCycles`

Inputs: $h, \eta_{\text{ch}}, \eta_{\text{dis}}, \delta_{\max}, \delta_{\min}, SoC_{\max}, SoC_{\min}$
Function: Optimal operation of storage with battery degradation
Initialize: $O_{cy}, b_0, \eta_{fric} = 1, \eta_{fric}^{previous} = 1$

$(O^*_{cy})_{\text{time}} = L_{cy}/L_{cal}$
while $(O_{cy} - (O^*_{cy})_{\text{time}}) > \epsilon$ **do**
  $x =$ Optimal arbitrage gains calculated using algorithm proposed in [182]
  Calculate $(\bar{B}_a)_{time} = 0.5((B_a)_{initial} + (B_a)_{time})$
  Calculate $(N_{100})_{time} =$ `DoDofVector`(x)
  Calculate $O_{cy} = \frac{(N_{100})_{time}}{(\bar{B}_a)_{time}}$
  if $O_{cy} > (O^*_{cy})_{\text{time}}$ **then**
    Reduce η_{fric} w.r.t. $\eta_{fric}^{previous}$ such that $\eta_{\text{fric}} \in [0, 1]$
  end if
  $\eta_{fric}^{previous} = \eta_{fric}$
  if $O_{cy} \lesssim (O^*_{cy})_{\text{time}}$ **then**
    Break While Loop
  end if
end while
Return the friction coefficient, η_{fric}

storage operation while performing arbitrage by introducing a friction coefficient in mode change. Adding friction will ensure that the battery does not operate for lower returns. This idea of creating dead-band of no operation is motivated by Eq.(5.4.1). The threshold based structure of the optimal solution indicates that the optimal decision for the battery when the condition $p_{\text{ch}}(i) > \mu > p_{\text{dis}}(i)$ is true, is to do nothing. This band signifies the additional profit the charge-discharge cycle of a battery should make in order to compensate the losses incurred due losses in charging and discharging. Increase of this band will indicate eliminating low returns transactions in arbitrage. We define modified charging and discharging cost as a function of friction coefficient denoted as $p^L_{\text{ch}}(i) = p_{\text{ch}}(i)/\eta_{\text{fric}}$ and $p^L_{\text{dis}}(i) = p_{\text{dis}}(i)\eta_{\text{fric}}$. Algorithm 10 uses the algorithms proposed in [182, 174] to control cycles of operation in such a way

that the calendar degradation is approximately equal to the cycle degradation, implying maximization of battery's operational life. Note that the proposed algorithm is sensitive to the accuracy of information, in this chapter we operate under deterministic setting as our objective is to identify the maximum dollar per cycle potential of a battery.

5.4.3 Open Source Codes

The equivalent depth-of-discharge and mechanism to calculate dollars per cycle is made open source. The link for the code is https://github.com/umar-hashmi/DollarsPerCycle.

5.5 Battery Participating in Ancillary Service

Ancillary services are essential components of power system to ensure reliable operation of the power grid. In this part of the chapter we focus on ancillary service market of PJM in the US. We list the compensation mechanism used under PJM and the amount of capacity needed to perform regulation. We also look into fluctuations of monthly regulation needs requested by PJM for the year 2017.

5.5.1 Compensation Mechanism

The value of regulation provided under PJM depends on the performance score, mileage ratio, market clearing prices. The compensation mechanism is described in this subsection. Performance score is calculated for each regulation resource for each hour. Performance scores reflect the benefits each resource provides to system control by focusing on the resource's response to PJM control signals. All ISO in the USA have some sort of performance evaluation mechanism for comparing service provided by regulating resources.

PJM's performance score has 3 components: Accuracy score, Delay score and Precision Score [143, 144, 39]. PJM calculates performance score for hourly data. The dynamic regulation signal is sampled every 2 seconds. Performance scores reflect how well the resource is following the regulation signal. Performance Score is defined as the equal weighted sum of accuracy score, delay score and precision score.

RegA and RegD represents the low and high frequency ancillary service requirement needs at PJM ISO. Batteries are suitable for tracking RegD regulation signal. Mileage is the absolute sum of movement of the regulation signal in a given time period with n samples. Mileage for RegA and RegD are denoted as $\text{Mileage}_{RegA} = \sum_{i=0}^{n} |RegA_i - RegA_{i-1}|$, $\text{Mileage}_{RegD} = \sum_{i=0}^{n} |RegD_i - RegD_{i-1}|$. Mileage is a proxy metric for measuring the amount of work done by regulation resources, i.e., their contribution towards area control error correction [97]. At the beginning of each hour, Hour Signal Mileage is measured for the previous operating hour. Hour Signal Mileage is the actual mileage used in settlements for service credits. Mileage ratio is defined as the ratio of Mileage_{RegD} and Mileage_{RegA}. Mileage ratio measures the relative work done or the movement of RegD resources relative to RegA [97].

The end user compensation is governed by hourly values of Regulation Market Capability Clearing Price (RMCCP), Regulation Market Performance Clearing Price (RMPCP), Mileage Ratio (M), Cumulative Regulation provided in MW (G) and performance score (η_{perf}). It is in the best interest for storage owners to maintain a high performance score. In order to maintain a high performance score battery owners must commit regulation appropriately. The integrated regulation provided in MW is used for calculating the compensation (Page 28 of [68]). The cumulative regulation provided for the k^{th} hour is denoted as $G_k = \sum_{i=i_{k-1}+1}^{i=i_k} |g_i|$, where g_i is the power output of regulation resource (MW) at i^{th}, i_k denotes the sample index of end of the k^{th} hour.

The RMCCP (USD/MWh) used in settlement is multiplied by the actual performance score and the hourly integrated megawatts operated each hour to determine capability revenues. Regulation RMCCP Credit for k^{th} hour is given as

$$\text{RMCCP}^k_{credit} = \eta^k_{perf} G_k \ \text{RMCCP}_k.$$

FERC order 755 provides the pay-for-performance in compensation design for regulating resources [117]. The RMPCP (USD/MWh) is used for calculating Regulation RMPCP Credit for hour index k, it is given as

$$\text{RMPCP}^k_{credit} = \eta^k_{perf} G_k \ \text{RMPCP}_k M_k.$$

Regulation Clearing Price Credit = Regulation RMCCP Credit + Regulation RMPCP Credit [68]. The typical variation of RMCCP and RMPCP is shown in Fig. 5.8.

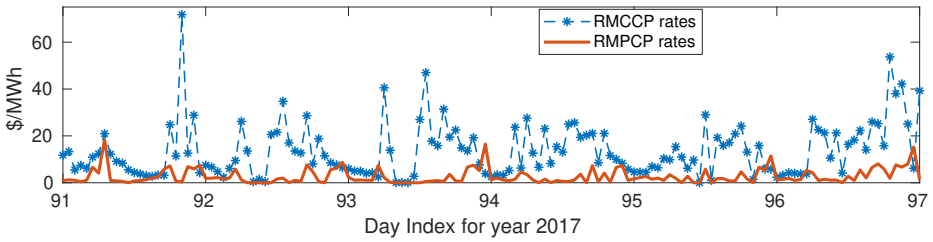

Figure 5.8: RMCP variation for 1st week of April, 2017 [152].

5.5.2 Controlling the Cycles

The design of regulation signal is done in such a way that energy storage owners participating in PJM's ancillary service market can track the regulation signal in a sustainable manner. Energy storage is a buffer of energy and consumes finite amount of power in charging and discharging cycles due to efficiency losses in power conversion. This implies if the regulation signal is not designed appropriately then battery charge level will drift to one of its boundaries and will not be able to provide regulation in the other direction. Fig. 5.9 shows the mean ramp-up and ramp-down required monthly for the year 2017 in PJM ISO. Mean

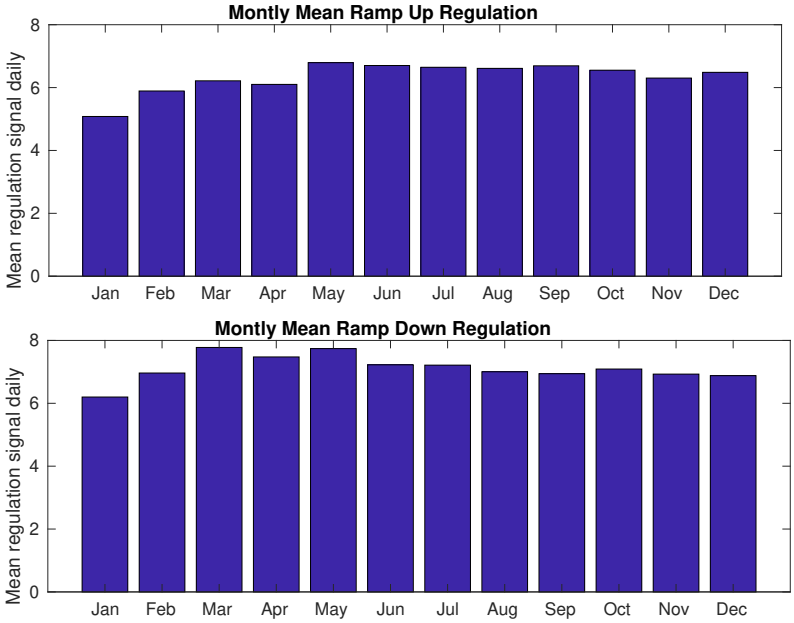

Figure 5.9: Monthly Average Ramp Up & Down Regulation, PJM 2017

ramp-up for M days in a month is calculated as $\frac{1}{M}\sum_{\tau=1}^{M}\sum_{i=0}^{T}[r_i]_\tau^+$, where $[r_i]_\tau^+$ denoted the up regulation for τ^{th} day and i^{th} instant. Similarly, mean ramp down for a month is calculated as $\frac{1}{M}\sum_{\tau=1}^{M}\sum_{i=0}^{T}[r_i]_\tau^-$. PJM's thoughtful design of regulation signal is evident from Fig. 5.9, where the ratio of cumulative mean ramp up over ramp down is maintained between 0.8 to 0.96 for each month in the year of 2017. Due to this attribute of regulation signal batteries can consume extra energy while performing ramping down (i.e. charging) compared to ramping up (i.e. discharging), compensating the loss in energy due to efficiency losses. Fig. 5.9 shows the histogram of mean regulation for each day in each month for ramping up and ramping down. The key take away from this figure is that the regulation requirements remain quite the same for the whole year and the variability is not governed by seasonality unlike price variability over the year.

The regulation provided by the batteries can be controlled by controlling the maximum ramp rate of the battery. The operational ramp rate can be adjusted such that $\delta_i \in [-\delta_{\text{op}}^{\max}, \delta_{\text{op}}^{\max}]$ where $\delta_{\text{op}}^{\max} \in [0, \min(\delta_{max}, -\delta_{\min})]$. The parameter used for controlling the cycles of operation is the operational maximum ramp rate of the battery, $\delta_{\text{op}}^{\max}$.

Algorithm 11 describes the mechanism to calculate the maximum capacity needed to track regulation signal sustainably for longer time horizons. It is observed that battery capacity is not a constraint for sustainable tracking of regulation signals using batteries pertaining to the design of regulation signal under PJM ISO.

5.6 Numerical Results

For the numerical results we use a Li-Ion battery with calendar life of 10 years and cycle life at 100% DoD is 4000 cycles. For degradation model, k_p is selected as 1.1, implying battery will perform approximately 5971 cycles at 70% DoD. We present simulation results at two different time scales, to make gains per cycle comparison between arbitrage and regulation more robust to short term volatilities. The shorter time scale is considered as 1 day and longer time scale is considered to be a year. The simulations are conducted using PJM real time price data and RegD data for the year 2017. In order to understand the volatility of price, data for the year 2016 is used. With our model we observe that the arbitrage and the regulation gains are affected by the ratio of ramp rate and storage capacity. Replacing a smaller battery with a big one with same ratio of ramp rate over storage capacity will increase the gains proportional to the factor of increase in battery capacity, assuming charging and discharging efficiencies are the same. This implies the current analysis is valid for different capacity battery with same ratio of the ramp rate and the capacity of the battery. For all numerical analysis we consider a $1kWh$ battery with $SoC_{\min} = 0.1$ and $SoC_{\max} = 0.98, \eta_{ch} = \eta_{dis} = 0.95$. The ratio of battery capacity over ramp rate is often used to denote battery type. For instance xC-yC battery will require 1/x hours to fully charge and 1/y hours to fully discharge. We use this nomenclature in results in this section. In order to calculate the financial potential of storage in ancillary service market, we assume that the performance index is equal to 0.95. The real time electricity data used for arbitrage simulation is of PJM [16] and ancillary service market parameters are downloaded from [152], [274].

Algorithm 11 `CapacityNeededRegulation`

Inputs: $r, k = 1$
Function: Maximum Capacity Needed to Perform Regulation

1: Calculate $N = \text{length}(r)$
2: **for** $i = 1 : N$ **do**
3: **for** $j = 1 : i$ **do**
4: $cum_{mat}(k) = cum_{mat}(k) + \eta_{ch}[r]^{+} - \frac{[r]^{-}}{\eta_{dis}}$
5: **end for**
6: k=k+1
7: **end for**
8: Return Capacity Needed, $b_{need} = \frac{h(max(cum_{mat}) - min(cum_{mat})}{SoC_{max} - SoC_{min}}$

5.6.1 Short Time-Scale: A typical Day

Arbitrage and regulation gains are calculated for price data and RegD signal for 2nd Feb. 2017. Storage with varying ramping capabilities are simulated for gains and gains per cycle. Results tabulated in Table

Table 5.2: Dollars/Cycle for storage performing arbitrage

Ramp Rate	Cycles Performed	Gain ($)	Dollars/Cycle
2C-2C	4.029	0.2015	0.0500
1C-1C	4.029	0.2015	0.0500
0.5C-0.5C	2.714	0.1675	0.0617
0.25C-0.25C	2.259	0.1380	0.0611

5.2 and Table 5.3 indicate that a high ramping storage will perform many more cycles while performing regulation. It is clear that gains per cycle is significantly higher for storage performing regulation compared to arbitrage.

For storage performing regulation, the number of 100% DoD cycles using the linear DoD model (i.e., $k_p = 1$) is more than 3 cycles. However, 100% cycles calculated for $k_p = 1.1$ is 1.121. Storage performing

Table 5.3: Dollars/Cycle for storage performing regulation

Ramp Rate	Cycles Performed	Gain ($)	Dollars/Cycle
2C-2C	11.045	9.0530	0.8196
1C-1C	5.153	4.5265	0.8785
0.5C-0.5C	2.404	2.2632	0.9415
0.25C-0.25C	1.121	1.1316	1.0091

regulation takes the advantage of short-cycling, evident from histogram of DoD shown in Fig. 5.10, while storage performing arbitrage performs deep discharge cycles, regulation due to shorter sampling time performs short DoD cycles, as pointed out earlier short DoD cycles significantly improves the cycle life of battery. It is evident from Table 5.3 that the efficient manner to calculate cycles of operation is by

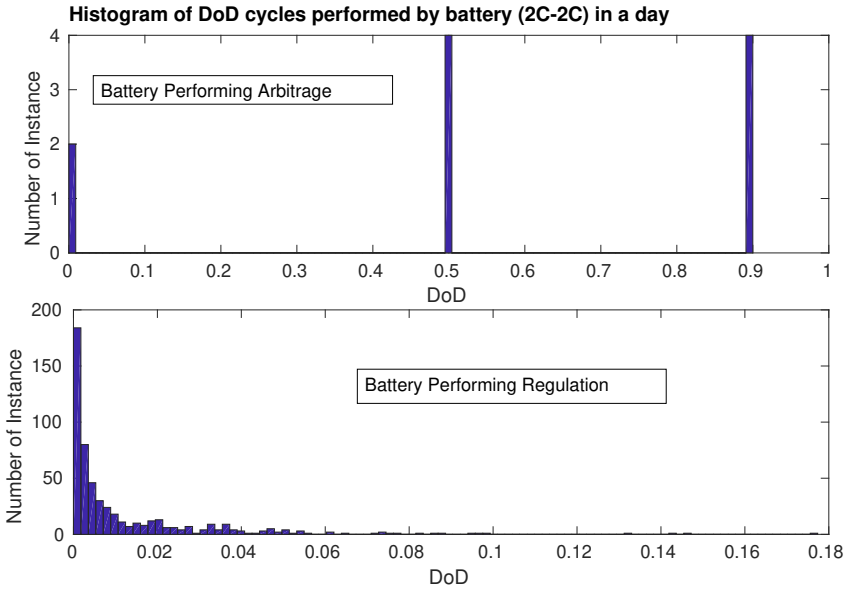

Figure 5.10: DoD variation of a battery performing arbitrage and regulation in PJM ISO in a day

adjusting the maximum ramping of battery. Furthermore, it is observed that storage operating at lower ramp rate has a higher dollars per cycle potential implying higher revenue in the long term.

5.6.2 Long Term Simulation - One Year

For the battery considered in this numerical example, the battery should perform $\approx$ 400 cycles per year in order to match the calendar and cycle degradation, thus maximizing battery life. Long term simulations for the year of 2017 is conducted. For arbitrage, the friction coefficient is adjusted to match the optimal number of cycles, as shown in Fig. 5.11. The dollar per cycle potential of storage performing regulation for the year 2017 is listed in Table 5.4. From the short term and long term simulations it is evident that

Table 5.4: Dollars/Cycle for storage performing regulation

Ramp Rate	Cycles Performed	Gain ($)	Dollars/Cycle
2C-2C	4451.34	7709.62	1.7320
1C-1C	2076.62	3854.81	1.8562
0.5C-0.5C	968.77	1927.40	1.9895
0.25C-0.25C	451.95	963.70	2.1323
0.125C-0.125C	210.84	481.85	2.2854

performing regulation is much more beneficial for storage owners compared to arbitrage.

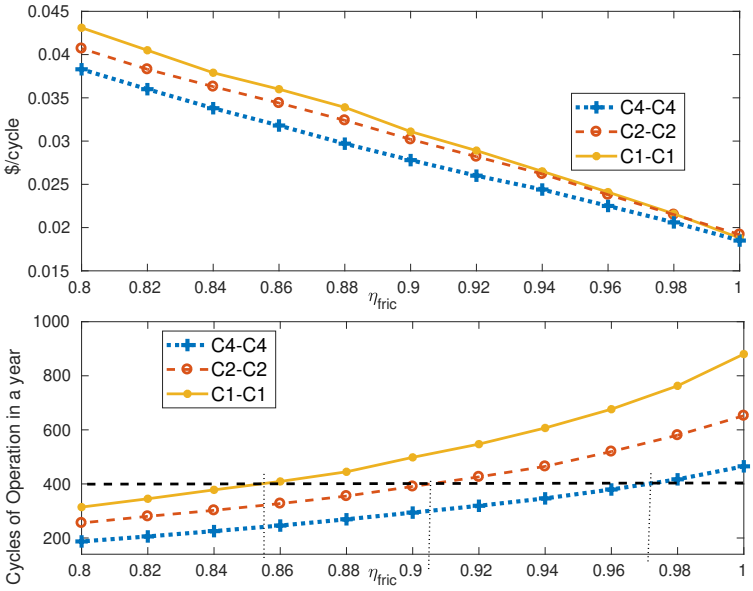

Figure 5.11: Arbitrage Gains, cycles of operation with η_{fric} for 2017

5.7 Conclusion and Perspectives

In order to maximize the battery life, the calendar life degradation has to be matched with cycle life degradation. For a battery performing arbitrage, the cycles can be controlled by tuning friction coefficient and for battery performing regulation the cycles can be controlled by adjusting the ramping rate. By adjusting ramp rate of the battery the amount of regulation provided by the battery is controlled. As the ramp rate increases the amount of regulation provided by the battery proportionally increases.

We propose an algorithm to calculate equivalent 100% cycles performed by battery. The financial potential of battery performing arbitrage and regulation is compared based on dollars per cycle potential identified using simulations based on real data from PJM ISO. The simulations results indicate that storage participating in ancillary services will gain significantly higher than storage performing energy arbitrage.

Dollars per cycle as a performance index is versatile. It can be used for (a) taking into account operational cycles, (b) this index can be normalized with respect to battery size for making it independent of storage size, which implies we can use it to select the right size of the battery. We used dollars per cycle to identify the optimal ramping battery in Chapter 7. Furthermore, the dollars per cycle can be used for identifying the profitability of battery. This is used in Chapter 8 and Chapter 9.

Part II

Energy Storage Co-Optimization for Electricity Consumers

Chapter 6

Arbitrage & Power Factor Correction

To the optimist, the glass is half full. To the pessimist, the glass is half empty. To the engineer, the glass is twice as big as it needs to be. -Unknown

Summary: The importance of reactive power compensation for power factor (PF) correction will significantly increase with the large-scale integration of distributed generation interfaced via inverters producing only active power. In this work, we focus on co-optimizing energy storage for performing energy arbitrage as well as local power factor corrections. The joint optimization problem is non-convex, but can be solved efficiently using a McCormick relaxation along with penalty-based schemes. Using numerical simulations on real data and realistic storage profiles, we show that energy storage can correct PF locally without reducing arbitrage gains. It is observed that active and reactive power control is largely decoupled in nature for performing arbitrage and PF correction (PFC). Furthermore, we consider a stochastic online formulation of the problem with uncertain load, renewable and pricing profiles. We develop a model predictive control based storage control policy using ARMA forecast for the uncertainty. Using numerical simulations we observe that PFC is primarily governed by the size of the converter and therefore, look-ahead in time in the online setting does not affect PFC noticeably. However, arbitrage gains are more sensitive to uncertainty for batteries with faster ramp rates compared to slow ramping batteries.

6.1 Introduction

With the growth of distributed generation (DG) and large-scale renewables, the need to understand their effects on power networks has become crucial. While bulk-renewable generators have well defined rules for performance including that for reactive power, distributed generation owned by small residential consumers have been exempted. This is primarily due to lack of measurement infrastructure and installed DG contributing to a small fraction of total generation. However, in recent years, growing incentives and environmental awareness have resulted in a large number of consumers installing distributed generation. In Chapter 3 and Chapter 4 we pointed that NEM policies have been a great success. Only in California almost a million consumers opted for DG installations by the end of 2018[1]. Understanding the effects, both operational and financial, of growth in distributed energy resources (DERs) is essential for Distribution System Operators (DSOs) to ensure reliable operation. Since DERs in current markets are not financially rewarded for providing reactive power support, small inverters connected to them primarily output active power and almost no reactive power [191]. This is also in compliance with IEEE Standard 1547, which specifies that DG shall not actively regulate the voltage at the point of common coupling [298]. As a result, there has been a degradation of the load power factor (PF) [344].

PF denotes the ratio of active power and the apparent power and is measured as $\cos(\phi)$, where ϕ denotes the angle between active and reactive power. As distribution grids are primarily designed to operate close to unity power factor, a systematic degradation in PF can lead to high current, excessive thermal losses, aggravated voltage profiles [199], and equipment damage. It has been shown that maintaining a high power factor leads to positive environmental effects due to increased grid efficiency [8]. To this end, several regional transmission organizations and system operators have operational rules for PF as stated in Table 2.2, though primarily for large loads.

[1] https://www.californiadgstats.ca.gov/, January, 2019

However, the PF of residential consumers is also a point of concern. For example, the Smart Islands Energy Systems (SMILE) project, initiated by the European Union in 2017 [13], involves data collection at multiple fronts including consumer smart meters in Madeira, Portugal. As a case study, 15 minute averaged household consumption and solar generation data on 18th May, 2018 for a representative residential consumer in the island of Madeira, Portugal is depicted in Fig. 6.1. Note that while PF at night is close to unity, during the day it degrades significantly due to solar output. Thus low load PF may be subjected to norms and penalties [344, 191]. Some household smart meters (Eg. Linky smart meters in France) already have reactive power monitoring capability that can implement PF norms [19]. The LV consumers in Uruguay have electricity bills with three different contracts [25] that include penalties for PF degradation. Section 6.6 presents a measurement case-study of degradation of power factor seen from a substation in the island of Madeira.

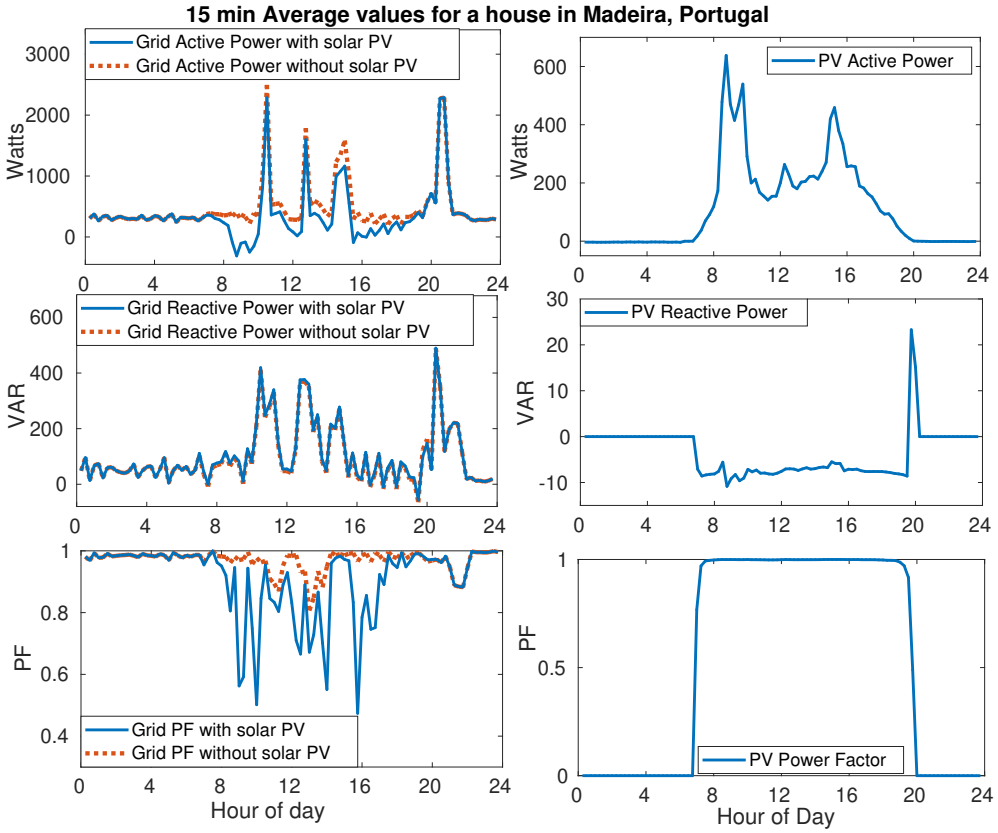

Figure 6.1: Variation of active, reactive power and absolute value of power factor for PV and load

6.1.1 Literature Review

While additional infrastructure such as capacitor banks [27, 186] have been proposed to improve power factor, we focus our work on using conventional energy storage/battery for performing power factor correction, in addition to other functions like arbitrage [283, 183]. Note that storage devices generate DC power and hence are connected to the grid through a DC/AC converter/inverter that are often over-sized compared to the installed DER facility [201]. Utilizing the storage converter/inverter and power electronics [296] for power factor correction averts additional investment. The overarching goal of this chapter is to demonstrate through novel co-optimization formulations that batteries can be used for PFC without any significant effect on arbitrage gains, for a range of price, consumption and PV settings. Note that due to the high cost of storage deployment, researchers have proposed using storage for co-optimization additional goals along with energy arbitrage (temporal shift of active load) for financial feasibility [207]. Inverter reactive power output depends on its control design [157], [313] and can be governed by terminal voltage and/or active power measurements [201], [85]. The authors in [254] use energy storage for maintaining voltages at wind facilities. Similarly, storage devices have been evaluated using power hardware-in-loop for minimizing losses and voltage fluctuations [307]. The authors in [136, 294] co-optimize storage for arbitrage, peak shaving and frequency regulation. Unlike the described prior work, we discuss storage for co-optimization of arbitrage and *power factor correction*. Note that contemporary solar inverters in low voltage operate close to unity power factor (UPF)[172] due to no reactive power obligations and hence are

practically ineffective for power factor correction. While we assume UPF for the solar inverter through the manuscript, we show that our approach can be used for controlling the solar inverter directly as a special case in Section 6.7.

6.1.2 Contribution

We are interested in using energy storage connected through an inverter for the joint task of arbitrage and PFC. In addition to commercial and residential electricity consumers, the formulation is also of interest for renewable integrators, transmission and distribution operators [4].

The contributions of this chapter are as follows

1. the development of a non-convex mixed-integer formulation to optimize storage for arbitrage and power factor correction in the presence of DG. While the co-optimization problem is non-convex, we demonstrate three different approximation schemes to solve the problem: (a) McCormick relaxation for original non-convex program, (b) receding horizon arbitrage with real-time PFC, and (c) arbitrage with penalty-based PFC. While the McCormick relaxation and real-time PFC policies routinely achieve the optimal solution, the penalty based approach is able to provide best alternatives in scenarios where no feasible solution satisfying PF limits exists.
2. we present a modified penalty-based algorithm that reduces converter usage along with arbitrage and PFC.
3. using realistic pricing, net load (consumption + solar) data and battery parameters, we extensively benchmark the achievable ability of storage devices to maintain PF limits without any significant degradation in arbitrage gains. This implies that household DG can follow PF limits as well if such regulations are created in future distribution grids.
4. we consider stochastic extensions of our algorithms for real-time implementation through Model Predictive Control (MPC). We use Auto-Regressive Moving Average (ARMA) processes to model temporally evolving signals in the MPC framework and demonstrate significant benefits from the online algorithms.

The chapter is organized in 7 sections. Section 6.2 provides the system details. Section 6.3 formulates the co-optimization problem of performing arbitrage and PFC using storage and discusses multiple solution strategies. Section 6.4 presents an online algorithm using ARMA forecasting and MPC in order to mitigate the effect of forecast error. Section 6.5 presents the numerical results. Section 6.6 provides a case study for a substation in Madeira where solar installations cause three phase unbalance, motivation for the imbalance reduction provided in Chapter 13. Section 6.7 provides PFC algorithm using solar inverter in absence of energy storage. Section 6.8 concludes the chapter and discusses future directions of research.

6.2 System Description

The system considered in this chapter consists of an electricity consumer with inelastic demand, renewable generation (rooftop solar) and battery. The energy storage will provide flexibility to deviate consumption in order to make gains by performing arbitrage and correct the power factor to satisfy utility prescribed limits. The block diagram of the system considered is shown in Fig. 2.20.

We denote time instant using variable i. The apparent power of the load shown in Fig. 2.20, at i^{th} time instant is denoted as $S_h^i = P_h^i + jQ_h^i$, where P_h^i and Q_h^i are the active and reactive power consumed. Apparent power of the solar inverter is given as $S_r^i = P_r^i$ where P_r^i is the active power supplied by solar inverter. We assume the solar inverter operates at unity PF. Let us denote the combined load and renewable active and reactive power by $P^i = P_h^i - P_r^i$ and $Q^i = Q_h^i$ respectively. The power factor seen by the grid is the ratio of real power supplied or extracted by the grid over the apparent power seen by the grid. In the absence of storage it is given by

$$\text{pf}_{\text{bc}}^i = P^i / \sqrt{P^{i\,2} + Q^{i\,2}}. \tag{6.2.1}$$

Observe that PF before correction, pf_{bc}^i, degrades as P_r^i and Q_h^i increases in magnitude. Next we discuss the battery model considered and its effect on PF.

Battery Model: The battery model is described in Chapter 2.5. The storage/battery converter can supply active and reactive power. The apparent power output of energy storage (connected through a converter which is an inverter or a rectifier) is given as $S_B^i = P_B^i + jQ_B^i$, where P_B^i, Q_B^i denote active and reactive power outputs respectively. We consider operation over a total duration T, with operations divided into N steps indexed by $\{1, ..., N\}$. The duration of each step is denoted as h. Hence, $T = hN$.

We denote the change in the energy level of the battery at i^{th} instant by x_i; $x_i > 0$ implies charging and $x_i < 0$ implies discharging. x_i/h denotes the corresponding storage ramp rate with $\delta_{\min} \leq 0$ and $\delta_{\max} \geq 0$ as the minimum and maximum ramp rates (kW) respectively. The storage active power P_B^i for the i^{th} instant is related to battery energy as $P_B^i = \frac{[x_i]^+}{h\eta_{ch}} - \frac{[x_i]^-\eta_{dis}}{h}$. Active power ramp rate constraint follows as

$$P_B^i \in [P_B^{\min}, P_B^{\max}] \text{ with } P_B^{\min}{=}\delta_{\min}\eta_{dis},\ P_B^{\max}{=}\frac{\delta_{\max}}{\eta_{ch}}, \tag{6.2.2}$$

Though the battery charge level is not affected by the reactive power output Q_B^i of the connected inverter, the amount of active power supplied or consumed is dependent upon it due to the line current limitations [208]. The converter rating is given by the maximum apparent power supplied/consumed, denoted as $S_B^{\max}$ which bounds the instantaneous apparent power S_B^i

$$(S_B^{\max})^2 \geq (S_B^i)^2 = (P_B^i)^2 + (Q_B^i)^2, \tag{6.2.3}$$

Let b_i denote the energy stored in the battery at the i^{th} step with $b_i = b_{i-1} + x_i$. To keep the charge in the battery within prescribed limits, the battery capacity constraint is imposed

$$b_i \in [b_{\min}, b_{\max}], \tag{6.2.4}$$

where $b_{\min} = SoC_{\min}B_{rated}$ and $b_{\max} = SoC_{\max}B_{rated}$. B_{rated} is the rated capacity and $SoC_{\min}$ and $SoC_{\max}$ are the minimum and maximum level of state of charge respectively.

6.2.1 Energy Arbitrage

In this chapter we assume that buying and selling prices of electricity at each instant i are the same and denote it by p_{elec}^i. Under this assumption, the arbitrage gains depend on the varying electricity price but not on the inflexible load. As monetary benefits from arbitrage is *based only on* active power, the operator seeks to minimize $\min_{P_B} \sum p_{\text{elec}}^i P_B^i$ with additional system constraints. Refer to Chapter 3 for details. The price of electricity is denoted as p_{elec}^i. The consumer optimization problem is given as [182]

$$\min \sum_{i=1}^{N} p_{elec}^i [P^i + P_B^i], \quad \text{subject to: Eqs. 6.2.2, 6.2.4}$$

Since there is no degree of freedom in P^i, it is equivalent to

$$(P_{arb}) \quad \min \sum_{i=1}^{N} p_{elec}^i P_B^i, \quad \text{subject to: Eqs. 6.2.2, 6.2.4}$$

In this problem the uncertainty will be due to variation of electricity price.

6.2.2 Power Factor Correction

The active power out of storage converter, $P_B^i \in [-P_B^{\max}, P_B^{\max}]$, and reactive power output ranges as $Q_B^i \in [-S_B^{\max}, S_B^{\max}]$. The utility sets the power factor limit $\text{pf}_{\min}$, which corresponds power angle $\theta_{\min} = \cos^{-1}(\text{pf}_{\min})$. The deep blue shaded region in Fig. 6.2 shows the feasible region of converter operation where output power factor lies within permissible limits of PF. In this plot we assume $P_B^{\max} \geq S_B^{\max}$. Note the power factor formulation in Eq. 6.2.1. In the presence of storage, it takes the form

$$pf_{\text{c}}^i = P_T^i / \sqrt{(P_T^i)^2 + (Q_T^i)^2}, \tag{6.2.5}$$

where total active power is denoted as $P_T^i = P^i + P_B^i$ and total reactive power is given as $Q_T^i = Q^i + Q_B^i$. It is clear that storage operations can negatively or positively affect the load PF. To ensure that the PF is within the permissible limits,

$$-k \leq \frac{Q_T^i}{|P_T^i|} = \frac{Q^i + Q_B^i}{|P^i + P_B^i|} \leq k, \quad \text{where } k = \tan(\theta_{\min}). \tag{6.2.6}$$

We assume that the limits in Eq. 6.2.6 are identical for both leading and lagging PF. Note that the feasible region for the PF constraint as shown in Fig. 6.2(a) is not convex. In the next section we will formulate a non-convex storage optimization problem and discuss solution strategies.

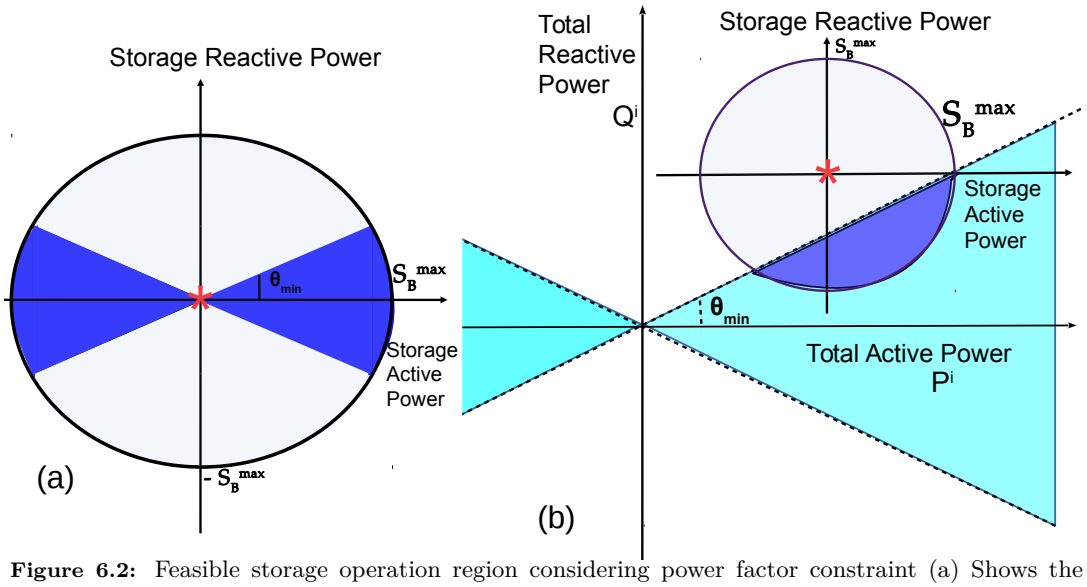

Figure 6.2: Feasible storage operation region considering power factor constraint (a) Shows the feasible region of storage in absence of load and DG. (b) Shows the feasible region of storage in presence of load and DG. The active and reactive power without storage is shown with red asterisk.

6.3 Arbitrage and PFC with Storage

We formulate the co-optimization problem for performing arbitrage and correcting power factor considering active (P_B^i) and reactive power (Q_B^i) output from storage connected via an inverter. Following the discussion in the preceding section, the objective function is given as

$$(P_{org}) \quad \min_{P_B^i, Q_B^i} \sum_{i=1}^{N} p_{elec}^i P_B^i, \quad \text{subject to, Eqs. 6.2.2, 6.2.3, 6.2.4, 6.2.6.}$$

Eq. 6.2.6 is non-convex but consists of two disjoint convex sets if the active power in the denominator is sign-restricted. This disjoint nature of PF constraint can be formulated as a mixed-integer convex problem by using McCormick relaxation as described in Section 6.3.1. Additional approaches to solve it are discussed in later sections. Section 6.3.2 presents the second sequential approach where arbitrage is optimized first and then PF constraints are corrected for the current instance only. Section 6.3.3 presents a third approach for this problem where we use a convex penalty for PF violations and solve the co-optimization problem by dynamic programming.

6.3.1 McCormick Relaxation based approach

We reformulate the non-convex PF constraint in (P_{org}) to a bi-linear constraint by introducing binary variables z as $|P_T^i| = (2z-1)P_T^i$. Here z is equal to 1 when total active power is positive and zero otherwise. Denoting the bi-linear term with variable $y = zP_T^i$, we use McCormick relaxation [244] to convert it to a mixed-integer linear constraint. As mentioned in [255], this McCormick relaxation is exact as one of the variables in the bi-linear term is a binary variable. After simplification, we get the following mixed-integer convex problem (P_{mr}).

McCormick envelopes are a type of relaxation used in bi-linear nonlinear programming problems as solving non-convex problems are difficult. The McCormick envelope guarantees convexity but keeps the bounds sufficiently tight [20]. In our setting, we use it to relax bi-linear representation of absolute value operator, say $|P_T^i| = (2z-1)(P_T^i)$ where z denotes a binary variable equal to 1 when $P_T^i > 0$ and zero otherwise. Let $y = zP_T^i$ denote the bi-linear variable. We then have

$$(2z-1)P_T^i \geq 0 \implies 2y - P_T^i \geq 0.$$

The McCormick relaxation for the bi-linear term is represented as follows

$$y \geq z_{lb}P_T^i + P_{lb}^i z - z_{lb}P_{lb}^i, \quad y \geq z_{ub}P_T^i + P_{ub}^i z - z_{ub}P_{ub}^i,$$
$$y \leq z_{lb}P_T^i + P_{ub}^i z - z_{lb}P_{ub}^i, \quad y \leq z_{ub}P_T^i + P_{lb}^i z - z_{ub}P_{lb}^i.$$

where z_{lb} (z_{ub}) and P^i_{lb} (P^i_{lb}) are the lower (upper) bounds for z and P^i_T respectively. As $z_{lb} = 0$ and $z_{ub} = 1$, the above constraints simplify to

$$y \geq P^i_{lb} z, \quad y \geq P^i_T + P^i_{ub} z - P^i_{ub}$$
$$y \leq P^i_{ub} z, \quad y \leq P^i_T + P^i_{lb} z - P^i_{lb},$$

The McCormick relaxation is known to be exact here as one of the variables in the bi-linear term is a binary variable. The optimization formulation including the above constraints is given as

$$(P_{mr}) \quad \min_{P_B, Q_B} \quad \sum_{i=1}^{N} p^i_{elec} P^i_B$$
$$\text{subject to, Eqs. 6.2.2, 6.2.3, 6.2.4}$$
$$\text{PF Constraint: } -2ky + kP^i_T - Q^i_T \leq 0,$$
$$-2ky + kP^i_T + Q^i_T \leq 0,$$
$$\text{McCormick Constraint:}$$
$$y \geq P^i_{lb} z, \quad y \geq P^i_T + P^i_{ub} z - P^i_{ub},$$
$$y \leq P^i_{ub} z, \quad y \leq P^i_T + P^i_{lb} z - P^i_{lb},$$
$$\text{Binary Variable: } z \in \{0, 1\}, \quad 2y - P^i_T \geq 0.$$

Here $P^i_{lb} = P^i + P^{\min}_B$ is the lower bound of total active power, and $P^i_{ub} = P^i + P^{\max}_B$ is the upper bound. Problem (P_{mr}) involving mixed-integer linear constraints can be solved by off the shelf solvers like Gurobi or Mosek that can be called by CVX [7]. Note that both (P_{org}, P_{mr}) consider arbitrage and PFC at equal footing for all time instances. To study the impact of PFC on arbitrage gains, we propose an approach next where PF of the current instance alone is considered while making optimal arbitrage decisions.

6.3.2 Receding horizon arbitrage with sequential PFC

We consider a receding horizon approach (P_{rh}) that solves two disjoint optimization problems, denoted as (P_{sub_1}) and (P_{sub_2}) below, for each time instant j and selects the solution with higher gains and feasibility.

$$(P_{sub_1}) \quad \min_{P_B, Q_B} \quad \sum_{i=j}^{N} p^i_{elec} P^i_B$$
$$\text{subject to, Eq. 6.2.2, Eq. 6.2.3, Eq. 6.2.4,}$$
$$-kP^j_T \leq Q^j_T \leq kP^j_T, \quad P^j_T \geq 0,$$

and the second sub problem is given as

$$(P_{sub_2}) \quad \min_{P_B, Q_B} \quad \sum_{i=j}^{N} p^i_{elec} P^i_B$$
$$\text{subject to, Eq. 6.2.2, Eq. 6.2.3, Eq. 6.2.4,}$$
$$-kP^j_T \geq Q^j_T \geq kP^j_T, \quad P^j_T < 0.$$

Note that both (P_{sub_1}),(P_{sub_2}) are convex and solve a cumulative arbitrage gains problem, but with PFC restricted to the current time-instant j only (no look-ahead PFC). The sub-problems only differ in the sign of the current total active power P^j_T. The feasible sub-problem with higher gains sets the storage actions for the current instant j, $(P^j_B)^*$ and $(Q^j_B)^*$. The approach then moves to the next instance $j + 1$.

Formulations (P_{org}), (P_{mr}), (P_{rh}) model the PF constraints as hard constraints and ensure their feasibility at every operational point. However, PF violations may be unavoidable and no feasible solution may exist. This may be due to converter limitations as well as storage constraints with regard to capacity and ramping. In such cases, we propose an alternate approach where we correct PF as best as possible.

6.3.3 Arbitrage with penalty based PFC

We redefine problem (P_{org}) using a penalty function $\theta(i)$ for the power factor. The objective of the new formulation (P_{plt}) is given by

$$\min_{P_B, Q_B} \quad \sum_{i=1}^{N} \left\{ p^i_{elec} P^i_B + \theta(i) \right\}, \tag{6.3.1}$$

where we define penalty function $\theta(i)$ as

$$\theta(i) = \lambda \max(0, |Q_T^i| - k|P_T^i|). \tag{6.3.2}$$

Here λ represents the constant associated with the linear cost of violating the PF. The shape of penalty function is shown in Fig. 6.3. The second term in Eq. 6.3.2 represents the amount of PF deviation from

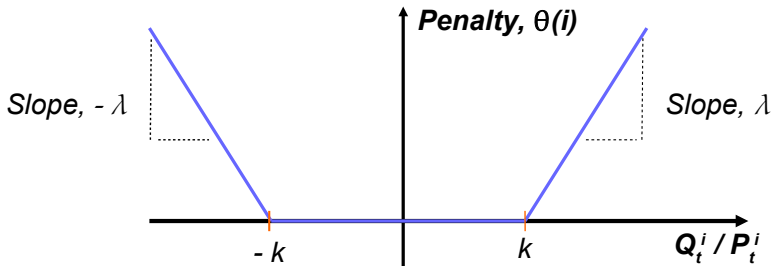

Figure 6.3: Penalty function with power factor variation

preset thresholds. This term will be equal to zero for cases where PF is within permissible limits. The max term can be modelled as two constraints

$$\theta(i) \geq 0, \quad \theta(i) \geq \lambda(|Q_T^i| - k|P_T^i|) \tag{6.3.3}$$

where absolute value function $|x|$ can further be represented as $(2z-1)x \geq 0$ with binary variable $z \in \{0, 1\}$. Eq. 6.3.3 can now be reformulated as

$$\begin{aligned} &\theta(i) \geq 0, \quad \theta(i) \geq \lambda(2y_1^i - Q_T^i - 2ky_2^i + kP_T^i). \\ &2y_1^i - Q_T^i \geq 0, \quad 2y_2^i - P_T^i \geq 0 \end{aligned} \tag{6.3.4}$$

Here y_1^i and y_2^i denote bi-linear variables

$$y_1^i = z_1^i Q_T^i, \quad y_2^i = z_2^i P_T^i \tag{6.3.5}$$

with binary variables z_1^i and z_2^i. z_1^i (z_2^i) is equal to 1 if the total reactive (active) power is greater than zero, and zero otherwise. As before, we use McCormick relaxation to convert the bi-linear terms in Eq. 6.3.5 to mixed-integer linear constraints

$$\begin{aligned} y_1^i &\geq Q_{lb}^i z_1^i, \quad y_1^i \geq Q_T^i + Q_{ub}^i z_1^i - Q_{ub}^i \\ y_1^i &\leq Q_{ub}^i z_1^i, \quad y_1^i \leq Q_T^i + Q_{lb}^i z_1^i - Q_{lb}^i \\ y_2^i &\geq P_{lb}^i z_2^i, \quad y_2^i \geq P_T^i + P_{ub}^i z_2^i - P_{ub}^i \\ y_2^i &\leq P_{ub}^i z_2^i, \quad y_2^i \leq P_T^i + P_{lb}^i z_2^i - P_{lb}^i. \end{aligned} \tag{6.3.6}$$

In these equations, $Q_{lb}^i = Q^i - S_B^{\max}$ and $Q_{ub}^i = Q^i + S_B^{\max}$ denote the lower and upper bounds respectively for total reactive power.

To summarize, the optimization problem for performing arbitrage and penalization PF violations and its associated constraints are given as

$$(P_{plt}) \quad \min_{P_B, Q_B} \quad \sum_{i=1}^{N} \left\{ p_{elec}^i P_B^i + \theta(i) \right\}$$

subject to, Eq. 6.2.2, Eq. 6.2.3, Eq. 6.2.4, Eq. 6.3.4, Eq. 6.3.6.

Note that while our approach uses linear costs for PF violations, the methodology can be extended to nonlinear penalties in a similar way.

6.3.4 Minimizing converter usage with arbitrage and PFC

Power electronic converters degrade with usage [336]. It is in the best interest of energy storage owners to minimize the converter operation, measured in apparent power output, to expand their lifetime. In order to emulate this we propose addition of converter usage component in the objective function of the new optimization problem (P_{plt}^{conv}). The new objective function consists of three components: (a) increase arbitrage gains, (b) reduce PF penalty and (c) reduce converter usage and is given as

$$\min_{P_B, Q_B} \sum_{i=1}^{N} \left\{ p_{elec}^i P_B^i + \theta(i) + \beta \left((P_B^i)^2 + (Q_B^i)^2 \right) \right\}$$

The optimization problem (P_{plt}^{conv}) is subject to the same constraints as (P_{plt}).

6.3.5 Open Source Codes

The co-optimization formulations and benchmarks presented in this chapter is made open source. The link for the code is https://github.com/umar-hashmi/powerfactorcorrection.

6.4 Modeling Uncertainty

The previous section discussed arbitrage and PFC under complete knowledge of future net loads and prices. In this section, we consider the setting where future values may be unknown. To that end, we first develop a forecast model for active and reactive power and electricity price for future times, where the forecast is updated after each time step. We develop the forecasting model for net load with solar generation using AutoRegressive Moving Average (ARMA) model and electricity price forecast using AutoRegressive Integrated Moving Average (ARIMA). The output of the forecast model is fed to model predictive control for real-time operation. The details of forecast model are provided in Section 2.4.1.

6.4.1 Model Predictive Control

The forecast values are fed to a Model Predictive Control (MPC) scheme [122] to identity the optimal modes of operation of storage for the current time-instance. Any of the developed schemes from the previous section can be used for the receding horizon optimization inside MPC. These steps (forecast and MPC) are repeated sequentially and highlighted in online Algorithm 9: `ForecastPlusMPCforCoOpt1`.

Algorithm 12 `ForecastPlusMPCforCoOpt1`

Global Inputs: $\eta_{\text{ch}}, \eta_{\text{dis}}, \delta_{\max}, \delta_{\min}, b_{\max}, b_{\min}, S_B^{\max}, b_0$
Inputs: $h, N, T, i = 0$

1: **while** $i < N$ **do**
2: $i = i + 1$
3: Forecast $\hat{P}, \hat{Q}$ from time step i to N using ARMA
4: Forecast $\hat{p}_{elec}$ from time step i to N using ARIMA
5: Co-optimize arbitrage and PFC using inputs $\hat{p}_{elec}, \hat{P}, \hat{Q}, h$, battery parameters
6: Find out battery output: P_B and Q_B
7: $b^{i^*} = b^{i-1} + [P_B(i)]^+ \eta_{\text{ch}} - [P_B(i)]^- / \eta_{\text{dis}}$
8: Update $b_0 = b^{i^*}$
9: **end while**

6.5 Numerical Results

In this section, we demonstrate the performance of our proposed optimization formulations through numerical simulations with real data. As described in Section 6.3, we consider multiple storage control policies in the presence of solar, as listed below.

- P_{arb}: Only arbitrage,
- P_{mr}: McCormick relaxation for arbitrage + PFC,
- P_{rh}: Receding horizon arbitrage + sequential PFC,
- P_{plt}: Arbitrage + penalized PFC,
- P_{plt}^{conv}: Arbitrage + penalized PFC+converter usage.

The price data for our simulations is taken from NYISO [29]. The load and generation data is taken from data collected at Madeira, Portugal. We use the following performance indexes to measure the performance of our simulations:

1. *Arbitrage Gains*: effectiveness in performing arbitrage,
2. *Power Factor Correction:* is gauged using 3 indices, using a prescribed PF limit of 0.9: (i) *No. of PF violations* denoted as VLT, (ii) *Mean PF*, and (iii) *Minimum PF*.

3. Converter Usage Factor (CUF): measures usage as

$$\text{CUF} = \frac{1}{N}\sum_{i=1}^{N}\frac{\sqrt{(P_B^i)^2+(Q_B^i)^2}}{S_B^{\max}}. \tag{6.5.1}$$

As a benchmark for PFC indices, in Table 6.1, we list the values over a representative day, for two nominal cases: (a)$NSNB$ (no solar with no battery), and (b)SNB (solar with no battery). It is evident that with

Table 6.1: Nominal Cases without Energy Storage for 1 day

Parameters	$NSNB$	SNB
No. of PF violations	8	25
mean PF	0.9735	0.9054
min PF	0.8201	0.1587

addition of solar, the PF seen by the grid deteriorates with number of PF violations increasing by 200% and minimum PF reached decreasing by 80%.

In order to rectify the PF and perform arbitrage we add inverter connected energy storage. In numerical results, we use four batteries with differing converter capacities for comparison. Their parameters are listed in Table 6.2. For fixed battery capacity, we consider four different ramp rates, each of which is described

Table 6.2: Battery Parameters

$B_{\min}$, $B_{\max}$, B_0	200Wh, 2000 Wh, 1000 Wh
$\eta_{\text{ch}} = \eta_{\text{dis}}$	0.95
$\delta_{\max} = -\delta_{\min}$	500 W for 0.25C-0.25C, 1000 W for 0.5C-0.5C 2000 W for 1C-1C, 4000 W for 2C-2C

as a ratio of battery capacity over ramp rate. For instance xC-yC ramp rate in Table 6.2 will require 1/x hours to fully charge and 1/y hours to fully discharge. By Eq. 6.2.2, the ramp rate also fixes the maximum power $P_B^{\max}$. We define maximum converter capacity $S_B^{\max}$ in terms of $P_B^{\max}$. We consider 4 different battery converters: (i) $S_B^{\max} = P_B^{\max}$, (ii) $S_B^{\max} = 0.9P_B^{\max}$ (i.e. under-designed), (iii) $S_B^{\max} = 1.25P_B^{\max}$ (i.e. over-designed), (iv) $S_B^{\max} = 1.5P_B^{\max}$ (i.e. over-designed). The sampling time h is 15 minutes, time horizon T is 24 hours and the power factor limit set is 0.9.

Table 6.3: Comparison of arbitrage gains for 1 day

Converter	Battery	P_{arb}	P_{mr}	P_{rh}	P_{plt}	P_{plt}^{conv}
$P_B^{\max}$	0.25C-0.25C	**0.1754**	N.F.	N.F.	0.1747	0.1747
	0.5C-0.5C	**0.2564**	0.2564	0.2564	0.2564	0.2564
	1C-1C	**0.3367**	0.3367	0.3367	0.3367	0.3367
	2C-2C	**0.4144**	0.4144	0.4144	0.4144	0.4144
$0.9P_B^{\max}$	0.25C-0.25C	**0.1728**	N.F.	N.F.	0.1704	0.1704
	0.5C-0.5C	**0.2523**	0.2511	0.2511	0.2511	0.2511
	1C-1C	**0.3314**	0.3314	0.3314	0.3314	0.3314
	2C-2C	**0.4098**	0.4098	0.4097	0.4098	0.4098
$1.25\times$ $P_B^{\max}$	0.25C-0.25C	**0.1754**	N.F.	N.F.	0.1753	0.1753
	0.5C-0.5C	**0.2564**	0.2564	0.2564	0.2564	0.2564
	1C-1C	**0.3367**	0.3367	0.3367	0.3367	0.3367
	2C-2C	**0.4144**	0.4144	0.4144	0.4144	0.4144
$1.5P_B^{\max}$	0.25C-0.25C	**0.1754**	0.1754	0.1754	0.1754	0.1754
	0.5C-0.5C	**0.2564**	0.2564	0.2564	0.2564	0.2564
	1C-1C	**0.3367**	0.3367	0.3367	0.3367	0.3367
	2C-2C	**0.4144**	0.4144	0.4144	0.4144	0.4144

We compare the arbitrage gains in Table 6.3 and PF violations in Table 6.4 respectively for different algorithms and battery settings over a day (96 time instances). Note the arbitrage gains with PFC matches

with arbitrage gains for P_{arb}, implying performing PFC does not deteriorated energy storage's ability to perform arbitrage. For PF violations, as expected, the no. of PF violations for P_{arb} remain close to

Table 6.4: Comparison of no. of PF violations for 1 day

Converter	Battery	P_{arb}	P_{mr}	P_{rh}	P_{plt}	P_{plt}^{conv}
$P_B^{\max}$	0.25C-0.25C	27	N.F.	N.F.	2	2
	0.5C-0.5C	27	0	0	0	0
	1C-1C	26	0	0	0	0
	2C-2C	24	0	0	0	0
$0.9P_B^{\max}$	0.25C-0.25C	26	N.F.	N.F.	4	4
	0.5C-0.5C	23	0	0	0	0
	1C-1C	25	0	0	0	0
	2C-2C	24	0	0	0	0
$1.25\times$ $P_B^{\max}$	0.25C-0.25C	26	N.F.	N.F.	1	1
	0.5C-0.5C	25	0	0	0	0
	1C-1C	26	0	0	0	0
	2C-2C	25	0	0	0	0
$1.5P_B^{\max}$	0.25C-0.25C	26	0	0	0	0
	0.5C-0.5C	25	0	0	0	0
	1C-1C	26	0	0	0	0
	2C-2C	25	0	0	0	0

SNB. P_{mr} and P_{rh} are not feasible (denoted as N.F. in results) for battery with slowest ramp rate and small converter, i.e., PF violations are unavoidable. However, the other schemes are able to reduce the number of violations drastically. In settings where feasible solution exist, all schemes considered are able to completely avoid any violation. Table 6.5 presents the mean PF. Note that for P_{mr} and P_{rh} in particular,

Table 6.5: Comparison of mean PF for 1 day

Converter	Battery	P_{arb}	P_{mr}	P_{rh}	P_{plt}	P_{plt}^{conv}
$P_B^{\max}$	0.25C-0.25C	0.9062	N.F.	N.F.	0.9581	0.9562
	0.5C-0.5C	0.8803	0.9571	0.9850	0.9616	0.9567
	1C-1C	0.9077	0.9615	0.9938	0.9426	0.9602
	2C-2C	0.8997	0.9656	0.9983	0.9378	0.9638
$0.9P_B^{\max}$	0.25C-0.25C	0.9058	N.F.	N.F.	0.9512	0.9554
	0.5C-0.5C	0.8837	0.9580	0.9772	0.9661	0.9580
	1C-1C	0.9080	0.9610	0.9909	0.9560	0.9603
	2C-2C	0.9012	0.9659	0.9972	0.9648	0.9642
$1.25\times$ $P_B^{\max}$	0.25C-0.25C	0.9062	N.F.	N.F.	0.9545	0.9567
	0.5C-0.5C	0.8803	0.9973	0.9903	0.9802	0.9802
	1C-1C	0.9077	0.9998	0.9962	0.9742	0.9742
	2C-2C	0.8997	0.9999	0.9987	0.9478	0.9478
$1.5P_B^{\max}$	0.25C-0.25C	0.9062	0.9934	0.9821	0.9850	0.9571
	0.5C-0.5C	0.8803	0.9987	0.9927	0.9832	0.9567
	1C-1C	0.9080	0.9999	0.9971	0.9839	0.9602
	2C-2C	0.8997	0.9999	0.9991	0.9244	0.9381

the mean PF for a large converter approaches close to 1, which demonstrates their ability in PFC. However this may lead to overuse of the converter, as evident from CUF listed in Table 6.7. Here P_{plt}^{conv} provides a way to balance CUF with mean PF as evident from both the tables. Table 6.6 lists the minimum PF measured over the same day which is greater or equal to the threshold for feasible cases. However, further analysis would be required to determine penalty functions that motivate or hinder converter usage.

It is clear from the mentioned results that storage devices over multiple settings can be used for PFC without any noticeable loss in arbitrage gains.

Fig. 6.4 presents the relationship between the PF threshold, mean PF and arbitrage gains for 1C-1C battery. As the effect of PF limit on the maximum possible arbitrage gains is almost non-existent except

Table 6.6: Comparison of minimum PF for 1 day

Converter	Battery	P_{arb}	P_{mr}	P_{rh}	P_{plt}	P_{plt}^{conv}
$P_B^{\max}$	0.25C-0.25C	0.1587	N.F.	N.F.	0.8443	0.8443
	0.5C-0.5C	0.0321	0.9000	0.9000	0.9000	0.9000
	1C-1C	0.1587	0.9000	0.9568	0.9000	0.9000
	2C-2C	0.0545	0.9000	0.9821	0.9000	0.9000
$0.9P_B^{\max}$	0.25C-0.25C	0.1587	N.F.	N.F.	0.8295	0.8295
	0.5C-0.5C	0.0321	0.9000	0.9000	0.9000	0.9000
	1C-1C	0.1587	0.9000	0.9000	0.9000	0.9000
	2C-2C	0.0545	0.9000	0.9000	0.9000	0.9000
$1.25\times$ $P_B^{\max}$	0.25C-0.25C	0.1587	N.F.	N.F.	0.8789	0.8789
	0.5C-0.5C	0.0321	0.9501	0.9303	0.9323	0.9000
	1C-1C	0.1587	0.9935	0.9681	0.9604	0.9000
	2C-2C	0.0545	0.9970	0.9842	0.9266	0.9000
$1.5P_B^{\max}$	0.25C-0.25C	0.1587	0.9015	0.9005	0.9000	0.9000
	0.5C-0.5C	0.0321	0.9739	0.9444	0.9638	0.9000
	1C-1C	0.1587	0.9935	0.9749	0.9765	0.9000
	2C-2C	0.0545	0.9993	0.9863	0.9124	0.9237

Table 6.7: Comparison of CUF for 1 day

Converter	Battery	P_{arb}	P_{mr}	P_{rh}	P_{plt}	P_{plt}^{conv}
$P_B^{\max}$	0.25C-0.25C	0.7154	N.F.	N.F.	0.9198	**0.7390**
	0.5C-0.5C	0.6056	0.6246	0.6387	0.6789	**0.6230**
	1C-1C	0.5520	0.5611	0.5709	0.6011	**0.5568**
	2C-2C	0.4970	0.5048	0.5059	0.5248	**0.4985**
$0.9P_B^{\max}$	0.25C-0.25C	0.7693	N.F.	N.F.	0.9386	**0.7823**
	0.5C-0.5C	0.6373	0.6552	0.6694	0.7088	**0.6541**
	1C-1C	0.5787	0.5876	0.5989	0.6183	**0.5842**
	2C-2C	0.5284	0.5375	0.5398	0.5395	**0.5302**
$1.25\times$ $P_B^{\max}$	0.25C-0.25C	0.5723	N.F.	N.F.	0.8045	**0.5992**
	0.5C-0.5C	0.4845	0.5605	0.5180	0.5513	**0.4984**
	1C-1C	0.4416	0.4796	0.4595	0.4648	**0.4454**
	2C-2C	0.3976	0.4106	0.4058	0.4208	**0.3988**
$1.5P_B^{\max}$	0.25C-0.25C	0.4770	0.5972	0.5277	0.6159	**0.5023**
	0.5C-0.5C	0.4037	0.4811	0.4379	0.4705	**0.4153**
	1C-1C	0.3680	0.4032	0.3844	0.4444	**0.3712**
	2C-2C	0.3311	0.3418	0.3387	0.3630	**0.3519**

for PF limit close to 1. This resonates with our claim that PFC and arbitrage are largely decoupled and performing PFC do not degrade energy storage's ability to perform arbitrage. From Fig. 6.4 we also observe that the mean PF during the day when solar generation is available drops to 0.81 significantly lower than the mean PF for the whole day in absence of solar generation which is 0.97.

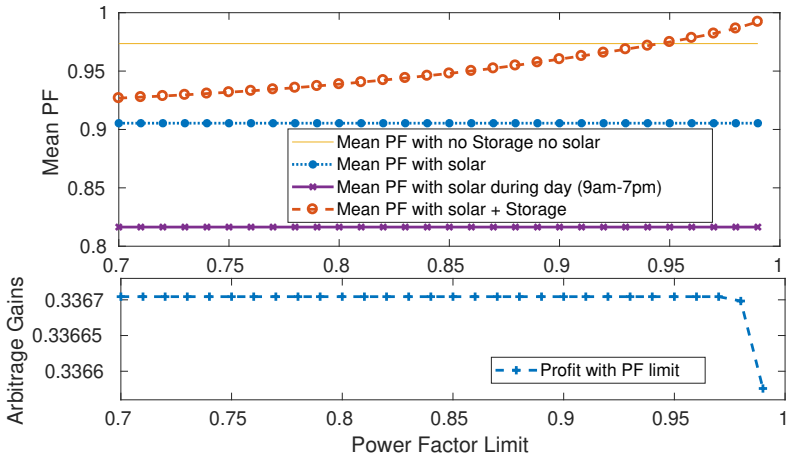

Figure 6.4: Arbitrage gains and mean PF with varying PF limit for 1C-1C

We present in Fig. 6.5 the variation for PF for different ramp rate batteries with same converter size for the same day for P_{plt}. The uncorrected PF is shown in Fig. 6.1. Fig. 6.6 shows the variation of active

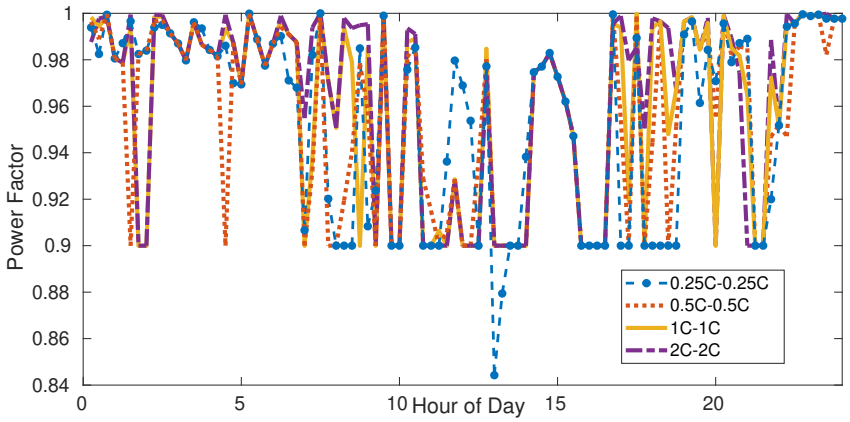

Figure 6.5: PFC + arbitrage for $S_B^{\max} = P_B^{\max} = \delta_{\max}/\eta_{ch}$

power, reactive power and PF variations with and without battery.

6.5.1 Results with uncertainty

In Section 6.8 we propose a real-time implementation for performing PFC with arbitrage under uncertainty. The forecast model is generated for load with solar generation and for electricity price. The ARMA based forecast use 9 weeks of data for training and generates forecast for the next week. `ForecastPlusMPC` is implemented in receding horizon. The training data for net load seen by the grid with and without PV is plotted in Fig. 6.7. Fig. 6.7 indicate that inclusion of solar PV have degraded the PF significantly.

The performance of forecast of electricity price signal is plotted in Fig. 6.8. The electricity price data used for this numerical experiment is taken from CAISO for the same days of load data. Note that the ARIMA model for price misses peaks beyond \$200/MW. However, this drawback of the forecast model is not dominant for batteries with slow ramp rates as for such batteries the optimal control action for any price above \$200/MW is discharge the battery at maximum rate. Note \$200/MW is significantly higher than the mean electricity price. To compare the effect of forecasting net load and electricity prices with perfect information, we present average arbitrage gains and PFC indices for one week starting from 1st June 2018 using (P_{plt}) as the optimization scheme inside PFC. Table 6.8 includes the deterministic results, while Table 6.9 includes the performance with uncertainty. Note that the arbitrage gain is more sensitive

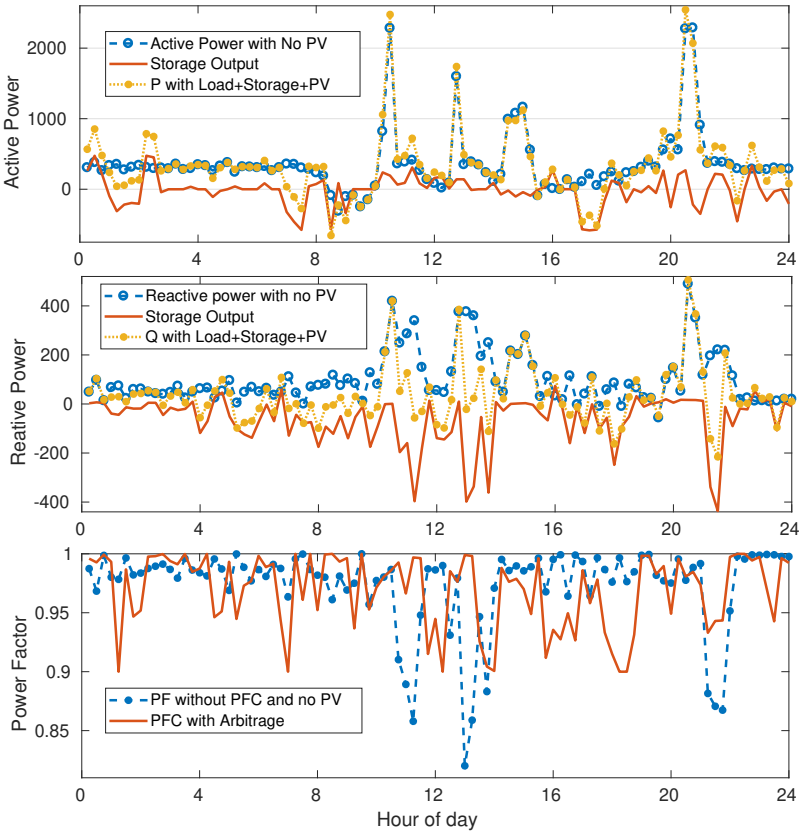

Figure 6.6: PFC with arbitrage for four quadrant storage operation

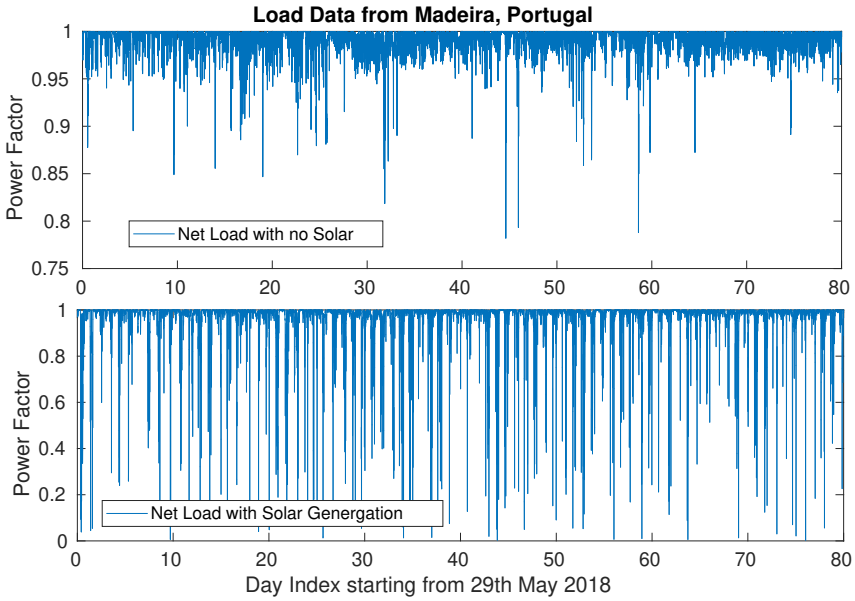

Figure 6.7: Variation of PF with and without solar PV

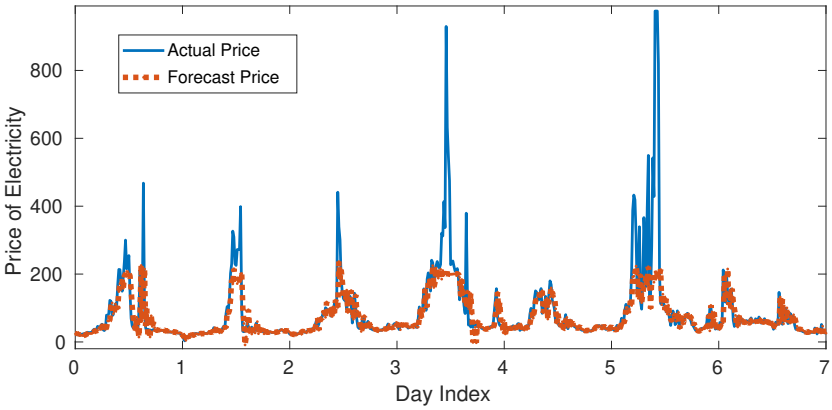

Figure 6.8: ARIMA Price Forecast

to uncertainty for fast ramping battery. This observation is in sync with [130]. PFC generally requires no-look-ahead as evident from comparison of (P_{mr}) and (P_{rh}). Note in Tables 6.8 and 6.9 that future uncertainty does not affect the power factor violations significantly. It is however true that an undersized converter for slow ramping battery have a high CUF compared to other cases.

Table 6.8: Deterministic Performance

Converter	Battery	Gains	Mean PF	VLT	CUF	Min PF
$P_B^{\max}$	0.25C-0.25C	3.0645	0.9705	11	0.8972	0.0487
	0.5C-0.5C	4.7840	0.9713	2	0.7508	0.6665
	1C-1C	7.0592	0.9433	0	0.6924	0.9000
	2C-2C	9.4113	0.9364	0	0.5868	0.9000
$0.9P_B^{\max}$	0.25C-0.25C	3.0385	0.9644	26	0.9278	0.0883
	0.5C-0.5C	4.7251	0.9618	19	0.7951	0.2141
	1C-1C	6.9569	0.9663	2	0.7128	0.6330
	2C-2C	9.3096	0.9754	1	0.6149	0.5688
$1.25\times$ $P_B^{\max}$	0.25C-0.25C	3.0647	0.9831	0	0.6985	0.9033
	0.5C-0.5C	4.7840	0.9799	0	0.6236	0.9352
	1C-1C	7.0593	0.9764	0	0.5495	0.9000
	2C-2C	9.4113	0.9769	0	0.4645	0.9000
$1.5P_B^{\max}$	0.25C-0.25C	3.0647	0.9803	0	0.6119	0.9000
	0.5C-0.5C	4.7840	0.9773	0	0.5267	0.9000
	1C-1C	7.0593	0.9762	0	0.4624	0.9000
	2C-2C	9.4113	0.9776	0	0.3874	0.9000

6.6 Case Study: Degradation of PF at a substation

We show the plots of data collected at a LV voltage substation in Madeira, Portugal. The data shows that degradation of power factor seen at the substation. The substation distributes the single phase distributed generation on each phase such that phases are balanced. However, due to deterioration of active power demand on each phase during the day as evident in Fig. 6.9. This dip is not observed in the reactive power plot shown as Fig. 6.10. Fig. 6.12 presents the zoomed in plot for Fig. 6.11. Fig. 6.12 shows that during the day when consumers generate part of their consumption using solar PV, leading to deterioration of power factor significantly. The degradation of PF is most prominent for Phase C.

Table 6.9: Performance with uncertainty model and MPC

Converter	Battery	Gains	Mean PF	VLT	CUF	Min PF
$P_B^{\max}$	0.25C-0.25C	2.9996	0.9704	13	0.9075	0.0488
	0.5C-0.5C	3.4962	0.9692	2	0.7746	0.6665
	1C-1C	4.6840	0.9465	0	0.7032	0.9000
	2C-2C	6.0345	0.9375	0	0.6142	0.9000
$0.9P_B^{\max}$	0.25C-0.25C	2.9718	0.9652	25	0.9324	0.0656
	0.5C-0.5C	3.3975	0.9630	21	0.8198	0.2152
	1C-1C	4.5934	0.9684	4	0.7258	0.6268
	2C-2C	5.9686	0.9771	1	0.6402	0.5762
$1.25\times$ $P_B^{\max}$	0.25C-0.25C	2.9997	0.9827	0	0.7166	0.9000
	0.5C-0.5C	3.4962	0.9796	0	0.6493	0.9146
	1C-1C	4.6841	0.9763	0	0.5680	0.9122
	2C-2C	6.0345	0.9765	0	0.4889	0.9083
$1.5P_B^{\max}$	0.25C-0.25C	2.9997	0.9789	0	0.6220	0.9248
	0.5C-0.5C	3.4962	0.9774	0	0.5540	0.9105
	1C-1C	4.6841	0.9747	0	0.4768	0.9058
	2C-2C	6.0345	0.9778	0	0.4071	0.9103

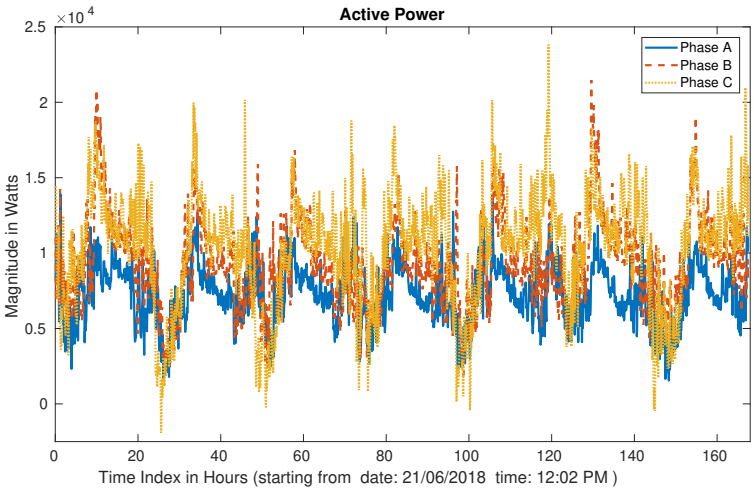

Figure 6.9: Active power seen from the sub-station

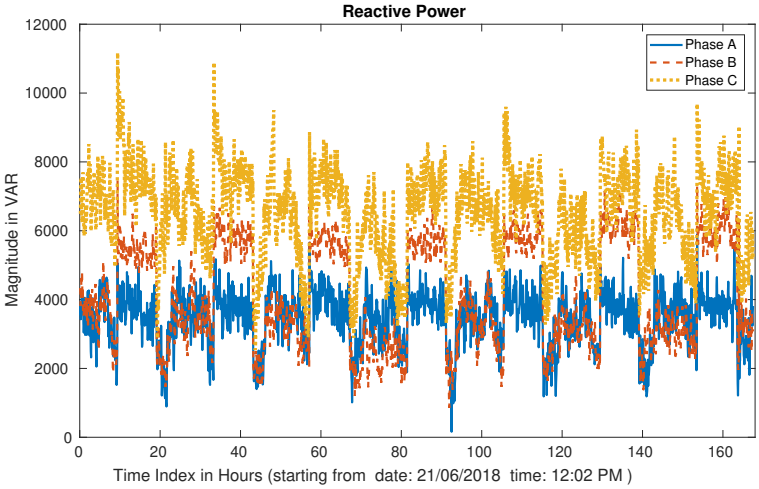

Figure 6.10: Reactive power seen from the substation

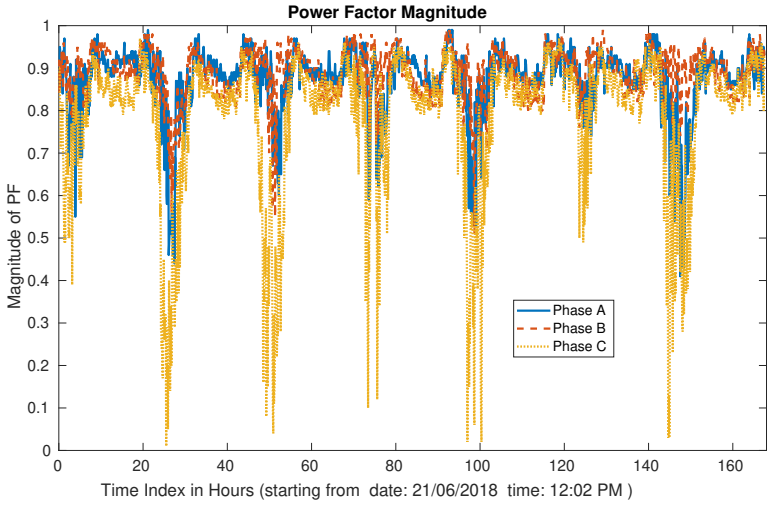

Figure 6.11: Power factor seen from the substation

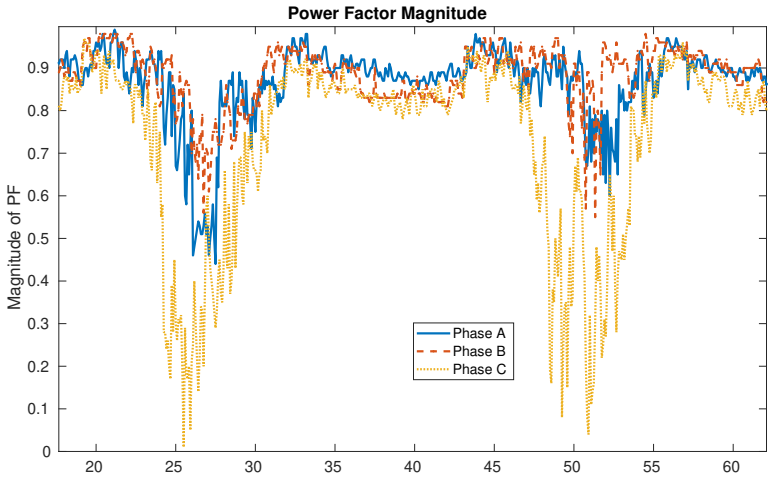

Figure 6.12: Power factor seen from the substation: zoomed in plot

6.7 Power Factor Correction with Solar Inverter

Traditionally solar inverters in LV distribution network operate at close to unity power factor, primarily due to no obligations to supply reactive power. This is financially sensible as the DG owner could size their solar inverted based on the maximum active power generation from rooftop solar panels. However, due to large scale DG connection the reactive power responsibilities needs to be shared. In this case study we present a special case of the power factor correction framework presented earlier for energy storage battery, modified for control of a solar inverter. The system considered here consists of a non-elastic consumer with active and reactive power demand and solar inverter with active power output governed by solar generation, thus an uncontrollable variable. The reactive power output of the solar inverter is controlled so as the power factor is corrected as much as possible. Fig. 6.13 shows the block diagram of the special case where consumer have solar generation interfaced with solar inverter but no storage.

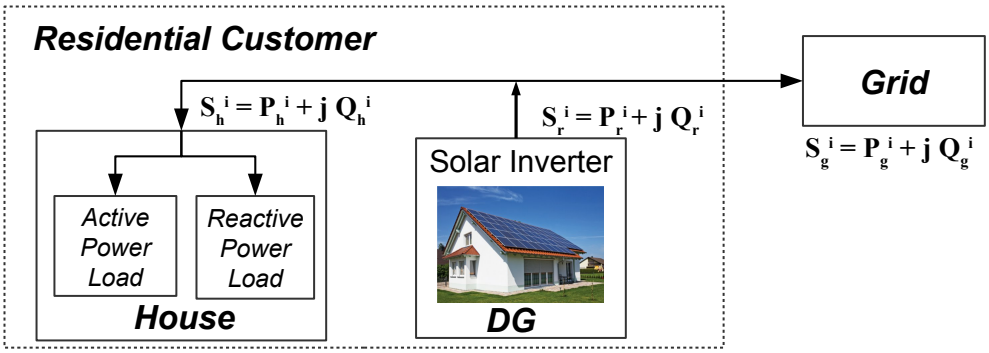

Figure 6.13: Residential consumer with solar generation

The optimization problem for solar inverter for PFC can be obtained by modifying optimization problem P_{plt} described for storage performing arbitrage and PFC. This optimization problem is denoted as P_{solPFC}

$$\min_{Q_r} \quad \sum_{i=1}^{N} \theta(i), \tag{6.7.1}$$

where we define penalty function $\theta(i)$ as

$$\theta(i) = \lambda \max(0, |Q_h^i + Q_r^i| - k|P_h^i - P_r^i|). \tag{6.7.2}$$

Note P_{solPFC} has only Q_r as the control variable and $P_h^i - P_r^i$ is known at each time instant i. Therefore, $|P_h^i - P_r^i|$ is a constant, we denote $M = |P_h^i - P_r^i|$.

The max term can be modeled as two constraints

$$\theta(i) \geq 0, \quad \theta(i) \geq \lambda(|Q_h^i + Q_r^i| - kM). \tag{6.7.3}$$

Eq. 6.7.3 can now be reformulated as

$$\begin{aligned} &\theta(i) \geq 0, \quad \theta(i) \geq \lambda(2y_1^i - (Q_h^i + Q_r^i) - kM). \\ &2y_1^i - (Q_h^i + Q_r^i) \geq 0, \end{aligned} \tag{6.7.4}$$

Here y_1^i denote bi-linear variable

$$y_1^i = z_1^i(Q_h^i + Q_r^i), \tag{6.7.5}$$

with binary variables z_1^i. z_1^i is equal to 1 if the total reactive power is greater than zero, and zero otherwise. We use McCormick relaxation to convert the bi-linear term in Eq. 6.7.5 to mixed-integer linear constraints

$$\begin{aligned} &y_1^i \geq Q_{lb}^i z_1^i, \quad y_1^i \geq (Q_h^i + Q_r^i) + Q_{ub}^i z_1^i - Q_{ub}^i \\ &y_1^i \leq Q_{ub}^i z_1^i, \quad y_1^i \leq (Q_h^i + Q_r^i) + Q_{lb}^i z_1^i - Q_{lb}^i \end{aligned} \tag{6.7.6}$$

In these equations, $Q_{lb}^i = Q_h^i - S_B^{\max}$ and $Q_{ub}^i = Q_h^i + S_B^{\max}$ denote the lower and upper bounds respectively for total reactive power. To summarize, the optimization problem for performing arbitrage and penalization PF violations and its associated constraints are given as

$$(P_{\text{solPFC}}) \quad \min_{Q_r} \quad \sum_{i=1}^{N} \theta(i)$$

subject to, Eq. 6.2.3, Eq. 6.7.4, Eq. 6.7.6.

The control of solar inverter for PFC has only one decision variable. Furthermore, if we assume that PF violation penalty is linear, i.e., the cost of violating is linearly proportional to the amount of violation then under such a case solar inverter can be controlled with no look-ahead.

We present an algorithm for linear PF violation penalty. In future work we will combine the control of the solar inverter with that of control of the storage inverter to maximize the arbitrage and PFC gains as well as compare it with gains from individual inverter controls.

Algorithm 13 `SolarInverterPFC`

Inputs: $Q_h^i, P_r^i, P_h^i, S_B^{\max}$

Calculate $M = |P_h^i - R_r^i|$,
Calculate Js $= |Q_h^i| - kM$
Calculate Slack $= \sqrt{(S_B^{\max})^2 - (P_h^i - P_r^i)^2}$.
if Js ≤ 0 **then**
    No PFC required as PF already within limits
    Set reactive power output of solar inverter $Q_r^i = 0$.
else
    if $Q_h^i > 0$ **then**
        $Q_r^i = \max(-Q_h^i + kM, -\text{Slack})$.
    else
        $Q_r^i = \min(|-Q_h^i - kM|, \text{Slack})$.
    end if
end if
Return Q_r^i.

6.8 Conclusion and Perspectives

In this chapter, we propose optimization formulations to operate inverter connected storage devices in distribution grids for co-optimizing arbitrage and power factor correction (PFC), both with or without perfect information. For a majority of cases, we show that the arbitrage gains with PFC converge to the gains achieved when storage performs only arbitrage. The primary reason for PFC being decoupled from arbitrage gains is due to the fact that in most instances, PF can be corrected by adjusting reactive power output. This is primarily governed by converter size and unlike storage active power output, which is constrained by capacity and ramp constraint. We also observe that arbitrage gain of batteries with higher ratio of ramp rate over capacity are more sensitive to uncertainty about future variables as they face capacity constraints more frequently.

It is also noteworthy that increasing the converter size would improve the mean PF without any significant change in arbitrage gains for the same ramping battery. In the current work, we consider a stringent case of maintaining PF for every operational point, though the methodology can be extended to the case with penalties on average PF. Moreover, in future work we will research further selection of optimal converter sizes and use solar and storage converter simultaneously. The control of active and reactive application proposed here is decoupled, however, further exploration is required to identify the extent of decoupling. Finally we will also research directions to incorporate network power flow constraints pertaining to flow and voltage limits [189] into our work on energy storage.

Chapter 7

Co-optimizing Storage for Prosumers

The electric light did not come from the continuous improvement of candles. -Oren Harari

Summary: In current distribution grids, energy storage devices can be used for multiple functions, often operating at different time-scales. The co-optimization formulation presented in Chapter 6 is extended to peak demand shaving. This chapter presents a new co-optimization formulation for energy storage for performing energy arbitrage and power factor correction in the time scale of minutes to hours, along with peak demand shaving in the time scale of a month. While the optimization problem is non-convex, we present an efficient penalty based convex relaxation to approximate it. Furthermore, we provide a mechanism to maximize the storage operational life by tuning the cycles of operation using a friction coefficient, and thereby make our formulation more realistic. To demonstrate the effectiveness of energy storage performing multiple tasks simultaneously, we present a case-study with real data for a time scale of several months. We demonstrate a real-time model predictive control based implementation of the proposed formulation with AutoRegressive forecasting of net-load and electricity price. Through our optimal storage control algorithm, we are able to show that energy storage can realistically correct power factor without significant change in either arbitrage gains or peak demand charges.

7.1 Introduction

In today's smart grid, many electricity consumers also generate part of their consumed electricity locally using renewable energy sources. Such consumers are referred to as electricity prosumers. In Chapter 10 we show that active participation of prosumers in electricity markets can lead to mutual benefits for both the utility as well as reduced cost of consumption for the prosumers [185]. While renewable energy sources are clean and cheap, they are also intermittent and hence unreliable. This leads to increased burden for control and ancillary services on the grid. In this context, energy storage devices such as batteries present a good alternative to act as a buffer and reduce the energy fluctuations due to renewables. The authors in [191] present the various roles energy storage can perform in future power networks due to their ability to absorb and deliver real and reactive power with very small response time. This capability of energy storage can be used for frequency regulation, voltage control to enhance power network stability. Further, using temporal differences in real-time electricity prices, energy storage bundled with intermittent generation can reduce electric bills and increase system reliability [191].

While energy storage devices can act as a technology enabler for power systems with non-trivial renewable energy sources, they are still expensive and often not financially viable for use in a specific application alone. In prior work, the authors in [182] present a deterministic case-study for identifying financial potential for different ramping batteries in North American and European energy markets. It is identified that performing only energy arbitrage is not fiscally profitable. It is thus necessary to combine various roles for operating energy storage for profitability as shown in the pioneering work [323]. However, a major challenge with co-optimizing for multiple applications is in dealing with *different revenue streams* and penalties with *differing time scales* of operation. Table 7.1 lists a non-exhaustive list of roles energy storage can perform and time scales at which these roles operate. The authors in [264] bifurcate energy storage applications into power or energy applications. The short-time scale applications such as ancillary service and frequency regulation can be viewed as high power applications as ramping needs are more essential compared to storage capacity. While arbitrage and peak shaving can be viewed as energy management

Table 7.1: Roles energy storage can play

Energy Storage Roles	Time scale
(1.) Frequency regulation	milliseconds to few sec.
(2.) Ancillary services	seconds to few minutes
(3.) Energy Arbitrage	minutes to hours
(4.) Power factor correction	minutes to hours
(5.) Peak demand reduction	days to months

applications. Frequency regulation and ancillary service participation is often exclusive for facilities which make service commitments prior to participation [218]. All ISOs in the USA have performance evaluation mechanisms for comparing services provided by regulating resources - often measured in terms of responsiveness to control signals [39, 144]. Such performance norms as well as lack of communication/monitoring equipment make it extremely difficult for low voltage electricity consumers to participate in dynamic regulation. Therefore, in this chapter we focus on co-optimizing the following storage applications for low voltage distribution grid consumers in the time-scale of minutes to several days for performing:
• **Energy Arbitrage**: Based on fluctuations of electricity price, end-users can charge their batteries when prices are low and discharge when prices are high and reduce their electricity bills [109, 338]
• **Peak Demand Charge**: The maximum demand dictates the size of power grid infrastructure, i.e. generators, transmission lines, transformers, circuit breakers etc. Many power utilities around the world have introduced peak demand charge [295, 320, 228] that a consumer may seek to minimize over a longer period (weeks or months).
• **Power Factor Correction** (PFC): Distributed generation (DG) often operate at close to unity power factor as they are not obliged to supply reactive, in compliance with IEEE Standard 1547 [298]. Hence all the reactive power is met by the distribution grid leading to issues. In this chapter we assume LV consumer is obliged to maintain a power factor greater than or equal to a threshold set by the power utility.

There has been multiple works in the past that have looked that individual battery goals. [250, 109, 338] have analyzed the usefulness of batteries in arbitrage or load shifting to benefit from price fluctuations. The authors in [263] use energy storage for peak demand shaving for industrial loads as the power demand payment for such loads reaches a level of 50% of the plant's electricity bill. On the other hand, the authors in [216, 339] present peak shaving in the context of residential electricity consumers. Power factor correction using energy storage converter is presented in [178, 326]. While such correction is currently mandated for large consumers [126], in the near future owing to PF issues related to domestic solar, PFC for domestic customers may be mandated. It is noteworthy that the co-optimization of energy storage usage has also been extensively researched. In Table 7.2 we list some of the works in this area.

Table 7.2: Co-optimization of energy storage

Paper	**Co-optimizing for**
[323], [92, 136]	Arbitrage and frequency regulation
[306]	Phase balancing with arbitrage
[245, 294, 330]	Peak shaving and frequency regulation
[187]	Arbitrage, peak shaving, energy backup

Prior work on co-optimization of storage operation for different time-scale applications such as [294], [330] do not explicitly propose a split of optimization horizon between the different time scales. In our work we overcome this by an efficient split.

Contribution: In this work, we focus on co-optimizing energy storage for performing energy arbitrage, peak demand shaving and power factor correction. The joint optimization problem is non-convex, but is solved efficiently using a penalty-based convex-relaxation scheme inspired by our prior work on *single* time-scale battery optimization for arbitrage and PFC [178]. To include the peak demand charges with *longer* time-scales, we use a memory variable, and furthermore split the longer optimization problem into smaller sections for efficient solution. Further battery degradation is taken into account by the formulation, and it is also amenable for addition of extra costs. To summarize, the key contributions of this chapter are:
• *Co-optimization* of energy arbitrage, power factor correction (time scale of minutes to hours), and peak demand charge saving (time scale of a month).
• *Control of cycles of operation* by the introduction of friction coefficient to manage cycle life degradation.

• *Numerical Case Study*: We present simulation of 80 days for load data from Madeira, Portugal with real-time electricity price data from CAISO and peak demand charge from PG&E in California.
• *Real-time implementation*:To account for real-time application, we consider a Model Predictive Control (MPC) framework where AutoRegressive forecasting is used to predict future prices and loads. In the context of the real-time implementation, peak demand shaving and arbitrage gains are affected by uncertainty modeling in for batteries with faster ramp rates, though PFC is not sensitive.

The overarching conclusion of this chapter is that energy storage devices can co-optimize these goals without any deterioration in individual gains and significantly higher total gains.

The chapter is organized as follows. Section 7.2 provides a description of the system. Section 7.3 formulates co-optimization problem for performing arbitrage, PF correction and peak demand charge saving. Section 7.5 presents the numerical results. Section 7.6 concludes the chapter.

7.2 System Description

In this chapter, similar to Chapter 3 to 6, we consider a low voltage electricity consumer with inelastic demand, rooftop solar generation and a battery. The block diagram of the system considered is shown in Fig. 2.20. The apparent power of the load is denoted as $S_h^i = P_h^i + jQ_h^i$, where P_h^i and Q_h^i are the active and reactive power consumed. Apparent power of the solar coupled with a converter is $S_r^i = P_r^i$. Total active power of load and solar PV is denoted as $P^i = P_h^i - P_r^i$. Similarly, the total reactive power of load and solar PV is denoted as $Q^i = Q_h^i$. The battery and system model used in this chapter is described in Chapter 2.5. The co-optimization formulation for arbitrage with PFC is presented in Chapter 6. In this chapter we extend this formulation for peak demand shaving along with PFC and arbitrage. Next we discuss the billing structure considered in this chapter.

7.2.1 Billing Structure

We consider the variable cost of electricity consists of three components. In our setting, each component has a value which automatically either blocks or prioritizes certain application, unlike [281] which prioritizes storage application. For instance, if ramping up for arbitrage is more profitable in certain time instant compared to peak shaving then the battery should ramp up. The three components are

(1) *Active energy cost*: equals the product of time varying cost of electricity denoted as p_{elec}^i and the amount of active energy consumed, is denoted as

$$C_P^i = p_{\text{elec}}^i \times P_T^i h. \tag{7.2.1}$$

(2) *Reactive energy cost/ PFC gains*: denoted as

$$C_Q^i = \lambda \max\left(0, \left|Q_T^i\right| - k\left|P_T^i\right|\right), \tag{7.2.2}$$

here λ denotes the penalty for reactive power if the PF dips below the limit prescribed. The mechanism for pricing reactive energy in Eq. 7.2.2 has similarities with charges imposed by UTE (Uruguay's government-owned power company) [25] and PF limits and penalty listed in Table 7.3, see [178].

Table 7.3: Power Factor Rules

Utility/Country	PF Limit	Reactive Cost
France [72]	$\lvert\tan(\phi)\rvert \leq 0.4$	$0.2 \times C_P^i$
Portugal [271]	$\lvert\cos(\phi)\rvert \geq 0.92$	0.016 to 0.18 $\times C_P^i$
Germany [303]	$\lvert\cos(\phi)\rvert \geq 0.95$	for Solar Generators
CAISO	$\lvert\cos(\phi)\rvert \geq 0.85$	LV consumers [23]

(3) *Peak demand cost*: denoted as

$$C_{peak} = \lambda_{\text{peak}} \max(P_T^i, \forall i \in \{1, ..., N_{\text{month}}\}\ ), \tag{7.2.3}$$

where the maximization is over a month. λ_{peak} denotes the peak-demand charged imposed on a time-scale of a month. Under this model, the total variable cost of electricity for a month is given as

$$C_T^{\text{month}} = C_{peak} + \sum_{i=1}^{N_{\text{month}}} \left\{C_P^i + C_Q^i\right\}. \tag{7.2.4}$$

where N_{month} denotes number of samples in the month considered.

7.3 Co-Optimization of Energy Storage

In this section we formulate the co-optimization problem for performing arbitrage, PFC and peak demand charge saving.

7.3.1 Energy Arbitrage

'Energy arbitrage' refers to buying electricity when price is low and selling it when price is high, and in effect making a profit. In this chapter we use the energy arbitrage formulation presented in Chapter 3 where the buying and selling prices of electricity at each instant i are the same and denote it by p^i_{elec}. As monetary benefits from arbitrage is *based only on* active power, the operator seeks to minimize the following problem

$$(P_{arb}) \min_{P_B, Q_B} \sum_{i=1}^{N} p^i_{elec} P^i_B h, \quad \text{subject to, Eq. 6.2.2, Eq. 6.2.3, Eq. 6.2.4.}$$

7.3.2 Arbitrage with PFC

Optimization problem (P_{plt}) is proposed in Chapter 6. The objective of this co-optimization formulation is given by

$$(P_{plt}) \qquad \min_{P_B, Q_B} \quad \sum_{i=1}^{N} \left\{ \; p^i_{elec} P^i_B h \quad + \quad \theta(i) \; \right\}. \tag{7.3.1}$$

Subject to: (a) Ramp *Eq.* 6.2.2, (b) Converter *Eq.* 6.2.3, (c) Capacity *Eq.* 6.2.4,

(d) Constraints which are Mixed-Integer type for the penalty function

$$\theta(i) \geq 0, \quad \theta(i) \geq \lambda(2y^i_1 - Q^i_T - 2ky^i_2 + kP^i_T).$$
$$2y^i_1 - Q^i_T \geq 0, \quad 2y^i_2 - P^i_T \geq 0$$

(e) McCormick Relaxations for bi-linear terms

$$y^i_1 \geq Q^i_{lb} z^i_1, \quad y^i_1 \geq Q^i_T + Q^i_{ub} z^i_1 - Q^i_{ub}$$
$$y^i_1 \leq Q^i_{ub} z^i_1, \quad y^i_1 \leq Q^i_T + Q^i_{lb} z^i_1 - Q^i_{lb}$$
$$y^i_2 \geq P^i_{lb} z^i_2, \quad y^i_2 \geq P^i_T + P^i_{ub} z^i_2 - P^i_{ub}$$
$$y^i_2 \leq P^i_{ub} z^i_2, \quad y^i_2 \leq P^i_T + P^i_{lb} z^i_2 - P^i_{lb}.$$

where total active power is denoted as $P^i_T = P^i + P^i_B$ and total reactive power is given as $Q^i_T = Q^i + Q^i_B$. y^i_1 and y^i_2 denote bi-linear variables

$$y^i_1 = z^i_1 Q^i_T, \quad y^i_2 = z^i_2 P^i_T \tag{7.3.2}$$

with binary variables z^i_1 and z^i_2. z^i_1 (z^i_2) is equal to 1 if the total reactive (active) power is greater than zero, and zero otherwise. $Q^i_{lb} = Q^i - S^{\max}_B$ and $Q^i_{ub} = Q^i + S^{\max}_B$ denote the lower and upper bounds respectively for total reactive power. $P^i_{lb} = P^i + P^{\min}_B$ is the lower bound of total active power, and $P^i_{ub} = P^i + P^{\max}_B$. $|x| = (2z-1)x \geq 0$ with $z \in \{0, 1\}$.

7.3.3 Peak Demand Shaving with PFC and arbitrage

We now add peak demand charge λ_{peak} (per units of power) to the formulation. The total cost is proportional to the peak electricity demand over a longer period of time (Eg. 1 month scale) unlike P_{arb} and P_{plt}. However, we split the optimization horizon to one day intervals. At each interval we add a memory variable to make the problem tractable as below.

$$(P^{\text{peak}}_{plt}) \min_{P_B, Q_B} \sum_{i=1}^{N} \left\{ p^i_{\text{elec}} P^i_B h + \theta(i) + \lambda_{\text{peak}} \max(P^i_T, P^{\text{previous}}_{\max}) \right\}$$

subject to, Eq. 6.2.2, Eq. 6.2.3, Eq. 6.2.4, Eq. 6.3.4, Eq. 6.3.6.

Variable $P^{\text{previous}}_{\max}$ here acts as the memory of peak loads in the previous days of the month. The $P^{\text{previous}}_{\max}$ is initialized, and updated if the peak power exceeds the current value. The overall optimization and update steps are shown in Algorithm 14. In order to obtain results not biased because of initialization

Algorithm 14 `PeakDemandThresholdUpdate`

Global Inputs: $\eta_{\text{ch}}, \eta_{\text{dis}}, \delta_{\max}, \delta_{\min}, b_{\max}, b_{\min}, S_B^{\max}$ **Inputs**: h, N, b_0
Initialize: $P_{\max}^{\text{previous}} = 0$

```
while days < Month do
    for i = 1 : N do
        Implement P_plt^peak for the day and find P_T^i,
        Update P_max^previous = max(P_T^i, P_max^previous) and Update battery capacity
    end for
    Update b_0 and increment days = days +1
end while
```

we select it as zero at the beginning of each month. In practical implementation we advice to initialize $P_{\max}^{\text{previous}}$ with more realistic functions of historical peak load and storage ramp rate. Other combinations of co-optimization (Eg. arbitrage with peak shaving) can be formed by dropping the unused functions (related to PFC).

7.3.4 Co-optimization with control of cycles

Note that the formulations discussed previously do not consider battery life that is affected by charge-discharge cycles. Battery manufacturers measure the life of a battery using two indices: cycle life and calendar life. Cycle life denotes the number of cycles a battery can operate at a certain depth-of-discharge before reaching its end-of-life or EoL[1]. Similarly, calendar life denotes the maximum probable age that the battery can be operational at before reaching end-of-life. The battery degradation model used in this chapter is described in detail in Chapter 5. The cycles of operation for batteries are controlled using friction coefficient. In this chapter, we define a friction function for the active power to model the degradation due to cycles of operation which eliminates low returning transactions while performing arbitrage in order to reduce cycles of operation of the battery.

$$P_{\text{fric}}^i = \frac{[P_B^i]^+}{\eta_{\text{fric}}} - [P_B^i]^- \eta_{\text{fric}} \tag{7.3.3}$$

Here η_{fric} denotes the friction coefficient. The new optimization function with battery degradation is presented as

$$(P_{cyc}) \min_{P_B, Q_B} \sum_{i=1}^{N} \left\{ p_{\text{elec}}^i P_{\text{fric}}^i h + \theta(i) + \lambda_{\text{peak}} \max(P_T^i, P_{\max}^{\text{previous}}) \right\}$$

subject to, Eq. 6.2.2, Eq. 6.2.3, Eq. 6.2.4, Eq. 6.3.4, Eq. 6.3.6.

The friction coefficient takes a value from 1 to 0. η_{fric} needs to be tuned so as the operational life is maximized. If the battery is not over operating then η_{fric} is set to 1. For cases where the battery is performing more cycles, the low returning transactions could be eliminated by decreasing the value of η_{fric}. Note that the control of cycles is only imposed on the arbitrage component of the objective function, as majority of cycles are performed for arbitrage. We would like to highlight that reactive power depends on converter size and does not affect storage cycles.

7.3.5 Open Source Codes

The co-optimization formulations and benchmarks presented in this chapter is made open source. The link for the code is `https://github.com/umar-hashmi/ConvexRelaxation`.

7.4 Real-time implementation

In real-world accurate information of parameters such as consumer load and renewable generation for future time is not known and required for the proposed optimization models. For real-time implementation we propose to implementation of the optimization algorithm in a model predictive framework with autoregressive forecasting. In Section 7.4.1 we describe the forecast model used and in Section 7.4.2 we describe the MPC algorithm as `CoOptimizationForecastMPC`.

[1]EoL is the state of the battery when the maximum battery capacity reduces to 80% of its initial rated capacity.

7.4.1 AutoRegressive Forecasting

The lookahead horizon of optimization is denoted as N_{opt}. Consider the number of decision samples in a month is denoted as N_{month}. At time k a rolling horizon forecast of N_{opt} number of samples is performed. We present a generalized ARMA model used for forecasting active power, reactive power and electricity price in terms of general variable V. We define the mean behavior of past values of parameter denoted as V at time step i as

$$\bar{V}^i = \frac{1}{D}\sum_{p=1}^{D} V_{(i-pN_{opt})} \quad \forall i \in \{k, ..., N_{opt}\}, k \geq 1, \tag{7.4.1}$$

where N_{opt} is the number of points in a time horizon of 1 day, and D is the number of days in the past whose values are considered in calculating $\bar{V}$. The forecast of V with $\hat{M}^i$ as the difference from mean behavior is given as

$$\hat{V}_i = \bar{V}_i + \hat{M}_i \quad \forall i \in \{k, ..., N_{opt} + k - 1\}, k \geq 1, \tag{7.4.2}$$

We define $\hat{M}_i \quad \forall i \in \{k, ..., N_{opt} + k - 1\}$ as

$$\hat{M}_k = \sum_{j=1}^{J} \alpha_j M_{k-j} + \sum_{u=1}^{U} \beta_u \delta_k^u, \tag{7.4.3}$$

where $\delta_k^m = (V_{k-mN} - \bar{V}_{k-mN})$ and $\alpha_i, \beta_i \forall i \in \{1, ..., U\}$ are constants. The weights used in ARMA model, $\alpha_j \forall j \in \{1, ..., J\}, \beta_u \forall u \in \{1, ..., U\}$, are tuned by solving Eq. 7.4.4

$$\min \sum_i \{||V_i - \hat{V}_i||^2 + ||\text{norm}([\alpha^i, \beta^i])||^1\}. \tag{7.4.4}$$

7.4.2 Model Predictive Control

ARMA models for active and reactive power and electricity price are tuned using historical data. The tuned ARMA model coefficients are calculated using Eq. 7.4.4. Using the tuned coefficients the forecast vectors are identified using Eq. 7.4.2. These forecast vectors are fed to MPC for calculating optimal energy storage actions for time step i. Similar steps are done for $i \in \{k+1, ..., N_{\text{opt}} + k\}$, till the end of time horizon is reached. Real-time algorithm is presented as `CoOptimizationForecastMPC`. A rolling horizon with N_{opt} number of samples is used for look-ahead. In this work we assume number of decision samples in 1 day as N_{opt}.

Algorithm 15 `CoOptimizationForecastMPC`

Storage Parameters: $\eta_{\text{ch}}, \eta_{\text{dis}}, \delta_{\max}, \delta_{\min}, b_{\max}, b_{\min}, b_0$.
Inputs: $h, N, T, i = 0$, Rolling horizon optimization time period N_{opt}, Historical load, renewable generation and price data, N_{month}.
Initialize: $P_{\max}^{\text{previous}} = 0$.

1: Use historical data to tune ARMA models for active power, reactive power and electricity price,
2: **while** $i < N_{month}$ **do**
3: Increment $i = i + 1$ and receive $p_{\text{elec}}(i)$ and load P_i, Q_i,
4: Forecast N_{opt} samples of $\hat{P}, \hat{Q}, \hat{p}_{elec}$ using ARMA,
5: Implement P_{plt}^{peak} for the rolling horizon and find P_T^i,
6: Calculate $P_{\max}^{\text{previous}} = \max(P_T^i, P_{\max}^{\text{previous}})$,
7: $b_i{}^* = b^{i-1} + \hat{x}^*(1)$ s.t. $\hat{x}^*(1) = [P_B{}^*(i)]^+ \eta_{\text{ch}} - [P_B{}^*(i)]^- / \eta_{\text{dis}}$,
8: Update $b_0 = b_i{}^*$, the initial capacity of battery is updated,
9: Return b^{i*}, $P_B{}^*(i)$, $Q_B{}^*(i)$.
10: **end while**

7.5 Numerical Results

In this section, we demonstrate the performance of our optimization formulations through numerical simulations with real data. We consider multiple storage control policies, as listed below.

- P_{arb}: Only arbitrage,
- P_{plt}: Arbitrage + PFC,

- P_{plt}^{peak}: Arbitrage + PFC+ Peak demand shaving,
- P_{pd}: Only peak demand shaving,
- P_{arb}^{peak}: Arbitrage + Peak demand shaving.

P_{cyc} with battery degradation is discussed subsequently. We use the following performance indexes to measure the performance of our simulations:

1. *Arbitrage Gains* G_{arb}: measures effectiveness in performing arbitrage,
2. *Power Factor Correction:* is gauged using 2 indices, using a prescribed PF limit of 0.9: (i) *No. of PF violations* and (ii) *Mean PF*,
3. Peak Demand Charge Savings (G_{pd}): Consider ΔP_{max} as the reduction in peak demand due to energy storage then the saving is given as $G_{pd} = \lambda_{\text{peak}} \Delta P_{max}$.
4. Gains of reactive energy: denoted as G_{reac} is the improvements in reactive/PF gains with respect to nominal case,
5. *Total Gains* G_T: is the sum of arbitrage gains, reactive compensation gains and peak demand charge saving, calculated with respect to nominal.
6. *Profit* is calculated as the ratio of the total gains and the nominal cost incurred,
7. *Converter Usage Factor*: measures usage of converter and presented in Eq. 6.5.1.
8. *Gains per cycle*: Calculated based on equivalent 100% Depth of Discharge (DoD) cycles. We consider the storage degradation model and algorithm to identify equivalent 100% DoD presented in Chapter 5 [181].

Table 7.4: Battery Parameters

$B_{\min}$, $B_{\max}$, B_0	200Wh, 2000 Wh, 1000 Wh
$\eta_{\text{ch}} = \eta_{\text{dis}}$	0.95
$\delta_{\max} = -\delta_{\min}$	500 W for 0.25C-0.25C 1000 W for 0.5C-0.5C 2000 W for 1C-1C 4000 W for 2C-2C 8000 W for 4C-4C
Cycle Life Calendar Life	4000 cycles at 100% DoD 10 years
Cost	$ 1000

For simulation results we consider a period of 80 days starting from 1st of June 2018. The load and generation data is taken from data collected at Madeira, Portugal. The price data for our simulations is taken from CAISO for the same dates [16]. We use PG&E peak demand rate which is $0.01826/ watt [295]. The gain λ for penalty function $\theta(i)$ is set to be equal to 0.4. Note different gains for the penalty function will place proportional importance in maintaining the instantaneous power factor within permissible limits. Under the *nominal case*, i.e., without any storage the consumer pays $207.88 for active energy, $46.485 for reactive energy and $246.138 for peak demand for 80 days period. The number of PF violations under the nominal case is 2894 time instants and the mean PF is 0.9399. The energy storage actions for deterministic case are decided based on the total optimization horizon of 80 days. The sampling time of this numerical experiment is 5 minutes (288 samples in a day).

Energy storage is interfaced via a converter which can supply active and reactive power based on its ratings. In numerical results, we use five batteries with different ramping capabilities for comparison. Their parameters are listed in Table 7.4. Battery model is denoted as xC-yC implies the battery takes 1/x hours to charge completely and 1/y hours to discharge completely. Fixing the total energy and varying ramping capability provides a sensitivity analysis of different ramping storage technologies. For computing storage profitability, we consider the 2 kWh battery to have a cost of $1000, approximately proportional to the cost of Tesla Powerwall per kWh [66]. For the battery given in Table 7.4, each 100% DoD cycle should make more that $0.2 in order to reach break-even, else this battery will not be profitable.

Fig. 7.1 shows the variation of nominal peak demand for each day along with $P_{\max}^{\text{previous}}$ for different battery models. It is clear that higher ramping battery can lower the peak demand up to a greater extent.

Table 7.5 lists detailed results comparing performance indices for different optimization problems and for different battery models. We wish to highlight that for 4C-4C battery, performing arbitrage with

Table 7.5: Performance indices for converter $S_B^{\max} = P_B^{\max}$

Performance Indices	P_{arb}	P_{plt}	P_{plt}^{peak}	P_{pd}	P_{arb}^{peak}
Battery 4C-4C					
mean PF	0.953	0.946	0.948	0.945	0.953
PF violation	2267	17	23	2622	2268
G_{pd} ($)	-12.526	-12.526	32.541	33.367	32.541
G_{arb} ($)	65.330	65.328	65.294	-25.418	65.296
G_{reac} ($)	6.136	46.847	46.847	4.162	6.180
G_T ($)	58.94	99.649	144.682	12.111	104.017
Profit %	11.78	19.91	**28.91**	2.42	20.78
Cycles	1243.0	1239.3	1239.1	38.79	1242.8
$/cycle	0.0474	0.0804	0.1168	0.3122	0.0837
CUF %	32.20	47.50	47.29	5.51	32.20
Battery 2C-2C					
mean PF	0.934	0.960	0.960	0.942	0.934
PF violation	3260	11	11	2758	3259
G_{pd} ($)	0.288	0.288	17.347	17.347	17.347
G_{arb} ($)	42.787	42.767	42.751	-12.756	42.771
G_{reac} ($)	-6.731	46.479	46.479	2.113	-6.636
G_T ($)	36.344	89.534	106.577	6.704	53.482
Profit %	7.26	17.89	21.29	1.34	10.69
Cycles	806.54	803.34	803.85	17.19	807.04
$/cycle	0.0451	0.1115	0.1326	0.3900	0.0663
CUF %	42.67	57.68	57.68	5.46	42.7
Battery 1C-1C					
mean PF	0.936	0.964	0.963	0.941	0.936
PF violation	3058	51	51	2811	3057
G_{pd} ($)	5.782	5.782	8.674	8.674	8.674
G_{arb} ($)	26.349	26.267	26.260	-6.380	26.342
G_{reac} ($)	-4.060	45.546	45.546	1.020	-4.021
G_T ($)	28.071	77.595	80.48	3.314	30.995
Profit %	5.55	15.35	15.92	0.66	6.13
Cycles	453.90	451.32	451.57	8.11	454.24
$/cycle	0.0618	0.1719	0.1782	0.4086	0.0682
CUF %	49.76	74.16	74.19	5.44	49.80
Battery 0.5C-0.5C					
mean PF	0.940	0.973	0.974	0.940	0.940
PF violation	3024	236	237	2839	3024
G_{pd} ($)	4.337	4.337	4.337	4.337	4.337
G_{arb} ($)	15.404	15.103	15.103	-3.189	15.401
G_{reac} ($)	-1.028	41.058	41.058	0.529	-1.006
G_T ($)	18.713	60.498	60.498	1.677	18.732
Profit %	3.74	12.09	12.09	0.34	3.74
Cycles	249.93	247.07	247.19	5.09	250.13
$/cycle	0.0749	0.2449	0.2447	0.3295	0.0749
CUF %	56.45	81.61	81.54	5.61	56.49
Battery 0.25C-0.25C					
mean PF	0.941	0.970	0.969	0.940	0.941
PF violation	2886	790	789	2868	2886
G_{pd} ($)	2.168	2.168	2.168	2.168	2.168
G_{arb} ($)	8.790	8.333	8.333	-1.590	8.788
G_{reac} ($)	0.205	31.971	37.971	0.187	0.214
G_T ($)	11.163	42.472	42.472	0.765	11.17
Profit %	2.21	8.40	8.40	0.15	2.21
Cycles	138.16	134.15	134.09	3.01	138.21
$/cycle	0.0808	0.3166	0.3167	0.2542	0.0808
CUF %	63.71	77.17	77.19	5.47	63.74

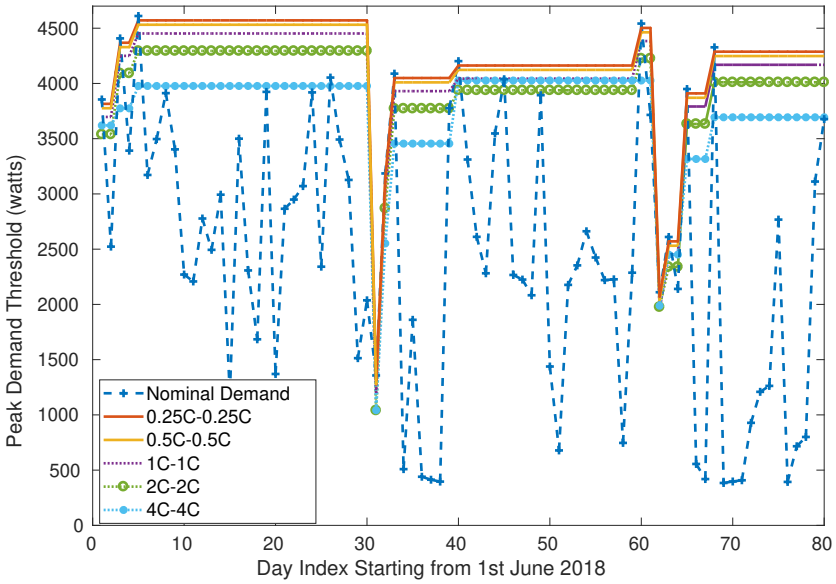

Figure 7.1: Variation of $P_{\max}^{\text{previous}}$ as the days progress

or without PFC, but without peak shaving leads to significant increase in peak demand charge. This drastically overshadows the marginal extra gain that energy storage makes by performing arbitrage. This observation is in sync with conclusions drawn by authors in [294], where super-linear gains were observed for co-optimizing storage. More significant are the results for P_{plt}^{peak}. Notice that for different batteries, it is able to reduce PF violations to as much as P_{plt}, while maintaining gains similar to ones in P_{arb}, P_{arb}^{peak}. This highlights the ability of batteries to do PFC over and above arbitrage and peak shaving. As expected, the gains of peak demand shaving increase as the ramping increases. Table 7.5 also lists that PF violations decrease with increased ramping. We believe these values are still pessimistic and can be improved with a more sophisticated penalty function, θ. To better elucidate the financial gains, we present Fig 7.2. Additional observations based on Table 7.5 are:
(1.) Co-optimizing clearly outperforms total financial gains over performing only one or few of the applications considered in this chapter. Co-optimizing could reduce the consumer bill by up to 28.9% for 4C-4C storage.
(2.) For slow ramping battery reactive compensation gains, G_{reac}, consists of a greater share of total gains compared to faster ramping battery. Consumer with 0.25C-0.25C battery makes up to 78.34% of their total gains by PFC.
(3.) Ignoring peak charges can lead to degraded total gains due to penalties- this is clear for performing only arbitrage for the 4C-4C battery.
(4.) The relatively low CUF for batteries performing peak demand saving solely indicates their under-utilization. Hence dedicating storage application only for peak-demand is sub-optimal.
(5.) For 0.25C-0.25C and 0.5C-0.5C battery, total gains for optimizations performing arbitrage with PFC matches with co-optimization gains for arbitrage, peak demand shaving and PFC, as the storage having a slow ramping capability does add much additional value.

Fig. 7.3 presents a visual representation of total gains made by P_{plt}^{peak} with different battery models. It is clear that total gains increases almost exponentially with decrease in charge-discharge time. This implies that financial potential of energy storage will increase significantly with faster batteries. However, such batteries will be more prone to uncertainty as pointed in [130]. It is worth noting in Table 7.5 that the storage device performs too many cycles and hence low gains per cycle. For example, the 4C-4C battery operates 1239 cycles of 100% DoD cycles in a 3 month period, which is equivalent to greater than 30% of its operational life. At this rate the battery would last less than a year. This motivates the use of P_{cyc} and inclusion of battery life into the model as discussed next.

7.5.1 Controlling and Tuning Cycles of Operation

In order to have an operational life equal to calendar life, the battery should operate 400 100% DoD cycles in a year. For our numerical simulation of 3 months, the battery should perform approximately 100 cycles

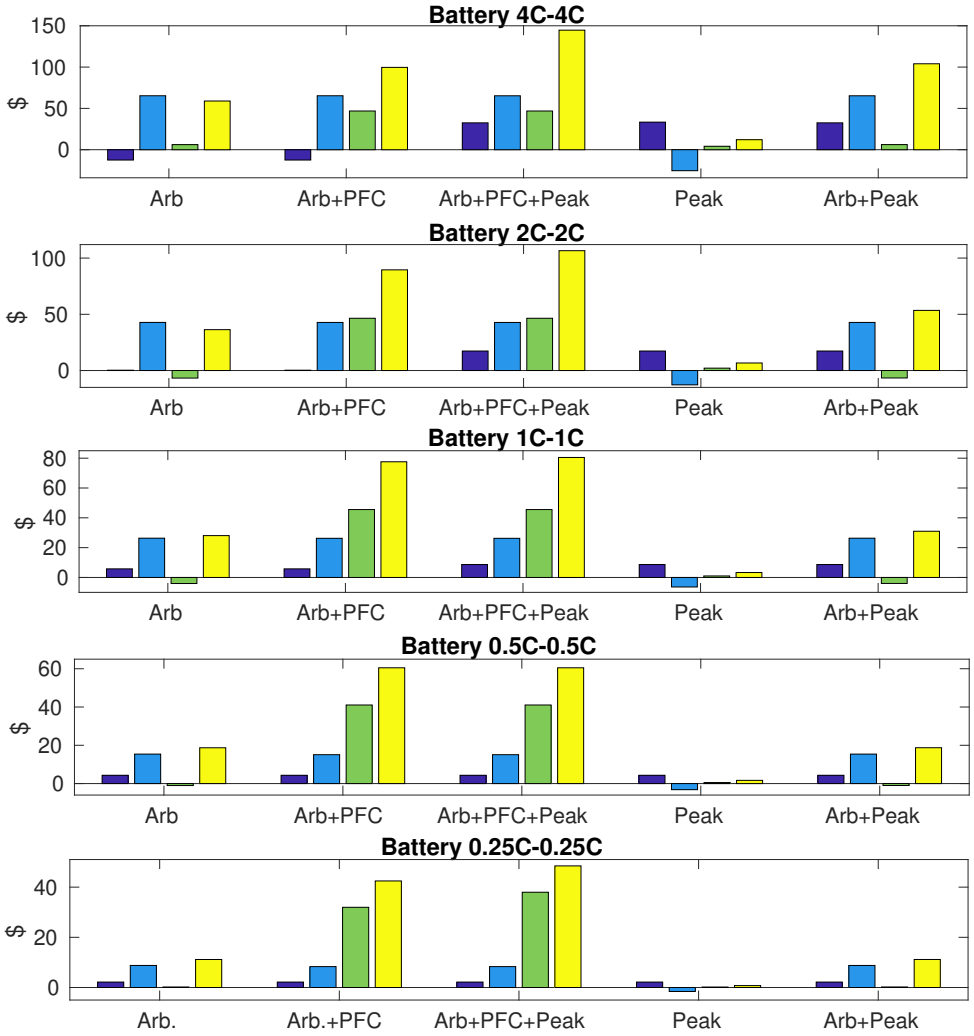

Figure 7.2: Gain plot: G_{pd}, G_{arb}, G_{reac}, G_T are shown as four bar

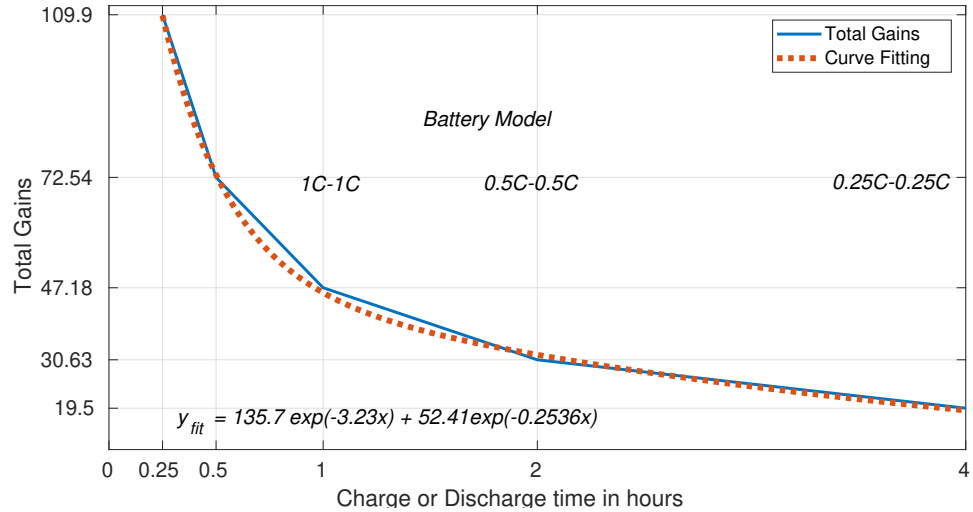

Figure 7.3: Total gain for the optimization problem P_{plt}^{peak} with different battery model and an approximate fit denoted as y_{fit}; The goodness of the fit parameters are: The sum of squares due to error (SSE) = 3.274, R-square = 0.9994, Adjusted R-square = 0.9975, Root mean squared error (RMSE) = 1.809.

(of 100% DoD). Depending on the storage model, the number of cycles of operation can be tuned using the friction coefficient. In order to demonstrate the effect of friction coefficient we show the effect of its variation on total gains, dollars per cycle, number of cycles and CUF in Table 7.6 for the 0.25C-0.25C battery. The following takeaways are clear from Table 7.6:
(1.) Dollars per cycle increases as η_{fric} decreases as low returning transactions are eliminated, in sync with findings in Chapter 3.6 [174].
(2.) Reducing friction coefficient from 1 to 0.8 has less than 2.1% effect on total gains, however, the number of cycles is reduced by more than 53.4%. This justifies the inclusion of degradation/life-cycle modeling into our formulation.
(3.) Decreasing η_{fric} below a certain level (0.4 for the case listed in Table 7.6) does not increase the total gain significantly, however, gains per cycle increases due to lower number of cycles of operation.

Table 7.6: Effect of η_{fric} for 0.25C-0.25C Battery for P_{cyc}

η_{fric}	G_T	cycles	**$/cycles**	CUF
1	42.601	134.10	0.3177	78.81
0.8	41.708	62.15	0.6711	59.73
0.6	40.053	27.70	1.446	55.04
0.4	38.215	18.986	2.013	51.5
0.2	36.704	15.005	2.446	53.62
0.1	34.557	12.53	2.758	53.39

Table 7.7 presents gains for different batteries for the friction coefficient at which their calendar life degradation approximates cycle life degradation. It is interesting to note that battery 2C-2C provides the highest dollars per cycle, which is even more than the fastest ramping battery 4C-4C. Note that for the faster ramping batteries, CUF is quite low. This implies that a smaller converter may be sufficient. Selection of optimal converter based on battery life-cycle is an objective of our future work in this domain.

Table 7.7: Tune η_{fric}: match calendar and cycle life degradation

Battery	η_{fric}	G_T	cycles	$/cycles	CUF
4C-4C	0.240	84.23	99.9	**0.8432**	22.5
2C-2C	0.532	86.07	99.9	**0.8617**	25.7
1C-1C	0.684	74.78	99.84	**0.7490**	50.5
0.5C-0.5C	0.802	58.92	100.2	**0.5890**	68.6
0.25C-0.25C	0.930	42.45	99.9	**0.4248**	69.3

Table 7.8: Deterministic and real-time implementation for March 2018

Battery Type	G_{arb}	G_{reac}	G_{peak}	G_T
Deterministic results: **rolling horizon of 1 day**				
0.5C-0.5C	3.723	5.855	4.337	13.914
1C-1C	6.523	5.855	8.674	21.051
2C-2C	10.719	5.855	16.221	32.794
Real-time implementation: **ARMA + MPC**				
0.5C-0.5C	2.819	5.855	4.337	13.010
1C-1C	5.073	5.855	5.590	16.518
2C-2C	9.226	5.855	10.800	25.880

7.5.2 Real-time Implementation

Simulation are performed for the month of March 2018. Data for the previous month is used to tune the ARMA model. ARMA models takes into account the previous 3 time intervals and 3 previous days, i.e., $D = 3$. The goal of the comparison is to understand the effect of parameter uncertainty on different revenue streams of the co-optimization formulation. Table 7.8 shows the comparison of arbitrage,

reactive compensation and peak demand gains for deterministic results with real-time implementations using `CoOptimizationForecastMPC` algorithm. The arbitrage gains are more sensitive to parameter uncertainty for battery with faster ramping battery. The results are in sync with observations made in [130]. The power factor correction gains are not influenced by future parameter uncertainties, as observed in [178]. The peak demand shaving similar to arbitrage gains are affected by parameter uncertainty more significantly for batteries with faster ramping.

7.6 Conclusion and Perspectives

We present a co-optimization formulation for arbitrage, power factor correction and peak shaving. These storage applications are motivated by three part electricity pricing used in new designs of pricing electricity. We consider realistic electricity billing mechanisms composed of three components: (i) active energy consumption cost, (ii) reactive energy cost and (iii) peak demand cost. Despite the different time-scales (minutes to a month), we show that using a memory variable for peak demand and a penalty-based formulation for power factor correction, the optimization problem can be efficiently solved. Using realistic battery parameters, real prices for arbitrage and peak demands, we demonstrate the efficiency of our co-optimization approach. Through numerical simulations we show that proposed co-optimization problem has higher consumer gains. We observe that total gains of the user would be lower for optimization problems which are a combination of one or two applications of the proposed optimization formulations.

We use different ramping batteries, and provide a sensitivity analysis of varying ramp rate batteries. We observe that faster ramping battery performs many more number of cycles compared to slow ramping battery. Since energy storage has a limited cycle life, therefore, control should consider the cycles of operation in control design. We propose inclusion of friction coefficient which acts as friction in mode changes and eliminating the low returning transactions. Comparing dollars per cycle indicate that faster ramping batteries need not be more profitable for the consumer. In numerical results we identify that after tuning the cycles of operation using friction coefficient, the battery model 2C-2C is most suitable with a value of \$0.8617 for each 100% DoD cycle.

We propose an online implementation of the proposed co-optimization formulation using Model Predictive Control. We observe that peak demand and arbitrage gains, but not power factor correction, are sensitive to uncertainties in forecast, with sensitivity being higher for faster ramp rates. In future work, we will analyze improvements in friction coefficient and penalty functions.

Further exploration is required for identification of more co-optimization roles and also prioritizing roles which can be more valuable at certain times compared to others. This is essential as the valuation of roles differ in time-scale, energy and power needs. Some storage applications require up-front commitments to be made by storage owners (for example dynamic regulation in PJM), modeling these into the storage control formulation is not straightforward.

Chapter 8

Co-optimizing Storage in Madeira

Multitasking the art of doing twice as much as you should half as well as you could. -Anonymous

Summary: Energy storage applications are explored from a prosumer (consumers with generation) perspective for the island of Madeira in Portugal. These applications could also be relevant to other power networks with similar consumer contracts. We formulate a convex co-optimization problem for: (a) performing arbitrage under zero feed-in tariff, (b) increasing self-sufficiency by increasing self-consumption of locally generated renewable energy, (c) providing peak shaving and (d) acting as a backup power source during anticipated and scheduled power outages. Using real data from Madeira we perform short and long time-scale simulations in order to select end-user contract which maximizes their gains considering storage degradation based on operational cycles. We observe energy storage ramping capability decides peak shaving potential, fast ramping batteries can significantly reduce peak demand charge. The numerical experiment indicates that storage providing backup does not significantly reduce gains performing arbitrage and peak demand shaving. Furthermore, we also use AutoRegressive Moving Average (ARMA) forecasting along with Model Predictive Control (MPC) for real-time implementation of the proposed optimization problem in the presence of uncertainty.

8.1 Introduction

Medium sized isolated power networks often restrict the share of renewables and enforce stringent rules necessary to maintain safety and stability of the electrical power system. Authors in [267] indicate that a high share of wind energy penetration could lead to large variations in active power generated due to sudden changes in wind speed. This in effect creates a huge mismatch between supply and demand, causing large variations in voltage and frequency leading to hazardous operating conditions. The enforcement regulations set by the Ministry of Industry and Energy of the Canary Government goes as far as restricting any further increase in wind farm installations directly connected to the power network. However, additional renewables are considered favourable if the generated energy is self-consumed locally [120]. In [111] the use of wind-powered hydro storage system for increasing the penetration of renewables is proposed for the island grid of Gran Canaria (part of Canarian Archipelago). In this solution, pumped storage acts as energy storage which is feasible due to the geography of the island and might not be applicable to similar isolated power networks.

The work in [321] presents a case study for Coimbra where residential solar and energy storage is locally consumed with goal of zero energy buildings. Authors observe that the electricity bill for the household reduces by more than 87%. Furthermore, self-consuming intermittent renewable generation locally is desired by the utilities, as such generation makes load balancing, frequency and voltage regulation more challenging. Thus self-consuming renewable generation assists the power grid to accommodate a larger share of renewables [232]. Often utilities set the feed-in-tariff lower than the retail rate, making self-consumption more desirable for electricity consumers. The details of compensation of active energy (as arbitrage) is described in Chapter 3 and Chapter 4. Authors in [101] observe that by increasing self-consumption of renewables, their financial feasibility could be achieved a decade before in some European countries. Although self-consumption holds multiple benefits for utilities, such a constraint creates a disparity for Distributed Generation (DG) owners, as excess generation cannot be fed back to the grid.

In order to mitigate this disparity, these DG owners should co-optimize for additional revenue streams. In Germany DG owners until 2012 were incentivized for self-consumption rather than feeding power back to

the grid [252]. Under the case where DG owners are not allowed to supply power back to the grid, energy storage can facilitate load-shifting in real-time, minimizing consumption cost, increasing self-sufficiency [232]. *Self-sufficiency* is the ratio of total energy demand met by local generation and/or storage with respect to cumulative energy needs. Storage acts as a buffer of electrical energy and assists in the temporal shift of energy usage. Authors in [191] describe the various applications for energy storage in future power networks. Furthermore, with greater integration of intermittent renewables performing arbitrage and ancillary services will be more profitable [185]. Co-optimizing energy storage for multiple applications has been proposed in many recent works. The authors in [136] co-optimize for arbitrage and frequency regulation, [294] co-optimizes peak saving and frequency regulation. In this chapter, we consider the case of Madeira Island, where utilities promote the inclusion of DG for self-consumption only. Hence this is a special case of arbitrage formulation presented in Chapter 4, with selling price set zero at all time instants. We propose the integration of a DG source along with energy storage. This battery facilitates self-consumption of locally generated energy, assist users in selecting a lower peak power contract, performing arbitrage and providing energy backup for instances of probable and scheduled power outages. The key contributions of this chapter are:

- *Co-optimization*: We propose a convex formulation for energy storage control for performing arbitrage, peak demand charge saving and backup reserve during power outages considering efficiency losses, ramping and capacity constraints for an energy storage.
- *Storage profitability*: The operational cycles govern storage degradation. The performance index for monetary value per cycle introduced in [181] is used. This index indicates that battery is financially profitable in Madeira.
- *Real time implementation*: We use Auto-Regressive Moving Average (ARMA) processes to model temporal evolution in the MPC framework for real-time implementation considering uncertainty, motivated by our prior work [183].

The key observations made from numerical results are:

- Storage owners would benefit more by performing *arbitrage* with contracts with more price variations.
- Ramping capability primarily decides the ability to reduce *peak demand* charge savings for consumers.
- When DG generation is smaller than or approximately equal to inelastic load in magnitude then *self-sufficiency* is governed by only the DG generator, otherwise, storage also contributes to it by increasing self-consumption.
- Providing *energy backup* does not noticeably reduce storage ability to perform peak demand and/or arbitrage.

The chapter is organized as follows. Section 8.2 introduces power system norms for consumers in Madeira. Section 8.3 formulates the co-optimization problem of performing arbitrage, peak shaving and energy backup. Section 8.4 presets the real-time control of storage under uncertainty. Section 8.5 presents the numerical results. Section 8.6 concludes the chapter.

8.2 Power System Norms in Madeira

Madeira is an archipelago in the North Atlantic Ocean, located about 1000 km southwest of mainland Portugal. It has a population of almost 270,000. 111,000 of which living in the capital city of Funchal.

8.2.1 Overview of the Madeira Electric Grid

Madeira relies on local generation for electricity. Empresa de Eletricidade da Madeira, S.A. (EEM) is the only DSO/TSO in Madeira, and is responsible for the activities related to production, transport, distribution and commercialization of electric energy. Energy generation sources used in Madeira are: thermal energy from fossil fuels like diesel and natural gas, hydro, wind, solid waste incineration (SWI), and photovoltaic (PV). In 2017, Madeira consumed 800GWh energy; thermal constituted about 70% of the energy mix, with the remaining 30% coming from renewable sources (hydro: 12.2%, wind: 9.5%, SWI: 4.8%, and PV: 3.6%) [83]. Thus 17% RES generation is controllable and 13% intermittent. The non-domestic sector (e.g., tourism and commerce), the domestic sector contributes 45% and 30% of total consumption respectively. The remaining 25% are contributed by public lighting (9%), public buildings (8%), industry (7%), and agriculture ($< 1\%$) [83].

8.2.2 Peak Power Contracts, Tariffs and Billing Cycles

As of 2018, LV customers can select between 8 levels of peak power contract (PPC), three power tariffs, and two billing cycles [320]. Thus, there are total 48 different contracts that users can select from.

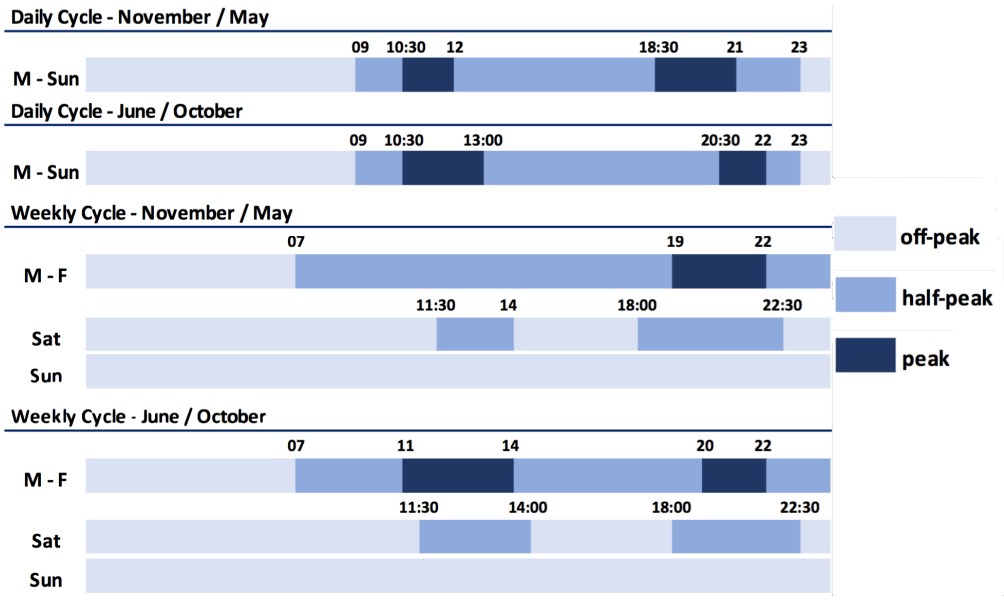

Figure 8.1: Billing cycle schemes currently in place.

LV customers are subject to a maximum peak power contract (kVA), ranging from 3.45 kVA to 20.70 kVA (see Tab.2.4). PPC value is selected by the customer based of their estimated electricity needs and should not be exceeded since the supply is shut-down when that happens. The disconnection of power is done locally and consumer can restart their energy-meter, however, sudden interruptions should be avoided as it may damage appliances.

Regarding the energy tariffs, there are three options for LV customers. *Single*, *dual* and *triple-rate* per kWh. In the *Single-rate* tariff the price is fixed at 0.1629 €/kWh. In the *dual-rate* tariff there are two *time-of-use* (ToU) prices (*peak* at 0.1894€/kWh, and *off-peak* at 0.0982€), whereas in the *triple-rate* tariffs have three ToU price levels (*peak* at 0.2153€, *off-peak* at 0.0982€, and *half-peak* at 0.1716€). The *off-peak*, *peak* and *half-peak* periods are defined in advance based on the notion of *daily* and *weekly* billing cycles. In the *daily* cycle there are no distinctions between weekend and workdays, whereas in the *weekly cycle* there are different *time-of-use* periods for work-days, Saturdays and Sundays. Fig. 8.1 summarizes the billing cycle schemes in practice as of 2018. For *dual-rate tariff*, the *peak* period includes also the *half-peak* period.

Consumer electricity bill consists of two components: a fixed component that depends on the contracted power (kVA), and a dynamic component governed by actual energy consumption (kWh). Note that the fixed component is governed by apparent power: a function of active and reactive power. In this work, we consider PPC levels to a function of only active power as apparent power is primarily governed by active power. Reactive power compensations as proposed in Chapter 6 [178] could be applied for the storage control in this chapter.

8.2.3 Self-Consumption and Renewables in Madeira

In Madeira island, since 2014, new mini and micro-producers are not allowed to feed-in excess production to the local grid, thus excess generation is wasted [83]. Due to such a constraint DGs are sized to maximize self-consumption and minimize excess production [277]. Counterintuitively, in a period that one should expect an explosion in the number of micro-producers leveraged by the relatively low prices of solar PV technologies, Madeira is experiencing an stagnation on the number of new solar PV installations due to the norms set by EEM. The main reason for this change in the local legislation is to protect the grid from the issues associated with the intermittent and uncertain nature of renewable production from solar in a total energy system. In case of the electrical LV networks in the rural areas of Madeira Island which are at the edge of the radial distribution network, when associated with low consumption and high production periods, it is very likely to observe the phenomena of voltage increase [83].

8.3 Co-optimizing Energy Storage

In this chapter we consider a prosumer with inelastic load and rooftop solar generation as DG and an energy storage. The battery serves four purposes: (i) increase self-consumption, thus reducing waste of excess generation if any, (ii) perform energy arbitrage, (iii) minimize the peak demand charge and (iv) maintain battery charge level for scheduled and/or anticipated power failures.

The battery and system model used in this chapter is described in Chapter 2.5. We use xC-yC notation to represent the relationship between ramp rate and battery capacity. xC-yC implies battery takes 1/x hours to charge and 1/y hours to discharge completely.

Optimizing the energy storage is essential due to its high cost. In this chapter we do not evaluate the fixed electricity cost as under such a case storage can only be used either for backing up excess generation and/or for peak demand shaving. Backing up energy will require no look-ahead and greedy behavior leads to optimality [305]. The optimal solution in such a case is governed by the sign of z_i and is given as

- if $z_i \geq 0$ then battery should discharge such that $s_i = \max\{-z_i, \delta_{\min} h \eta_{dis}, (b_{i-1} - b_{\max})\eta_{dis}\}$,
- if $z_i < 0$ then battery should charge such that $s_i = \min\{-z_i, \delta_{\max} h/\eta_{ch}, (b_{i-1} - b_{\min})/\eta_{ch}\}$.

Next we formulate co-optimization problem for storage control for arbitrage, peak shaving and backup.

8.3.1 ToU pricing + zero feed-in-tariff + Peak-Shaving

The total load is denoted as $l_i = z_i + s_i$. The optimal arbitrage problem with battery (P_{arb}) is defined as the minimization of the cost of total energy consumed denoted as $\min \sum_{i=1}^{N} [l_i]^+ p_{\text{elec}}(i)$ subject to the battery constraints, see Chapter 2.5. $p_{\text{elec}}(i)$ denotes the electricity price for consuming electricity, i.e. $l_i > 0$, for instant i. Here we assume the feed-in-tariff to be zero. This optimization framework is a special case of the problem studied in [182], [148]. Under zero feed-in-tariff, only consumed energy is charged and end-user gets no incentive in supplying power back to the grid (i.e. $l_i < 0$). This is emulated using a variable $\theta_i = \max(0, l_i)$. Keeping $l_i \geq 0$ will maximize the self-consumption of renewable generation.

In this formulation we also consider peak demand shaving by reducing the peak demand contract the end-user should opt for. Consider the maximum demand of the user without storage is $P_{\max}$ then the inclusion of energy storage would bring this maximum demand lower proportional to its ramp rate, considering look-ahead optimization ensures battery has enough capacity to discharge during peak demand. The end user operates the energy storage for minimizing the cost of consumption, increasing self-consumption by reducing the waste of excess of generation and restraining peak demand. This optimization problem

$$(P_{opt}) \quad \min_{s_i} \quad \sum_{i=1}^{N} p_{elec}(i)\theta_i h,$$

subject to, (i.) Ramp Constraint Eq. 6.2.2, (ii.) Capacity constraint Eq. 6.2.4,

(iii.) $\theta_i \geq 0$, (iv.) $\theta_i \geq [z_i + s_i]$,

(v.) Peak Shaving: (PPC)$[z_i + s_i]/h \leq P^{set}_{\max}$.

$P^{set}_{\max}$ is selected by the electricity consumer as a PPC contract with the utility in Madeira. Note that selecting a low level of $P^{set}_{\max}$ might be impossible to maintain using a given energy storage. The peak power threshold, $P^{set}_{\max}$, is selected close to the power level $(P_{\max} + \delta_{\min})$, subject to $P^{set}_{\max} \geq (P_{\max} + \delta_{\min})$.

8.3.2 Storage for BackUp with Arbitrage + Peak Shaving

The valuation of energy storage devices performing energy backup is hard to quantify and often ignored in assessing the value of energy storage devices. Regions where power network is not very reliable, consumers install energy storage devices and a power converter to charge the battery while power is available through the grid and immediately start discharging when the grid supply is not active. Installing such devices provides uninterrupted power supply to the user, enhancing the reliability of power supply at the consumer end. Abrupt disconnection of power supply drastically affects the life of certain appliances. Energy storage is also used for energy backup in developed countries; loads like data centers and hospitals are critical and therefore, local backup of energy is essential. Here we consider two types of backup modes:

• *Pre-scheduled unavailability of power*: Due to scheduled maintenance power outages could occur. It is essential to consider such incidents in case of Madeira as being an isolated power network it has less inertia

and less redundancy making it more prone to scheduled outages. In such cases the time of the outage denoted as i_{incident}, is known a priori and users can maintain the battery level above b_{set}, so as in absence of grid supply users can meet its energy needs. This is represented as an additional constraint denoted as $b_i = b_{i_{\text{incident}}} \geq b_{\text{set}}$.

• *Probability of power loss*: based on past failure incidents a probability of power failure can be calculated; for instance, the chances of power failure due to load shedding are much more probable during morning and evening peak than any other time of the day. $\mathbb{P}_i$ denotes the probability of power failure during the instant i. If $\mathbb{P}_i$ is high than the user should maintain a greater charge level in the battery. The co-optimization problem combined with planned and probable outages is given as follows

$$(P_{\text{madeira}}) \quad \min_{s_i} \quad \sum_{i=1}^{N} \{p_{elec}(i)\theta_i h - \lambda \mathbb{P}_i b_i\},$$
$$\text{subject to, (i.) Eq. 6.2.2, (ii.) Eq. 6.2.4,}$$
$$\text{(iii.) } \theta_i \geq 0, \quad \text{(iv.) } \theta_i \geq [l_i], \quad \text{(v.) } [l_i]/h \leq P_{\max}^{set},$$
$$\text{(vi.) } b_i = b_{i_{\text{incident}}} \geq b_{\text{set}}; \text{ where } \lambda \text{ is scaling factor.}$$

Note P_{opt} and P_{madeira} are convex in nature as the objective function and associated constraints are convex.

Using this, the co-optimization problems for performing arbitrage, peak shaving and backup can be solved by by off the shelf solvers like Gurobi or Mosek through CVX [7].

8.3.3 Open Source Codes

The co-optimization formulations and benchmarks presented in this chapter is made open source. The link for the code is `https://github.com/umar-hashmi/MadeiraStorage`.

8.4 Real-time Control under Uncertainty

The decision variables for the optimization problem P_{opt} and P_{madeira} is the energy storage output s_i. The stochastic variable in these settings is the the net-load excluding energy storage output, z_i. We use AutoRegressive Moving Average (ARMA) forecasting for modeling z_i. The details of the model is described in Section 8.4.1 (for more details refer to Section 2.4.1) and model predictive control algorithm is described in Section 8.4.2.

8.4.1 Modeling Uncertainty: ARMA Forecasting

We define the mean behavior of past values of net load without storage at time step i as

$$\bar{z}_i = \frac{1}{D} \sum_{p=1}^{D} z_{i-pN} \quad \forall i \in \{k, ..., N\}, k \geq 1, \tag{8.4.1}$$

where D is the number of days in the past whose values are considered in calculating $\bar{z}$. The forecasted net load given as $\hat{z}_i = \bar{z}_i + \hat{X}_i \quad \forall i \in \{k, ..., N\}, k \geq 1$, where $\hat{X}_i$ represents the forecasted difference from the mean behavior. We define $\hat{X}_i \quad \forall i \in \{k, ..., N\}$ as

$$\hat{X}_{\text{k}} = \alpha_1 \hat{X}_{\text{k}-1} + \alpha_2 \hat{X}_{\text{k}-2} + \alpha_3 \hat{X}_{\text{k}-3} + \beta_1 \delta_{\text{k}}^1 + \beta_2 \delta_{\text{k}}^2 + \beta_3 \delta_{\text{k}}^3, \tag{8.4.2}$$

where $\delta_k^m = (z_{k-mN} - \bar{z}_{k-mN})$ and $\alpha_i, \beta_i \forall i \in \{1, 2, 3\}$ are constant. We use the errors in net load without storage for the past three time steps and the error in the same time step for past three days. At time step $i = k - 1$ we calculate $\hat{X}_k$ as shown in Eq 8.4.2. Using $\hat{X}$ we calculate $\hat{z}$.

8.4.2 Model Predictive Control

The vector $\hat{z}$ for instants i to N is fed to MPC for calculating optimal energy storage actions for time step i. Similar steps are done for $i \in \{k+1, ..., N\}$, till the end of time horizon is reached. Real-time algorithm is presented as `ForecastPlusMPCforCoOpt3`.

Algorithm 16 `ForecastPlusMPCforCoOpt3`

Inputs: $\eta_{\text{ch}}, \eta_{\text{dis}}, \delta_{\max}, \delta_{\min}, b_{\max}, b_{\min}, b_0, p_{elec}, h, N, T, i = 0$

1: **while** $i < N$ **do**
2: Increment i=$i+1$
3: Forecast $\hat{z}$ from time step i to N
4: Solve for $s^* = P_{\text{madeira}}(p_{elec}, \hat{z}, h, N, T)$
5: $b_i^* = b_{i-1} + [s^*]^+ \eta_{ch} - [s^*]^- / \eta_{dis}$
6: Update $b_0 = b_i^*$
7: **end while**

8.5 Numerical Results

For the numerical evaluation we use a battery with initial charge level, b_0=1kWh, $b_{\max}$=2kWh, $b_{\min}$=0.2kWh, η_{ch}=η_{dis}=0.95. The home has 6.25 kWp solar PV. The performance indices used for evaluating simulations are:

• *Arbitrage Gains* (G_{arb}),

• *Peak shaving gains* (G_{peak}): difference between nominal Peak Power Contract (PPC) and the new PPC contract after adding storage.

• *Self-sufficiency* (SS): calculated using total energy consumed, PV generation and storage output.

• *Gains per cycle*: In our prior work [181] we develop a mechanism to measure the number of cycles of operation based on depth-of-discharge of energy storage operational cycles. We use total gains, G_T=G_{arb}+G_{peak}, to calculate €/cycles gained by operating energy storage as one of the performance index. This index puts a financial value to operational cycles of the battery.

We perform deterministic simulations for arbitrage and peak demand shaving in Section 8.5.1. Section 8.5.2 presents numerical results for energy storage performing backup along with arbitrage and peak shaving. Section 8.5.3 compares forecast plus MPC with results for a week with respect to the deterministic results.

8.5.1 Deterministic Solution for P_{opt}

We compare various pricing contracts and propose the best contract that energy storage owners can select for maximizing their gains. Here we consider only the daily cycles since this is the most commonly selected option in Madeira. Two types of simulations results are presented: simulation on a shorter-time scale, (i.e., for a day) and for longer time-scale, (i.e., for a month). The load data is collected from a facility in Madeira. Single-rate tariff is used as the nominal case with respect to which profit and performance improvements are calculated.

Shorter Time Scale: A day

Simulations using 2 and 3-level ToU price for 4 different batteries are conducted for load data of 18th May, 2018.

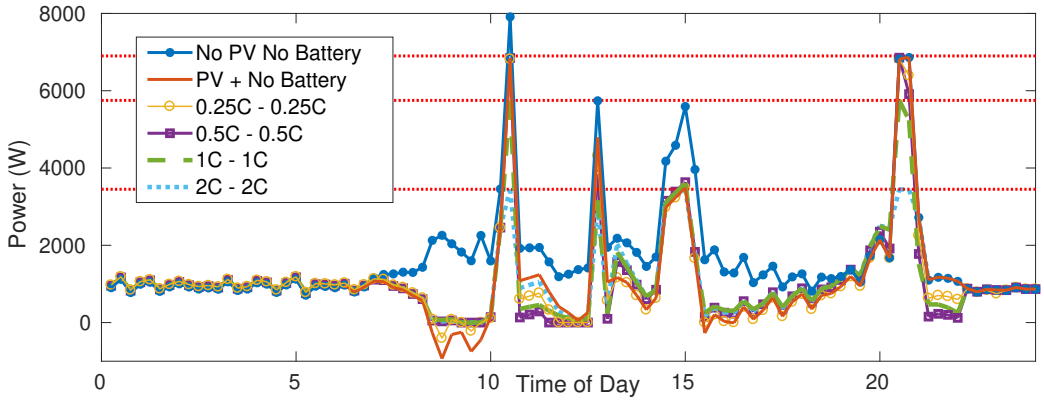

Figure 8.2: Net Load with/without solar and with/without battery for $h = 0.25$ hours; here we consider *4 different batteries*

From Table 8.1 we can conclude that 3-level ToU provides higher gains for end-user, fast ramping battery can increase G_{peak}, however, G_{arb} deteriorates due to greater contribution of the battery performing peak reduction. Fig. 8.2 shows the variation of net load for 3-level ToU.

Table 8.1: Comparison for 1 day

Case	G_{arb} €	PPC kVA	G_{peak} €	SS %	G_T €	**€/cyc**
No Battery						
No PV	-	10.35	-	-	-	-
PV	-	6.9	0.144	32.9	0.144	-
2 Level ToU with Battery						
0.25C-0.25C	**0.240**	6.9	0.144	36.2	0.384	0.568
0.5C-0.5C	0.235	6.9	0.144	36.6	0.379	0.561
1C-1C	0.235	5.75	0.192	36.6	0.427	**0.631**
2C-2C	0.212	**3.45**	**0.287**	36.3	**0.499**	0.363
3 Level ToU with Battery						
0.25C-0.25C	0.333	6.9	0.144	36.2	0.477	**0.704**
0.5C-0.5C	**0.366**	6.9	0.144	36.2	0.510	0.376
1C-1C	0.351	5.75	0.192	36.1	0.543	0.346
2C-2C	0.301	**3.45**	**0.287**	36.1	**0.587**	0.379

Table 8.2: Comparison for Longer Time Scale

Case	G_{arb} €	PPC kVA	G_{peak} €	SS %	G_T €	**€/cyc**	SPB yrs.
No Battery							
No PV	-	17.25	-	-	-	-	-
PV	-	17.25	0	34.1	0	-	-
2 Level ToU with Battery							
0.25C-0.25C	18.38	13.8	4.27	34.9	22.65	**0.855**	3.2
0.5C-0.5C	18.38	13.8	4.27	34.9	22.65	0.855	3.2
1C-1C	18.38	13.8	4.27	34.9	22.65	0.855	3.2
2C-2C	18.37	**10.35**	**8.54**	34.9	**26.92**	0.669	4.1
3 Level ToU with Battery							
0.25C-0.25C	25.01	13.8	4.27	34.9	29.28	**1.035**	2.7
0.5C-0.5C	25.89	13.8	4.27	34.7	30.16	0.640	4.3
1C-1C	**26.08**	13.8	4.27	34.7	30.36	0.589	4.7
2C-2C	26.06	**10.35**	**8.54**	34.6	**34.60**	0.568	4.8

Integration of storage leads to approximately 3% saving of electricity bills. Prior to installation of storage, 5.8% of solar generation was wasted and with addition of storage the waste is reduced to zero. The simulations also shows that additional gains are possible by reducing the PPC shown in Fig 8.2 and Table 8.1.

Longer Time-Scale: A month

Longer time scale simulations are conducted for the month of June, 2018. Table 8.2 shows that energy storage does not contribute significantly towards self-sufficiency. Fig. 8.3 shows the variation of SS for each day due to PV. Long time scale simulations also indicate that 3 level ToU is more beneficial. Further the gains per cycle indicate that energy storage is highly profitable. A typical LiIon battery costing around €500/kWh could perform around 4000 cycles at 100% DoD. Thus such a battery (of 2kWh size) to be profitable should make more than €0.25/cycle. Table 8.1 and Table 8.2 show that €/cycle is significantly more than €0.25. Table 8.2 also list the simple payback period (SPB) in years by extrapolating the gains linearly based on gains made in 1 month.

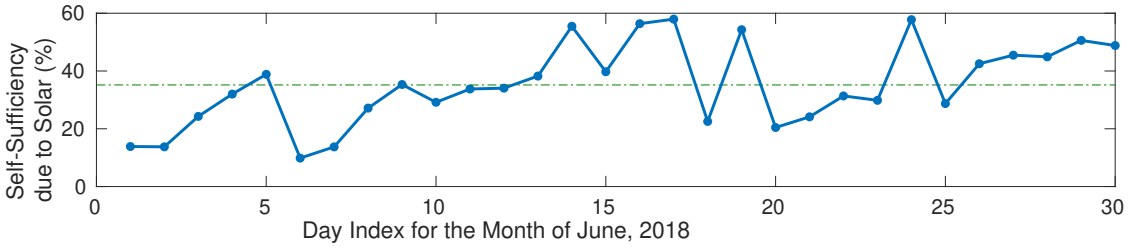

Figure 8.3: Self-Sufficiency due to Solar for June 2018

8.5.2 Co-optimizing with Power Backup

The probability of power failure used for scheduling energy storage backup is shown in Fig. 8.4(a). The probability of power failure on a typical day is primarily because of load-shedding, which happens more during peak consumption hours.

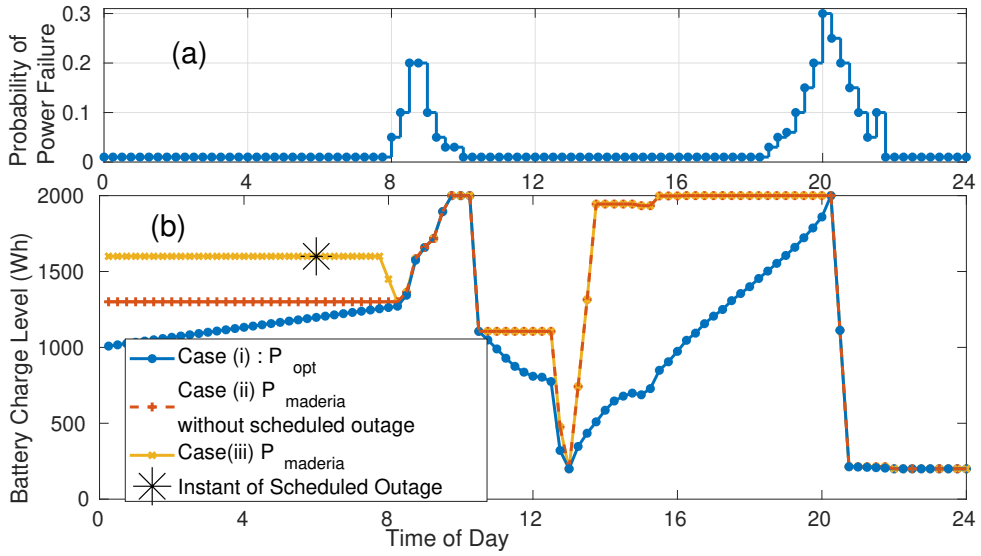

Figure 8.4: (a) Probability of power failure, (b) Battery charge level

We assume that there is a scheduled power outage incident at i_{incident}=6 am. During this time storage should maintain an state of charge of 80% or higher, therefore, $b_{set} = 0.8b_{\max}$.

Table 8.3: Comparison of gains for power backup

Index	Case (i) P_{opt}	Case (ii)	Case (iii) $P_{madeira}$
G_{arb}	0.3006	0.3006	0.2976
G_{peak}	0.2867	0.2867	0.2867

Fig. 8.4(b) shows battery charge level for three cases: (i) P_{opt}: arbitrage with peak shaving, (ii) Arbitrage with peak shaving and backup for probable outage governed by failure probability in Fig. 8.4(a) and (iii) $P_{madeira}$: arbitrage, peak shaving, probable outage with scheduled outage. As evident from Fig. 8.4(b) the charge level for Case (iii) maintains a higher charge level during i_{incident}. For case (ii) and case (iii) maintains a high charge level during probable outage during morning and evening peak. As shown in Table 8.3, the effect on gains due to performing backup is insignificant, less than 1% in this case. For these cases self-sufficiency remains fairly similar.

8.5.3 Real-Time Implementation (Forecast plus MPC)

The coefficients of the ARMA forecast model is tuned using regression. For this case, we use a battery of 1C-1C type. The comparison of total load for deterministic and MPC simulations is shown in Fig. 8.5. The

state of charge (SoC) of the battery is shown in Fig. 8.6. It can be observed that for stochastic simulations the battery capacity is maintained at high SoC level in order to minimize probable outage component of the objective function.

The arbitrage gains for the deterministic case for the week is €5.50 and for ARMA with MPC the gains are €5.01. Loss of opportunity (LoO) is defined as = 1−(actual arbitrage gains)/(deterministic arbitrage gains). The LoO for this numerical experiment is 8.91%. A low value of LoO indicates the robustness of our proposed real time framework. Peak demand shaving for this week is €0.336 for both deterministic and ARMA with MPC case. Although in this numerical experiment the peak demand is in compliance with the same contract as for the deterministic case, however, it would be advised to select a higher level of peak demand contract pertaining to forecast errors.

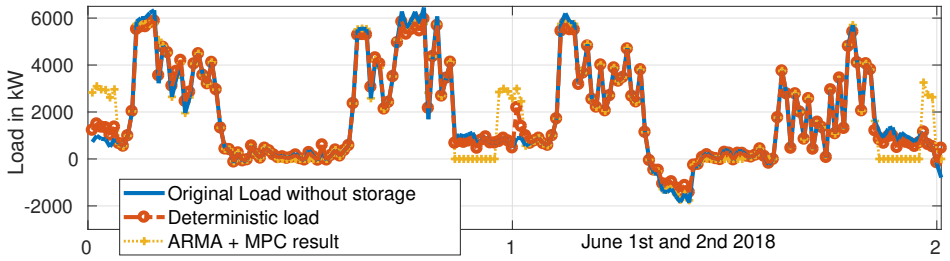

Figure 8.5: Net load comparison for June 1 and June 2, 2018

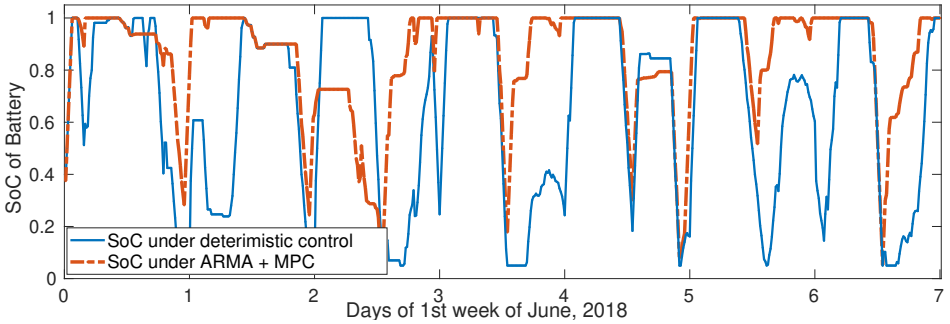

Figure 8.6: Battery Capacity for 1st week of June, 2018

8.6 Conclusion and Perspectives

We present a case study for the island of Madeira and formulate a convex co-optimization problem for performing arbitrage, peak-shaving and providing backup during power outages. Using numerical simulations we observe that storage owners benefit more under greater volatility, evident from higher gains electricity customers can make with 3-level ToU compared to 2-level. We believe an increase in storage size will make more volatile consumer contracts more beneficial. Energy storage adds to economic value while solar PV increases self-sufficiency for scenarios where distributed generation is lower or comparable to the magnitude of the inelastic load. For DG generating more than inelastic load, storage also contributes to self-sufficiency by increasing self-consumption. We show that using storage for power backup during probable and scheduled outages do not undermine its ability to perform arbitrage and peak demand shaving. Considering storage operational cycle degradation, we calculated gains per cycle indicating the storage could be financially viable in Madeira (simple payback period ≈3 years). Numerical simulation for real-time control using ARMA based forecast with MPC shows the efficacy of the proposed scheme for storage co-optimization.

The dependency of inelastic load and DG generation on storage sizing and NEM rules requires more exploration. Consider a planning problem which takes into account historical data and provides best-suited battery and the consumer contract the user should opt for given investment constraints. Of course, such formulations need to be redesigned for other power networks depending on local network rules. Further work is required to select an optimal battery size based on historical data. The storage parameter selection would be governed by inelastic load and solar generation of the consumer.

Chapter 9

Storage for low voltage consumers in Uruguay

Earth provides enough to satisfy every man's needs, but not every man's greed. -Mahatma Gandhi

Summary: Energy storage can be used for many applications in the Smart Grid such as energy arbitrage, peak demand shaving, power factor correction, energy backup to name a few, and can play a major role at increasing the capacity of power networks to host renewable energy sources. Often, storage control algorithms will need to be *tailored* according to power networks billing structure, reliability restrictions, and other local power networks norms. In this chapter we explore residential energy storage applications in Uruguay, one of the global leaders in renewable energies, where interesting low-voltage consumer contracts were recently introduced. Based on these billing mechanisms, we focus on energy arbitrage and reactive energy compensation with the aim of minimizing the cost of consumption of an end-user. Given that in the new contacts the buying and selling price of electricity are equal and that reactive power compensation is primarily governed by the installed converter, the storage operation is not sensitive to parameter uncertainties and, therefore, no lookahead is required for decision making (refer to Chapter 3). A threshold-based *hierarchical* controller is proposed which decides on the optimal active energy for arbitrage and uses the remaining converter capacity for reactive power compensation, which is shown to increase end-user profit. Numerical results indicate that storage could be profitable, even considering battery degradation, under some but not all of the studied contracts. For the cases in which it is not, we propose the best-suited contract. Results presented here can be naturally applied whenever the tariff structure satisfies the hypothesis considered in this work.

9.1 Introduction

Electric power systems are undergoing major transformations because of changes in the generation mix, in the structure of the network, and in the means and profiles of electricity consumption. The increased share of intermittent generation requires large amount of reserves and costly infrastructure expansions, while the electrification of energy consumption will significantly distort the aggregate electricity consumption profile. This is mainly due to EVs that consume as much as the rest of the loads in a typical household over a small charging period [173]. The negative consequences of such distributed energy resources can be avoided by an adequate response from active energy participants with flexible energy consumption and/or generation (prosumers). In order to achieve such a response, incentives are provided to interested participants, who receive economic rewards in exchange of their flexibility services. In Chapter 10 we observe that with the growth of renewable share the need for such responsive users is going to increase. This represents an opportunity for energy participants to start providing services to the grid. Energy storage devices such as batteries are at the focal point of such applications, as these are gradually becoming profitable thanks to increasing flexibility opportunities and rewards and to continuous drop of their cost.

Authors in [214] present the economic analysis of storage in Southern California Homes. They highlight that earlier Net-Energy Metering or NEM policies allowed only excess renewable generation to be supplied back to the grid. However, new NEM policy allows distributed generation along with solar to participate in NEM making it more conducive for consumers to invest in energy storage.

For low voltage consumers, performing energy arbitrage is one of the prominent applications of storage devices. Optimizing storage for performing energy arbitrage is studied in numerous works, some examples

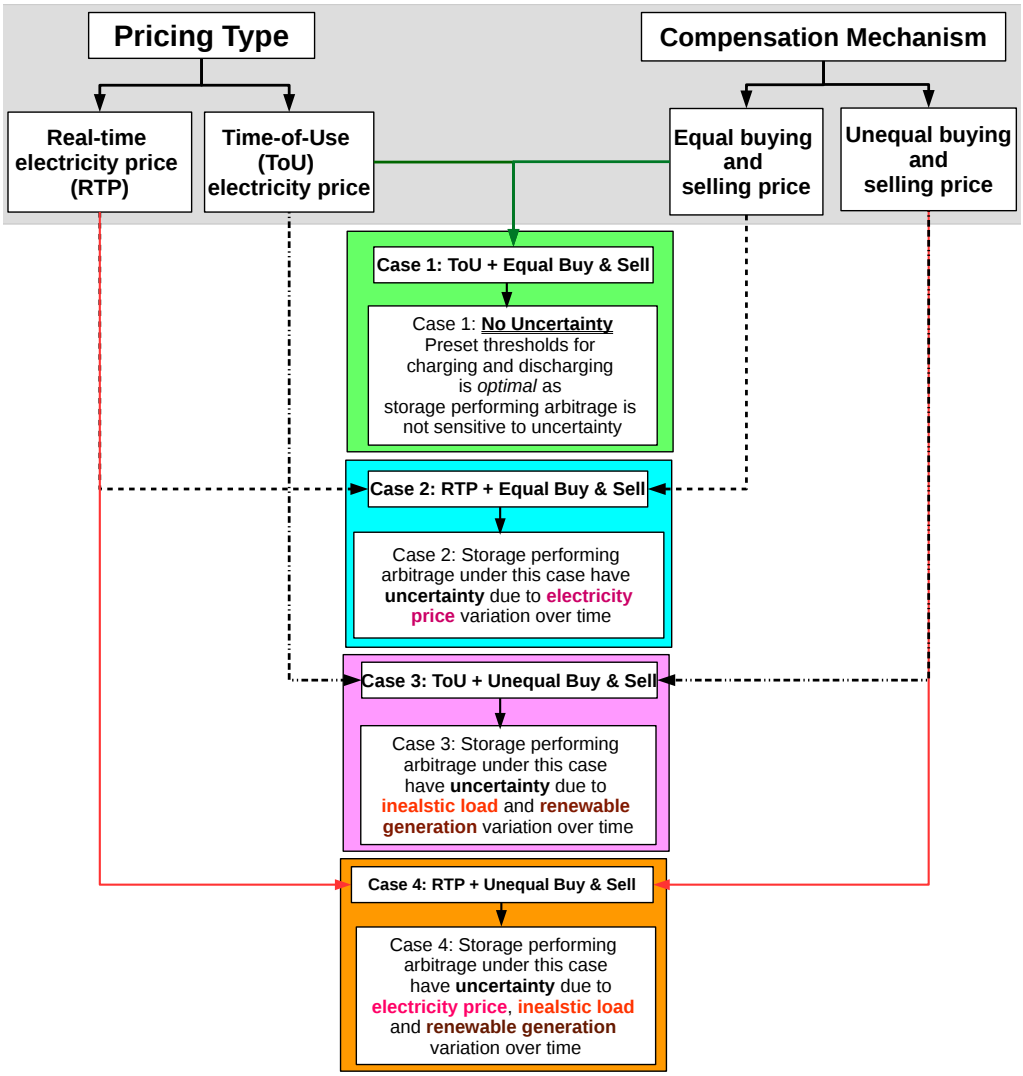

Figure 9.1: Uncertainty under storage performing arbitrage; Consider the consumer have an inelastic load, local renewable generation and storage. Under this setting storage operation is prone towards uncertainty depending on pricing type and excess generation compensation mechanism.

are [217], [257], [182]. In [217], the authors propose an algorithm mixture of dynamic programming and particle swarm optimization to schedule a battery in presence of a wind turbine. The time-of-use or ToU has 3 leaves and they manage to obtain a 5.6 % saving in the energy bill each month. Authors in [257] use linear programming for storage control under ToU pricing for PG&E residential and consumers in San Francisco.

Co-optimizing energy storage for multiple revenue streams could drastically enhance the gains made by storage owners [323], [294], [177]. Pioneering work on co-optimization, [323], presents an application of batteries performing arbitrage and frequency regulation for a New York ISO case-study. They show that storage batteries might not be profitable for a single dedicated application due to its high cost. Authors in [294] claim that combining several applications could lead to greater gains compared to cumulative gains obtained by performing few of the tasks at a time. This is essential, as having one dedicated goal might maximize gains in that application but might lead to unexpected penalties or undermine other applications. For instance storage performing only energy arbitrage could increase the peak demand charge paid by the consumer, in effect reducing the total gain made by the storage owner [177]. A fine understanding of the billing mechanism is essential to avoid incurring such a penalty.

Profitability is an essential question from a consumer perspective, who needs to decide whether to invest in energy storage devices. The storage battery having a limited operational and aging life [174], economic analysis should consider the operational cycles in analyzing the gains made by using energy storage. Authors in [80] observe that ignoring storage degradation could inflate the gains made by operating the

storage battery. They also highlight the importance of forecasting parameters such as consumer load and electricity price for maximizing prosumer profit. In Chapter 8 we present a case-study for Madeira island power network, where we explore residential storage applications and their economic viability. We also provide recommendation about the best-suited contract among 46 different options for low voltage consumers based on short-term and long-term simulations of 1 day and 1 month respectively. In [127], the authors assess the profitability of storage in Ontario under various pricing schemes, without the possibility to sell energy back to the grid, showing that for several cases it cannot be achieved. Authors in [116] evaluate the feasibility of energy arbitrage (without selling back to the grid) in Australia using time of use pricing. For several batteries they found the probability of earnings depending on battery size. Profitability of storage devices is governed by grid norms which represent the eagerness and needs of power networks to incentivize consumers for installing energy storage. The compensation mechanisms are also influenced by political will, as electricity is not just any commodity in a market for profit making but also a necessity in today's world.

In this work, we consider storage control and applications for LV consumers in Uruguay, where new contracts were proposed in early 2019, providing unique opportunities for consumers to include storage to modify the consumption profile seen by the utility meter. We present a co-optimization formulation for the energy storage device performing arbitrage and power factor correction (PFC), considering storage degradation. We find that some consumer contracts could be profitable enough for consumers to invest on storage. In Chapter 6 we identify that when co-optimizing storage for arbitrage and PFC, these objectives are largely decoupled as arbitrage is governed by storage charge level while the reactive power capability is constrained by instantaneous active power and converter size. Furthermore, we also identify that lookahead for reactive power compensation is not essential, allowing us to consider myopic reactive compensation. For energy arbitrage, the control in the context of LV electricity consumer in Uruguay has following properties:

- *No uncertainty in electricity price*: In Time-of-Use the instants and levels of price variations are known a priori thus no uncertainty in storage control due to electricity price. This is an advantage over real real-time electricity pricing schemes, where prices need to be forecasted.

- *Net metering - Compensation of excess generation based on equal buying and selling price level*: Electricity buying price vary over time (for ToU these variations are known), however, at every time instant the buying price and selling price remain the same in magnitude. For example, consider the buying price of electricity between 9 am and 10 am is 0.05$/kWh; the consumer consumes say 20 kWh, making the cost of consumption equal to $1. In the same time period had the prosumer instead of consuming generated 20 kWh of energy, he/she would have received compensation of $1. Under such a compensation mechanism, the objective to minimize the cost of consumption of the user which includes inelastic load, renewable generation, and storage output is equivalent to maximizing the profit made by only energy storage performing arbitrage [182]. In other words, optimal storage control decisions are independent of variations in inelastic load and renewable generation at consumer end, which was also observed in [335]. Refer to Appendix A.7 for more details. Fig. 9.1 shows the effect of uncertainty based on pricing mechanism and compensation of excess consumer generation. Thus, storage active power can be operated based on precomputed thresholds which minimize the stress on the battery as the optimal solution, therefore, active power output of storage also does not require lookahead. The proposed consumer contracts make consumers completely not sensitive to uncertainty in inelastic load, renewable generation and electricity price variation, furthermore, no lookahead of such parameters are required. This should be very attractive for consumers as storage operation in a more dynamic market could affect consumer gains made by storage operation due to the real-time variation of system parameters causing a loss of opportunity. In Chapter 3, Section 3.6 we present a case-study for identifying the effect of price uncertainties on arbitrage gains. We observe that consumer gains can be up to 59% lower for the stochastic case in comparison to the deterministic one. Furthermore, authors in [213, 309] propose storage control for performing arbitrage, taking into consideration uncertainty in real time storage operation. These control mechanisms are computationally intensive, however, in our work we observe that energy storage operation becomes immune to uncertainty due to pricing of electricity and excess generation compensation.

The chapter is organized in sections. Section 9.2 provides a brief summary of the power system landscape in Uruguay. Section 9.3 presents the new electricity consumer contracts applicable for low voltage consumers in Uruguay. Section 9.4 outlines the various applications energy storage can be used for the consumer contracts detailed in the previous section. Section 9.5 describes the storage control algorithm applicable for different contracts. The proposed storage algorithm considers storage ramping and capacity constraint, charging and discharging efficiency losses. Section 9.6 presents the numerical results using the storage control algorithm. Section 9.7 concludes the chapter.

9.2 Energy Landscape in Uruguay

Uruguay is a country with 3.5 million inhabitants located in the south of South America, that has become a world leader in renewable energies. Historically, this small country has relied upon hydro power, mainly from two dams: Salto Grande (co-owned with Argentina in the Uruguay river) and Rio Negro, thermal power plants, and importing energy from neighboring countries: Argentina and Brazil. As of today, Uruguay has completely changed their energy mix, consuming mostly from renewable resources and becoming a purely exporting country. In the year 2017, only 1% of the energy was produced from thermal power stations, while 65% corresponded to hydro generation, and the remaining 34% was composed of a mix between biomass, wind and photovoltaic energy. With more than 600 wind turbines in 2018 wind power provided up to 49 % of the energy consumed, which positions Uruguay as the second country in the world with the highest share of wind power in their electricity mix, behind Denmark.

The main actor in the energy sector is UTE, a public company that acts as the only retailer, DSO and TSO, and it is also one of the main producers of electricity. In a country with a surface of 176,215 km^2, the distribution and transmission lines span 84,245 km and 5561 km respectively as of 2017. As a matter of comparison, France with 3.6 times the extension of Uruguay, has 18.8 times more kilometers of transmission lines [288]. Of the above mentioned mix, the residential sector consumes approximately 3500 GWh yearly, while big customers represent a load of 2000 GWh and medium consumers account for 1500 kWh. The peak power consumption registered in the years 2016 and 2017 was of 1964 MW and 1916 MW respectively and occurred during the winter (mid July), while the yearly load factor was of 64.3 %.

Uruguay's energy sector is still evolving towards a smarter landscape. UTE has several demand response programs in place. Among them, they offer time-of-use tariff to residential consumers, 60% price rebates for big consumers who increase their demand during periods of renewable energy surplus, and price rebates on efficient household appliances such as class A water heater. Regarding distribution of residential clients among tariffs, 47 % of total clients subscribe to a flat rate tariff while 53% use a more complex contract such as time-of-use.

9.3 Electricity Consumer Contracts

Low Voltage (LV) electricity consumers can opt for new billing mechanisms introduced by UTE in January 2019 [316], leading residential consumers to choose among three different consumer contracts. Next we describe the three contracts denoted as C1, C2 and C3 in this document for easy referencing. They are structured with a variable fee that depends on the amount or the time of active energy consumption, a part that is proportional to the contracted peak power and a fixed charge that is applied to all contracts every month, irrespective of their variable energy or power consumption. Furthermore, consumers pay a reactive energy charge. The details of the contracts can be found Portal of Electricity operator in Uruguay[1]. The electricity prices are listed in Uruguayan peso[2].

This section is divided into five sub-sections. In Section 9.3.1 we list the fixed and variable active energy rates for the different contracts. In Section 9.3.2 the peak contracted power is given. Note that consumers need to select the peak power contracts beforehand, as it determines the cabling and metering requirements and therefore, do not have a flexibility in real-time to optimize. In turn, this will determine the fixed costs incurred by the consumer. The billing of reactive power under the three contracts are presented in Section 9.3.3. Section 9.3.4 presents the total and variable cost of electricity consumption. In this chapter, we use the variable component to minimize the cost of consumption of user using a battery. Consumers with distributed generation such as rooftop solar generation can opt for net-metering in Uruguay. Section 9.3.5 presents the net-metering policies for different consumer contracts.

9.3.1 Fixed and Active Energy Cost

Table 9.1, Table 9.2 and Table 9.3 lists the fixed, power and energy charges for contracts C1, C2 and C3. The fixed cost for contract Ci is denoted as C^{Ci}_{fixed} for $i \in \{1, 2, 3\}$. We also present the active energy charge calculated under the different contracts for consumers.

[1] https://tinyurl.com/y5ug28jh

[2] 1 Uruguayan Peso equals 0.031 USA Dollar on 21st Feb. 2019.

Table 9.1: C1: Simple Residential Rate

Category	Price
Charge for energy consumption:	
1 kWh to 100 kWh monthly	5.160 peso/kWh
101 kWh to 600 kWh monthly	6.470 peso/kWh
601 kWh onwards	8.065 peso/kWh
Charge for contracted power	61.6 peso/kW
Fixed monthly charge	198.9 peso

Table 9.2: C2: Two-level ToU Residential Rate

Category	Price
Charge for energy consumption:	
Peak hours: from 17:00 to 23:00	8.623 peso/kWh
Off-peak hours: 00:00 to 17:00 and 23:00 to 24:00 hrs	3.453 peso/kWh
Charge for contracted power	61.6 peso/kW
Fixed monthly charge	359.4 peso

C1: Simple Residential Flat Rate

Simple residential contracts are applicable for consumers with voltage level 230V and 400V and the contracted power is less than or equal to 40 kW. The cost of active energy is given as:

$$C_{\text{active}}^{C1} = \lambda_{\text{fixed}} E_a, \tag{9.3.1}$$

where E_a denotes the active energy consumed and expressed in kWh and λ_{fixed} denotes the flat rate electricity cost under C1.

C2: Two level Time-of-Use (ToU) Rates

Two level ToU residential contracts are applicable for consumers with voltage level 230V and 400V and the contracted power greater than 3.3 kW and less than or equal to 40 kW. The cost of active energy is given as:

$$C_{\text{active}}^{C2} = \lambda_{\text{peak}} E_a^{\text{peak}} + \lambda_{\text{off-peak}} E_a^{\text{off-peak}}, \tag{9.3.2}$$

where E_a^{peak} denotes the active energy consumed during peak period over the month, $E_a^{\text{off-peak}}$ denotes the active energy consumed during off-peak period over the month, and expressed in kWh and λ_{peak} denotes peak electricity cost, $\lambda_{\text{off-peak}}$ denotes off-peak electricity cost under C2 contract.

C3: Three-level ToU Rates

Three level ToU residential contracts are applicable for consumers with voltage level 230V and 400V and the contracted power greater than 3.7 kW and less than or equal to 40 kW. The cost of active energy is

Table 9.3: C3: Three-level ToU Residential Rate

Category	Price
Charge for energy consumption:	
Peak hours: from 17:00 to 23:00 hrs	8.623 peso/kWh
Mid-peak hours: 07:00 to 17:00 and 23:00 to 24:00 hrs	4.676 peso/kWh
Off-peak hours: 00:00 to 7:00 hrs	1.803 peso/kWh
Charge for contracted power	61.6 peso/kW
Fixed monthly charge	359.4 peso

Table 9.4: Power Contracted: 1-phase LV consumers

Power levels
3.7 kW, 4.6 kW, 7.4 kW, 9.2 kW

Table 9.5: Power Contracted: 3-phase LV consumers

Power levels (kW)
12, 20, 25, 30, 35, 40 kW, 41 to 50 kW

given as:

$$C^{C3}_{\text{active}} = \lambda_{\text{peak}} E^{\text{peak}}_a + \lambda_{\text{mid-peak}} E^{\text{mid-peak}}_a + \lambda_{\text{off-peak}} E^{\text{off-peak}}_a, \tag{9.3.3}$$

where $E^{\text{mid-peak}}_a$ denotes the active energy consumed during mid-peak period over the month and expressed in kWh and $\lambda_{\text{mid-peak}}$ denotes mid-peak electricity cost under C3 contract.

9.3.2 Peak Power Contract for LV Consumers

For low voltage consumers in Uruguay should specify the peak power contracted. This is essential as the utility provides the connection and safety features based on the contracted power.

Single phase consumers in LV network can select the contracted power from following levels presented in Table 9.4. Three phase consumers in LV network can select the contracted power from following levels presented in Table 9.5. Based on Table 9.4 and Table 9.5 consumers select their power contract denoted as $P_{\text{contracted}}$. The charge for power contracted for contract $i \in \{1, 2, 3\}$ is denoted as C^{Ci}_{power}. The cost of power contracted is given as:

$$C^{Ci}_{\text{power}} = \lambda_{\text{power}} P_{\text{contracted}}. \tag{9.3.4}$$

The value of λ_{power} is listed in Table 9.1, Table 9.2 and Table 9.3 for contracts C1, C2 and C3 respectively. Note the peak power charge is same for C1/C2/C3.

9.3.3 Billing of Reactive Energy

Traditionally, LV consumers were not obliged to regulate reactive power. There where many well thought reasons why it made sense, we list a few below:

• Majority of loads used by low voltage consumers consisted of resistive loads, thus, the inherent power factor seen by the grid used to be close to unity.

• Utility neither had the infrastructure nor the motivation for making it obligatory for small LV consumers to comply reactive power norms normally well-defined for commercial establishments.

However, the reasons why utilities across the world do not meter reactive power in LV networks is rapidly changing due to some of the following reasons:

• Evolution of many new loads have significantly increased the reactive power of the LV consumers. In absence of regulation utilities would have to face degradation of efficiency of LV distribution network [8] and additional stress on distribution transformer.

• Most countries have been promoting distributed generation (DG) such as rooftop solar PV installations. These DGs operate at close to unity power factor, implying that while an important part of the active power is locally met by the DG, all the reactive power is provided/absorbed by the grid [178].

Due the above mentioned transformation, the utilities are designing penalties for consumers with a low power factor. Uruguay is in the fore front globally in implementing reactive power penalties and incentives for small LV consumers to control their power factor.

Next we describe the mechanisms of charging for degraded power factor for each of the three consumer contracts.

Reactive power cost under C1

Consumers billed in accordance to C1, or simple residential contract, need to pay a penalty if the power factor calculated for the month deteriorates below 0.92. The power factor is calculated as a function of

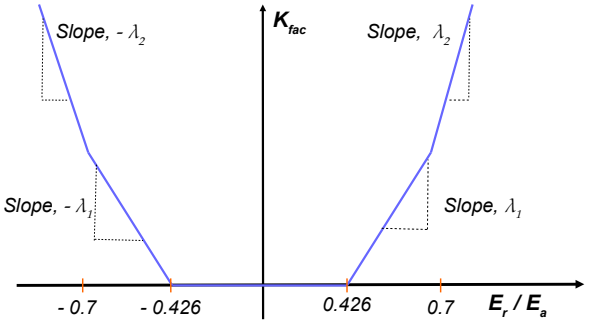

Figure 9.2: Graphical representation of K_{fac} for C1 with respect to the PF; where $\lambda_1 = 0.4$ and $\lambda_2 = 1$.

aggregate reactive power (E_r) and active power (E_a) as follows

$$\text{pf}_{\text{month}} = \cos\left(\arctan\left(\frac{E_r}{E_a}\right)\right). \tag{9.3.5}$$

The cost or reactive power for contract C1 is given as

$$C^{C1}_{\text{reactive}} = K_{\text{fac}} \times E_r. \tag{9.3.6}$$

Where K_{fac} is the coefficient of surcharge for reactive consumption and is governed by the following conditions:

$$K_{\text{fac}} = \begin{cases} 0, & \text{if } \frac{E_r}{E_a} \leq 0.426, \\ 0.4\left(\frac{E_r}{E_a} - 0.426\right), & \text{if } \frac{E_r}{E_a} \in (0.426,\ 0.7], \\ 0.4\left(\frac{E_r}{E_a} - 0.426\right) + 0.6\left(\frac{E_r}{E_a} - 0.7\right), & \text{if } \frac{E_r}{E_a} > 0.7. \end{cases} \tag{9.3.7}$$

Reactive power cost under C2

Consumers billed in accordance to C2, or two-level ToU residential contract, need to pay a penalty if the power factor calculated for the month deteriorates below 0.92. Consumers under C2 are also provided incentives for cases where the pf_{month} exceeds 0.92. The coefficient of surcharge or consumption bonus for reactive consumption is governed by following conditions:

$$K_{\text{fac}} = \begin{cases} \frac{B}{100}\left(\frac{E_r}{E_a} - 0.426\right), & \text{if } \frac{E_r}{E_a} \leq 0.7, \\ \frac{B}{100}\left(\frac{E_r}{E_a} - 0.426\right) + \frac{100-B}{100}\left(\frac{E_r}{E_a} - 0.7\right), & \text{if } \frac{E_r}{E_a} > 0.7, \end{cases} \tag{9.3.8}$$

where the value of B is 36 or 34 depending on the contract. For consumers under C2, the coefficient K_{fac} acts as penalty for case where $\frac{E_r}{E_a} > 0.426$. However, if $\frac{E_r}{E_a} \leq 0.426$ then it provides incentives for the consumer as the cost of reactive power would be negative. Coefficient K_{fac} is applied to the total active energy consumed during the peak period over the whole month. The total active energy is denoted as

$$E_a = E_a^{\text{off-peak}} + E_a^{\text{peak}}, \tag{9.3.9}$$

The cost or reactive power for contract C2 is given as

$$C^{C2}_{\text{reactive}} = K_{\text{fac}} \times E_a^{\text{peak}}. \tag{9.3.10}$$

Reactive power cost under C3

The power factor applied for C3 consumers is given as

$$\text{pf}^{+}_{\text{month}} = \cos\left(\arctan\left(\frac{E_{rQ1}}{E_{a+}}\right)\right), \tag{9.3.11}$$

where E_{rQ1} is the absolute value of reactive energy in Quadrant 1 over a month expressed in kVAR and E_{a+} denotes the absolute value of active energy in the month expressed in units kWh. Consumers

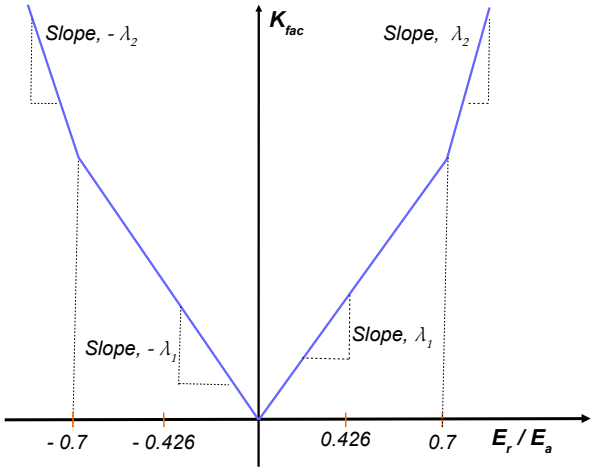

Figure 9.3: Graphical representation of K_{fac} for C2 with respect to the PF; where $\lambda_1 = \frac{B}{100}$ and $\lambda_2 = 1$.

Table 9.6: Value of B under C3

Voltage level	Value of B
230 to 400 V	23
6.4 - 12 - 22 kV	18
31.5 kV	12

billed in accordance to C3, or three level ToU residential contract, need to pay a penalty if the power factor, calculated with aggregate reactive power (E_{rQ1}) and active power (E_{a+}), calculated for the month deteriorates below 0.92. Similar to C2, Consumers under C3 are also provided incentives for cases where the $\text{pf}^{+}_{\text{month}}$ exceeds 0.92.

The coefficient of surcharge or consumption bonus for reactive consumption is governed by following conditions:

$$K_{\text{fac}} = \begin{cases} \frac{A}{100}\left(\frac{E_{rQ1}}{E_{a+}} - 0.426\right), & \text{if } \frac{E_{rQ1}}{E_{a+}} \leq 0.7, \\ \frac{A}{100}\left(\frac{E_{rQ1}}{E_{a+}} - 0.426\right) + \frac{100-B}{100}\left(\frac{E_{rQ1}}{E_{a+}} - 0.7\right), & \text{if } \frac{E_{rQ1}}{E_{a+}} > 0.7, \end{cases} \tag{9.3.12}$$

where the value of B depends on supply voltage listed in Table 9.6. Coefficient K_{fac} is applied to the total active energy consumed during the peak period over the whole month. The total active energy is denoted as

$$E_{a+} = E_{a+}^{\text{off peak}} + E_{a+}^{\text{mid peak}} + E_{a+}^{\text{peak}}, \tag{9.3.13}$$

where $E_{a+}^{\text{off peak}}$ denotes the total energy consumed during off-peak hours over the month, $E_{a+}^{\text{mid peak}}$ denotes the total energy consumed during mid-peak hours over the month and E_{a+}^{peak} denotes the total energy consumed during peak hours over the month. The cost or reactive power for contract C3 is given as

$$C_{\text{reactive}}^{C3} = K_{\text{fac}} \times E_{a+}. \tag{9.3.14}$$

9.3.4 Cost of Consumption

The cost of electricity consists of four components:

(1.) *Fixed electricity cost*: depending on the contract type, consumers are charged a fixed cost which is independent of the consumed electricity,

(2.) *Power contracted cost*: the consumer specifies the peak power level before the utility provides a connection. From the utility perspectives this contract determines the protection settings, fuse settings, cable ratings, meter type etc.

(3.) *Active energy cost*: The cost of consuming active energy is decided by the contract type.

(4.) *Reactive energy cost*: This component of electricity cost is decided by the power factor, voltage level, total active energy consumed and contract type.

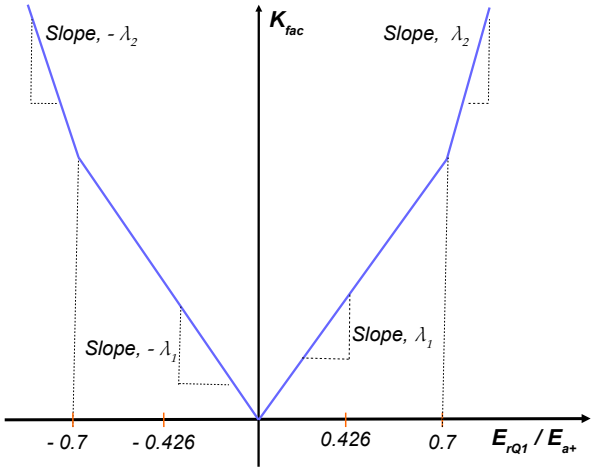

Figure 9.4: Graphical representation of K_{fac} for C3 with respect to the PF; where $\lambda_1 = \frac{A}{100}$ and $\lambda_2 = 1$.

Table 9.7: Variable cost component based on contract type

Contract	C^{Ci}_{variable}
C1	$\lambda_{\text{fixed}} E_a + K_{\text{fac}} \times E_r$
C2	$\lambda_{\text{peak}} E_a^{\text{peak}} + \lambda_{\text{off-peak}} E_a^{\text{off-peak}} + K_{\text{fac}} \times E_a^{\text{peak}}$
C3	$\lambda_{\text{peak}} E_a^{\text{peak}} + \lambda_{\text{mid-peak}} E_a^{\text{mid-peak}} + \lambda_{\text{off-peak}} E_a^{\text{off-peak}} + K_{\text{fac}} \times E_{a+}^{\text{peak}}$

Therefore, the total cost of consumption under contract Ci is given as

$$C^{Ci}_{\text{Total}} = C^{Ci}_{\text{fixed}} + C^{Ci}_{\text{power}} + C^{Ci}_{\text{active}} + C^{Ci}_{\text{reactive}}. \tag{9.3.15}$$

The variable component of the cost would consists of the cost of active and reactive power given as

$$C^{Ci}_{\text{variable}} = C^{Ci}_{\text{active}} + C^{Ci}_{\text{reactive}}. \tag{9.3.16}$$

The variable component of electricity price could only be reduced if the electricity consumer optimizes their consumption locally using load flexibility and/or energy storage. The cost component $C^{Ci}_{\text{fixed}} + C^{Ci}_{\text{power}}$ have no degree of freedom and therefore, cannot be reduced.

9.3.5 Net-Metering in Uruguay

Net-energy metering (NEM) for small wind power, solar, biomass and mini-hydro systems is allowed since 2010 by Decree 173/010[3] on micro-generation. The government-owned national electric company, UTE[4], is mandated to buy at retail price all the excess electricity produced by consumers for a period of ten years [74]. Generated electricity must be low-voltage and the maximum power of installations is the lower between 6 kW and the peak power contracted by consumer, although higher power is possible with additional authorization before installation[5]. The buying and selling electricity prices for LV consumers in Uruguay under contracts C1, C2 and C3 are depicted in Fig. 9.5, Fig. 9.6 and Fig. 9.7 which shows that buy and sell price have the same level. Note that consumer needs to opt for NEM separately by notifying the utility which may require the installation of different hardware.

In this chapter we use net-metering for contracts C2 and C3. The rationale behind not opting for net-metering for contract C1 is described in Section 9.4.1.

[3] http://tinyurl.com/y2ccr2o2
[4] https://portal.ute.com.uy/
[5] https://tinyurl.com/y2gydsu7

Figure 9.5: Buying and selling price of electricity over a day under contract C1 with NEM

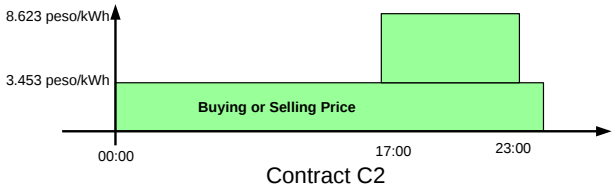

Figure 9.6: Buying and selling price of electricity over a day under contract C2 with NEM

9.4 Storage for LV Prosumers in Uruguay

The system considered in this chapter consists of an electricity consumer with inelastic demand, renewable generation source (rooftop solar) and an energy storage. The battery provides flexibility to deviate consumption in order to make profit by performing arbitrage and provide reactive energy compensation. The system is shown in Fig. 1.2. The energy storage interfaced via a converter provides flexibility to the consumer to modify the active and reactive power seen by the grid. Energy storage with converter can act as source and/or sink of active and reactive power. Opportunities for prosumers with storage in Uruguay are:

Arbitrage: the ToU cost structure makes the selection of arbitrage decisions fairly simple for storage owners. Furthermore, since under Net-metering policies in Uruguay, the buy and sell price is equal for each time instant, shown in Fig. 9.5, Fig. 9.6 and Fig. 9.7, this implies that the control energy storage becomes independent of the inelastic load and solar generation.

From the structure of ToU prices, clearly the storage needs to charge during the off-peak period and discharge during the peak period. Storage remains idle during mid-peak periods except for very slow ramping batteries which could not be completely charged in off-peak duration or discharged completely during peak period duration.

Avoiding power factor penalty: previously we described the billing mechanism for reactive power for LV consumers in Section 9.3.3. The thresholds indicate that as power factor (PF) seen by the grid deteriorates the cost of consumption increases in proportion to peak energy consumed; this penalty for low PF could be avoided by maintaining the PF locally. Energy storage interfaced via a converter could be used for PF improvement locally.

Maintaining a high PF so as the consumer receives additional rebate on electricity consumption cost. Note that the consumers maintaining a unity PF could reduce the active power cost under C2 by almost 13.6% of the cost energy consumed under the peak period of ToU. For contract C3, the cost of consumption could be reduced by utmost 9.8% of the cost of energy consumed during peak period. However, for C1, there is no additional incentive for consumers improving the PF above 0.92. Users opting for C1 could make profit by reactive power compensation if the PF without any such correction is lower than 0.92.

The battery and system model used in this chapter is described in Chapter 2.5.

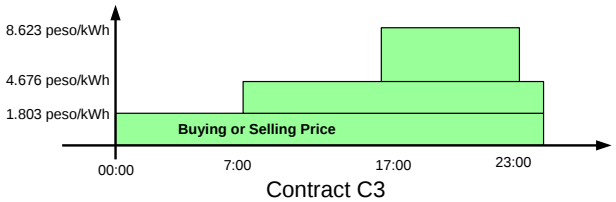

Figure 9.7: Buying and selling price of electricity over a day under contract C3 with NEM

Table 9.8: Storage Operation under C1 without NEM

Min Load without solar	Max Load without solar	Installed Solar kWp	Storage Role
$L_{\min}$	$L_{\max}$	below $L_{\min}$	No storage active energy management required
$L_{\min}$	$L_{\max}$	between $L_{\min}$ and $L_{\max}$	Storage might increase self-consumption
$L_{\min}$	$L_{\max}$	above $L_{\max}$	Storage increases self-consumption

9.4.1 Active Power Management

Energy storage active power could serve two purposes: (1.) increase self-consumption of locally generated energy under the absence of NEM and (2.) perform arbitrage under ToU electricity pricing.

Under Contract C1

Energy price is fixed for the day and, therefore, no arbitrage is possible. Under fixed electricity price storage could maximize self-consumption locally in absence of NEM. However, self-consumption could only be increased for cases where the instantaneous generation is more than the instantaneous load [187].

Table 9.8 lists the effect on self-consumption with the size of installed solar in absence of net-metering, which implies consumers have no incentive to supply power back to the grid and therefore, would attempt to increase the self-consumption as much as possible [187]. In Table 9.8 $L_{\min}$, $L_{\max}$ denotes the minimum and maximum load without solar, $0 \leq L_{\min} \leq L_{\max}$. For case where installed solar is comparable or larger than maximum load without solar generation, storage substantially contributes in increasing self-consumption.

Theorem 9.4.1

For arbitrage to be profitable following condition should be valid:

$$p_s^j \eta_{dis} > \frac{p_b^i}{\eta_{ch}},$$

where p_s^j denotes the selling price at time instant j and p_b^i denotes the buying price at time instant i, such that $j > i$ and $j, i \in \{1, 2, , ..., N\}$. Here N denotes the number of time instants in the horizon.

The proof of Theorem 9.4.1 is provided in Appendix A.9.

Performing arbitrage with contract C1 with NEM will not be profitable as Theorem 9.4.1 is not valid, since $p_s^j = p_b^i \ \forall j, i$ and $\eta_{\text{ch}}, \eta_{\text{dis}} < 1$. In this chapter we explore the usage of energy storage for different contracts. Optimizing the energy storage is essential pertaining to its high cost. In context of C1 storage can only be used either for backing up excess generation and/or for peak demand shaving. Recall, the net load without storage is denoted as $z_i = d_i - r_i$, where d_i denotes the inelastic load and r_i denotes the renewable generation. Backing up energy will require no look-ahead and greedy behavior leads to optimality. The optimal solution in such a case is governed by the sign of active power, $P^i = z_i/h$ and is given as

- If $P^i \geq 0$ then battery should discharge such that $P_B^i = \max\left\{-P^i, \delta_{\min} h \eta_{dis}, (b_{i-1} - b_{\max})\eta_{dis}\right\}$,
- If $P^i < 0$ then battery should charge such that $P_B^i = \min\left\{-P^i, \delta_{\max} h/\eta_{ch}, b_{i-1} - b_{\min}/\eta_{ch}\right\}$.

With C2 or C3 with NEM

Optimal energy storage arbitrage under net-energy metering is introduced in Chapter 3. The proposed algorithm provides a unique solution. However, performing arbitrage under time-of-use setting often has infinite possible optimal solutions as many different charging and discharging trajectories would lead to optimal arbitrage gains.

A battery performing arbitrage under contracts C2 and C3 in Uruguay will perform at maximum 1 cycle over a day of depth-of discharge equal to $\text{SoC}_{\max} - \text{SoC}_{\min}$. Consider the the battery capacity denoted as b_{rated} could charge from $\text{SoC}_{\min}$ to $\text{SoC}_{\max}$ at off-peak period then the storage buying cost including charging losses would be $\lambda_{\text{off-peak}}(\text{SoC}_{\max} - \text{SoC}_{\min})b_{\text{rated}}/\eta_{\text{ch}}$. Similarly, for battery discharging from $\text{SoC}_{\max}$ to $\text{SoC}_{\min}$ during peak period of ToU price, λ_{peak}, would provide a revenue of $\lambda_{\text{peak}}(\text{SoC}_{\max} -$

$\text{SoC}_{\min})b_{\text{rated}}\eta_{\text{dis}}$. The storage owner profit is the difference of the revenue made by discharging and cost incurred during charging, shown as

$$G_{\text{arb}} = (\text{SoC}_{\max} - \text{SoC}_{\min})b_{\text{rated}}\Big\{\lambda_{\text{peak}}\eta_{\text{dis}} - \lambda_{\text{off-peak}}/\eta_{\text{ch}}\Big\}. \tag{9.4.1}$$

Storage ramp rate selection under ToU is governed by the relationship between (a.) $T_{\text{off-peak}}$ and T_{ch} and (b.) T_{peak} and T_{dis}. For contract C2 we define $T_{\text{off-peak}}$ as the period of 17 hours (from 00:00 to 17:00) and T_{peak} as the period of 6 hours (from 17:00 to 23:00). Refer to Fig. 9.6.

For contract C3 we define $T_{\text{off-peak}}$ as the period of 7 hours (from 00:00 to 7:00) and T_{peak} as the period of 6 hours (from 17:00 to 23:00). Refer to Fig. 9.7.

Based on relationship between (a.) $T_{\text{off-peak}}$ and T_{ch} and (b.) T_{peak} and T_{dis} following cases are proposed for storage performing arbitrage under ToU prices:

Case 1: $T_{\text{off-peak}} > T_{\text{ch}}$ and $T_{\text{peak}} > T_{\text{dis}}$: For this case the battery can be fully charged during off-peak period and fully discharged during peak period. In this case the ramp rate of the battery should be selected so the stress on battery (which is proportional to square of ramp rate) is minimized. The storage ramp rate is as follows:

- If $\{p^i_{elec} = \lambda_{\text{peak}}\}$ then discharge at $\delta^*_{\text{peak}} = \max((b_{\min} - b_{\max})/T_{\text{peak}}, (b_{\min} - b_{i-1})/h, \quad \delta_{\min})$,
- If $\{p^i_{elec} = \lambda_{\text{off-peak}}\}$ then charge at $\delta^*_{\text{off-peak}} = \min((b_{\max} - b_{\min})/T_{\text{off-peak}}, (b_{\max} - b_{i-1})/h, \quad \delta_{\max})$,

Case 2: $T_{\text{off-peak}} > T_{\text{ch}}$ and $T_{\text{peak}} < T_{\text{dis}}$: Battery should only be charged to a level which could be discharged completely during peak period. The storage ramp rate is as follows:

- If $\{p^i_{elec} = \lambda_{\text{peak}}\}$ then discharge at $\delta^*_{\text{peak}} = \delta_{\min}$,
- If $\{p^i_{elec} = \lambda_{\text{off-peak}}\}$ then charge at $\delta^*_{\text{off-peak}} = \min((b_{\max} - b_{\min})/T_{\text{off-peak}}, (b_{\max} - b_{i-1})/h, \quad \delta_{\max})$,

Case 3: $T_{\text{off-peak}} < T_{\text{ch}}$ and $T_{\text{peak}} > T_{\text{dis}}$: For this case battery cannot be charged completely from $b_{\min}$ to $b_{\max}$ within $T_{\text{off-peak}}$ time period. The storage ramp rate is as follows:

- If $\{p^i_{elec} = \lambda_{\text{peak}}\}$ then discharge at $\delta^*_{\text{peak}} = \max((b_{\min} - b_{\max})/T_{\text{peak}}, (b_{\min} - b_{i-1})/h, \quad \delta_{\min})$,
- If $\{p^i_{elec} = \lambda_{\text{off-peak}}\}$ then charge at $\delta^*_{\text{off-peak}} = \delta_{\max}$,

Case 4: $T_{\text{off-peak}} < T_{\text{ch}}$ and $T_{\text{peak}} < T_{\text{dis}}$: For this case the storage ramp rate is given as follows:

- If $\{p^i_{elec} = \lambda_{\text{peak}}\}$ then discharge at $\delta^*_{\text{peak}} = \delta_{\min}$,
- If $\{p^i_{elec} = \lambda_{\text{off-peak}}\}$ then charge at $\delta^*_{\text{off-peak}} = \delta_{\max}$,

It is clear that for Case 1 described above, the battery will perform 1 cycle per day at a Depth-of-Discharge equal to $\text{DoD} = \frac{(b_{\max} - b_{\min})}{b_{\text{rated}}} = \text{SoC}_{\max} - \text{SoC}_{\min}$. Based on the degradation model proposed in Chapter 5, the number of cycles of operation could be controlled by increasing $\text{SoC}_{\min}$ and/or by decreasing $\text{SoC}_{\max}$. The control of cycles of operation using friction coefficient is introduced in Chapter 5.

We would like to highlight that similar to prior works [174, 181] and Chapter 5 for mid-peak period under contract C3, the optimal action is to do nothing (i.e. stay idle with $\delta^*_{\text{mid-peak}} = 0$). Note that the proposed ramp rate thresholds presented also minimized the stress on the battery; stress as defined earlier on the battery is proportional to the square of the ramp rate [242, 164].

9.4.2 Compensation Strategy for Reactive Power

The unique attribute of contracts in Uruguay is the mechanism used for billing reactive power. The utility have two thresholds for charging for reactive power. First we list the penalty
• For PF $\in [0.92, 1]$: Consumes pay no penalty under contract C1,
• For PF $\in [0.82, 0.92]$: Consumes pay penalty under contract C1, C2 and C3,
• For PF $\in [0, 0.82]$: Consumes pay higher penalty compared to case where PF $\in [0.82, 0.92]$ under contract C1, C2 and C3,

Consumers could reduce there cost of consumption by maintaining a high PF for contracts C2 and C3:
• Maintaining a PF above 0.92 could provide additional gains to consumers opting for C2 and C3. However, consumers under C1 hold no incentive in improving the PF beyond 0.92.
• Improving PF which under nominal case is lower than 0.92 would reduce the cost of consumption under all contracts.

Next we describe the control mechanism for improving power factor or in other words reactive power compensation using energy storage.

Reactive Power Compensation using Energy Storage interfaced via a Converter

In Chapter 6 we present that reactive compensation using energy storage interfaced via a converter performing arbitrage is largely decoupled. This is due to reactive power capability is governed by converter size and instantaneous active power. However, if the converter is slightly over-sized then converter could supply reactive power without being constrained primarily by instantaneous active power. Furthermore, since the converter size is static and a non-varying parameter, therefore, lookahead in time is not required. This implies myopic reactive power compensation matches in optimal solution. In Chapter 6, we show through numerical results that no lookahead reactive power compensation along with arbitrage (which requires lookahead) matches very closely with the co-optimization results where the storage performs arbitrage and PF compensation. The former optimization problem is denoted as P_{rh} and the later optimization problem is denoted as P_{plt} in Chapter 6. Based on these findings, we propose myopic reactive power compensation for all contracts. For users opting for C1, must not correct the PF beyond 0.92.

9.5 Control Algorithm for Storage in Uruguay

In previous sections we discussed the new contracts available for LV consumers in Uruguay and what roles energy storage could play for such consumers. In this section we present the storage control algorithm for the different contracts in Uruguay. The storage control algorithm consists of two algorithms: `UruguayStorageControl` and `CalculateKfac`.

These algorithms could be used for contracts C1, C2 or C3. The consumer needs to specify storage parameters, converter size, initial battery capacity. The code updates the storage control decision based on battery capacity available until the end of month is reached. At the end of month the algorithm calculates the profit due to storage integration for the consumer compared to the nominal case where no storage is considered.

9.5.1 Storage Operation Immune to Uncertainty

Uncertainty in Active Power Control in Uruguay: Control of energy storage is coupled in time. For the active power, if the battery is charged in the present time then the amount of energy available in subsequent time instant will be higher. In Chapter 4 identify that storage performing only active power arbitrage have uncertainty due to two parameters: (a.) uncertainty due to electricity price variation and (b.) uncertainty due net load without storage variation. These sources of uncertainty was for the case of real-time electricity price and where the selling price have an arbitrary ratio varying between 0 and 1 with respect to the buying price [183], refer to Case 4 in Figure 9.1. However, for the case of Uruguay, the LV consumers respond to Time-of-Use prices which vary in a deterministic manner, thus no uncertainty due to electricity price variations.

In Chapter 3 we have identified that energy storage control under equal instantaneous buy and sell price becomes independent of the net load without storage. This implies that active power control faces no uncertainty with respect to contracts in Uruguay which have ToU pricing structure and NEM which provides equal buy and sell price at each time instant. Refer to Appendix A.7 and Figure 9.1 for details.

Uncertainty in Reactive Power Control in Uruguay: Numerical results in Chapter 6 and Chapter 7 show that storage interfaced via a converter operating with no lookahead is close to optimality. Furthermore, we show in numerical results that valuation of reactive power compensation is significantly lower than incentive in performing arbitrage. Therefore, in the algorithm presented for active and reactive energy compensation, the active power is adjusted to maximize arbitrage gains and the available energy storage converter is utilized for reactive power compensation, thus prioritizing active power over reactive power compensation.

9.6 Numerical Experiments

The numerical results presents three scenarios. In Section 9.6.1 the potential of performing energy arbitrage is identified based on gains made by performing arbitrage for a month. In Section 9.6.2 consumer cost of consumption is compared with nominal case with storage to that of consumer load with energy storage performing active and/or reactive energy compensation. Based on 2 standard models of Tesla PowerWall we recommend the suitable contracts. A similar analysis would be required with consumer of different

Algorithm 17 `UruguayStorageControl`

Global Inputs: Battery Characteristics: $\eta_{\text{ch}}, \eta_{\text{dis}}, \delta_{\max}, \delta_{\min}, b_{\max}, b_{\min}$.

Inputs: Sampling time h, Number of points in a month N_{month}, Time instant index $i = 0$,

Function: Computes optimal Active and Reactive Power of Energy Storage Output for Contracts C1, C2 and C3

Initialize b_0, and Input electricity prices $\lambda_{\text{peak}}, \lambda_{\text{mid-peak}}, \lambda_{\text{off-peak}}$,
Input periods of peak, mid-peak and off-peak as $T_{\text{peak}}, T_{\text{mid-peak}}, T_{\text{off-peak}}$,
Set $E_a^{\text{peak}}, E_a^{\text{mid-peak}}, E_a^{\text{off-peak}}, E_{a+}^{\text{peak}}, E_{a+}^{\text{mid-peak}}, E_{a+}^{\text{off-peak}} = 0$, Set $E_r, E_{rQ1} = 0$,
Input the converter rating $S_B^{\max}$, b_0
while $i < N_{\text{month}}$ **do**
  $i = i + 1$,
  if Contract is C1 **then** Storage can only be used for increasing self-consumption as no Arbitrage possible
    if Net load without solar $z_i \geq 0$ **then** Battery should discharge s.t. $x_i^* = \max\{-z_i/\eta_{dis}, \delta_{\min}h, (b_{i-1} - b_{\max})\}$,
    else Battery should charge such that $x_i^* = \min\{-z_i\eta_{ch}, \delta_{\max}h, b_{i-1} - b_{\min}\}$.
    end if
  else if Contract is C2 or C3 **then**
    if $p_{elec}^i == \lambda_{\text{peak}}$ **then** Battery should discharge, $x_i^* = h\max\left((b_{\min} - b_{\max})/T_{\text{peak}}, (b_{\min} - b_0)/h, \ \delta_{\min}\right)$,
    else if $p_{elec}^i == \lambda_{\text{mid-peak}}$ **then** Battery should do nothing, $x_i^* = 0$,
    else if $p_{elec}^i == \lambda_{\text{off-peak}}$ **then** Charge, $x_i^* = h\min((b_{\max} - b_{\min})/T_{\text{off-peak}}, (b_{\max} - b_0)/h, \ \delta_{\max})$,
    end if
  end if
  $s_i^* = [x_i^*]^+/\eta_{ch} - [x_i^*]^-\eta_{dis}$ and Set $P_B^i = sign(s_i^*) \times \min\left(|s_i^*|, S_B^{\max}\right)$,
  if Contract is C2 and C3 **then** Set $Q_B^i = -sign(Q^i) \times \min\left(|Q^i|, \ \sqrt{(S_B^{\max})^2 - (s_i^*)^2}\right)$,
  else Select Q_B^i such that power factor is no more then 0.92, as C1 consumers have no additional incentive
  end if
  if $p_{elec}^i == \lambda_{\text{peak}}$ **then** Calculate $E_a^{\text{peak}} = E_a^{\text{peak}} + (P^i + P_B^i)h$, and calculate $(E_a^{\text{peak}})_{\text{nominal}} = (E_a^{\text{peak}})_{\text{nominal}} + (P^i)h$,
  else if $p_{elec}^i == \lambda_{\text{mid-peak}}$ **then** Calculate $E_a^{\text{mid-peak}} = E_a^{\text{mid-peak}} + (P^i + P_B^i)h$, and calculate $(E_a^{\text{mid-peak}})_{\text{nominal}} = (E_a^{\text{mid-peak}})_{\text{nominal}} + (P^i)h$,
  else if $p_{elec}^i == \lambda_{\text{off-peak}}$ **then** Calculate$E_a^{\text{off-peak}} = E_a^{\text{off-peak}} + (P^i + P_B^i)h$, and calculate $(E_a^{\text{off-peak}})_{\text{nominal}} = (E_a^{\text{off-peak}})_{\text{nominal}} + (P^i)h$,
  end if
  Aggregate reactive power, $E_r = E_r + (Q^i + Q_B^i)h$,
  Aggregate reactive power in Quadrant 1, $E_{rQ1} = E_{rQ1} + |(Q^i + Q_B^i)h|$,
  $b_i^* = b_0 + x_i^*$ and Update $b_0 = b_i^*$,
end while
if Contract is C1 **then**
  Calculate $(K_{\text{fac}})_{\text{nominal}}$ with C1 contract using `CalculateKfac` defined as Algorithm 18,
  Calculate K_{fac} with C1 contract using `CalculateKfac`,
  Nominal Cost $= (\lambda_{\text{fixed}} + (K_{\text{fac}})_{\text{nominal}})(E_a)_{\text{nominal}}$,
  New Cost $= (\lambda_{\text{fixed}} + K_{\text{fac}})E_a$,
else if Contract is C2 **then**
  Calculate $(K_{\text{fac}})_{\text{nominal}}$ with C2 contract using `CalculateKfac` defined as Algorithm 18,
  Calculate K_{fac} with C2 contract using `CalculateKfac`,
  Nominal Cost $= \left(\lambda_{\text{peak}} + (K_{\text{fac}})_{\text{nominal}}\right)(E_a^{\text{peak}})_{\text{nominal}} + \lambda_{\text{off-peak}}\left((E_a^{\text{mid-peak}})_{\text{nominal}} + (E_a^{\text{off-peak}})_{\text{nominal}}\right)$,
  New Cost $= \left(\lambda_{\text{peak}} + K_{\text{fac}}\right)E_a^{\text{peak}} + \lambda_{\text{off-peak}}\left(E_a^{\text{mid-peak}} + E_a^{\text{off-peak}}\right)$,
else if Contract is C3 **then**
  Calculate $E_{a+}^{\text{peak}} = |E_a^{\text{peak}}|$, $E_{a+}^{\text{mid-peak}} = |E_a^{\text{mid-peak}}|$, $E_{a+}^{\text{off-peak}} = |E_a^{\text{off-peak}}|$,
  Calculate $(K_{\text{fac}})_{\text{nominal}}$ with C3 contract using `CalculateKfac`,
  Calculate K_{fac} with C3 contract using `CalculateKfac`,
  Nominal Cost$=\lambda_{\text{peak}}(E_a^{\text{peak}})_{\text{nominal}} + \lambda_{\text{mid-peak}}(E_a^{\text{mid-peak}})_{\text{nominal}} + \lambda_{\text{off-peak}}(E_a^{\text{off-peak}})_{\text{nominal}} + (K_{\text{fac}})_{\text{nominal}}(E_{a+}^{\text{peak}})_{\text{nominal}}$,
  New Cost $= \lambda_{\text{peak}}E_a^{\text{peak}} + \lambda_{\text{mid-peak}}E_a^{\text{mid-peak}} + \lambda_{\text{off-peak}}E_a^{\text{off-peak}} + K_{\text{fac}}E_{a+}^{\text{peak}}$,
end if
Profit = Nominal Cost of Consumption − New Cost of Consumption with inclusion Storage,
Return Vectors x^*, Q_B and Profit.

Algorithm 18 `CalculateKfac`

Inputs: $E_a^{\text{peak}}, E_a^{\text{mid-peak}}, E_a^{\text{off-peak}}, (E_a^{\text{peak}})_{\text{nominal}}, (E_a^{\text{mid-peak}})_{\text{nominal}}, (E_a^{\text{off-peak}})_{\text{nominal}}, E_r, E_{rQ1}$

Function: Computes K_{fac} for Contracts C1, C2 and C3 for Uruguay LV consumers

Initialize A, B,

if Contract is C1 **then**
  Calculate $E_a = E_a^{\text{peak}} + E_a^{\text{mid-peak}} + E_a^{\text{off-peak}}$,
  Calculate $(E_a) = (E_a^{\text{peak}})_{\text{nominal}} + (E_a^{\text{mid-peak}})_{\text{nominal}} + (E_a^{\text{off-peak}})_{\text{nominal}}$,
  if $E_r/E_a \leq 0.426$ **then**
    Assign $K_{\text{fac}} = 0$,
  else if $0.426 < E_r/E_a \leq 0.7$ **then**
    Assign $K_{\text{fac}} = 0.4\left(\frac{E_r}{E_a} - 0.426\right)$,
  else
    Assign $K_{\text{fac}} = 0.4\left(\frac{E_r}{E_a} - 0.426\right) + 0.6\left(\frac{E_r}{E_a} - 0.7\right)$,
  end if
  if $(E_r)_{\text{nominal}}/(E_a)_{\text{nominal}} \leq 0.426$ **then**
    Assign $(K_{\text{fac}})_{\text{nominal}} = 0$,
  else if $0.426 < (E_r)_{\text{nominal}}/(E_a)_{\text{nominal}} \leq 0.7$ **then**
    Assign $(K_{\text{fac}})_{\text{nominal}} = 0.4\left(\frac{(E_r)_{\text{nominal}}}{(E_a)_{\text{nominal}}} - 0.426\right)$,
  else
    Assign $(K_{\text{fac}})_{\text{nominal}} = 0.4\left(\frac{(E_r)_{\text{nominal}}}{(E_a)_{\text{nominal}}} - 0.426\right) + 0.6\left(\frac{(E_r)_{\text{nominal}}}{(E_a)_{\text{nominal}}} - 0.7\right)$,
  end if

else if Contract is C2 **then**
  Calculate $E_a = E_a^{\text{peak}} + E_a^{\text{mid-peak}} + E_a^{\text{off-peak}}$,
  Calculate $(E_a)_{\text{nominal}} = (E_a^{\text{peak}})_{\text{nominal}} + (E_a^{\text{mid-peak}})_{\text{nominal}} + (E_a^{\text{off-peak}})_{\text{nominal}}$,
  if $E_r/E_a \leq 0.7$ **then**
    Assign $K_{\text{fac}} = \frac{B}{100}\left(\frac{E_r}{E_a} - 0.426\right)$,
  else
    Assign $K_{\text{fac}} = \frac{B}{100}\left(\frac{E_r}{E_a} - 0.426\right) + \frac{100-B}{100}\left(\frac{E_r}{E_a} - 0.7\right)$,
  end if
  if $(E_r)_{\text{nominal}}/(E_a)_{\text{nominal}} \leq 0.7$ **then**
    Assign $(K_{\text{fac}})_{\text{nominal}} = \frac{B}{100}\left(\frac{(E_r)_{\text{nominal}}}{(E_a)_{\text{nominal}}} - 0.426\right)$,
  else
    Assign $(K_{\text{fac}})_{\text{nominal}} = \frac{B}{100}\left(\frac{(E_r)_{\text{nominal}}}{(E_a)_{\text{nominal}}} - 0.426\right) + \frac{100-B}{100}\left(\frac{(E_r)_{\text{nominal}}}{(E_a)_{\text{nominal}}} - 0.7\right)$,
  end if

else if Contract is C3 **then**
  Calculate $E_{a+}^{\text{peak}} = |E_a^{\text{peak}}|, \quad E_{a+}^{\text{mid-peak}} = |E_a^{\text{mid-peak}}|, \quad E_{a+}^{\text{off-peak}} = |E_a^{\text{off-peak}}|$,
  Calculate $E_{a+} = E_{a+}^{\text{peak}} + E_{a+}^{\text{mid-peak}} + E_{a+}^{\text{off-peak}}$,
  Calculate $(E_{a+})_{\text{nominal}} = (E_{a+}^{\text{peak}})_{\text{nominal}} + (E_{a+}^{\text{mid-peak}})_{\text{nominal}} + (E_{a+}^{\text{off-peak}})_{\text{nominal}}$,
  if $E_{rQ1}/E_a \leq 0.7$ **then**
    Assign $K_{\text{fac}} = \frac{A}{100}\left(\frac{E_{rQ1}}{E_{a+}} - 0.426\right)$,
  else
    Assign $K_{\text{fac}} = \frac{A}{100}\left(\frac{E_{rQ1}}{E_a} - 0.426\right) + \frac{100-A}{100}\left(\frac{E_{rQ1}}{E_{a+}} - 0.7\right)$,
  end if
  if $(E_{rQ1})_{\text{nominal}}/(E_{a+})_{\text{nominal}} \leq 0.7$ **then**
    Assign $(K_{\text{fac}})_{\text{nominal}} = \frac{A}{100}\left(\frac{(E_{rQ1})_{\text{nominal}}}{(E_{a+})_{\text{nominal}}} - 0.426\right)$,
  else
    Assign $(K_{\text{fac}})_{\text{nominal}} = \frac{A}{100}\left(\frac{(E_{rQ1})_{\text{nominal}}}{(E_{a+})_{\text{nominal}}} - 0.426\right) + \frac{100-A}{100}\left(\frac{(E_{rQ1})_{\text{nominal}}}{(E_{a+})_{\text{nominal}}} - 0.7\right)$,
  end if

end if

Return $(K_{\text{fac}})_{\text{nominal}}$, K_{fac}.

Table 9.9: Arbitrage Gains Potential for a Month

b_{rated} kWh	Contract C2	Contract C3
1	106.68	147.32
2	213.36	294.65
5	533.40	736.62
10	1066.81	1473.23
20	2133.62	2946.46

Table 9.10: Nominal load of a LV consumer

Load Consumed during	kWh
Peak Period	200
Mid Peak	200
Off-peak	100

consumption pattern. In Section 9.6.3 we present that based on storage operational cycles and degradation, the battery under certain contracts and size could be profitable for consumers. The financial returns of storage in Uruguay are significantly higher than several ISOs in the USA and Europe as observed in a case-study presented in Chapter 3 Section 3.4.

9.6.1 Arbitrage Potential

In Table 9.9 we list the arbitrage gains the storage owners would make for $\text{SoC}_{\max} = 0.98$, $\text{SoC}_{\min} = 0.2$, η_{dis}=η_{ch} =0.95. From Table 9.9 it is clear that storage is hugely profitable. Storage owner would make 3.56 peso per day per kWh for contract C2 and 4.91 peso per day per kWh for contract C3. For a user with a 1000 peso per month as electricity bill under C3 would have to pay nothing perpetually if they install a 7kWh battery (performing arbitrage only) which could charge completely within the off-peak time period and discharge completely during peak periods.

9.6.2 Consumer gains with/without storage

For this numerical experiment we assume a consumer with active energy consumed over a month listed in the table 9.10. We assume the cumulative absolute value of reactive power is $E_{rQ1} = 1.2 \times E_r$ and cumulative value of absolute of active power $E_{a+} = E_a$. For the consumer load listed in Table 9.10 we vary the amount of reactive load and see the effect without and with inclusion of energy storage providing active and/or reactive energy compensation.

Nominal Case

The nominal case consists of inelastic load with DG output in absence of energy storage. Thus the nominal case is described for no compensation of active and reactive energy at consumer end. It is essential to analyze the effect on consumer load listed in Table 9.10 on the cost of consumption based on the different contracts. Note the presented analysis will vary with consumer load and we wish to present the mechanism of analysis for the case described, of course a similar analysis needs to be performed for a specific user who wish to select the appropriate contract based on their consumption behavior.

Fig. 9.8 presents the the cost of active energy with increasing share of reactive energy. It is clear that cost of active energy is independent of increase in reactive energy. In absence of flexibility to alter the active energy consumption, clearly contract C1 is best suited for the consumer presented in Table 9.10. Fig. 9.9 presents the cost of reactive energy under contract C1, C2 and C3. With increase in share of reactive energy, cost paid by consumer under C1 is significantly higher compared to C2 and C3.

Fig. 9.10 plots the variable cost component denoted as C^{Ci}_{variable}. It is clear that the cost of active power dominates the variable cost. The same trends are visible in Fig. 9.12 which presents the total cost of consumption which includes the variable cost, fixed cost and power cost. Note that the fixed cost for C2 and C3 is almost double the cost paid by consumer under C1. Fig. 9.11 presents the ratio of the cost of reactive energy and the cost of active energy in percentage. For consumers consuming equal quantities

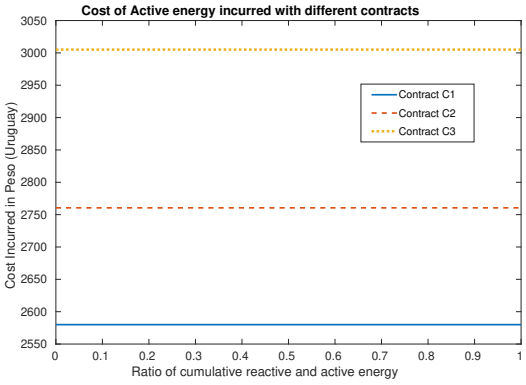

Figure 9.8: Active energy cost with different contracts

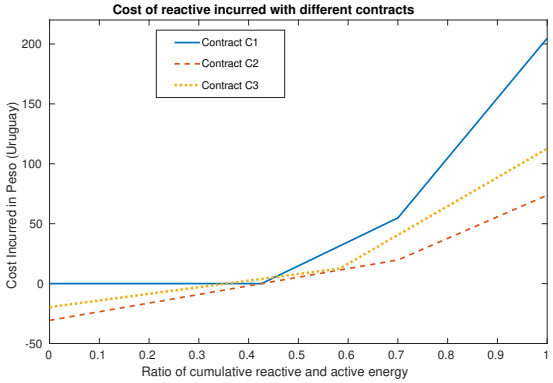

Figure 9.9: Reactive energy cost with different contracts

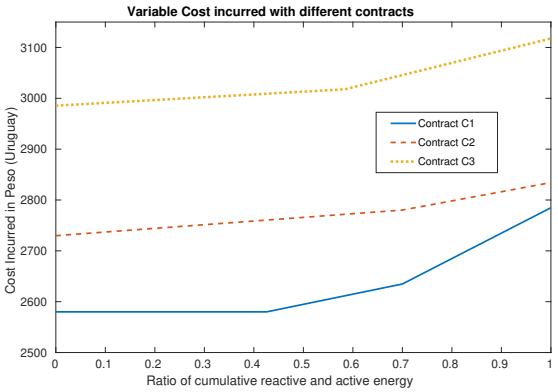

Figure 9.10: Variable cost with different contracts

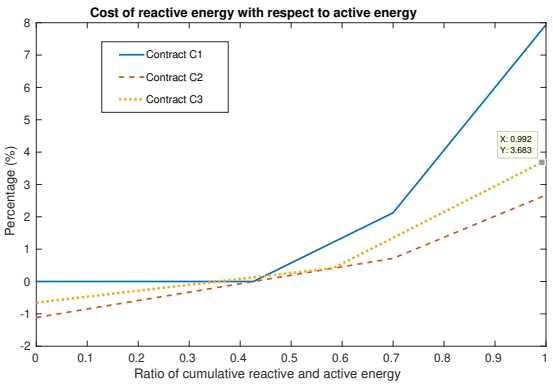

Figure 9.11: Cost of reactive energy compared to active energy cost with different contracts

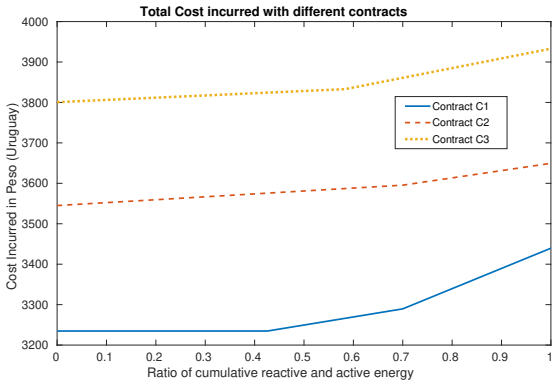

Figure 9.12: Total energy cost with different contracts

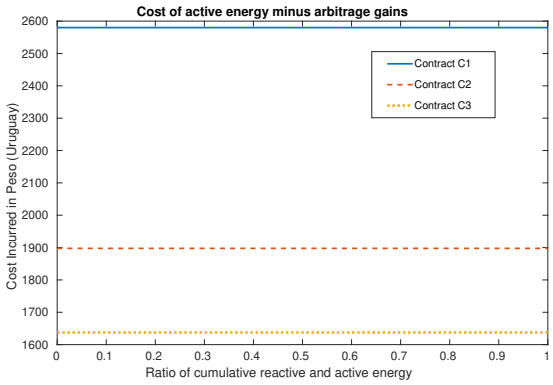

Figure 9.13: Cost of active energy with arbitrage

active and reactive energy end up paying almost 8% of active energy cost under C1, less than 4% of active energy cost under C2 and less than 3% of active energy cost under C3. Clearly, the value of reactive energy compensation is highest under contract C1. We would like to bring to notice that the cost paid by consumer for active energy is significantly higher than that of the reactive energy. In the proposed algorithm the energy storage converter active power output is selected based on maximization of arbitrage gains and remaining converter capacity is used for supplying reactive power for correcting the PF in accordance to the contract selected by the LV consumer.

Inclusion of Tesla PowerWall 1 (6.4 kWh)

The total arbitrage gains made by consumer owning Tesla PowerWall 1 which has a rated capacity of 6.4 kWh is 682.4733 pesos under contract C2 and 942.5827 pesos under contract C3. Fig. 9.13 presents the cost of active energy with inclusion of energy storage performing only arbitrage. Now we can see that inclusion of storage have turned contract C3 most profitable for the consumer.

Fig. 9.14 presents the total cost with inclusion of energy storage performing only arbitrage. In this case, total cost under C2 and C3 are comparable. Assuming energy storage converter could supply all the reactive energy that the user consumed, which is fairly reasonable as the utility aggregates reactive power over the month. Fig. 9.15 presents the total cost of consumption (includes fixed and power cost) with energy storage performing arbitrage and reactive power compensation. Clearly, contract C3 consumer pays the least and consumer under C1 pays the maximum electricity bill in this scenario. Fig. 9.16 shows the percentage of consumer would make with respect to the nominal case under the same contract. Consumers with C3 would make a profit exceeding 25% by installing Tesla PowerWall 1. Note since consumer under C1 could perform only reactive power compensation, it makes a profit only if the ratio of reactive energy and active energy exceeds 0.426.

Inclusion of Tesla PowerWall 2 (13.5 kWh)

The total arbitrage gains made by consumer owning Tesla PowerWall 2 which has a rated capacity of 13.5 kWh is 1439.6 pesos under contract C2 and 1988.3 pesos under contract C3.

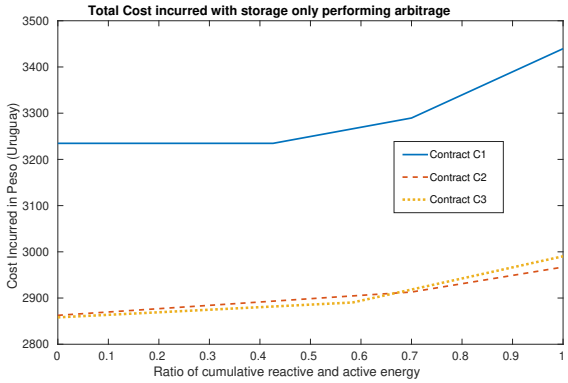

Figure 9.14: Total cost with only arbitrage

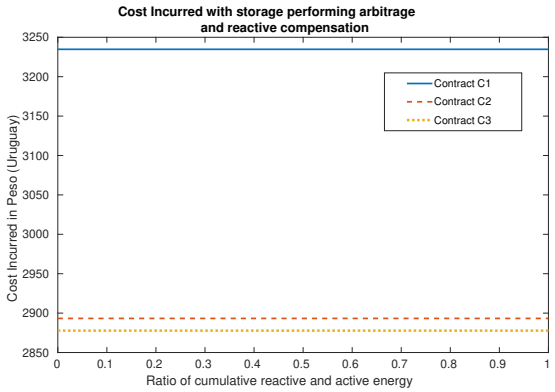

Figure 9.15: Total cost of electricity

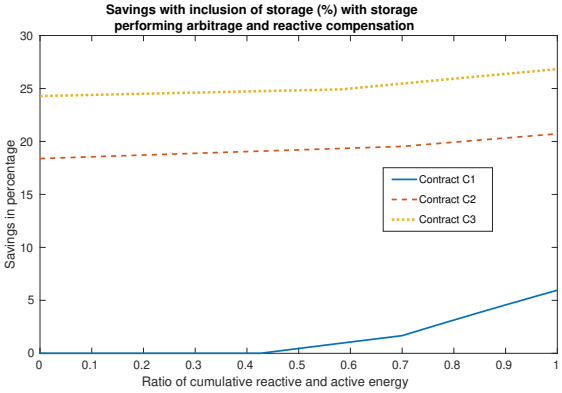

Figure 9.16: Profit due to inclusion of storage in terms of savings in percentage

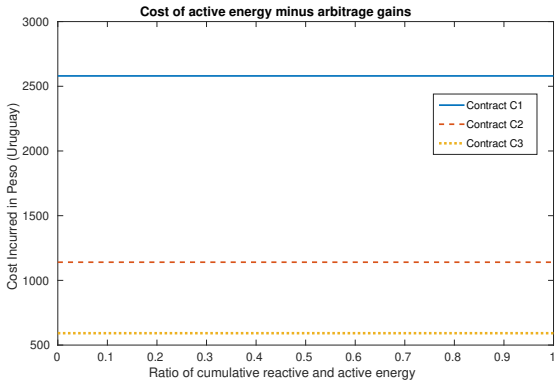

Figure 9.17: Active energy cost with arbitrage for PowerWall 2

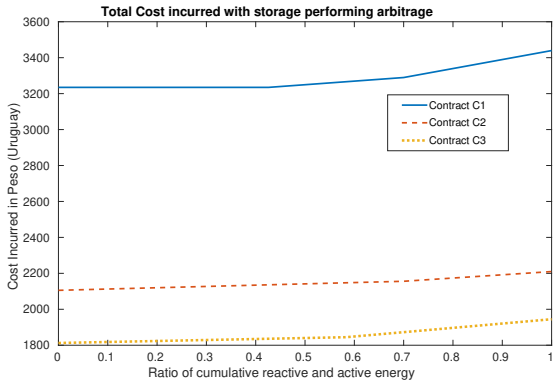

Figure 9.18: Total cost with only arbitrage for PowerWall 2

Fig. 9.17 presents the cost of active energy with inclusion of energy storage performing only arbitrage. Now we can see that inclusion of storage have turned contract C3 most profitable for the consumer. Note that the gap between C2 and C3 increases as the storage size increases, as the amount of profit under C3 is higher for performing arbitrage compared to C2. Compare Fig. 9.13 and Fig. 9.17.

Fig. 9.18 presents the total cost with inclusion of energy storage performing only arbitrage. In this case, total cost under C2 and C3 are not comparable. Consumer would pay around 150 pesos lower under C3 then under C2.

Fig. 9.19 presents the total cost of consumption (includes fixed and power cost) with energy storage performing arbitrage and reactive power compensation. Clearly, contract C3 consumer pays the least and consumer under C1 pays the maximum electricity bill in this scenario with Tesla PowerWall 2. Fig. 9.20 shows the percentage of consumer would make with respect to the nominal case under the same contract. Consumers with C3 would make a profit exceeding 50% by installing Tesla PowerWall 2. Consumers with C2 would make a profit exceeding 40% by installing Tesla PowerWall 2. Note since consumer under C1 could perform only reactive power compensation, it makes a profit only if the ratio of reactive energy and active energy exceeds 0.426.

We observe that consumers with storage should opt for C3, i.e., three level time-of-use electricity pricing rather than fixed pricing under C1. Note that the selection of contract also depends on the reactive energy consumed, load and storage size. In this analysis we assume that conditions $T_{\text{off-peak}} > T_{\text{ch}}$ and $T_{\text{peak}} > T_{\text{dis}}$ are true.

9.6.3 Energy Storage Profitability

The cost of Tesla Powerwall 1 is $3000 and Tesla Powerwall 2 is $5500 (for the year 2017), making the per kWh cost of $470 and $398 [66]. Consider the storage could perform 3000 cycles of 100% depth-of-discharge over a maximum calendar life of 10 years. We use the degradation model presented in [181]. In order to have the storage application profitable the per cycle gains should satisfy

• For Tesla Powerwall 1: the battery should earn more than $1 for each cycle in order to be profitable,

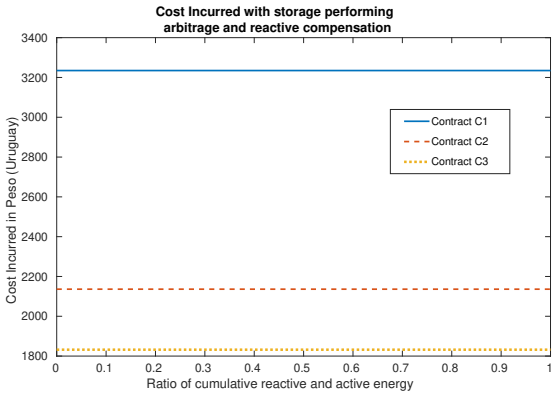

Figure 9.19: Total cost of electricity for Tesla PowerWall 2

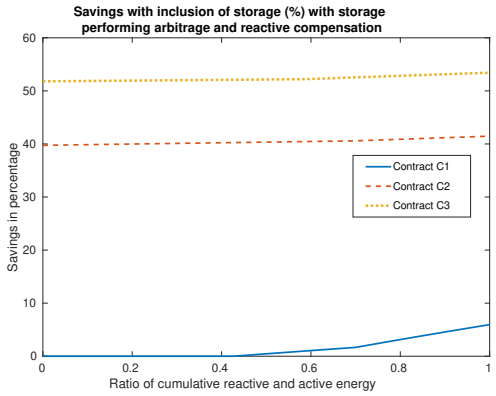

Figure 9.20: Profit due to inclusion of storage in terms of savings in percentage for Tesla PowerWall 2

• For Tesla Powerwall 2: the battery should earn more than \$1.8333 for each cycle in order to be profitable.

The depth-of-discharge of battery for each day is equivalent to $\text{DoD}_{\text{daily}} = \text{SoC}_{\text{max}} - \text{SoC}_{\text{min}}$. Thus, the battery performs 0.7608 cycles of 100% DoD each day and 277.7 cycles each day.

Of course the storage gains are dependent on the load active and reactive energy consumed during different times of the day. For the nominal load profile storage gains by only performing arbitrage appears to be profitable as the dollar per cycle gain exceeds the dollars per cycle cost calculated based on the cost and life ratings of the battery. Adding the reactive compensation gains would further improve the dollars per cycle of the battery, in effect reducing the payback period. The simple payback period for cases where storage is profitable would lie between 3-4 years, similar to storage returns in the island of Madeira as presented in Chapter 8.

9.7 Conclusion and Perspectives

The details of electricity billing and net-metering policy under the new electricity consumer contracts applicable to the low voltage electricity consumers in Uruguay are summarized. The consumer contracts

Table 9.11: Profitability

Parameter	Tesla Powerwall 1	Tesla Powerwall 2
Desired \$/cycle	\$1.0	\$1.833
Month gain in pesos	C2: 682.5, C3:942.6	C2: 1439.6, C3:1988.3
Month gain in dollars	C2: 20.29, C3:28.02	C2: 42.8, C3:59.11
Total cycles in month	22.83	22.83
Profit in \$/cycle	C2: 0.889, C3: 1.227	C2: 1.874, **C3: 2.589**

make it attractive for consumers to install energy storage and distributed generation. Due to the huge difference between peak and off-peak electricity pricing, installing energy storage could be rewarding for LV consumers. Furthermore, consumers could use the storage converter for reactive power compensation which could provide an additional revenue stream for the consumer. For each contract threshold-based uncertainty insensitive algorithm based on hierarchical control of active energy for arbitrage and reactive energy compensation is proposed. In the present work, the question of whether energy storage is profitable for three new energy contracts in Uruguay is assessed. These contracts are of particular interest for two reasons. Firstly, the buying price and selling price are the same, for which it is shown that policy for performing arbitrage is insensitive to load and generation. Secondly, reactive power compensation is monetarily compensated in some of those cases. With data from real batteries and taking into account battery degradation, it is shown that for some of the new contracts it will be profitable to buy a battery, while for others it will not. For the latter case, an evaluation of the best contract available is also provided. Using numerical results we show that arbitrage is more profitable than reactive energy compensation, but Chapter 6 identifies that reactive compensation can still be performed without compromising the former. Energy markets with similar pricing and net-metering policy could use this analysis.

Chapter 10

Effect of Electricity Pricing on Ancillary Service

What we know is a drop, what we don't know is an ocean. - Issac Newton

Summary: The objective of this chapter is to analyze the effect of real time electricity price (RTP) on the amount of ancillary services required for load balancing in presence of responsive users, information asymmetry and forecast errors in demand and renewable energy sources (RES) generation. We consider a RTP that is determined by the forecasted generation and ramping cost. A community choice aggregator manages the load of all the consumers by setting the price. The consumer's objective is to minimize their overall cost of consumption. Ancillary services are called upon to balance the load in real time.

With zero RES in the power network and a high degree of load flexibility, the proposed RTP flattens and the volatility in demand vanishes. However, in presence of RES the volatility in price and demand is reduced up to an extent and ancillary services are required for load balancing. The amount of ancillary services required increases with forecast errors. We also propose a real time algorithm that approximates the optimal consumer behavior under the complete information setting. Extensive numerical simulations are provided using real data from Pecan Street and Elia Belgium.

10.1 Introduction

European Union has set the goal of 20% renewable generation by 2020 and 27% by 2030 [61]. India has set an ambitious goal of achieving 40% cumulative electric power capacity from non fossil fuel sources by 2030 [69]. A cost efficient solution to achieve load balancing, essential for reliable operation of power system, is to encourage retail customers and other market participants to take part in price based demand response in slower time scales and ancillary services in real time. The objective of this chapter is to propose a RTP design that is implementable and effective in incentivizing consumers to use their load flexibility to manage the volatility in the generation with a high proportion of intermittent RES. This enables the system operator to reduce the overall cost by not having to deploy the more expensive fast ramping generators.

10.1.1 Related Work

There is extensive work on real time pricing that addresses the peak load issues. Authors in [337] propose a controller for residential HVAC systems that significantly reduce peak loads and electricity bills with modest variations in thermal comfort. Authors in [279, 291] propose a real time electricity pricing scheme that reduces the peak-to-average load ratio, i.e. flattens the load, leading to peak shaving for the grid. Authors in [302] present how price based demand side management programs assist in reduction of peak demand and present a case study of impact of real time pricing on power network in the city of Gothenburg, Sweden. Note that demand side management includes DR, energy-efficiency and conservation programs [319]. Primary objective of the works [310, 302, 337, 279, 291] is peak shaving. In our work we show that dynamic pricing not only helps in reducing peaks and generating profit for the consumer but also assists in reducing the ramping requirement in the power network.

In addition, there are many works that propose an equilibrium price process that maximizes social welfare. Authors in [166] show the existence of a competitive equilibrium when players are price-takers.

They establish that under the equilibrium price process, players selfish response coincide with the social welfare-maximizing policy computed by a social planner. Authors in [147] claim that at the Nash equilibrium, with multiple stores of sufficient size, the stores collectively erode their own profits. Essentially, each store attempts to increase its own profit over time by over-competing at the expense of the others. All of the above works study the equilibrium price process in the presence of flexible loads and/or energy storage.

10.1.2 Contributions

We assume consumers have a portion of flexible load, which they shift in time to minimize their consumption cost. The generation side consists of schedulable generators and RES generation. These generators can be turned on when needed. The generator starting time constraints are ignored in this chapter. We also assume the aggregate demand and the RES generation used for setting the price of electricity contains forecast errors. The contributions of this chapter are:
• *Effect of RTP on ancillary service needs*: We analyze the effect of RTP design which considers information asymmetry in presence of responsive users on the amount of ancillary services needed for load balancing.
• *Real Time Price* design in presence of RESs and price-responsive users. We show that the greedy behavior of consumers to minimize its own cost of consumption lowers the volatility of price and demand, increases profit for consumers and lowers the ancillary service required for load balancing. We also show that in the presence of RES with forecast error, as the level of flexibility increases the ancillary service requirements saturate to a level.
• *Implementable Price Design under information asymmetry*: We consider price design under the setting where ex-ante (before real time) price is set by an aggregator. Information asymmetry is caused by the time delay between setting RTP, consumption decision and intermittent generation. Setting RTP requires the prediction of aggregate demand and RES generation by the utility if the price is set ex-ante and prediction of price by the consumers if the price is set ex-post [287]. In our work, price design accounts for this information asymmetry which has been largely ignored in prior works on real time electricity price design. Most prior works consider time interval as a point, which worked well due to price inelasticity of demand. However, due to increased energy awareness and technological advancements the future consumers cannot be assumed to be inelastic to price fluctuations.
• *Volatility of electricity price and demand*: We show that the volatility in demand and price lowers with increased fraction of load flexibility at the consumer end in presence of forecast errors.
• *Sensitivity Analysis*: We study (i) the effect of load flexibility and its variation on the amount of ancillary service required for load balancing, (ii) the effect of variation of RES penetration for a fixed forecast error on the amount of ancillary service required, (iii) the effect of variation of forecast error for a fixed renewable penetration on the amount of ancillary service required.
• *Real Time Algorithm for Consumer's Scheduling*: Proposed real time algorithm approximates the optimal consumer scheduling under the complete information setting.

10.1.3 Key Observations

We would like to remind the reader of the key observations,
• With schedulable generation (no intermittent generation), the proposed price design completely balances the load, with sufficient amount of flexibility in consumption.
• For power networks with intermittent generation, price by itself is not sufficient to balance load and so ancillary services are required. With increase in forecast error for RES, the size of ancillary services needed for balancing load increases.
• In presence of responsive consumers and RES, the proposed price design can lower the volatility of price and aggregated demand but does not eliminate the volatility completely.

10.2 System Description

We propose an electricity RTP design for a power network consisting of generators, aggregator, consumers and ancillary service participants. The aggregator's objective is to minimize peak to average ratio of the aggregate power consumption and induce responsiveness from the consumers so as the amount of ancillary service needed for load balancing is as low as possible. The consumer's objective is to minimize their cost of consumption.

10.2.1 Consumer Model

Consumers are assumed to be price responsive and alter their consumption based on price variations, with the constraint that the aggregate energy consumed by users under nominal operation without any load flexibility equals the new power consumption trajectory with load flexibility. Note in this chapter we do not consider energy saving, rather shifting load in time like demand response. Denote the time horizon as T. Let the time horizon be sampled in to N intervals of sampling time h. Denote by D^o the nominal demand profile of the consumer. The nominal demand is the power consumption at a time given there is no load flexibility. Let the electricity price corresponding to the nominal demand profile be p^o_{elec}. Let $x \in [0, 1]$ be the fraction of the load of the nominal demand that is flexible. Also, let D denote the power consumption trajectory of the consumer with load flexibility x and p_{elec} denote the electricity price corresponding to the demand profile D. Note that p^o_{elec} and p_{elec} differ because consumer's response influences the market price in our setup. The consumer's optimization problem (P) is given by

$$\min \sum_{i=1}^{N} p_{\text{elec}}(i) D_i, \text{ s.t. } \sum_{i=1}^{N} D(i) = \sum_{i=1}^{N} D^o_i, D_i \in [D_{\min}(i), D_{\max}(i)] \tag{P}$$

where $D_{\min}(i) = (1 - x)D^o_i$ and $D_{\max}(i) = (1 + x)D^o_i$. Load flexibility is assumed to have power and energy constraint, much like an energy storage device [182].

10.2.2 Generation Scheduling

At time instant i the controllable portion of generation, $P_c(i)$, is scheduled based on forecasted demand $\hat{D}_i$ and forecasted RES generation $\hat{P}_r(i)$ such that total generation $P_g(i) = P_c(i) + \hat{P}_r(i)$. However, the actual demand D_i and actual RES generation $P_r(i)$ are know at the next time instant $i + 1$. Therefore, the task of load balancing cannot be performed by ex-ante RTP design due to this information asymmetry. Furthermore, RTP can only partly facilitate the load balancing as the time scales of RTP is 5 min to an hour. Hence, ancillary services are required to balance load. Our motivation for this chapter is to

Table 10.1: Information and Decisions Asymmetries

	Time Instant	i	$i+1$
Aggregator	Information Decisions	$\hat{D}_i, \hat{P}_r(i)$ $p_{\text{elec}}(i)$	$D_i, P_r(i)$
Consumers	Information Decisions	$p_{\text{elec}}(i)$ D_i	

understand the role of load flexibility in compensating volatility, load balancing and minimizing peak to average ratio in electricity markets.

10.2.3 Price Model

In Community Choice Aggregation or a microgrid the per unit cost of power generation at time instant i is defined as

$$f(P_g(i)) = \frac{C^R_{pu} E_r(i) + C^A_{pu} E_A(i) + C^B_{pu} E_B(i) + ...}{E_r(i) + E_A(i) + E_B(i) + ...} \tag{10.2.1}$$

where C^A_{pu} is the per unit energy generation cost (LCOE) of generation type A and $E_A(i)$ is the amount of energy generation from generation type A at time instant i. R represent the renewable energy generators. The amount of energy generated at any time instant 'i' by source R, i.e. $E_r(i) = P_r(i)h$, is accommodated at all times in $P_g(i)$. $E_r(i)$ is not scheduled generation and depends on exogenous parameters like solar insolation, wind velocity etc. The total energy generated at time instant i is defined as $E_g(i) = P_g(i)h = E_r(i)+E_A(i)+E_B(i)+E_C(i)+....$ The total cost of generation is represented as $C_{gen}(i) = f\left(P_g(i)\right) \times E_g(i)$.

Our proposed electricity price structure has two components: generation cost and ramping cost. As identified in [311], the price of electricity is not only governed by generation but also by the amount of change in generation with respect to the previous time period. However, unlike [311], we consider information asymmetry in the price design. This ramp is performed due to volatility in demand and

uncertainty in RES generation. The ramping component of the proposed price model will increase the price as the power network becomes more volatile, is given as

$$P_{\Delta}(i) = \gamma |P_c(i) - P_c(i-1)|, \tag{10.2.2}$$

where γ is a positive scalar. The factor γ has to be tuned so as the ramping component does not dominate and to ensure the stability of the price design. Therefore, the proposed price of electricity for per unit of energy is defined as

$$p_{\text{elec}}(i) = f\big(P_g(i)\big) + P_{\Delta}(i). \tag{10.2.3}$$

The cost incurred by agent Q at time instant 'i' for consuming energy $e_Q(i)$ is given as, $C_Q(i) = p_{\text{elec}}(i)e_Q(i)$.

For scheduling generation we use forecasted aggregate demand. The aggregate demand in the immediate previous time instant which is already known is used as the forecast in the present time instant. The generation scheduled at time instant i equals the demand in immediate past time instant $i-1$, given as $P_g(i) = \hat{D}_i = D_{i-1}$. This *persistence model* model has been statistically evaluated in [167], [287] for wind power generation with forecast uncertainty.

Remark 9. *As the fraction of flexibility in consumption increases, the incentives for users will increase or remain the same. Consider two scenarios with different levels of flexibility x_1, x_2, such that $x_1 > x_2$ and $\sum D_1^* = \sum D_2^* = \sum D^o$ is met where D_1^* is the optimal demand trajectory with flexibility x_1 and D_2^* is the optimal demand trajectory with flexibility x_2, then*

$$\sum p_{elec}^{x_1}(i) D_1^*(i) \leq \sum p_{elec}^{x_2}(i) D_2(i) \leq \sum \hat{p}_{elec}(i) D_i^o,$$

where D^o represents the nominal demand curve with no flexibility.

10.2.4 Real time Operation

The optimization problem (P) for aggregate consumer model cannot be implemented in real time because of the cumulative power constraint. In this section we present an algorithms that consumers can implement for approximating the optimal solution under deterministic scenario. The calculation of instantaneous demand using proposed algorithm is sequential and therefore, implementable in real time. We propose

Algorithm 19 `RealTimeControl`$(i, x, \bar{d}, D_i^o, \bar{r}, \hat{P}_r(i))$

1: Calculate $D_{\min}(i) = (1-x)D_i^o$
2: Calculate $D_{\max}(i) = (1+x)D_i^o$.
3: $(D_i^*)_{RT} = \min |D_i - \bar{d} + \bar{r} - \hat{P}_r(i)|$, s.t. $D_i \in [D_{\min}(i), D_{\max}(i)]$

Algorithm 19 for computing the new aggregate load trajectory for consumers with load flexibility for a power network with RES generation. The input to the algorithm is the time instant, degree of load flexibility, mean nominal demand for the user, instantaneous nominal load and forecasted RES generation. The algorithm use the mean nominal load and mean RES generation to ensure total energy consumed in the time horizon is matched to the nominal energy consumed in the time horizon. The mean of the nominal demand is denoted as $\bar{d} = \frac{1}{N}\sum_{i=1}^{N} D_i^o$. The mean renewable energy generated in the time horizon is denoted as $\bar{r} = \frac{1}{N}\sum_{i=1}^{N} \hat{P}_r$. Note Alg. 1 assumes a homogeneous population of loads, for heterogeneous loads respective mean load and mean RES generation has to be estimated.

10.3 Indices Used for Measurement

In this section we define indices to measure volatility in price, demand and generation. We also list the indices to measure ancillary services required for achieving load balancing.

10.3.1 Volatility Indices

RTP design considering variable generation cost and ramping cost components, as proposed in the chapter, will become more volatile with increase in uncertainty in generation, demand, scheduling mismatch and ramping constraints. This volatility in prices will induce users to alter their consumption behavior. These

users responding to these prices will reduce the volatility of price to a level where no further deviation is profitable [147]. This implies that with high degree of load flexibility the disparity for non-responsive consumers will reduce.

Measuring Volatility of Generation and Aggregate Demand

• Case 1– No responsive users and no renewables: The generators are all controllable and the volatility is due to change in demand.

$$\hat{D}(i) = D^o_{i-1},$$
$$P_g(i) = P_c(i) = D^o_{i-1},$$

$$\text{Demand and Grid volatility, } V_c^{\text{non}} = \sum \left|\hat{D}_i - D^o_{i-1}\right|, \tag{10.3.1}$$

where D^o_{i-1} is the nominal demand in time instant $i-1$.
• Case 2– No responsive users and with renewables: The total generation consists of controllable generators and intermittent RES generation. The volatility in power network is not only because of demand but also because of uncertainty in RES generation

$$P_g(i) = P_c(i) + \hat{P}_r(i) = D^o_{i-1},$$
$$\text{volatility of RES, } V_r = \sum \left|\hat{P}_r(i) - P_r(i)\right|,$$

where $\hat{P}_r(i)$ is forecasted RES generation. The volatility in the power network is due to mismatch in actual versus the forecasted demand and RES generation. The grid volatility is defined as

$$\text{Grid volatility, } V_{non} = V_c^{\text{non}} + \frac{V_r \max P_r(i)}{\max D^o}. \tag{10.3.2}$$

The volatility in demand in this case is equal to V_c^{non}.
• Case 3– Responsive users and no renewables: The generators are all controllable and the volatility is due to change in demand.

$$\hat{D}_i = D_{i-1},$$
$$P_g(i) = P_c(i) = D_{i-1},$$

$$\text{Demand and Grid volatility, } V_c^{\text{res}} = \sum \left|D_i - D_{i-1}\right|. \tag{10.3.3}$$

• Case 4– With responsive users and with renewables: The volatility with new load trajectory D is denoted as

$$P_g(i) = P_c(i) + \hat{P}_r(i) = D_{i-1},$$

$$\text{Grid volatility, } V_{responsive} = \sum \left|D_i - D_{i-1}\right| + \frac{V_r \max P_r}{\max D}. \tag{10.3.4}$$

The volatility in demand in this case is equal to V_c^{res}.

Measuring Volatility of Price

The nominal volatility in price is given as

$$V^{price}_{nominal} = \sum \left|p^o_{\text{elec}}(i) - p^o_{\text{elec}}(i-1)\right|, \tag{10.3.5}$$

where p^o_{elec} is the nominal price corresponding to nominal demand, D^o, with no load flexibility. In a power network with responsive users, the volatility in price will be denoted as

$$V^{price}_{responsive} = \sum \left|p_{\text{elec}}(i) - p_{\text{elec}}(i-1)\right|. \tag{10.3.6}$$

where p_{elec} is the price corresponding to new optimal demand curve, D, with load flexibility x.

10.3.2 Measuring Ancillary Service Required

The instantaneous power mismatch is communicated to ancillary service participants to respond. We define the residual or the load imbalance as the difference of generation and demand.
With only controllable generation: the residual is denoted as

$$R(i) = P_g(i) - D_i, \tag{10.3.7}$$

The residual represents the mismatch between supply and demand.

Mismatch with RES: The actual renewable generation is not known because of the intermittent nature. If forecasted value is given as $\hat{P}_r$. The error in magnitude of energy is represented as $P_r^{err}(i) = P_r(i) - \hat{P}_r(i)$. The residual in this case is given as

$$R(i) = P_g(i) - D_i + P_r^{err}(i), \tag{10.3.8}$$

where $P_g(i) = P_c(i) + \hat{P}_r(i)$, $P_c(i)$ is the controllable portion of generation. The residual for electricity grid with schedulable generation plus RES depends on the generation and demand mismatch and the error in forecast of RES energy. The balancing problem with only schedulable generators had uncertainty at the consumer end, however with RES there is also uncertainty in generation. Based on the sign of $R(i)$:
Case 1: $R(i) < 0$ implies $D(i) > P_g(i)$ and it is desirable that the consumers reduce consumption for load balance and it is incentivized to reduce the load.
Case 2: $R(i) > 0$ implies $D(i) < P_g(i)$ and it is desirable that the consumers increase their consumption and it is incentivized to increase the consumption.

We define four scalar values to measure the amount of ancillary service required for achieving load balancing as:

- Total ramp up capacity needed, $R_{\text{up}} = \sum_{i=1}^{N} [R(i)]^+$
- Total ramp down capacity needed, $R_{\text{down}} = \sum_{i=1}^{N} [R(i)]^-$
- Maximum ramp up needed, $M_{\text{up}} = \max[R(i)]^+ \quad \forall i$
- Minimum ramp up needed, $M_{\text{down}} = \max[R(i)]^- \quad \forall i$

The ancillary service requirement will be governed by quadruplet, $AC_{\text{needed}} = \{R_{\text{up}}, R_{\text{dowm}}, M_{\text{up}}, M_{\text{down}}\}$. AC_{needed} will decide the size of ancillary services needed for load balancing.

10.4 Numerical Results

The proposed electricity price signal is evaluated for completely schedulable generation and for schedulable generation with RES. The simulation parameters used are $\gamma = 0.5$, $T = 24$ and $h = 0.25$.

10.4.1 Results with only schedulable generations

We consider a 1000 MW capacity system where the power system is formed with different types of generators with different cost of generation (LCOE) as listed below. The per unit generation cost is approximated

Generation Type	A	B	C	D	E	F	G
Cost in \$/MWh	40	60	100	120	150	180	200
Share in %	35	25	20	5	5	5	5

by $6e - 5P_g^2(t) - 0.022P_g(t) + 41$ \$/MWh.

We normalize the load consumption data of Belgium on 6th January 2017 [46] to our rated maximum capacity. Fig. 10.1 shows the nominal value of demand with no flexibility [46] and demand trajectories with increasing degrees of load flexibility over a period of one day. Note, the optimal consumption trajectory becomes flatter with increased load flexibility, this is a desired scenario for the aggregator as the peak consumption is reduced and power ramp needs are reduced as much as possible. Fig. 10.1 indicate that the optimal strategy for consumers partially responsive to proposed real time electricity price is to flatten their aggregate consumption trajectory. Therefore, for controllable generators with increase of load flexibility

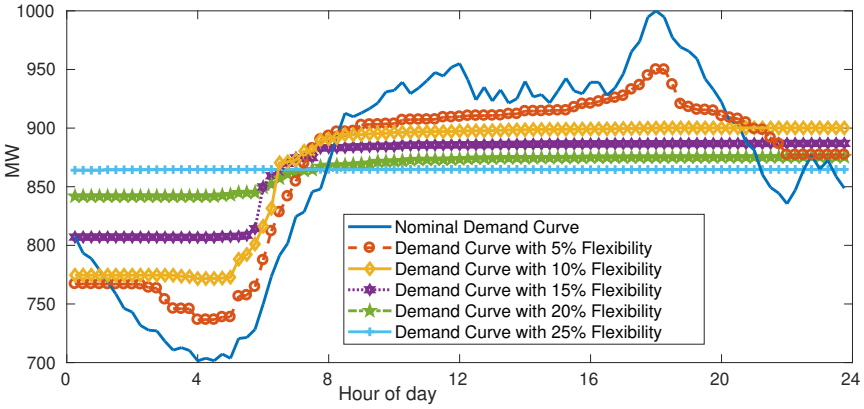

Figure 10.1: Optimal demand trajectories with load flexibility

we can say $\sum |D_i^* - D_i^*| \to 0$ as $x \uparrow$. From Fig. 10.1 it is evident that the ramping cost component tends to zero for flexibility greater that 25%, for this numerical example. Fig. 10.2 shows the comparison of mean, variance and maximum value of price for the day decreases with increase in consumer responsiveness for the optimal solution and proposed real time algorithm. The performance of real time algorithm matches that of the optimal solution as the load flexibility increases. Note the correlationship between maximum value of price and the fraction of flexibility is not as strong as the mean and variance of the price. Fig. 10.3

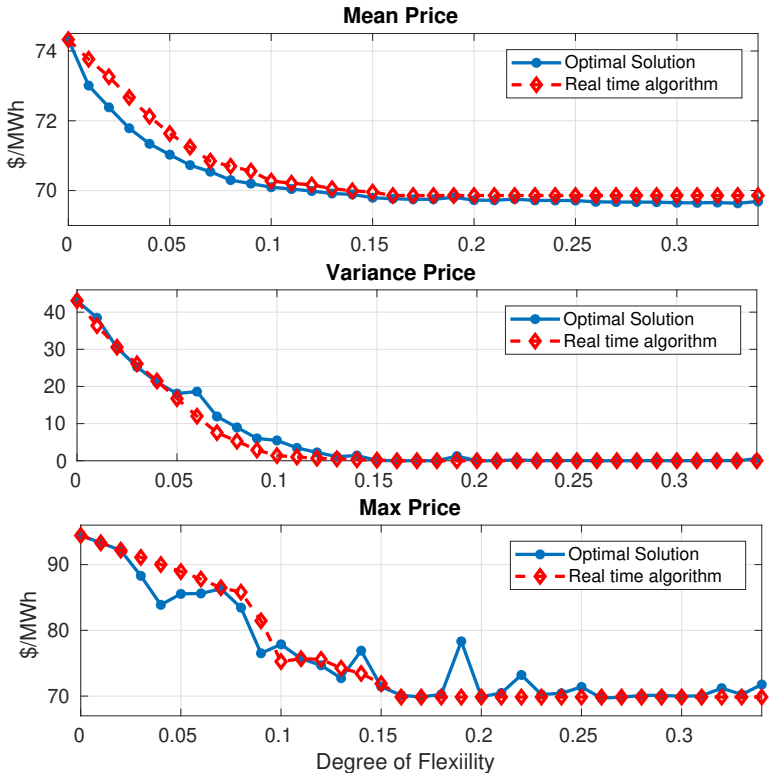

Figure 10.2: Volatility in price with load flexibility

compares the demand volatility and consumer profit for the optimal scenario with the real time algorithm. It is evident that the consumer greedy behavior is leading to reduction in price and demand volatility. The volatility of demand with responsive users is lower compared to nominal demand without responsiveness, given as $(V_c^{\text{res}})_x^* \leq V_c^{\text{non}}$ is true. Fig. 10.3 also reveals that the consumer's profit saturates at a certain level of load flexibility. From the consumer point of view, this is the optimal level of flexibility because the profit increases up to this level and saturates for any further increase in the flexibility. Note the amount of flexibility required for flattening the demand depends on the nominal demand curve and cannot be generalized from the presented numerical results. Fig. 10.4 shows the four indices measuring the ancillary

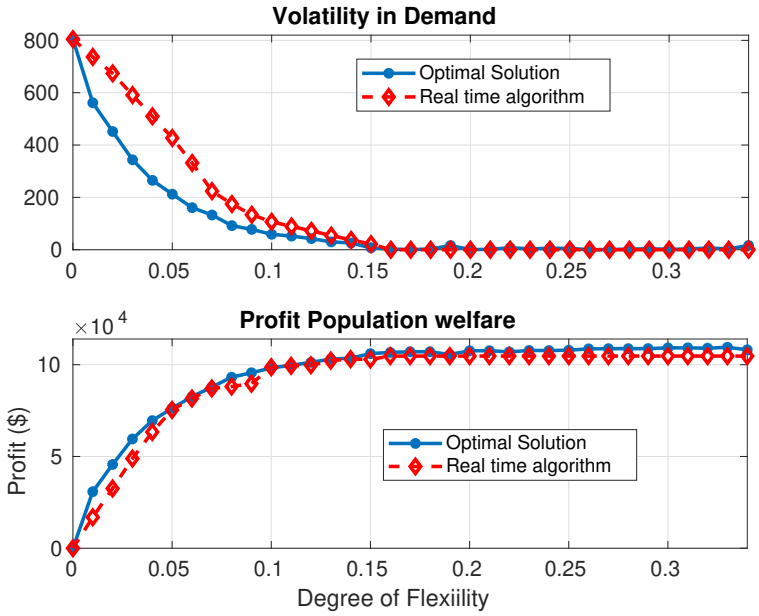

Figure 10.3: Demand volatility and consumer profit with x

services for achieving load balancing in the power network. It is evident from the figure that cumulative ramp up and down capacity required are negatively correlated with fraction of flexibility. This implies increase in consumers flexibility lowers required ancillary services. We conduct a numerical experiment

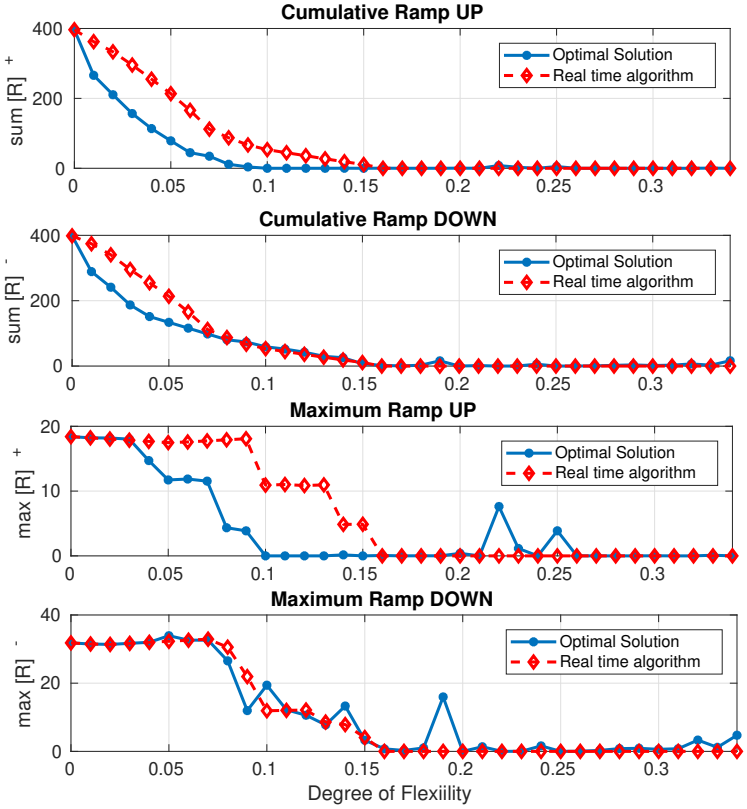

Figure 10.4: Ancillary Services needed with load flexibility

with two different user groups with different consumption profiles. Fig. 10.5 shows that the consumers with two user groups with different load profiles, `Load1` and `Load2`. The consumers with more volatility in demand have more incentive in having a higher degree of load flexibility, evident from the profit of these

user groups.

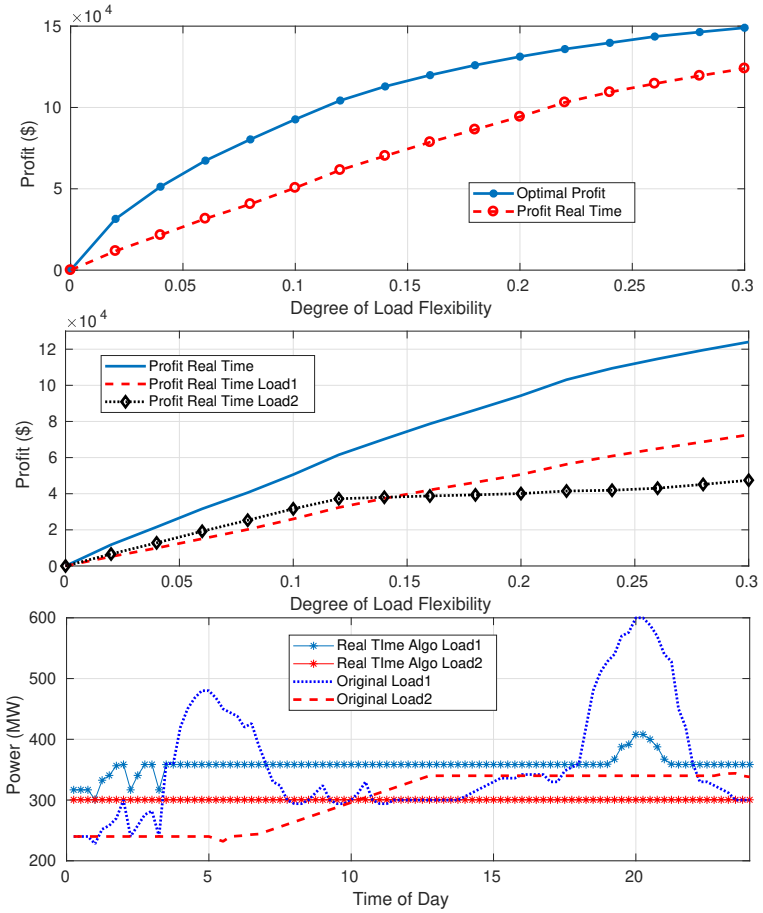

Figure 10.5: Consumer profit with Nominal Load Profiles

10.4.2 With RES Generation

The generation mix described in Section 4.1 is extended here. Let us assume 33.3% of total generation is solar generation (500 MW maximum capacity) and the cost of generation is $\$35/MWh$, equal to the cheapest controllable generator. We assume ±30% forecast error. The solar generation data is taken from Pecan Street [58] and normalized for our rated solar generation. The actual and forecasted values are related as $P_r(i) = \hat{P}_r(i)(1 + err)$, where err is an uniform random variable representing the forecast error at that time instant. We would like to highlight that the generation from RES has to be accommodated in total generation mix at all times.

Fig. 10.8 compares the performance of real time algorithm (Algo. 19) with respect to the optimal solution of the power network with 33% RES share and ±30% forecast error and increasing consumer responsiveness. Fig. 10.7 shows the mean, variance, maximum value and standard deviation of price with intermittent solar generation with variation of consumer load flexibility. Note that variance is much higher compared to Fig. 10.2. Fig. 10.8 shows the demand volatility and aggregate consumer profit with increase in consumer load flexibility. Fig. 10.9 shows the ancillary service requirement with increasing flexibility. It is interesting to note that the cumulative ramp up and down requirement is minimum for just 3% consumer load flexibility and it saturates at a higher level for any further increase in consumer load flexibility, which is still lower than the nominal required ancillary service for achieving load balancing. Fig. 10.10 shows the ancillary service requirement with increasing error in forecast. 100 simulations are conducted for 0%, 10%, 20%, 30%, 40% and 50% error in forecast with 20% load flexibility and 33.3% RES in the power network by capacity. It is evident that accuracy in the forecast of power generation by RES is essential to limit the ancillary services required, and as the forecast error increases the amount of ancillary services required will increase. Therefore, integration of RES will increase the load balancing needs of the power network. Thus, planning of increasing in RES share should duly consider load balancing aspect of the power system in order

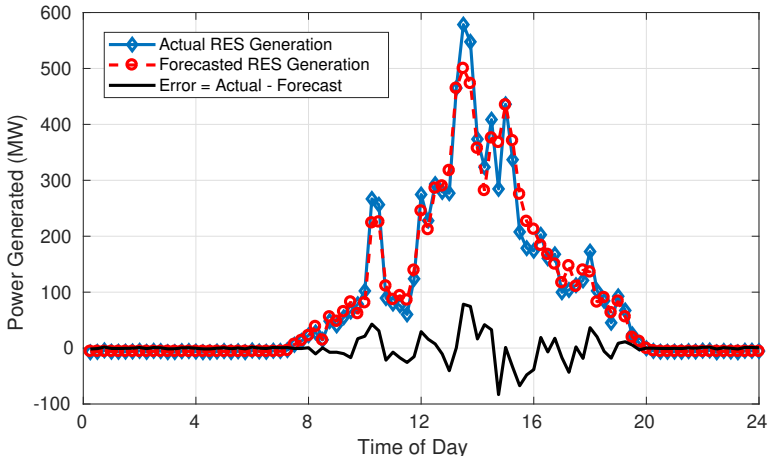

Figure 10.6: Solar Generation

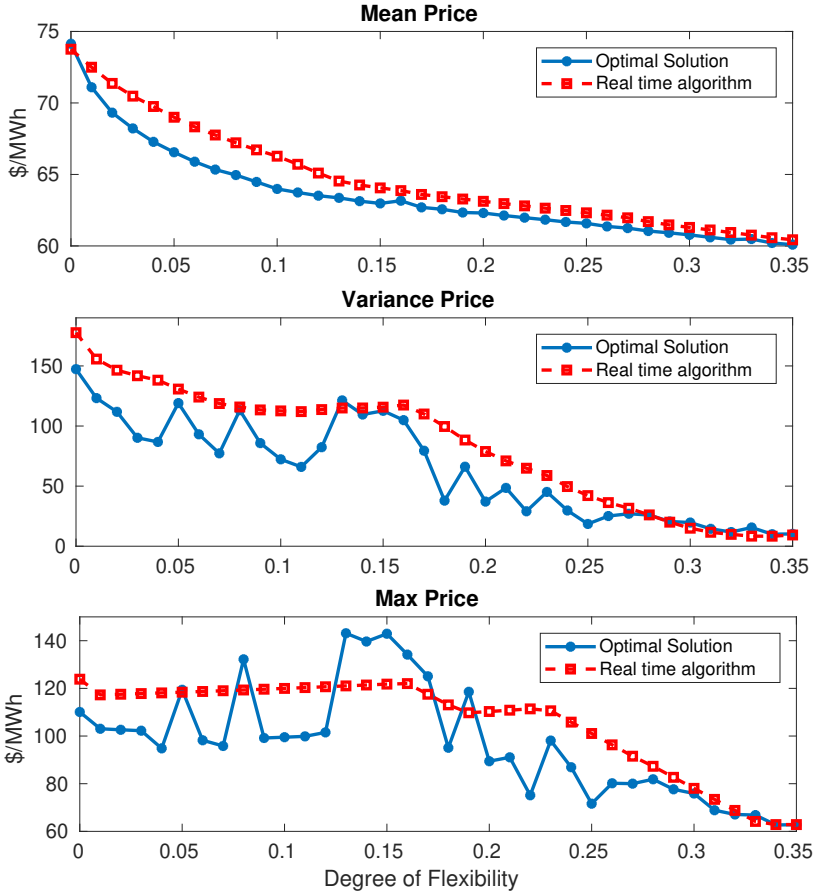

Figure 10.7: Indexes of price with respect to varying degrees of flexibility and in presence of 33.3% solar generation

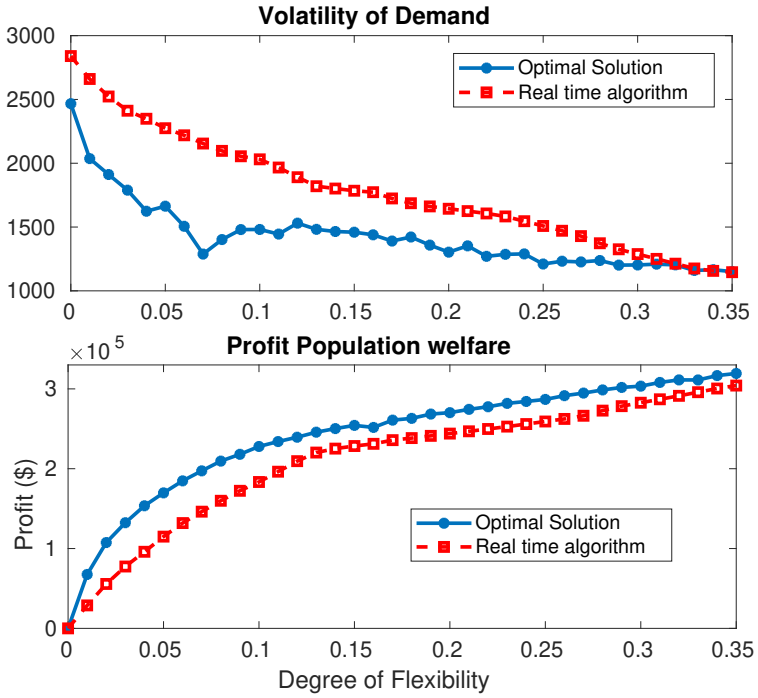

Figure 10.8: Demand Volatility and consumer profit with load flexibility with 33.3% solar and ±30% forecast error

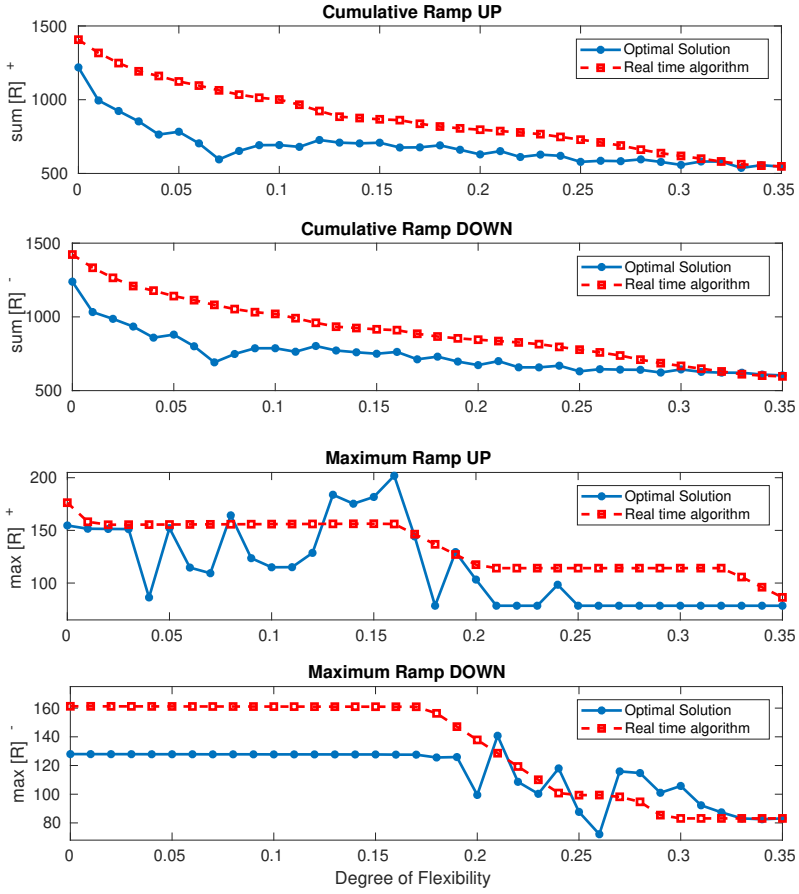

Figure 10.9: Ancillary Services needed with load flexibility with 33.3% solar

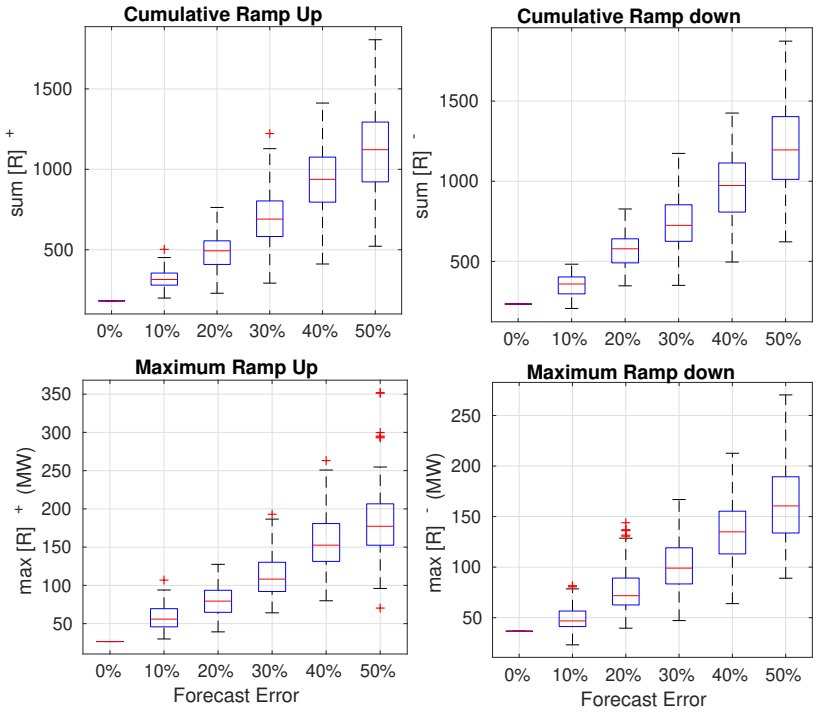

Figure 10.10: Size of ancillary services with forecast error

to ensure its reliable operation. Fig. 10.11 presents a sensitivity analysis of variation of renewable share and consumer flexibility on the ancillary service requirement, price and demand volatility and aggregate consumer profit. The forecast error for this result is fixed at ±30%. It is evident that prices become more volatile with increased share of renewable sources under the proposed price model. The increased volatility also provides an opportunity for users with load flexibility to increase their profit by responding to the price variations. The ancillary service requirement increases with increased share of renewables in the power network. The uncertainty in RES generation cannot be completely compensated with ex-ante price design. For 50% RES with ±30% forecast error, the cumulative ramp up reduced by ≈ 40%, the cumulative ramp down reduced by ≈ 44%, profit increased from 0 to 6.29e5, standard deviation of price reduced from 39.5 to 27.4 for the increase in load flexibility from 0 to 55%.

10.5 Conclusion and Perspectives

In this chapter, we propose an implementable real time electricity price design for a power system with a high proportion of the uncontrollable and highly variable RESs in the generation mix. Their highly variable nature requires rethinking of how current power systems are organized and operated. A part of the solution is the utilization of consumption flexibility. This requires a price design that incentivizes the consumers to alter their consumption in a way that meets the needs of the grid.

RTP design, considering information asymmetry, assists in lowering but not eliminating, price and demand volatility in presence of flexible loads, RES forecast errors and demand uncertainty. Therefore, commissioning of large scale RES should consider proportional expansion of the ancillary market for reliable operation of a power network by ensuring load balancing at all times. With an increased share of RESs and forecast error in the generation, the required ancillary services should proportionally increase to ensure power network reliability.

The observations made in this chapter raises the question of optimal resource sharing in real-time price market and ancillary service market. It needs to be identified that based on response time, degree of flexibility scheduling resources in which market can assist the grid the most. In this thesis we dealt with energy storage participating in the real-time electricity market in Chapter 3 to Chapter 9 and distributed/bulk storage participating in ancillary services in Chapter 11. Resource allocation is not dealt with in this thesis and would be a crucial question to answer as these resources are costly.

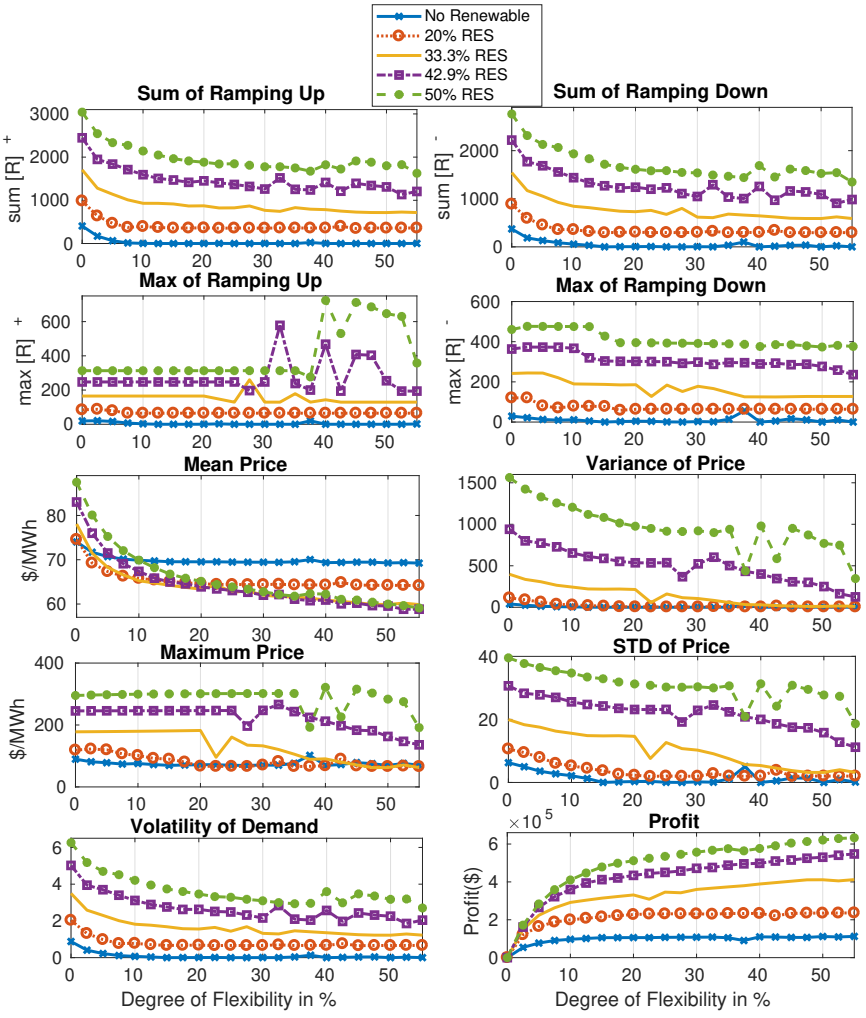

Figure 10.11: Effect of variation of consumer responsiveness and RES share in power network on price and demand volatility and ancillary service needs

Part III

Large-scale storage applications and Quality-of-Service of storage

Chapter 11

Control of a fleet of batteries

By failing to prepare, you are preparing to fail. - Benjamin Franklin

Summary: Battery storage is increasingly important for grid-level services such as frequency regulation, load following, and peak-shaving. The management of a large number of batteries presents a control challenge: How can we solve the apparently combinatorial problem of coordinating a large number of batteries with discrete, and possibly slow rates of charge/discharge? The control solution must respect battery constraints, and ensure that the aggregate power output tracks the desired grid-level signal.

A distributed stochastic control architecture is introduced as a potential solution. Extending prior research on distributed control of flexible loads [134], a randomized decision rule is defined for each battery of the same type. The power mode at each time-slot is a randomized function of the grid-signal and its internal state. The randomized decision rule is designed to maximize idle time of each battery, and keep the state-of-charge near its optimal level, while ensuring that the aggregate power output can be continuously controlled by a grid operator or aggregator. Numerical results show excellent tracking, and low stress to individual batteries.

11.1 Introduction

Future power grids will have greater volatility due to the higher percentage of weather dependent renewable energy sources connected to the grid. These sources are intermittent, and their power generation has sharp peaks and valleys. This makes load balancing and frequency regulation challenging.

Storage systems have enormous potential value for a range of services. Individual consumers can use storage to enable more effective use of residential solar power, or to reduce electricity costs in regions with time-of-use pricing. Battery energy storage systems (BESS) are increasingly important for grid-level services such as frequency regulation, load following, peak-shaving, and deferral of investment in transmission and generation resources [162].

The value of responsive regulation is now recognized and incentivized through FERC Order 755, issued in 2011. FERC 755 report [270, pages 23-24] contains a survey of experiments conducted by Beacon Power and Primus Power to determine the value of highly responsive resources for ancillary service. Primus claims that batteries provide approximately 76% more "area control error" (ACE) correction when compared with traditional service from generation.

Among the goals of the present chapter are:

- Address the apparent combinatorial problem of coordinating a large number of geographically distributed batteries to provide grid services.
- Ensure that each battery within the fleet does not violate local constraints, such as bounds on the state of charge (SoC).

One challenge is that the grid level signals exhibit ramps and volatility that may be beyond reach for any individual battery. Another is that many battery technologies exhibit strong asymmetry with respect to charging/discharging rates; this is particularly true for lithium-ion technology.

Whether the batteries are distributed across a region or in a central location, techniques are required to ensure that the fleet of batteries can perform desired grid services reliably and accurately, while respecting

the inherent constraints of individual batteries [212, 124, 200]. For most cell chemistries, the effective capacity of a battery is increased with slow discharge rates [215]. It is argued in [285] that the battery lifetime is reduced when discharge current is subject to high variance.

Distributed control is adopted so that the complexity of the control solution does not grow with the number of batteries. It is useful to employ randomization to introduce additional degrees of freedom for control. Each battery in the fleet is modeled as a controlled Markov chain, in which the controlled transition probabilities are common among each battery of the same type; this defines a local randomized control architecture. The randomized decision rule is designed to encourage idle time for each battery, and keep the state-of-charge near its optimal level, while ensuring that the aggregate power output can be continuously controlled by a grid operator or aggregator.

The aggregate behavior is approximated by a mean field model, which is a nonlinear input-output system, as in [233, 247]. This concept was brought to the power systems community in [237]. In numerical results it is found that linearized dynamics are nearly flat over a large bandwidth. An additional macro feedback loop is used to ensure accurate tracking; integral control is justified because of the simple aggregate dynamics.

It is found in numerical experiments that the goals can be achieved with this hierarchical control architecture: the aggregate of batteries accurately tracks the grid signal, and constraints on the battery SoC are strictly enforced. It is also found that individual batteries behave in a nearly deterministic manner – randomization leads to smooth input-output dynamics without causing "chattering" of individual batteries.

Related literature

The basic distributed control architecture developed in this chapter is based upon prior work on "demand dispatch" – the creation of virtual energy storage from flexible loads [247, 133, 134]. For loads whose power consumption cannot be varied continuously, a distributed randomized control architecture provides the needed degrees for freedom to track a smooth power reference signal, despite the discrete nature of each load. The use of randomization has been adopted in other work, such as [209, 241, 343]. A significant difference is the design approach: it is argued here and in prior research that with appropriate local control at the load or individual battery, the aggregate of resources will appear to the grid operator as an input-output system that is easily controlled. Local control also ensures that strict bounds on quality of service to the load are maintained.

While there are many papers on BESS, we are not aware of any work with a comparable distributed control architecture, or comparable results. The prior work [121, 233] considers low-frequency services such as "valley filling", based on BESS in which each battery is a residential electric vehicle. There are many recent papers on managing generation along with grid level storage, such as [96, 276].

The recent work [200] surveys mathematical models for estimating the cost of running LiIon batteries, emphasizing the importance of maintaining the SoC near its optimal level. This chapter and [333] focus on control loops to regulate the SoC level, and the latter focuses on estimating potential revenue from BESS in typical ancillary service markets. Reference [243] considers a nonlinear model for a single battery, and compares control techniques to address the conflicting goals of managing SoC and tracking a regulation signal. These papers provided part of the motivation for the present work in this chapter.

While the setting is entirely different, [285] provides insights and control techniques for managing batteries in portable electronic devices. An MDP (Markov Decision Process) model is proposed to obtain good performance for the device, while ensuring that the battery is not subject to stress. It is claimed that the battery control system will extend the battery service lifetime by more than 20%. It is not clear if the methodology of [285] can be extended to grid applications.

This chapter is divided into four sections. Section 11.2 provides the distributed control design, nominal battery model, controlled Markov model of an individual battery and the mean field model for aggregate behavior of the fleet. Section 11.3 provides the numerical results for different battery models tracking PJM RegD signal with efficiency losses. Section 11.4 concludes the chapter and provides some perspectives on the topic.

11.2 Distributed control design

Consider a large collection of batteries, potentially distributed across a large geographical region within a single balancing authority (BA). In numerical experiments we will consider data from PJM; the largest BA in the U.S. [75]. A BA maintains supply-demand balancing within its operating region by regulating

frequency to its nominal value (60 Hz in the U.S.), and regulating power flow between adjacent BAs. This requires resources to provide ancillary services – traditionally, power output from generators is ramped up and down to track a signal broadcast from the BA. At PJM, for frequency regulation there are two signals: RegA and RegD. The latter is distinguished by its higher frequency content, and it is also conditioned so that it is approximately zero energy over long time-horizons. Fig. 11.1 shows the cumulative sum of the RegD signal over a typical day in 2015. While the sum eventually returns to zero, on this day it took a long positive excursion before returning to zero at midnight.

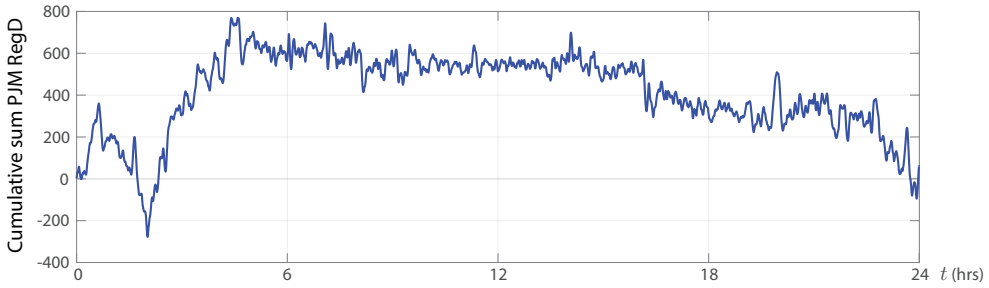

Figure 11.1: Cumulative sum of PJM RegD – data from January 4, 2015.

The distributed control approach of [247, 115] is based on a Markovian nominal model for an individual resource (flexible loads in these papers). The main difficulty of extending this approach to batteries is that the nominal behavior for batteries is highly deterministic: if there is no need for storage, the batteries should stay idle at the mid-range SoC value. This will extend battery life, and also ensure that there is ancillary service capacity in each direction (both charging and discharging). The first step in this proposed design is to construct a stochastic nominal model that is close to this deterministic nominal behavior.

11.2.1 Nominal model design

Fig. 11.2 illustrates the overall control architecture in which design is based on two components: there is a local decision rule at each battery based on a common signal $\{\zeta_t\}$ that is broadcast to all batteries. Error feedback based on the regulation signal $\{r_t\}$ and measurements of aggregate power is used to ensure accurate tracking.

Time is discrete with time steps of h seconds. In the next section, for PJM RegD signal tracking we will use $h = 2$ seconds. We assume that an individual battery can be in three different modes of operation: charging, discharging and idle. The state of a battery has two components, the mode and the state of charge (SoC):

$$x = (m, s),$$

where $m \in \{\text{ch}, \text{dis}, \text{id}\}$ and $s \in [0, 1]$, with 1 corresponding to a fully charged battery.

While a battery is in a charging mode ($m = \text{ch}$), it is charging with a constant rate denoted δ_{ch}. Its new state after h seconds is $(\text{ch}, s + h\delta_{\text{ch}})$. Similarly, if a battery is discharging, then its new state after h seconds is $(\text{dis}, s - h\delta_{\text{dis}})$. A battery that is idle does not change its SoC, so the new state after h seconds is (id, s).

We describe next the change of mode of operation of a battery. Denote by $p_{\text{ch}}, p_{\text{dis}}, p_{\text{id}} : [0, 1] \to [0, 1]$ the functions that model the probability to stay in the charging, discharging or idle mode respectively. Bounds on SoC impose the constraint $p_{\text{ch}}(s) = 0$, for all $s > 1 - h\delta_{\text{ch}}$ and $p_{\text{dis}}(s) = 0$ for all $s < h\delta_{\text{dis}}$.

In a state (m, s), a first decision (first coin flip) is made to decide if there is a change of mode of the battery. If so then the second decision is made to decide which of the remaining two modes the battery is

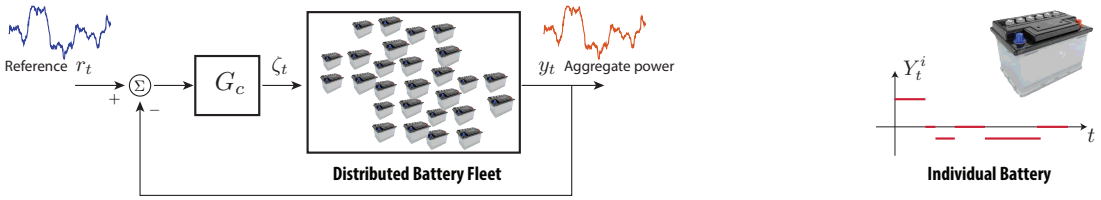

Figure 11.2: BESS control architecture: Local control at each battery combined with error feedback based on aggregate power is used to track the regulation signal. The power output of an individual battery Y_t^i takes on a finite number of values.

going to switch to. This choice is done with the probabilities proportional to the values of the p functions of the remaining two modes.

As an example, suppose the current state is $x = (\text{ch}, s)$. The new state, after h seconds is then:

$$\begin{array}{lll} x^+ := (\text{ch}, s + h\delta_{\text{ch}}), & \text{with probability} & p_0^+(x) \\ x^0 := (\text{id}, s), & \text{with probability} & p_0^0(x) \\ x^- := (\text{dis}, s - h\delta_{\text{dis}}), & \text{with probability} & p_0^-(x) \end{array} \tag{11.2.1}$$

where $p_0^+(x) = p_{\text{ch}}(s)$,

$$p_0^0(x) = (1 - p_{\text{ch}}(s)) \frac{p_{\text{id}}(s)}{p_{\text{id}}(s) + p_{\text{dis}}(s)}$$

$$\textit{and} \quad p_0^-(x) = (1 - p_{\text{ch}}(s)) \frac{p_{\text{dis}}(s)}{p_{\text{id}}(s) + p_{\text{dis}}(s)}$$

The design of $p_{\text{ch}}, p_{\text{dis}}, p_{\text{id}}$ used in the numerical results of this chapter is given in Fig. 11.3. In this design, the target SoC interval was set to 40 - 80% SoC. If the battery is charging, it will remain charging with probability almost 1 until it reaches 40% SoC. The probability to keep charging then decreases and reaches almost 0 at 80% SoC. The design of p_{dis} is symmetrical. The function p_{id} has values almost 1 for 50-70% SoC values and it is almost 0 outside the target interval.

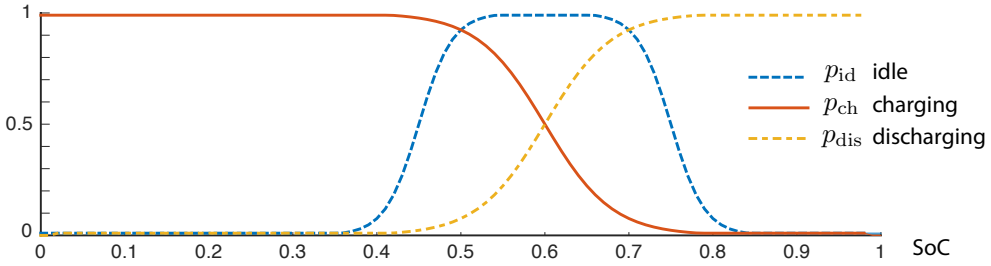

Figure 11.3: Design of switching probability functions $p_{\text{ch}}, p_{\text{dis}}, p_{\text{id}}$.

The nominal Markov model for an individual battery is then given by a transition kernel P_0. Its state space X is the union of three intervals; let $\mathcal{B}$ denotes its Borel sigma field. For any state x, the probability measure $P_0(x, \cdot)$ is supported on at most three states. From (11.2.1) we see that for the state $x = (\text{ch}, s)$, and for any $A \in \mathcal{B}$, $P_0(x, A) =$

$$p^+(x)\mathbb{I}\{x^+ \in A\} + p^0(x)\mathbb{I}\{x^0 \in A\} + p^-(x)\mathbb{I}\{x^- \in A\}$$

11.2.2 Controlled Markov model for an individual battery

Based on this nominal model, a controlled Markov model for an individual battery can be obtained following similar steps as in [115]. The main difference is that the proposed model evolves on a continuous state space compared to the discrete state space design in this previous work.

Let $\mathcal{U}(x)$ denote the power output at state x; it is assumed that this takes on just three values: $\mathcal{U}(x) = 0$ for $x = (\text{id}, s)$, and the remaining values are consistent with the Markov model:

$$\frac{|\mathcal{U}(\text{ch}, s)|}{\mathcal{U}(\text{dis}, s)} = \frac{\delta_{\text{ch}}}{\delta_{\text{dis}}}, \quad 0 \le s \le 1.$$

For any fixed value of ζ, the probability measure $P_\zeta(x, \cdot)$ is also supported on at most three states. For the family of transition matrices, the three states (x^+, x^0, x^-) depend on x but not on ζ: $P_\zeta(x, A) = p_\zeta^+(x)\mathbb{I}\{x^+ \in A\} + p_\zeta^0(x)\mathbb{I}\{x^0 \in A\} + p_\zeta^-(x)\mathbb{I}\{x^- \in A\}, \quad x \in \mathsf{X}, \ A \in \mathcal{B}$.

The values of $p_\zeta^+(x)$, $p_\zeta^0(x)$ and $p_\zeta^-(x)$ are set as follows:

$$\begin{aligned} p_\zeta^+(x) &= p_0^+(x) \exp\big(\zeta \mathcal{U}(x^+) - \Lambda_\zeta(x)\big) \\ p_\zeta^0(x) &= p_0^0(x) \exp\big(\zeta \mathcal{U}(x^0) - \Lambda_\zeta(x)\big) \\ p_\zeta^-(x) &= p_0^-(x) \exp\big(\zeta \mathcal{U}(x^-) - \Lambda_\zeta(x)\big) \end{aligned} \tag{11.2.2}$$

with $\Lambda_\zeta(x) = \log\Big(\sum_{m \in \{-,0,+\}} p_0^m(x) \exp\big(\zeta \mathcal{U}(x^k)\big)\Big)$.

This is similar to the *myopic design* introduced in [240]. It can be interpreted as an instance of the optimal design introduced in [247], but with a time-horizon of *one* rather than infinite. This transformation of the nominal model will encourage discharge when $\zeta > 0$, and charging when $\zeta < 0$.

11.2.3 Mean Field Model

The family of transition kernels $\{P_\zeta : \zeta \in \mathbb{R}\}$ is constructed to define local decision making: Each battery evolves as a controlled Markov chain on a finite state space, with common input $\zeta = (\zeta_{\mathbf{0}}, \zeta_{\mathbf{1}}, \dots)$. It is assumed that the scalar signal ζ is broadcast to each battery. If a battery is in state x at time t, and the value ζ_t is broadcast, then the battery transitions to the state x' according to the probability measure $P_{\zeta_t}(x, \cdot)$.

Let $X_t^i = (M_t^i, S_t^i)$ denote the state of the ith battery at time t. The dynamics of the first component are governed by the randomized policy; the second component denotes SoC, which evolves as a controlled random walk:

$$\begin{aligned} S_{t+1}^i &= S_t^i + h\delta_{\text{ch}} && \text{charge mode, } M_t^i = 1 \\ S_{t+1}^i &= S_t^i - h\delta_{\text{dis}} && \text{discharge mode, } M_t^i = -1 \\ S_{t+1}^i &= S_t^i && \text{idle, } M_t^i = 0 \end{aligned} \tag{11.2.3}$$

The empirical probability measure is defined as the average,

$$\mu_t^N(A) = \frac{1}{N}\sum_{i=1}^N \mathbb{I}\{X_t^i \in A\}, \qquad A \in \mathcal{B}.$$

As in prior work for the discrete state space [247, 133, 115], we assume that average power output is obtained through measurements or state estimation. At time t, this is expressed in terms of the empirical probability measure:

$$y_t^N = \frac{1}{N}\sum_{i=1}^N Y_t^i = \int \mathcal{U}(x)\mu_t^N(dx), \qquad t \ge 0,\ x \in \mathsf{X},$$

where $Y_t^i = \mathcal{U}(X_t^i)$ as shown in Fig. 11.2.

The mean field model is defined by the recursion

$$\mu_{t+1}(A) = \int P_{\zeta_t}(x, A)\, \mu_t(dx) \tag{11.2.4}$$

Under general conditions on the model and on μ_0 it can be shown that μ_t^N is approximated by μ_t. One condition is that the input ζ_t is a continuous function of $(y_0^N, \dots, y_{t-1}^N, \dots)$ that depends upon t, but does not depend upon N.

Under these conditions, the average power output is approximated using the mean-field model:

$$y_t = \int \mathcal{U}(x)\mu_t(dx), \quad t \ge 0. \tag{11.2.5}$$

In prior work on demand dispatch it is found that although the input-output mean field dynamics are nonlinear, the dynamics are accurately approximated by a linear model, and often the linearized dynamics are minimum phase [247]. Desirable aggregate behavior can also be obtained through design [115, 240].

11.3 Numerical results

The following three scenarios were considered, differentiated by their time-to-charge T_{ch}, time-to-discharge T_{dis}, and power ratings:

Scenario	T_{ch}	$\mathcal{U}(\text{ch}, s)$	T_{dis}	$\mathcal{U}(\text{dis}, s)$
S1:	2hr	-0.5kW	2hr	0.5kW
A1:	2hr	-0.5kW	1hr	1kW
A2:	2hr	-0.5kW	30min	2kW

(11.3.1)

In each case, a collection of 1,000 batteries can deliver at most 500kW of power. In the symmetric model the lower limit is -500kW. The regulation signal was scaled to respect these constraints.

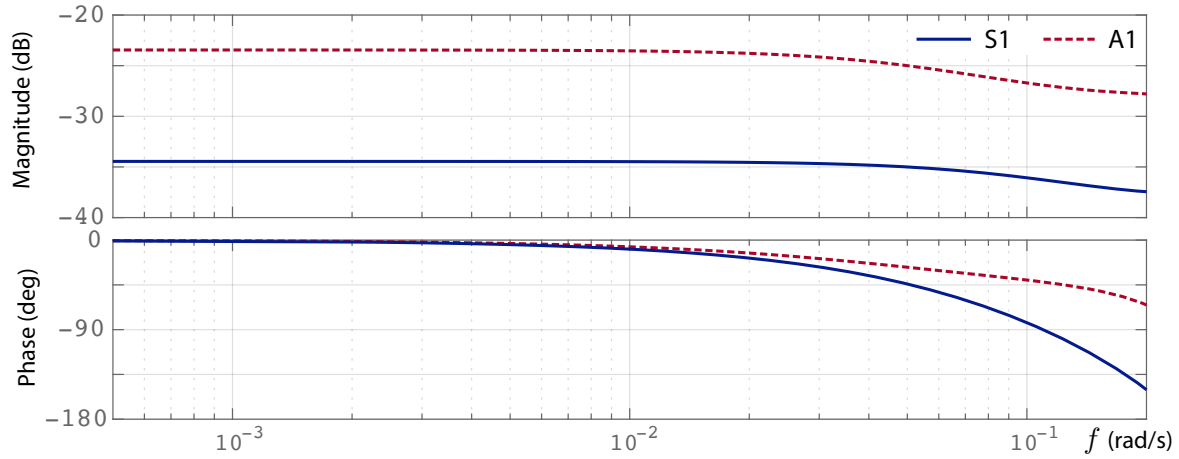

Figure 11.4: Bode plots for linear models obtained using Least Squares.

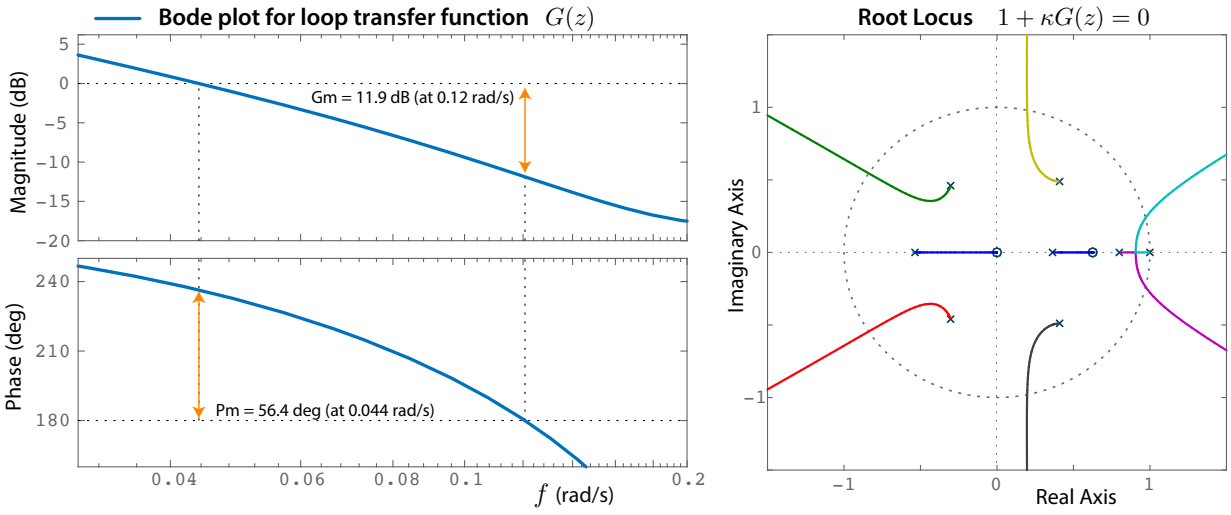

Figure 11.5: Bode plot, margins and root locus for the loop transfer function.

In each of these three scenarios, a linear approximation of the input-output dynamics was obtained using Least Squares. A seventh order model was sufficient in all cases.

Fig. 11.4 shows the Bode plots obtained for models S1 and A1. In each case, the magnitude plot is nearly constant over the frequency range of interest, $f \in [10^{-4}, 5 \times 10^{-2}]$.

While the magnitude plots are nearly perfectly flat, the true dynamics are only approximately linear. To achieve accurate tracking we introduce error feedback, with input ζ_t, error $e_t = r_t - y_t^N$, and "plant transfer function" G_p: the linear model for input-output dynamics.

Consider the symmetric model S1 for which the Bode plot of G_p is shown in Fig. 11.4. Design of the compensator G_c is simplest in continuous time. The loop transfer function is the product $G = G_c G_p$, and the compensator G_c is constructed so that it has high gain at low frequencies, and the crossover frequency f_c is chosen at the desired closed-loop bandwidth. Since by definition $|G(jf_c)|_{dB} = 0$, a glance at Fig. 11.4 implies that $|G_c(jf_c)|_{dB} \approx 35$ if $f_c \in [10^{-4}, 5 \times 10^{-2}]$.

The flat magnitude plot for G_p motivates the use of pure integral control, $G_c(s) = K_I^\circ s^{-1}$, with $K_I^\circ = 50 f_c$ (using $|50|_{dB} \approx 35$). This is implemented in discrete time:

$$\zeta_t = K_I \sum_{i=0}^{t} e_i \,, \qquad K_I = h K_I^\circ \tag{11.3.2}$$

where $h = 2$ is the sampling time in seconds.

On choosing $f_c = 5 \times 10^{-2}$ we obtain $K_I^\circ = 250 \times 10^{-2}$, and hence $K_I = 5$. Fig. 11.5 shows a Bode plot of the loop transfer function with this design (represented in continuous time), along with the root locus plot for the discrete-time loop transfer function.

11.3.1 Tracking and SoC Performance

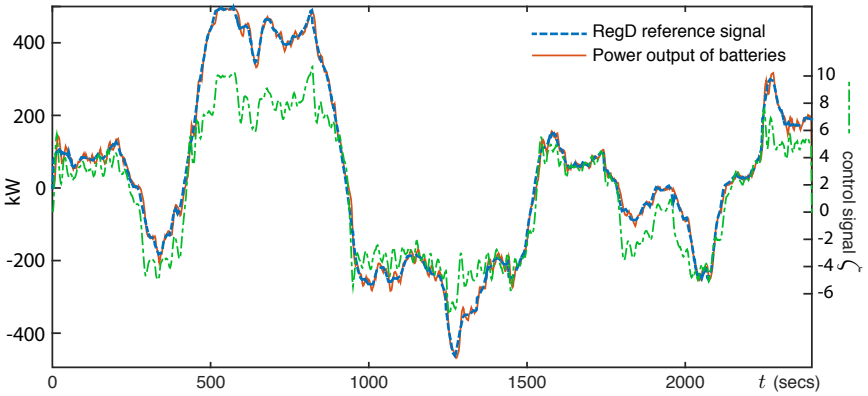

Figure 11.6: Tracking of PJM's RegD Normalized Signal Test in Scenario S1 with 1000 batteries. Also shown is the control signal (11.3.2).

All experiments use PJM's Normalized Signal Test for RegD to define the reference signal $\{r_t\}$ [75]. The initial condition for each battery was at rest, with SoC at 50%. The impact on the initial condition was insignificant in these and other experiments.

Consider first the symmetric model, Scenario S1, in which each battery requires 2hr to fully charge (resp. discharge), and draws 0.5 kW when charging. The tracking results and control signal obtained using the integral gain $K_I = 5$ are displayed in Fig. 11.6.

It is found that an individual battery operates in a nearly deterministic manner, and the SoC is maintained to the desired limits, even though the local control is randomized. The plots marked "$\eta = 1.0$" in Fig. 11.7 show a comparison of the mean SoC and the evolution of SoC for an individual battery. All goals have been achieved: grid level tracking is nearly perfect, and battery constraints are maintained.

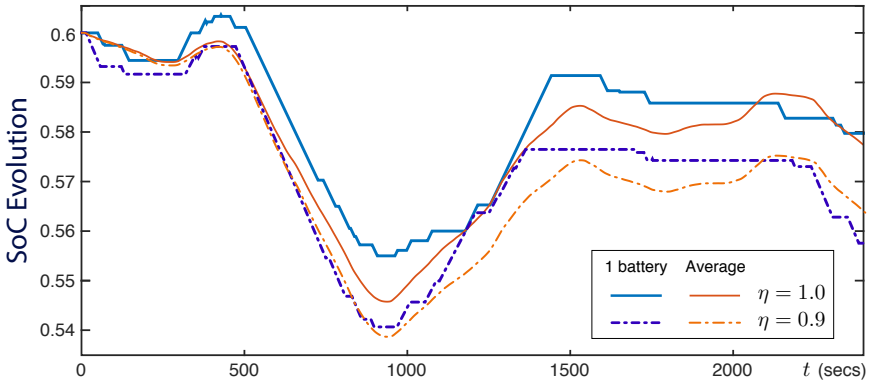

Figure 11.7: Evolution of SoC for the symmetric model.

Tracking results obtained with only 200 batteries are shown in Fig. 11.8. There is some extra high-frequency error due to quantization, but the performance is well within the requirements of PJM.

The PI design was repeated in the two asymmetric models. Tracking is more challenging in these cases. This is true in part because there is a capacity reduction associated with asymmetry. It is also found that nonlinear effects are more apparent in asymmetric models.

Results for the asymmetric case A2 are displayed in Fig. 11.9. It is clear that the true system is nonlinear: when the regulation signal is large and positive, the closed loop system appears to be under-damped (oscillation is observed). When the regulation signal is negative then the closed loop system appears over-damped. Similar but less extreme results were observed in the case A1.

11.3.2 Impact of efficiency loss

In the preceding experiments efficiency losses have been ignored. For example, the round trip efficiency of Tesla's Powerwall is just 92.5%. A linear model was used to test the impact of efficiency losses. For an efficiency parameter $\eta_{\mathbf{ch}}, \eta_{\mathbf{dis}} \in (0, 1]$, the evolution of the state of charge of battery i is given by

$$\begin{aligned} S^i_{t+1} &= S^i_t + \eta_{\mathbf{ch}} \times h\delta_{\text{ch}} \quad \text{charge mode, } M^i_t = 1 \\ S^i_{t+1} &= S^i_t - h\delta_{\text{dis}}/\eta_{\mathbf{dis}} \quad \text{discharge mode, } M^i_t = -1 \end{aligned} \tag{11.3.3}$$

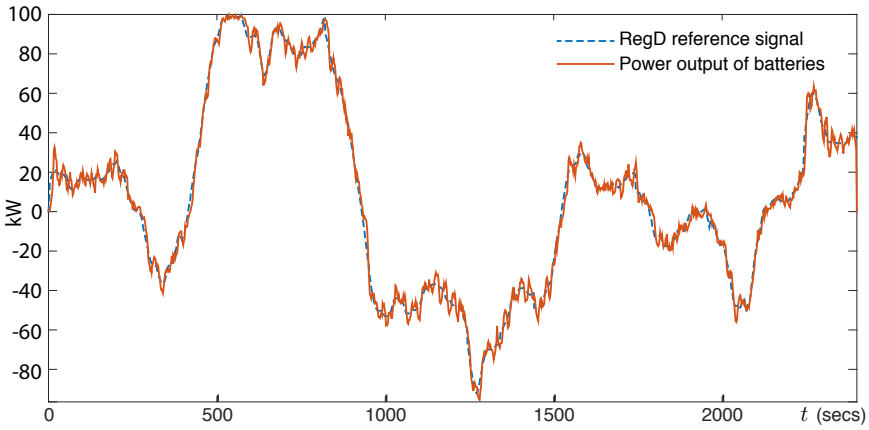

Figure 11.8: Tracking of PJM's RegD Normalized Signal Test in Scenario S1 with *only 200 batteries*.

The power output of the battery remains the same: $Y_t^i = \mathcal{U}(X_t^i)$ for each t and i.

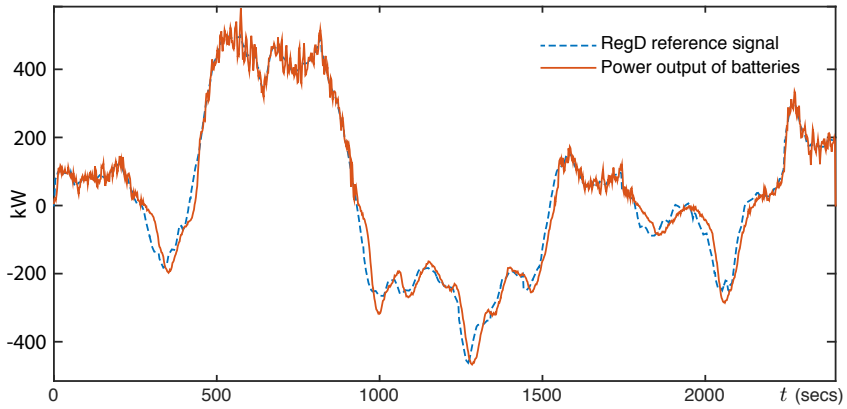

Figure 11.9: Tracking of PJM's RegD Normalized Signal Test in Scenario A2.

In the results described below we take $\eta = 0.9$. For the 40 minute PJM test signal, this loss presents no impact on tracking performance. There is an observable negative drift in SoC over this time interval – typical results are shown in Fig. 11.7 in Scenario S1 with 1,000 batteries. The SoC at the end of the experiment is slightly smaller than observed with $\eta = 1$. This would be unacceptable on a 24 hour run: an additional feedback loop is required to draw additional power to make up for losses.

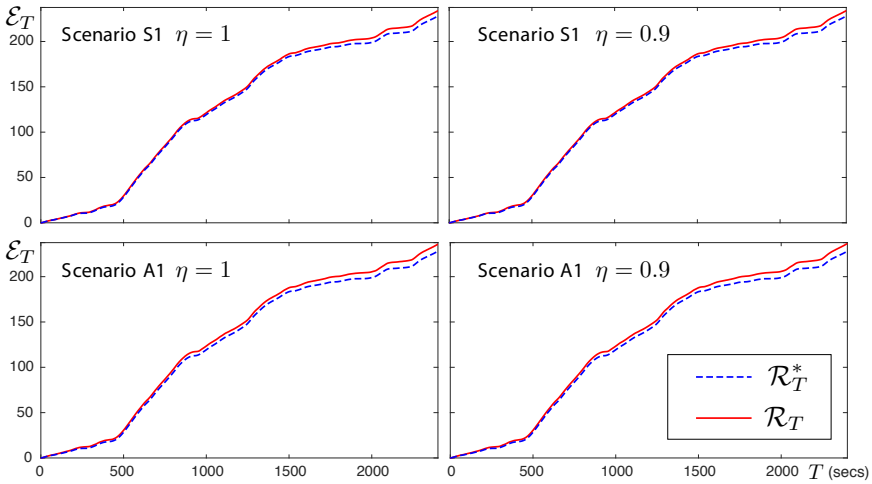

Figure 11.10: Mileage nearly reaches the ideal with and without losses. The error at the end of the run is under 3% in case S1.

Excess operation of the fleet of batteries was computed based on *mileage* – a traditional metric of service from batteries [270]. For an individual battery, the cumulative mileage by time T and its average

are defined by

$$\mathcal{R}_T^k = \sum_{t=1}^{T} |\mathcal{U}(X_t^k)|\,, \quad \mathcal{R}_T = \frac{1}{N}\sum_{k=1}^{N} \mathcal{R}_T^k \qquad T \geq 1\,. \tag{11.3.4}$$

The following sequence is regarded as a metric for *excess operation*:

$$\mathcal{E}_T = \frac{\mathcal{R}_T - \mathcal{R}_T^*}{\mathcal{R}_T^*}\,, \quad \text{where} \;\; \mathcal{R}_T^* = \frac{1}{T}\sum_{t=1}^{T} |r_t|$$

It can be shown using Jensen's inequality that $\mathcal{E}_T \geq 0$ in the ideal case of perfect tracking. We obtain $\mathcal{E}_T = 0$ if *each* battery tracks the reference exactly.

With $\mathcal{E}$ defined to be the final value at the end of the 40min PJM test signal, the following are typical values:

Scenario	$\mathcal{E}$, $\eta = 1$	$\mathcal{E}$, $\eta = 0.9$
S1	2.51%	2.54%
A1	3.30%	3.62%

with scenario data given in (11.3.1). The impact of losses is negligible in these experiments. In all cases, it is surprising to see only about 3% beyond the ideal mileage using a distributed randomized control strategy.

The evolution of mileage in these four cases is shown in Fig. 11.10. The close match with the ideal means that most batteries in the fleet are cooperating, in the sense that the sign of $\mathcal{U}(X_t^i)$ matches the sign of r_t, or is equal to zero, for the overwhelming majority of indices $i = 1, \dots, 1,000$.

11.4 Conclusions and Perspectives

It is remarkable that a fleet of 'dumb, slow batteries' can accurately track a grid level signal with much faster temporal characteristics, while maintaining individual SoC within desired bounds. We observe that for sampling time $h = 2$ seconds and $\min(T_{ch}, T_{dis}) \geq 1800$ seconds, the myopic control with no lookahead leads to less than 4% regret, implying near optimal solution. Note that $h << \min(T_{ch}, T_{dis})$.

There is of course much more work to be done on local control design, and control techniques for the aggregate. What is the best way to resolve the asymmetric behavior observed in Fig. 11.9? One approach is at the macro-level: gain scheduling could be used, in which the gain K_I is reduced when the regulation signal is positive, and increased when it is negative. An alternative is to refine the local control design to make the aggregate appear more linear, as in [240].

Further research is needed to investigate the heterogeneous setting (e.g. with respect to the capacity, charging and discharging rates), and the robustness to un-modelled dynamics (e.g. charging/discharging rates that depend on the current SoC level). Another direction concerns state estimation both for the aggregate power consumption used as a control feedback and state estimation for the local control.

Chapter 12

Drift Control for a Fleet of Batteries

A ship is always safe at shore but that is not what it's built for. - Albert Einstein

Summary: A distributed fleet of batteries participating in fast dynamic regulation should accurately track the regulation signal denoting the system imbalance and at the same time battery charge level is maintained which will ensure the battery can track the regulation signal sustainably without reaching minimum or maximum charge level. In such a case the battery cannot either ramp-up or ramp-down. We propose an additional drift compensation layer of control to the distributed stochastic control of a fleet of batteries proposed in Chapter 11, in order to maintain state-of-charge (SoC) of the battery in the optimal band of operation. The proposed control layers are redesigned using Linear Quadratic Regulator (LQR) which minimizes the input energy and tracking error for aggregate power and maintaining SoC. Further, gain scheduling is proposed for adaptive proportional gain for larger deviation of SoC from the desired level. Using numerical simulations we show that the addition of this layer of control does not deteriorate the ability of distributed fleet of batteries to perform fast dynamic regulation and it assists in the stable operation of batteries in presence of efficiency losses and non-zero mean regulation signal. We use PJM's performance evaluation metrics to show the efficacy of the proposed controller in presence of storage efficiency losses.

12.1 Introduction

Many believe that there will be a battery revolution over the next decade − energy storage systems will be distributed across the grid at residential homes, electric vehicles, data centres, etc. Resources such as pumped storages, small hydro plants, compressed gas, flywheels, aggregate load flexibility can act as virtual batteries. With increasing share of intermittent renewable energy sources connected to the grid, the need for fast ramping ancillary service will grow. In Chapter 11 we present a mechanism to control distributed fleet of batteries for providing ancillary services to the grid. The solution proposed in this chapter ensures that battery's quality-of-service (QoS) is met. The QoS of a battery in context of this chapter is defined considering two operational features of Li-ion based batteries. First, Li-ion should not be over-charged or over-discharged, which is ensured by the proposed nominal design of battery limiting the SoC level within the pre-decided optimal SoC band. Second aspect of QoS is achieved by limiting cycles of operation by maximizing idle time of the battery. It is essential to duly regulate energy storage cycle of operation as identified in [174]. Overusing the battery will reduce the operational life of the battery.

In this chapter, we redesign the control of the fleet of the batteries introduced in Chapter 11 with an additional control layer for ensuring that the mean SoC of the fleet of battery remains in the desired band. The proposed solution is scalable and require minimum communication infrastructure. The characteristics of the nominal model are the same as described in Chapter 11. Unlike flexible loads, the nominal design of batteries are not as natural, since nominal behavior of a battery is to stay idle. The battery in [114] is modeled as continuous time Markov chain with transition probabilities calculated based on centralized control signal. The proposed stochastic control tend to maximize idle time of batteries which will provide the time for battery capacity recovery. Minimizing the variance of discharge current profile of a battery leads to maximizing battery lifetime [286].

Authors in [150] consider a power system consisting of a high penetration of wind generation and storage systems for regulation of frequency. The feedback controller proposed maintains the SoC at the optimal operating point. Authors in [262] identify the importance of maintaining the SoC level close to 50%. A

grid-connected EV supplies a distributed spinning reserve according to the frequency deviation at the plug-in terminal, which is used as a signal of supply and demand imbalance in the power grid. The importance of maintaining SoC is identified in [195, 235, 227, 340, 137, 312]. Authors in [195] propose supervisory controller for AC/DC microgrid with objectives to maximize utilization of renewables, maintaining SoC of battery banks and managing power exchange. [235, 340] describe battery energy system with focus on control mechanism for SoC balancing of battery units. Authors in [227] proposed the control of EV batteries for performing frequency regulation while charging to the desired level. For battery in [137] the SoC needs to be maintained between 10% and 90% of the rated capacity. The battery controller in [312] ensures through local optimization that battery SoC is constant for plug-in-hybrid vehicle. Distributed stochastic control is used for controlling fleet of batteries and flexible loads having an error feedback based on the measurements or estimates of aggregate power and the local decision rule based on a common scalar signal that is broadcast to all the loads and/or batteries [135]. In order to ensure the longevity of a battery, the constraints on SoC, ramping and temperature should be respected by the controller.

12.1.1 Frequency Regulation in PJM

PJM, a balancing authority, is part of Eastern interconnection in the USA. Each balancing authority must comply with standards set by North American Electric Reliability Corporation (NERC). The "Real Power Balancing Control Performance" standard requires each balancing authority to control its area control error (ACE) within specified limits in terms of yearly averages and on minute-by-minute basis [3]. Frequency regulation is the tool to smooth out the real-time supply and demand imbalances, or ACE.

Due to fast ramping characteristics of batteries, a 2008 study by Pacific Northwest National Laboratory [236] suggests that 1 MW of fast-responding resources can provide the same regulation service as 1.7 MW of an average hydropower plant, 2.7 MW of an average combustion turbine, or 29 MW of an average steam turbine. The advantage of using batteries for fast response regulation is evident, due to the high precision in tracking [218]. However, energy storage devices have finite ability to absorb or inject power due to its finite capacity. In comparison, conventional power plants can be more flexible in adjusting its output, constrained by its starting/stopping time restricting their ramping ability. Thus, fast ramping resources performing dynamic regulation (complements traditional generation) if cannot sustain the output which accurately tracks the regulation signal for a long time then their performance advantage decreases. In order to use resources like batteries, *energy neutrality* is essential. Energy neutrality is defined as the case when cumulative energy input equals the cumulative output energy in a time window considered.

In 2011, FERC's Order 755 required grid operators to compensate frequency regulation providers, including new fast ramp-rate resources, according to their actual performance and technical ability to support the grid system. On October 1, 2012, with the purpose of incorporating accurate but energy-limited storage resources, PJM split the frequency regulation signal into two signals: slow-responding Regulation A (RegA) and fast-responding Regulation D (RegD). In the initial construction of this split-signal system, RegA was designed for resources "with the ability to sustain energy output for long periods of time, but with limited ramp rates," while RegD was designed for resources "with the ability to quickly adjust energy output, but with limited ability to sustain energy output for long periods of time" [218].

Using the study conducted by KEMA, PJM developed a valuation system to determine the optimal mix of RegA and RegD resources [17], the study simulates different combinations of RegA and RegD for achieving load balancing. It is observed that introducing RegD resources reduces the overall amount of regulation needed until a certain point, increasing RegD resources beyond leads to diminishing returns from using RegD. According to PJM, the reason that an excessive share of RegD resources can worsen the reliability as to maintain energy neutrality, sometimes the RegD control signal "moves in opposite control direction than desired by dispatch" [238]. The concepts of optimal mix and relative benefits are captured by the marginal benefits factor, which measures how well a RegD resource can substitute for RegA, while still satisfying the regulation requirement. The benefit factor for RegD is almost always greater than 1 and for RegA is always 1, making RegD tracking more beneficial for participants. In early 2015 PJM noticed that larger participation of RegD tracking makes it difficult to ensure its energy neutrality as sometimes the regulation signal was maintained by manually intervening to correct the fast regulation signal moving in the wrong direction [171]. To avoid larger participation of RegD, PJM implemented the following changes: (a) in December 2015, PJM deteriorated the benefit factor making RegD tracking less lucrative [261], (b) reduced the maximum amount of RegD resources to be procured from 62 to 40%, and (c) finally in early 2017 PJM re-engineered the frequency regulation signals to achieve "conditional neutrality" for RegD resources. The new RegA and RegD signals now work together so as energy neutrality is only supported for RegD resources when there are excess RegA resources available with extra capacity [218].

The conditionally neutral RegD signal makes the usage of batteries as regulation services very difficult. This is evident from the decline of front of the meter energy deployment which reduced from 51.4 MW in Q3 2015 to just 2.3 MW in Q3 2016. The non-zero mean regulation makes it essential for battery based dynamic regulation to maintain SoC tightly close to optimal level which would ensure sustained operation of batteries. Due to the above reasoning, the fleet of batteries needs to maintain their mean SoC close to the desired level which will ensure that the fleet has both ramp-up and ramp-down capability at all times. With this motivation, we propose a drift control layer along with accurate tracking feedback layer to ensure the SoC level do not drift drastically. We show through numerical results that inclusion of such a layer would not deteriorate the performance indices which measures the quality of regulation provided.

Regulation resources currently receive a two-part payment that consists of capability payment and performance payment, both of which are scaled according to the performance score, are shown below. Performance score is a measure the quality of regulation provided by a participant.

$$\begin{aligned}\text{Capacity Payment} &= \lambda^{\text{cap}} C^{\text{reg}} P_{\text{score}},\\ \text{Performance Payment} &= \lambda^{\text{perf}} C^{\text{reg}} R^{\text{mileage}} P_{\text{score}},\end{aligned}$$

where λ^{cap} is the regulation market capability clearing price, λ^{perf} is the regulation market performance clearing price, C^{reg} is the committed regulation capacity, R^{mileage} is the mileage ratio of RegD over RegA and P_{score} is the performance score calculated hourly. A good performance score is essential for maximizing gains for a participant in regulation market. The key contributions of this chapter are:

• *Drift compensation control layer*: due to tracking a non-zero mean regulation signal and/or losses in charging and discharging, the SoC of batteries can drift outside the optimal band. Thus a lower available capacity to either ramp up or ramp down. We redesign the proposed control in Chapter 11 with the inclusion of additional control layer compensating the mean SoC drift while ensuring good tracking.

• *Drift update at a lower time scale*: The drift compensation requires SoC measurement. We propose updating the drift layer at a much slower time scale at least for every half the charging or discharging time of the batteries.

• *Controller design*: We linearize the non-linear system model. Across this fixed point, the parameter fitting is formed using the least square method. The augmented state space model is used for identifying control gains which minimizes control energy and tracking error of aggregate power and SoC drift using LQR control design. Further, gain scheduling is performed which prioritizes maintaining state-of-charge for larger deviation of SoC from the desired levels.

• *Performance evaluation*: Using PJM's performance evaluation metrics, combination of accuracy, precision and delay scores for tracking, we show that distributed fleet of batteries can track faster temporal dynamic regulation signal in presence of efficiency losses (charging efficiency (η_{ch}) and discharging efficiency (η_{dis})) without deterioration in performance index.

A demand dispatch architecture is proposed in Chapter 11 where a geographically distributed fleet of batteries not only provides ancillary services to the grid but also takes into consideration the health of batteries by reducing the operational cycles (increases cycle life) and increasing idle time (increases calender life). Often life of a battery is defined as the combined effect of cycle and calender life, see Chapter 5. State space for an individual battery is again the Cartesian product: a particular state is denoted as $x = (m, s)$, where $m = \{\text{ch,dis,id}\}$ represents the mode of operation which could be either charging (m =ch), discharging (m=dis) or idle (m =id), and $s \in [0, 1]$ denotes the SoC. Normalized power delivery at state x depends on the mode of operation: $\mathcal{U}(\text{ch})=-1, \mathcal{U}(\text{id})=0, \mathcal{U}(\text{dis})=1$. We use the nominal battery model proposed in Chapter 11 Section 11.2.1.

This chapter is organized in six sections. Section 12.2 describes the drifting of SoC because of efficiency loss. Section 12.3 presents the controller design using linearization, LQR control and gain scheduling. Section 12.4 introduces the performance indices used by PJM for evaluating the dynamic tracking. Section 12.5 presents the numerical results and Section 12.6 concludes the chapter.

12.2 Drift compensation for a fleet of batteries

Batteries can act as generators momentarily, however, they have limited capacity and the charge level has to be replenished. Furthermore, batteries incur losses in charging, discharging and ac/dc and dc/ac conversion cycle, thus they consume finite amount of energy. This lost energy in cycling has to be compensated, ensuring the mean SoC of the fleet of batteries remain in the optimal band of operation.

For guaranteeing the objective achievement of providing dynamic regulation using batteries, as proposed in Chapter 11, the mean SoC of 'N' batteries should remain in optimal SoC band at all times. Mean SoC drifting to its boundaries will limit the capability of the fleet to either ramp up or ramp down thus constraining its ability to accurately track the regulation signal. The controller minimizes the error through feedback control. The feedback error e_t is given as $e_t = r_t - y_t^N$, where $r_t \in [-1, 1]$ is the regulation signal and $y_t^N \in [-1, 1]$ is the normalized aggregate behavior of the fleet at time t is

$$y_t^N = \frac{1}{N} \sum_{k=1}^{N} \mathcal{U}(X_t^k). \tag{12.2.1}$$

For a perfect feedback controller tracking will have the feedback error approximately equal to zero, $e_i \approx 0$. This would imply that the normalized response of all the participants will be equal to the regulation signal, i.e., $r_t \approx y_t^N$.

Definition: Perfect Controller In order to gauge the performance of control of distributed fleet of batteries, an index is introduced in Chapter 11 as the *excess operation* of the fleet of batteries was computed based on *mileage* [270]. The metric *excess operation* is defined as $\mathcal{E}_T = \frac{\mathcal{R}_T - \mathcal{R}_T^*}{\mathcal{R}_T^*}$, where $\mathcal{R}_T^* = \frac{1}{T}\sum_{t=1}^{T} |r_t|$. We obtain $\mathcal{E}_T = 0$ if *each* battery tracks the reference exactly, referred here as perfect controller. For a controller to be perfect the excess of operation is zero, given by following condition

$$\sum_{t=1}^{T} \{|r_t| - |y_t^N|\} = 0. \tag{12.2.2}$$

12.2.1 Lossless batteries with zero mean tracking signal

Let us consider an operational case where the batteries are lossless ($\eta_{ch} = \eta_{dis} = 1$) and the tracking signal is a zero mean regulation signal. This implies $\sum_{t=1}^{T} r_t = 0$, and the controller will force $\sum_{t=1}^{T} y_t^N = 0$. For lossless scenario the state change is given as

$$s_{t+1}^k = \begin{cases} s_t^k + h\delta_{ch}, & \text{if } M_t^k = 1, \text{ Charging} \\ s_t^k - h\delta_{dis}, & \text{if } M_t^k = -1, \text{ Discharging} \\ s_t^k, & \text{if } M_t^k = 0, \text{ Idle .} \end{cases}$$

In Eq. 12.2.1 the aggregate power output is calculated based on homogeneous population of batteries with each storage of unity capacity, therefore, the aggregate capacity of the fleet equals the total number of batteries in the fleet, i.e., N. The mean SoC of the fleet of battery is denoted as

$$y_t^B = \frac{\sum_{k=1}^{N} s_t^k}{\sum_{k=1}^{N} b_{\max}^k}, \tag{12.2.3}$$

where $b_{\max}^k$ denotes the maximum battery capacity of kth battery and $C_{\text{agg}} = \sum_{k=1}^{N} b_{\max}^k$ denotes the aggregated rated capacity of the fleet. Note that C_{agg} is a constant and $y_t^B \in [0, 1]$. C_{agg} equals N for homogeneous population of batteries with each storage of unity capacity, see Eq. 12.2.1. The tracking signal can be re-written for perfect tracking

$$\sum_{t=1}^{T} y_t^N = \frac{1}{C_{\text{agg}}} \sum_{t=1}^{T} \sum_{k=1}^{N} \mathcal{U}(X_t^k) = 0,$$

this implies that the amount charging and discharging cancels each other and is given as

$$\frac{1}{C_{\text{agg}}} \sum_{t=1}^{T} \sum_{k=1}^{N} \Big\{ - h\delta_{ch} \mathbb{1}(M_t^k = 1) + h\delta_{dis} \mathbb{1}(M_t^k = -1) \Big\} = 0.$$

This implies the total amount of charging energy supplied to the battery is equivalent to the amount of energy supplied by discharging for a zero mean regulation signal.

Proposition 1. *For a perfect controller tracking a zero mean regulation signal using lossless batteries, the mean SoC of the population at the end of tracking period will be equal to the mean SoC of the population at the beginning of tracking period.*

Proof: Lets assume the mean SoC of the population of batteries at the beginning of tracking time horizon is given as $y_0^B = \frac{1}{C_{\text{agg}}} \sum_{k=1}^{N} s_0^k$. The end SoC will be

$$y_{\text{end}}^B = y_0^B + \frac{1}{C_{\text{agg}}} \sum_{t=1}^{T} \sum_{k=1}^{N} \Big\{ h\delta_{ch} \mathbb{1}(M_t^k{=}1) - h\delta_{dis} \mathbb{1}(M_t^k{=}-1) \Big\}.$$

We know for a perfect controller tracking zero mean signal with lossless batteries

$$\frac{1}{C_{\text{agg}}} \sum_{t=1}^{T} \sum_{k=1}^{N} \Big\{ h\delta_{ch} \mathbb{1}(M_t^k = 1) - h\delta_{dis} \mathbb{1}(M_t^k = -1) \Big\} = 0.$$

Therefore, $y_{\text{end}}^B = y_0^B$. This shows that for an ideal controller for lossless batteries tracking a zero mean signal the mean SoC of the population will not drift at all from its initial value. □

12.2.2 Lossy batteries with zero mean tracking signal

The change of state of the battery is given as

$$s_{t+1}^k = \begin{cases} s_t^k + h\delta_{ch}\eta_{ch}, & \text{if } M_t^k = 1, \text{ Charging} \\ s_t^k - \frac{h\delta_{dis}}{\eta_{dis}}, & \text{if } M_t^k = -1, \text{ Discharging} \\ s_t^k, & \text{if } M_t^k = 0, \text{ Idle .} \end{cases}$$

for perfect tracking $e_t \approx 0 \implies r_t \approx y_t^N$. The tracking signal can be re-written for perfect tracking as

$$\sum_{t=1}^{T} y_t^N = \frac{1}{C_{\text{agg}}} \sum_{t=1}^{T} \sum_{k=1}^{N} \Big\{ -h\delta_{ch} \mathbb{1}(M_t^k{=}1) + h\delta_{dis} \mathbb{1}(M_t^k{=}-1) \Big\} = 0.$$

Proposition 2. *For a perfect controller tracking a zero mean regulation signal through lossy energy storage batteries, the mean SoC of the population at the end of tracking period will be strictly lower than the mean SoC of the population at the beginning of tracking period.*

Proof: The end SoC of the population is given as

$$y_{\text{end}}^B = y_0^B + \frac{1}{C_{\text{agg}}} \sum_{t=1}^{T} \sum_{k=1}^{N} \Big\{ h\delta_{ch}\eta_{ch} \mathbb{1}(M_t^k{=}1) - \frac{h\delta_{dis}}{\eta_{dis}} \mathbb{1}(M_t^k{=}-1) \Big\}.$$

Since the signal is zero mean we know for a perfect controller tracking zero mean signal with lossless batteries will satisfy

$$\sum_{t=1}^{T} \sum_{k=1}^{N} h\delta_{ch} \mathbb{1}(M_t^k = 1) = \sum_{t=1}^{T} \sum_{k=1}^{N} h\delta_{dis} \mathbb{1}(M_t^k = -1).$$

Substituting this in y_{end}^B we get

$$y_{\text{end}}^B = y_0^B + \frac{1}{C_{\text{agg}}} \sum_{t=1}^{T} \sum_{k=1}^{N} \Big\{ h\delta_{ch} \mathbb{1}(M_t^k = 1) \Big(\eta_{ch} - \frac{1}{\eta_{dis}} \Big) \Big\}.$$

We know that $0 < \eta_{ch}, \eta_{dis} < 1$, therefore $\left(\eta_{ch} - \frac{1}{\eta_{dis}} \right) < 0$ This implies $s_{\text{end}} < s_0$. □

Proposition 2 shows that the end SoC is strictly lower than the mean initial SoC of the population, for a fleet of batteries tracking a zero mean regulation signal in presence of efficiency losses. If the time horizon T is large (i.e. the positive/negative ramp is high) and/or η_{ch}, η_{dis} is low than end SoC, s_{end}, could go below lower boundary of optimal SoC band, in such a scenario we would not be able to guarantee the objective achievement of dynamic regulation using population of batteries.

12.2.3 Why drift compensation?

Batteries store energy for later usage. A battery that is fully charged cannot store any further energy, similarly a battery completely discharged can supply no further energy. In order to ensure that the batteries can ramp up and/or ramp down the charge level should be maintained somewhere around mid-SoC level of 50%. The mid-SoC can vary depending on lower SoC and upper SoC limits governed by storage technology. The target SoC is denoted as $y_{\text{tar}} = 0.5(y^u_{\text{opt}} - y^l_{\text{opt}})$, where y^u_{opt} is the upper boundary of optimal SoC band and y^l_{opt} is the lower boundary of optimal SoC band. We define the drift term for zero mean signal as

$$\tilde{y}^B_t = y^B_t - y_{\text{tar}}. \tag{12.2.4}$$

Clearly, as $\tilde{y}^B_t$ increases in magnitude the SoC drifts further away from the desired SoC level. This could happen because: (a) batteries incur losses as shown in Section 12.2.1 and 12.2.2, (b) the regulation signal is not zero mean and (c) for imperfect controller, i.e., $\mathcal{E}_T \neq 0$. All above mentioned cases are probable and therefore, SoC in real world will drift because of one or multiple of above mentioned causes.

How can we avoid a scenario where y^B_t goes outside the optimal SoC band? In order to ensure that the mean SoC of the population does not go beyond the optimal SoC band we add a drift compensation control layer is proposed in addition to regulation tracking layer.

What does it mean to control? How does it stabilize the operation of a fleet of batteries? This additional drift control layer replicates the greedy behavior (prioritizing SoC compensation) of population of batteries where in addition to providing dynamic regulation, the population of batteries tries to maintain their SoC close to the target SoC. This greedy behavior of batteries will deteriorate the performance indexes used to measure the quality of regulation. However, the question is how badly it deteriorates the performance scores. In the next section we will define the performance score indices used by PJM for evaluating the quality of dynamic regulation.

12.3 Drift Compensation Controller design

In the previous section, we described the need for compensating mean SoC of a fleet of batteries in the presence of a perfect controller, zero mean regulation signal and storage efficiency losses. Similar drift in SoC is anticipated for non-zero mean regulation signal and/or imperfect controller with $\mathcal{E}_T \neq 0$. The control loops with drift compensation is shown in Fig 12.1. There are two objectives for control design: (i) maintaining mean state-of-charge (SoC) of the fleet of batteries close to its target SoC level and (ii) track the regulation signal. These two objectives could be in conflict sometimes, in those cases both these objectives cannot be met simultaneously. Under such a case where tracking is not possible due to charge level of batteries, the battery may opt out and try to maintain the SoC level close to its target level. In PJM ISO, the regulation signal is designed to be conditionally neutral and provides storage owners to adjust SoC. However, storage control should duly consider maintaining SoC as in absence of such a control would severely undermine fleets ability to track regulation signal sustainably for longer period of time.

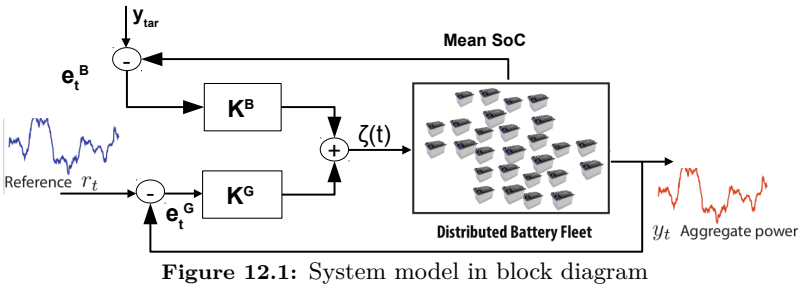

Figure 12.1: System model in block diagram

In the subsequent part of this section, we enumerate the steps for identifying suitable controller gains for the dual objective of accurate tracking and maintaining SoC. In Section 12.3.1 linearized system model of the nonlinear system is presented. In Section 12.3.2 least-square method is used for identifying the state matrices based on simulation data. For tractable state space analysis the discrete state model in transformed to continuous state space model in Section 12.3.3. The accumulated integral error is kept within bounds using a discount factor. In the absence of resetting integral error, the stability and performance of the control can be compromised. Section 12.3.4 presents the augmented state space matrices taking into account integral discount factors for the two control loops shown in Fig 12.1. Using the

augmented state space model LQR controller gains are obtained which minimizes the tracking error and the penalty on SoC deviation. This is presented in Section 12.3.5. For instances where SoC is farther away from the desired level, the controller in such cases should prioritize SoC compensation. This is achieved using the gain scheduling is presented in Section 12.3.6. Section 12.3.7 presents the LQR gain in form of controller gains to be used. A test simulation is performed using a swept sine as an input signal, showing the controller stability for the frequency range of interest. The input and output of this test simulation validate the efficacy of the proposed controller which assists in SoC recovery. The test simulation is presented in Section 12.3.8. The variables used are described in Table 12.1.

12.3.1 Linearized System Model

For nonlinear system such as the control of a fleet of batteries, zooming in close the fixed point(s)[1], the dynamics around those fixed point could be linearized. The state vector is defined as $S_t^T = [y_t^N, \tilde{y}_t^B]$. We linearize a nonlinear system across a fixed point $\bar{S}$ such that the derivative at fixed point is equal to zero, i.e., $\dot{\bar{S}} \approx 0$. We linearize our model across the nominal mean SoC equal to target SoC, implying $\tilde{y}_t^B \approx 0$. The control signal for this mean SoC value should be small enough so as the SoC deviation do not reaches to the point where such linearizations would not be valid. For the drift compensator model presented in Eq. 12.3.1 and Eq. 12.3.2 we linearize such that the aggregate power output is small and mean SoC is close to the target SoC. $-\alpha, -g, \beta$ denotes coefficients.

$$\begin{bmatrix} y_{t+1}^N \\ \tilde{y}_{t+1}^B \end{bmatrix} = \begin{bmatrix} -\alpha & 0 \\ -g & 1 \end{bmatrix} \begin{bmatrix} y_t^N \\ \tilde{y}_t^B \end{bmatrix} + \begin{bmatrix} \beta \\ 0 \end{bmatrix} \zeta_t + \begin{bmatrix} \text{Uncertainty in } \zeta_t \to y_t^N \text{ model} \\ \text{Uncertainty in } \zeta_t \to y_t^B \text{ model} \end{bmatrix} \tag{12.3.1}$$

$$\text{Output of System, } \begin{bmatrix} y_1 \\ y_2 \end{bmatrix} = \begin{bmatrix} 1 & 0 \\ 0 & 1 \end{bmatrix} \begin{bmatrix} y_t^N \\ \tilde{y}_t^B \end{bmatrix} + \begin{bmatrix} \text{Measurement noise in } y_t^N \text{ model} \\ \text{Measurement noise in } y_t^B \text{ model} \end{bmatrix} \tag{12.3.2}$$

Table 12.1: Variable Description

Variable	Description
y_t^N	Normalized aggregate power output
y_t^B	Normalized mean SoC (energy) level of fleet
$\tilde{y}_t^B$	Deviation of y_t^B from y_{tar}
y_{tar}	Target SoC level of the fleet
r_t	Regulation signal to be tracked by the fleet
ζ_t	Control Input fed to the fleet of batteries
K^B	Controller for tracking SoC deviation from y_{tar}
K^G	Controller for tracking regulation signal
K_r	LQR optimal gains
A_{augment}	Augmented state matrix A
B_{augment}	Augmented state matrix B
ρ_G	Discount factor for cumulative power deviation error
ρ_B	Discount factor for cumulative battery deviation error

12.3.2 Least Square Fitting

Fig 12.1 shows that the states used to calculate control signal ζ is based on (a) Power error $r_{t+1} - y_{t+1}^N$ and (b) SoC error $\tilde{y}_{t+1}^B$. We redefine our state space model given as Eq. 12.3.3.

$$\begin{bmatrix} r_{t+1} - y_{t+1}^N \\ \tilde{y}_{t+1}^B \end{bmatrix} = \begin{bmatrix} a_{11} & a_{12} \\ a_{21} & a_{22} \end{bmatrix} \begin{bmatrix} r_t - y_t^N \\ \tilde{y}_t^B \end{bmatrix} + \begin{bmatrix} b_1 \\ b_2 \end{bmatrix} \zeta_t \tag{12.3.3}$$

The unknown coefficients in Eq. 12.3.3 are defined as $\theta = [a_{11} \;\; a_{12} \;\; a_{21} \;\; a_{22} \;\; b_1 \;\; b_2]$.

$$\psi_1 = [(r_t - y_t^N) \;\; \tilde{y}_t^B \;\; 0 \;\; 0 \;\; \zeta_t \;\; 0], \qquad \psi_2 = [0 \;\; 0 \;\; (r_t - y_t^N) \;\; \tilde{y}_t^B \;\; 0 \;\; \zeta_t]. \tag{12.3.4}$$

[1] Operating points at which the nonlinear system provides steady states are called fixed points. Fixed points can be stable or unstable. For example, a pendulum has two fixed points one at zero degrees (stable) and another in an inverted position at 180 degrees (unstable).

The matrix ψ is denoted as the concatenation of ψ_1 and ψ_2 denoted as $\psi = [\psi_1; \quad \psi_2]$. The unknown coefficients of the state space model described in Eq. 12.3.3 is solved as shown in Eq. 12.3.5.

$$\theta_{\text{LS}} = (\psi^T\psi)^{-1}\psi^T \begin{bmatrix} r_{t+1} - y^N_{t+1} \\ \tilde{y}^B_{t+1} \end{bmatrix} \tag{12.3.5}$$

$$\begin{bmatrix} r_{t+1} - y^N_{t+1} \\ \tilde{y}^B_{t+1} \end{bmatrix} = \begin{bmatrix} \theta_{\text{LS}}(1) & \theta_{\text{LS}}(2) \\ \theta_{\text{LS}}(3) & \theta_{\text{LS}}(4) \end{bmatrix} \begin{bmatrix} r_t - y^N_t \\ \tilde{y}^B_t \end{bmatrix} + \begin{bmatrix} \theta_{\text{LS}}(5) \\ \theta_{\text{LS}}(6) \end{bmatrix} \zeta_t. \tag{12.3.6}$$

12.3.3 Discrete to Continuous Transformation

The control analysis is more intuitive in continuous time-domain. However, the system defined is discrete. The state space matrices are defined for continuous time domain as follows

$$S^D_{t+1} = A_{\text{discrete}} S^D_t + B\zeta_t,$$
$$\frac{S^D_{t+1} - S^D_t}{T_s} = \frac{A_{\text{discrete}} - I}{T_s} S^D_t + \frac{B}{T_s}\zeta_t,$$

Continuous state matrices for the system are given as $A_{\text{continuous}} = \frac{A_{\text{discrete}} - I}{T_s}$, $B_{\text{continuous}} = \frac{B}{T_s}$, denoted as

$$A_{\text{continuous}} = \frac{\begin{bmatrix} \theta_{\text{LS}}(1) - 1 & \theta_{\text{LS}}(2) \\ \theta_{\text{LS}}(3) & \theta_{\text{LS}}(4) - 1 \end{bmatrix}}{T_s}, \quad B_{\text{continuous}} = \frac{\begin{bmatrix} \theta_{\text{LS}}(5) \\ \theta_{\text{LS}}(6) \end{bmatrix}}{T_s}. \tag{12.3.7}$$

12.3.4 Augmented State Matrix

The cumulative integral gains for aggregate power and SoC deviation should be discounted for stable controller operation. Consider the discount factor for cumulative power deviation is denoted as ρ_G and the discount factor for cumulative SoC deviation is denoted as ρ_B.

$$A_{\text{lag}} = \begin{bmatrix} (\rho_G - 1)/T_s & 0 \\ 0 & (\rho_B - 1)/T_s \end{bmatrix}. \tag{12.3.8}$$

The augmented state matrices are denoted as

$$A_{\text{augment}} = \begin{bmatrix} A_{\text{continuous}} & 0 \\ C & A_{\text{lag}} \end{bmatrix}, \quad B_{\text{augment}} = \begin{bmatrix} B_{\text{continuous}} \\ 0 \\ 0 \end{bmatrix}, \tag{12.3.9}$$

The dimension of A_{augment} is 4x4, B_{augment} is 4x1 and C is 2x2.

12.3.5 Linear Quadratic Regulator Gain

The best suited controller gains which minimizes (a) input energy cost and (b) control energy cost is selected using Linear Quadratic Regulator (LQR). The details of LQR for different system models are summarized in Appendix A.10.

For system to be controllable $\mathcal{C}$ should be full rank matrix. The Matlab script for checking controllability is given as

```
>> C = ctrb(A_augment, B_augment)
>> Check = (rank(C) - size (A_augment) == 0)
```

If variable `Check` = 1 then then the system is controllable. For controllable systems the LQR eigenvalue placement can be achieved by following code:

```
>> K_r = lqr(A_augment, B_augment, Q, R)
```

here Q and R denotes the penalty for not meeting the desired states and input energy respectively.

Table 12.2: Controller parameters for test example in Section 12.3.8

Variable	Value
R	0.5
Q	$\begin{bmatrix} 1 & 0 & 0 & 0 \\ 0 & 1 & 0 & 0 \\ 0 & 0 & 1000 & 0 \\ 0 & 0 & 0 & 100 \end{bmatrix}$
C	$\begin{bmatrix} 1 & 0 \\ 0 & 1 \end{bmatrix}$
$\theta_{\text{LS}}(1)$	0.644644
$\theta_{\text{LS}}(2)$	0.370062
$\theta_{\text{LS}}(3)$	0.000428
$\theta_{\text{LS}}(4)$	1.001226
$\theta_{\text{LS}}(5)$	0.000358
$\theta_{\text{LS}}(6)$	-2.09904×10^{-05}
ρ_G	0.991
ρ_B	0.99
K_r	[-149.58 -6453.34 -17.80 -2.45]

12.3.6 Gain Scheduling

Define the proportional gain for the battery as

$$K_P^B(y_t^B) = K_P^B \tilde{y}_t^B. \tag{12.3.10}$$

$$K_P^B(\tilde{y}_t^B) = \lambda_1 \tilde{y}_t^B + \lambda_2 (\tilde{y}_t^B)^3. \tag{12.3.11}$$

$$\lambda_1 = \frac{d}{dy} K_P^B(0) = K_r^{\text{small}}(2), \qquad \frac{d}{dy} K_P^B(0.2) = K_r^{\text{big}}(2),$$

$$\lambda_2 = \frac{K_r^{\text{big}}(2) - K_r^{\text{small}}(2)}{3 \times (0.2)^2}$$

For the proportional battery gain K_P^B is made to vary depending on the SoC of the battery, depicted in Fig. 12.2.

$$Q_{big} = \begin{bmatrix} 1 & 0 & 0 & 0 \\ 0 & 10^8 & 0 & 0 \\ 0 & 0 & 1000 & 0 \\ 0 & 0 & 0 & 100 \end{bmatrix} \quad Q_{small} = \begin{bmatrix} 1 & 0 & 0 & 0 \\ 0 & 1 & 0 & 0 \\ 0 & 0 & 1000 & 0 \\ 0 & 0 & 0 & 100 \end{bmatrix}$$

We identify gains as $K_r^{\text{small}}(2) = -6453, \quad K_r^{\text{big}}(2) = -45284.$

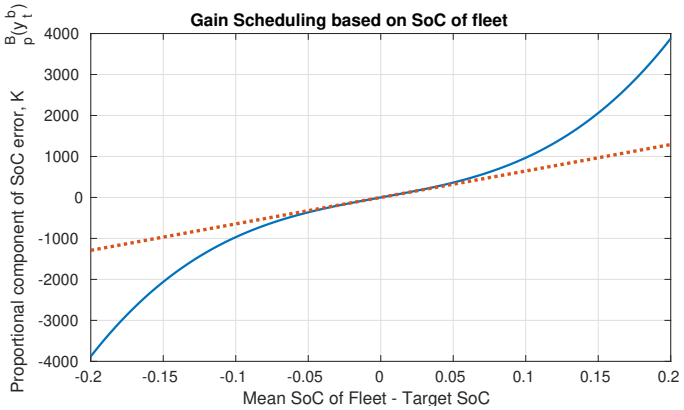

Figure 12.2: Proportional gain of SoC deviation from target levels based on the SoC

Table 12.3: LQR gain and controller gains

Controller Element	LQR matrix element
K_P^G	$= K_r(1)$
K_P^B	$= K_r(2)$
K_I^G	$= K_r(3)$
K_I^B	$= K_r(4)$

12.3.7 Optimal Controller Gain

$$\zeta_t = K_P^G(r_t - y_t^N) + K_P^B \tilde{y}_t^B + K_I^G \sum_{j=1}^{t} \rho_G \ (r_j - y_j^N) + K_I^B \sum_{j=1}^{t} \rho_B \ \tilde{y}_j^B \tag{12.3.12}$$

Table 12.4: Sign of controller gain

Parameter	Positive for discharge	Negative for charge
ζ	$\zeta > 0$ promotes discharging	$\zeta < 0$ promotes charging
$\text{err}_G = (r_t - y_t^N)$	$\text{err}_G > 0$ then battery should discharge	$\text{err}_G < 0$ then battery should charge
$\text{err}_B = \tilde{y}_t^B$	err_B increases then battery should discharge	err_B decrease then battery should charge

LQR provides $K_r = [K_p^G \quad K_p^B \quad K_i^G \quad K_i^B]$.

12.3.8 Test Simulation

The target SoC used for test simulations is set at 0.6 with the starting mean SoC of the fleet with 1000 batteries is equal to 0.5. The charging and discharging efficiency is set at 0.9. The simulation results for swept sine input signal and tracking performance is plotted in Fig. 12.3. Fig. 12.4 shows the mean SoC and cumulative sum of regulation signal. SoC recovery is visible from first plot of Fig. 12.4.

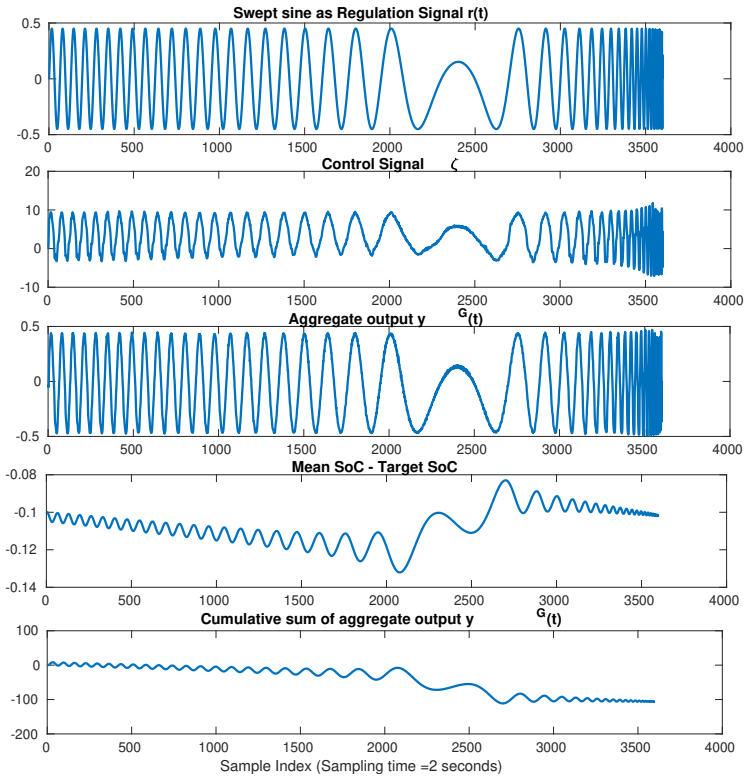

Figure 12.3: Simulation result

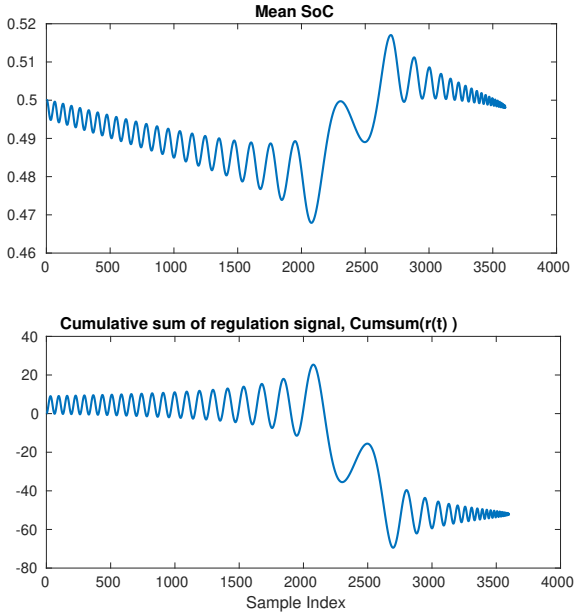

Figure 12.4: SoC recovery due to drift compensation

12.4 PJM Performance Scores

Performance score is calculated for each regulation resources for each regulating hour. Performance scores reflects the benefits each resource provides to system control by focusing on the resource's response to PJM control signals. All ISO in the USA have some sort of performance evaluation mechanism for comparing service provided by regulating resources. To qualify for the regulation market, resources must pass three consecutive regulation tests with a performance score of 75% or higher. Resource MW output must be telemetered and activated before testing. Once the resources are part of regulation resources, the resources must continue to demonstrate minimum performance requirements. Firstly, the historical performance score must be greater the 40%. The historical performance score is the mean of past 100 hours of performance score, its a rolling horizon average. Secondly, the individual hour performance must be greater than 25% to be compensated. Note that these are the minimum performance indexes essential to be part of regulation market, however, resources with poor performance indexes might rarely be called for participating in regulation by PJM's Ancillary Service Optimizer (ASO), therefore, it is essential for regulating resources to maintain a high performance score. ASO runs one hour in advance of operating hour to procure least cost set of resources.

PJM's performance score has 3 components: Accuracy score, Delay score and Precision Score. PJM calculates performance score for hourly data. The dynamic regulation signal is sampled every 2 seconds. The components of performance score measures are described as [143, 144, 39]:

• *Accuracy Score*: measures correlationship between regulation signal and the response of regulation providing units. The correlationship is calculated for a 5 min rolling time window with sampling granularity of 10 seconds for the regulation signal and the response. Accuracy score corresponds to the time index where the correlationship between regulation signal and time-shifted response (up to 5 min) is the highest. Accuracy Score $= \max_{t_j=0:10:300\text{sec}} \Big\{\text{corr }(\text{signal}(t_0 : t_0 + 3600),\ \text{response}(t_0 + t_j : t_0 + t_j + 3600)\Big\}$.

• *Delay Score*: There could be delay between regulation signal and the point of highest correlation. Delay is given as $t_k = \arg\max_{t_j}\{\text{corr }(\text{signal},\ \text{response}\}$. The delay score is calculated as

$$\text{Delay Score } = \max\left\{1, \text{abs}\left\{\frac{(t_k - 10) - 300}{300}\right\}\right\}$$

The PJM wants a 10 second delay in control signal and response signal. This is primarily because the communication round trip delay is approximately 9-11 seconds.

• *Precision*: difference between the area under the curve for the control signal and the regulating

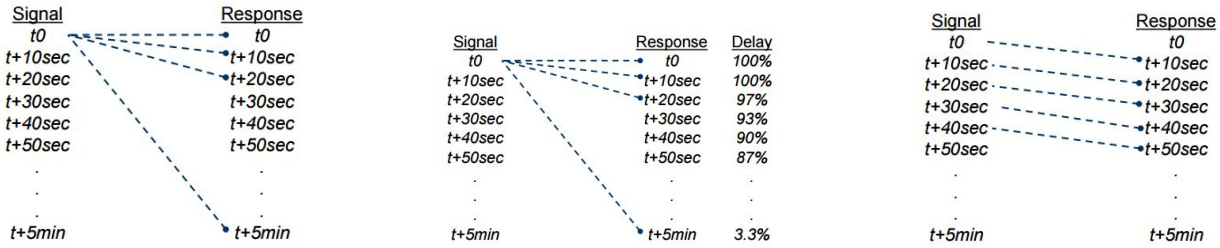

(a) Accuracy Score **(b)** Delay Score **(c)** Precision Score

Figure 12.5: Performance Score Indices used by PJM ISO [39].

unit's response.

$$\text{Precision Score } = 1 - \text{Average of } \left| \frac{\sum \text{ Response} - \sum \text{ Control Signal}}{\sum \text{ Control Signal}} \right|$$

Performance scores reflect how well the resource is following the regulation signal. Performance Score is defined as the equal weighted sum of accuracy, delay and precision score.

12.5 Numerical Evaluation

In the previous section we showed that additional compensation is essential to guarantee objective achievement of dynamic regulation. The concern with such a modification in control is the deterioration in indexes measuring performance of the regulation provided by fleet of batteries. In this section we will numerically evaluate the performance of control with drift compensation. We wish to understand the degradation in performance indexes due to inclusion of greedy behavior of population of batteries.

The battery parameters used are: maximum capacity is 1 kWh, maximum charge rate is 0.5 kW, maximum discharge rate is 0.5 kW and initial SoC is 0.6.

Table 12.5 and Table 12.6 shows performance indexes and SoC of population at the end of the day for control without and with drift control respectively. In practical application of fleet of batteries, it would

Table 12.5: No Drift Compensation

η_{ch}, η_{dis}	Roundtrip Efficiency	Average Accuracy	Average Delay	Average Precision	Mean SoC	End SoC
1	1	0.9974	1.00	0.9833	0.542	0.592
0.95	0.9025	0.6582	1.00	0.9809	0.364	0.144

Table 12.6: With Drift Compensation point-by-point

$\eta_{\text{rt}} = \eta_{ch}\eta_{dis}$	Average Accuracy	Average Delay	Average Precision	Perf. Score	Mean SoC	End SoC
1	0.9955	1.00	0.9829	0.993	0.599	0.612
0.9025	0.9955	1.00	0.9803	0.992	0.593	0.603
0.81	0.9953	1.00	0.9766	0.991	0.586	0.593
0.7225	0.9952	1.00	0.9725	0.989	0.580	0.583
0.64	0.9951	1.00	0.9685	0.988	0.572	0.572
0.5625	0.9949	1.00	0.9640	0.986	0.564	0.561

be non-realistic to update the drift signal for each time instant. The drift signal updated at a slower time scale could lead to results which match real time update of the drift signal. This is showcased in Table 12.7 where results are generated for the case where the drift signal is updated once in an hour, based on mean SoC of the fleet at the beginning of the hour. However, if the duration of drift signal is extended beyond a certain period (this period is governed by ramp rate of the battery and regulation signal) then quality of tracking deteriorates drastically, as evident from Table 12.8. Numerical results indicate a slight drop in

Table 12.7: With Drift Compensation hourly update

$\eta_{\text{rt}} = \eta_{ch}\eta_{dis}$	Average Accuracy	Average Delay	Average Precision	Perf. Score	Mean SoC	End SoC
1	0.9970	1.00	0.9810	0.993	0.598	0.616
0.9025	0.9970	1.00	0.9804	0.993	0.592	0.607
0.81	0.9970	1.00	0.9770	0.991	0.585	0.597
0.7225	0.9967	1.00	0.9730	0.990	0.577	0.586
0.64	0.9967	1.00	0.9686	0.988	0.569	0.575
0.5625	0.9964	1.00	0.9642	0.987	0.560	0.563

Table 12.8: With Drift Compensation two hourly update

$\eta_{\text{rt}} = \eta_{ch}\eta_{dis}$	Average Accuracy	Average Delay	Average Precision	Perf. Score	Mean SoC	End SoC
1	0.9814	1.00	0.8971	0.960	0.596	0.403
0.9025	0.9915	1.00	0.9021	0.965	0.586	0.396
0.81	0.9898	1.00	0.9077	0.966	0.576	0.395
0.7225	0.9910	1.00	0.9144	0.969	0.566	0.403
0.64	0.9891	1.00	0.9228	0.971	0.555	0.420
0.5625	0.9640	1.00	0.9375	0.967	0.545	0.447

performance indexes which is of the order of $\approx 1\%$ if the batteries which is completely efficient is replaced by $\approx 56\%$ efficient batteries. The drop in performance indexes, which is almost insignificant, comes at the cost of keeping SoC of the population of batteries within the optimal SoC band. This is crucial for sustainable tracking of regulation signal. The results with no drift compensation (Table 1) fails even for $\eta_{ch} = \eta_{dis} = 0.95$, because SoC drops below the lower boundary of optimal band. Fig. 12.6 shows the

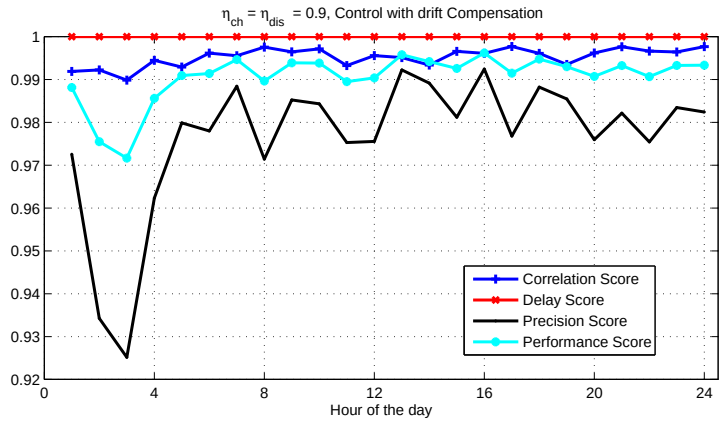

Figure 12.6: Performance Score for point-by-point drift compensation

variations in performance index parameters for a 24 hour simulation.

12.6 Conclusion and Perspectives

In this chapter, we propose a drift compensation control layer for stochastic control of a geographically distributed fleet of batteries, in order to maintain the charge level of batteries in the optimal range. We show that the inclusion of drift compensation leads to the stable operation of providing dynamic regulation with a fleet of batteries with efficiency losses. The control design is performed using Linear Quadratic Regulator which minimizes control energy required and also ensures accurate tracking and SoC being close to the desired level. This controller is made adaptive using gain scheduling, where the proportional gain increases in a cubic function for larger deviation of SoC from the desired level. Using PJM's performance evaluation metrics we show that the objective of accurate tracking and maintaining SoC of the fleet can be simultaneously performed without noticeable deterioration in performance score. We also numerically

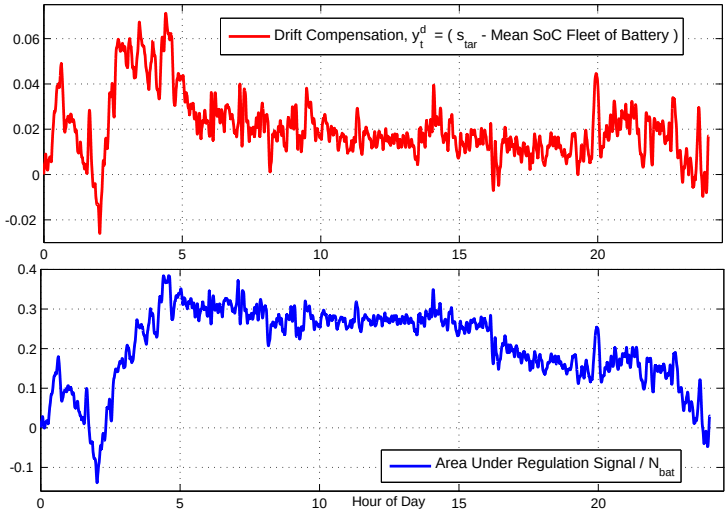

Figure 12.7: Deriving drift compensation - Alternative ways

show that lower time scale update of drift compensation layer can still provide good tracking. It is observed that the drift layer update should be done at least half the charging or discharging time. To bring time scales into perspective, the dynamic regulation is performed at a sampling rate of 2 seconds, the charging and discharging time of battery considered is in hours.

There is of course much more work to be done on estimating drift compensation signal from know regulation signal, as shown in Fig. 12.7. Ideally, the state of all batteries in the fleet will be unknown and calculating mean SoC of the population at each time instant will be impractical. Further research is needed to investigate the relationship between initial mean SoC and the regulation signal on the drift compensating signal.

Chapter 13

Phase Balancing using Storage

The key to keeping your balance is knowing when you've lost it. -Anonymous

Summary: Most bulk transmission of electrical energy is done in three phases. However, distribution of electrical energy in low voltage level is often performed in single phase. The three phases independently act as three single phase lines. Phase imbalance can introduce additional power losses and limit the loading capability of distribution transformer [102]. With ad hoc deployment of renewables the chances of power unbalances among phases will increase with increase in share of distributed renewable energy installations. In this chapter we introduce the phase unbalance problem and the effects of unbalanced generation and load on three phase radial distribution network. We present storage based control architectures for achieving phase balancing.

This chapter is divided into 5 sections. Section 13.1 provides an introduction of phase unbalance in power system. In Section 13.2 we perform OpenDSS based radial distribution network simulations for identifying the effect of connecting single phase generation and load in three phase system. We observe losses in line increase significantly with such unbalance. Section 13.3 present storage architectures for phase balancing. Section 13.4 presents a case-study of Madeira in Portugal. In Chapter 2 Section 2.2.6 we describe a case study of EV charging in Pasadena, California. Section 13.5 concludes the chapter and provides some perspectives.

13.1 Introduction to Phase Balancing

Unbalance describes a condition in a poly-phase system in which the phasors of voltage or current are not equal in magnitude and/or the phase angle between consecutive phasors. For example, a three phase system have unbalanced voltage if the rms value[1] of phase voltages are not the same and/or the phase angle between voltage phases are not exactly 120 degrees [95], [10].

Fortescue in 1918 developed symmetrical components for representation of any set of unbalanced phasors [165]: (i) a direct or *positive* sequence in order (abc), (ii) an inverse or *negative* sequence in order (acb), (iii) a homopolar or *zero* sequence system in same direction.

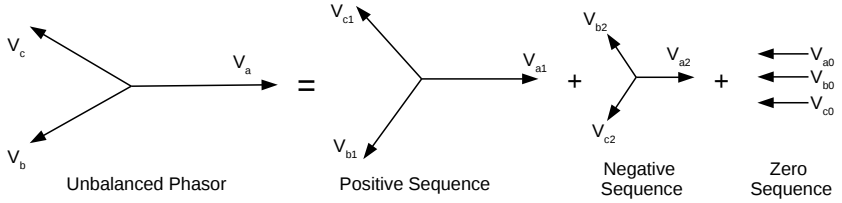

Figure 13.1: Sequence Component of an unbalanced phasor

The transformation of unbalanced phasor is given as [165], [88]

$$\begin{bmatrix} V_{a0} \\ V_{a1} \\ V_{a2} \end{bmatrix} = \frac{1}{3} \begin{bmatrix} 1 & 1 & 1 \\ 1 & e^{\frac{j2\pi}{3}} & e^{\frac{-j2\pi}{3}} \\ 1 & e^{\frac{-j2\pi}{3}} & e^{\frac{j2\pi}{3}} \end{bmatrix} \begin{bmatrix} V_a \\ V_b \\ V_c \end{bmatrix} \tag{13.1.1}$$

[1] RMS or root mean square is defined as the square root of the mean of the square of the parameter; for three phase voltages the rms voltage is calculated as $V_{rms} = \sqrt{\frac{1}{3}(V_a^2 + V_b^2 + V_c^2)}$.

where $e^{\frac{j2\pi}{3}} = 1\angle 120^0$, $\{V_a, V_b, V_c\}$ are phase voltages.

Current unbalance is related to voltage unbalance through network impedances. If the network impedances are asymmetric then voltage unbalance can occur even though the currents are perfectly balanced. In this work we balance power in each phase leading to reduction in unbalance in current and voltage. The remaining part of this section we discuss the reasons, effects and mitigation of unbalance. We list the indices used to measure unbalance in voltage. We present the effects of large scale distributed generation (DG) such as photovoltaic and electric vehicle (EV) will have on unbalance in three phase low distribution power network.

13.1.1 Cause of unbalance in three-phase power network

Asymmetries in each of the three phases can be because of unbalanced loading and cable length. Here we highlight the unbalance which could be caused of large scale EV deployment and DG installation.

With larger integration of single-phase intermittent and stochastic distributed generation and evolution of end user consumption requires detailed assessment of voltage unbalance and effective mitigation [229]. The connection of single phase EVs and DGs are random and often clustered in a certain area. In addition both EVs and PVs tend to be active in a synchronized manner, i.e., majority of the EVs are getting charged in the evening when people reach their homes after work and with high probability all the PVs generate electricity when it is sunny. Such a synchronized operation of these loads and generation aggravates the problems for distribution system operators who are obliged to ensure power quality at all times.

Electric vehicles require high charging current, longer periods of charging which tend to coincide with charging of other EVs. EVs with 30kWh battery stores as much as the average US residence consumes in a day, making it significant portion of total household load [163]. Furthermore, often EV charging is single phase which could cause voltage unbalance [278]. This should be a concern for distribution system operators as EVs are expected to grow drastically in near future. The sale of EV will contribute to 10-50% of all new cars by 2030 [163]. Authors in [278] note that voltage imbalance caused by EVs is unlikely to exceed the prescribed limits set by the utility provided EVs are reasonably distributed among three phases. Phase distribution often could not consider such asymmetrical evolution of new loads. This could have adverse effect on voltage unbalance of a three-phase distribution network [293]. Furthermore, the effect of connection of EVs on unbalance is significant if they are connected farther away in the feeder, causing greater unbalance [293].

Distributed generation (such as PV, wind etc.) is intermittent, interfaced via single phase converter and solar PV also have a high impedance and low short circuit current making it more prone to cause unbalance in the power network [229], [155]. Within Europe the voltage characteristic standard, EN50160 [128], states that the 10-min rms voltage should be between 90% and 110% of the nominal voltage most of the time and between 85% and 110% all of the time. The distribution feeders are designed such that the voltage magnitude becomes lower when moving along the feeder. Integrating DGs at distribution level makes the design condition of feeders invalid and thus over-voltages could occur [104], see Chapter 2, Section 2.2.8 for an example demonstrating the change in voltage profile due to inclusion of EVs and DGs. The introduction of DG changes the fault currents and will also increase the risk of an incorrect protection operation. Uncertainty in generation and drastic ramping up/down of generation could be difficult to handle by DSOs. For example the solar generation can reduce by 70% in few seconds due to passing clouds [142].

Thus, larger integration of DGs and PVs will increase the chances of voltage unbalance.

13.1.2 Effect of unbalance in three-phase power network

Unbalance causes negative sequence power flow which contributes to thermal aging, reduction of equipment life and derating the capacity of induction machines. In induction machine magnetic field and torque are proportional to positive sequence of the machine. Negative sequence generates an inverse torque forcing the machine to decelerate. Thus total torque is reduced and the machine cannot rotate at full speed. Voltage unbalance can create a current unbalance 6-10 times the magnitude of voltage unbalance [37]. Negative sequence for synchronous generator causes overheating in the inner construction of damper windings [229].

For transformers zero sequence flow could inverse the temperature of windings and positive and negative sequence cause parasitic losses in the transformer structure [155]. It is estimated that there are 2.4 GWh equivalent to $134,000 additional annual losses due to presence of unbalance based on 17,600 transformers in Brazil [290]. The capacity of transformer, cables and overhead lines in order to carry negative sequence current, the amount of positive sequence must be downgraded. This leads to reduction in capacity for

carrying positive sequence current is reduced [129, 149]. Phase unbalance can, therefore, limit the power transferred on a feeder [327]. Unbalance could also lead to preventive breaker or relay tripping and shutdown of a feeder [327], as pointed in Section 13.1.1.

The voltage unbalance of low-voltage feeder maybe seen by other feeders fed from the same distribution transformer. Furthermore, current unbalance can be propagated through the distribution transformer to the higher voltage network [95, 138]. It is evident that voltage unbalance affects only three phase customers.

13.1.3 Indices for measuring of unbalance in three-phase power network

There are various indices to measure unbalance in three-phase power network. We list some of the definitions we use in this work. The selection of which definition to use depends on available data from real measurements, details to be provided in case studies in next sections.

Definition 1: International Electrotechnical Commission or IEC defines voltage unbalance factor (VUF) as the ratio of the magnitudes of negative sequence over positive sequence denoted as

$$\text{VUF}_1 = \frac{|V_{a2}|}{|V_{a1}|}. \tag{13.1.2}$$

VUF_1 denotes the true definition of VUF [273]. The remaining definitions are approximations of VUF_1. The alternate definitions are required as sequence components which require sophisticated measurement devices are often not measured.

Definition 2: Alternative definition using magnitudes of line-to-line fundamental component voltages. The VUF in this case is given as

$$\text{VUF}_2 = \sqrt{\frac{1-\sqrt{3-6\beta}}{1+\sqrt{3-6\beta}}}, \quad \text{where } \beta = \frac{V_{ab}^4 + V_{bc}^4 + V_{ca}^4}{(V_{ab}^2 + V_{bc}^2 + V_{ca}^2)^2}. \tag{13.1.3}$$

The approximation of VUF_1 using VUF_2 is valid provided zero sequence component is negligible [10]. In presence of zero sequence there will be an error in approximating the VUF and the measured VUF will lie in the range $\text{VUF} \in [\text{VUF}_2 - \frac{|V_{a0}|}{|V_{a1}|}, \text{VUF}_2 + \frac{|V_{a0}|}{|V_{a1}|}]$ [169].

Definition 3: National Electrical Manufacturers Association or NEMA defines VUF by the ration of maximum deviation from average voltage

$$\text{VUF}_3 = \frac{\max(V_{ab}, V_{bc}, V_{ca}) - \text{mean}(V_{ab}, V_{bc}, V_{ca})}{\text{mean}(V_{ab}, V_{bc}, V_{ca})}. \tag{13.1.4}$$

VUF_3 is also called phase voltage unbalance rate (PVUR). NEMA definition uses only magnitude information. A comparison of VUF calculated shows a discrepancy of up to 13% from actual VUF [301].

Definition 4: Similarly, for line voltage unbalance rate (LVUR) is defined as [273]

$$\text{VUF}_4 = \frac{\max(V_{an}, V_{bn}, V_{cn}) - \text{mean}(V_{an}, V_{bn}, V_{cn})}{\text{mean}(V_{an}, V_{bn}, V_{cn})}. \tag{13.1.5}$$

VUF_4 is also known as the IEEE definition of voltage unbalance. NEMA definitions are good approximations of actual unbalance for cases where VUF is less than 5% [273].

Authors in [169] point that the line-to-neutral voltages rather than the specified line-to-line voltage values for calculating VUF_3 can give errors only if there is significant zero sequence component present in unbalance phasors, otherwise this approximation is valid. [301] states that voltage unbalance assessment is a steady-state event and recommends measurement of voltage at high sampling rate. Often voltage measurements are done in time scales of several minutes. Due to averaging of voltage over the interval, the unbalance calculated using average values is more than 50% lower than the average of the unbalance for the same interval [169].

Definition for VUF_3 is created based on the fact that many commercially available electricity meters are not able to measure the angular difference between each phase. The VUF rules are listed in Table 2.5. The mitigation of three-phase network is introduced in Chapter 2.2.5.

13.2 Understanding the effects of phase unbalance

In this section we perform phase unbalance simulations on a radial distribution network by connecting single phase renewable generation and electric vehicle loads on a three phase four wire distribution system.

We identify that system unbalance should be gauged by (a) losses in the neutral, (b) line losses and (c) voltage unbalance factor. Considering only voltage unbalance factor does not provide the complete picture of system unbalance especially if the network is compact. We observe that effect on system unbalance is affected by: (i) the location of network where single phase loads or generation is connected in the network, (ii) the effect of connecting single phase load and generation is nearly symmetrical for VUF, however, the effect of neutral and line losses are not symmetrical for loads and generation, (iii) networks which are sparse or congested with significant voltage drop could lead to significant VUF values. We present the voltage drop, VUF, line losses, neutral loss, active power, reactive power and current magnitudes at each of the nodes of the network.

13.2.1 Simulation Results

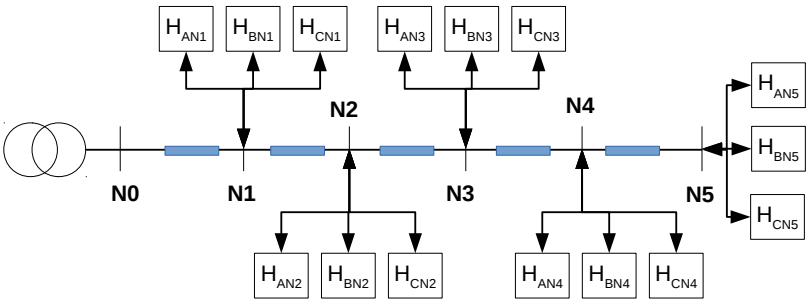

Figure 13.2: Simulation Baseline Model

We perform a sensitivity analysis by placing different levels of RES (0%, 10%, 20%, ..., 90%, 100% of max load in each phase) at points N1 (closed to feeder) and N5 (furtherest to feeder). For evaluation we are interested in observing the variations of following parameters at nodes:

1. Voltage Unbalance Factor: for each node,
2. Per-unit voltage: for each phase at each node,
3. Active power: for each phase at each node,
4. Reactive power: for each phase at each node,
5. Losses incurred in each of the phases and
6. Losses incurred in the neutral conductor.

For this we assume the nominal case has a balanced load in each phases as we aim to understand the variation caused due to integration of DGs/EVs in one of the phase. In this experiment we assume the worst-case condition where all these single phase DGs/EVs are connected to one of the phases.

The key observations using simulations for a radial network shown Fig. 13.2 are as follows:

- VUF is not affected until the lines have significant voltage drop due to high resistance or overloaded and/or network is sparse with significant line losses. For a compact network with low drop in voltage with respect to voltage at the generation feeder in a radial distribution network, VUF is not significant even for a large share of DGs/EVs connected to only one phase, refer to Fig. 13.4. The VUF limits are listed in Table 2.5. Clearly, the VUF limit lies within 1-3%. For compact network the VUF rises to less than 0.22% for 120% (compared to phase load) of DGs/EVs connected to N1 (refer to Table 13.1) and 0.9% for DGs/EVs connected to N5 (refer to Table 13.2). However, VUF is a crucial index for networks which are either congested and/or sparse, refer to Table 13.3 to Table 13.6.
- For single phase DG connected close to the feeder has a near to uniform effect on VUF compared to DG connected farther away which affects the distant nodes much more than nodes closer to the feeder. Fig. 13.4 shows that increase in share of DG connected at Node 5 or N5 almost linearly increases the VUF.
- Contrary to prevalent notion that adding renewables would help in reducing voltage drop if connected at distant nodes, however, DG not well balanced along the phases could reduce the losses in a phases (note Phase A losses in Fig. 13.3) but increases the losses in the neutral conductor drastically. Thus the total losses in effect are very large for large share of renewables. However, with increase integration of EVs the losses increase in phase and neutral without any ambiguity.

- Imbalance in power distribution network is observed using three parameters: VUF, losses in the neutral conductor and losses in the phase.
- The 3 phase 4 wire system is used when a mixture of single-phase and three-phase loads are to be served, such as mixed lighting and motor loads, where each customer may be only fed from one phase and the neutral (which is common to the three phases). When a group of customers sharing the neutral draw unequal phase currents, the common neutral wire carries the currents resulting from these imbalances. Electrical engineers try to design the three-phase power system for any one location so that the power drawn from each of three phases is the same, as far as possible at that site. However, we observe that connecting large amount of single phase DG could aggravate the system unbalance by increasing losses in the neutral conductor. Substation authorities in Madeira have reported the major concern for them regarding unbalance manifests in form of blowing up of neutral conductor due to over-current.
- The last plot of Fig. 13.3 shows that DGs can be designed to reduce the total loss in the distribution network. These results further improve if we assume DG placement to be balanced in each phase.
- Considerable increase (almost 3 to 4 times) voltage drop in the injecting phase reduces with DG connected at N5 compared to DG connected at N1. However, this configuration increases the voltage drop in one of the phase.
- Fig. 13.3 shows the total phase losses, neutral losses and total losses for DGs/EVs connected at N1 and N5. The total losses for DG/EV connected at the distant feeder are significantly higher compared to the case where the DG/EV integration close to the feeder.
- Fig. 13.5, Fig. 13.6, Fig. 13.7, Fig. 13.8 shows the voltage drop in percentage for integration of DG/EV at N1 and N5. The drop in voltage decreases in the phase where DG is connected and increases when EV is connected.
- Fig. 13.9, Fig. 13.10 and Fig. 13.11 shows the active, reactive power and phase current variation with respect to nodes due to integration of DG/EV at nodes N1 and N5.

Table 13.1: Performance Indices for 5kW total phase load with DG or EV connected at N1

EV/DG at N1	Mean VUF	Max VUF	Neutral Losses	Total Phase losses	Sum of Voltage drop at N1	Sum of Voltage drop at N5
Nominal Balance Case	7.50e-08	1.19e-07	0	118.47668	-1.46091	-3.6141
Balanced + 40% DG	6.95e-08	1.03e-07	0	88.71856	-1.0968	-3.2472
Balanced + 40% EV	8.77e-08	1.70e-07	0	163.1242	-1.82691	-3.9828
Unbalanced + 120% DG	0.22105	0.2222	39.8537	103.57916	-1.09782	-3.2484
Unbalanced + 120% EV	0.22514	0.22639	41.0473	178.62513	-1.82810	-3.98393

Table 13.2: Performance Indices for 5kW total phase load with DG or EV connected at N5

EV/DG at N5	Mean VUF	Max VUF	Neutral Losses	Total Phase losses	Sum of Voltage drop at N1	Sum of Voltage drop at N5
Nominal Balance Case	7.50e-08	1.19e-07	0	118.47668	-1.46091	-3.6141
Balanced + 40% DG	5.85e-08	1.12e-07	0	43.8494	-1.0909	-2.0587
Balanced + 40% EV	7.57e-08	1.34e-07	0	269.9494	-1.8410	-5.1984
Unbalanced + 120% DG	0.5137	0.8088	193.1352	117.3938	-1.1128	-2.0621
Unbalanced + 120% EV	0.5586	0.8812	222.0076	359.8447	-1.8675	-5.2065

13.2.2 Honeymoon and Divorce Cases

Two distinct and contradictory ideologies exists when it comes to renewable energy sources (RES) and specifically DGs. Some believe that RES is not only environmentally friendly but also solves many problems of power network such as (a) reducing transmission losses: DGs integrating close to their consumption point could eliminate the losses which is incurred by traditional generation sources, (b) congestion relief and

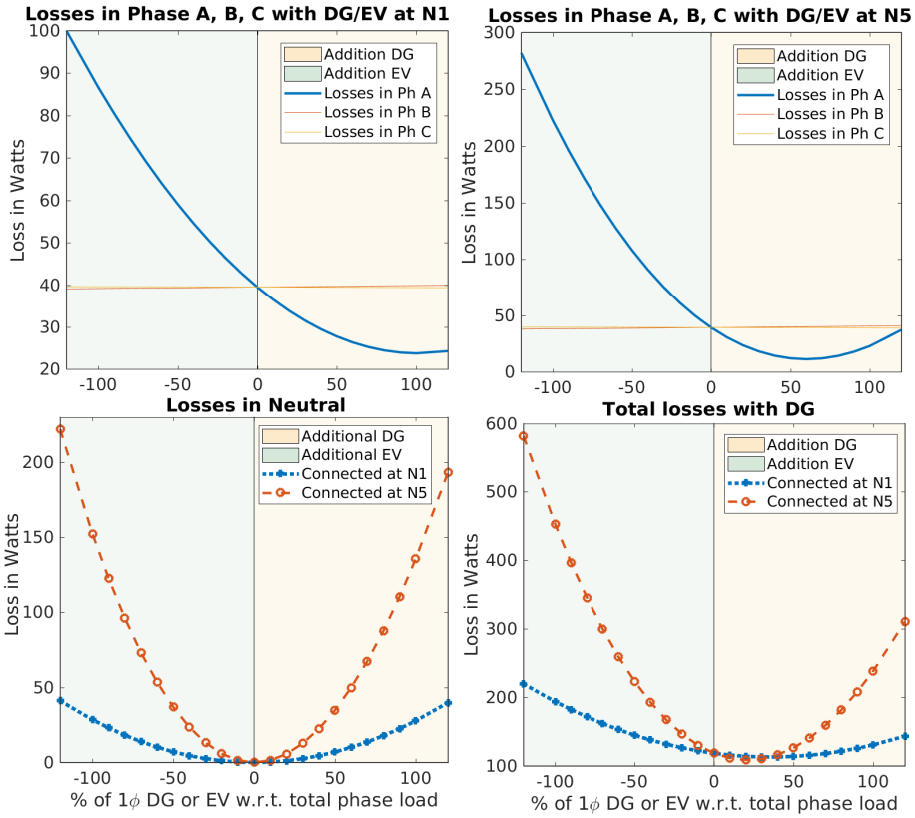

Figure 13.3: Losses in the distribution network with two scenarios: (i) DG/EV connected at N1 and (ii) DG/EV connected at N5

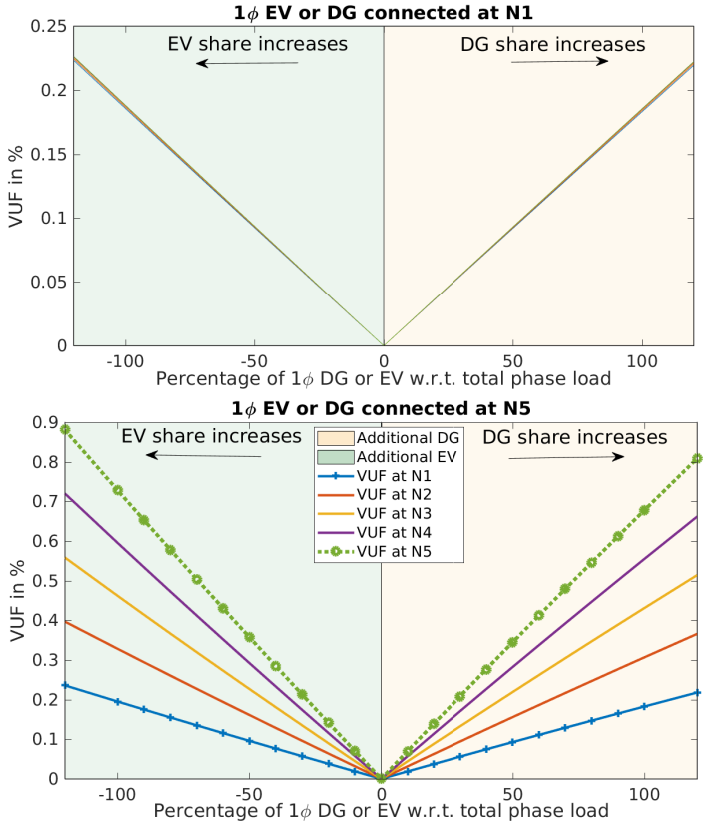

Figure 13.4: VUF with (i) DG/EV connected at N1 and (ii) DG/EV connected at N5

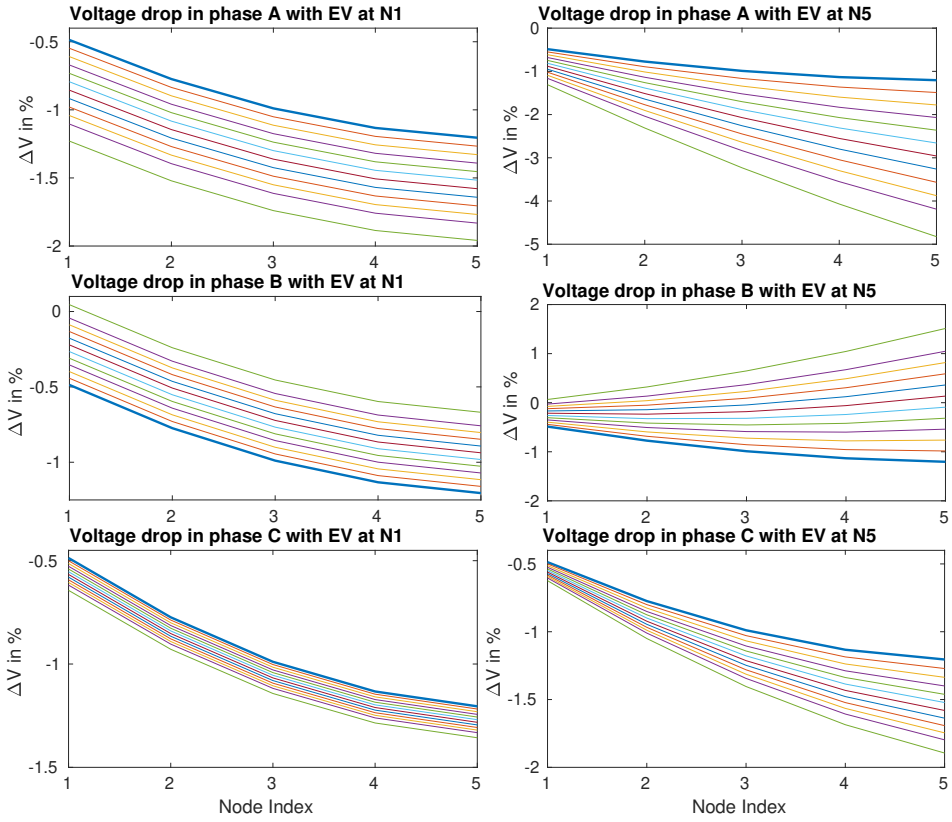

Figure 13.5: Voltage drop with (i) EV connected at N1 and (ii) EV connected at N5

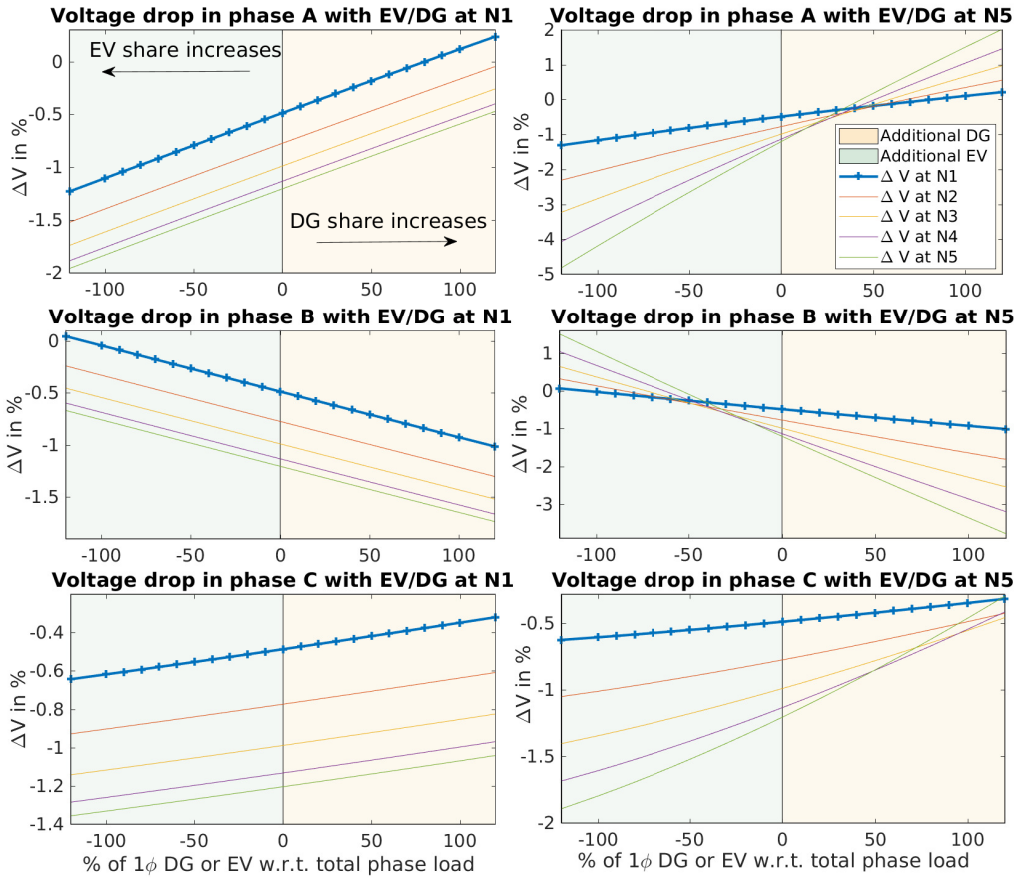

Figure 13.6: Voltage drop with (i) DG/EV connected at N1 and (ii) DG/EV connected at N5

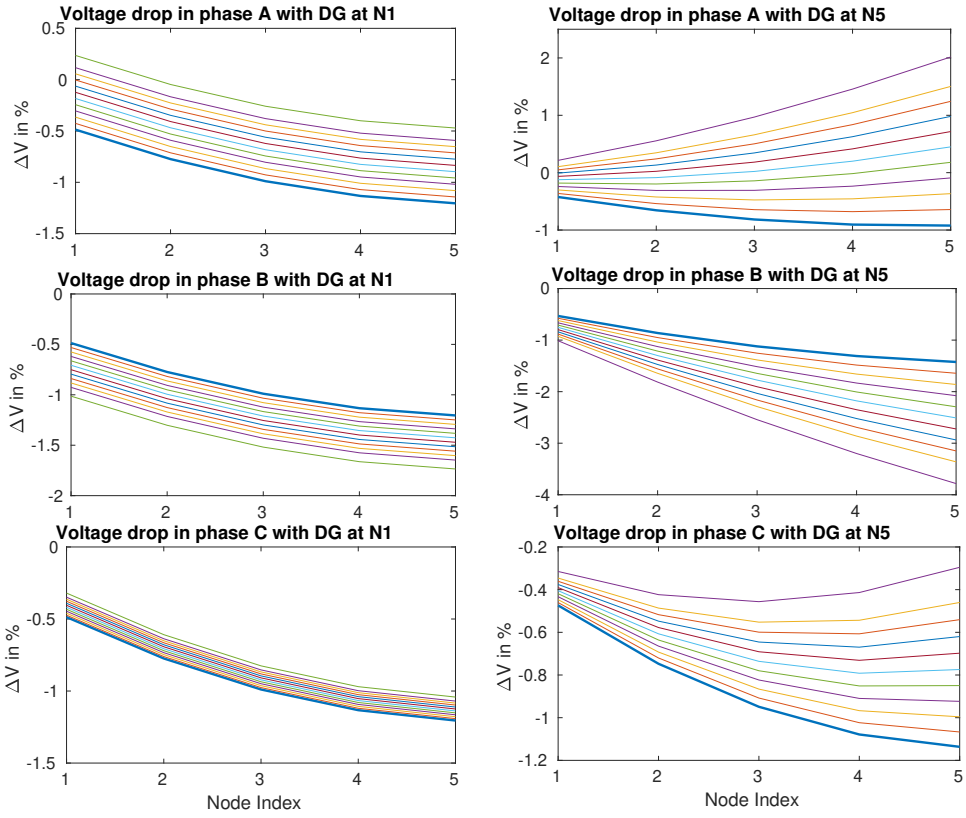

Figure 13.7: Voltage drop with (i) DG connected at N1 and (ii) DG connected at N5

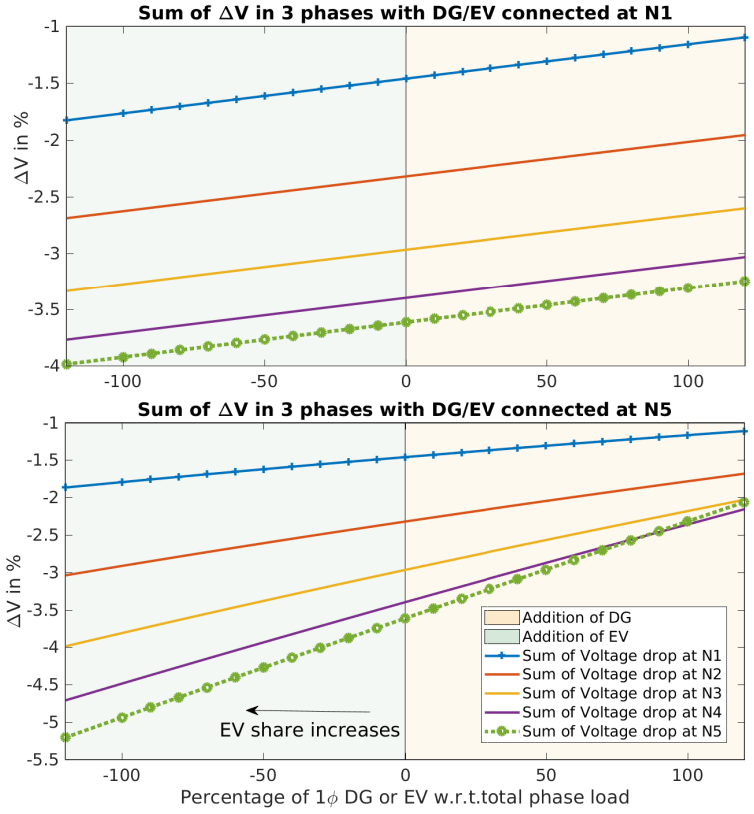

Figure 13.8: Sum of Voltage drop in 3 phases with (i) DG connected at N1 and (ii) DG connected at N5

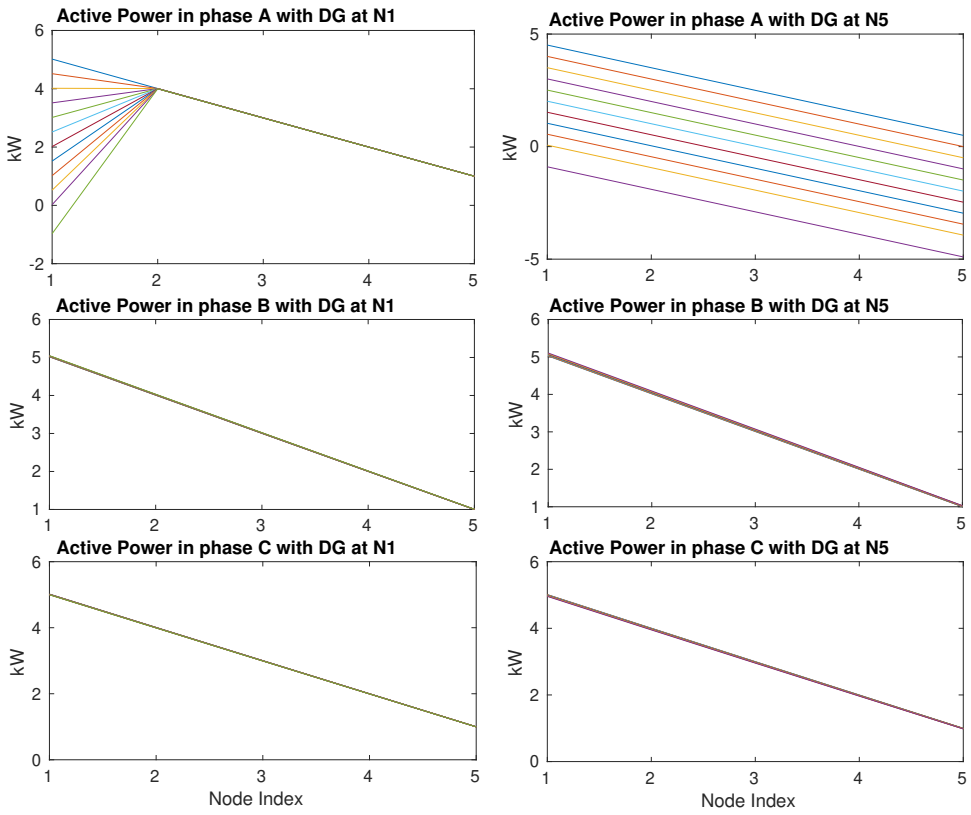

Figure 13.9: Active power with (i) DG connected at N1 and (ii) DG connected at N5

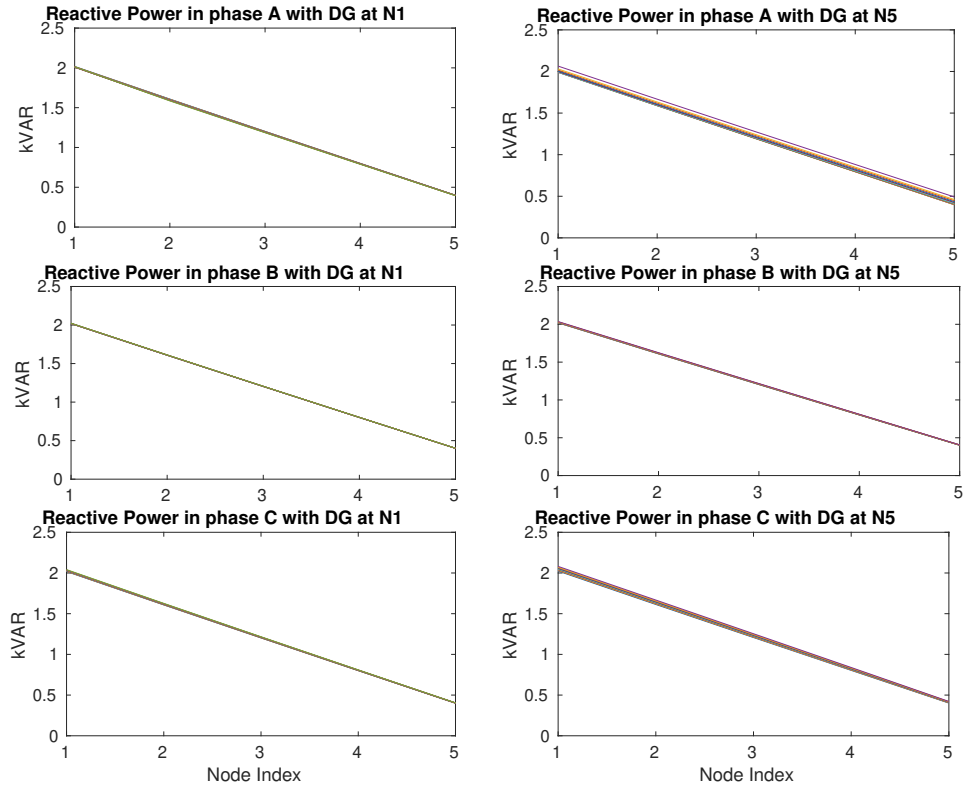

Figure 13.10: Reactive power with (i) DG connected at N1 and (ii) DG connected at N5

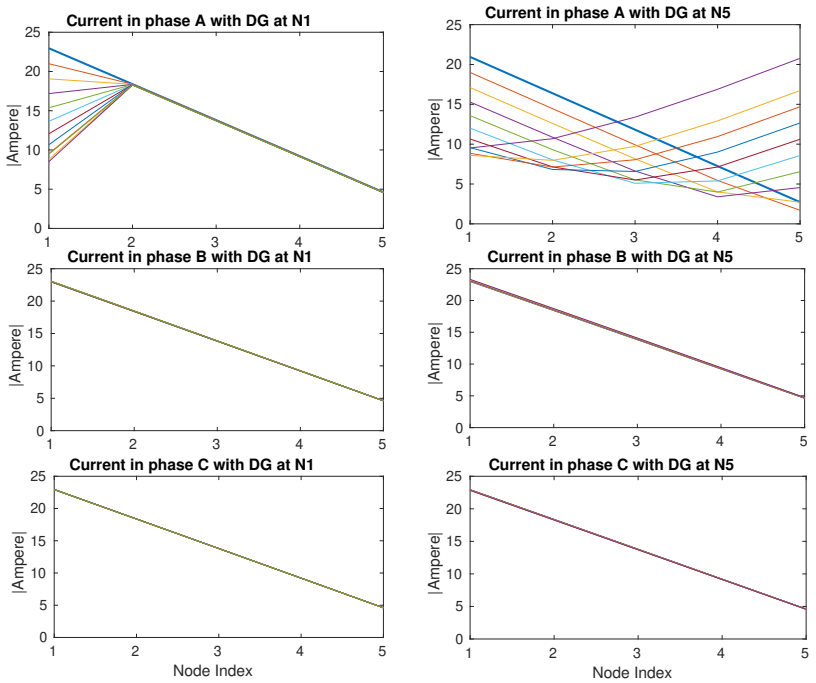

Figure 13.11: Current magnitude with (i) DG connected at N1 and (ii) DG connected at N5

voltage profile flattening: since the DGs are connected in the distribution network which lifts the voltage profile at nodes far away from the generation feeder or substation. DGs (often intrinsically assumed balanced) would decrease the losses in the network thus improving the efficiency of the network. This philosophy of distributed renewable energy generation propagators is referred to as *the Honeymoon case*.

The second line of thought considers renewable energy sources a menace for power networks reliability (of course not undermining the low carbon footprint aspect of renewable energy sources). The intermittent and uncertain nature of the generation they believe causes many problems in system balancing essential to maintain the system frequency. The localized injections of DG energy could cause over-voltage problems at a localized level leading to false tripping of circuit breakers and relays. Furthermore, the unplanned DG growth in distribution network could create unbalance in the network leading to increased losses in distribution network. The phase and supply and demand balancing which was difficult with stochastic evolution of load only, gets more difficult with uncertainty in DGs. This philosophy of distributed renewable energy generation propagators is referred to as *the Divorce case*.

Both these line of thinking are in some way extreme cases. A more sensible way of thinking would combine the goods that DGs offer and minimizes the difficulties associated with them.

Table 13.3: Performance Indices for 50kW total phase load, Overloaded, with DG or EV connected at N1

EV/DG at N1	Mean VUF	Max VUF	Neutral Losses	Total Phase losses	Sum of Voltage drop at N1	Sum of Voltage drop at N5
Balanced + 40% DG	1.12e-07	1.82e-07	0	10996.1153	-12.4467	-36.5481
Balanced + 40% EV	7.62e-08	1.15e-07	0	20621.7336	-21.0819	-46.0758
Unbalanced + 120% DG	2.8155	3.1089	4264.5506	13099.4897	-12.6841	-36.8959
Unbalanced + 120% EV	4.3865	5.0357	7064.8551	25068.9811	-21.7348	-47.0552

13.3 Architectures of Storage Solutions

In our present work we consider balancing active and reactive power between phases using energy storage battery. We consider storage is owned by the utility and placed at selected node of the network. The battery model used in this chapter is described in Chapter 2 Section 2.5. Next we present the storage control architectures for facilitating phase balancing.

Table 13.4: Performance Indices for 50kW total phase load, Overloaded, with DG or EV connected at N5

EV/DG at N5	Mean VUF	Max VUF	Neutral Losses	Total Phase losses	Sum of Voltage drop at N1	Sum of Voltage drop at N5
Balanced + 40% DG	1.19e-07	1.43e-07	0	4988.4956	-11.6358	-22.0773
Balanced + 40% EV	1.23e-07	2.71e-07	0	40753.8467	-23.8587	-66.8436
Unbalanced + 120% DG	5.2444	8.1075	22111.61	16063.4889	-14.531	-24.2719
Unbalanced + 120% EV	4.7895	7.2048	7005.75	22851.0115	-18.378	-44.3698

Table 13.5: Performance Indices for 5kW total phase load with Sparse network; DG or EV connected at N1

EV/DG at N1	Mean VUF	Max VUF	Neutral Losses	Total Phase losses	Sum of Voltage drop at N1	Sum of Voltage drop at N5
Balanced + 40% DG	9.25e-08	2.21e-07	0	1066.2160	-9.0111	-32.7123
Balanced + 40% EV	1.04e-07	1.45e-07	0	1972.4848	-15.7299	-40.0998
Unbalanced + 120% DG	2.0373	2.306	41.5705	1261.3842	-9.0739	-32.8439
Unbalanced + 120% EV	2.841	3.3052	59.6847	2310.5699	-15.9015	-40.4231

Table 13.6: Performance Indices for 5kW total phase load with Sparse network; DG or EV connected at N5

EV/DG at N5	Mean VUF	Max VUF	Neutral Losses	Total Phase losses	Sum of Voltage drop at N1	Sum of Voltage drop at N5
Balanced + 40% DG	7.91e-08	1.25e-07	0	484.264	-8.4588	-18.7116
Balanced + 40% EV	1.24e-07	1.67e-07	0	3825.694	-17.4885	-58.9971
Unbalanced + 120% DG	4.4593	7.2123	224.0432	1573.9655	-10.4382	-20.2429
Unbalanced + 120% EV	4.3512	6.8105	80.3176	2367.5169	-13.8983	-40.0262

13.3.1 Solution with one battery and phase selector

A single battery is used to install to compensate imbalance in three-phases. A phase selection algorithm selects the phase with which battery is connected and the storage charges or discharges to minimize the imbalance as much as possible. Fig. 1.4 shows the architecture of this proposed solution. In this figure the battery is placed at the substation close to the transformer. However, we observe from simulations that the best-suited location to install phase balancing storage resource will depend on network architecture. For a radial distribution network the storage device should be places on the furthest node for maximum cumulative correction of voltage and losses. The phase selector algorithm should consider maintaining state-of-charge of the battery close to 50%, so that the battery could charge or discharge for reducing the phase imbalance.

13.3.2 Solution with three storage with each dedicated to each phase

Three dedicated batteries interfaced via a converter are connected to three phases. Fig. 13.12 shows the architecture of this solution. The storage controller takes into account the phase imbalance and also maintains the SoC of each of these batteries.

13.3.3 Solution with three storage with phase selector for each battery

The objective of performing phase balancing using energy storage is to compensate active and reactive power unbalance in each phases and maintain the state of charge (SoC) of each of the battery. We achieve these goals using two-step algorithm The first step is a scheduling algorithm which identifies which battery should compensate which phase based on SoC and historical variation of each phase. Note the scheduling algorithm is implemented at a longer time scale, in our case hourly. The second step consists of active and reactive power compensation, in a manner that the sum of square of active and reactive power unbalances are minimized over the time horizon under consideration.

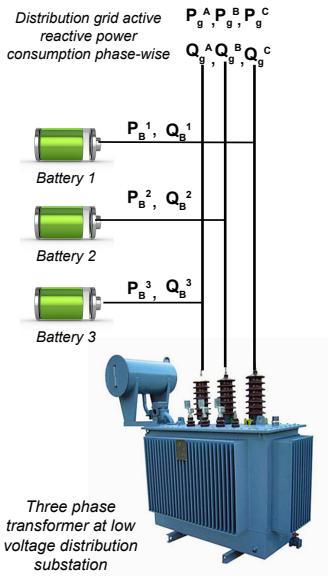

Figure 13.12: Block diagram of phase-wise compensation at with dedicated battery for each phase

Notation

The active power supplied by distribution transformer (in absence of energy storage) for phase A at time instant i is denoted as $P_g^A(i)$. Similarly, $P_g^B(i)$ and $P_g^C(i)$ represents the active power supplied for phase B and C respectively.

The reactive power supplied by distribution transformer (in absence of energy storage) for phase A at time instant i is denoted as $Q_g^A(i)$. Similarly, $Q_g^B(i)$ and $Q_g^C(i)$ represents the reactive power supplied for phase B and C respectively.

The battery supplies active and reactive power denoted as $P_B(i)$ and $Q_B(i)$ respectively. The active power supplied a battery is bounded by its ramp rate and capacity constraint and the reactive power supplied is governed by active power output and converter size. In this work we consider four-quadrant storage operation.

The active power unbalance in phase A at time instant i is given as

$$\Delta_P^A(i) = P_g^A(i) - \bar{P}_g(i), \tag{13.3.1}$$

where $\bar{P}_g(i)$ is the mean of active power in all phases given as

$$\bar{P}_g(i) = \frac{1}{3}\left(P_g^A(i) + P_g^B(i) + P_g^C(i)\right). \tag{13.3.2}$$

If $\Delta_P^A(i) > 0$ then active power supplied in phase A is higher than the mean active power supplied in each phase. Therefore, in order to provide compensation for this unbalance, the battery should discharge. Similarly, unbalance in active power for phase B and C are calculated.

The reactive power unbalance in phase A at time instant i is given as

$$\Delta_Q^A(i) = Q_g^A(i) - \bar{Q}_g(i), \tag{13.3.3}$$

where $\bar{Q}_g(i)$ is the mean of reactive power in all phases given as

$$\bar{Q}_g(i) = \frac{1}{3}\left(Q_g^A(i) + Q_g^B(i) + Q_g^C(i)\right). \tag{13.3.4}$$

If $\Delta_Q^A(i) > 0$ then reactive power supplied in phase A is higher than the mean reactive power supplied in each phase. Therefore, in order to provide compensation for this unbalance, the battery should supply reactive power. Similarly, unbalance in reactive power for phase B and C are calculated.

Scheduling Algorithm

The sampling time of control decisions for operating energy storage is h. The scheduling algorithm is implemented every N samples. The scheduling algorithm allots which energy storage should compensate

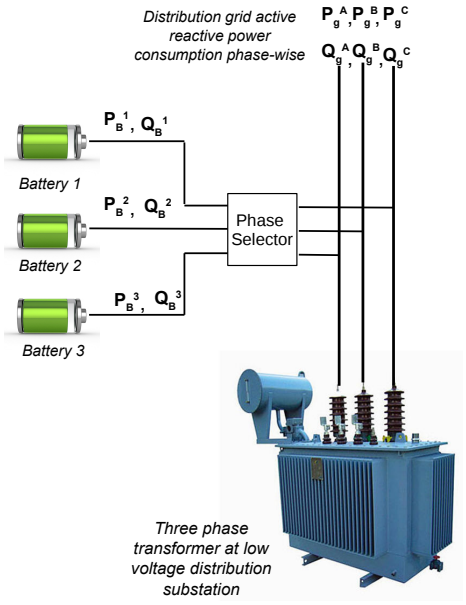

Figure 13.13: Block diagram of phase-wise compensation with phase allocation for each storage

which phase for the next N samples, based on SoC of all the batteries and historical variation of each phase. In this work we consider hourly energy storage allotments.

Hourly average forecasted imbalance of active power for phase x and hour k is denoted as

$$\hat{H}_P^x(k) = -\frac{1}{N}\sum_{h}^{N}\hat{\Delta}_P^x, \tag{13.3.5}$$

where N_h is the number of samples in 1 hour.

The hourly forecasted imbalance is sorted in ascending order and stored in a vector M_k. M_k is given as

$$M_k = \text{sort}(\hat{H}_P^A(k), \hat{H}_P^B(k), \hat{H}_P^C(k)).$$

The SoC of batteries is stored in vector Z_k and is given as

$$Z_k = \text{sort}(SoC_k^{B1}, SoC_k^{B2}, SoC_k^{B3}).$$

Higher value of hourly average forecasted imbalance imply more charging opportunity. Therefore, this value should be matched with lowest SoC value. $M_k(1)$ is matched with $Z_k(3)$.

The reactive power supplying capability is a function of converter size and active power magnitude. In scheduling we only consider active power imbalance as the battery SoC is governed by active power and reactive power does not affect the SoC of the battery [208].

Phase-wise Compensation

Suppose after running algorithm Phase A is compensated using battery $g1$, Phase B is compensated using battery $g2$ and Phase C is compensated using battery $g3$.

The objective function for battery $g1$ is given as

$$(P_{bat}^{g1}) \quad \min \sum_i \left\{ \left(\Delta_P^A(i) + P_B^{g1}(i)\right)^2 + \left(\Delta_Q^A(i) + Q_B^{g1}(i)\right)^2 \right\}$$

$$\text{s.t. (i) } b_i^{g1} \in [b_{\min}, b_{\max}] \forall i,$$

$$\text{(ii) } P_B^{g1}(i) \in [P_B^{\min}, P_B^{\max}] \forall i,$$

$$\text{(iii) } (P_B^{g1}(i))^2 + (Q_B^{g1}(i))^2 \leq (S_B^{\max})^2 \forall i$$

Note that the optimization problem (P_{bat}^{g1}) is convex as the objective function and constraints are convex functions. Similar to (P_{bat}^{g1}) the objective functions for battery $g2$ and $g3$ can be implemented.

13.3.4 Phase Balancing with Storage: Stylized Example

In our exhaustive simulations on identifying the effect of connection of EVs and PVs on a radial distribution network we identified that the indicators of unbalance: (a) Neutral conductor losses, (b) line losses and (c) VUF has the most pronounced effect on the furtherest node of the radial distribution network, therefore, we select storage battery to be placed at this point. Nominal case is described for 1 day with bulk PV generation at N3 Phase A during the day and bulk EV consumption during the evening at N3 Phase C, see Fig. 13.14. The imbalance magnitude is 5 times higher than the storage placed at farther end of the radial distribution network. Fig. 13.15, Fig. 13.16 and Fig. 13.17 shows that the storage compensates the unbalance caused due to EV and PV and in effect reduces the unbalance indices described above.

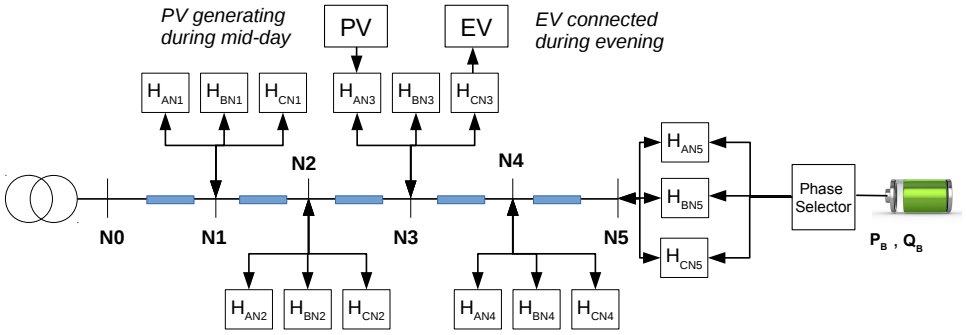

Figure 13.14: Simulation scenario for the stylized example.

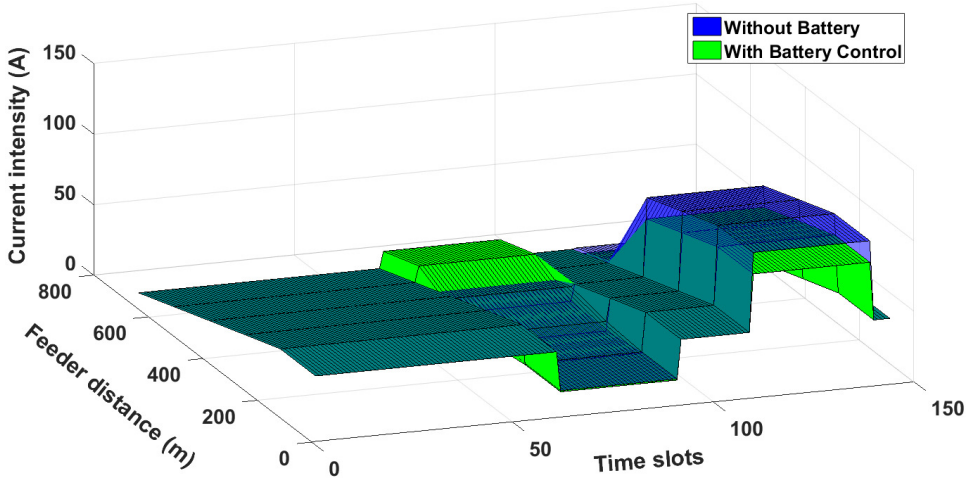

Figure 13.15: Impact on current intensity.

13.4 Case Study : Madeira Substation[2]

This section presents a case study of phase balancing in Madeira Island, Portugal. First, an overview of the local grid is provided, in order to give some context to the reader. Second, the case of a specific distribution substation in Madeira is presented, in order to motivate the need to improved grid control through the introduction of Battery Energy Storage Systems (BESS) at the distribution station level. Finally, this section concludes with a Q&A that was conducted with staff from the planning department of Madeira's DSO/TSO.

13.4.1 Overview of the Local Grid

Madeira is a total energy island, and all the energy is generated locally. There is only one DSO/TSO in Madeira and it is responsible for the activities related to production, transport, distribution and commer-

[2]This section is prepared by Dr. Lucas Pereira at ITI/LARSyS, Tecnico Lisboa, Portugal.

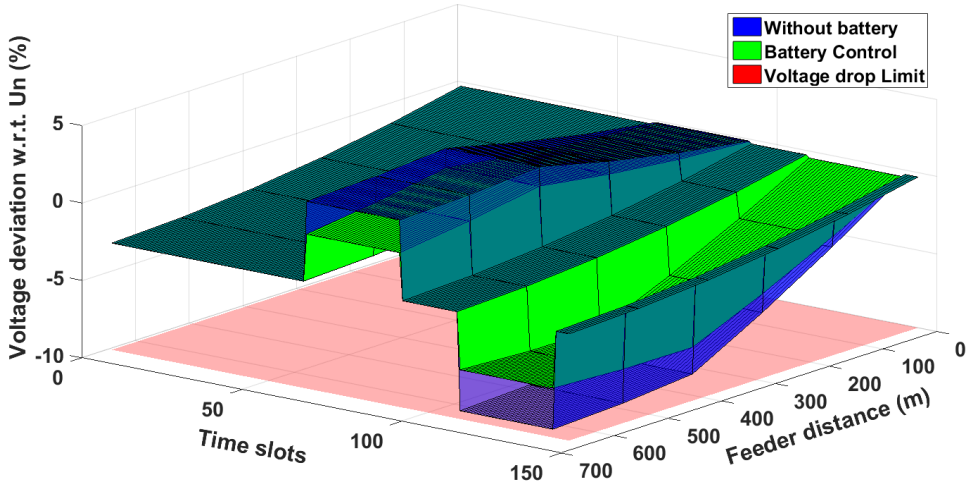

Figure 13.16: Impact on Voltage deviation.

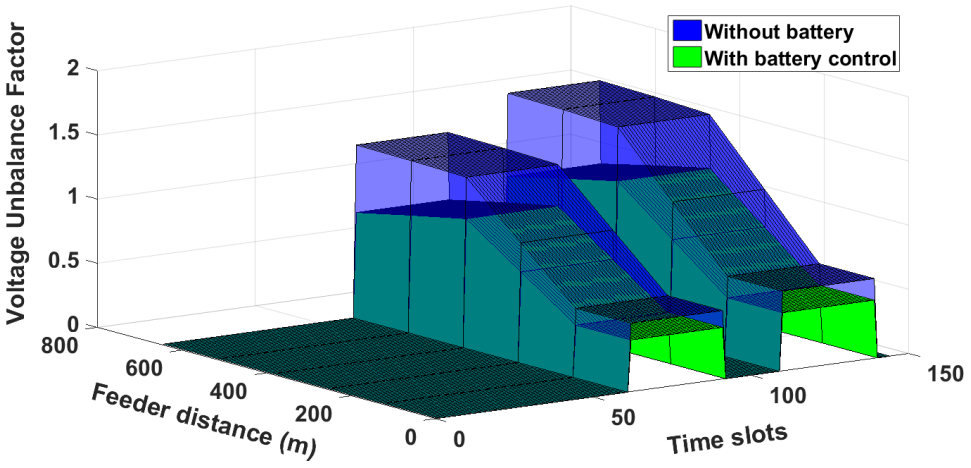

Figure 13.17: Impact on Voltage Unbalance Factor.

cialization of electric energy. The DSO is also the entity that acquires the electric energy that is produced by private micro- and mini-producers.

The electric grid in Madeira island is fed by five sources of energy, namely: hydro, wind, photovoltaic, solid waste incineration, and thermal energy from burning fossil fuels like diesel and natural gas. As of this writing the electric energy production in Madeira island is guaranteed by two thermal plants, 10 hydro plants, eight wind farms, one solid waste plant, three solar farms with 7 MW, 2 MW and 6 MW respectively, and 770 distributed solar micro and mini-producers, with full injection to the grid. The grid is composed of: 20 x 30/6.6 kV substations, 4 x 60/6.6 kV substations 3 x 60/30 kV substations and 2 x 60/30/6.6 kV substations.

The grid total losses amount to 8.6% of the total emission (2016). From that value, 0.5% are the responsibility of the HV networks (60 kV), 2.5% are losses at the MV level (30 and 6.6 kV), with the remaining 5.6% losses happen low voltage network. It should be noted that LV losses include commercial losses.

Power Quality Norms and Control Mechanisms for Voltage and Frequency

In Portugal, electric grids must primarily comply with the national Quality of Service Regulation (RQS) parameters (depicted in table 13.7), while also respecting the European Norm NP EN 50160:2010, which is the Portuguese version of the European Norm EN 50160: 1994 [3].

With respect to the control mechanism in the Madeira grid, in the present, voltage and frequency fluctuation are controlled by the thermal power stations through the available spinning reserve. Hydro power plants also provide some frequency control capability but only in situations where there are plenty of available hydro resources or the power plants are close to their rated power. In any case, the hydro plants are slower than the thermal ones, so they are not usually considered for voltage and frequency control.

Overall, the frequency is controlled by the largest generation group in the grid, whereas voltage at the LV substation can be regulated either at the HV/LV substation level, or locally through the transformer tap-changer.

Regulation for Mini/Micro-Production and Self-Consumption

The current legislation for micro-production and self-consumption of energy is defined by the Decree-Law no 153/2014 of October 20^{th} of 2014. This Decree-Law defines two types of Units of Production, the UPP (Unit of Small Production), and the UPAC (Unit Production for Self-Consumption).

UPPs are units of production, based on a single technology (e.g., solar or wind). All the energy produced by a UPP must be injected to in the Public Service Electric Grid (RESP). On the other hand, UPACs, are units of production that can be either off-grid or grid-connected. The energy produced by an UPAC, must be first used for self-consumption, and only then injected to the grid.

In Madeira, since the publication of the Decree-Law 153/2014, the local DSO does not accept new UPPs, and UPACs are not allowed to inject the excess energy to the RESP (i.e., excess production must be curtailed). This imposition is owing to the isolated nature of the Madeira electric grid that is very sensitive to variations in the energy produced by RES, hence the need to avoid direct injection to the grid. Nevertheless, EEM still maintains the 785 installations that were contracted prior to this decision.

13.4.2 Case of a Distribution Substation in Madeira

The selected low voltage (LV) distribution substation is located in one of the most western villages of Madeira Island. This substation has a transformer with an apparent power of 250 kVA, connected in

Metric	Nominal Value	Unit	Thresholds	
			Min	Max
Voltage	230	V	-10% (207)	+10% (253)
Frequency	50	Hz	-2% (49)	+2% (51)
Harmonics	-	-	THD $< 8\%$	
Flicker	-	-	Plt $< 1\%$	

Table 13.7: Grid Quality of Service thresholds as defined by the national Quality of Service Regulation, after the European norm EN 50160:2010.

[3] EN 50160: 1994, https://www.pasma.com.au/pdf/GuideToEN50160.pdf

delta-wye, which transforms voltage from the transmission grid (6600 V) to the distribution grid (400 V). The feeder capacity is of 62.5 kVA, i.e., 25% of the transformer capacity.

The substation has a daily average load of 27 kW, an Off-Peak power of 1 kW and a Peak power of 63 kW. At the moment the transformer's capacity is relatively high when compared with the power requested by the grid, mostly due to the expectation of growth in farming activities and local accommodation businesses in this rural area. This transformer feeds a low voltage distribution board (Quadro Geral de Baixa Tensão - QGBT) with five outputs outputs that distributes the electricity throughout the public grid, supplying around 100 customers consisting mostly of domestic, small businesses and agricultural facilities, with just a few three-phase installations (see figure 13.18 for an overview of the grid; the yellow dots represent the position of the UPP sites.).

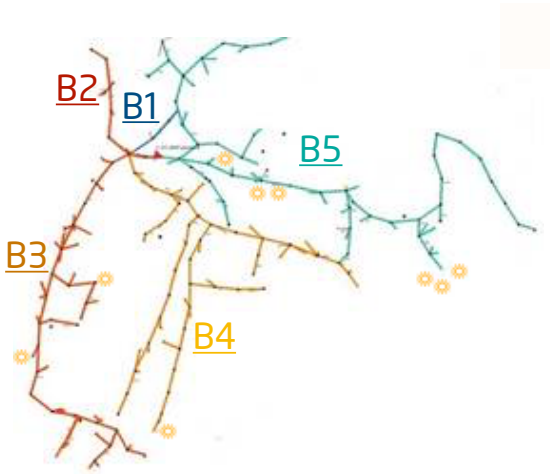

Figure 13.18: Madeira substation transformer five output branches and the nine connected UPPs

Presently, this is one of Madeira's LV substations with higher micro PV generation, with a total capacity of 36 kWp, distributed over nine UPPs (see table 13.8 for details), which is about 14% of the feeder capacity. As such, there is still a lot of room to connect new UPPs and UPACs, which will require additional efforts to keep the grid properly balanced.

Table 13.8: UPPs connected to the selected substation in the low voltage grid, and the respective installed PPV capacities.

UPP	kWp	Branch	Connected Phases
1	5.17	5	A B C
2	3.3	5	A B C
3	1.95	5	A B C
4	3.45	3	A
5	3.45	3	B
6	3.45	4	C
7	5.17	5	A
8	5.17	5	B
9	5.17	5	C

Phase Balancing

Presently, the Madeira electric grid is empirically or inherently balanced, i.e., the DSO/TSO relies on the experience of the distribution team to carefully plan and manage the grid, by always trying to do the best distribution of the installations in each phase (thus minimizing the potential for phase unbalance), and having the adequate extensions of the conductors (thus avoiding voltage fluctuations and the edge of the grid). Furthermore, before 2014, when deciding on the installation of a new UPP, extensive simulations were conducted in order to assess the potential effects of adding additional renewable storage in the energy mix. Any candidate installation that yielded grid quality parameters outside the accepted thresholds (shown in table 13.7), would not be accepted in order to avoid potential disturbances in the grid.

Still, and despite the best efforts, due to the stochastic nature of energy, and especially renewable production, there is still some considerable phase unbalance. For example, figure 13.19, presents the per

phase average active power between 11 and 17 March of 2019, showing an evident unbalance between the three phases. This unbalance in active power also leads to an unbalance in voltage, as shown in figure 13.20.

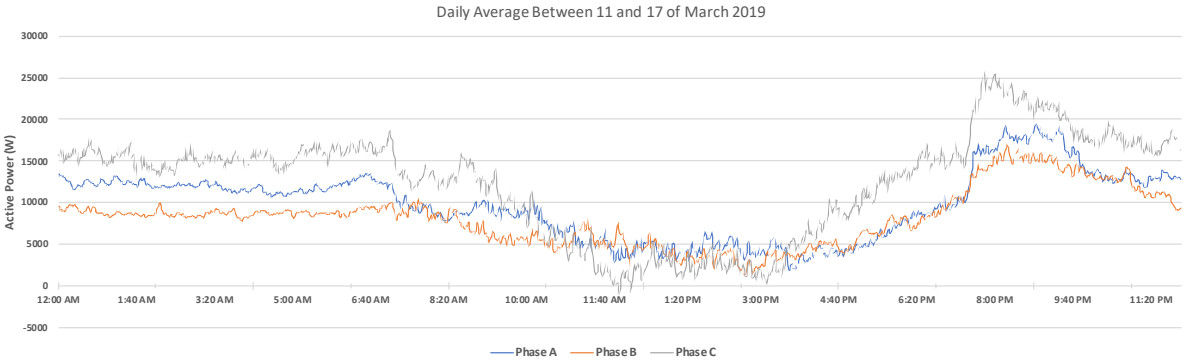

Figure 13.19: Active power per phase, averaged by minute between 11 and 17 of March 2019

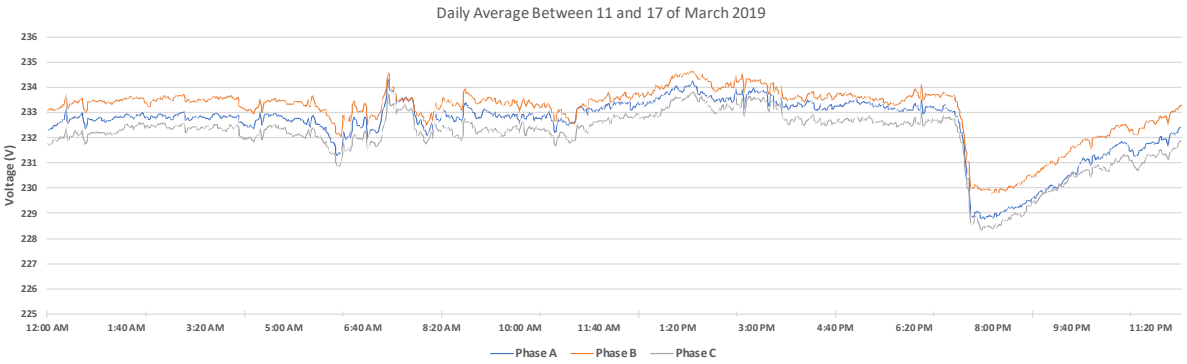

Figure 13.20: Voltage per phase, averaged by minute between 11 and 17 of March 2019

Ultimately, in a LV network, like the one presented here, phase unbalance can lead to an overload of the neutral conductor due to current leakage (show in Figure 13.21), and can ultimately lead to the presence of harmonics that in the long-term will affect the operation of inductive equipment (e.g., overheating, and speed variations).

Against this background, it is very relevant to study the possibility of providing improved grid control through the introduction of Battery Energy Storage Systems (BESS) at the distribution station level. Ultimately, the ability to coordinate active and reactive power balances at the distribution level would represent a major step towards safely increasing the injection of renewable energy sources in the Madeira electric grid. Furthermore, considering that most of the LV substations in Madeira Island have the same characteristics of this one with respect to load consumption (i.e., are mostly resistive), such a solution could be easily replicated in other substations since the only difference will be the amount of energy injected in the grid by the UPPs.

This is even more important when one considers that in the neat future grid-injection from renewable sources will be allowed once more. This will necessarily lead to an increase in the number of UPPs and UPACs connected to the Island's distribution stations, many of which should be from single-phase installations, which will cause further perturbation to the grid.

13.4.3 Q&A with the EEM Madeira

Which are the greatest problems that phase imbalance can cause in the grid?

In LV networks, the biggest problem of phase imbalance is the overload in the neutral conductor, given the leakage current. Furthermore, this can also lead to the presence of harmonics, that in the long-term will affect the operation of inductive equipment (overheating, speed variations).

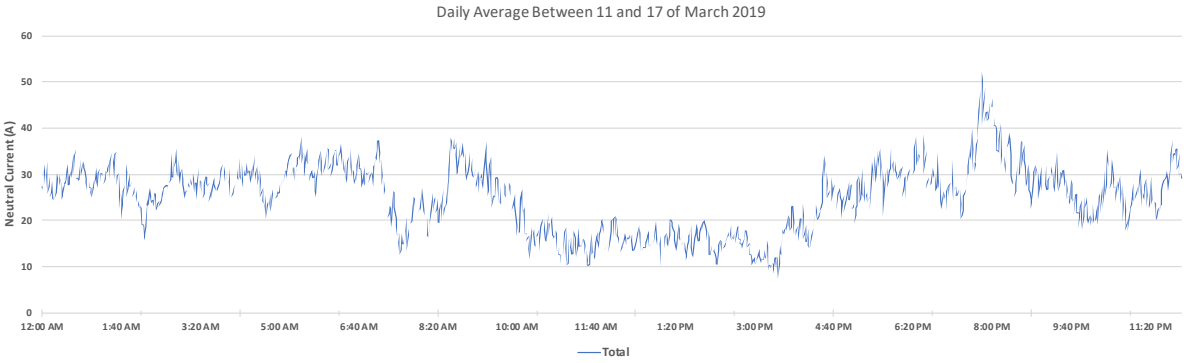

Figure 13.21: Neutral currents, averaged by minute between 11 and 17 of March 2019

What causes the larger imbalance: voltage, power distribution across the phases, or are they both related? I.e., if we solve one of the causes, does it solve the other?

The larger phase unbalance (of current) in LV happens at the phase distribution level, i.e., if all the clients had three-phase systems this problem would not occur. No, because voltage unbalance can also happen due to issues in the MV network.

What are the current solutions? Is there any norm to follow?

The current "solutions" are basically the careful planning and management of the grid: always try to do the best distribution of the installations in each phase, and try to have adequate extensions for the conductors (thus avoiding voltage fluctuations at the edge of the grid). Yes, in ML and LV networks the energy distribution must follow the NP EN 50160 norm[4].

How realistic is it to assume that the other DS in Madeira will behave similarly to this one?

The distribution grid at this DS, like with most LV networks in Madeira, is primarily resistive. Consequently, what will differentiate this from other DS is the amount of energy injected by the UPPs.

When there is a new request for an UPP, is there any defined process that must be followed to assess the impact of the installation?

Yes, the DSO/TSO performs a number of simulations using a proprietary planning software.

Is there any reference to the acceptable Power Factor values in the grid code?

The grid code is still under development. Nevertheless, we already have an estimate of the voltage and frequency control that was done through the modulation of active and reactive power in different installations.

Are there any active voltage compensation mechanisms? I ask this because at this point the Voltage is very well balanced, despite the presence of 9 UPPs

No. Instead, the distribution services make sure that all the consumers are qualitatively distributed across the three phases. In this end, this results in an empirical phase balancing.

What is the feeder capacity of this substation?

The apparent power of the transformer is 250 kVA, and the peak apparent power is about 68 kVA. As such, there is still a very big margin to connect new consumers. Nevertheless, and since the new grip-code is still to approve, the feeder capacity of any LV substation is of 25% of the transformers' capacity. For example, in Fazendinha this would be 62.5 kVA, meaning that there is still room for an additional 26.5 kWp of micro-production.

[4]NP EN 50160, https://paginas.fe.up.pt/ ee86007/pagina_norma_np_en_501602001.htm

13.5 Conclusion and Perspectives

The three phase network could face greater unbalance due to unequal distributed generation and/or load connected to each of the phases. Based on simulations of a radial distribution network on OpenDSS software platform we identify the indices that should be used for measuring three phase system unbalance: (a) VUF, (b) neutral losses and (c) line losses. Further, we observe that compensating phase imbalance is most effective if it is performed on the distant feeder in a radial distribution network.

Two case studies demonstrating phase imbalance is presented. The first case study is derived from data collected from Madeira Portugal. The utility in Madeira allots the phase in which new DGs in a network is to be connected, such a planned allocation of DG is aimed to achieve a balanced three phase network. However, unbalances are still observed as the DG production is not uniform in the phases (refer to Fig. 6.9 and Fig. 6.10 for imbalance in three phases). The second case study deals with EV charging testbed located at Caltech in Pasadena, California (refer to Chapter 2 Section 2.2.6).

We present three architectures of storage compensating system unbalance which might be caused due to unbalance load and/or distributed generation. It is observed that significantly smaller sized storage compared to imbalance magnitude can assist in reducing such an imbalance in three phases. More rigorous algorithm development is the future goal and not performed in this chapter.

Chapter 14

Conclusions and Future Directions

Life is like riding a bicycle. To keep your balance you must keep moving. - Albert Einstein

14.1 Conclusions

This thesis explores applications of energy storage in the context of power network participants, such as low and medium voltage consumers and large-scale storage applications for generators and aggregators. The contributions made in this thesis are categorized into four blocks: (i) energy arbitrage, (ii) co-optimization of storage, (iii) large-scale application and (iv) health consideration of battery.

The first contribution is the development of energy arbitrage algorithm in the presence of time-varying buying and selling price of electricity, charging and discharging efficiency losses, storage ramping and capacity constraint, inelastic load and renewable generation variation. The proposed algorithm is applicable for a piecewise linear convex cost function which is developed in the context of electricity consumers with inelastic load and renewable generation. This formulation can be applied for net-energy metering based compensation of excess generation. The proposed algorithm is compared with linear programming and convex optimization formulation to demonstrate the computational efficiency. We show that the worst-case run-time complexity is quadratic in the time horizon. Auto-regressive forecast models are implemented for rolling horizon or receding horizon model predictive control to take into account real-world uncertainties in electricity price, consumer load and renewable generation. The applicability of this proposed algorithm is demonstrated in case-studies using real data from several ISOs. Some key observations are presented as follows:

- Slow ramping batteries are less sensitive to uncertainties compared to faster-ramping batteries.
- Sensitivity analysis of the varying ratio of selling and buying price without and with net load (inelastic load and/or renewable generation) variation is performed. A high value of the ratio of selling and buying price affects more the sensitivity of arbitrage gains due to uncertainty in parameters. Storage operation can be profitable for the low selling price in the presence of consumer load and renewable generation, although only storage operation under the same compensation may not be profitable. This implies the value of storage under low selling price compared to buying price increases due to the presence of load and generation.
- Using a stylized example we show that the intermediate ramp rate (other than idle, minimum or maximum ramp) can be an optimal action for performing energy arbitrage under the assumption that decisions can be made only at discrete time-steps.
- Quantification of parameter uncertainties based on the compensation mechanism and pricing type is presented in Fig. 9.1. The pricing type is categorized into (a) real-time electricity price whose variations are not known a priori and (b) time-of-use pricing whose variations are known and the excess generation compensation can be categorized based one net-metering or NEM policy into (i) NEM 1.0 denotes selling price equal to buying price and (ii) NEM 2.0 denotes selling price lower than or equal to buying price. Combination of pricing type and excess generation compensation decides the parameters whose uncertainties affect the arbitrage gains. For instance, in Chapter 9 with a time-of-use price and NEM 1.0 excess generation compensation, we observe that the performing arbitrage is completely insensitive to future uncertainties in parameters.

Theoretical and analytical observations help us identify the governing parameters of following:

- *Sub-horizon*: is governed by (a) electricity price, (b) charging and discharging efficiency, (c) sampling time, (d) ratio of ramp rate and the rated storage capacity and (e) initial storage capacity,
- *Shadow price*: is governed by (a) electricity price and (b) charging and discharging efficiency,
- *Thresholds of storage operation*: are governed by (a) consumer inelastic load, (b) renewable generation, (c) electricity price, (d) storage ramp rate, (e) charging and discharging efficiency and (f) ratio of ramp rate and the rated capacity,
- *Effect of uncertainty* on arbitrage gains: governed by (a) relationship between sampling time [204] and the ratio of ramp rate and the rated storage capacity, (b) charging and discharging efficiency.

The dependencies listed above are identified for piecewise convex cost function for NEM 1.0 and NEM 2.0 in this thesis and require further exploration to quantify their relationship with each other. The proposed energy arbitrage algorithm is made open source in the form of arbitrage toolbox. The MATLAB code for the proposed algorithm is developed along with benchmark algorithms using convex optimization and linear programming. These benchmarks are also made open source.

Energy storage due to its high cost is often not financially viable to perform one dedicated task. The second key contribution of the thesis is co-optimizing formulations for increasing the total gains made by operating the battery. We present three co-optimization formulations in this thesis:

- Formulation 1: arbitrage + power factor correction : *showing active and reactive power control are largely decoupled* (a) the co-optimization problem for controlling the active and reactive power output of storage battery interfaced via a converter is almost decoupled. This is inferred based on no reduction in active power arbitrage gains due to reactive power compensations, (b) although active power output of storage requires lookahead over the time-horizon for maximizing arbitrage gains, the reactive power control requires no lookahead in time (in almost all cases), (c) uncertainty in parameters affects arbitrage gains, however, due to the independence of reactive power control over future uncertainties, the reactive power control is not affected by uncertainties in the near future.

- Formulation 2: arbitrage + power factor correction + peak demand shaving: *efficient formulation considering drastically different time-scales of the tasks* (a) co-optimization formulation considers the time scales of these tasks. Energy arbitrage and PFC are performed in a time-scale of minutes to an hour. However, peak demand shaving is performed in a time-scale of a month. Combining these time scales together makes this optimization problem intractable. We propose a memory variable for tracking the previous maximum power for applying peak demand shaving only if the power peak exceeds the previous maximum and reduce the optimization horizon to one day, in which the proposed co-optimization problem can be solved efficiently. (b) The benefits of co-optimizing are significantly greater than performing a dedicated or a few of these tasks together, see Fig. 7.2. For instance, performing only arbitrage and PFC could significantly increase the peak demand charge paid by the consumer, undermining the gains made by the consumer. Co-optimizing can reduce the consumer bill by up to 28.9% for a prosumer integrating 2 kWh 4C-4C[1] battery. Furthermore, control of battery operation cycles is proposed by the introduction of friction coefficient to manage cycle life degradation. (c) Simulation of 80 days of load data from Madeira, Portugal with real-time electricity price data from CAISO and peak demand charge from PG&E in California is performed. The uncertainty of system parameters is modeled using auto-regressive models and sequentially implemented as model predictive control of storage operation.

- Formulation 3: arbitrage + peak demand shaving + energy backup + self-sufficiency: *storage operation is tailored according to consumer contracts applicable to LV consumers in Madeira, Portugal.* (a) A convex formulation is proposed for storage control for co-optimizing arbitrage, peak demand charges saving and backup reserve during power outages considering efficiency losses, ramping and capacity constraints for a battery. (b) Considering storage operational cycle degradation, we calculate gains per cycle indicating the battery can be financially viable in Madeira with a simple payback period of approximately 3 years. (c) Numerical results indicate the following: (i) ramping capability primarily decides the ability to reduce peak demand charge savings for consumers, (ii) providing energy backup for probable and scheduled power outages does not noticeably reduce storage ability to perform peak demand and/or arbitrage and (iii) for DG generating more than inelastic load, storage

[1] xC-yC notation represent the relationship between ramp rate and battery capacity. xC-yC implies battery takes 1/x hours to charge and 1/y hours to discharge completely.

also contributes to self-sufficiency by increasing self-consumption. (d) The proposed co-optimization formulation is used for recommending the best-suited consumer contract based on inelastic load and renewable generation variation. In Madeira, LV consumers select from an array of a total of 48 different contracts. This framework can be used for the selection of the best-suited consumer contract depending on consumption pattern, renewable generation and available storage (or flexibility).

A case-study of storage applications for LV consumers in Uruguay is also performed. Storage operation is used for co-optimizing energy arbitrage along with reactive energy compensation. It is observed that due to the net-metering policy and time-of-use pricing, the storage operation is immune to any parameter uncertainty. In this special case, storage can be operated using pre-decided thresholds and optimal profit can be ensured. We observe that depending on consumer inelastic load and renewable generation integrating storage can be profitable.

The third key contribution of this thesis is proposing *large scale applications of batteries*, such as

- Distributed control of a fleet of batteries: control architecture for a distributed fleet of batteries is proposed which can accurately track a grid level signal with much faster temporal characteristics (compared to amount of energy charged or discharges in one sample of time) using a fleet of batteries, while maintaining individual SoC within desired bounds. Proposed control solution also maintains the SoC of the fleet of batteries in the desired of operation and increases the idle time of each battery. This controller consists of a centralized decision maker and local control design. Each of the battery in the fleet has their independent local controller and there is no information exchange among these local controllers. From simulation results, we observe: (a) the fleet of batteries cooperates in tracking a regulation signal and do not chatter. In case of chattering, some batteries will compensate each other by charging and discharging. This will increase the operational cycles causing the battery to reach its end-of-life faster. (b) Properties of the distributed control proposed: (i) minimum communication requirement as the centralized control sends a scalar signal which the local control use for taking decisions, (ii) considering Quality-of-Service (QoS) for batteries by including bounds on SoC. Further, the stochastic control increases the idle time of the batteries thus increasing battery life, (iii) scalability: the complexity of the control solution (using randomization) does not grow with the number of batteries.
- Phase balancing: The bulk of behind the meter resources such as rooftop solar generation and electric vehicle charging are single phase connected to three-phase distribution systems. Ad hoc growth of single phase connected DGs and EVs can lead to unbalanced three phases with negative consequences on power network efficiency. We conducted stylized simulations on a 3 phase 4 wire radial distribution network using an openDSS-based simulator to understand the effects of phase unbalance. We measure Voltage Unbalance Factor and we identify the negative impacts of phase unbalance which increases: (i) voltage drop/rise, (ii) neutral losses and (iii) phase losses in 3 phase 4 wire distribution network. We evaluate the integration of storage in the distribution network aimed to balance load across phases. It is observed that relatively small-sized storage (compared to unbalance magnitude; storage size upto 10% of imbalance) can significantly reduce the radial distribution network unbalance. We identify that the best location to install a battery in such a distribution network is at the end node of the distribution feeder, regardless of the location where the imbalance is created. We propose three storage control architectures for balancing active and reactive power: (a) three batteries dedicated for each phase, (b) three batteries with phase selector ensuring SoC level in each battery and (c) single battery with phase selector. The implementation of control mechanisms for all these architectures can be considered as the future extension of this topic. Then, unbalance case study of a substation in Madeira in Portugal due to DG integration is presented. We detail the mechanism in which power network operators plan to locate the DGs in the distribution network so as balancing by design could be achieved. However, in spite of controlled placement of DGs, substation operators observed imbalance in the distribution side. Their primary concern happened to be high neutral conductor current which often leads to a significant amount of losses. We also show some of the data collected at the substation. We list the DG allocation procedure in context of Madeira. Note that such a meticulous phase allocation might not be possible in more densely populated regions, therefore, the problem of unbalance will be more pronounced compared to the substation case study presented.

The fourth key contribution of the thesis is to bring health or life aspect of batteries in control design. Batteries have a limited life and need to be utilized appropriately so as the operational life can be increased.

1. Nominal design of battery: Note that over-charging and over-discharging for Li-Ion battery raises safety concerns and also drastically affects battery operational life. Batteries, unlike loads, do not have a nominal behavior. For instance, the water heater should operate during morning and evening when hot water is needed by the consumer. The batteries, on the other hand, should remain idle when not needed. A continuous Markov model with two components is proposed with the following properties:
   - The first component have three states: charging, discharging or idle,
   - The second component of Markov model is the state-of-charge of a battery (continuous variable),
   - Battery should charge with high probability when the SoC is lower than a certain level and discharge with high probability for a higher level of SoC. This probability distribution keeps the battery SoC in the pre-decided desired band. The probability to remain idle is high in if the SoC remains in this band. This nominal design of batteries increases the idle time in effect reduces stress on each of the batteries.

   The proposed nominal battery model (a) increases idle time, (b) avoids battery overcharging and over-discharging.
2. Energy storage devices have finite ability to absorb or inject power due to its finite capacity. Batteries participating in fast dynamic regulation should operate ensuring the regulation signal denoting the system imbalance is tracked accurately and at the same time battery charge level is maintained which will ensure the battery can track the dynamic signal sustainably without reaching minimum or maximum charge level. In such a case the battery cannot either ramp-up or ramp-down. We propose an drift compensation layer of control to the distributed stochastic control of a fleet of batteries proposed in Chapter 11, in order to maintain state-of-charge (SoC) of the battery in the optimal band of operation. The proposed controller is designed using Linear Quadratic Regulator (LQR) which minimizes the input energy and tracking error for aggregate power and SoC, and gain scheduling for adaptive proportional gain for larger deviation of battery charge level. Using numerical simulations we show that the addition of this layer of control does not deteriorate the ability of distributed fleet of batteries to perform fast dynamic regulation and it assists in the stable operation of a fleet of batteries in presence of efficiency losses and non-zero mean regulation signal. We use PJM's performance evaluation metrics to compare scenarios.

3. We consider cycle and calendar life of the battery and propose mechanisms to control operational cycles such that the battery operational life is increased: Batteries have a limited operational life, often bounded by its calendar life and cycle life. Calendar life refers to the maximum age of a battery. For example, if the calendar life is 10 years, then even if the battery is not used the battery with high probability will reach its end-of-life in this period. The second index is cycle life, which bounds the maximum number of operational cycles that a battery can perform. The operation cycles measurement should consider the depth-of-discharge of each cycle. For instance cycle with 10% change in SoC cannot be directly compared with 80% change in SoC cycle. We propose an algorithm for calculating equivalent operation cycles based on ramping trajectory. We claim that the operational life battery will be increased if the degradation of battery due to ageing matches that to the degradation due to operation cycles. The rationale to select this degradation model of battery is based on battery datasheet which often mentions the cycle and calendar life of the battery and also provides the relationship of operation cycles and depth-of-discharge.

   The next step in increasing battery operational life is to control the operation cycles. For storage performing arbitrage we propose a friction coefficient which can be tuned to control the cycles that the battery operates. This friction coefficient is motivated by increasing the dead-band where optimal action for a battery is to remain idle. Therefore, the inclusion of friction coefficient only eliminates the low returning transactions and do not affect the arbitrage gains significantly. In a numerical experiment performed in Chapter 7, we observe that reducing friction coefficient from 1 to 0.8 has less than 2.1% effect on total gains, however, the number of cycles is reduced by more than 53.4%. The operation cycles for storage performing dynamic regulation can be controlled by tuning the ramping commitments[2] made by storage owners.

[2]Fast regulation signal sent to ancillary service providing resources which commit to ramp up or ramp down; these commitments are often made in terms of peak ramping capabilities that the resource can perform.

14.2 Future Directions

14.2.1 Selection of best-suited energy storage

In this thesis, we made several interesting observation which can help in selecting the best-suited battery in terms of financial returns. Some of these observations are:

- Ramping capability (maximum discharging and charging power constraint) of battery decides the peak demand shaving performed by the storage device for a given peak load. This implies installing storage device for only peak demand shaving should aim to maximize the ramping capability of storage for a given cost (refer to Chapter 7 and Chapter 8).
- Cycles of operation decided based on the storage application, the ratio of ramp rate and storage capacity, efficiency losses etc. Storage installations should consider that $/cycle of storage devices is enough to be financially feasible.
- The lookahead time horizon depends on (a) initial storage capacity, (b) electricity price variation, (c) storage efficiency, (d) ratio of ramp rate overcapacity and (e) sampling time of decision making (refer to the case study provided in Chapter 3.5).
- Storage in presence of renewable energy and inelastic load can still be profitable for selling price relatively smaller compared to buying price of electricity. Note that for the same compensation, without renewable generation and inelastic load energy storage cannot be profitable as inelastic load and local generation adds value to energy storage, [176], as the ratio of selling price and buying price is closer to zero, see Fig. 4.8.

From the contributions made in this thesis, one can say that best-suited storage selection will be governed by the following four factors:

1. *Applications* for which storage is to be installed: as discussed in this thesis, storage can be used for different applications. The tasks allocated to storage decides the operational cycle of storage and thus affect the returns and life of the battery. Refer to Chapter 2.2 for some of the storage applications summarized.
2. *External factors* affecting size and storage type are: (i) sampling time of storage operation, (ii) incentive mechanism of applications for example for arbitrage it will be a variation in electricity price, (iii) inelastic load, (iv) renewable generation.
3. *Storage parameters*: A more thorough analysis of how to select energy storage parameters are required. Selecting battery parameters 1- charging and discharging efficiency, 2- ramp rates/battery capacity (defines the charging and discharging time required), 3- available capacity, 4- cycles of operation, 5- calender life, 6- self-discharge or leakage, 7- converter size, 8- converter losses and operational life, 9- nonlinear constraints such as charging and discharging ramp rate which is governed by SoC, 10- degradation characteristic of storage would lead to increased internal losses, lowering of useful capacity.
4. *Financial feasibility*: In this thesis, we proposed a new mechanism to identify storage profitability. We proposed the calculation of $/cycle which takes into account storage operational cycle and returns. This way identifying the value of storage intrinsically considers storage degradation into account.

The four governing factors are correlated and coupled. Statistical tools need to be developed for selecting the best-suited storage for an application or several applications.

We believe that there is a gap in battery selection problem based on parameters. The statistical tool would also help investors answer the question of selection of best-suited storage technology for some application(s), from (see Table 2.1): (a) Lithium Ion, (b) lead acid, (c) flow battery, (d) pumped hydro, (e) flywheel, (f) ultra-capacitor (etc.).

14.2.2 Optimal lookahead horizon for hydro generation facilities

Hydro facilities can be modeled as a battery with dynamic parameters. The power ramping capability is a nonlinear function of the height of the water head in the reservoir. Since the ratio of ramp rate over battery capacity for hydro is significantly smaller compared to Li-Ion batteries, the lookahead required for decision making for hydro facilities will be longer, see CAISO case-study presented in Chapter 3.5. Choosing an optimal lookahead horizon would ensure the best use of computational resources and avoid oversizing or under-sizing issues.

14.2.3 Storage/DG/Load placement based on voltage profile

Power network is evolving, new loads such as electric vehicles and distributed generation will be disruptive on how traditional power system used to work. The problem of placement of new loads such as EV charging facility, data-centers etc, flexibility such as battery and distributed generation will be critical to the healthy operation of the power network. There are many different directions for these problems, some of which could be:

- development of the new standards and protocols for energy participants: consumers, producers and energy traders,
- infrastructure deployment planners which aim to minimize the expenditure required for power network upgrades,
- redesigning relays and adjust the settings of relays for ensuring two-way power flow in power network with an especial focus to the distribution network,
- reanalyzing optimal power flow constraints which could get modified due to such an evolution of the power network,
- localized flexibility planning in the form of responsive loads and/or storage for mitigation of congestion at the local level.

Using a case-study we show in Chapter 2.2.8 that the voltage profile of a network distorts due to the integration of DGs or EVs (see Fig. 2.8). New storage, DG and EV charging placement is critical for the stability of the power system. Identification of best location should consider (a) local voltage profile, (b) the effect inclusion of new loads or generation on the rest of the network. Similarly, storage placement should consider buses where it could provide the maximum support for the voltage.

Consider the nominal voltage of bus i of a network is denoted as V_i^N. The voltage constraint states that the bus voltages should be within the lower and upper voltage level denoted as $V_i^N \in [V_l, V_u] \ \forall \ i$, where V_l denotes the lower voltage level and V_l denotes the upper voltage level. Consider the network under consideration has B buses.

Consider we add DG and/or EV in one of the buses of the network denoted by bus index j. Such inclusion will modify the voltage profile in the complete network. We denote the new voltage at bus i with new load/DG/flexibility as $V_i^{T_j}$, here T_j denotes the change in network at bus j.

Next we define two indices which measures the cumulative distance of voltage from the boundaries as: upper and lower slack defined as

$$I_u^N = \sum_{i=1}^{B} (V_u - V_i^N), \qquad I_l^N = \sum_{i=1}^{B} (V_i^N - V_l)$$

The indices with inclusion of DG and/or load connected at bus j is denoted as

$$I_u^{T_j} = \sum_{i=1}^{B} (V_u - V_i^{T_j}), \qquad I_l^{T_j} = \sum_{i=1}^{B} (V_i^{T_j} - V_l)$$

Using the above definitions we define differential slack (compares the nominal case with the modified network case) denoted as

$$\Delta I_u^j = I_u^N - I_u^{T_j} \tag{14.2.1}$$

$$\Delta I_l^j = I_l^N - I_l^{T_j} \tag{14.2.2}$$

DG integration

With the integration of DGs, the voltage profile will be lifted above the nominal case for any network considering other loads and generation remains the same. Thus if a large amount of DGs is included the voltage profile would probably violate the upper boundary. Therefore, in the DG integration case, the network operator should consider minimizing the value of ΔI_u^j by selecting the j to place those DGs. This problem is given is as

$$J_{DG} = \min_{j \in \{1,2,\ldots,B\}} \Delta I_u^j. \tag{14.2.3}$$

Note that ΔI_u^j is calculated for buses $i \in \{1, 2, ..., B\}$ by connecting the same rating of DG at each bus.

For a network, we rank the buses $j_1, j_2, j_3, ..., j_B$ such that $\Delta I_u^{j_1} \leq \Delta I_u^{j_2} \leq \Delta I_u^{j_3} \leq ... \leq \Delta I_u^{j_B}$. If DG placement is considered then DGs should be placed in j_1 then in j_2 and so on. This ranking shows that connecting same amount of DG at a different bus of the network has a different impact on the whole network. By identifying J_{DG} by solving Eq. 14.2.3 we minimize the impact of adding DG in the network.

Feeder hosting capacity for some buses is higher compared to others in a network. Such buses should be selected for planned DG installations. Solving Eq. 14.2.3 provides such buses with higher feeder hosting capacity.

New load integration

Loads such as electric vehicle charging facility, data centers have the flexibility to be placed in a network. With the integration of new loads, the voltage profile will be pulled lower than the nominal case for any network considering other loads and generation remains the same. Thus if a large number of new loads are included the voltage profile would probably violate the lower boundary. Therefore, in a new load integration case, the network operator should consider minimizing the value of ΔI_l^j by selecting the j to place those new loads. This problem is given is as

$$J_{\text{load}} = \min_{j \in \{1,2,...,B\}} \Delta I_l^j. \tag{14.2.4}$$

Note that ΔI_l^j is calculated for buses $i \in \{1, 2, ..., B\}$ by connecting the same rating of loads at each bus. For a network, we rank the buses $j_1, j_2, j_3, ..., j_B$ such that $\Delta I_l^{j_1} \leq \Delta I_l^{j_2} \leq \Delta I_l^{j_3} \leq ... \leq \Delta I_l^{j_B}$. If load placement is considered then new loads should be placed in j_1 then in j_2 and so on. This ranking shows that connecting the same amount of new loads at a different bus of the network has a different impact on the whole network. By identifying J_{load} by solving Eq. 14.2.4 we minimize the impact of new load in the network. Solving Eq. 14.2.4 the utility can decide the locations for new loads such as EV charging stations for instance.

Storage integration

Storage can ramp up or ramp down or it could act as a load while charging and a DG while discharging. Thus energy storage could help the network not only in resolving network congestion (under-voltage) but also in over-voltage cases that might happen due to DG generation. The storage owner would like to place their storage at the bus where the value created by such placement on the network could be maximized. Therefore, in DG integration case the network operator should consider to minimize the value of $\Delta I_l^j + \Delta I_u^j$ by selecting the j to place those storage devices. This problem is given is as

$$J_{\text{store}} = \min_{j \in \{1,2,...,B\}} (\Delta I_l^j + \Delta I_u^j). \tag{14.2.5}$$

We define $\Delta I^j = \Delta I_l^j + \Delta I_u^j$. For a network, we rank the buses $j_1, j_2, j_3, ..., j_B$ such that $\Delta I^{j_1} \leq \Delta I^{j_2} \leq \Delta I^{j_3} \leq ... \leq \Delta I^{j_B}$. If storage placement is considered then storage should be placed in j_1 then in j_2 and so on. This ranking shows that connecting the same amount of storage at a different bus of the network have a different impact on the whole network. By identifying J_{store} by solving Eq. 14.2.5 we minimize the impact of adding storage in the network.

Note that by solving Eq. 14.2.5 we can comment only about the desired power rating of the energy storage to be placed, however, for identifying storage capacity, extended simulations for longer time horizon should be considered.

14.2.4 Modeling flexible loads as batteries

In a preliminary work presented as [173] we evaluate the control of flexible loads based on electricity price variation. This work divides flexible loads into (i) loads which can be shifted in time and their nominal consumption profile can we steered, for example electric vehicle charging which can be shifted in time as well the charging profile can be altered ensuring the EV battery is charged to a desired level within the specified window, (ii) loads which can be modified in time within a flexible window, however, their consumption profile cannot be altered. For example, motor based loads such as washing machine, dishwasher etc. Using this framework a numerical experiment using real consumption data from Pecan Street [58] and electricity price data from ERCOT [16] is presented for home ID 5357 for 3rd and 4th January 2017.

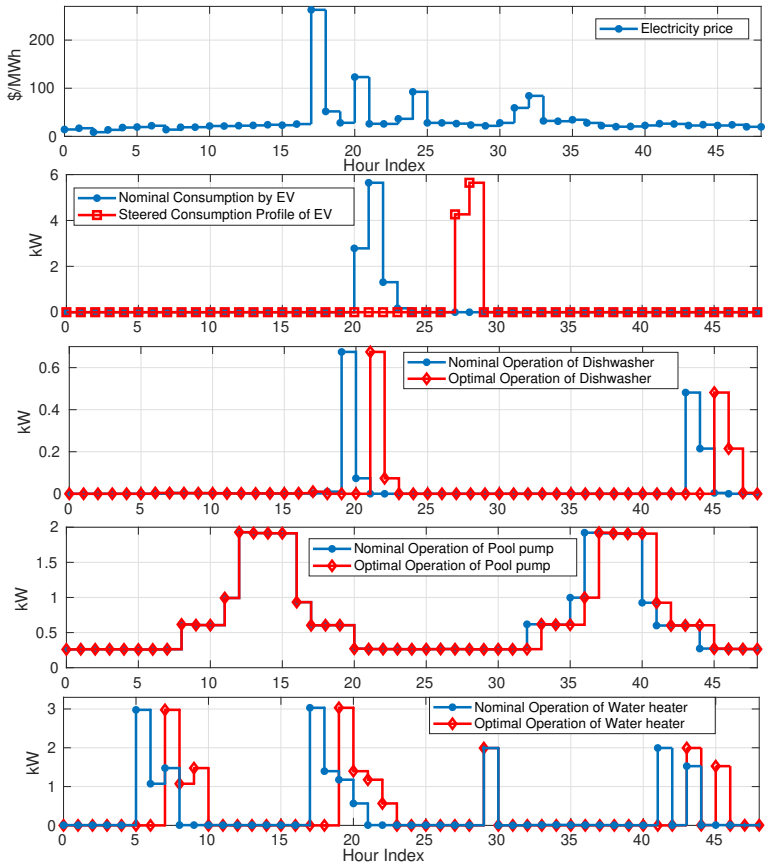

Figure 14.1: The nominal operation versus the optimal operation of flexible loads considering electricity price, flexibility window [173].

Fig. 14.1 shows the nominal and optimal operation of flexible devices considering price variations considering the window of flexibility and end-time, refer to [173] for details of the experiment.

The deviation of new consumption profile is denoted as

$$L_{\Delta}(t) = \text{Optimal Load at time } t - \text{Nominal load at time } t, \tag{14.2.6}$$

Fig. 14.2 shows the deviation from the nominal operation. Note L_{Δ} is a zero mean signal.

Clearly, L_{Δ} shown in Fig. 14.2 can be modeled as $\eta_{\text{ch}} = \eta_{\text{ch}} = 1$ battery. L_{Δ} denoting the ramp rate of this virtual battery. The advantages of modeling flexible loads as a battery is that the insights developed on storage control in this thesis can be applied to controlling loads. Further work is required for robust *virtual battery* model for (i) aggregating homogeneous and heterogeneous size of the same type of flexible load (ii) aggregating homogeneous and heterogeneous size of different types of flexible loads.

14.2.5 Minimizing renewable energy curtailment

Consider using renewable generators used as conventional generators, where these facilities commit a certain power output during a certain time of the day. In order to match these commitments, renewable generation facility owners install energy storage. The storage device helps in matching commitments and also in reducing wastage of renewable generation. Such a storage integration can only be effective with forecast accuracy, which will also decide the size of the battery. Note that the marginal value of integrating storage deteriorates with size, thus the sizing should consider financial limitations into decision making cycle.

14.2.6 Extension of topics covered in thesis

(1) *Energy arbitrage*:

- Extending the proposed optimal arbitrage algorithm for any convex function. The convex function can be approximated using to k linear segment piecewise linear components. It will of interest to compare the sensitivity of the number of segments and the optimality gap.

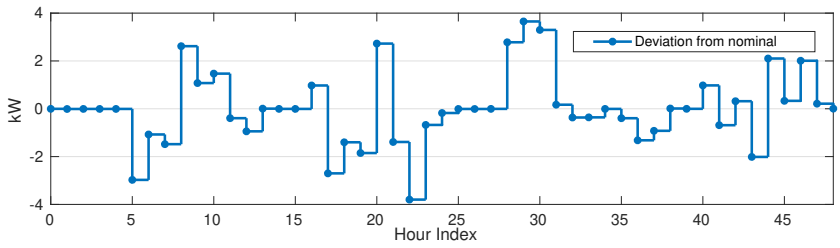

Figure 14.2: Deviation from the nominal operation

- Presenting an algorithm which applies for positive and negative electricity prices with optimal guarantees.
- Price maker problem: market impact factor and storage usage applicable to the storage of large size affecting electricity markets with their operation.
- Closed form rule to identify the sub-horizon; In chapters 3 and 4, we identify that the length of sub-horizon depends on (a) initial storage capacity, (b) electricity price variation, (c) storage efficiency, (d) ratio of ramp rate overcapacity and (e) sampling time of decision making. Further work is required to quantify the effect of these factors and perform a sensitivity analysis.

(2) *Co-optimization* exploring storage applications not considered here: congestions, reserve allocation and spectral decomposition of imbalance signal for ancillary services for different time scales.

(3) *Health* - dynamic degradation model taking into account battery chemistry.

(4) *Forecast model* - more efficient forecast model taking into account computation required to perform forecast; comparing computation required and loss in opportunity. Parameter uncertainty can be compensated more effectively with more sophisticated forecast models.

(5) *Fleet of batteries*: redesigning the nominal model to account for storage ramping asymmetries. Discretization of storage ramp levels into more finer levels which would require the nominal model to be adapted.

(6) *Spectral demand decomposition* and reserve planning problem for installing different ramping batteries in order to balance and supply more accurately.

(7) Storage/flexibility allocations for different time scale operation for enhancing grid reliability.

In this thesis, we consider batteries for various applications for electricity consumers, and aggregator/utility. Storage is becoming more and more financially relevant and near future storage, deployments are going to grow. However, with the growth of advanced communication infrastructure, artificial intelligence-based decision making load flexibility modeled as virtual batteries will eventually replace real batteries.

Appendix A

Appendix 1

A.1 Proof of Theorem 3.2.1

We first prove existence of (x^*, α^*, β^*) such that:

1. x^* is the primal optimal solution,
2. (α^*, β^*) is the dual optimal solution, and
3. the optimality gap is zero (strong duality).

Since the constraints of the primal problem are all linear, weak Slater's constraint qualification conditions (which imply strong duality) follow simply from the feasibility of the primal problem. Clearly, under the assumptions $b_{\min} \leq b_{\max}, \delta_{\min} \leq \delta_{\max}$, $b_0 \in [b_{\min}, b_{\max}]$, $0 \in [\delta_{\min}, \delta_{\max}]$ a feasible solution exists ($x_i = 0$ for all $i = 1, 2, \ldots, N$ is feasible). Furthermore, since the primal objective function is continuous and the constraints define a convex compact set, its minimum must be finite and achieved at the some x^* in the feasibility region. According to the strong duality theorem, the above facts imply that the dual problem must be maximized at some (α^*, β^*) and the duality gap must be zero.

From the above reasoning it also follows that (x^*, α^*, β^*) must be the saddle point satisfying the KKT conditions. Hence, using RHS inequality of the Saddle Point conditions,

$$\mathscr{L}(x^*, \alpha^*, \beta^*) \leq \mathscr{L}(x, \alpha^*, \beta^*)$$

$$\implies \sum_{i=1}^{N} \left\{ C^{(i)}_{\text{storage}}(x_i^*) + \alpha_i^*(b_{\min} - b_i^*) + \beta_i^*(b_i^* - b_{max}) \right\}$$

$$\leq \sum_{i=1}^{N} \left\{ C^{(i)}_{\text{storage}}(x_i) + \alpha_i^*(b_{min} - b_i) + \beta_i^*(b_i - b_{max}) \right\}$$

Substituting $b_i = b_0 + \sum_{j=1}^{i} x_j$ we get,

$$\sum_{i=1}^{N} \left\{ C^{(i)}_{\text{storage}}(x_i^*) - \mu_i^* x_i^* \right\} \leq \sum_{i=1}^{N} \left\{ C_{\text{storage}}(x_i) - \mu_i^* x_i \right\} \tag{A.1.1}$$

where $\mu_i^* = \sum_{j=i}^{N} (\alpha_j^* - \beta_j^*)$. μ_i^* is the accumulated Lagrange multiplier for time instant i to N. Hence,

$$\mu_k^* - \mu_{k+1}^* = (\alpha_k^* - \beta_k^*) \tag{A.1.2}$$

The complementary slackness conditions for the Lagrangian are defined as

$$\alpha_i(b_{\min} - b_i) = 0, \quad \beta_i(b_i - b_{\max}) = 0, \forall i \text{ s.t. } \alpha_i, \beta_i \geq 0$$

Equation (8) derived above and complementary slackness conditions implies following relation of μ_k^* and μ_{k+1}^* ,

$$\mu_{k+1}^* \begin{cases} = \mu_k^*, & \text{if } b_{min} < b_k^* < b_{max} \quad \text{as} \quad \alpha_k^* = \beta_k^* = 0 \\ \leq \mu_k^*, & \text{if } b_k^* = b_{min} \quad \text{as} \quad \alpha_k^* \geq 0 \text{ and } \beta_k^* = 0 \\ \geq \mu_k^*, & \text{if } b_k^* = b_{max} \quad \text{as} \quad \alpha_k^* = 0 \text{ and } \beta_k^* \geq 0 \end{cases}$$

The accumulated Lagrangian i.e. μ for the N^{th} (last) instant is $\mu_N^* = \alpha_N^* - \beta_N^*$, therefore

$$\mu_N^* = \begin{cases} = 0^*, & \text{if } b_{min} < b_N^* < b_{max} \\ \geq 0, & \text{if } b_N^* = b_{min} \\ \leq 0, & \text{if } b_N^* = b_{max} \end{cases}$$

Such a x^* solves the optimal arbitrage problem (P_{NEM1}) and α^*, β^* solves the dual problem. □

A.2 Convex Optimization: Conditions of Optimality

A.2.1 Convex Function and Subdifferential

Let $f : X \to \mathbb{R}$ be a function. The function f is convex if:

- $\mathbf{dom}(f)$ is convex in $\mathbb{R}^n$ *(convex set in a real vector space)*
- $f\big(\alpha x_1 + (1-\alpha)x_2\big) \leq \alpha f(x_1) + (1-\alpha) f(x_2)\ \forall\ x_1, x_2 \in \mathbf{dom}(f)$ and $\alpha \in [0,1]$
- Second Order Condition: $\nabla^2 f(x) \geq 0\ \forall\ x \in \mathbf{dom}(f)$
- First Order Condition: $f(z) \geq f(x) + \nabla f(x)^T (z - x)\ \forall\ x, z \in \mathbf{dom}(f)$

Let us analyze the First Order Condition (FOC) described above. By the definition of differentiation:

$$f'(a) = \lim_{h \to 0} \frac{f(a+h) - f(a)}{h}$$
$$\implies f(a+h) = f(a) + h \times f'(a)$$

For convexity to hold by FOC, the following condition must be valid:

$$f(a+h) \geq f(a) + h \times f'(a)$$

For the above equation to be valid $f'(a) \geq 0$ which implies the derivative of f is monotonically non-decreasing in the whole interval $\mathbf{dom}(f)$ i.e. $\nabla f(x)$ is either equal or more than what it was in the preceding value for which the function is evaluated.

Subgradient: g is a subgradient of f (not necessarily convex) at x if

$$f(z) \geq f(x) + g^T (z - x) \quad \forall z$$
$$\implies -g^T z + f(z) \geq -g^T x + f(x)$$

If $f(x) > -\infty\ \forall \quad x \in \mathbb{R}^n$, then

$$\mathbf{epi} f = \Big((x, \omega) | f(x) \leq \omega, \quad x \in \mathbb{R}^n \Big)$$

$$\begin{bmatrix} -g^T \\ 1 \end{bmatrix} \times \begin{bmatrix} x \\ f(x) \end{bmatrix} \leq \begin{bmatrix} -g^T \\ 1 \end{bmatrix} \times \begin{bmatrix} y \\ \omega \end{bmatrix} \quad (x, \omega) \in \mathbf{epi} f$$

The Hyperplane H is defined as,

$$H = \big[(y, \omega) \in \mathbb{R}^{n+1} | \quad (-g, 1)^T (y, \omega) = (-g, 1)^T (x, f(x)) \big]$$

The hyperplane H supports **epi** f at the vector $(x, f(x))$. The interpretation of g is a subgradient at x iff the hyper-plane in $\mathbb{R}^{n+1}$ has a normal $(-g, 1)$ and passes through $(x, f(x))$ supports the epigraph of f.

The set of all subgradients of f at point x in $\mathbf{dom}(f)$ is called the subdifferential of f at x and denoted as $\partial f(x)$.

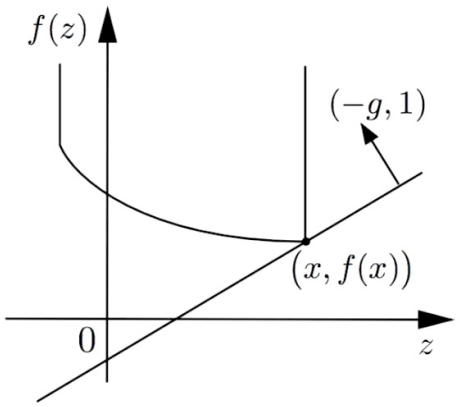

Figure A.1: The Subgradients [99]

A.2.2 Optimality condition for unconstrained problem

The cost function $f(x)$ is to be minimized is subjected to no constraints and $x \in X$
Case 1: If f is convex and differentiable then the optimal solution x^* is defined as,

$$f(x^*) = \inf_x f(x) \quad \implies \nabla f(x^*) = 0 \text{ from FOC.}$$

Case 2: Generalizations to nondifferentiable convex function f will also be valid:

$$f(x^*) = \inf_x f(x) \quad \implies \partial f(x^*) = 0$$

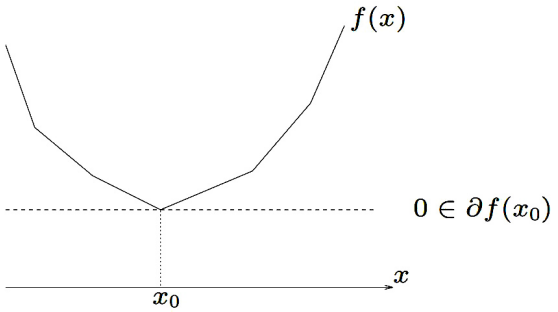

Figure A.2: Generalization of FOC for non-smooth functions [108]

Figure 14 provides us a clear interpretation of applicability of FOC for non-smooth convex functions. This intuition is essential as a constrained optimization problem can be converted into unconstrained minimization of the Lagrangian, in that case we should anticipate that $0 \in \partial \mathscr{L}$.

A.2.3 Constrained Optimization Primal Problem (P)

In practice we have equality and inequality constraints that are imposed on the objective function like minimization of cost or maximization of revenue. We define a general constrained optimal problem and use the same notation as [284].

$$\begin{aligned} \textbf{(P)} \quad & \text{minimize } f_0(x) \quad \text{over } C \in \mathbb{R}^n \\ & \text{subject to: } f_1(x) \leq 0, \quad \ldots. \quad , f_r(x) \leq 0 \\ & f_{r+1}(x) = 0, \quad \ldots. \quad , f_m(x) = 0 \end{aligned}$$

Where:
f_i is finite convex function on C for $i = 0, 1, 2, \quad \ldots. \quad , r$
f_i is affine function on C for $i = r+1, \quad \ldots. \quad , m$

A vector x will be called a feasible solution to **(P)** if $x \in C$ and x satisfies $'m'$ constraints of **(P)**. The set of feasible solutions to **(P)** is (possibly empty) convex set, given as:

$$C_0 = C \cap C_1 \cap C_2 \cap \quad ... \quad \cap C_m$$
$$\text{where } C_i = \{x | f_i(x) \leq 0\} \quad \text{for } i = 1, 2, ..., r$$
$$C_i = \{x | f_i(x) = 0\} \quad \text{for } i = r+1, ..., m$$

Let's define the objective function for **(P)** as F on $\mathbb{R}^n$ as,

$$F(x) = f_0(x) + \delta(x|C_0) = \begin{cases} f_0(x) & \text{if} x \in C_0 \\ +\infty, & \text{otherwise} \end{cases}$$

A point $x \in C_0$ is feasible point solving **(P)**. A vector $x^* = (x_1, ..., x_n) \in C_0$ minimizes the objective function is called the optimal solution. The value is defined as:

$$p^* = \inf\{f_0(x) | f_i(x) \leq 0, i = 1, ..., r \text{ and } f_i(x) = 0, i = r+1, ..., m\}$$

If p^* is $+\infty$ the problem (P) is infeasible, if p^* is $-\infty$ the problem (P) is unbounded below [108].

Lagrangian Dual Problem (D)

Convex optimization problems can be transformed to their dual problem. This transformation provides another perspective to the original problem **(P)**. Among the various duality formulations, the Lagrangian duality is most popular. The Lagrangian dual of **(P)** is denoted as **(D)**. The Lagrangian Dual function is $\theta : \mathbb{R}^r \times \mathbb{R}^{m-r} \to \mathbb{R}$

$$\begin{aligned} \textbf{(D)} \qquad & \text{maximize } \theta(\mu, \lambda) \\ & \text{subject to:} \quad \mu \geq 0 \end{aligned}$$

Where

$$\theta(\mu, \lambda) = \inf_{x \in X} \{f_0(x) + \sum_{i=1}^{r} \mu_i f_i(x) + \sum_{i=r+1}^{m} \lambda_i f_i(x)\}$$

The dual problem provides a lower bound to the original optimization problem i.e. for $\mu \geq 0$, $\theta(\mu, \lambda) \leq p^*$. θ is concave and can be $-\infty$ for some μ, λ [108].
Note the Lagrangian (weighted sum of objective and constraint functions) is defined as,

$$\mathscr{L}(\mathbf{x}, \mu, \lambda) = f_0(x) + \sum_{i=1}^{r} \mu_i f_i(x) + \sum_{i=r+1}^{m} \lambda_i f_i(x)$$

In the next part of this report we will extend the concept of primal and dual problem to understand the Saddle point but before that we need to evaluate whether or not optimality conditions for smooth convex function is similar to non-smooth convex function? The significance of Lagrangian is that it converts a constrained optimal problem to an unconstrained optimal problem at the cost of solving for extra number of variables (which implies $0 \in \nabla \mathscr{L}(x^*, \mu, \lambda)$ or $0 \in \partial \mathscr{L}(x^*, \mu, \lambda)$)

Weak and Strong Duality

The optimal value of Primal problem is $p^* = f_0(x^*)$ and the optimal value of dual problem is $d^* = \theta(\mu^*, \lambda^*)$. Weak duality garantees that the dual solution d^* is the lower bound of primal solution p^*. This implies

$$d^* \leq p^*$$

The above inequality holds even if the original problem is not convex. This is called weak duality [108]. The value $p^* - d^*$ is called Duality Gap (as shown in figure below).
Strong duality is a concept in optimization such that the primal and dual solutions are equivalent. This implies for strong duality the duality gap is zero.

If the primal solution is $-\infty$ implying unbounded below, then the dual solution is also $-\infty$ and the dual problem is infeasible. When the dual problem is unbounded above implying $d^* = \infty$ then the primal problem is infeasible [108].

(a) Weak Duality. **(b)** Strong Duality.

Figure A.3: Duality [211]

Slater's Condition

This condition is sufficient condition for strong duality to hold for a convex optimization problem. It states that the feasible region must have an interior point.

$$\exists \quad x \in \textbf{relint } C_0 : f_i(x) \leq 0 \forall i = 1, ..., j \cap f_i(x) < 0 \forall i = j+1, ..., r \cap f_i(x) = 0 \forall i = r+1, ..., m$$

Strict inequality is only required for nonlinear constraint functions [108].

Theorem A.2.1

Convex Optimization problem satisfying Slater's Constraint Qualification has x^* as the Primal Optimal and μ^*, λ^* is Dual Optimal iff

- $f_i(x^*) \leq 0, \mu_i^* \geq 0 \ \forall i \in \{1, 2, ..., r\}$
- $0 \in \partial f_0(x) + \sum_{i=1}^{r} \mu_i \partial f_i(x) + \sum_{i=r+1}^{m} \lambda_i \partial f_i(x)$ *this is equivalent to* $0 \in \nabla_x \mathscr{L}$ *or* $0 \in \partial \mathscr{L}$
- $\mu_i^* f_i(x^*) = 0 \ \forall i \in \{1, 2, ..., r\}$

This generalizes KKT conditions for nondifferentiable $f_i(x) for given (i = 0, 1, ..., r)$.

[Refer Theorem 28.3 [284] for Proof].

Saddle Point Optimality

If Slater's Constraint Qualification is valid implying that strong duality holds implies that (x^*, μ^*, λ^*) minimizes the Lagrangian $\mathscr{L}(\mathbf{x}, \mu, \lambda)$ is called the saddle point.
Definition $(x^*, \mu^*, \lambda^*) \in \mathbb{R}^n \times \mathbb{R}^r \times \mathbb{R}^{m-r}$ and is called a saddle point of $\mathscr{L}(\mathbf{x}, \mu, \lambda)$ if [112]

- $x^* \in X$
- $\mu^* \geq 0$
- $\mathscr{L}(\mathbf{x}^*, \mu, \lambda) \leq \mathscr{L}(\mathbf{x}^*, \mu^*, \lambda^*) \leq \mathscr{L}(\mathbf{x}, \mu^*, \lambda^*) \quad \forall x \in X, \mu \in \mathbb{R}^r, \lambda \in \mathbb{R}^{m-r}$

The existence of a saddle point solution to the Lagrangian function is a necessary and sufficient condition for the absence of a duality gap.

Theorem A.2.2

(x^*, μ^*, λ^*) is a saddle point solution to $\mathscr{L}(\mathbf{x}, \mu, \lambda)$ iff

1. $\mathscr{L}(\mathbf{x}^*, \mu^*, \lambda^*) = minimize_{x \in X} \ \mathscr{L}(\mathbf{x}, \mu^*, \lambda^*)$
2. $f_i(x) \leq 0, i = 1, ..., r$ *and* $f_i(x) = 0, i = r+1, ..., m$
3. $\mu^{*T} f_i(x) = 0 \quad \forall i = 1, ..., r$
4. $\mu^* \geq 0$

A.3 Proof of Theorem 4.2.1

Let $\psi(t) = a[t]^+ - b[t]^-$ with $a \geq b \geq 0$. Using $t = [t]^+ - [t]^-$ we have $\psi(t) = (a-b)[t]^+ + bt$. Since both $[t]^+$ and t are convex in t and $a - b, b \geq 0$ we have that ψ is convex since it is the positive sum of two convex functions.

Now let $f(x) = \frac{1}{\eta_{ch}}[x]^+ - \eta_{dis}[x]^-$ (as defined in Eq. 4.2.1) and $h_i(s) = [z_i + s]^+ p_b(i) - [z_i + s]^- p_s(i)$. Then by the above reasoning we have that for $p_b(i) \geq p_s(i) \geq 0$ and $\eta_{ch}, \eta_{dis} \in (0, 1]$, h_i is convex in s and f is convex in x. Also, note that h_i is non-decreasing in s. Hence, for $\lambda \in [0, 1]$ we have

$$h_i\big(f(\lambda x + (1-\lambda)y)\big) \leq h_i\big(\lambda f(x) + (1-\lambda)f(y)\big) \tag{A.3.1}$$
$$\leq \lambda h_i(f(x)) + (1-\lambda)h_i(f(y)) \tag{A.3.2}$$

In the above, the first inequality follows from the convexity of f and non-decreasing nature of h_i and the second inequality follows from convexity of h_i. Therefore, we have that $h_i \cdot f = h_i(f())$ is a convex function in x. This shows that the objective function of (P) is convex in x since $C^i_{nm} = h_i \cdot f$. Finally, since the constraints are linear in x, we have that problem (P) is convex. □

Cost function of the optimization problem (P) is plotted for visual inspection of the convexity of the function. The cost function is denoted as $C_{nm}(i)$ which equals $[z_i + s_i]^+ p^i_b - [z_i + s_i]^- p^i_s$. Reiterating our convention: consuming electricity is considered to be positive, thus for $x_i > 0$ implies battery is consuming or in other words charging. Net load without storage is positive implies load seen from the grid is charged for consumption. For plotting the cost function with respect to the optimization variable x_i we consider following two cases:

A.3.1 For $z_i > 0$

Under the condition that $z_i > 0$, we have following cost function based on storage operation:

- For charging we have $[z_i + x_i/\eta_{\text{ch}}]p^i_b$,
- For discharging we have following conditions:
  - If $-z_i < x_i\eta_{\text{dis}}$ then $[z_i + x_i\eta_{\text{dis}}]p^i_b$,
  - Else $[z_i + x_i\eta_{\text{dis}}]p^i_s$.

A.3.2 For $z_i < 0$

Under the condition that $z_i < 0$, we have following cost function based on storage operation:

1. For charging we have following conditions:
   (a) If $|z_i| < x_i/\eta_{\text{ch}}$ then $[z_i + x_i/\eta_{\text{ch}}]p^i_b$,
   (b) Else $[z_i + x_i/\eta_{\text{ch}}]p^i_s$.
2. For discharging we have $[z_i + x_i\eta_{\text{dis}}]p^i_s$.

A.4 Proof of Theorem 4.2.2

We first prove existence of (s^*, α^*, β^*) such that:

1. s^* is the primal optimal solution,
2. (α^*, β^*) is the dual optimal solution, and
3. the optimality gap is zero (strong duality).

Since the constraints of the primal problem are all linear, weak Slater's constraint qualification conditions (which imply strong duality) follow simply from the feasibility of the primal problem. Clearly, under the assumptions $b_{\min} \leq b_{\max}, \delta_{\min} \leq \delta_{\max}$, $b_0 \in [b_{\min}, b_{\max}]$, $0 \in [\delta_{\min}, \delta_{\max}]$ a feasible solution exists ($s_i = 0$ for all $i = 1, 2, \ldots, N$ is feasible). Furthermore, since the primal objective function is continuous and the

constraints define a convex compact set, its minimum must be finite and achieved at the some s^* in the feasibility region. According to the strong duality theorem, the above facts imply that the dual problem must be maximized at some (α^*, β^*) and the duality gap must be zero.

From the above reasoning it also follows that (s^*, α^*, β^*) must be the saddle point satisfying the KKT conditions. Hence, using RHS inequality of the Saddle Point conditions,

$$\begin{aligned}
&\mathscr{L}(x^*, \alpha^*, \beta^*) \leq \mathscr{L}(x, \alpha^*, \beta^*) \\
\implies &\sum_{i=1}^{N} \Big\{ C_{\text{nm}}^{(i)}(x_i^*) + \alpha_i^*(b_{\min} - b_i^*) + \beta_i^*(b_i^* - b_{max}) \Big\} \\
&\leq \sum_{i=1}^{N} \Big\{ C_{\text{nm}}^{(i)}(x_i) + \alpha_i^*(b_{min} - b_i) + \beta_i^*(b_i - b_{max}) \Big\}
\end{aligned}$$

Substituting $b_i = b_0 + \sum_{j=1}^{i} x_j$ we get,

$$\sum_{i=1}^{N} \Big\{ C_{\text{nm}}^{(i)}(x_i^*) - \mu_i^* x_i^* \Big\} \leq \sum_{i=1}^{N} \Big\{ C_{\text{nm}}(x_i) - \mu_i^* x_i \Big\} \tag{A.4.1}$$

where $\mu_i^* = \sum_{j=i}^{N} (\alpha_j^* - \beta_j^*)$. μ_i^* is the accumulated Lagrange multiplier for time instant i to N. Hence,

$$\mu_k^* - \mu_{k+1}^* = (\alpha_k^* - \beta_k^*) \tag{A.4.2}$$

The complementary slackness conditions for the Lagrangian are defined as

$$\alpha_i(b_{\min} - b_i) = 0, \quad \beta_i(b_i - b_{\max}) = 0, \forall i \text{ s.t. } \alpha_i, \beta_i \geq 0$$

Equation (8) derived above and complementary slackness conditions implies following relation of μ_k^* and μ_{k+1}^* ,

$$\mu_{k+1}^* \begin{cases} = \mu_k^*, & \text{if } b_{min} < b_k^* < b_{max} \quad \text{as} \quad \alpha_k^* = \beta_k^* = 0 \\ \leq \mu_k^*, & \text{if } b_k^* = b_{min} \quad \text{as} \quad \alpha_k^* \geq 0 \text{ and } \beta_k^* = 0 \\ \geq \mu_k^*, & \text{if } b_k^* = b_{max} \quad \text{as} \quad \alpha_k^* = 0 \text{ and } \beta_k^* \geq 0 \end{cases}$$

The accumulated Lagrangian i.e. μ for the N^{th} (last) instant is $\mu_N^* = \alpha_N^* - \beta_N^*$, therefore

$$\mu_N^* = \begin{cases} = 0^*, & \text{if } b_{min} < b_N^* < b_{max} \\ \geq 0, & \text{if } b_N^* = b_{min} \\ \leq 0, & \text{if } b_N^* = b_{max} \end{cases}$$

Such a x^* solves the optimal arbitrage problem (P_{NEM2}) and α^*, β^* solves the dual problem.

A.5 Proof of Remark 6

For a given $\mu_i^* = \mu$ the optimal decision $s_i^*(\mu)$ is given by minimizing Eq. A.5.1.

$$[z_i + s_i]^+ p_b(i) - [z_i + s_i]^- p_s(i) - \mu\Big(\eta_{\text{ch}}[s_i]^+ - \frac{1}{\eta_{\text{dis}}}[s_i]^-\Big) \tag{A.5.1}$$

Hence, in order to minimize Eq. A.5.1 we consider the sign of $(z_i + s_i)$ and s_i. This will provide the following cases

J1: $s_i(p_b(i) - \mu\eta_{\text{ch}})$ s.t. $z_i + s_i \geq 0$ and $s_i \in [0, S_{\max}]$,

J2: $s_i(p_s(i) - \mu\eta_{\text{ch}})$ s.t. $z_i + s_i \leq 0$ and $s_i \in [0, S_{\max}]$,

J3: $s_i\Big(p_b(i) - \frac{\mu}{\eta_{\text{dis}}}\Big)$ s.t. $z_i + s_i \geq 0$ and $s_i \in [S_{\min}, 0]$,

J4: $s_i\Big(p_s(i) - \frac{\mu}{\eta_{\text{dis}}}\Big)$ s.t. $z_i + s_i \leq 0$ and $s_i \in [S_{\min}, 0]$.

Table A.1: Conditions to check

Tag	$[z_i + s_i]$	$[s_i]$	min Condition	Desired scenario
J1	+ve	+ve	$s_i(p_b(i) - \mu\eta_{\text{ch}})$	$(p_b(i) - \mu\eta_{\text{ch}}) \leq 0$
J2	-ve	+ve	$s_i(p_s(i) - \mu\eta_{\text{ch}})$	$(p_s(i) - \mu\eta_{\text{ch}}) \leq 0$
J3	+ve	-ve	$s_i(p_b(i) - \frac{\mu}{\eta_{\text{dis}}})$	$(p_b(i) - \frac{\mu}{\eta_{\text{dis}}}) \geq 0$
J4	-ve	-ve	$s_i(p_s(i) - \frac{\mu}{\eta_{\text{dis}}})$	$(p_s(i) - \frac{\mu}{\eta_{\text{dis}}}) \geq 0$

The accumulated Lagrange multiplier, μ, can be viewed as the shadow price of decision making. Based on conditions J1 to J4, the value of μ will divide the price levels into nine cases. Table A.1 lists the constraints and minimizing conditions, we will use this table to find optimal value of s_i^*. From Table A.1 we can see the conditions of desired scenarios. Based on conditions J1 to J4, we can observe there will be four distinct levels in price signal which will subsequently divide the real line into nine possible levels for the accumulated Lagrange multiplier (μ) as shown in Fig **??**.

Based on four levels of prices shown in Fig A.4, the range is divided into into nine possible bands for the accumulated Lagrange multiplier.

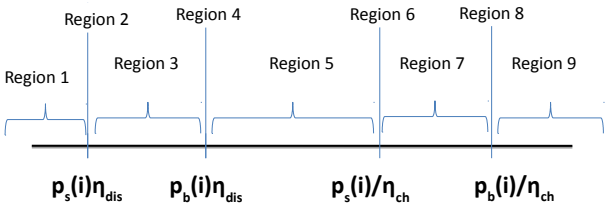

Figure A.4: Cases based on levels of μ

Region 1: $\mu < \eta_{\text{dis}} p_s(i)$: The minimizing conditions will be achieved by J3 and J4 as shown below

Tag	$[z_i + s_i]$	$[s_i]$	min Condition	Sign	Comment
J1	+ve	+ve	$s_i(p_b(i) - \mu\eta_{\text{ch}})$	+ (+)	Undesired
J2	-ve	+ve	$s_i(p_s(i) - \mu\eta_{\text{ch}})$	+ (+)	Undesired
J3	+ve	-ve	$s_i(p_b(i) - \frac{\mu}{\eta_{\text{dis}}})$	- (+)	Desired
J4	-ve	-ve	$s_i(p_s(i) - \frac{\mu}{\eta_{\text{dis}}})$	- (+)	Desired

From J4 if $(z_i + s_i) < 0$ then $s_i^* = [S_{\min}, S_{\min}]$ and from J3 if $(z_i + s_i) \geq 0$ then $s_i^* = [S_{\min}, S_{\min}]$. Therefore, irrespective the sign of z_i the optimal value is $[S_{\min}, S_{\min}]$.

Region 2: $\mu = \eta_{\text{dis}} p_s(i)$: The minimizing conditions will be achieved by J3 and J4 is a don't care condition with only constraint on s_i being negative or zero.

Tag	$[z_i + s_i]$	$[s_i]$	min Condition	Sign	Comment
J1	+ve	+ve	$s_i(p_b(i) - \mu\eta_{\text{ch}})$	+ (+)	Undesired
J2	-ve	+ve	$s_i(p_s(i) - \mu\eta_{\text{ch}})$	+ (+)	Undesired
J3	+ve	-ve	$s_i(p_b(i) - \frac{\mu}{\eta_{\text{dis}}})$	- (+)	Desired
J4	-ve	-ve	$s_i(p_s(i) - \frac{\mu}{\eta_{\text{dis}}})$	- (0)	Don't Care

Sub-Case 1: from J3 if $z_i \geq 0$ then $s_i^* = [\max\{-z_i, S_{\min}\}, \max\{-z_i, S_{\min}\}]$.
Sub-Case 2: from J4 if $z_i < 0$ then $s_i^* = [S_{\min}, 0]$.

Region 3: $\mu \in (\eta_{\text{dis}} p_s(i), \eta_{\text{dis}} p_b(i))$: The minimizing conditions will be achieved by minimizing J3. All other conditions, i.e., J1, J2 and J4 are undesired.

Tag	$[z_i + s_i]$	$[s_i]$	min Condition	Sign	Comment
J1	+ve	+ve	$s_i(p_b(i) - \mu\eta_{\text{ch}})$	+ (+)	Undesired
J2	-ve	+ve	$s_i(p_s(i) - \mu\eta_{\text{ch}})$	+ (+)	Undesired
J3	+ve	-ve	$s_i(p_b(i) - \frac{\mu}{\eta_{\text{dis}}})$	- (+)	Desired
J4	-ve	-ve	$s_i(p_s(i) - \frac{\mu}{\eta_{\text{dis}}})$	- (-)	Unesired

Sub-Case 1: from J3 if $z_i \geq 0$ then $s_i^* = [\max\{-z_i, S_{\min}\}, \max\{-z_i, S_{\min}\}]$.
Sub-Case 2: from J2 and J4 $s_i^* = [0, 0]$.

Region 4: $\mu = \eta_{\text{dis}} p_b(i)$:

Tag	$[z_i + s_i]$	$[s_i]$	min Condition	Sign	Comment
J1	+ve	+ve	$s_i(p_b(i) - \mu\eta_{\text{ch}})$	+ (+)	Undesired
J2	-ve	+ve	$s_i(p_s(i) - \mu\eta_{\text{ch}})$	+ (+)	Undesired
J3	+ve	-ve	$s_i(p_b(i) - \frac{\mu}{\eta_{\text{dis}}})$	- (0)	Don't Care
J4	-ve	-ve	$s_i(p_s(i) - \frac{\mu}{\eta_{\text{dis}}})$	- (-)	Undesired

Sub-Case 1: from J3 if $z_i \geq 0$ then $s_i^* = [\max\{-z_i, S_{\min}\}, 0]$.
Sub-Case 2: from J2 and J4, if $z_i < 0$ then $s_i^* = [0, 0]$.

Region 5: $\mu \in (\eta_{\text{dis}} p_b(i), \frac{p_s(i)}{\eta_{\text{ch}}})$:

Tag	$[z_i + s_i]$	$[s_i]$	min Condition	Sign	Comment
J1	+ve	+ve	$s_i(p_b(i) - \mu\eta_{\text{ch}})$	+ (+)	Undesired
J2	-ve	+ve	$s_i(p_s(i) - \mu\eta_{\text{ch}})$	+ (+)	Undesired
J3	+ve	-ve	$s_i(p_b(i) - \frac{\mu}{\eta_{\text{dis}}})$	- (-)	Undesired
J4	-ve	-ve	$s_i(p_s(i) - \frac{\mu}{\eta_{\text{dis}}})$	- (-)	Undesired

Sub-Case 1: from J1 and J3 if $z_i \geq 0$ then $s_i^* = [0, 0]$.
Sub-Case 2: from J2 and J4, if $z_i < 0$ then $s_i^* = [0, 0]$.

Region 6: $\mu = \frac{p_s(i)}{\eta_{\text{ch}}}$:

Tag	$[z_i + s_i]$	$[s_i]$	min Condition	Sign	Comment
J1	+ve	+ve	$s_i(p_b(i) - \mu\eta_{\text{ch}})$	+ (+)	Undesired
J2	-ve	+ve	$s_i(p_s(i) - \mu\eta_{\text{ch}})$	+ (0)	Don't Care
J3	+ve	-ve	$s_i(p_b(i) - \frac{\mu}{\eta_{\text{dis}}})$	- (-)	Undesired
J4	-ve	-ve	$s_i(p_s(i) - \frac{\mu}{\eta_{\text{dis}}})$	- (-)	Undesired

Sub-Case 1: from J1 and J3 if $z_i \geq 0$ then $s_i^* = [0, 0]$.
Sub-Case 2: from J2 if $z_i < 0$ then $s_i^* = [0, \min\{-z_i, S_{\max}\}]$.

Region 7: $\mu \in (\frac{p_s(i)}{\eta_{\text{ch}}}, \frac{p_b(i)}{\eta_{\text{ch}}})$: The minimizing conditions will be achieved by J2. All other cases will be undesirable.

Tag	$[z_i + s_i]$	$[s_i]$	min Condition	Sign	Comment
J1	+ve	+ve	$s_i(p_b(i) - \mu\eta_{\text{ch}})$	+ (+)	Undesired
J2	-ve	+ve	$s_i(p_s(i) - \mu\eta_{\text{ch}})$	+ (-)	Desired
J3	+ve	-ve	$s_i(p_b(i) - \frac{\mu}{\eta_{\text{dis}}})$	- (-)	Undesired
J4	-ve	-ve	$s_i(p_s(i) - \frac{\mu}{\eta_{\text{dis}}})$	- (-)	Undesired

Sub-Case 1: from J2 if $z_i < 0$ then $s_i^* = [\min\{-z_i, S_{\max}\}, \min\{-z_i, S_{\max}\}]$.
Sub-Case 2: if $z_i \geq 0$ then do nothing, $s_i^* = [0, 0]$. This is because J1 and J3 covers two direction of movement i.e. charging and discharging, both of which will increase the objective function

Region 8: $\mu = \frac{p_b(i)}{\eta_{\text{ch}}}$: The minimizing conditions will be achieved by J2 and J1 is a don't care condition.

Tag	$[z_i + s_i]$	$[s_i]$	min Condition	Sign	Comment
J1	+ve	+ve	$s_i(p_b(i) - \mu\eta_{\text{ch}})$	+ (0)	Don't Care
J2	-ve	+ve	$s_i(p_s(i) - \mu\eta_{\text{ch}})$	+ (-)	Desired
J3	+ve	-ve	$s_i(p_b(i) - \frac{\mu}{\eta_{\text{dis}}})$	- (-)	Undesired
J4	-ve	-ve	$s_i(p_s(i) - \frac{\mu}{\eta_{\text{dis}}})$	- (-)	Undesired

Sub-Case 1: from J2 if $z_i < 0$ then $s_i^* = [\min\{-z_i, S_{\max}\}, \min\{-z_i, S_{\max}\}]$.
Sub-Case 2: from J1 is $z_i \geq 0$ then $s_i^* = [0, S_{\max}]$.

Region 9: $\mu > \frac{p_b(i)}{\eta_{\text{ch}}}$: The minimizing conditions will be achieved by J2 and J1.

Tag	$[z_i + s_i]$	$[s_i]$	min Condition	Sign	Comment
J1	+ve	+ve	$s_i(p_b(i) - \mu\eta_{\text{ch}})$	+ (-)	Desired
J2	-ve	+ve	$s_i(p_s(i) - \mu\eta_{\text{ch}})$	+ (-)	Desired
J3	+ve	-ve	$s_i(p_b(i) - \frac{\mu}{\eta_{\text{dis}}})$	- (-)	Undesired
J4	-ve	-ve	$s_i(p_s(i) - \frac{\mu}{\eta_{\text{dis}}})$	- (-)	Undesired

Irrespective of sign of z_i, $s_i^* = [S_{\max}, S_{\max}]$.

A.6 Proof of Remark 7

Based on four levels of prices shown in Fig A.5, the range is divided into into nine possible bands for the accumulated Lagrange multiplier.

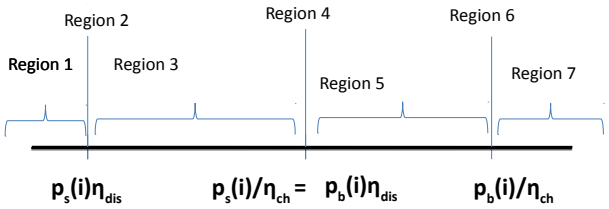

Figure A.5: Cases based on levels of μ

Region 1: $\mu < \eta_{\text{dis}} p_s(i)$: The minimizing conditions will be achieved by J3 and J4 as shown below

Tag	$[z_i + s_i]$	$[s_i]$	min Condition	Sign	Comment
J1	+ve	+ve	$s_i(p_b(i) - \mu\eta_{\text{ch}})$	+ (+)	Undesired
J2	-ve	+ve	$s_i(p_s(i) - \mu\eta_{\text{ch}})$	+ (+)	Undesired
J3	+ve	-ve	$s_i(p_b(i) - \frac{\mu}{\eta_{\text{dis}}})$	- (+)	Desired
J4	-ve	-ve	$s_i(p_s(i) - \frac{\mu}{\eta_{\text{dis}}})$	- (+)	Desired

From J4 if $(z_i + s_i) < 0$ then $s_i^* = [S_{\min}, S_{\min}]$ and from J3 if $(z_i + s_i) \geq 0$ then $s_i^* = [S_{\min}, S_{\min}]$. Therefore, irrespective the sign of z_i the optimal value is $[S_{\min}, S_{\min}]$.

Region 2: $\mu = \eta_{\text{dis}} p_s(i)$: The minimizing conditions will be achieved by J3 and J4 is a don't care condition with only constraint on s_i being negative or zero.

Tag	$[z_i + s_i]$	$[s_i]$	min Condition	Sign	Comment
J1	+ve	+ve	$s_i(p_b(i) - \mu\eta_{\text{ch}})$	+ (+)	Undesired
J2	-ve	+ve	$s_i(p_s(i) - \mu\eta_{\text{ch}})$	+ (+)	Undesired
J3	+ve	-ve	$s_i(p_b(i) - \frac{\mu}{\eta_{\text{dis}}})$	- (+)	Desired
J4	-ve	-ve	$s_i(p_s(i) - \frac{\mu}{\eta_{\text{dis}}})$	- (0)	Don't Care

Sub-Case 1: from J3 if $z_i \geq 0$ then $s_i^* = [\max\{-z_i, S_{\min}\}, \max\{-z_i, S_{\min}\}]$.
Sub-Case 2: from J4 if $z_i < 0$ then $s_i^* = [S_{\min}, 0]$.

Region 3: $\mu \in (\eta_{\text{dis}} p_s(i), \eta_{\text{dis}} p_b(i))$: The minimizing conditions will be achieved by minimizing J3. All other conditions, i.e., J1, J2 and J4 are undesired.

Tag	$[z_i + s_i]$	$[s_i]$	min Condition	Sign	Comment
J1	+ve	+ve	$s_i(p_b(i) - \mu\eta_{\text{ch}})$	+ (+)	Undesired
J2	-ve	+ve	$s_i(p_s(i) - \mu\eta_{\text{ch}})$	+ (+)	Undesired
J3	+ve	-ve	$s_i(p_b(i) - \frac{\mu}{\eta_{\text{dis}}})$	- (+)	Desired
J4	-ve	-ve	$s_i(p_s(i) - \frac{\mu}{\eta_{\text{dis}}})$	- (-)	Unesired

Sub-Case 1: from J3 if $z_i \geq 0$ then $s_i^* = [\max\{-z_i, S_{\min}\}, \max\{-z_i, S_{\min}\}]$.
Sub-Case 2: from J2 and J4 $s_i^* = [0, 0]$.

Region 4: $\mu = \eta_{\text{dis}} p_b(i)$:

Tag	$[z_i + s_i]$	$[s_i]$	min Condition	Sign	Comment
J1	+ve	+ve	$s_i(p_b(i) - \mu\eta_{\text{ch}})$	+ (+)	Undesired
J2	-ve	+ve	$s_i(p_s(i) - \mu\eta_{\text{ch}})$	+ (+)	Undesired
J3	+ve	-ve	$s_i(p_b(i) - \frac{\mu}{\eta_{\text{dis}}})$	- (0)	Don't Care
J4	-ve	-ve	$s_i(p_s(i) - \frac{\mu}{\eta_{\text{dis}}})$	- (-)	Undesired

Sub-Case 1: from J3 if $z_i \geq 0$ then $s_i^* = [\max\{-z_i, S_{\min}\}, 0]$.
Sub-Case 2: from J2 and J4, if $z_i < 0$ then $s_i^* = [0, \min\{-z_i, S_{\max}\}]$.

Region 5: $\mu \in (\frac{p_s(i)}{\eta_{\text{ch}}}, \frac{p_b(i)}{\eta_{\text{ch}}})$: The minimizing conditions will be achieved by J2. All other cases will be undesirable.

Tag	$[z_i + s_i]$	$[s_i]$	min Condition	Sign	Comment
J1	+ve	+ve	$s_i(p_b(i) - \mu\eta_{\text{ch}})$	+ (+)	Undesired
J2	-ve	+ve	$s_i(p_s(i) - \mu\eta_{\text{ch}})$	+ (-)	Desired
J3	+ve	-ve	$s_i(p_b(i) - \frac{\mu}{\eta_{\text{dis}}})$	- (-)	Undesired
J4	-ve	-ve	$s_i(p_s(i) - \frac{\mu}{\eta_{\text{dis}}})$	- (-)	Undesired

Sub-Case 1: from J2 if $z_i < 0$ then $s_i^* = [\min\{-z_i, S_{\max}\}, \min\{-z_i, S_{\max}\}]$.
Sub-Case 2: if $z_i \geq 0$ then do nothing, $s_i^* = [0, 0]$. This is because J1 and J3 covers two direction of movement i.e. charging and discharging, both of which will increase the objective function

Region 6: $\mu = \frac{p_b(i)}{\eta_{\text{ch}}}$: The minimizing conditions will be achieved by J2 and J1 is a don't care condition.

Tag	$[z_i + s_i]$	$[s_i]$	min Condition	Sign	Comment
J1	+ve	+ve	$s_i(p_b(i) - \mu\eta_{\text{ch}})$	+ (0)	Don't Care
J2	-ve	+ve	$s_i(p_s(i) - \mu\eta_{\text{ch}})$	+ (-)	Desired
J3	+ve	-ve	$s_i(p_b(i) - \frac{\mu}{\eta_{\text{dis}}})$	- (-)	Undesired
J4	-ve	-ve	$s_i(p_s(i) - \frac{\mu}{\eta_{\text{dis}}})$	- (-)	Undesired

Sub-Case 1: from J2 if $z_i < 0$ then $s_i^* = [\min\{-z_i, S_{\max}\}, \min\{-z_i, S_{\max}\}]$.
Sub-Case 2: from J1 is $z_i \geq 0$ then $s_i^* = [0, S_{\max}]$.

Region 7: $\mu > \frac{p_b(i)}{\eta_{\text{ch}}}$: The minimizing conditions will be achieved by J2 and J1.

Tag	$[z_i + s_i]$	$[s_i]$	min Condition	Sign	Comment
J1	+ve	+ve	$s_i(p_b(i) - \mu\eta_{\text{ch}})$	+ (-)	Desired
J2	-ve	+ve	$s_i(p_s(i) - \mu\eta_{\text{ch}})$	+ (-)	Desired
J3	+ve	-ve	$s_i(p_b(i) - \frac{\mu}{\eta_{\text{dis}}})$	- (-)	Undesired
J4	-ve	-ve	$s_i(p_s(i) - \frac{\mu}{\eta_{\text{dis}}})$	- (-)	Undesired

Irrespective of sign of z_i, $s_i^* = [S_{\max}, S_{\max}]$.

A.7 Arbitrage with NEM 1.0

Energy arbitrage refers to buying energy when the price of electricity is low and selling it when price is high. Another interpretation could be shifting consumptions from high price periods to low price periods. The problem of energy arbitrage is considered from consumer or end-user perspective. The consumer of electricity has its goal to minimize the overall cost of consumption by installing energy storage device such as a battery for performing energy arbitrage. The price of electricity is denoted as $p_{elec}(i)$. The consumer optimization problem is given as [182]

$$(P^0_{arbitrage}) \qquad \min_{P^i_B \in \left[\eta_{\text{dis}}\delta_{\min}h, \frac{\delta_{\max}h}{\eta_{\text{ch}}}\right]} \sum_{i=1}^{N} [P_i + P^i_B] p_{elec}(i)$$

$$\text{subject to,(i.)} \;\; b_{\min} - b_0 \leq \sum_{j=1}^{i} x_j \leq b_{\max} - b_0.$$

The optimization problem $(P^0_{arbitrage})$ is equivalent to min $\sum_{i=1}^{N}\{p_{elec}(i)P_i + p_{elec}(i)P^i_B\}$. Since there is no degree of freedom in $p_{elec}(i)P_i$ for all i, therefore, $(P^0_{arbitrage})$ is equivalent to

$$(P^{equi}_{arbitrage}) \qquad \min_{P^i_B \in \left[\eta_{\text{dis}}\delta_{\min}h, \frac{\delta_{\max}h}{\eta_{\text{ch}}}\right]} \sum_{i=1}^{N} P^i_B p_{elec}(i)$$

$$\text{s.t. (i.) } b_{\min} - b_0 \leq \sum_{j=1}^{i} x_j \leq b_{\max} - b_0, \forall i \in \{1, .., N\}$$

A.8 Arbitrage with Convex Optimization using CVX

There could be several different ways of formulating optimal arbitrage problem using convex optimization toolbox. We propose one of the many ways of solving optimal arbitrage problem with convex piecewise linear cost function using CVX in MATLAB. Since in the optimization formulation we do not have any binary variable, this optimization problem could be solved using the default solver, SDPT3[1].

The decision variable x_i is fragmented into two variable given as

$$x_i = x^{ch}_i - x^{ds}_i, \tag{A.8.1}$$

where $x^{ch}_i \in [0, X_{\max}]$ and $x^{ds}_i \in [0, -X_{\min}]$, denotes the charging and discharging values.

A.8.1 Only storage with NEM and losses

We use following Matlab pseudo code is presented below:

```
>> cvx_begin
>> variables x^ch(N,1) x^ds(N,1) delB(N,1)
>> minimize sum(p_b^T*x^ch/η_ch − p_s^T*x^ds η_dis)
>> subject to
>>      zeros(N,1)<= x^ch <= x_upper;
>>      zeros(N,1)<= x^ds <= -x_lower;
>>      delB == x^ch − x^ds;
>>      b_min ≤ b_0 + M * delB ≤ b_max;
>> cvx_end
>> profit = (p_b^T*x^ch/η_ch-p_s^T*x^ds η_dis)
```

where M is lower triangular matrix, x_upper and x_lower are row matrix of size N with upper and lower limit of optimization variable.

A.8.2 Arbitrage with load, renewable generation with NEM and losses

We use following Matlab pseudo code is presented below:

```
>> cvx_begin
>> variables x^ch(N,1) x^ds(N,1) delB(N,1) lhouse(N,1)
>> minimize sum(p_b^T*subplus(lhouse)−p_s^T*min(0,lhouse)))
>> subject to
>>      zeros(N,1)<= x^ch <= x_upper;
>>      zeros(N,1)<= x^ds <= -x_lower;
>>      delB == x^ch − x^ds;
>>      lhouse == x^ch/η_ch − x^ds η_dis + z;
>>      b_min ≤ b_0 + M * delB ≤ b_max;
>> cvx_end
>> profit = (p_b^T*subplus(z)-p_s^T*subplus(-z))- (p_b^T*subplus(lhouse)-p_s^T*subplus(-lhouse))
```

where `lhouse` denotes the total load seen by the energy meter including storage output.

[1] http://www.math.nus.edu.sg/~mattohkc/sdpt3.html

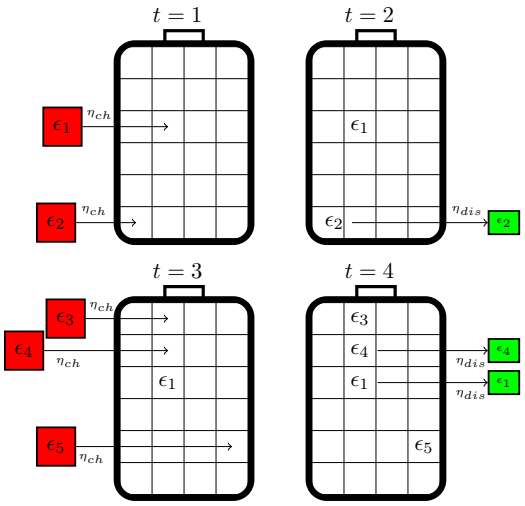

Figure A.6: Demonstrating the proof of Theorem 9.4.1

A.9 Proof of Theorem 9.4.1

Let ϵ denote a sufficiently small amount of energy, and w.l.o.g assume that inside every time slot, all energy packets arrive sequentially. That is, we can define $E=\{\epsilon_1, \epsilon_2, .., \epsilon_K\}$ as a complete order of all energy packets that charged the battery. Let I_k denote the time slot at which the packet ϵ_k entered the battery and O_k when it left it. If the packet never left (that is, if there is remaining energy in the battery at the end of the arbitrage) we let $k = \infty$ and $p_s^\infty = 0$. Let n_{ij} denote the number of packets that charged the battery during time slot i and discharged at time slot j.

$$n_{ij} = \sum_{k=0}^{K} \mathbb{I}\{I_k = i, O_k = j\}$$

The price of charging the battery ϵ at time i is given by $\epsilon \frac{p_b^i}{\eta_{ch}}$. The earnings of discharging the battery at time slot j is given by $\epsilon \eta_{dis} p_s^j$. Finally, the total profit obtained by the arbitrage is given by:

$$\text{Profit} = \sum_{i\in[N], j\in[N]\setminus\{1\}\cup\{\infty\}} \epsilon n_{ij} \left[\eta_{dis} p_s^j - \frac{p_b^i}{\eta_{ch}}\right]$$

Because $m_{ij} \in \mathbb{N}$, if $p_s^j \eta_{dis} \leq \frac{p_b^i}{\eta_{ch}}$, then $Profit \leq 0$.

In Fig. A.6 the size of the squares represents the amount of energy. Red squares (before been charged in the battery) are bigger than the squares composing the battery. This in turn, are bigger than the green squares that output the battery. Regarding the case presented: initially, the battery is empty. At $t = 1$, 2 energy packets arrive ϵ_1 and ϵ_2, so $I_1 = I_2 = 1$. In the next time-slot, ϵ_2 leaves so we can update $O_2 = 2$. At time-slot $t = 3$, three energy packets arrive (3,4,5) so we have $I_3 = I_4 = I_5 = 3$. Finally, in the last time-slot the energy packets ϵ_1 and ϵ_4 leave so $O_1 = O_4 = 4$. Because the battery is still fully charged at the end of the horizon, $O_3 = O_5 = \infty$. In this example $n_{12} = 1$, $n_{14} = 1$, $n_{34} = 1$ and $n_{3\infty} = 2$. With this information the final profit can be found.

A.10 Control Design Using LQG in Matlab©

A.10.1 System Type I: Open Loop System

An open loop system is given as

$$\dot{x} = Ax.$$

For such a system to be stable, matrix A should have negative real part eigenvalues as

$$x(t) = e^{At}x(0).$$

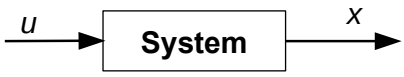

Figure A.7: Open loop system

Consider λ as an eigenvalue such that $\lambda = a \pm ib$ then by Euler formula

$$e^{\lambda t} = e^{at}(\cos(bt) \pm i\sin(bt)).$$

Clearly if $a > 0$ then e^{at} grows to infinity with progress of time t, implying an unstable system.

A.10.2 System Type II: Closed Loop Full-feedback

Closed loop system with full feedback

$$\dot{x} = Ax + Bu,$$
$$\dot{x} = (A - BK)x.$$

For such a system to be stable the eigenvalues of the matrix $(A - BK)$ should have negative real part. Choosing appropriate values of K, eigenvalues of $(A - BK)$ can be controlled.

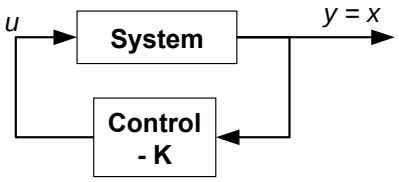

Figure A.8: Full feedback system

Such a system is shown in Fig. A.8. Note for equation $y = Cx$, for full feedback system C equals unity row matrix.

In Matlab placement of eigenvalues for a full feedback system is easily done using eigenvalue placement at points denoted as `eigs` in the code.

```
>> K = place(A,B, eigs)
```

However, often we do not know where to place the eigenvalues. For such cases we use Linear Quadratic Regulator or LQR. LQR controller solves this optimization problem:

$$J_{\text{LQR}} = \int_0^\infty \{x^T Q x + u^T R u\} dt,$$

here Q and R denotes the penalty for not meeting the desired states and input energy respectively.

Note that for LQR eigenvalue placement controllability of system is essential. The controllability matrix is denoted as

$$\mathcal{C} = [B \quad AB \quad ... \quad A^{n-1}B].$$

For system to be controllable $\mathcal{C}$ should be full rank matrix. The Matlab script for checking controllability is given as

```
>> C = ctrb(A,B)
>> Check = (rank(C) - size (A) == 0)
```

If variable `Check` = 1 then then the system is controllable. For controllable systems the LQR eigenvalue placement can be achieved by following code:

```
>> K = lqr(A,B, Q, R)
```

A.10.3 System Type III: Limited Measurement Feedback System

Limited measurement feedback system, therefore, the system becomes

$$\dot{x} = Ax + Bu,$$
$$y = Cx.$$

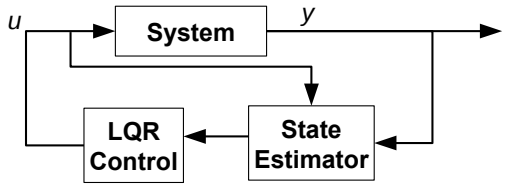

Figure A.9: Limited measurement feedback system

For estimating the states required for control design, we should check for observability. The observability matrix is denoted as

$$\mathcal{G} = \begin{bmatrix} C \\ CA \\ .. \\ CA^{n-1} \end{bmatrix}.$$

For system to be observable $\mathcal{G}$ should be full rank matrix. The Matlab script for checking observability is given as

```
>> G = obsv(A,B)
>> Check = (rank(G) - size (A) == 0)
```

For an observable system full estimator can be developed

$$\dot{\hat{x}} = A\hat{x} + Bu + K_f(y - \hat{y}),$$
$$\hat{y} = Cx.$$

Rearranging the system equation we get

$$\dot{\hat{x}} = (A - K_f C)\hat{x} + [B \quad K_f]\begin{bmatrix} u \\ y \end{bmatrix}.$$

Let the error is defined as $\epsilon = x - \hat{x}$, therefore, $\dot{\epsilon} = (A - K_f C)\epsilon$. Thus if system is observable then we can place eigenvalues by choosing estimator gain K_f.

A.10.4 System Type IV: Limited Measurement Noisy Feedback System

Limited measurement feedback system with disturbance in model and noise in measurements; realistic system would have exogenous disturbance and sensor noise. The model for such a system is give as

$$\dot{x} = Ax + Bu + GW_d, \quad \{\text{State Equation}\}$$
$$y = Cx + W_n \quad \{\text{Measurement Equation}\}.$$

where W_d denotes system disturbance and W_n denotes measurement noise. If we assume

- W_d denotes Gaussian white disturbance process with covariance V_d; $V_d = \mathbb{E}[W_d W_d^T]$ and
- W_n denotes Gaussian white noise process with covariance V_n; $V_n = \mathbb{E}[W_n W_n^T]$,

then we can develop full estimator of the system using Kalman Filter.

Cost function of the estimator

$$J_{\text{estimator}} = \mathbb{E}[(x - (\hat{x}))^T (x - (\hat{x}))]$$

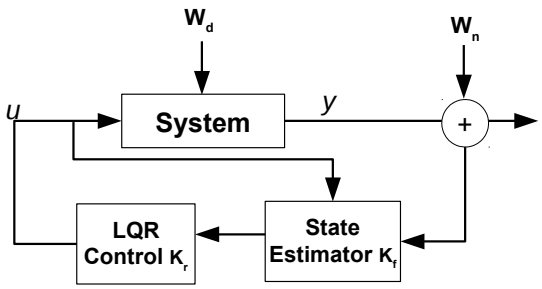

Figure A.10: Limited measurement feedback system with disturbance and noise

The Matlab code for estimator is

```
>> K_f = lqe(A,G, C, V_d,V_n)
```

`lqe` denotes linear quadratic estimator. V_d is a square matrix with size of matrix A. V_n is a square matrix with number of columns of matrix C.

Alternatively, this could be done using command `kalman`.

```
>> sys = ss(A, B, C, D, Ts)
>> [K_est, K_f, P] = kalman( sys, V_d, V_n)
```

where `Ts` denotes the sampling time.

The estimator generates estimate $\hat{x}$ to be fed to LQR control design. For implementing this following lines of Matlab code is executed:

```
>> sysKf = ss(A−K_fC, [B K_f], eye(size(A)), 0*[B K_f ] , Ts )
>> [x̂, t] = lsim ( sysKf, [u,y], t)
```

Linear optimal control design: If we have a linear system that is observable then we develop optimal full state feedback control using LQE and subsequently use LQR to place the eigenvalues of the system

$$\epsilon = x - \hat{x}$$
$$\dot{\hat{x}} = A\hat{x} + Bu + W_d$$

Substitute the input $u = -K_r\hat{x}$. The error model after algebraic simplification is given as

$$\dot{\epsilon} = (A - K_fC)\epsilon + W_d - K_fW_n$$

These equations in matrix form is given as

$$\begin{bmatrix}\dot{x}\\ \dot{\epsilon}\end{bmatrix} = \begin{bmatrix}A - BK_r & BK_r\\ 0 & A - K_fC\end{bmatrix}\begin{bmatrix}x\\ \epsilon\end{bmatrix} + \begin{bmatrix}I & 0\\ I & -K_f\end{bmatrix}\begin{bmatrix}W_d\\ W_n\end{bmatrix}$$

The LQR control design can be implemented with $\hat{x}$ generated by the estimator for designing K_r. We use following Matlab code for finding K_r

```
>> [A_kf, B_kf, C_kf, D_kf] = ssdata(sysKf)
>> K_r = lqr (A_kf, B_kf, Q, R )
```

where `Q, R` are penalty matrix, $\hat{u} = -K_r\hat{x}$.

$$A_{\text{new}} = A - K_fC - [B \quad K_f]K_r,$$
$$B_{\text{new}} = [B \quad K_f]K_r.$$

The linear quadratic Gaussian (LQG) controller is a combination of a Kalman filter (a linear quadratic state estimator (LQE)) together with a linear quadratic regulator (LQR).

Acknowledgements The author would like to thank Prof. Steve Brunton from University of Washington for his lectures and lucid explanation of the topic [110].

Appendix B

Arbitrage using Linear Programming

Summary: We formulate the optimal energy arbitrage problem for a piecewise linear cost function for energy storage devices using linear programming (LP). The LP formulation is based on the equivalent minimization of the epigraph. This formulation considers ramping and capacity constraints, charging and discharging efficiency losses of the storage, inelastic consumer load and local renewable generation in presence of net-metering which facilitates selling of energy to the grid and incentivizes consumers to install renewable generation and energy storage. We consider the case where the consumer loads, electricity prices, and renewable generations at different instances are uncertain. These uncertain quantities are predicted using an Auto-Regressive Moving Average (ARMA) model and used in a model predictive control (MPC) framework to obtain the arbitrage decision at each instance.

B.1 Introduction

Energy storage devices provide flexibility to alter the consumption behavior of an electricity consumer. In Chapter 3 and Chapter 4 we identify that storage operation under net-metering policies have a piece-wise line structure in presence of renewable generation and inelastic load. The cost function considered in this chapter includes inelastic load, renewable generation and storage charging and discharging efficiency, and ramping and capacity constraints. We formulate the optimal arbitrage problem for such a cost function for an electricity consumer with inelastic load and renewable generation adopting NEM by using Linear Programming (LP).

Authors in [341] provide a summary of storage control methodologies used in power distribution networks among which LP based formulations can be solved efficiently using commercially available solvers. The complexity of LP based algorithms is polynomial [203]. Therefore, these algorithms can be used to efficiently solve the arbitrage problem for the duration of a day divided into smaller time steps ranging from 5 minutes to an hour. A day is the typical time horizon over which arbitrage is performed [251, 196].

Authors in [146] observe that the energy arbitrage problem for storage is convex in nature and under the price-taker assumption the cost function will have a piecewise linear structure [182] and hence LP tools could be used. LP techniques for energy storage arbitrage have been used in several prior works: [269], [118], [139], [309], [109], [258], [325]. Authors in [109, 118, 325] consider storage operation in presence of time-varying electricity price. However, in these formulations no renewable energy source or consumer load is assumed to be present. Authors in [139, 309] consider optimal scheduling of storage battery for maximizing energy arbitrage revenue in presence of distributed energy resources and variable electricity price. Formulations presented in [258, 269] consider storage performing arbitrage in a residential setting with inelastic load and local generation. Most common LP formulations for energy arbitrage such as in [269], [325], [309], [118] consider separation of charging and discharging components. In these formulations, they do not include constraint enforcing only one of the charging or the discharging component to be active at any particular time as the inclusion of such a constraint makes these formulations nonlinear. Therefore, in these formulations, optimal results cannot be guaranteed. Authors in [139, 109] do not consider energy storage charging and discharging efficiencies in the cost minimization, making it straight forward to apply LP. Authors in [258] consider a special case of optimization with zero-sum aggregate storage power output. For such a case LP tools could be used, however, generalizing the formulations needs to be explored further.

The key contributions of this section are as follows:

- *LP formulation for storage control*: We formulate the LP optimization problem for piecewise linear

convex cost function, for storage with efficiency losses, ramping and capacity constraints and a consumer with inelastic load and renewable generation. The buying and selling price of electricity are varying over time. The selling price is assumed to be at best equal to buying price for each time instant, this assumption is in sync with most net-metering policies worldwide. We describe the LP formulations for lossy battery with inelastic consumption, renewable generation and selling price less than or equal to buying price. The reduction of this formulation for cases (a) lossless battery with equal buying and selling price of electricity and (b) lossy battery with selling price less than or equal to buying price, is trivial and also included in this section. Based on the structure of the cost function we apply an epigraph based minimization described in [108] to the arbitrage problem.

• *Real-time implementation:* We implement an auto-regressive based forecast model along with model predictive control.

Battery operational life is often quantified using cycle and calendar life which decides the cycles a battery should perform over a time period. Friction coefficient, denoted as $\eta_{\text{fric}} \in [0, 1]$, and introduced in [174] assists in reducing the operational life of the battery such that low returning transactions of charging and discharging are eliminated, thus increasing the operational life of the battery. In subsequent work, authors in [181] propose a framework to tune the value of friction coefficient for increasing operational life of battery. In a prior work, [177], we show that redefining η_{ch} equal to $\eta_{\text{ch}}\eta_{\text{fric}}$ and η_{dis} equal to $\eta_{\text{dis}}\eta_{\text{fric}}$, we can control the cycles of operation by eliminating the low returning transactions by reducing the value of η_{fric}.

The section is organized as follows. Section B.2 presents the linear programming formulation of storage performing arbitrage with inelastic load, renewable generation and net-metering based compensation. Section B.3 presents the matrix formulation for solving the arbitrage problem using linear programming. Section B.4 presents an online algorithm using the proposed optimal arbitrage algorithm along with auto-regressive forecasting in the MPC framework. Finally, Section B.5 concludes the section.

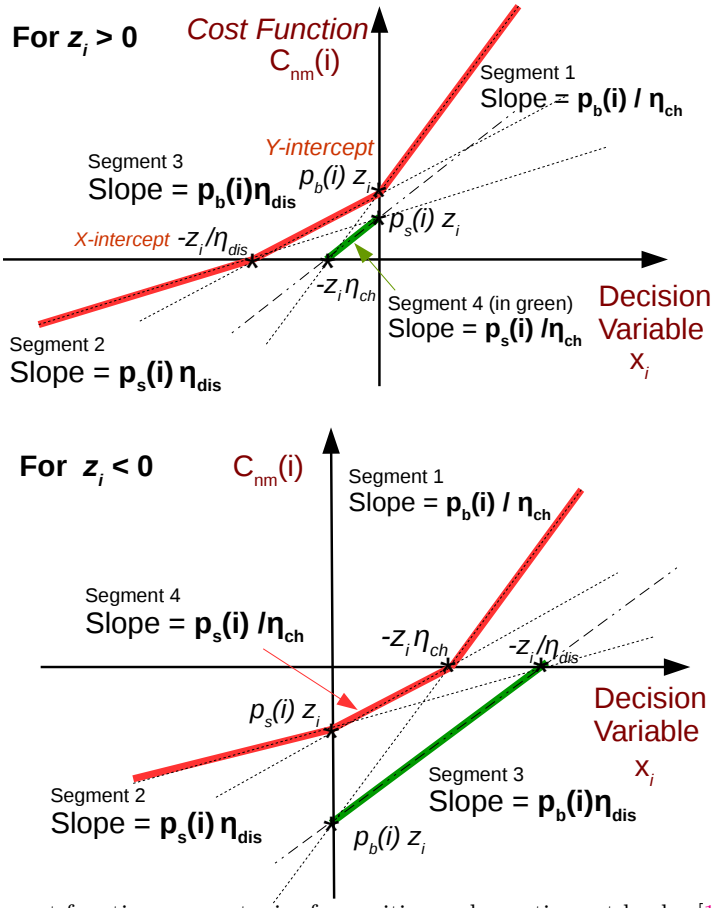

Figure B.1: The cost function segment wise for positive and negative net load z [183]. The decision variable is storage change in charge level, x_i, and cost function, $C_{nm}(i)$ is formed with 4 line segments.

Table B.1: Cost function for storage with load under NEM

Segment	Slope	x-intercept	y-intercept
Segment 1	$p_b(i)/\eta_{ch}$	$-z_i\eta_{ch}$	$z_i p_b(i)$
Segment 2	$p_s(i)\eta_{dis}$	$-z_i/\eta_{dis}$	$z_i p_s(i)$
Segment 3	$p_b(i)\eta_{dis}$	$-z_i/\eta_{dis}$	$z_i p_b(i)$
Segment 4	$p_s(i)/\eta_{ch}$	$-z_i\eta_{ch}$	$z_i p_s(i)$

B.2 Optimal Arbitrage with Linear Programming

The optimal arbitrage problem, (P), can be solved using linear programming as the cost function is (i) convex and (ii) piecewise linear, and (iii) the associated ramping and capacity constraints are linear. In this section, we provide an LP formulation for the optimal arbitrage of the storage device under net-metering and consumer inelastic load and renewable generation, leveraging the epigraph based minimization presented in [108]. A summary of the epigraph based formulation for a piecewise linear convex cost function is presented in Appendix B.2.1. The optimal arbitrage formulation for storage under net-metering and consumer inelastic load and renewable generation using the epigraph formulation is presented in this section. Fig. B.1 shows the two cost functions depending on the net-load without storage output, i.e. for $z_i > 0$ and $z_i < 0$. Note that there are 4 unique segments which form the cost function $C_{nm}(i)$. The slope, x-intercept and y-intercept of these linear segments are given in Table B.1. The epigraph based LP formulation is possible as irrespective of the sign of the load, the cost function is given as

$$C_{nm}(i) = \max\big(\text{Segment 1, Segment 2, Segment 3, Segment 4}\big). \tag{B.2.1}$$

Since, Eq.B.2.1 is independent of the sign of load and based on the intercepts, Eq.B.2.1 is valid for $p_b(i) \geq p_s(i)$ and for $\eta_{ch}, \eta_{dis} \in (0, 1]$ (conditions of convexity), therefore, we could formulate this problem as an LP. Using the epigraph equivalent formulation for piecewise linear convex cost function we formulate the optimal arbitrage problem using linear programming, denoted as $\mathrm{P_{LP}}$

$$(\mathrm{P_{LP}}) \quad \min \quad \{t_1 + t_2 + ... + t_N\},$$

$$\text{subject to,} \quad \text{(a) Segment 1: } \frac{p_b^i}{\eta_{ch}} x_i + z_i p_b^i \leq t_i, \ \forall i$$

$$\text{(b) Segment 2: } p_s^i \eta_{dis} x_i + z_i p_s^i \leq t_i, \ \forall i$$

$$\text{(c) Segment 3: } p_b^i \eta_{dis} x_i + z_i p_b^i \leq t_i, \ \forall i$$

$$\text{(d) Segment 4: } \frac{p_s^i}{\eta_{ch}} x_i + z_i p_s^i \leq t_i, \ \forall i$$

$$\text{(e) Ramp constraint: } x_i \in [X^i_{\min}, X^i_{\max}], \ \forall i$$

$$\text{(f) Capacity constraint: } \sum x_i \in [b_{\min} - b_0, b_{\max} - b_0], \ \forall i.$$

The cost function for only lossy storage operation under NEM would have two-piecewise linear segments and it would be linear for equal buying and selling price of electricity with lossless battery. Authors in [139, 109] present this case in their LP formulation. This case could be obtained by simplifying the more general case depicted as $\mathrm{P_{LP}}$ in Fig. B.1.

We make our code open source on formulating optimal arbitrage problem using linear programming[1].

B.2.1 Epigraph formulation of Linear Programming

An unconstrained minimization problem of a convex piecewise-linear function, $h(x)$, could be transformed to an equivalent linear programming problem by forming the epigraph problem [108], [318]. Consider the convex piecewise cost function minimization problem is denoted as $(P_{org}) \quad \min h(x)$, where $h(x) = \max_{i=1,\ldots,m}(a_i^T x + b_i)$. For cases where the decision variable x is scaler, a_i^T is also a scaler. Thus, $a_i x + b_i$ is a two-dimensional line with b_i denoting the y-intercept and a_i the slope of the line. The equivalent epigraph problem for the original problem P_{org} is denoted as $(P_{epi}) \quad \min t, \quad$ subject to, $a_i x + b_i \leq$

[1] https://github.com/umar-hashmi/linearprogrammingarbitrage

$t, \quad i = 1, ..., m,$ where t denotes auxiliary scalar variable. The LP matrix notation for the optimization problem P_{epi} is represented as: minimize $\tilde{f}^T\tilde{x}$, subject to $\tilde{A}\tilde{x} \leq \tilde{b}$; where $\tilde{f} = \begin{bmatrix}0\\1\end{bmatrix}, \quad \tilde{x} = \begin{bmatrix}x\\t\end{bmatrix}, \quad \tilde{A} = \begin{bmatrix}a_1 & -1\\ : & :\\ a_m & -1\end{bmatrix}, \quad \tilde{b} = \begin{bmatrix}-b_1\\ :\\ -b_m\end{bmatrix}$. Now consider extending this minimization problem for two time instants with a unique cost function for each time instant. The optimization problem is denoted as $(P_{epi}) \quad \min \quad t_1 + t_2,$ s.t., (i) $a_{1i}x + b_{1i} \leq t_1,$ (ii) $a_{2i}x + b_{2i} \leq t_2, \; i = 1, ..., m,$ The equivalent LP matrices are denoted as

$$\tilde{f}=\begin{bmatrix}0\\0\\1\\1\end{bmatrix}, \tilde{x}=\begin{bmatrix}x_1\\x_2\\t_1\\t_2\end{bmatrix}, \tilde{A}=\begin{bmatrix}a_{11} & 0 & -1 & 0\\ : & : & : & :\\ a_{1m} & 0 & -1 & 0\\ 0 & a_{21} & 0 & -1\\ : & : & : & :\\ 0 & a_{1m} & 0 & -1\end{bmatrix}, \tilde{b}=\begin{bmatrix}-b_{11}\\ :\\ -b_{1m}\\ -b_{21}\\ :\\ -b_{2m}\end{bmatrix}.$$

A similar LP formulation for N time steps with piecewise linear cost function could be formulated.

B.3 Formulating LP Matrices

In this section we provide LP formulations for storage device for performing arbitrage. We present three versions of the LP problem for energy arbitrage. Firstly, a lossless storage performing arbitrage under equal buying and selling price of electricity, i.e. $\kappa_i = 1, \; \forall i$. Secondly, storage under net-metering, i.e. $\kappa_i \in [0, 1]$, with charging and discharging losses and finally storage with inelastic load and renewable generation at consumer end with net-metering and storage losses. The progressive formulations shows the evolution of complexity and the manner we deal with such challenges. We apply the epigraph based minimization presented in [108] for optimal storage arbitrage.

B.3.1 Lossless Storage with equal buy and sell price

The LP formulation for lossless energy storage device with time varying electricity price is given as:

$$\text{Ojective function: } p_{elec}^T x, \text{subject to: (a)} A_{c1}x \leq b, \text{ (b) } lb \leq x \leq ub,$$

where x and p_{elec} denote row vectors of dimension Nx1. The constraint (a) takes care of the capacity constraint which ensures instantaneous battery charge level is within minimum and maximum bounds and constraint (b) takes into account the ramp constraint of the battery. The capacity constraint could be rewritten as two constraints given as $(i) \sum_i x_i \leq \{b_{\max} - b_0\}, \; (ii) - \sum_i x_i \leq \{b_0 - b_{\min}\} \forall i$. The capacity constraints, $A_{c1}x \leq b$, in matrix is given as

$$\begin{bmatrix}1 & 0 & 0 & .. & 0 & 0\\ 1 & 1 & 0 & .. & 0 & 0\\ : & : & : & .. & : & :\\ 1 & 1 & 1 & .. & 1 & 1\\ -1 & 0 & 0 & .. & 0 & 0\\ -1 & -1 & 0 & .. & 0 & 0\\ : & : & : & .. & : & :\\ -1 & -1 & -1 & .. & -1 & -1\end{bmatrix}\begin{bmatrix}x_1\\x_2\\ :\\ x_N\end{bmatrix} = \begin{bmatrix}b_{\max} - b_0\\ b_{\max} - b_0\\ :\\ b_{\max} - b_0\\ b_0 - b_{\min}\\ b_0 - b_{\min}\\ :\\ b_0 - b_{\min}\end{bmatrix}. \tag{B.3.1}$$

The dimension of matrix A_{c1} is 2NxN, and b is of the order 2Nx1. Note that in this formulation we do not consider storage efficiency losses and also assume price of electricity for buying and selling to be equal for each time instant. The lower bound (lb) and upper bound (ub) in constraint (b) is given as

$$lb = \begin{bmatrix}X_{\min}\\X_{\min}\\ :\\ X_{\min}\end{bmatrix} \leq \begin{bmatrix}x_1\\x_2\\ :\\ x_N\end{bmatrix} \leq ub = \begin{bmatrix}X_{\max}\\X_{\max}\\ :\\ X_{\max}\end{bmatrix}. \tag{B.3.2}$$

B.3.2 Only Storage Case with net-metering and efficiency losses

Consider the operation of energy storage under time varying buying and selling price of electricity. It is assumed the selling price is at best equal to buying price, however, we do not assume for this formulation to have a fixed ratio of selling and buying price of electricity. The storage is considered to have charging and discharging efficiency losses. The cost function for optimal arbitrage problem for storage with change in charge level, x_i, as the decision variable is presented in Fig. B.2. Clearly, the cost function, C_{storage}, is a combination of two lines. The equation of these line segments are denoted as Seg.1: $Y_{1i}(x_i) = \frac{p_b(i)}{\eta_{ch}} x_i$, Seg.2: $Y_{2i}(x_i) = p_s(i)\eta_{dis} x_i$,

The cost function is denoted as $C_{\text{storage}} = \max(Y_{1i}(x_i), Y_{2i}(x_i))$. Note that y-intercept of segment 1 and segment 2 are equal to zero, therefore, $b_{1i} = 0$ and $b_{2i} = 0$ for all i. The electricity price, p_{bat}, is denoted as (equivalent to the slopes of the cost function with respect to the decision variable). $p_{\text{bat}}(i)$ is equal to $\frac{p_b(i)}{\eta_{ch}}$ for $x_i \geq 0$ and $p_s(i)\eta_{dis}$ for otherwise. The epigraph based LP formulation (see Appendix B.2.1) could be applied for the optimal arbitrage problem with cost function denoted as C_{storage}, as the cost function is convex and piecewise linear.

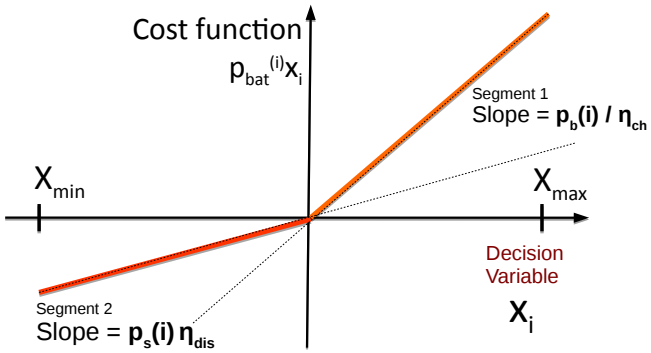

Figure B.2: The cost function segment wise for storage performing arbitrage with $\kappa_i \in [0, 1]$. We would like to highlight that this cost function also applies for equal buying and selling price in presence of load and renewable generation, as under such cases operation of storage becomes independent of load and renewable variations [182].

Using the epigraph equivalent formulation for piecewise linear convex cost function we formulate the optimal arbitrage problem using LP, given as

$$\begin{aligned} \min \quad & \{t_1 + t_2 + ... + t_N\} \\ \text{subject to,} \quad & \frac{p_b^i}{\eta_{ch}} x_i - t_i \leq 0, \; p_s^i \eta_{dis} x_i - t_i \leq 0, \forall i \\ & x_i \in [X_{\min}, X_{\max}], \sum x_i \in [b_{\min} - b_0, b_{\max} - b_0], \forall i. \end{aligned}$$

The matrix format for the above problem is denoted as minimize $f^T X$, subject to $A_{c2} X \leq b_{c2}$, and $X \in [lb, ub]$.

$$f = \begin{bmatrix} 0 \\ : \\ 0 \\ 1 \\ : \\ 1 \end{bmatrix}, X = \begin{bmatrix} x_1 \\ : \\ x_N \\ t_1 \\ : \\ t_N \end{bmatrix}, lb = \begin{bmatrix} X_{\min} \\ X_{\min} \\ : \\ X_{\min} \\ T_{\min} \\ T_{\min} \\ : \\ T_{\min} \end{bmatrix} \leq \begin{bmatrix} x_1 \\ x_2 \\ : \\ x_N \\ t_1 \\ t_2 \\ : \\ t_N \end{bmatrix} \leq ub = \begin{bmatrix} X_{\max} \\ X_{\max} \\ : \\ X_{\max} \\ T_{\max} \\ T_{\max} \\ : \\ T_{\max} \end{bmatrix}. \tag{B.3.3}$$

where $T_{\min}$ and $T_{\max}$ are bounds on t_i. Since these bounds are not known to us, we choose $T_{\min}$ to be negative with a large magnitude and $T_{\max}$ to be positive with a large magnitude. The dimension of A_{c2} is 4Nx2N, b_{c2} is 4Nx1, X and f is 2Nx1.

$$A_{c2} = \begin{bmatrix} \frac{p_b(1)}{\eta_{ch}} & 0 & 0 & ... & 0 & -1 & 0 & 0 & ... & 0 \\ 0 & \frac{p_b(2)}{\eta_{ch}} & 0 & ... & 0 & 0 & -1 & 0 & ... & 0 \\ : & : & : & ... & : & : & : & : & ... & : \\ 0 & 0 & 0 & ... & \frac{p_b(N)}{\eta_{ch}} & 0 & 0 & 0 & ... & -1 \\ p_s(1)\eta_{dis} & 0 & 0 & ... & 0 & -1 & 0 & 0 & ... & 0 \\ 0 & p_s(2)\eta_{dis} & 0 & ... & 0 & 0 & -1 & 0 & ... & 0 \\ : & : & : & ... & : & : & : & : & ... & : \\ 0 & 0 & 0 & ... & p_s(N)\eta_{dis} & 0 & 0 & 0 & ... & -1 \\ 1 & 0 & 0 & ... & 0 & 0 & 0 & 0 & ... & 0 \\ 1 & 1 & 0 & ... & 0 & 0 & 0 & 0 & ... & 0 \\ : & : & : & ... & : & : & : & : & ... & : \\ 1 & 1 & 1 & ... & 1 & 0 & 0 & 0 & ... & 0 \\ -1 & 0 & 0 & ... & 0 & 0 & 0 & 0 & ... & 0 \\ -1 & -1 & 0 & ... & 0 & 0 & 0 & 0 & ... & 0 \\ : & : & : & ... & : & : & : & : & ... & : \\ -1 & -1 & -1 & ... & -1 & 0 & 0 & 0 & ... & 0 \end{bmatrix}, \quad b_{c2} = \begin{bmatrix} 0 \\ 0 \\ : \\ 0 \\ 0 \\ 0 \\ : \\ 0 \\ b_{\max} - b_0 \\ b_{\max} - b_0 \\ : \\ b_{\max} - b_0 \\ b_0 - b_{\min} \\ b_0 - b_{\min} \\ : \\ b_0 - b_{\min} \end{bmatrix}, \tag{B.3.4}$$

B.3.3 Storage performing arbitrage with inelastic load and renewable generation under net-metering and storage losses

The matrix format for the optimization problem P_{LP} is denoted as minimize $f^T X$, subject to $A_{c3}X \leq b_{c3}$, and $X \in [lb, ub]$. The variables for LP formulation is denoted as The lower bound and upper bound of the state variable same as the previous case as Eq. B.3.3. The dimension of A_{c3} is 6Nx2N, b_{c3} is 6Nx1, X and f is 2Nx1, N denotes number of samples in the horizon of optimization.

$$A_{c3} = \begin{bmatrix} \frac{p_b(1)}{\eta_{ch}} & 0 & 0 & ... & 0 & -1 & 0 & 0 & ... & 0 \\ 0 & \frac{p_b(2)}{\eta_{ch}} & 0 & ... & 0 & 0 & -1 & 0 & ... & 0 \\ : & : & : & ... & : & : & : & : & ... & : \\ 0 & 0 & 0 & ... & \frac{p_b(N)}{\eta_{ch}} & 0 & 0 & 0 & ... & -1 \\ p_s(1)\eta_{dis} & 0 & 0 & ... & 0 & -1 & 0 & 0 & ... & 0 \\ 0 & p_s(2)\eta_{dis} & 0 & ... & 0 & 0 & -1 & 0 & ... & 0 \\ : & : & : & ... & : & : & : & : & ... & : \\ 0 & 0 & 0 & ... & p_s(N)\eta_{dis} & 0 & 0 & 0 & ... & -1 \\ \frac{p_s(1)}{\eta_{ch}} & 0 & 0 & ... & 0 & -1 & 0 & 0 & ... & 0 \\ 0 & \frac{p_s(2)}{\eta_{ch}} & 0 & ... & 0 & 0 & -1 & 0 & ... & 0 \\ : & : & : & ... & : & : & : & : & ... & : \\ 0 & 0 & 0 & ... & \frac{p_s(N)}{\eta_{ch}} & 0 & 0 & 0 & ... & -1 \\ p_b(1)\eta_{dis} & 0 & 0 & ... & 0 & -1 & 0 & 0 & ... & 0 \\ 0 & p_b(2)\eta_{dis} & 0 & ... & 0 & 0 & -1 & 0 & ... & 0 \\ : & : & : & ... & : & : & : & : & ... & : \\ 0 & 0 & 0 & ... & p_b(N)\eta_{dis} & 0 & 0 & 0 & ... & -1 \\ 1 & 0 & 0 & ... & 0 & 0 & 0 & 0 & ... & 0 \\ 1 & 1 & 0 & ... & 0 & 0 & 0 & 0 & ... & 0 \\ : & : & : & ... & : & : & : & : & ... & : \\ 1 & 1 & 1 & ... & 1 & 0 & 0 & 0 & ... & 0 \\ -1 & 0 & 0 & ... & 0 & 0 & 0 & 0 & ... & 0 \\ -1 & -1 & 0 & ... & 0 & 0 & 0 & 0 & ... & 0 \\ : & : & : & ... & : & : & : & : & ... & : \\ -1 & -1 & -1 & ... & -1 & 0 & 0 & 0 & ... & 0 \end{bmatrix}, \quad b_{c3} = \begin{bmatrix} -z_i p_b(1) \\ -z_i p_b(2) \\ : \\ -z_i p_b(N) \\ -z_i p_s(1) \\ -z_i p_s(2) \\ : \\ -z_i p_s(N) \\ -z_i p_s(1) \\ -z_i p_s(2) \\ : \\ -z_i p_s(N) \\ -z_i p_b(1) \\ -z_i p_b(2) \\ : \\ -z_i p_b(N) \\ b_{\max} - b_0 \\ b_{\max} - b_0 \\ : \\ b_{\max} - b_0 \\ b_0 - b_{\min} \\ b_0 - b_{\min} \\ : \\ b_0 - b_{\min} \end{bmatrix}. \tag{B.3.5}$$

B.4 Real-time implementation

The previous section discussed optimal storage arbitrage under complete knowledge of future net loads and prices. In this section, we consider the setting where future values may be unknown. To that end, we first develop a forecast model for net load without storage (which includes inelastic consumer load and consumer distributed generation) and electricity price for future times, where the forecast is updated after each time step. Then, we develop the forecasting model for net load with solar generation using AutoRegressive Moving Average (ARMA) model and electricity price forecast using AutoRegressive Integrated Moving Average (ARIMA).

The forecast models based on ARMA and ARIMA model developed in [178] are used in this work. The forecast values are fed to a Model Predictive Control (MPC) scheme to identity the optimal modes of operation of storage for the current time-instance. Any of the developed schemes from the previous section can be used for the optimization inside MPC. These steps (forecast and MPC) are repeated sequentially and highlighted in online Algorithm 20: `ForecastMPClinearProgram`.

Algorithm 20 `ForecastMPClinearProgram`

Storage Parameters: $\eta_{\text{ch}}, \eta_{\text{dis}}, \delta_{\max}, \delta_{\min}, b_{\max}, b_{\min}, b_0$.
Inputs: $h, N, T, i = 0$, Rolling horizon optimization time period N_{opt}, Historical inelastic load, renewable generation and electricity price data.

Use historical data to tune ARMA and ARIMA models,
while $i < N$ **do**
    Increment $i = i + 1$,
    Real-time electricity price value $p_{\text{elec}}(i)$ and load z_i,
    Forecast $\hat{z}$ from time step $i + 1$ to $i + N_{\text{opt}}$ using ARMA,
    Forecast $\hat{p}_b$ and $\hat{p}_s$ from time $i + 1$ to $i + N_{\text{opt}}$ using ARIMA,
    Calculate $\hat{\kappa}$ as the ratio of $\hat{p}_s$ and $\hat{p}_b$,
    Build LP matrices for time step i to N,
    Solve the Linear Optimization problem for forecast vectors,
    Calculate ${b_i}^* = b_{i-1} + \hat{x}^*(1)$,
    Update $b_0 = {b_i}^*$, the initial capacity of battery is updated.
    Return ${b_i}^*$, ${x_i}^*$.
end while

B.5 Conclusion

We formulate energy storage arbitrage problem using linear programming. The linear programming formulation is possible due to piecewise linear convex cost functions. In this formulation we consider: (a) net-metering compensation (with selling price at best equal to buying price) i.e. $\kappa_i \in [0, 1]$, (b) inelastic load, (c) consumer renewable generation, (d) storage charging and discharging losses, (e) storage ramping constraint and (f) storage capacity constraint. Net-load and electricity price are modeled with AutoRegressive models for model predictive control.

Bibliography

[1] Alabama Power Company: Rules and Regulations for Electric Service 2017. Online, https://www.alabamapower.com/content/dam/alabamapower/Rates/APCRulesRegulations.pdf.

[2] Ancillary Services. Online, http://www.elia.be/en/products-and-services/ancillary-services.

[3] Balancing and frequency control: North American Electric Reliability Corporation. Online, https://tinyurl.com/y4x69u2u, journal=NERC, Princeton.

[4] Battery Energy Storage System: The power to control energy by Ved Sinha (ABB). Online, https://tinyurl.com/y9qle48y.

[5] BPA Balancing Authority Load and Total Wind, Hydro, Fossil/Biomass, and Nuclear Generation, Near-Real-Time. Online, https://transmission.bpa.gov/Business/Operations/Wind/baltwg.aspx.

[6] Current System Imbalance. Online, http://www.elia.be/en/grid-data/balancing/current-system-imbalance.

[7] CVX: Matlab Software for Disciplined Convex Programming, version 2.0. Online, http://cvxr.com/cvx.

[8] Energy efficiency improvement through optimization of the power factor correction. Online, http://www2.schneider-electric.com/documents/technical-publications/en/shared/electrical-engineering/technical-papers/medium-voltage/energy_efficiency_CIRED_2007.pdf.

[9] Energy storage possibilities for expanding electric grid flexibility. Online, https://www.nrel.gov/docs/fy16osti/64764.pdf.

[10] ES55 Design Standards - Voltage Unbalance. Online, https://tinyurl.com/yye7wgwb.

[11] Essential Services Commission Victoria: Electricity Distribution Code, Dec. 2015. Online, https://www.esc.vic.gov.au/sites/default/files/documents/Electricity-Distribution-Code-Version-9.pdf.

[12] FirstEnergy Corp: Customer Guide for Electric Service – Ohio, 2017. Online, https://tinyurl.com/y29gottk.

[13] Horizon 2020 Project Smile: Deliverable 4.1, 2018. Online, http://www.h2020smile.eu/wp-content/uploads/2018/06/Deliverable-D4.1.pdf.

[14] Hydro Ottawa Ltd: Conditions of Service 2017. Online, http://static.hydroottawa.com/documents/corporate/policies/HOL-COS-V6-EN-FINAL-04-01-2017.pdf.

[15] Imbalance Prices. Online, http://www.elia.be/en/grid-data/balancing/imbalance-prices.

[16] Industry Data Energy Online. Online, http://www.energyonline.com/Data/.

[17] KERMIT Study Report: PJM Interconnection - To determine the effectiveness of the AGC in controlling fast and conventional resources in the PJM frequency regulation market. Online, https://tinyurl.com/y87lntbx.

[18] Lansing Board of Water and Light: Rules and Regulations for Electric Service 2017. Online, https://tinyurl.com/y2fvd8fd.

[19] Linky Single-Phase Smart Meters. Online, https://www.enedis.fr/sites/default/files/Notice_compteur_Linky_Monophase_anglais.pdf.

[20] McCormick envelopes. Online, https://optimization.mccormick.northwestern.edu/index.php/McCormick_envelopes.

[21] NEMA Standards Publication MG 1-2009: Motors and Generators. Online, https://law.resource.org/pub/us/cfr/ibr/005/nema.mg-1.2009.pdf.

[22] Net Metering. Online, https://tinyurl.com/ybgzerct.

[23] Pacific Gas and Electric Company Electric Tariff. Online, https://www.pge.com/tariffs/tm2/pdf/ELEC_4795-E.pdf.

[24] Paris Climate Change Agreement. Online, https://en.wikipedia.org/wiki/Paris_Agreement.

[25] Pliego Tarifario, Gerencia Análisis Tarifario, UTE Uruguay. Online, http://tinyurl.com/y5ug28jh.

[26] POST NOTE Number 372 February 2011 Future Electricity Networks. Online, https://www.parliament.uk/documents/post/postpn_372-future-electricity-networks.pdf.

[27] Power Factor Correction (PFC) in solar power plants. Online, https://tinyurl.com/y3njurn4.

[28] Power factor design and reactive power capabilities - PJM ISO. Online, https://tinyurl.com/yyv6ddv2.

[29] Real Time LMP, New York ISO. Online, https://tinyurl.com/2flowo6.

[30] Residential On Call. Online, https://www.fpl.com/save/programs/on-call.html.

[31] Rule 21: Pacific Gas and Electric. Online, https://www.pge.com/tariffs/tm2/pdf/ELEC_RULES_21.pdf.

[32] Rule 21: San Diego Gas & Electric. Online, http://regarchive.sdge.com/tm2/pdf/ELEC_ELEC-RULES_ERULE21.pdf.

[33] Rule 21: Southern California Edison. Online, https://www1.sce.com/NR/sc3/tm2/pdf/Rule21_1.pdf.

[34] The IRC: Shaping Our Energy Future. Online, https://isorto.org/.

[35] Today's Outlook - Net demand (demand minus solar and wind) . Online, http://www.caiso.com/TodaysOutlook/Pages/default.aspx.

[36] Voltage Disturbances Standard EN 50160. Online, http://copperalliance.org.uk/uploads/2018/03/542-standard-en-50160-voltage-characteristics-in.pdf.

[37] Voltage Unbalance and Motor: Pacific Gas and Electric. Online, https://www.pge.com/includes/docs/pdfs/mybusiness/customerservice/energystatus/powerquality/voltage_unbalance_rev2.pdf.

[38] Wind Generation and Total Load in The BPA Balancing Authority. Online, https://tinyurl.com/y3zwf643.

[39] Pjm performance scoring. Online, http://www.pjm.com/-/media/committees-groups/task-forces/rmistf/postings/performance-scoring-design-component.ashx?la=en, 2016.

[40] Abb ess pro datasheet. Online, https://library.e.abb.com/public/4ac5cde207f4fe9283257cf3006af87a/9AKK106103A6303_EssPro_PCS_DataSheet-WEB.pdf, 2017.

[41] Aentron off grid battery system. Online, http://www.aentron.com/wp-content/uploads/2017/05/OFF_GRID_BATTERY_SYSTEM_EN.pdf, 2017.

[42] Aes energy storage: Advancion energy storage for the grid. Online, http://aesenergystorage.com/wp-content/uploads/2017/01/010517-Advancion-4-Brochure.pdf, 2017.

[43] Best go power. Online, http://www.bestgopower.com/faq/30-what-is-depth-of-discharge-dod.html, 2017.

[44] Bosch energy storage solutions. Online, http://boschenergystoragesolutions.resource.bosch.com/media/bess/pdfs/BoschStorageSolution_Power_EN.pdf, 2017.

[45] Byd home based energy storage solution. Online, https://tinyurl.com/nsh9dml, 2017.

[46] Elia data download page. Online, http://www.elia.be/en/grid-data/data-download, 2017.

[47] Energy government usa. Online, https://tinyurl.com/y82qdfq5, 2017.

[48] Featherweight lithium ion battery li tel 48-170 c. Online, http://www.cdtechno.com/pdf/lit/12_1093_1214.pdf, 2017.

[49] Forsee power lithium ion he 48. Online, https://drive.google.com/open?id=0BxK92uSDJ7PENlczWURjelNnUlU, 2017.

[50] Iso storage pilot projects: Advancing a smarter grid. Online, https://www.caiso.com/Documents/FastFacts_ISOStoragePilotProjects-AdvancingSmarterGrid.pdf, 2017.

[51] Lg chem: Resu 6.4 ex. Online, https://drive.google.com/open?id=0BxK92uSDJ7PEbFFLamRTTXA2NFk, 2017.

[52] Li-ion battery temperature trends during charge and discharge. Online, https://tinyurl.com/yxfl2sc3, 2017.

[53] Lithium battery failures. Online, http://www.mpoweruk.com/lithium_failures.htm, 2017.

[54] Methode tactivenergy ac6000. Online, http://www.methode.com/Documents/TechnicalLibrary/AC6000-Lithium-Ion-UPS-data-sheet.pdf, 2017.

[55] Net energy metering. Online, http://www.cpuc.ca.gov/General.aspx?id=3800, 2017.

[56] Net metering. Online, https://www.nrel.gov/technical-assistance/basics-net-metering.html, 2017.

[57] Panasonic storage battery system using lithium ion batteries. Online, https://tinyurl.com/y6et4u2s, 2017.

[58] Pecan street dataport. Online, https://dataport.cloud/, 2017.

[59] Qinous ess compact, medium, large. Online, https://drive.google.com/open?id=0BxK92uSDJ7PEVmJUcWpQcHYwVkU, 2017.

[60] Refu elektronik gmbh: Refubox rb-003-003-001-0300. Online, http://www.refu-energy.de/uploads/tx_edxproductman/1405_Datenblatt_eng_REFUbox_AnsichtEinzels.pdf, 2017.

[61] Renewable energy: Catalyst for a clean energy transition. Online, https://tinyurl.com/lgl3u3y, 2017.

[62] Saft batteries: Evolion, proven ultra-compact solution for on and off-grid installations. Online, https://tinyurl.com/yyx8asdl, 2017.

[63] Saft batteries: Li ion battery life. Online, https://drive.google.com/open?id=0BxK92uSDJ7PEbHVjRGk3MXE0YUE, 2017.

[64] Tesla built a huge solar energy plant on the island of kauai. Online, https://www.theverge.com/2017/3/8/14854858/tesla-solar-hawaii-kauai-kiuc-powerpack-battery-generator, 2017.

[65] Tesla powerwall 1 datasheet. Online, http://mcelectrical.com.au/wp-content/uploads/2017/02/Tesla_Powerwall-1_Datasheet_v3-3_English.pdf, 2017.

[66] Tesla powerwall, wikipedia. Online, https://en.wikipedia.org/wiki/Tesla_Powerwall, 2017.

[67] Tesvolt energy storage: Tps storage. Online, https://drive.google.com/open?id=0BxK92uSDJ7PETGFubTFQLXg5bnM, 2017.

[68] PJM Market Settlements Developement Department, Manual 28, http://www.pjm.com/-/media/documents/manuals/m28.ashx, 2018.

[69] Wikipedia renewable energy in india. Online, https://en.wikipedia.org/wiki/Renewable_energy_in_India, 2018.

[70] BU-1003: Electric Vehicle (EV) . Online, https://batteryuniversity.com/learn/article/electric_vehicle_ev, 2019.

[71] California DG Stats. Online, https://www.californiadgstats.ca.gov/, 2019.

[72] Power Factor Correction Enerdis France. Online, http://www.enerdis.com/sites/default/files/documents/guide_compensation_906211239_bd.pdf, 2019.

[73] Understanding electric car charging. Online, https://www.spiritenergy.co.uk/kb-ev-understanding-electric-car-charging, 2019.

[74] International Renewable Energy Agency. Renewable Energy Policy Brief: URUGUAY. Online, https://tinyurl.com/y2gydsu7, 2015.

[75] Markets and operations at PJM. Online, http://tinyurl.com/PJMregs, 2015.

[76] Real time electricity price data. Online, Energinet.dk, 2016.

[77] 100% renewable energy, wikipedia,. Online, https://tinyurl.com/jq7r4jd, 2019.

[78] California dg stats. Online, http://tinyurl.com/yymlx3x2, 2019.

[79] Energy online california iso real-time price. Online, https://tinyurl.com/p2ac2lh, 2019.

[80] K. Abdulla, J. de Hoog, V. Muenzel, F. Suits, K. Steer, A. Wirth, and S. Halgamuge. Optimal operation of energy storage systems considering forecasts and battery degradation. *IEEE Transactions on Smart Grid*, 9(3):2086–2096, May 2018.

[81] Khalid Abdulla, Julian De Hoog, Valentin Muenzel, Frank Suits, Kent Steer, Andrew Wirth, and Saman Halgamuge. Optimal operation of energy storage systems considering forecasts and battery degradation. *IEEE Transactions on Smart Grid*, 9(3):2086–2096, 2018.

[82] Khalid Abdulla, Kent Steer, Andrew Wirth, Saman Halgamuge, and Julian de Hoog. Accounting for forecast uncertainty in the optimized operation of energy storage. In *Innovative Smart Grid Technologies-Asia (ISGT-Asia), 2016 IEEE*, pages 183–189. IEEE, 2016.

[83] ACIF-CCIM, Prsma, EEM, M-ITI, and Route Monkey. Madeira Pilot Case Study Specification and Assessment. Technical report 4.1, European Commission, Funchal, Portugal, October 2017.

[84] René Aid. An introduction to electricity markets and derivatives Lecture 1 — Electricity markets.

[85] MJE Alam, KM Muttaqi, and Darmawan Sutanto. Distributed energy storage for mitigation of voltage-rise impact caused by rooftop solar pv. In *Power and Energy Society General Meeting, 2012 IEEE*, pages 1–8. IEEE, 2012.

[86] Abdulwahab Alhamali, Mohamed Emad Farrag, Geraint Bevan, and Donald M Hepburn. Review of energy storage systems in electric grid and their potential in distribution networks. In *2016 Eighteenth International Middle East Power Systems Conference (MEPCON)*, pages 546–551. IEEE, 2016.

[87] Hunt Allcott. Rethinking real-time electricity pricing. *Resource and energy economics*, 33(4):820–842, 2011.

[88] Ariana Amberg, Alex Rangel, et al. Tutorial on symmetrical components. *Selinc. Cachefly. Net*, 1:1–6, 2014.

[89] Dyreson Ana, Hoffman Chris, Prichard Aaron, and Schienebeck Amanda. Effects of Salt River Project Demand Based Rate Change on the Rooftop Solar Market in Maricopa County, Arizona. Online, https://emp.lbl.gov/sites/default/files/uwisconsin-srp_solar_event_study_final051117.pdf, 2017.

[90] Erling D Andersen and Knud D Andersen. Presolving in linear programming. *Mathematical Programming*, 71(2):221–245, 1995.

[91] Kyle Anderson and Abbas El Gamal. Co-optimizing the value of storage in energy and regulation service markets. *Energy Systems*, pages 1–19, 2016.

[92] Kyle Anderson and Abbas El Gamal. Co-optimizing the value of storage in energy and regulation service markets. *Energy Systems*, 8(2):369–387, 2017.

[93] V Arangarajan, A Maung Than Oo, Jaideep Chandran, G Shafiullah, and Alex Stojcevski. Role of energy storage in the power system network. *Renewable energy and sustainable development*, pages 201–225, 2015.

[94] Prabir Barooah, Ana Buic, and Sean Meyn. Spectral decomposition of demand-side flexibility for reliable ancillary services in a smart grid. In *2015 48th Hawaii International Conference on System Sciences*, pages 2700–2709. IEEE, 2015.

[95] Shiva Beharrysingh. *Phase unbalance on low-voltage electricity networks and its mitigation using static balancers*. PhD thesis, © Shiva Beharrysingh, 2014.

[96] A. I. Bejan, R. J. Gibbens, and F. P. Kelly. Statistical aspects of storage systems modelling in energy networks. In *46th Annual Conference on Information Sciences and Systems*, pages 1–6, 2012.

[97] Scott Benner. Performance, Mileage and the Mileage Ratio, https://tinyurl.com/y7m5lbmj, 2015.

[98] Bente Klein. Renewable energy policy database and support. Online, https://tinyurl.com/ybtrnohs, 2017.

[99] Dimitri P Bertsekas. *Convex optimization theory*. Athena Scientific Belmont, 2009.

[100] Dimitris Bertsimas, Eugene Litvinov, Xu Andy Sun, Jinye Zhao, and Tongxin Zheng. Adaptive robust optimization for the security constrained unit commitment problem. *IEEE Transactions on Power Systems*, 28(1):52–63, 2013.

[101] Ramchandra Bhandari and Ingo Stadler. Grid parity analysis of solar photovoltaic systems in germany using experience curves. *Solar Energy*, 83(9):1634–1644, 2009.

[102] M Tavakoli Bina and A Kashefi. Three-phase unbalance of distribution systems: Complementary analysis and experimental case study. *International Journal of Electrical Power & Energy Systems*, 33(4):817–826, 2011.

[103] BloombergNEF. A behind the scenes take on lithium ion battery prices. Online, https://tinyurl.com/y3xbu8xt, 2019.

[104] MHJ Bollen, Yongtao Yang, and Fainan Hassan. Integration of distributed generation in the power system-a power quality approach. In *Harmonics and Quality of Power, 2008. ICHQP 2008. 13th International Conference on*, pages 1–8. IEEE, 2008.

[105] Severin Borenstein. The long-run efficiency of real-time electricity pricing. *The Energy Journal*, pages 93–116, 2005.

[106] Severin Borenstein. The long-run efficiency of real-time electricity pricing. *The Energy Journal*, 26(3):93–116, 2005.

[107] B Bouillon. Prepared Statement of Brad Bouillon on Behalf of the California Independent System Operator Corporation.

[108] Stephen Boyd and Lieven Vandenberghe. *Convex optimization*. Cambridge university press, 2004.

[109] Kyle Bradbury, Lincoln Pratson, and Dalia Patiño-Echeverri. Economic viability of energy storage systems based on price arbitrage potential in real-time us electricity markets. *Applied Energy*, 114:512–519, 2014.

[110] Steve Brunton. Control Bootcamp Video Lectures.

[111] C Bueno and Jose A Carta. Wind powered pumped hydro storage systems, a means of increasing the penetration of renewable energy in the canary islands. *Renewable and Sustainable Energy Reviews*, 10(4):312–340, 2006.

[112] James V. Burke. Convex Optimization: Saddle Point Theory, and Lagrangian Duality. Online, https://sites.math.washington.edu/~burke/crs/516/notes/saddlepoints.pdf, 2019.

[113] Michael Burnett. Energy Storage and the California "Duck Curve".

[114] Ana Bušić, Md Umar Hashmi, and Sean Meyn. Distributed control of a fleet of batteries. In *2017 American Control Conference (ACC)*, pages 3406–3411. IEEE, 2017.

[115] Ana Bušić and Sean Meyn. Distributed randomized control for demand dispatch. In *IEEE Conference on Decision and Control*, pages 6964–6971, Dec 2016.

[116] C. Byrne and G. Verbic. Feasibility of residential battery storage for energy arbitrage. In *2013 Australasian Universities Power Engineering Conference (AUPEC)*, pages 1–7, Sep. 2013.

[117] Raymond H Byrne, Ricky J Concepcion, and César A Silva-Monroy. Estimating potential revenue from electrical energy storage in pjm. In *Power and Energy Society General Meeting (PESGM), 2016*, pages 1–5. IEEE, 2016.

[118] Raymond H Byrne and César A Silva-Monroy. Potential revenue from electrical energy storage in ercot: The impact of location and recent trends. In *2015 IEEE Power & Energy Society General Meeting*, pages 1–5. IEEE, 2015.

[119] Raymond H Byrne and Cesar Augusto Silva-Monroy. Estimating the maximum potential revenue for grid connected electricity storage: Arbitrage and regulation. *Sandia National Laboratories*, 2012.

[120] Roque Calero and José Antonio Carta. Action plan for wind energy development in the canary islands. *Energy Policy*, 32(10):1185–1197, 2004.

[121] D.S. Callaway and I.A. Hiskens. Achieving controllability of electric loads. *Proceedings of the IEEE*, 99(1):184 –199, January 2011.

[122] Eduardo F Camacho and Carlos Bordons Alba. *Model predictive control*. Springer Science & Business Media, 2013.

[123] MC Campi and G Calafiore. Decision making in an uncertain environment: the scenario-based optimization approach. *Multiple Participant Decision Making*, pages 99–111, 2004.

[124] Rachel Carnegie, Douglas Gotham, David Nderitu, and Paul Preckel. Utility scale energy storage systems. Technical report, State Utility Forecasting Group, Purdue University, West Lafayette, Indiana, 2013.

[125] Rachel Carnegie, Douglas Gotham, David Nderitu, and Paul V Preckel. Utility scale energy storage systems. *State Utility Forecasting Group. Purdue University*, 1, 2013.

[126] Daniel J Carnovale and Ansel Barchowsky. Energy savings—realistic expectations for commercial facilities. pages 1–16, 2015.

[127] T. Carpenter, S. Singla, P. Azimzadeh, and S. Keshav. The impact of electricity pricing schemes on storage adoption in ontario. In *2012 Third International Conference on Future Systems: Where Energy, Computing and Communication Meet (e-Energy)*, pages 1–10, May 2012.

[128] EN50160 CENELEC. 50160. *Voltage characteristics of electricity supplied by public distribution systems*, 2001.

[129] T-H Chen. Evaluation of line loss under load unbalance using the complex unbalance factor. *IEE Proceedings-Generation, Transmission and Distribution*, 142(2):173–178, 1995.

[130] Yize Chen, Md Umar Hashmi, Deepjyoti Deka, and Michael Chertkov. Stochastic battery operations using deep neural networks. In *2019 IEEE Power & Energy Society Innovative Smart Grid Technologies Conference (ISGT)*, pages 1–5. IEEE, 2019.

[131] Yize Chen, Xiyu Wang, and Baosen Zhang. An unsupervised deep learning approach for scenario forecasts. In *2018 Power Systems Computation Conference (PSCC)*, pages 1–7. IEEE, 2018.

[132] Yize Chen, Yishen Wang, Daniel Kirschen, and Baosen Zhang. Model-free renewable scenario generation using generative adversarial networks. *IEEE Transactions on Power Systems*, 33(3):3265–3275, 2018.

[133] Yue Chen, Ana Bušić, and Sean Meyn. Individual risk in mean field control with application to automated demand response. In *53rd IEEE Conference on Decision and Control*, pages 6425–6432, Dec 2014.

[134] Yue Chen, Ana Bušić, and Sean Meyn. State estimation for the individual and the population in mean field control with application to demand dispatch. *CoRR and to appear, IEEE Transactions on Auto. Control*, 2016.

[135] Yue Chen, Md Umar Hashmi, Joel Mathias, Ana Bušić, and Sean Meyn. Distributed control design for balancing the grid using flexible loads. In *Energy Markets and Responsive Grids*, pages 383–411. Springer, 2018.

[136] Bolong Cheng and Warren Powell. Co-optimizing battery storage for the frequency regulation and energy arbitrage using multi-scale dynamic programming. *IEEE Transactions on Smart Grid*, pages 1–1, 2016.

[137] Feng Cheng, Steve Willard, Jonathan Hawkins, Brian Arellano, Olga Lavrova, and Andrea Mammoli. Applying battery energy storage to enhance the benefits of photovoltaics. In *Energytech, 2012 IEEE*, pages 1–5. IEEE, 2012.

[138] M Chindriş, A Cziker, Anca Miron, H Bălan, and A Sudria. Propagation of unbalance in electric power systems. In *9th International Conference Electrical Power Quality and Utilisation, EPQU*, volume 7, 2007.

[139] Sridhar Chouhan, Deepak Tiwari, Hakan Inan, Sarika Khushalani-Solanki, and Ali Feliachi. Der optimization to determine optimum bess charge/discharge schedule using linear programming. In *2016 IEEE Power and Energy Society General Meeting (PESGM)*, pages 1–5. IEEE, 2016.

[140] Kein Huat Chua, Jianhui Wong, Yun Seng Lim, Phil Taylor, Ezra Morris, and Stella Morris. Mitigation of voltage unbalance in low voltage distribution network with high level of photovoltaic system. *Energy Procedia*, 12:495–501, 2011.

[141] KH Chua, Yun Seng Lim, Phil Taylor, Stella Morris, and Jianhui Wong. Energy storage system for mitigating voltage unbalance on low-voltage networks with photovoltaic systems. *IEEE Transactions on power delivery*, 27(4):1783–1790, 2012.

[142] George Crabtree, Jim Misewich, Ron Ambrosio, Kathryn Clay, Paul DeMartini, Revis James, Mark Lauby, Vivek Mohta, John Moura, Peter Sauer, et al. Integrating renewable electricity on the grid. In *AIP Conference proceedings*, volume 1401, pages 387–405. AIP, 2011.

[143] Danielle Croop. Online, http://www.pjm.com/~/media/committees-groups/task-forces/rmistf/20160413/20160413-item-02-performance-scoring.ashx.

[144] Danielle Croop. Online, http://www.pjm.com/-/media/committees-groups/task-forces/rmistf/20160830/20160830-item-04-performance-scoring.ashx.

[145] James Cruise, Lisa Flatley, Richard Gibbens, and Stan Zachary. Optimal control of storage incorporating market impact and with energy applications. *arXiv preprint arXiv:1406.3653*, 2014.

[146] James Cruise, Lisa Flatley, Richard Gibbens, and Stan Zachary. Control of energy storage with market impact: Lagrangian approach and horizons. *Operations Research*, 2019.

[147] James Cruise, Lisa Flatley, and Stan Zachary. Impact of storage competition on energy markets. *arXiv preprint arXiv:1606.05361*, 2016.

[148] James R Cruise, Richard J Gibbens, and Stan Zachary. Optimal control of storage for arbitrage, with applications to energy systems. In *Information Sciences and Systems (CISS), 2014 48th Annual Conference on*, pages 1–6. IEEE, 2014.

[149] Leszek S Czarnecki. Power related phenomena in three-phase unbalanced systems. *IEEE Transactions on Power Delivery*, 10(3):1168–1176, 1995.

[150] Jie Dang, John Seuss, Luv Suneja, and Ronald G Harley. Soc feedback control for wind and ess hybrid power system frequency regulation. In *Power Electronics and Machines in Wind Applications (PEMWA), 2012 IEEE*, pages 1–7. IEEE, 2012.

[151] Naïm R Darghouth, Ryan H Wiser, Galen Barbose, and Andrew D Mills. Net metering and market feedback loops: Exploring the impact of retail rate design on distributed pv deployment. *Applied Energy*, 162:713–722, 2016.

[152] PJM RegD data. Pjm ancillary services. http://www.pjm.com/markets-and-operations/ancillary-services.aspx, 2018.

[153] Deloitte. European energy market reform Country profile: France. Online, https://tinyurl.com/y39wycf9.

[154] KC Divya and Jacob Østergaard. Battery energy storage technology for power systems—an overview. *Electric Power Systems Research*, 79(4):511–520, 2009.

[155] Johan Driesen and Thierry Van Craenenbroeck. Voltage disturbances: Introduction to unbalance. *Power Quality Application Guide, Copper Development Association*, 5(3), 2002.

[156] Cherrelle Eid, Javier Reneses Guillén, Pablo Frías Marín, and Rudi Hakvoort. The economic effect of electricity net-metering with solar pv: Consequences for network cost recovery, cross subsidies and policy objectives. *Energy Policy*, 75:244–254, 2014.

[157] Abraham Ellis, R Nelson, E Von Engeln, R Walling, J MacDowell, L Casey, E Seymour, W Peter, C Barker, B Kirby, et al. Review of existing reactive power requirements for variable generation. In *Power and Energy Society General Meeting, 2012 IEEE*, pages 1–7. IEEE, 2012.

[158] EpexSpot. Negative prices q&a. https://www.epexspot.com/en/company-info/basics_of_the_power_market/negative_prices, April 2019.

[159] Nicholas Etherden and Math HJ Bollen. Overload and overvoltage in low-voltage and medium-voltage networks due to renewable energy–some illustrative case studies. *Electric Power Systems Research*, 114:39–48, 2014.

[160] Robert L Fares and Michael E Webber. The impacts of storing solar energy in the home to reduce reliance on the utility. *Nature Energy*, 2(2):17001, 2017.

[161] Robert L Fares and Michael E Webber. What are the tradeoffs between battery energy storage cycle life and calendar life in the energy arbitrage application? *Journal of Energy Storage*, 16:37–45, 2018.

[162] Garrett Fitzgerald, James Mandel, Jesse Morris, , and Hervé Touati. The economics of battery energy storage: How multi-use, customer-sited batteries deliver the most services and value to customers and the grid. Technical report, Rocky Mountain Institute, September 2015.

[163] Garrett Fitzgerald, Chris Nelder, and James Newcomb. Electric vehicles as distributed energy resources. *Rocky Mountain Institute, Boulder, CO*, 2016.

[164] Philipp Fortenbacher, Johanna L Mathieu, and Göran Andersson. Modeling and optimal operation of distributed battery storage in low voltage grids. *IEEE Transactions on Power Systems*, 32(6):4340–4350, 2017.

[165] Charles L Fortescue. Method of symmetrical co-ordinates applied to the solution of polyphase networks. *Transactions of the American Institute of Electrical Engineers*, 37(2):1027–1140, 1918.

[166] Nicolas Gast, Jean-Yves Le Boudec, Alexandre Proutière, and Dan-Cristian Tomozei. Impact of storage on the efficiency and prices in real-time electricity markets. In *Proceedings of the fourth international conference on Future energy systems*, pages 15–26. ACM, 2013.

[167] Nicolas Gast, DanCristian Tomozei, and JeanYves Le Boudec. Optimal storage policies with wind forecast uncertainties. *ACM SIGMETRICS Performance Evaluation Review*, 40(3):28–32, 2012.

[168] Steffen Görtz. Battery energy storage for intermittent renewable electricity production: A review and demonstration of energy storage applications permitting higher penetration of renewables, 2015.

[169] Victor J Gosbell, HMSC Herath, Sarath Perera, and DA Robinson. Sources of error in unbalance measurements. 2002.

[170] Frank Graves, Thomas Jenkin, and Dean Murphy. Opportunities for electricity storage in deregulating markets. *The Electricity Journal*, 12(8):46–56, 1999.

[171] Howard Haas. Regulation Market Review. PJM – Online, http://pjm.com/~/media/committees-groups/committees/oc/20150505/20150505-item-17-regulation-market-review.ashx, July 2015.

[172] Md Umar Hashmi. Design and development of upf rectifier in a microgrid environment. Master's thesis, Indian Institute of Technology Bombay, 2012.

[173] Md Umar Hashmi. Load Flexibility for Price based Demand Response. working paper or preprint, November 2018.

[174] Md Umar Hashmi and Ana Busic. Limiting energy storage cycles of operation. In *Green Technologies Conference (GreenTech), 2018*, pages 71–74. IEEE, 2018.

[175] Md Umar Hashmi, Ana Bušić, and Sean Meyn. Drift compensation for maintaining soc of a fleet of batteries. 2020.

[176] Md Umar Hashmi, Jonathan Cavaleiro, Lucas Pereira, and Ana Busic. Sizing and profitability of energy storage for prosumers in madeira, portugal. *2020 IEEE ISGT NA, Washington DC*.

[177] Md Umar Hashmi, Deepjyoti Deka, Ana Busic, Lucas Pereira, and Scott Backhaus. Co-optimizing energy storage for prosumers using convex relaxations. *2019 20th International Conference on Intelligent System Application to Power Systems (ISAP), New Delhi India*.

[178] Md Umar Hashmi, Deepjyoti Deka, Ana Busic, Lucas Pereira, and Scott Backhaus. Arbitrage with power factor correction using energy storage. *IEEE Transactions on Power Systems*, 2020.

[179] Md Umar Hashmi, Jose Horta, Diego Kiedanski, Lucas Pereira, Ana Bušić, and Daniel Kofman. Energy storage applications for low voltage consumers in uruguay. *arXiv preprint arXiv:2002.04192*, 2020.

[180] Md Umar Hashmi, José Horta, Lucas Pereira, Zachary Lee, Ana Bušić, and Daniel Kofman. Towards phase balancing using energy storage. *arXiv preprint arXiv:2002.04177*, 2020.

[181] Md Umar Hashmi, Wael Labidi, Ana Bušić, Salah-Eddine Elayoubi, and Tijani Chahed. Long-term revenue estimation for battery performing arbitrage and ancillary services. In *2018 IEEE International Conference on Communications, Control, and Computing Technologies for Smart Grids (SmartGridComm)*, pages 1–7. IEEE, 2018.

[182] Md Umar Hashmi, Arpan Mukhopadhyay, Ana Bušić, and Jocelyne Elias. Optimal control of storage under time varying electricity prices. In *2017 IEEE International Conference on Smart Grid Communications (SmartGridComm)*, pages 134–140. IEEE, 2017.

[183] Md Umar Hashmi, Arpan Mukhopadhyay, Ana Bušić, and Jocelyne Elias. Storage optimal control under net metering policies. *arXiv preprint arXiv:2002.01524*, 2020.

[184] Md Umar Hashmi, Arpan Mukhopadhyay, Ana Bušić, Jocelyne Elias, and Diego Kiedanski. Optimal storage arbitrage under net metering using linear programming. In *2019 IEEE International Conference on Communications, Control, and Computing Technologies for Smart Grids (SmartGridComm), Beijing China*, pages 1–7. IEEE, 2019.

[185] Md Umar Hashmi, Deepan Muthirayan, and Ana Bušić. Effect of real-time electricity pricing on ancillary service requirements. In *Proceedings of the Ninth International Conference on Future Energy Systems*, pages 550–555. ACM, 2018.

[186] Md Umar Hashmi, Michael Paul Nowak, Clay Lynwood Fellers, Karl Eric Fender, Santosh Kumar Sharma, Hassan Al-Atat, Damian Antonio Gonzalez, and Nudurupati Naga Vasishta Pratap. Monitoring system for a capacitor bank, January 22 2019. US Patent 10,184,969.

[187] Md Umar Hashmi, Lucas Pereira, and Ana Bušić. Energy storage in madeira, portugal: co-optimizing for arbitrage, self-sufficiency, peak shaving and energy backup. In *2019 IEEE Milan PowerTech*, pages 1–6. IEEE, 2019.

[188] Md Umar Hashmi and Jayesh G Priolkar. Simulation and analysis of modified droop control using virtual impedance to improve stability and transient response. In *Electrical, Computer and Communication Technologies (ICECCT), 2015 IEEE International Conference on*, pages 1–6. IEEE, 2015.

[189] A. Hassan, R. Mieth, M. Chertkov, D. Deka, and Y. Dvorkin. Optimal load ensemble control in chance-constrained optimal power flow. *IEEE Transactions on Smart Grid*, pages 1–1, 2018.

[190] Guannan He, Qixin Chen, Chongqing Kang, Pierre Pinson, and Qing Xia. Optimal bidding strategy of battery storage in power markets considering performance-based regulation and battery cycle life. *IEEE Transactions on Smart Grid*, 7(5):2359–2367, 2016.

[191] Cody A Hill, Matthew Clayton Such, Dongmei Chen, Juan Gonzalez, and W Mack Grady. Battery energy storage for enabling integration of distributed solar power generation. *IEEE Transactions on smart grid*, 3(2):850–857, 2012.

[192] Jesse Honig. The price is right: Investigating net metering policies for rooftop solar in california. 2016.

[193] José Horta, Daniel Kofman, David Menga, and Mathieu Caujolle. Augmenting der hosting capacity of distribution grids through local energy markets and dynamic phase switching. *arXiv preprint arXiv:1807.09584*, 2018.

[194] Jahangir Hossain and Apel Mahmud. *Large scale renewable power generation: advances in technologies for generation, transmission and storage*. Springer Science & Business Media, 2014.

[195] Mehdi Hosseinzadeh and Farzad Rajaei Salmasi. Power management of an isolated hybrid ac/dc micro-grid with fuzzy control of battery banks. *IET Renewable Power Generation*, 9(5):484–493, 2015.

[196] Weihao Hu, Zhe Chen, and Birgitte Bak-Jensen. Optimal operation strategy of battery energy storage system to real-time electricity price in denmark. In *Power and Energy Society General Meeting, 2010 IEEE*, pages 1–7. IEEE, 2010.

[197] C ISO. What the duck curve tells us about managing a green grid. *Calif. ISO, Shap. a Renewed Futur*, pages 1–4.

[198] JST JOHN. Eia data reveals california's real and growing duck curve. *Greentech Media*, 25, 2017.

[199] MN Kabir, Yateendra Mishra, Gerard Ledwich, Zhao Yang Dong, and Kit Po Wong. Coordinated control of grid-connected photovoltaic reactive power and battery energy storage systems to improve the voltage profile of a residential distribution feeder. *IEEE Trans. Industrial Informatics*, 10(2):967–977, 2014.

[200] S. Karagiannopoulos, A. Rigas, N. Hatziargyriou, G. Hug, and A. Oudalov. Battery energy storage capacity fading and control strategies for deterministic and stochastic power profiles. In *2016 Power Systems Computation Conference (PSCC)*, pages 1–7, June 2016.

[201] Stavros Karagiannopoulos, Petros Aristidou, and Gabriela Hug. Hybrid approach for planning and operating active distribution grids. *IET Generation, Transmission & Distribution*, 11(3):685–695, 2017.

[202] Georges Kariniotakis, Luciano Martini, Chris Caerts, Helfried Brunner, and Nicolas Retière. Challenges, innovative architectures and control strategies for future networks: the web-of-cells, fractal grids and other concepts. In *CIRED 2017-24th International Conference on Electricity Distribution*, page 1287, 2017.

[203] Narendra Karmarkar. A new polynomial-time algorithm for linear programming. In *Proceedings of the sixteenth annual ACM symposium on Theory of computing*, pages 302–311. ACM, 1984.

[204] Diego Kiedanski, Md Umar Hashmi, Ana Bušić, and Daniel Kofman. Sensitivity to forecast errors in energy storage arbitrage for residential consumers. In *2019 IEEE International Conference on Communications, Control, and Computing Technologies for Smart Grids (SmartGridComm)*, pages 1–7. IEEE, 2019.

[205] Olli Kilkki, Antti Alahäivälä, and Ilkka Seilonen. Optimized control of price-based demand response with electric storage space heating. *IEEE Transactions on Industrial Informatics*, 11(1):281–288, 2015.

[206] Jae Ho Kim and Warren B Powell. Optimal energy commitments with storage and intermittent supply. *Operations research*, 59(6):1347–1360, 2011.

[207] Brendan Kirby, Ookie Ma, and Mark O'Malley. The value of energy storage for grid applications. *National Renewable Energy Laboratory. May. http://www. nrel. gov/docs/fy13osti/58465. pdf (accessed October 21, 2014)*, 2013.

[208] Mithat C Kisacikoglu, Burak Ozpineci, and Leon M Tolbert. Reactive power operation analysis of a single-phase ev/phev bidirectional battery charger. In *Power Electronics and ECCE Asia (ICPE & ECCE), 2011 IEEE 8th International Conference on*, pages 585–592. IEEE, 2011.

[209] Stephan Koch, Johanna L. Mathieu, and Duncan S. Callaway. Modeling and control of aggregated heterogeneous thermostatically controlled loads for ancillary services. In *Proc. 17th Power Systems Computation Conference*, pages 1–7, 2011.

[210] Iordanis Koutsopoulos, Vassiliki Hatzi, and Leandros Tassiulas. Optimal energy storage control policies for the smart power grid. In *Smart Grid Communications (SmartGridComm), 2011 IEEE International Conference on*, pages 475–480. IEEE, 2011.

[211] Alexandre Kowalczyk. SVM - Understanding the math - Duality and Lagrange multipliers. Online, https://www.svm-tutorial.com/2016/09/duality-lagrange-multipliers/, 2019.

[212] Elena Marie Krieger. *Effects of variability and rate on battery charge storage and lifespan.* PhD thesis, Princeton University, 2013.

[213] Dheepak Krishnamurthy, Canan Uckun, Zhi Zhou, Prakash R Thimmapuram, and Audun Botterud. Energy storage arbitrage under day-ahead and real-time price uncertainty. *IEEE Transactions on Power Systems*, 33(1):84–93, 2018.

[214] Richard K Lam, Duc Hoai Tran, and Hen-Geul Yeh. Economics of residential energy arbitrage in california using a pv system with directly connected energy storage. In *2015 IEEE Green Energy and Systems Conference (IGESC)*, pages 67–79. IEEE, 2015.

[215] Barrie Lawson. Electropaedia: Energy storage and power generation technologies. online http://www.mpoweruk.com/performance.htm, 2016.

[216] Jason Leadbetter and Lukas Swan. Battery storage system for residential electricity peak demand shaving. *Energy and buildings*, 55:685–692, 2012.

[217] T. Lee. Operating schedule of battery energy storage system in a time-of-use rate industrial user with wind turbine generators: A multipass iteration particle swarm optimization approach. *IEEE Transactions on Energy Conversion*, 22(3):774–782, Sep. 2007.

[218] Thomas Lee. Exploring frequency regulation market transformation. 2017.

[219] Zachary J. Lee. Acn-data webpage. https://ev.caltech.edu/dataset, April 2019.

[220] Zachary J Lee, Daniel Chang, Cheng Jin, George S Lee, Rand Lee, Ted Lee, and Steven H Low. Large-scale adaptive electric vehicle charging. In *2018 IEEE International Conference on Communications, Control, and Computing Technologies for Smart Grids (SmartGridComm)*, pages 1–7. IEEE, 2018.

[221] Zachary J. Lee, Daniel Johansson, and Steven H. Low. ACN-Sim — An Open-Source Simulator for Data-Driven Electric Vehicle Charging Research. In *Proceedings of the Tenth International Conference on Future Energy Systems*, e-Energy '19, June 2019.

[222] Zachary J. Lee, Tongxin Li, and Steven H. Low. ACN-Data: Analysis and Applications of an Open EV Charging Dataset. In *Proceedings of the Tenth International Conference on Future Energy Systems*, e-Energy '19, June 2019.

[223] Huijuan Li. Hosting Capacity for Distributed Energy Resources on Distribution Feeders. Online, https://cigre-usnc.org/wp-content/uploads/2017/10/Li-2017GOTF_HostingCap.pdf.

[224] Xiao Hui Li and Seung Ho Hong. User-expected price-based demand response algorithm for a home-to-grid system. *Energy*, 64:437–449, 2014.

[225] Pasqualino Lico, Mattia Marinelli, Katarina Knezović, and Samuele Grillo. Phase balancing by means of electric vehicles single-phase connection shifting in a low voltage danish grid. In *Power Engineering Conference (UPEC), 2015 50th International Universities*, pages 1–5. IEEE, 2015.

[226] Marco Liserre, Thilo Sauter, and John Y Hung. Future energy systems: Integrating renewable energy sources into the smart power grid through industrial electronics. *IEEE industrial electronics magazine*, 4(1):18–37, 2010.

[227] Hui Liu, Zechun Hu, Yonghua Song, and Jin Lin. Decentralized vehicle-to-grid control for primary frequency regulation considering charging demands. *IEEE Transactions on Power Systems*, 28(3):3480–3489, 2013.

[228] L. Liu, W. Miller, and G. Ledwich. Solutions for reducing electricity costs for communal facilities. australian ageing agenda. https://www.australianageingagenda.com.au/2017/10/27/solutions-reducing-facility-electricity-costs/, 2017.

[229] Zhixuan Liu. *Probabilistic assessment of unbalance in distribution networks based on limited monitoring*. PhD thesis, University of Manchester, 2014.

[230] PJM Interconnection LLC. Pjm manual 11: Energy & ancillary services market operations. Technical report, Tech. rep, 2014.

[231] J. Löfberg. Yalmip : A toolbox for modeling and optimization in matlab. In *In Proceedings of the CACSD Conference*, Taiwan, 2004.

[232] Rasmus Luthander, Joakim Widén, Daniel Nilsson, and Jenny Palm. Photovoltaic self-consumption in buildings: A review. *Applied Energy*, 142:80–94, 2015.

[233] Z. Ma, D. Callaway, and I. Hiskens. Decentralized charging control for large populations of plug-in electric vehicles. In *49th IEEE Conference on Decision and Control*, pages 206–212, Dec 2010.

[234] Ivan Machado and Itzel Arias. Grid codes comparison. 2006.

[235] Laxman Maharjan, Shigenori Inoue, Hirofumi Akagi, and Jun Asakura. State-of-charge (soc)-balancing control of a battery energy storage system based on a cascade pwm converter. *IEEE Transactions on Power Electronics*, 24(6):1628–1636, 2009.

[236] Yuri V Makarov, Shuai Lu, Jian Ma, and Tony B Nguyen. Assessing the value of regulation resources based on their time response characteristics. Technical report, Pacific Northwest National Lab.(PNNL), Richland, WA (United States), 2008.

[237] R. Malhame and C.-Y. Chong. Electric load model synthesis by diffusion approximation of a high-order hybrid-state stochastic system. 30(9):854 – 860, Sep 1985.

[238] Danielle Martini. Regulation Problem Statement Issue Charge Options. PJM – Online, http://www.pjm.com/~/media/committees-groups/committees/oc/20150526-rpi/20150526-item-02-regulation-problem-statement-options.ashx, December 2015.

[239] Julia Matevosyan. ERCOT Renewable Integration. Online, https://tinyurl.com/y5bss7zx.

[240] J. Mathias, A. Bušić, and S. Meyn. Demand dispatch with heterogeneous intelligent loads. In *Proc. 50th Annual Hawaii International Conference on System Sciences (HICSS), and arXiv 1610.00813*, 2017.

[241] J.L. Mathieu, S. Koch, and D.S. Callaway. State estimation and control of electric loads to manage real-time energy imbalance. 28(1):430–440, 2013.

[242] Johanna L Mathieu and Joshua A Taylor. Controlling nonlinear batteries for power systems: Trading off performance and battery life. In *Power Systems Computation Conference (PSCC), 2016*, pages 1–7. IEEE, 2016.

[243] Johanna L Mathieu and Joshua A Taylor. Controlling nonlinear batteries for power systems: Trading off performance and battery life. In *2016 Power Systems Computation Conference (PSCC)*, pages 1–7. IEEE, 2016.

[244] Garth P McCormick. Computability of global solutions to factorable nonconvex programs: Part i—convex underestimating problems. *Mathematical programming*, 10(1):147–175, 1976.

[245] Olivier Mégel, Johanna L Mathieu, and Göran Andersson. Scheduling distributed energy storage units to provide multiple services. In *Power Systems Computation Conference (PSCC), 2014*, pages 1–7. IEEE, 2014.

[246] Sean Meyn, Prabir Barooah, Ana Bušić, and Jordan Ehren. Ancillary service to the grid from deferrable loads: The case for intelligent pool pumps in florida. In *52nd IEEE Conference on Decision and Control*, pages 6946–6953. IEEE, 2013.

[247] Sean Meyn, Prabir Barooah, Ana Bušić, Yue Chen, and Jordan Ehren. Ancillary service to the grid using intelligent deferrable loads. 60(11):2847–2862, Nov 2015.

[248] Sean P Meyn, Prabir Barooah, Ana Bušić, Yue Chen, and Jordan Ehren. Ancillary service to the grid using intelligent deferrable loads. *IEEE Transactions on Automatic Control*, 60(11):2847–2862, 2015.

[249] Aditya Mishra, David Irwin, Prashant Shenoy, Jim Kurose, and Ting Zhu. Smartcharge: Cutting the electricity bill in smart homes with energy storage. In *Proceedings of the 3rd Internat. Conference on Future Energy Systems: Where Energy, Computing and Communication Meet*. ACM, 2012.

[250] Amir-Hamed Mohsenian-Rad and Alberto Leon-Garcia. Optimal residential load control with price prediction in real-time electricity pricing environments. *IEEE Trans. Smart Grid*, 1(2):120–133, 2010.

[251] Pedram Mokrian, Moff Stephen, et al. A stochastic programming framework for the valuation of electricity storage. In *26th USAEE/IAEE North American Conference*, pages 24–27. Citeseer, 2006.

[252] Janina Moshövel, Kai-Philipp Kairies, Dirk Magnor, Matthias Leuthold, Mark Bost, Swantje Gährs, Eva Szczechowicz, Moritz Cramer, and Dirk Uwe Sauer. Analysis of the maximal possible grid relief from pv-peak-power impacts by using storage systems for increased self-consumption. *Applied Energy*, 137:567–575, 2015.

[253] Joshua Michael Mueller. *Evaluating storage technologies for wind and solar energy*. PhD thesis, Massachusetts Institute of Technology, 2018.

[254] Eduard Muljadi, Charles Butterfield, Robert Yinger, and Harold Romanowitz. Energy storage and reactive power compensator in a large wind farm. In *42nd AIAA Aerospace Sciences Meeting and Exhibit*, page 352, 2004.

[255] Harsha Nagarajan, Mowen Lu, Emre Yamangil, and Russell Bent. Tightening mccormick relaxations for nonlinear programs via dynamic multivariate partitioning. In *International Conference on Principles and Practice of Constraint Programming*, pages 369–387. Springer, 2016.

[256] K-H Ng and Gerald B Sheble. Direct load control-a profit-based load management using linear programming. *IEEE Transactions on Power Systems*, 13(2):688–694, 1998.

[257] Tu A Nguyen and Raymond H Byrne. Maximizing the cost-savings for time-of-use and net-metering customers using behind-the-meter energy storage systems. In *2017 North American Power Symposium (NAPS)*, pages 1–6. IEEE, 2017.

[258] Tu A Nguyen, Raymond H Byrne, Babu R Chalamala, and Imre Gyuk. Maximizing the revenue of energy storage systems in market areas considering nonlinear storage efficiencies. In *2018 International Symposium on Power Electronics, Electrical Drives, Automation and Motion (SPEEDAM)*, pages 55–62. IEEE, 2018.

[259] Anna Nordling, Ronja Englund, Alexander Hembjer, and Andreas Mannberg. Electricity storage technologies IVA's Electricity Crossroads project. Online, https://www.iva.se/globalassets/rapporter/vagval-el/201604-iva-vagvalel-ellagring-rapport-english-e-ny.pdf.

[260] United States Department of Energy. International energy outlook. *Energy Information Administration (EIA) USA*, 2016.

[261] Michael Olaleye. Benefits Factor. PJM – Online, http://www.pjm.com/~/media/committees-groups/task-forces/rmistf/20151111/20151111-item-04-benefits-factor-additional-info.ashx, July 2015.

[262] Yutaka Ota, Haruhito Taniguchi, Tatsuhito Nakajima, Kithsiri M Liyanage, Jumpei Baba, and Akihiko Yokoyama. Autonomous distributed v2g (vehicle-to-grid) satisfying scheduled charging. *IEEE Transactions on Smart Grid*, 3(1):559–564, 2012.

[263] Alexandre Oudalov, Rachid Cherkaoui, and Antoine Beguin. Sizing and optimal operation of battery energy storage system for peak shaving application. In *Power Tech, 2007 IEEE Lausanne*, pages 621–625. IEEE, 2007.

[264] Alexdandre Oudalov, Daniel Chartouni, Christian Ohler, and G_ Linhofer. Value analysis of battery energy storage applications in power systems. In *Power Systems Conference and Exposition, 2006. PSCE'06. 2006 IEEE PES*, pages 2206–2211. IEEE, 2006.

[265] Peter Palensky and Dietmar Dietrich. Demand side management: Demand response, intelligent energy systems, and smart loads. *IEEE transactions on industrial informatics*, 7(3):381–388, 2011.

[266] G Ernest Palomino, John Wiles, John Stevens, and Frank Goodman. Performance of a grid connected residential photovoltaic system with energy storage. In *Photovoltaic Specialists Conference, 1997., Conference Record of the Twenty-Sixth IEEE*, pages 1377–1380. IEEE, 1997.

[267] M Papadopoulos, P Malatestas, and N Hatziargyriou. Simulation and analysis of small and medium size power systems containing wind turbines. *IEEE Transactions on Power Systems*, 6(4):1453–1458, 1991.

[268] Alessandra Parisio, Luca Fabietti, Marco Molinari, Damiano Varagnolo, and Karl H Johansson. Control of hvac systems via scenario-based explicit mpc. In *Decision and Control (CDC), 2014 IEEE 53rd Annual Conference on*, pages 5201–5207. IEEE, 2014.

[269] Yong-Gi Park, Jong-Bae Park, Namsu Kim, and Kwang Lee. Linear formulation for short-term operational scheduling of energy storage systems in power grids. *Energies*, 10(2):207, 2017.

[270] Rich Pedroncelli. Frequency Regulation Compensation in the Organized Wholesale Power Markets – FERC 755. FERC Docket Nos. RM11-7-000 and AD10-11-000; Order No. 755 – Online, http://tinyurl.com/FERC755, October 20 2011.

[271] Jacques Peronnet. Power factor correction kvar policy in countries. Online, https://tinyurl.com/y437cpyd.

[272] Marek Petrik and Xiaojian Wu. Optimal threshold control for energy arbitrage with degradable battery storage. In *UAI*, pages 692–701, 2015.

[273] P Pillay and M Manyage. Definitions of voltage unbalance. *IEEE Power Engineering Review*, 21(5):50–51, 2001.

[274] PJM. PJM Regulation Zone Preliminary Billing Data, https://tinyurl.com/y85ezqco, 2018.

[275] Northwest Power and Conservation Council. White paper on the value of energy storage to the future power system. Online, https://www.nwcouncil.org/reports/white-paper-value-energy-storage-future-power-system.

[276] I. Prodan and E. Zio. An optimization-based control approach for reliable microgrid energy management under uncertainties. In *IEEE Workshop on Integration of Stochastic Energy in Power Systems (ISEPS)*, pages 4–7, Nov 2013.

[277] Prsma, M-ITI, EEM, and ACIF-CCIM. Data Collection, Modelling, Simulation and Decision. Technical report 4.3, European Commission, Funchal, Portugal, June 2018.

[278] GA Putrus, Pasist Suwanapingkarl, David Johnston, EC Bentley, and Mahinsasa Narayana. Impact of electric vehicles on power distribution networks. In *Vehicle Power and Propulsion Conference, 2009. VPPC'09. IEEE*, pages 827–831. IEEE, 2009.

[279] Li Ping Qian, Ying Jun Angela Zhang, Jianwei Huang, and Yuan Wu. Demand response management via real-time electricity price control in smart grids. *IEEE Journal on Selected areas in Communications*, 31(7):1268–1280, 2013.

[280] Junjie Qin, Raffi Sevlian, David Varodayan, and Ram Rajagopal. Optimal electric energy storage operation. In *Power and Energy Society General Meeting, 2012 IEEE*, pages 1–6. IEEE, 2012.

[281] Mohammad Rasouli, Camille Pache, Patrick Panciatici, Jean Maeght, Ramesh Johari, and Ram Rajagopal. Cloud storage for multi-service battery operation (extended version). *arXiv preprint arXiv:1906.00732*, 2019.

[282] Elizabeth L Ratnam, Steven R Weller, and Christopher M Kellett. An optimization-based approach for assessing the benefits of residential battery storage in conjunction with solar pv. In *Bulk Power System Dynamics and Control-IX Optimization, Security and Control of the Emerging Power Grid (IREP), 2013 IREP Symposium*, pages 1–8. IEEE, 2013.

[283] Hongbo Ren, Qiong Wu, Weijun Gao, and Weisheng Zhou. Optimal operation of a grid-connected hybrid pv/fuel cell/battery energy system for residential applications. *Energy*, 113:702–712, 2016.

[284] Ralph Tyrell Rockafellar. *Convex analysis*. Princeton university press, 2015.

[285] Peng Rong and M. Pedram. Battery-aware power management based on Markovian decision processes. *IEEE Transactions on Computer-Aided Design of Integrated Circuits and Systems*, 25(7):1337–1349, July 2006.

[286] Peng Rong and Massoud Pedram. Battery-aware power management based on markovian decision processes. *IEEE Transactions on Computer-Aided Design of Integrated Circuits and Systems*, 25(7):1337–1349, 2006.

[287] Mardavij Roozbehani, Munther A Dahleh, and Sanjoy K Mitter. Volatility of power grids under real-time pricing. *IEEE Transactions on Power Systems*, 27(4):1926–1940, 2012.

[288] RTE France. RTE figures. Online, https://www.rte-france.com/en/screen/europe-s-biggest-transmission-system, 2019.

[289] Nerea Ruiz, Iñigo Cobelo, and José Oyarzabal. A direct load control model for virtual power plant management. *IEEE Transactions on Power Systems*, 24(2):959–966, 2009.

[290] Rogerio Salustiano, Estacio Neto, and Manuel Martinez. The unbalanced load cost on transformer losses at a distribution system. 2013.

[291] Pedram Samadi, Amir-Hamed Mohsenian-Rad, Robert Schober, Vincent WS Wong, and Juri Jatskevich. Optimal real-time pricing algorithm based on utility maximization for smart grid. In *Smart Grid Communications (SmartGridComm), 2010 First IEEE International Conference on*, pages 415–420. IEEE, 2010.

[292] Jeremias Schmidli, Line Roald, Spyros Chatzivasileiadis, and Göran Andersson. Stochastic ac optimal power flow with approximate chance-constraints. In *Power and Energy Society General Meeting (PESGM), 2016*, pages 1–5. IEEE, 2016.

[293] Farhad Shahnia, Arindam Ghosh, Gerard Ledwich, and Firuz Zare. Predicting voltage unbalance impacts of plug-in electric vehicles penetration in residential low-voltage distribution networks. *Electric Power Components and Systems*, 41(16):1594–1616, 2013.

[294] Yuanyuan Shi, Bolun Xu, Di Wang, and Baosen Zhang. Using battery storage for peak shaving and frequency regulation: Joint optimization for superlinear gains. *IEEE Transactions on Power Systems*, 33(3):2882–2894, 2018.

[295] Cal Silcox. PG&E Rates Overview. Online, https://www.arb.ca.gov/msprog/asb/workshop/pge.pdf.

[296] Bhim Singh, Kamal Al-Haddad, and Ambrish Chandra. A review of active filters for power quality improvement. *IEEE transactions on industrial electronics*, 46(5):960–971, 1999.

[297] Ramteen Sioshansi, Paul Denholm, Thomas Jenkin, and Jurgen Weiss. Estimating the value of electricity storage in pjm: Arbitrage and some welfare effects. *Energy economics*, 31(2):269–277, 2009.

[298] JW Smith, W Sunderman, R Dugan, and Brian Seal. Smart inverter volt/var control functions for high penetration of pv on distribution systems. In *Power Systems Conference and Exposition (PSCE), 2011 IEEE/PES*, pages 1–6. IEEE, 2011.

[299] Kandler Smith, Ying Shi, and Shriram Santhanagopalan. Degradation mechanisms and lifetime prediction for lithium-ion batteries—a control perspective. In *American Control Conference (ACC), 2015*, pages 728–730. IEEE, 2015.

[300] Kandler Smith, E Wood, S Santhanagopalan, GH Kim, J Neubauer, and A Pesaran. Models for battery reliability and lifetime. Technical report, National Renewable Energy Laboratory (NREL), Golden, CO., 2014.

[301] IEEE Standard. Ieee p1159.1: Guide for recorder and data acquisition requirements for characterization of power quality events. Online, http://grouper.ieee.org/groups/1159/1/IE1159_95e.pdf, 2000.

[302] David Steen, Tuan Le, and Lina Bertling. Price-based demand-side management for reducing peak demand in electrical distribution systems–with examples from gothenburg. In *NORDAC 2012*, 2012.

[303] Thomas Stetz. German Guidelines and Laws for PV Grid Integration. Online, https://tinyurl.com/yyc7dkcw.

[304] Steven Stoft. Power system economics. *Journal of Energy Literature*, 8:94–99, 2002.

[305] Han-I Su and Abbas El Gamal. Modeling and analysis of the role of energy storage for renewable integration: Power balancing. *IEEE Transactions on Power Systems*, 28(4):4109–4117, 2013.

[306] Sun Sun, Ben Liang, Min Dong, and Joshua A Taylor. Phase balancing using energy storage in power grids under uncertainty. *IEEE Transactions on Power Systems*, 31(5):3891–3903, 2016.

[307] Zach Taylor, Hossein Akhavan-Hejazi, and Hamed Mohsenian-Rad. Power hardware-in-loop simulation of grid-connected battery systems with reactive power control capability. In *Power Symposium (NAPS), 2017 North American*, pages 1–6. IEEE, 2017.

[308] Enrico Telaretti, Mariano Ippolito, and Luigi Dusonchet. A simple operating strategy of small-scale battery energy storages for energy arbitrage under dynamic pricing tariffs. *Energies*, 9(1):12, 2015.

[309] Anupam A Thatte, Le Xie, Daniel E Viassolo, and Sunita Singh. Risk measure based robust bidding strategy for arbitrage using a wind farm and energy storage. *IEEE Transactions on Smart Grid*, 4(4):2191–2199, 2013.

[310] Jacopo Torriti. Price-based demand side management: Assessing the impacts of time-of-use tariffs on residential electricity demand and peak shifting in northern italy. *Energy*, 44(1):576–583, 2012.

[311] John N Tsitsiklis and Yunjian Xu. Pricing of fluctuations in electricity markets. *European Journal of Operational Research*, 246(1):199–208, 2015.

[312] P Tulpule, Vincenzo Marano, and Giorgio Rizzoni. Effects of different phev control strategies on vehicle performance. In *American Control Conference, 2009. ACC'09.*, pages 3950–3955. IEEE, 2009.

[313] Konstantin Turitsyn, Petr Sulc, Scott Backhaus, and Michael Chertkov. Local control of reactive power by distributed photovoltaic generators. In *Smart Grid Communications (SmartGridComm), 2010 First IEEE International Conference on*, pages 79–84. IEEE, 2010.

[314] Rahul Urgaonkar, Bhuvan Urgaonkar, Michael J Neely, and Anand Sivasubramaniam. Optimal power cost management using stored energy in data centers. In *Proceedings of the ACM SIGMETRICS joint international conference on Measurement and modeling of computer systems*, pages 221–232. ACM, 2011.

[315] Energy Information Administration (US). U.S. Battery Storage Market Trends. Online, https://www.eia.gov/analysis/studies/electricity/batterystorage/pdf/battery_storage.pdf.

[316] UTE Uruguay. Pliego tarifario. Online, https://tinyurl.com/y5ug28jh, 2019.

[317] Peter M van de Ven, Nidhi Hegde, Laurent Massoulié, and Theodoros Salonidis. Optimal control of end-user energy storage. *IEEE Transactions on Smart Grid*, 4(2):789–797, 2013.

[318] Prof. L. Vandenberghe. Online, https://tinyurl.com/yytfnmnx.

[319] John S Vardakas, Nizar Zorba, and Christos V Verikoukis. A survey on demand response programs in smart grids: Pricing methods and optimization algorithms. *IEEE Communications Surveys & Tutorials*, 17(1):152–178, 2015.

[320] VCharge, AAU, Route Monkey, CERTH, Prsma, and RINA-C. Most Appropriate DR Services for each Pilot. Technical report 5.1, European Commission, Bristol, UK, February 2018.

[321] Filomeno M Vieira, Pedro S Moura, and Aníbal T de Almeida. Energy storage system for self-consumption of photovoltaic energy in residential zero energy buildings. *Renewable Energy*, 103:308–320, 2017.

[322] C Vlahoplus, G Litra, P Quinlan, and C Becker. Revisiting the california duck curve: An exploration of its existence, impact, and migration potential. Technical report, Tech. rep., Scottmadden, Inc.(Aug. 2016), 2016.

[323] Rahul Walawalkar, Jay Apt, and Rick Mancini. Economics of electric energy storage for energy arbitrage and regulation in new york. *Energy Policy*, 35(4):2558–2568, 2007.

[324] Hao Wang and Baosen Zhang. Energy storage arbitrage in real-time markets via reinforcement learning. *arXiv preprint arXiv:1711.03127*, 2017.

[325] Hao Wang and Baosen Zhang. Energy storage arbitrage in real-time markets via reinforcement learning. In *2018 IEEE Power & Energy Society General Meeting (PESGM)*, pages 1–5. IEEE, 2018.

[326] Hui Wang et al. Energy storage for power factor correction in battery charger for electric-powered vehicles, October 16 2014. US Patent App. 14/139,059.

[327] Kai Wang, Steven Skiena, and Thomas G Robertazzi. Phase balancing algorithms. *Electric Power Systems Research*, 96:218–224, 2013.

[328] Wei Wang and Nanpeng Yu. Phase balancing in power distribution network with data center. *ACM SIGMETRICS Performance Evaluation Review*, 45(2):64–69, 2017.

[329] Sam Weckx and Johan Driesen. Load balancing with ev chargers and pv inverters in unbalanced distribution grids. *IEEE Transactions on Sustainable Energy*, 6(2):635–643, 2015.

[330] Corey D White and K Max Zhang. Using vehicle-to-grid technology for frequency regulation and peak-load reduction. *Journal of Power Sources*, 196(8):3972–3980, 2011.

[331] Xiaomin Xi, Ramteen Sioshansi, and Vincenzo Marano. A stochastic dynamic programming model for co-optimization of distributed energy storage. *Energy Systems*, 5(3):475–505, 2014.

[332] Bolun Xu et al. Degradation-limiting optimization of battery energy storage systems operation. 2013.

[333] Bolun Xu, Alexandre Oudalov, Jan Poland, Andreas Ulbig, and Göran Andersson. Bess control strategies for participating in grid frequency regulation. *IFAC Proceedings Volumes*, 47(3):4024–4029, 2014.

[334] Bolun Xu, Jinye Zhao, Tongxin Zheng, Eugene Litvinov, and Daniel S Kirschen. Factoring the cycle aging cost of batteries participating in electricity markets. *IEEE Transactions on Power Systems*, 2017.

[335] Yunjian Xu and Lang Tong. Optimal operation and economic value of energy storage at consumer locations. *IEEE Transactions on Automatic Control*, 62(2):792–807, 2017.

[336] Shaoyong Yang, Dawei Xiang, Angus Bryant, Philip Mawby, Li Ran, and Peter Tavner. Condition monitoring for device reliability in power electronic converters: A review. *IEEE Transactions on Power Electronics*, 25(11):2734–2752, 2010.

[337] Ji Hoon Yoon, Ross Baldick, and Atila Novoselac. Dynamic demand response controller based on real-time retail price for residential buildings. *IEEE Transactions on Smart Grid*, 5(1):121–129, 2014.

[338] Dimitrios Zafirakis, Konstantinos J Chalvatzis, Giovanni Baiocchi, and Georgios Daskalakis. The value of arbitrage for energy storage: Evidence from european electricity markets. *Applied energy*, 184:971–986, 2016.

[339] Menglian Zheng, Christoph J Meinrenken, and Klaus S Lackner. Smart households: Dispatch strategies and economic analysis of distributed energy storage for residential peak shaving. *Applied Energy*, 147:246–257, 2015.

[340] Haihua Zhou, Tanmoy Bhattacharya, Duong Tran, Tuck Sing Terence Siew, and Ashwin M Khambadkone. Composite energy storage system involving battery and ultracapacitor with dynamic energy management in microgrid applications. *IEEE transactions on power electronics*, 26(3):923–930, 2011.

[341] Matija Zidar, Pavlos S Georgilakis, Nikos D Hatziargyriou, Tomislav Capuder, and Davor Škrlec. Review of energy storage allocation in power distribution networks: applications, methods and future research. *IET Generation, Transmission & Distribution*, 10(3):645–652, 2016.

[342] Ray Daniel Zimmerman, Carlos Edmundo Murillo-Sánchez, Robert John Thomas, et al. Matpower: Steady-state operations, planning, and analysis tools for power systems research and education. *IEEE Transactions on power systems*, 26(1):12–19, 2011.

[343] Charalampos Ziras, Evangelos Vrettos, and Goran Andersson. Primary frequency control with refrigerators under startup dynamics and lockout constraints. In *IEEE Power & Energy Society General Meeting*, pages 1–5, 2015.

[344] Michael Zuercher-Martinson. Smart pv inverter benefits for utilities. *Renewable Energy World*, 2012.

RÉSUMÉ

Cette thèse est motivée par les transformations des systèmes d'énergie électrique, dues à une plus grande intégration des énergies renouvelables et à un modèle de consommation en évolution. Le stockage d'énergie est une solution possible pour faciliter une transition en douceur, garantissant la stabilité du système d'alimentation électrique. Dans cette thèse, la batterie Li-Ion a un double rôle de stockage d'énergie. Premièrement, il est utilisé par les consommateurs individuels pour minimiser le coût de l'électricité. Cela se fait par un arbitrage énergétique basé sur le prix de l'électricité, la correction du facteur de puissance, la réduction de la demande de pointe et la préservation de l'énergie. Ensuite, il est également utilisé pour augmenter la fiabilité et la stabilité du réseau électrique, en effectuant une régulation dynamique et une phase d'équilibrage. Le coût des batteries étant toujours élevé, l'importance est également accordée à la santé de la batterie compte tenu de sa dégradation dans les formulations d'optimisation et de contrôle. Plusieurs études de cas utilisant des données réelles sont menées pour évaluer les performances des algorithmes de contrôle et d'optimisation du stockage. Nous notons que la baisse des prix des batteries et la part croissante des énergies renouvelables intermittentes ne feront qu'augmenter la pertinence de ces travaux pour les futurs réseaux électriques.

MOTS CLÉS

Stockage d'énergie, optimisation, contrôle, systèmes d'alimentation électrique.

ABSTRACT

This thesis is motivated by the electric power system transformations due to more renewable integration and changing consumption patterns. Energy storage is one possible solution to facilitate a smooth transition, ensuring the stability of the power system. In this thesis Li-Ion battery is used both at the level of individual consumers, minimizing the cost of electricity by performing energy arbitrage under time-varying electricity price, power factor correction, peak demand shaving and energy backup, and at the grid level for increasing reliability and stability of the power network by performing dynamic regulation and phase balancing. The cost of the batteries being still high, the importance is also given to the health of the battery taking into account its degradation in optimization and control formulations. Several case studies using real data are conducted to evaluate the performance of the storage control and optimization algorithms. We observe that the ever-decreasing prices of batteries and the growing share of intermittent renewables will only increase the relevance of this work for future power networks.

KEYWORDS

Energy storage, optimization, control, electrical power systems.